UNIVERSITY OF CAMBRIDGE

The Development of Peroxide-Responsive Arylboronic Acids for Antibody-Drug Conjugates and Small-Molecule Prodrugs

Nicola Ashman

Lucy Cavendish College

University of Cambridge

June 2023

Supervised by Professor David R. Spring

This thesis is submitted for the degree of **Doctor of Philosophy**

Declaration

This thesis is the result of my own work and includes nothing which is the outcome of work done in collaboration except as declared in the Preface and specified in the text. I further state that no substantial part of my thesis has already been submitted, or, is being concurrently submitted for any such degree, diploma or other qualification at the University of Cambridge or any other University or similar institution except as declared in the Preface and specified in the text. It does not exceed the prescribed word limit for the Physics and Chemistry Degree Committee.

Nicola Ashman

June 2023

Lucy Cavendish College, University of Cambridge

The Development of Peroxide-Responsive Arylboronic Acids for Antibody-Drug Conjugates and Small-Molecule Prodrugs

Nicola Ashman

Cancer cells exhibit oxidative stress, which results in the over-production of reactive-oxygen species (ROS), such as hydrogen peroxide. Hence, there are elevated levels of hydrogen peroxide in cancer compared to healthy cells, which can be exploited for the targeted delivery of drugs.

Section I of this thesis describes the design, synthesis, and evaluation of antibody-drug conjugates (ADCs) comprising arylboronic acid linkers, which give responsive drug release in the presence of the elevated hydrogen peroxide in cancer. ADCs are a continually expanding therapeutic area, and the linker used for the antibody-drug connection is of upmost importance in determining the stability of the conjugate and the specificity of drug release. Arylboronic acids are known to undergo C-B bond oxidation by action of hydrogen peroxide, and when combined with a suitable self-immolative aryl ring, can subsequently undergo spontaneous 1,6-elimination to release a free drug. Hence, initial studies evaluated a panel of model linkers with a fluorescent reporter molecule and confirmed the linker reactivity with peroxide but otherwise high stability. Trastuzumab peroxide-cleavable ADCs were then synthesised and evaluated *in vitro* against a panel of breast cancer cell lines, and preliminary evidence is presented which suggests the ADCs may not require internalisation for payload release. Hence, peroxide-cleavable ADCs comprising anti-PD-L1 antibody durvalumab were also synthesised and evaluated *in vitro*, with preliminary evidence suggesting the generation of an efficacious non-internalising ADC.

Section II of this thesis describes the application of peroxide-responsive arylboronic acids towards the generation of small-molecule prodrugs. Non-targeted drugs, such as olaparib and navitoclax, often suffer from poor tolerability and toxicity because they exert their function on healthy cells as well as target cancer cells. Thus, to improve their efficacy and safety profile, inactive prodrugs of olaparib and navitoclax were designed by capping key amines with the arylboronic acid self-immolative motif. This would enable site-specific release of the free drugs upon encounter with the high levels of hydrogen peroxide in cancer. Synthetic efforts and preliminary investigations towards the peroxide-responsive prodrugs is presented.

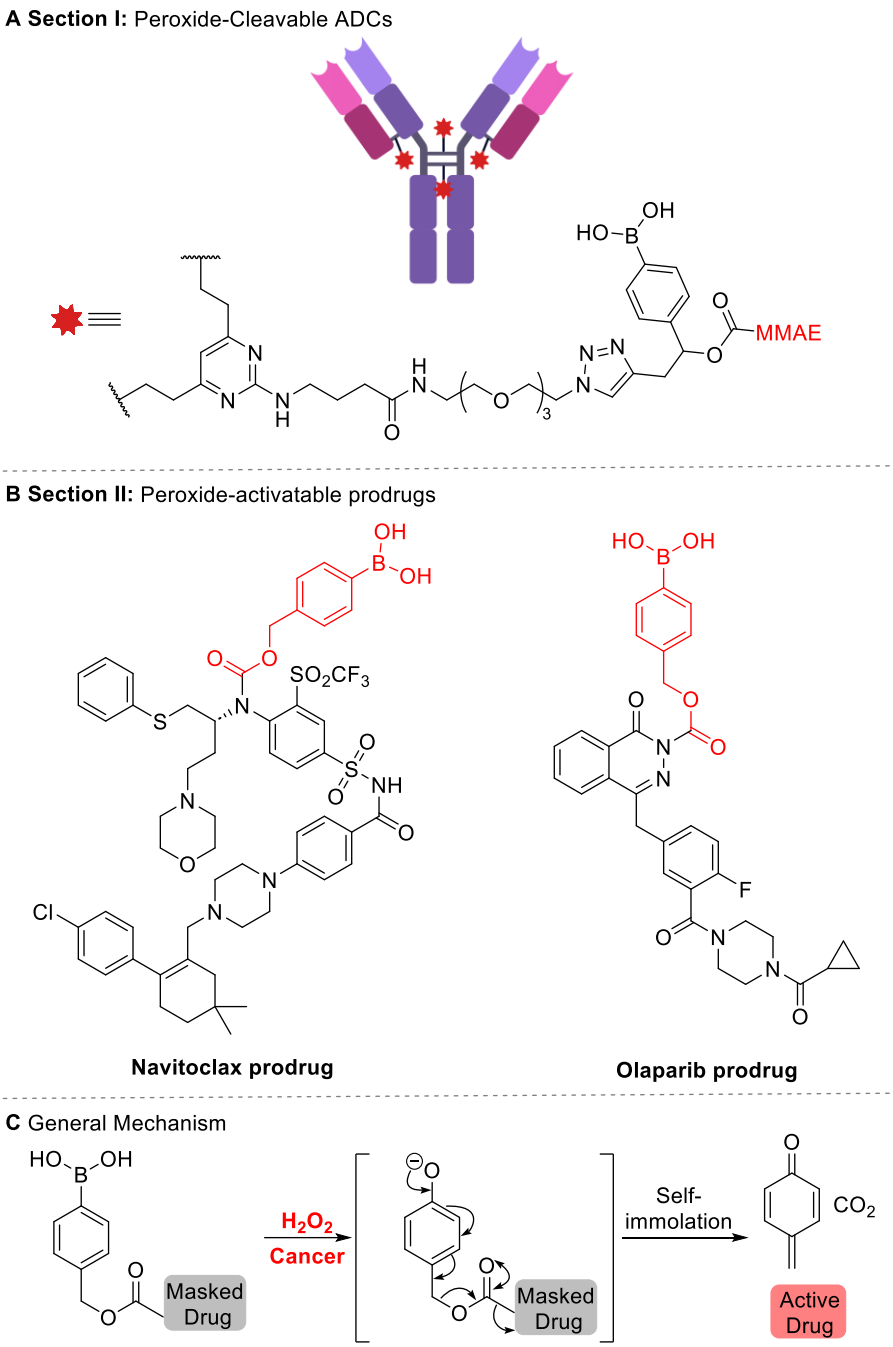

Figure 1: A) Section I: peroxide-cleavable ADCs, MMAE = monomethyl auristatin E B) Section II: peroxide-activatable small molecule prodrugs of navitoclax and olaparib and C) general mechanism of arylboronic acid reaction with hydrogen peroxide in cancer, followed by self-immolation to release free drug.

Acknowledgments

First and foremost, I would like to thank Prof. David Spring for his continued support and welcome advice throughout the years. Completing a PhD in your group has been a pleasure and I am very glad to have had the opportunity. I would also like to thank AstraZeneca for my funding, and in particular the support of my supervisors Ryan Greenwood and Arnaud Tiberghien.

Special thanks to Jonathan Bargh who not only supervised me in the group, but also continued to supervise my work remotely from AZ Sweden. The quality of my research has undoubtedly been greatly improved thanks to your continued sound advice and valued mentorship.

Thanks also extends to Stephen Walsh who acquainted me to the wonderful (read: challenging) world of cellular biology. Your expertise and advice were in no doubt essential for the completion of my PhD. Thanks to Prof. Jason Carroll, Jill Temple, and the rest of the Carroll lab at CRUK who were extremely welcoming and incredibly kind to allow a bunch of chemists to infiltrate the TC room with bacteria-infested compounds and weird blue lights. A massive thanks to Mahri Park for her companionship in our quest to conquer tissue culture: there's no-one else I'd rather have by my side to spend endless hours pipetting.

Jiyan and Hikaru: thank you to your friendship and company in lab bay 1. It will be hard to forget some of our weird conversations, and I will greatly miss the eclectic music that underscored our lab work. Thanks also for tolerating all of my stupid questions.

The NMR team at Cambridge goes above and beyond to support research, so thanks to Peter Gierth, Andrew Mason, and Duncan Howe for their incredible help. Thanks also to David Longmire at AZ for assistance with a tricky NMR.

Thanks to Prof. Mike Murphy for a valuable discussion about ROS, and thanks to Sarah, Tomas, Jonny and Mahri for proofreading this thesis. Figures were created using BioRender.com.

To the Kerrs: John, Linda, Laura, Emma & Archie, thank you for always being there - be it for dog walks, a bad game of poker, or a Sunday dinner – I am forever grateful and lucky to be a part of mi familia extendida. Andrew: I will always be grateful for your continued support, encouragement, and comfort, especially in the more difficult times. I could not have done this without you.

And finally, thanks to my family. I've never known such resilience, strength, and selflessness and I am proud of you all. Mum: you have always enabled me to do whatever I set out to and I am eternally in your debt.

Abbreviations

^{t}	Tertiary
°C	degrees Celsius
µ	Micro
5-FU	5-Fluorouracil
A	Absorbance
Ac	Acetyl
ADC	Antibody-Drug Conjugate
ALL	Acute lymphoblastic leukemia
AMC	7-Amino-4-methyl coumarin
AML	Acute myeloid leukemia
AMT	Aminotrexate
aq	Aqueous
ATCC	American Type Culture Collection
Bak	Bcl-2 antagonist/killer 1
Bax	Bcl-2-associated X protein
Bcl-2	B-cell lymphoma 2
Bcl-w	Bcl-2-like protein 2
Bcl-xL	B-cell lymphoma-extra large
Bid	BH3 interacting-domain death agonist
Bik	Bcl-2-interacting killer
Bmf	Bcl-2-modifying factor
Boc	*tert*-Butoxycarbonyl
Boc_2O	Boc anhydride
Bok	Bcl-2 related ovarian killer
Bpin	Pinacol boronate
br	Broad
BRCA	Breast Cancer Associated
BTFFH	Fluoro-*N*,*N*,*N*′,*N*′-bis(tetramethylene)formamidinium hexafluorophosphate
Calcd	Calculated
CAT	Catalase
CD20, 21 etc	Cluster of differentiate
CEACAM5	Carcinoembryonic antigen cell adhesion molecule 5
Cem	Cemadotin

Ces1c	Carboxylesterase 1c
CLL	Chronic lymphatic leukemia
conc.	Concentrated
COSHH	Control of substances hazardous to health
COSY	Correlation spectroscopy
CuAAC	Copper-catalyzed azide-alkyne cycloaddition
d	Doublet
Da	Dalton
DAB	Diazaborine
DAR	Drug-to-antibody ratio
DCE	1,2-Dichloroethane
DCM	Dichloromethane
DIPEA	*N*,*N*,-Diisopropylethylamine
DM1	Emtansine
DM4	Ravtansine
DMAP	4-(Dimethylamino)pyridine
DMB	Di-methoxy benzyl
DME	1,2-Dimethoxyethane
DMEM	Dulbecco's Modified Eagle Medium
DMF	*N,N*-Dimethylformamide
DMSO	Dimethyl sulfoxide
DNA	Deoxyribonucleic acid
DOX	Doxorubicin
dppf	1,1'-Bis(diphenylphosphino)ferrocene
DVP	Divinyl pyrimidine
EC_{50}	Half maximal effective concentration
ECACC	European Collection of Authenticated Cell Cultures
EDG	Electron-donating group
EPR	Enhanced permeability and retention
eq.	Equivalent(s)
equiv.	Equivalent(s)
ESI	Electrospray ionisation
Et	Ethyl
et al.	And others

EWG	Electron-withdrawing group
Fab	Fragment, antigen-binding
FBS	Fetal bovine serum
Fc	Fragment, crystallisable
FCC	Flash column chromatography
FDA	Food and Drug Administration
Fmoc	9-Fluorenylmethoxycarbonyl
g	gram(s)
Gal-3-BP	Galectin-3-binding protein
Gem	Gemcitabine
GSH	L-Glutathione
h	Hour(s)
HATU	1-[Bis(dimethylamino)methylene]-1*H*-1,2,3-triazolo[4,5-*b*]pyridinium 3-oxide hexafluorophosphate
HC	Heavy chain
HDAC	Histone deacetylase
HEK	Human embryonic kidney
HER2	Human epidermal growth factor receptor 2
HIC	Hydrophobic interaction chromatography
HMBC	Heteronuclear multiple bond correlation spectroscopy
HMPA	Hexamethylphosphoramide
HOBt	1-Hydroxybenzotriazole
HOMO	Highest occupied molecular orbital
HPLC	High performance liquid chromatography
HR	Homologous recombination
HRMS	High resolution mass spectrometry
HSQC	Heteronuclear single-quantum correlation spectroscopy
Hz	Hertz
IC_{50}	Half-maximal inhibitory concentration
IEDDA	Inverse-electron demand Diels-Alder
IgG	Immunoglobulin G
IR	Infrared
J	Coupling constant
Ki	Inhibition constant

L	Litres
LC	Light chain
LCMS	Liquid chromatography mass spectrometry
LDA	Lithium diisopropylamide
LG	Leaving group
LiHMDS	Lithium hexamethyldisilazide
LRG1	Leucine-rich alpha-2-glycoprotein 1
LUMO	Lowest unoccupied molecular orbital
M	Molar
m	Milli
m	Multiplet
mAb	Monoclonal antibody
MC	Maleimidocaproyl
Mcl-1	Induced myeloid leukemia cell differentiation protein
Me	Methyl
min(s)	Minute(s)
MLT	Melatonin
MMAE	Monomethyl Auristatin E
MMAF	Monomethyl Auristatin F
MMP	Matrix Metalloproteinase
MMPi	Matrix metalloproteinase inhibitors
MO	Molecular orbital
Mol	mole(s)
MTX	Methotrexate
MWCO	Molecular weight cut off
N	Normal
NAD	Nicotinamide adenine dinucleotide
NaHMDS	Sodium hexamethyldisilazide
Nav	Navitoclax
Nav-gal	Galacto-conjugated navitoclax prodrug
NGM	Next generation maleimide
NKA	Sodium-potassium pump
NMR	Nuclear magnetic resonance
p	*para*

p	Pico
PAB	*para*-Amino benzyl
PABE	*para*-Aminobenzyl ether
PAR	Poly(ADP-ribose)
PARP	Poly(ADP-ribose)polymerases
PARPi	PARP inhibitors
PBD	Pyrrolobenzodiazepine
PBS	Phosphate buffered saline
PD-1	Programmed cell death protein 1
PDB	Protein data bank
PD-L1	Programmed cell death-ligand 1
PE	Petroleum ether
Ph	Phenyl
PMB	*para*-Methoxy benzyl
PNGase F	Peptide: *N*-glycosidase F
PNP	*para*-Nitrophenyl
ppm	Parts per million
PROTAC	Proteolysis targeting chimera
Puma	p53 upregulated modulator of apoptosis
R	Undefined chemical group
Rf	Retention factor
ROESY	Rotating Frame Overhauser Enhancement Spectroscopy
ROS	Reactive-Oxygen Species
RP	Reverse-phase
RPMI	Roswell Park Memorial Institute
rt	Room temperature
s	Singlet
SAHA	Vorinostat
SAR	Structure-activity relationship
sat.	Saturated
scFv	Single chain variable fragment
SDS-page	Sodium dodecyl sulfate-polyacrylamide gel electrophoresis
SEC	Size-exclusion chromatography
SIP	Small immune protein

SLL	Small lymphocytic lymphoma
SMCC	Succinimidyl-4-(*N*-maleimidomethyl) cyclohexane-1-carboxylate
S_N2	Bimolecular nucleophilic substitution
S_NAr	Nucleophilic aromatic substitution
SOD	Superoxide dismutase
SPAAC	Strain-promoted azide-alkyne cycloaddition
TAG	Tumour-associated glycoprotein 72
TBS	Tris buffered saline
TCEP	Tris(2-carboxyethyl)phosphine
THF	Tetrahydrofuran
THPTA	Tris(3-hydroxypropyltriazolylmethyl)amine
TIC	Total ion count
TLC	Thin-Layer Chromatography
U	Enzyme unit
UV	Ultraviolet
V	Volts
Val-Ala	Valine Alanine
Val-Cit	Valine Citrulline
Val-Leu-Lys	Valine leucine lysine
VHL	Von Hippel-Lindau
WHO	World Health Organisation
wt%	Weight percent
δ	Chemical shift
ε	Extinction coefficient

Table of Contents

Section II: Peroxide-Activatable Prodrugs

Section I

Chapter 1: Peroxide-Cleavable Antibody-Drug Conjugates

1.1 Introduction

1.1.1 Cancer Therapy

Cancer is an umbrella term that encompasses a wide range of diseases characterised by the abnormal and uncontrollable growth of cancer cells.[1] It is often regarded as the second leading cause of death worldwide, with nearly 10 million deaths in 2020 attributed to cancer by the world health organisation (WHO).[2]

Currently, standard cancer treatment utilises small-molecule drugs which target rapidly dividing cells (chemotherapy), often in combination with radiotherapy or surgery. Chemotherapeutic drugs function by a number of mechanisms such as blocking cancer cell proliferation, promoting cell cycle regulation, or initiating apoptosis.[3] However, a major disadvantage is the inability for chemotherapeutic agents to discriminate between healthy and cancerous cells, which can lead to off-target toxicity and cause severe side-effects. Hence, there has been significant interest in the development of targeted cancer therapies, which aim to achieve greater selectivity towards cancerous cells.

1.1.2 Antibody-Drug Conjugates

Antibody-drug conjugates have emerged as an effective method for targeted drug delivery, ensuring that the chemotherapeutic agent is only delivered to cancer cells. This is achieved by conjugation of the small-molecule cytotoxic chemotherapeutic (often termed a "warhead" or "payload") to an antibody *via* a linker (Figure 2). The number of drugs conjugated to the antibody is defined by the drug-to-antibody ratio (DAR).

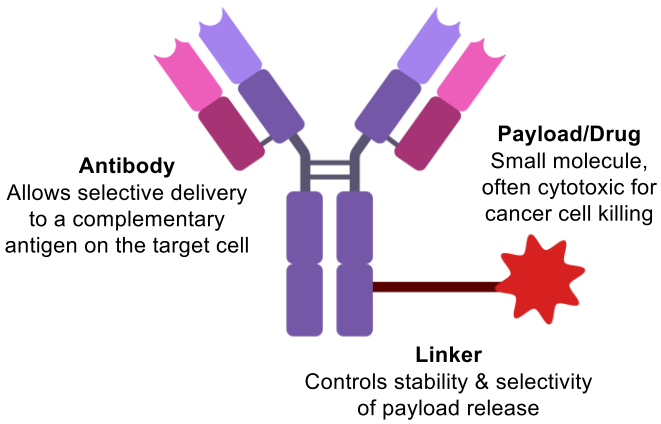

Figure 2: Generic structure of an antibody-drug conjugate (ADC).

The ADC field is continually expanding, with 8 ADCs approved by the Food and Drug Administration (FDA) in 2019-2022, and an additional 249 ADC clinical trials initiated in 2022.[4] Currently, 12 ADCs are approved by the FDA, for a wide range of cancer indications (Figure 3, Figure 4).

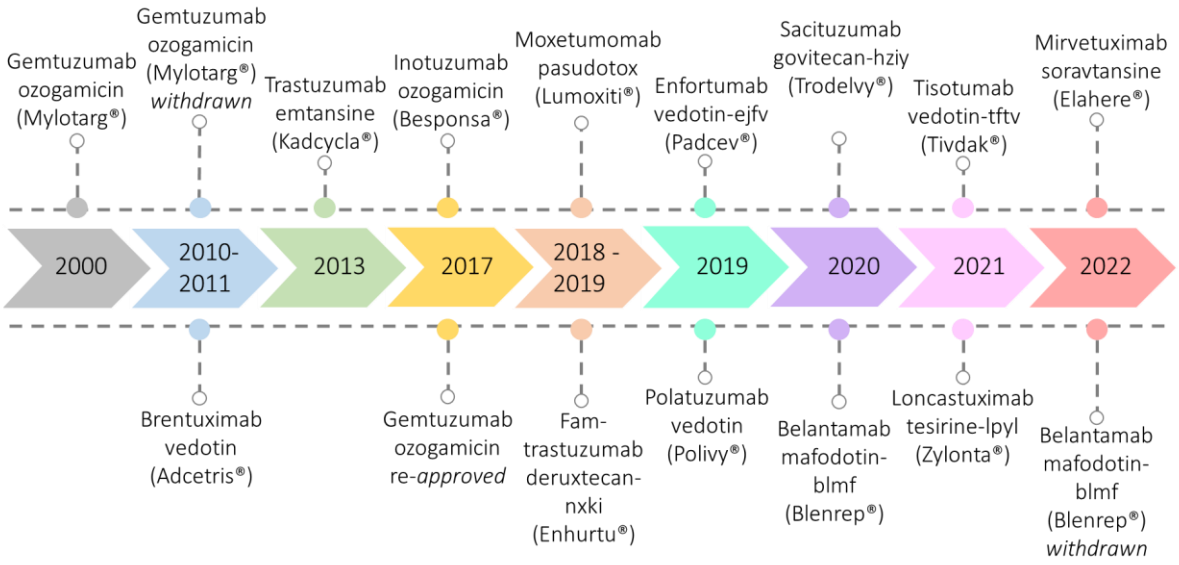

Figure 3: Historic timeline of FDA-approved ADCs.

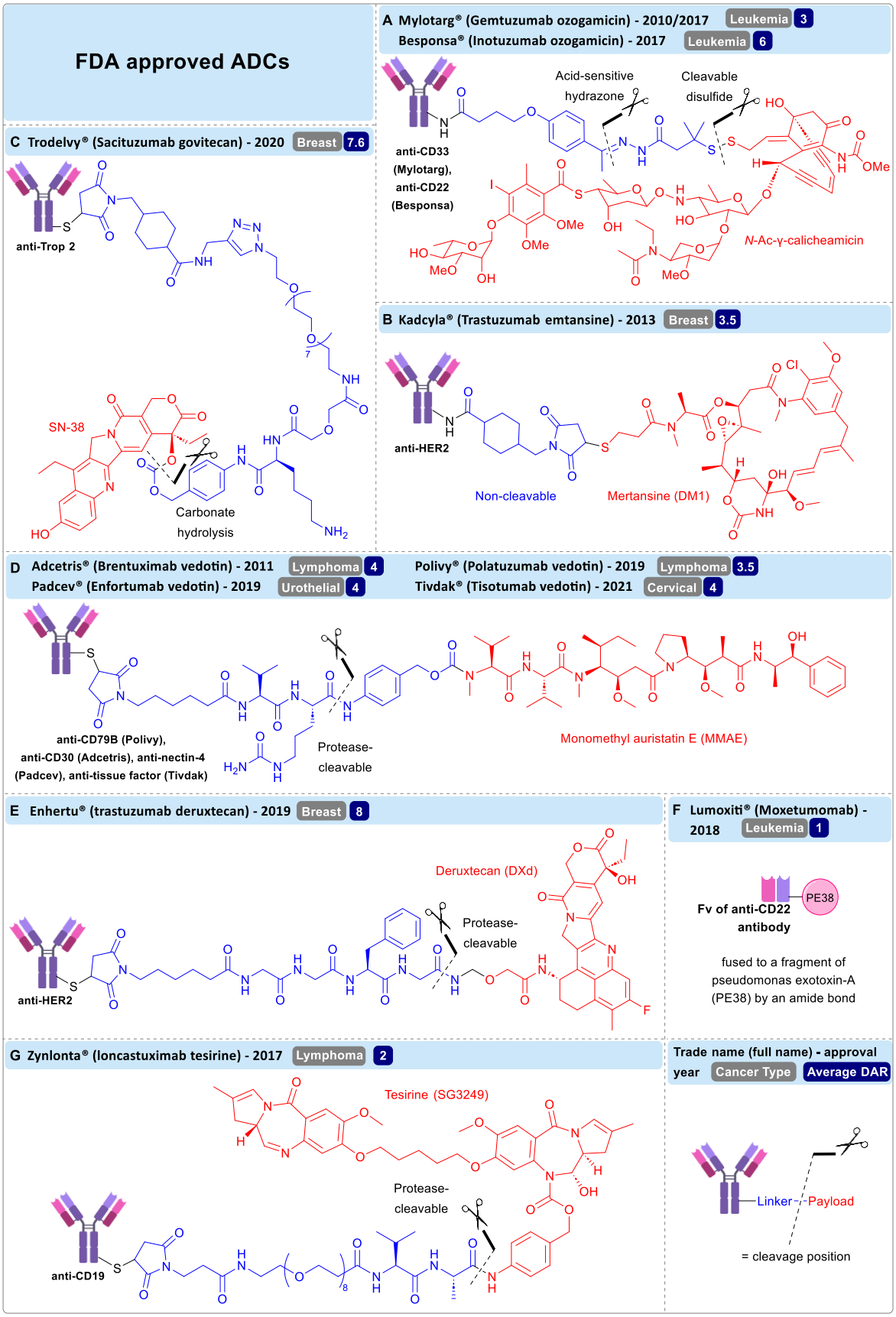

Figure 4: Structure of FDA-approved ADCs, including the type of antibody, linker cleavage mechanism, approval year, treatment indication and average drug-to-antibody ratio (DAR).

1.1.3 Mechanism of Action

The antibody of an ADC is specific for binding a cancer-associated antigen, typically overexpressed by cancer cells compared to healthy cells. Most ADCs function by an internalising mechanism of action (Figure 5A). Upon encounter with the target antigen, antibody-antigen binding occurs which triggers internalisation of the ADC. The ADC is trafficked from an early endosome to a lysosome, wherein the ADC is degraded, releasing the payload either by cleavage of the linker, or by proteolytic degradation of the antibody. In both cases, an active payload species is released which can then act on the target cell to cause cancer cell death by a variety of mechanisms depending on the drug. For example, cell death can occur by DNA alkylation (by DNA cross-linkers e.g. cisplatin); DNA topoisomerase inhibition (e.g. camptothecin, doxorubicin); or inhibition of microtubule formation (e.g. vinca alkaloids, taxanes). If the released payload species is suitably membrane-permeable, it can diffuse out of the cell in which it was released and into surrounding "bystander cells". This "bystander effect" can be beneficial as it allows the payload to act upon surrounding cancer cells which may not display the target antigen.

In contrast, a non-internalising ADC does not require internalisation for the release of the payload. Instead, after antibody-antigen binding, internalisation does not occur quickly/at all, and instead the linker is designed to be cleaved extracellularly, releasing a payload which can then diffuse into the target cell (Figure 5B). Non-internalising ADCs may target a number of different cancer-associated components beyond cell-surface antigens, such as components of the tumour microenvironment, tumour stroma or vasculature.[5]

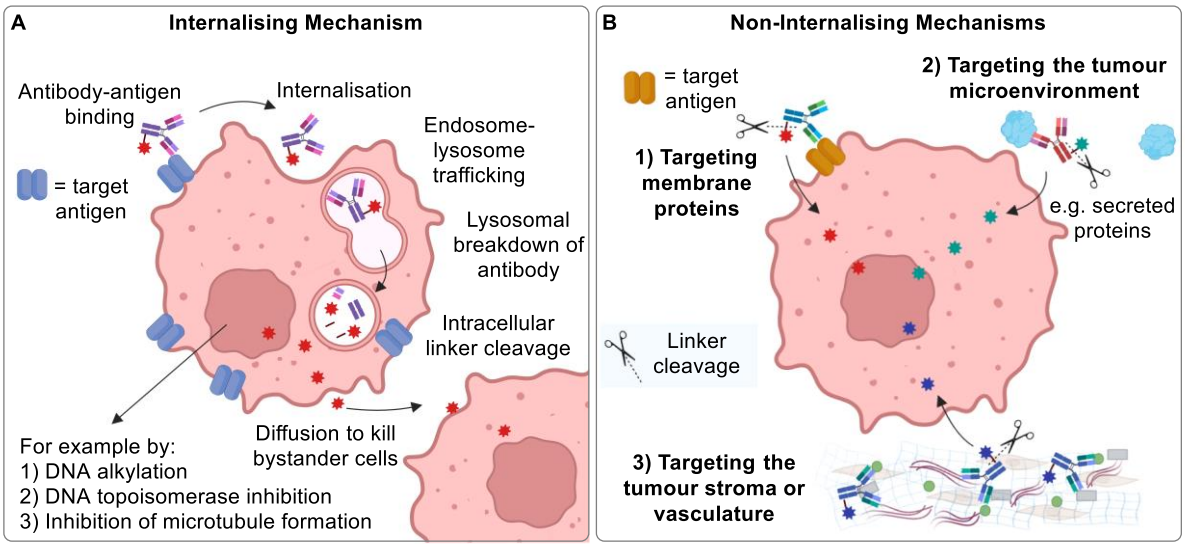

Figure 5: (A) Internalising and (B) non-internalising mechanisms of action of ADCs.

1.1.4 Monoclonal Antibodies

Antibodies are large (~150 kDa) glycoproteins consisting of four polypeptide chains, and the term monoclonal indicates that the antibodies are synthetically generated from identical cells. All currently approved ADCs comprise antibodies with the immunoglobulin (IgG) structure, which consists of two heavy chains and two light chains (Figure 6). Each light chain is divided into a variable (V_L) and constant (C_L) region, and each heavy chain is divided into a variable (V_H) and three constant domains, (C_H^1, C_H^2, C_H^3). The excellent selectivity of ADC targeting is achieved by binding of the antibody Fab (fragment antigen binding) region. The Fc (fragment crystallisable) domain is responsible for the long serum half-lives of antibodies and recognition by immune cells. Finally, the polypeptide chains are held together by four interchain disulfide bonds, as well as a network of non-covalent interactions.

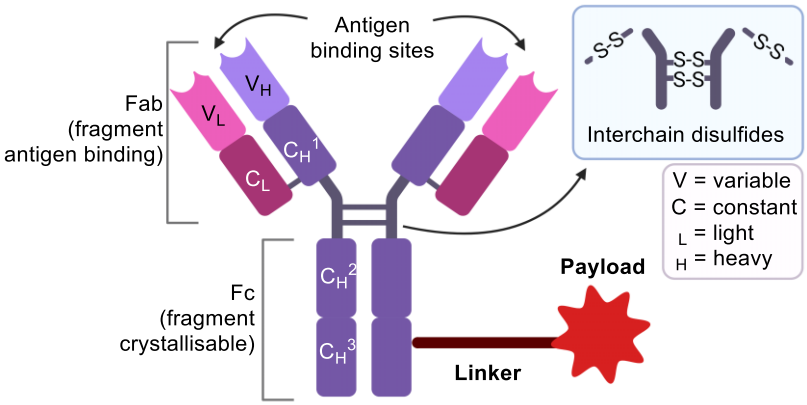

Figure 6: Structure of an IgG antibody.

For successful use in ADCs, the antibody must not trigger a host immune response; must allow effective discrimination between healthy/cancer cells by recognition of an antigen preferentially expressed only on target cells; and enable effective release of the payload at the site of action.

1.1.5 ADC Payloads

A major benefit of ADC technology is the capacity to use drugs with significantly higher toxicity than could be safely administered as sole agents, due to the ability to selectively deliver the drug to the target cell. Moreover, highly cytotoxic payloads are often a necessity for efficacious ADCs, since only a fraction reaches the desired site of action. For example, the delivery of payloads to target cells is restricted by the levels of target antigen expression; efficiency of ADC internalisation; efficiency of payload release by linker cleavage; and limited DAR (3-4). Hence, payloads for ADCs often require sub-nanomolar IC_{50}s. In addition, ADC payloads should not be too hydrophobic as this may cause antibody aggregation and fast clearance, limiting the efficacy of the therapeutic.[6–8]

Monomethyl auristatins E and F (MMAE and MMAF respectively) are highly potent synthetic analogues of natural product dolastatin 10 (Figure 7). They are anti-mitotic agents which block tubulin polymerisation to inhibit cell division. MMAE and MMAF are usually conjugated to linkers *via* their terminal secondary amines and are employed in FDA-approved ADCs: Adcetris®, Polivy®, Padcev® and Tivdak® (Figure 4). Unlike MMAE, MMAF contains a carboxylic acid functional group which is negatively charged under physiological conditions. Therefore, upon release extra- or intra-cellularly, MMAF is not membrane permeable and cannot exert the bystander effect.

Derived from the natural product maytansine, maytansinoids are synthetic analogues which inhibit the assembly of microtubules by binding to tubulin, causing mitotic arrest. Emtansine (DM1) and ravtansine (DM4) are highly stable, highly soluble and contain thiol functional groups often conjugated to antibodies *via* disulfide linkers, for example in FDA-approved ADC Kadcyla® (Figure 4, Figure 7).

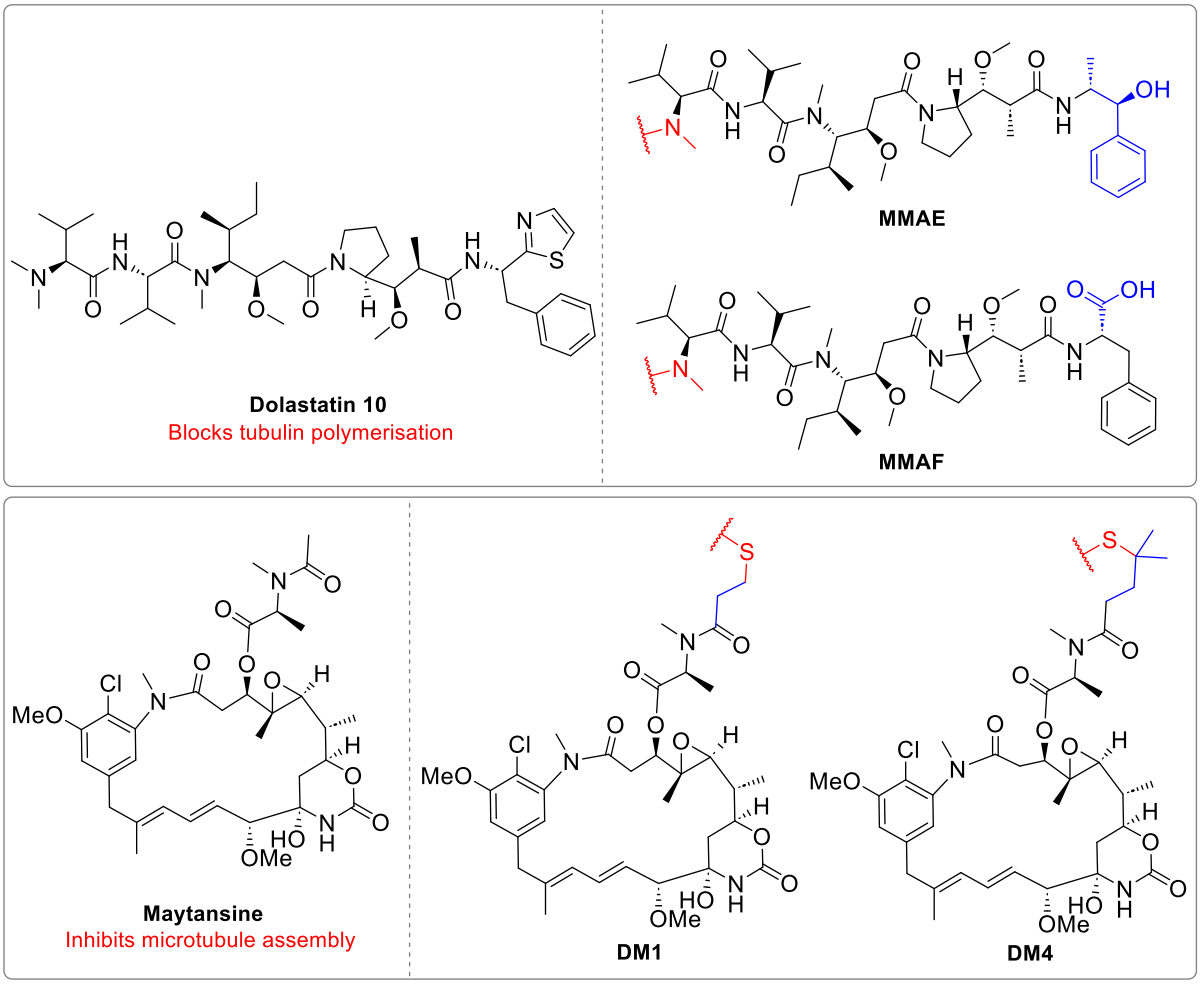

Figure 7: Structure of common ADC payloads MMAE, MMAF, DM1 and DM4. Natural products are shown on the left, with the analogues utilised in ADCs on the right. The structural modifications from the natural product are highlighted in blue, and the site for linker conjugation highlighted in red.

Calicheamicin payloads are a class of enediyne antitumour antibiotics and derivatives such as *N*-acetyl-γ-calicheamicin have been employed in Mylotarg® and Besponsa® (Figure 4, Figure 8). Its mode of action involves binding to the minor groove of DNA and eventually causing DNA strand scission by the formation of a diradical species which abstracts hydrogen atoms from the deoxyribose DNA backbone. Like the maytansinoids, calicheamicin analogues are conjugated to the ADC linker *via* disulfide bonds.

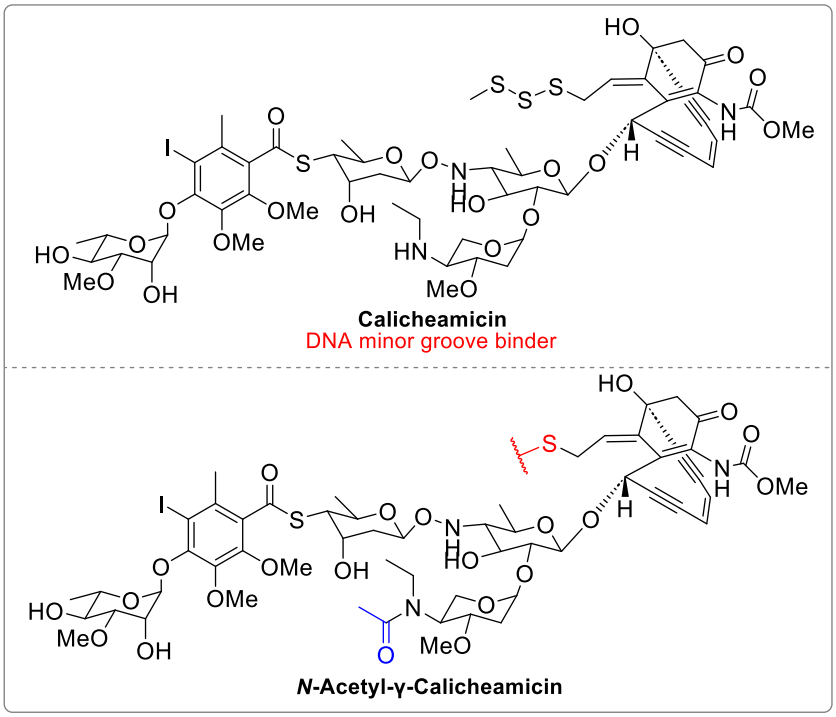

Figure 8: Structure of common ADC payload *N*-acetyl-γ-calicheamicin. Structural differences from the calicheamicin natural product are highlighted in blue, and the site for linker conjugation highlighted in red.

Enhertu® and Trodelvy® incorporate topoisomerase inhibitors DXd and SN-38 (Figure 9). They are synthetic analogues of natural product camptothecin, which binds to and stabilises the topoisomerase I-DNA complex, causing DNA damage that results in apoptosis.

Finally, a more recent class of ADC payloads are pyrrolobenzodiazepine (PBD) dimers (Figure 9).[9] They are derived from the anthramycin family of antitumour antibiotics and act by cross-linking the minor groove of DNA. The PBD dimer tesirine is employed in Zynlonta® (Figure 4).

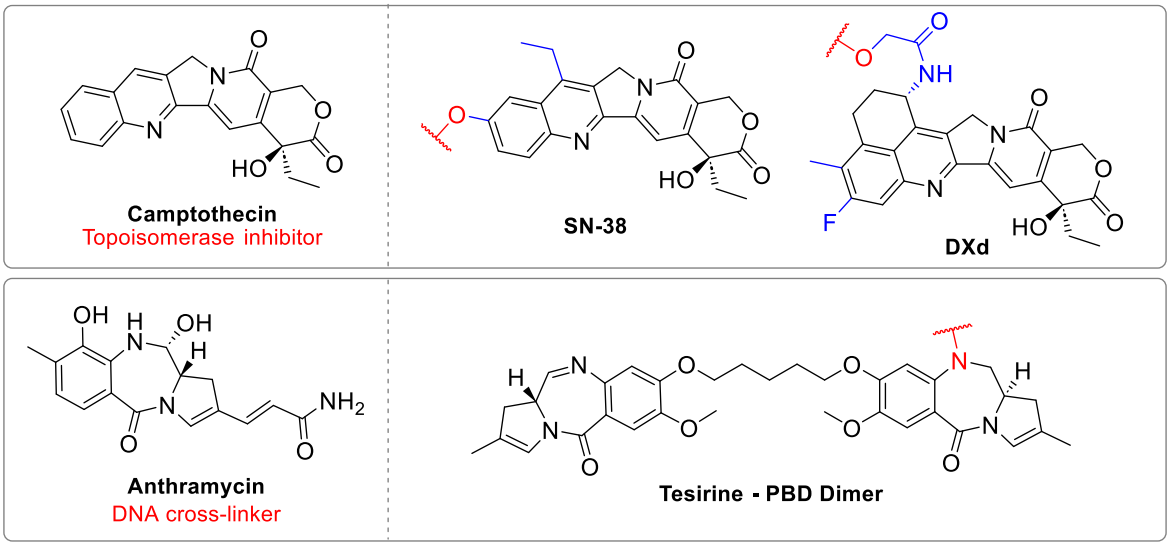

Figure 9: Structure of common ADC payloads PBD dimer tesirine, SN-38 and DXd. Natural products are shown on the left, with the analogues utilised in ADCs on the right. The structural modifications from the natural product are highlighted in blue, and the site for linker conjugation highlighted in red.

1.1.6 Linker-Antibody Connection

The method of conjugation of the linker-drug construct to the antibody is important in determining how many linker-drug species are attached (DAR), the stability of the linkage, and the homogeneity of the ADC product. Generating homogenous ADCs with a defined DAR and conjugation sites is desirable to avoid problems associated with heterogenous mixtures. For example, heterogenous mixtures may contain species with differing properties and pharmacokinetics, and thus potentially result in sub-optimal therapeutic efficacy. The site of conjugation is also an important consideration, as it should not impede antigen recognition by the Fab region and must generate a stable conjugate.

Historically, as for Kadcyla® and Mylotarg®, the native antibody lysine residues (of which there are approximately 30) were used as nucleophilic amines for linker conjugation. This produced an average DAR of 3-4,[10] however, conjugates were generated non-site-selectively and thus produced heterogenous ADCs with a mixture of different conjugation sites.

Cysteine conjugation later emerged as an alternative method: the four interchain disulfide bonds of an IgG antibody can be reduced to their reactive thiols, revealing 8 defined sites for conjugation. Distant from the antigen binding site, conjugation to these sites was also attractive since it would not impact antibody-antigen binding. Many different linkers have been developed for reaction with antibody cysteines (maleimides,[11] bromomaleimides,[12] disulfides,[13] phenyloxadiazoles,[14] 3-arylpropiolonitriles,[15] quaternized vinyl- and alkylpyridines,[16] carbonylacrylates,[17] α-halocarbonyl linkers,[18] and palladium-mediated cysteine arylation[19] (Figure 10).

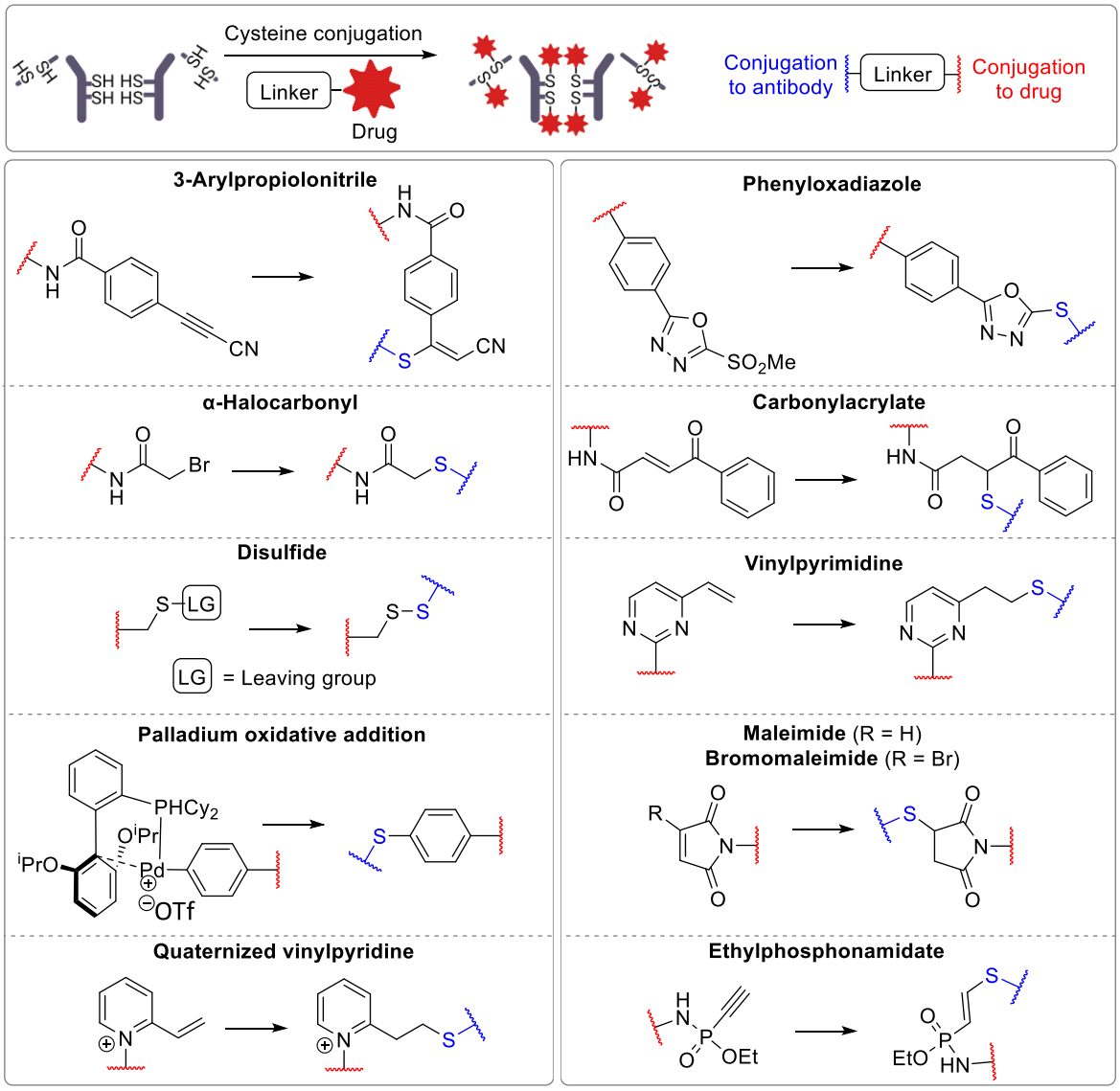

Figure 10: Several methods to conjugate the native cysteines of an antibody. Red attachment points indicate connection to a drug. Blue attachment points indicate conjugation to an antibody cysteine.

However, whilst cysteine conjugation afforded less heterogenous mixtures than with lysine conjugation, heterogenous mixtures are still obtained from the unselective reaction of 8 available thiols. Thus, antibody re-bridging was developed. After reduction of the interchain disulfides to the reactive thiols, they are reacted with a *bis*-electrophilic linker which can re-form the native covalent bonds between the antibody chains (Figure 11). In an ideal case, all the native covalent bonds are re-formed, generating a homogenous species with 4 linker-drugs per antibody (DAR of 4).

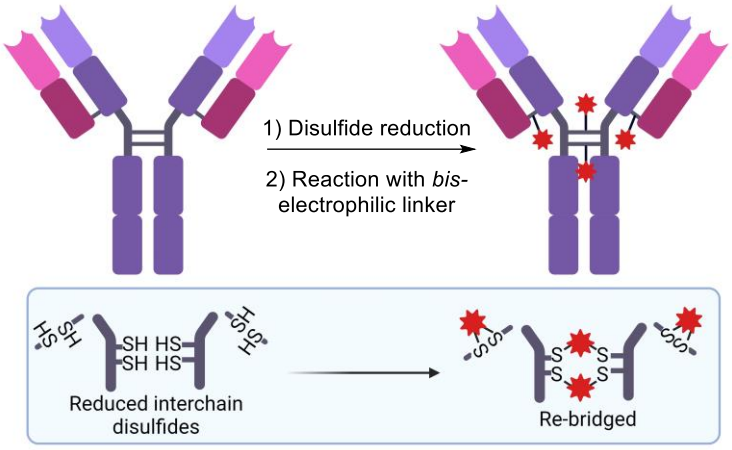

Figure 11: Generic illustration of antibody re-bridging with *bis*-electrophilic linkers to generate homogenous ADCs.

Multiple re-bridging agents have been described,[20] which include *bis*-sulfones,[21–23] next-generation maleimides (NGMs), [12,24–27] pyridazinediones (PDs),[28–32] dibromomethyl heteroaryls,[33] arylene-dipropiolonitrile,[34] dichloroacteones,[35] and divinylpyrimidines[36,37] (Figure 12).

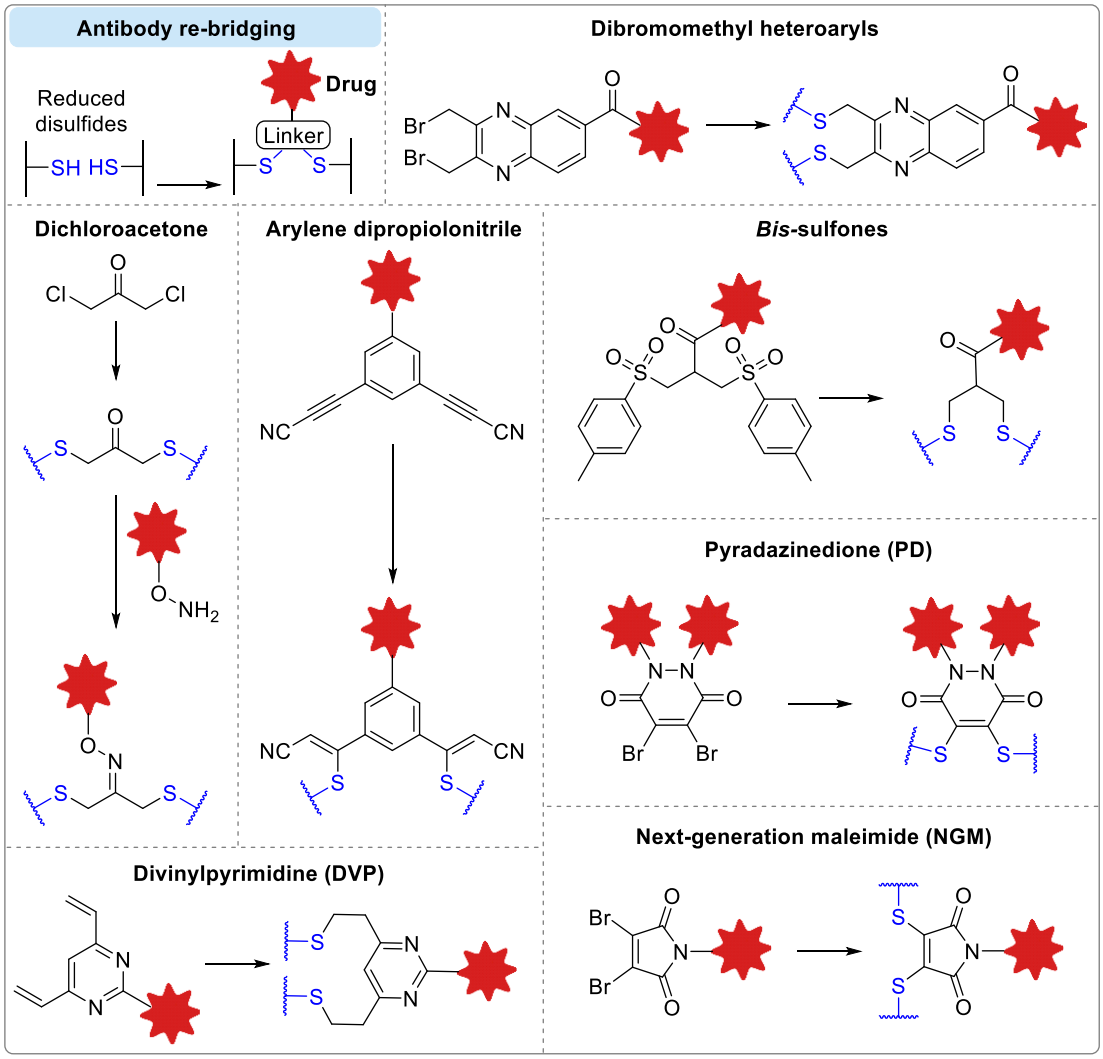

Figure 12: Selection of reported antibody re-bridging methods. Blue connection points indicate connection to the antibody disulfides.

In addition to disulfide re-bridging, there are many other methods for conjugation to antibodies, such as antibody engineering which can introduce additional cysteine residues (THIOMAB™ conjugates[38,39]) or other unnatural amino acids,[40] and modification of native amino acids by enzymatic methods.[41–47]

1.1.7 Linker-Payload Connection

The nature of the chemical linker that connects the payload to the antibody is essential at imparting stability, specificity, and efficacy of the ADC. Linkers are often categorised as “cleavable” or “non-cleavable”.

1.1.7.1 Non-Cleavable Linkers

Common non-cleavable linkers include succinimidyl-4-(*N*-maleimidomethyl) cyclohexane-1-carboxylate (SMCC) and maleimidocaproic acid (MC) (Figure 13). These non-cleavable linkers lack any cleavable functionality, and instead, payload release occurs due to proteolytic degradation of the

antibody in lysosomes following ADC internalisation. Thus, the payload-species that is released remains appended to the terminal amino acid which was used for conjugation to the antibody. This charged payload species is poorly membrane permeable and thus unable to diffuse out of the cell in which it was released, so the bystander effect is not possible with non-cleavable linkers. It should be considered that the amino acid appendage must not negatively impact the potency of the drug or impede its cytotoxic action. Additionally, since internalisation of the ADC into lysosomes is required for payload release, non-cleavable linkers are unsuitable for application to non-internalising ADCs. As a result, non-cleavable ADCs are usually only applicable to treat cancers with high internalising antigen expression. Despite this potential limitation, they are generally considered to have superior stability in circulation than ADCs bearing cleavable linkers, which may reduce off-target toxicity and improve the safety of the therapy.

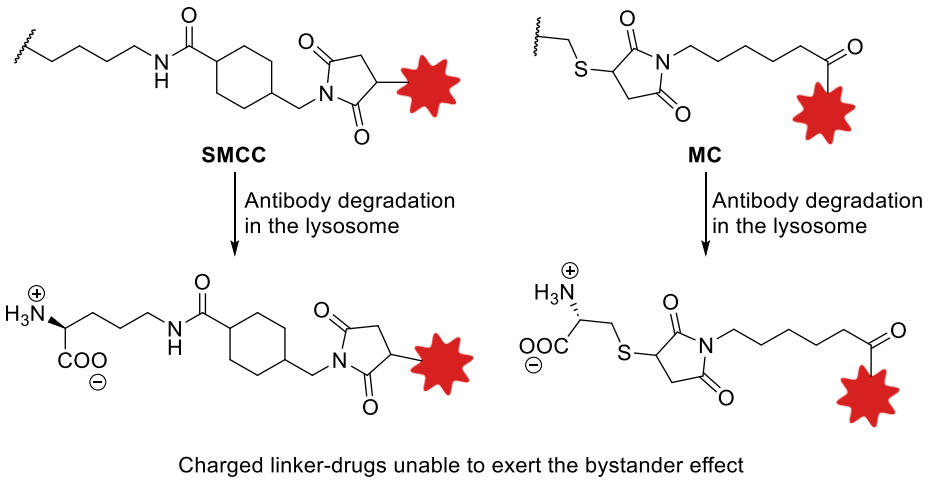

Figure 13: SMCC and MC non-cleavable linkers. After proteolytic degradation in a lysosome, a charged payload-linker species is released, which is unable to exert the bystander effect.

1.1.7.2 Cleavable Linkers

Cleavable linkers contain a reactive moiety that can be cleaved in the presence of cancer-specific triggers, or upon internalisation into a cancer cell. Cleavable linkers can further be classified as chemically cleavable, or enzymatically cleavable.

A class of chemically cleavable linkers contain moieties susceptible to cleavage in the acidic lysosomes (pH 4.5 – 5.0)[48] after internalisation into a target cell (Figure 14A). Acid labile hydrazones, carbonates or esters can be utilised for acid-cleavable linkers such as in FDA-approved ADCs Mylotarg®, Trodelvy® and Bensponsa® (Figure 4).

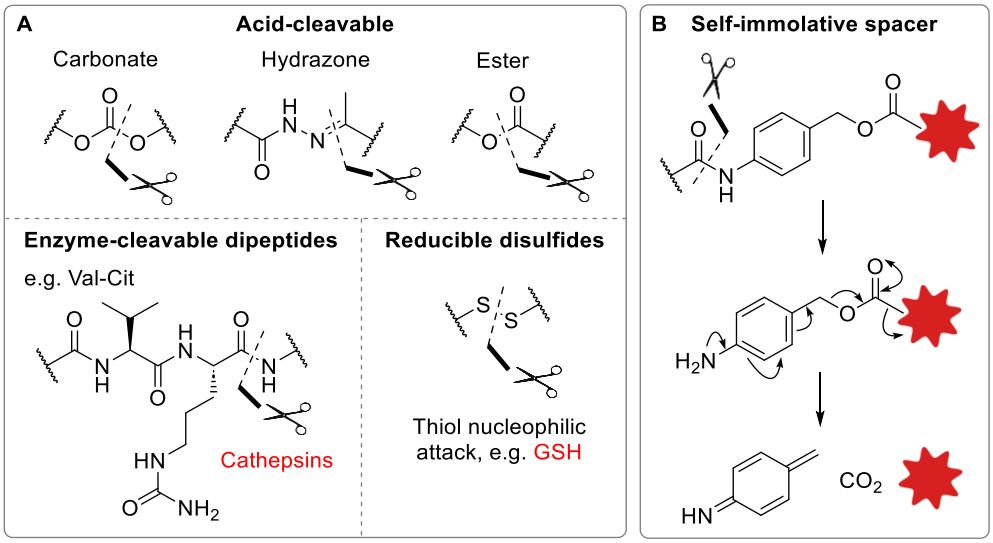

Figure 14: (A) Cleavable linkers, including chemically cleavable and enzyme-cleavable linkers. (B) 1,6-elimination of a self-immolative *para*-aminobenzyl carbamate spacer.

Disulfide moieties can be incorporated into ADC linkers to exploit the elevated levels of reactive nucleophiles such as glutathione (GSH) in cancer compared to healthy cells.[49] Upon nucleophilic attack, the disulfide cleavable linker can reveal a thiol-containing drug, such as with FDA-approved ADCs Mylotarg® and Besponsa®. It has recently been demonstrated that disulfide-containing ADC linkers can generate efficacious non-internalising ADCs, since dying tumour cells can release a high concentration of reductants in the extracellular tumour microenvironment.[50] To this effect, Giansanti *et al.* utilised a "linkerless" ADC, connecting a thiol-containing maytansinoid to an antibody targeting galectin-3-binding protein (Gal-3-BP), which is secreted into the tumour microenvironment.[5,51] GSH-mediated cleavage of the disulfide bond at the site of cancer thus enabled release of the free thiol drug.

Despite their employment in FDA-approved ADCs, acid- or glutathione-cleavable linkers are generally found to be too hydrolytically unstable *in vivo*, which can lead to premature payload release and off-target effects.[52–54] In particular, acid-cleavable linkers are required to discriminate between small pH differences, from circulation in plasma (pH 7.4), to within lysosomes (pH 4.5-5.0). Hence, it is challenging to achieve absolute circulatory stability of acid-cleavable linkers.[48] For example, Mylotarg® was withdrawn in 2010 following its first approval in 2000 due to its sub-optimal circulatory half-life.[55,56] For glutathione-cleavable linkers, instability is proposed to result from disulfide exchange reactions with proteins containing free sulfhydryl groups in plasma.[53] Hence, most ADCs in current development utilise enzyme-cleavable linkers, with 6 of the 12 FDA-approved ADCs employing cathepsin-cleavable dipeptides.

Often, cathepsin-cleavable dipeptidic linkers (Val-Cit or Val-Ala) are combined with self-immolative spacer units (Figure 14B), which enable the release of a completely unmodified payload. A *para*-

aminobenzyl (PAB) spacer can be appended *via* an amide bond to the dipeptide linker. Following cathepsin cleavage, the free aniline can undergo spontaneous 1,6-elimination to release an unmodified amine-containing payload. For more detailed discussion of self-immolative spacers beyond the PAB spacer most commonly used in ADCs, please refer to Section II of this report.

Whilst it was initially thought that cathepsin-cleavable linkers require internalisation into lysosomes for cleavage, more evidence is emerging to suggest the presence of these enzymes is not limited to within lysosomes. Dying tumour cells are proposed to release high concentrations of intracellular enzymes into the tumour microenvironment.[57] For example, Javaid *et al.* demonstrated that cisplatin-induced death of cancer cells generated sufficient levels of extracellular cathepsins *in vitro*.[5,58] This enabled extracellular cleavage of a Val-Cit linker, resulting in an efficacious non-internalising ADC targeting extracellular leucine-rich alpha-2-glycoprotein 1 (LRG1).[5,58] Other non-internalising ADCs have also utilised cathepsin cleavable linkers.[59–62] However, validating the performance of such cathepsin-cleavable ADCs *in vivo* is complicated by their susceptibility to cleavage by a mouse hydrolase, carboxylesterase 1C (Ces1C).[63–65] For example, although the non-internalising LRG1 ADC inhibited tumour growth *in vivo* in a mouse model, the contribution of Ces1c to linker cleavage (and resulting ADC efficacy) was not elucidated. In general, the Ces1c instability of cathepsin-cleavable linkers is a major hinderance to their *in vivo* evaluation in mouse models.[60,66] Another drawback of dipeptidic linkers is their high hydrophobicity and subsequent tendency to cause faster clearance, antibody aggregation, and limit their use with highly hydrophobic payloads.[67,68]

Sulfatase-cleavable linkers were previously developed in the Spring group, which exploit the elevated levels of lysosomal sulfatases in cancer compared to healthy cells (Figure 15).[69–72] These linkers have superior solubility compared to dipeptides, are stable in human and mouse plasma and have produced anti-HER2 ADCs with potent anti-cancer activity *in vitro*.[73]

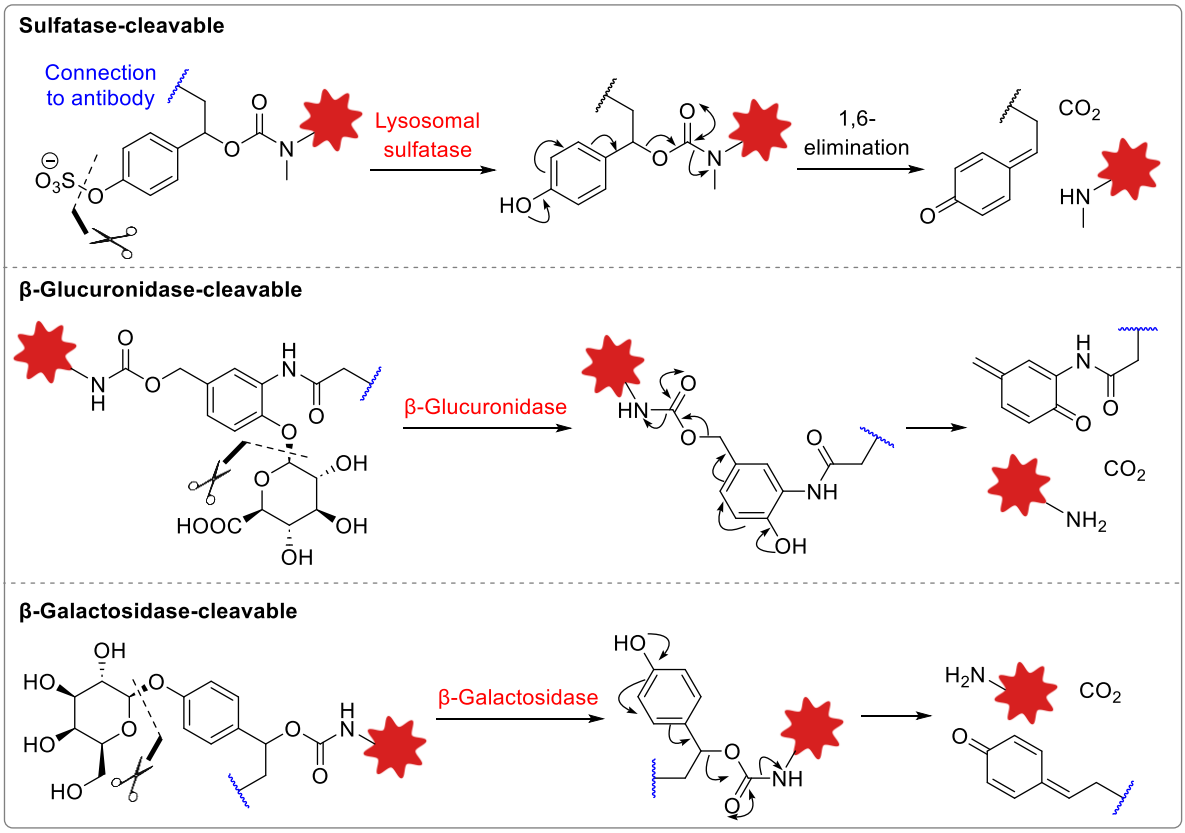

Figure 15: Enzyme cleavable linkers targeting sulfatases, β-glucuronidases and β-galactosidases.

β-glucuronidase and β-galactosidase enzymes are similarly overexpressed in tumours, so linkers comprising β-glucuronic acids and β-galactose units have been explored as alternative enzyme-cleavable linkers (Figure 15). Due to their high hydrophilicity, β-glucuronidase ADCs could be synthesised with high-drug loading (DAR 8), minimal aggregation and reduced clearance.[8,68,74,75] The linkers had high stability in rodent plasma and had potent anti-tumour activity *in vitro* and *in vivo.* Similarly, β-galactosidase ADCs have been demonstrated to have superior efficiency and potency compared to a Val-Cit analogue.[76]

Linkers targeting phosphatases and pyrophosphatases have also been utilised as cleavage motifs, alone or in combination with cathepsin cleavable dipeptides (Figure 16).[77–79] The highly hydrophilic charged phosphates allowed conjugation to highly hydrophobic glucocorticoid payloads without significant antibody aggregation.

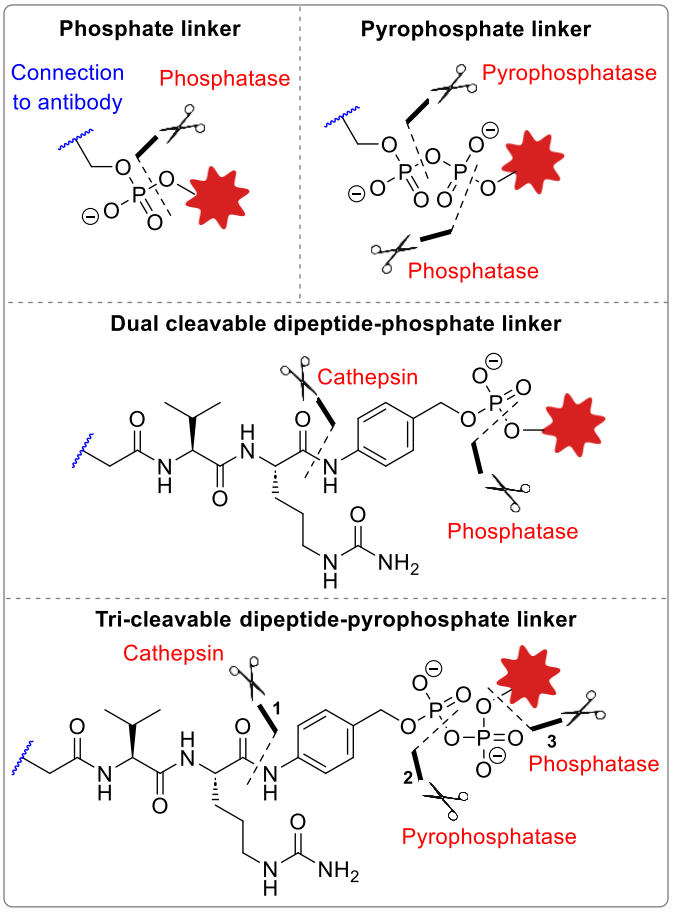

Figure 16: Phosphatase- and pyrophosphatase-cleavable linkers.[77–79] Blue connection points indicate connection to an antibody.

Another example of an ADC which requires dual linker cleavage combined a β-galactose unit with a sulfatase-cleavable motif, for sequential cleavage and selective payload release (Figure 17).[80] Anti-HER2 ADCs bearing the dual-cleavable linker gave potent cytotoxicity against breast cancer cells *in vitro*, and the improved lipophilicity of the dual-cleavable linker may offer benefits for conjugation of more hydrophobic payloads.

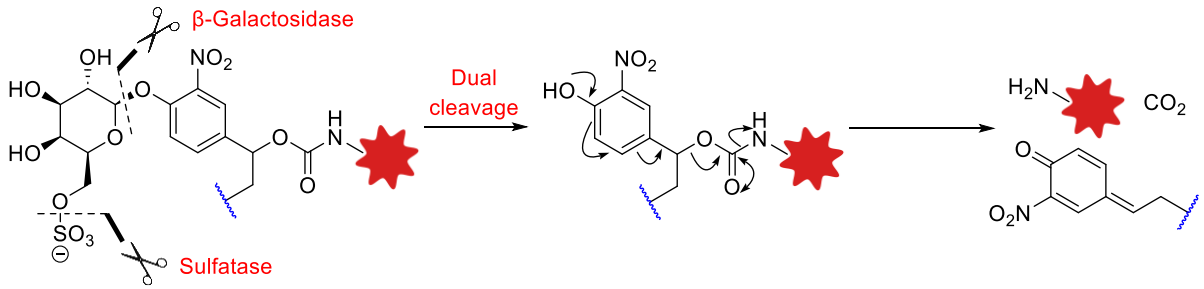

Figure 17: Dual β-galactosidase and sulfatase cleavable linker. Blue connection points indicate connection to an antibody.

1.1.8 Non-internalising ADCs

Since most ADCs were designed to internalise into the target cell following antigen binding, the design of cleavable ADC linkers largely centred around intracellular cleavage stimuli. However, it is being increasingly recognised that some cancer-associated stimuli classically targeted by internalising ADCs are not constrained to inside the cell.[5] In fact, dying tumour cells can release high concentrations of intracellular species into the tumour microenvironment, sufficient for linker cleavage extracellularly. Hence, many cleavable motifs classically used for internalising ADCs are being applied for the generation of efficacious non-internalising ADCs.[5]

1.1.8.1 Cathepsin-cleavable

During the development of non-internalising ADCs, it was discovered that cathepsins may have sufficient extracellular concentrations for efficacious payload release extracellularly. Poorly internalised antigens CD20, CD21 and CD72 were targeted with ADCs comprising disulfide or Val-Cit cleavable linkers and MMAE (Figure 18).[81] The Val-Cit and disulfide ADCs were efficacious *in vivo*, whereas those containing non-cleavable linkers were not. This suggests a lack of internalisation of the ADCs, since a non-cleavable linker would still be expected to enable cell killing if internalised (the linker-MMAE construct released after proteolytic degradation retains some activity).[82] Furthermore, replacement of MMAE with MMAF rendered the Val-Cit ADC inactive, which is rationalised by the poor cell membrane permeability of charged MMAF compared to MMAE. This supports the proposed mechanism of extracellular payload release, since only membrane permeable payloads (MMAE) gave potent activity.

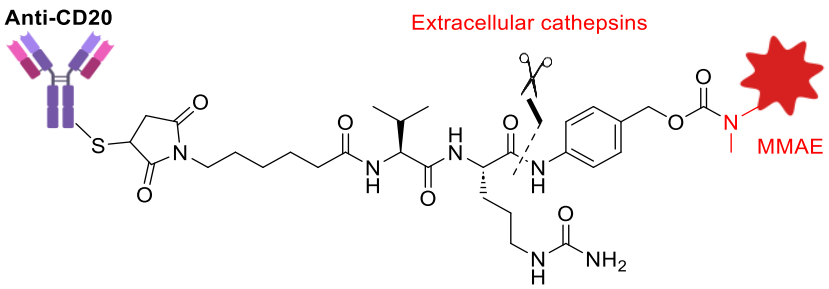

Figure 18: Structure of an anti-CD20 non-internalising ADC comprising a Val-Cit cleavable dipeptide. The antibody connection shown is for illustrative purposes only and should not be interpreted as site of connection or DAR.

Val-Cit linkers were also incorporated into a non-internalising ADC targeting leucine-rich alpha-2-glycoprotein 1 (LRG1). LRG1 is a glycoprotein which is secreted into the microenvironment of many tumours.[58] Anti-LRG1-Val-Cit-MMAE ADCs were only effective *in vitro* when cells were pre-treated with cisplatin, which created sufficient initial concentrations of extracellular cathepsins from the dying cells to allow Val-Cit linker cleavage. With cisplatin co-treatment *in vitro*, the anti-LRG1 ADC achieved an impressive IC_{50} of 15 pM, and without cisplatin treatment, the ADC achieved potent tumour growth

inhibition in an *in vivo* mouse melanoma model. However, the known instability of Val-Cit dipeptides to the mouse Ces1c hydrolase complicates conclusions from the latter *in vivo* study. It remains unclear whether the potency of ADCs with Val-Cit linkers arises solely from at cleavage by target tumoural cathepsins, or as a result of circulatory instability in mouse models. This is a key shortfall of the *in vivo* evaluation of Val-Cit ADCs in mice.

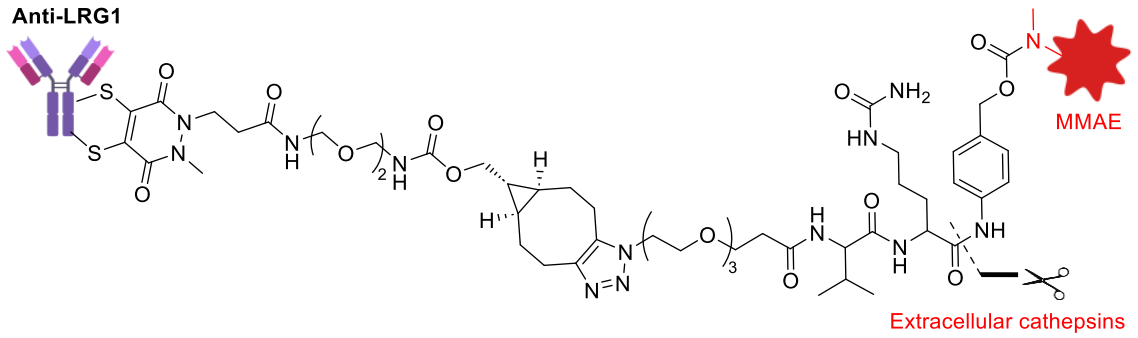

Figure 19: Structure of non-internalising anti-LRG1 ADC bearing a Val-Cit cleavable linker. The antibody connection shown is for illustrative purposes only and should not be interpreted as site of connection or DAR.

Tenascin-C is a protein with high abundance in the stroma of solid tumours, and limited presence in healthy tissues.[83–85] The F16 antibody is used to target the A1 domain of tenascin-C and was used to generate a non-internalising ADC comprising Val-Cit cleavable linkers and MMAE. The resulting ADC cured 100% of treated mice in mouse xenograft models, however the ADC was unstable in mouse plasma due to mouse Ces1c hydrolysis. Hence, once again, the *in vivo* efficacy of the Val-Cit non-internalising ADC cannot solely be attributed to the desired mechanism of action.

1.1.8.2 Acid labile

Despite being designed with the internalising mechanism of action in mind, FDA-approved ADC Mylotarg®, which targets internalising antigen CD33, has been shown to be potent even against tumours with undetectable levels of cell surface CD33. This suggests a mechanism of payload release other than intracellular linker cleavage. Moreover, when the acid-sensitive hydrazone in Mylotarg® was replaced with an acid-stable linker, its activity against CD33-negative cells was diminished. Hence, extracellular linker cleavage in the acidic tumour microenvironment (pH 5.5-7.0)[86] is suggested as an alternative mechanism of this ADC, in combination with the enhanced permeability and retention effect (EPR), whereby ADCs passively accumulate in tumours due to their enhanced vascular permeability.

Anti-CD20 ADCs with acid-labile linkers have also demonstrated that the extracellular environment of tumour cells is sufficiently acidic for extracellular payload release.[87] An anti-CD20 antibody was conjugated to calicheamicin *via* an acid-cleavable dimethyl hydrazide AcBut linker, or acid-stable amide

linker (Figure 20A). Only the acid-labile linked ADC gave potent growth inhibition *in vivo*, suggesting that internalisation of the ADC did not occur and instead, extracellular linker cleavage was responsible for activity. This was supported by replacement of the CD20 antibody for an anti-CD22 antibody, which is an internalising target. In this case, the acid-cleavable and acid-stable ADCs had similar efficacy.

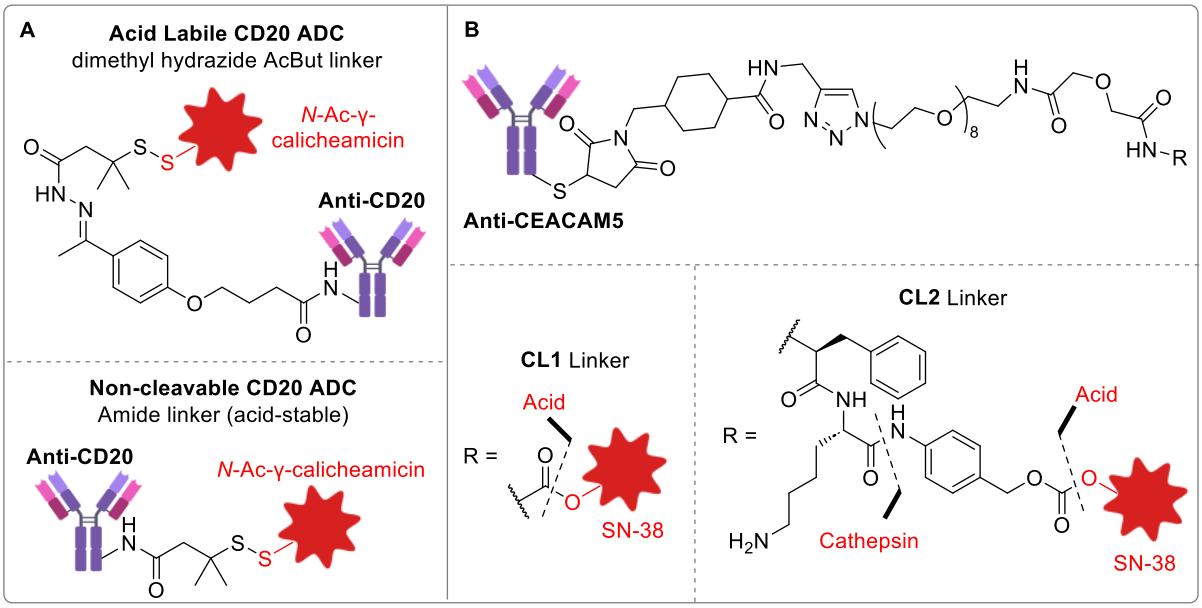

Figure 20: Structure of non-internalising anti-CD20 (A) and anti-CEACAM5 (B) ADCs.

Esters and carbonates are also acid-labile motifs, and have been incorporated into non-internalising ADCs targeting carcinoembryonic antigen cell adhesion molecule 5 (CEACAM5) (Figure 20B).[88–90] CEACAM5-targeting ADCs with ester linkers (CL1) or dual cleavable dipeptidic and carbonate linker (CL2) were able to release SN-38 in the extracellular tumour microenvironment, achieving 100% survival in a lymphoma tumour model. It is noted that the ester and carbonate linkers have only intermediate stability,[89] therefore activity is likely due to slow SN-38 release local to the tumour, which may not be appropriate for payloads with greater potency than SN-38. FDA-approved internalising ADC Trodelvy® also contains the carbonate functionality: when its acid-labile linker was replaced with a highly stable linker, efficacy was significantly reduced, suggesting that gradual release of SN-38 from the labile carbonate likely contributes to efficacy.[91]

Esters were also utilised in non-internalising ADCs targeting stromal collagen (Figure 21A).[92] Again, the hydrolytic lability of the ester bond was used for the gradual release of SN-38 in the tumour microenvironment. The ADCs with a DAR of 7-8 gave potent antitumour activity *in vivo*, with enhanced activity in a stroma-rich vs. stroma-poor pancreatic mice xenografts, and achieved inhibition of tumour growth for as long as 3 months (presumably due to the slow release of SN-38). A similar stromal-targeting ADC was explored with antibodies targeting fibrin, a fibrous protein abundant in the stroma of solid tumours (Figure 21B).[93]

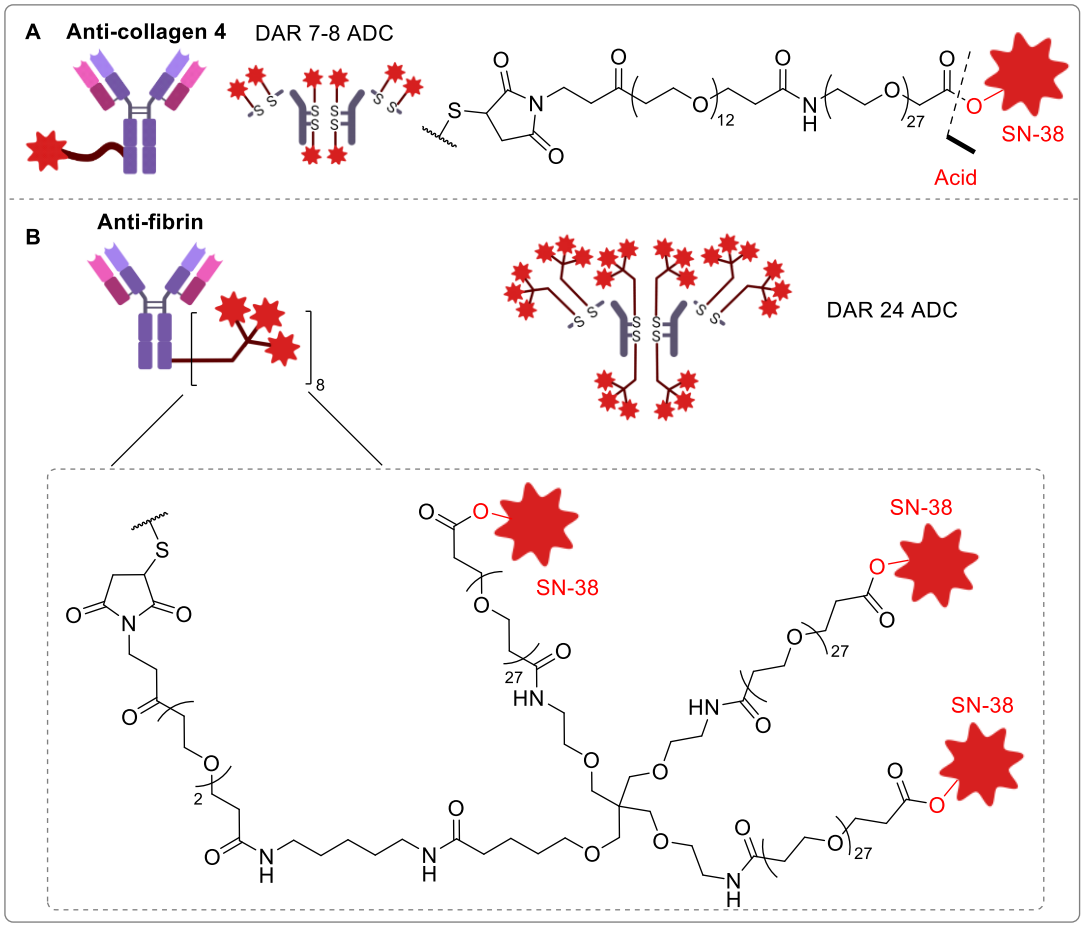

Figure 21: Structure of acid-labile linkers employed for non-internalising anti-collagen (A) and anti-fibrin (B) ADCs. The antibody connection shown is for illustrative purposes only.

1.1.8.3 Disulfides

Bernardes *et al.* have demonstrated that sufficient concentrations of reductants are present in the extracellular tumour microenvironment to enable extracellular payload release from disulfide linkers.[57] An F8 antibody was utilised for binding to the EDA domain of fibronectin: a glycoprotein associated with cancer cell angiogenesis, located in the subendothelial extracellular matrix of tumour blood vessels. Conjugation of thiol-containing dolastatins or maytansinoids was achieved in a "linkerless" fashion, simply by disulfide exchange with the cysteines on the F8 antibody (Figure 22A). Following cleavage by the extracellular tumoural reductants, such as GSH, only free drug and parent antibody is released.

The linkerless technology was also used to target galectin-3-binding protein (Gal-3-BP), which is secreted into the microenvironment of the majority of cancers (Figure 22B).[51] Anti-Gal-3-BP disulfide-containing ADCs achieved potent tumour growth inhibition *in vivo*, with a DM3 conjugate achieving long-lasting and complete remission in a mice xenograft model.

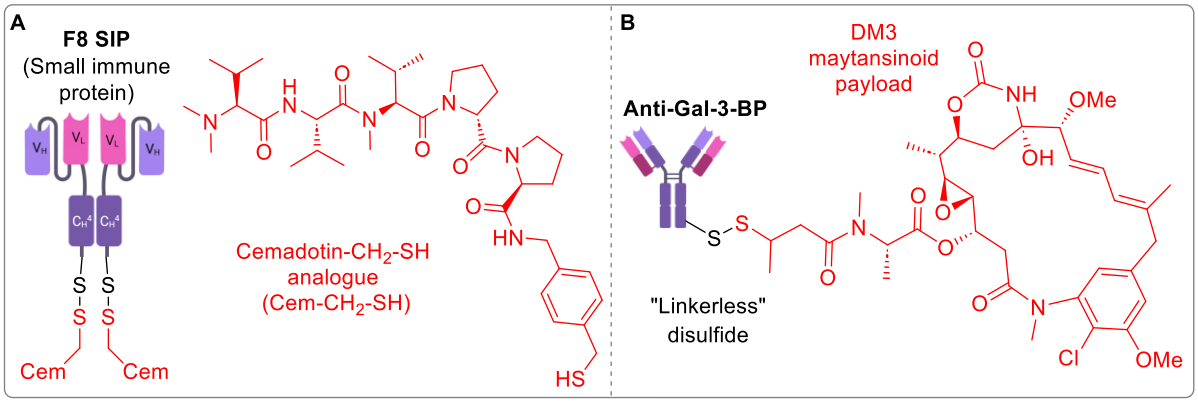

Figure 22: Structure of non-internalising ADCs comprising disulfide cleavable linkers. The antibody connection shown is for illustrative purposes only.

Disulfide linkers may benefit from a so called “chain reaction” whereby the first instance of cancer cell killing by the cytotoxin results in further release of reductants such as GSH from the dying cancer cell, which in turn can cleave more disulfide linkers, and amplify the release of payload and thus amplify cell death (Figure 23).

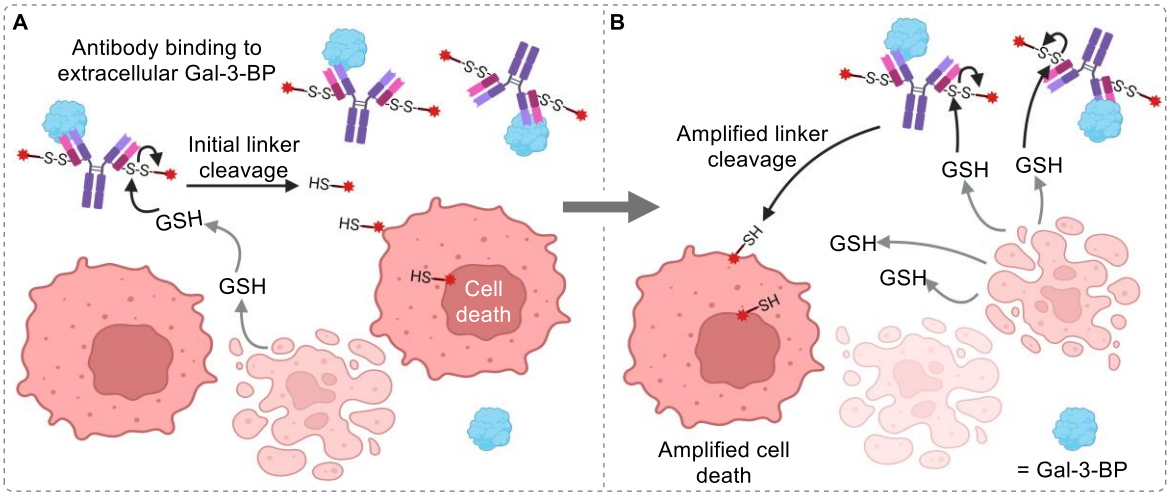

Figure 23: Illustration of the amplified cell death that can occur from disulfide-cleavable ADCs, for example those targeting Gal-3-BP. (A) Initial linker cleavage from reductants released from dying cancer cells results in further cancer cell death. Thus, increased levels of reductants are released in the tumour microenvironment. (B) This amplifies linker cleavage, which then amplifies cancer cell killing by the released payload species.

1.1.8.4 Other approaches

In addition to the use of classical cleavage triggers to achieve extracellular payload release, a host of new linkers have emerged for use in non-internalising ADCs.

Plasmin is a protease which is only produced in its active form in the presence of fibrin. Thus, a plasmin-cleavable linker was utilised in an anti-fibrin ADC to enhance the selectivity of payload release, which would only occur after targeting fibrin in the tumour stroma, followed by linker cleavage by active

plasmin.[94] The tripeptide Val-Leu-Lys conjugated to MMAE *via* a self-immolative spacer afforded ADCs with significant inhibition of tumour growth *in vivo*.

Cleavable linkers are not a requirement for effective non-internalising ADCs. Other approaches have tethered inhibitors to the antibody to allow proximity-induced selectivity. For example, Love *et al.* conjugated a pan-MMP inhibitor to an antibody selective for MMP9, thus bringing the unselective inhibitor only in close proximity to MMP9 (Figure 24A).[95] Inhibition of MMP9 could be achieved without linker cleavage or conjugate breakdown. Similarly, an inhibitor of the Na^+/K^+ ATPase (NAK), was conjugated to an antibody targeting dysadherin. Dysadherin is a cell-membrane glycoprotein which interacts with NKA and is overexpressed in many cancers.[96] Hence, antibody targeting of dysadherin brought the NKA inhibitor in close-proximity to NKA, allowing inhibition without linker cleavage or ADC breakdown (Figure 24B).

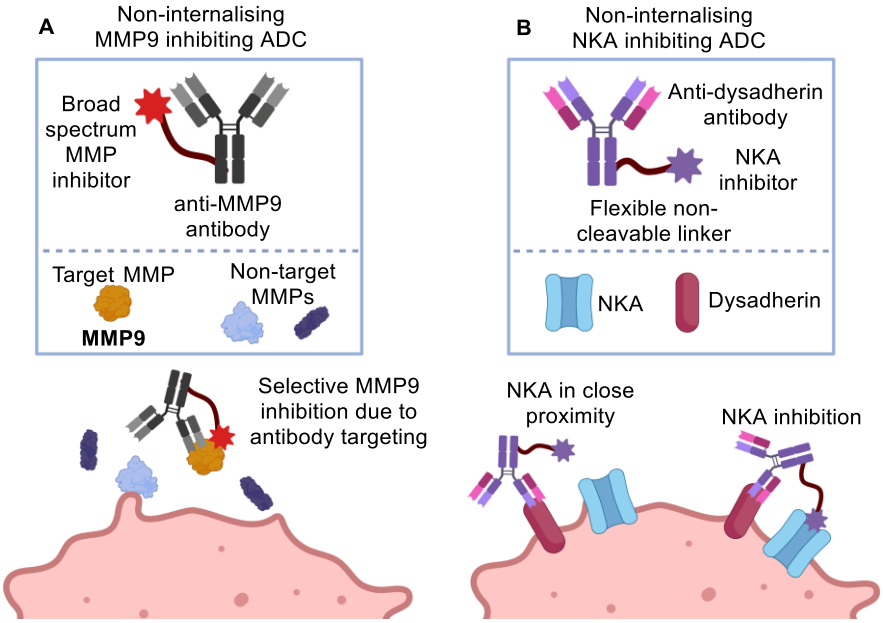

Figure 24: (A) A non-internalising ADC capable of selectively inhibiting MMP9 with a pan-MMP inhibitor by selective antibody binding to MMP9, and (B) a non-internalising ADC capable of inhibiting NKA by binding to close-proximity protein dysadherin.

Finally, linkers have been designed for activation and payload release by the introduction of exogenous triggers. Rossin *et al.* utilised the inverse-electron demand Diels Alder (IEDDA) to allow payload release from a *trans*-cyclooctene linker of an anti-TAG72 ADC upon administration of exogenous tetrazines.[62,97] Stenton *et al*. utilised a propargyl carbamate linker which could be cleaved upon administration of a palladium activator, to generate an anti-tenascin C ADC.[98] Finally, Oliveira *et al*. generated anti-tenascin C ADCs with linkers susceptible to platinum de-caging for payload release.[99]

1.1.8.5 Benefits

Clearly, non-internalising ADCs greatly expand the number of cellular targets that can be exploited by ADCs. Whilst internalising ADCs are reliant on high, homogenous internalising antigen expression, non-internalising ADCs can target non-internalising cell membrane antigens, extracellular proteins and components of the stroma or vasculature unique to cancer. Additionally, a non-internalising approach may be attractive for the treatment of cancers which develop resistance against internalising ADCs (mechanisms of which include reducing internalising antigen expression or acquiring defects in the internalisation process).[100,101] It has also been suggested that extracellular payload release may facilitate deeper tumour penetration and improve the bystander effect, which may be useful in the treatment of solid tumours where antibody diffusion is limited.[102]

1.1.9 Peroxide and Cancer

The high metabolism of cancer cells, as well as other factors such as mitochondrial dysfunction, increased cellular receptor signalling, increased activity of oxidases and oncogene activity, leads to an increase in reactive-oxygen species (ROS) and oxidative stress.[103–105] ROS are radicals, molecules or ions with an unpaired electron, including hydroxyl radicals $^{\bullet}OH$, superoxide O_2^- and hydrogen peroxide, H_2O_2.[106] Signalling pathways which rely on ROS are often elevated in many types of cancers, where they contribute to cell growth, proliferation, and cell survival. Under normal physiological conditions, the concentrations of ROS are carefully maintained to prevent cellular damage,[106] however, cancer cells become adapted to high levels of oxidative stress.

H_2O_2 is the most stable and long-lived ROS, and consequently is the most well studied. Intracellular H_2O_2 is produced from superoxide (O_2^-) by superoxide dismutase (SOD) enzymes. Elevated SOD expression in cancer cells can result in abnormally high levels of H_2O_2, as well as by the inactivation of H_2O_2 scavenging enzymes, such as catalase, which decomposes H_2O_2 to water and oxygen. Whilst mainly produced intracellularly at mitochondria, H_2O_2 is highly diffusible and may cross cell membranes through membrane channels.[106,107] The concentrations of H_2O_2 have been known to reach as high as 100 µM in cancer cells, approx. 100 times higher than in healthy cells.[108,109] It is this distinction that makes ROS promising to exploit for targeted drug delivery.

Jourden and Cohen were the first to describe a small-molecule matrix metalloproteinase inhibitor (MMPi) prodrug which was activated selectively by H_2O_2.[110] Since then, a number of small-molecule H_2O_2-activatable prodrugs have been developed to achieve site-selective drug activity, which are discussed in detail later in this report (see Section II). Common ROS-responsive motifs are boronic esters and acids, which are capable of selective oxidation by H_2O_2 to hydroxyl moieties (Figure 25). The boronic esters or acids can thus be used to mask a hydroxyl essential for the function of a drug, to

render it inactive until it reaches the tumour site and is revealed by the elevated levels of H_2O_2. Alternatively, arylboronates or arylboronic esters can be coupled *via* self-immolative spacers to allow release of drugs bearing functional groups other than alcohols, such as amines through carbamate bonds (Figure 25B). Following C-B bond oxidation, the self-immolative linker can undergo spontaneous 1,6-elimination to release an active drug with liberation of CO_2 and a quinone methide side-product.

The released quinone methide is highly reactive and electrophilic, and is known to undergo reactions with water, glutathione (GSH), and other biological nucleophiles such as DNA bases.[111,112] In the case of cancer treatment, the toxicity of the quinone methide by-product may contribute to the therapeutic effect, providing it is only released at the site of action.[113]

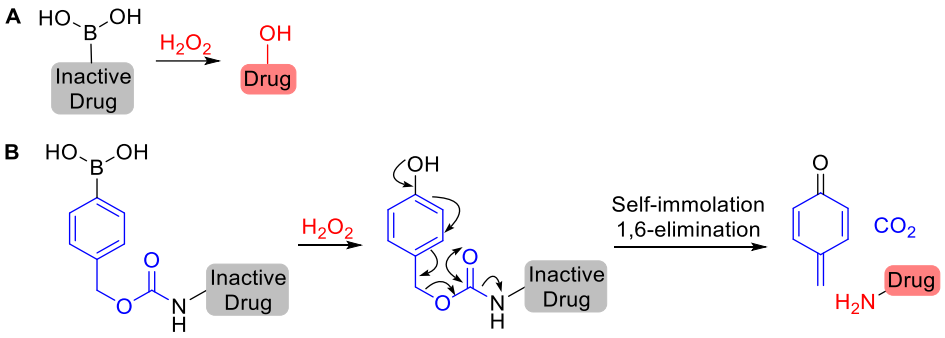

Figure 25: General reactivity of boronic acids with H_2O_2 (A) to reveal a native hydroxyl of a drug, (B) to reveal a phenol of a self-immolative spacer, which can then undergo 1,6-elimination to release the unmodified drug. The self-immolative spacer is depicted in blue.

For drug release from arylboronate or arylboronic acid self-immolative linkers, the kinetics of two processes need to be considered: 1) oxidation of the C-B bond by H_2O_2, and 2) quinone methide formation by elimination. Aryl ring electronics have conflicting influence on both steps. C-B bond oxidation is facilitated by electron-withdrawing groups on the aromatic ring and hampered by electron-donating groups.[114] Conversely, electron-donating groups enhance the rate of self-immolation and quinone methide formation by lowering the energy barrier to dearomatisation and stabilising the positive charge that develops at the benzylic position.[115] Whilst some studies report that the 1,6-elimination step is rate-limiting,[116] it is not totally understood what the effects of aromatic substitutions may be in the overall process. For example, a study which trapped quinone methides after peroxide activation of arylboronates showed that whilst nitro group (NO_2) substitution of the aryl ring did significantly slow the kinetics of quinone methide formation, because C-B oxidation was much faster than analogues bearing electron-donating OMe/Me substituents, more of the nitro-quinone methide trapped product was observed.[114] Therefore, it is challenging to predict what structural modifications might yield a prodrug with the fastest payload release *in vivo*. Additionally, the success

of H_2O_2-activatable prodrugs may also be influenced by other factors such as their membrane permeability and general pharmacokinetics.

1.1.9.1 ROS-cleavable ADCs

During the preparation of this report, António *et al.* described the development of a ROS-responsive antibody fragment-conjugate.[117] The authors utilised diazaborine (DAB) motifs, which can be oxidised by H_2O_2 to reveal a phenol and hydrazone (Figure 26A). The authors propose that 1,6-elimination through the *para*-hydroxybenzyl ether linker can then release alcohol payloads such as SN-38. Accordingly, SN-38 was attached to the benzylic position of a DAB via an ether linkage and conjugated to a V_L single-domain antibody fragment for targeting and internalisation into B-cell lymphoma cells (Figure 26B).

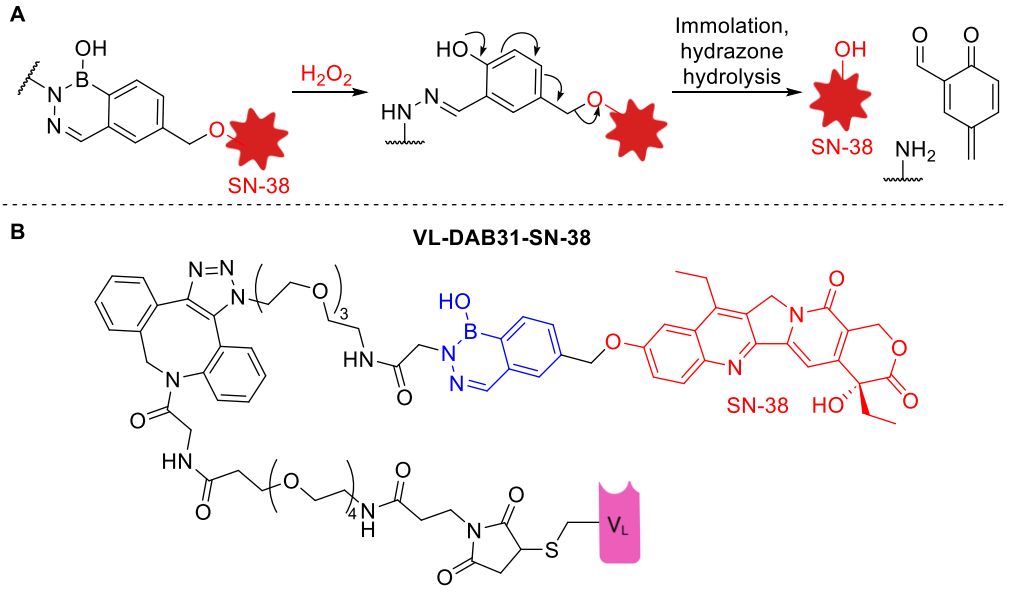

Figure 26: (A) Proposed mechanism of action by H_2O_2 DAB linker cleavage and drug immolation and (B) structure of the antibody fragment conjugate VL-DAB31-SN-38 containing cleavable diazaborine linker connecting SN-38.

In vitro evaluation of VL-DAB31-SN-38 revealed cytotoxicity against B-Cell lymphoma CLBL-1 cell line, but no toxicity against a control Jurkat cell line. However, the antibody fragment conjugate was approx. 11-fold less potent than treatment of SN-38 (IC_{50} = 54.1 nM vs. 4.67 nM of SN-38), suggesting incomplete liberation of SN-38 *in vitro*. Additionally, the *in vitro* mechanism of action of this antibody fragment conjugate was not fully explored, and it remains to be seen whether the cytotoxicity arises solely from action of H_2O_2 cleavage of the linker and efficient 1,6-elimination to release free SN-38 or by other mechanisms.

1.2 Project Aims & Overview

1.2.1 Project Aims

Given the importance of the linker chemistry in defining the stability, selectivity and efficacy of ADCs, there is need to expand the toolbox of cleavable motifs. Arylboronates and arylboronic acids are well-established cleavable motifs, and their ability to generate efficacious small-molecule prodrugs activated by the elevated levels of H_2O_2 in cancer has been well-explored (see Section II of this report). This project aims to develop the first full IgG ADC comprising a H_2O_2-cleavable arylboronic acid linker. The effect of aryl ring electronics will be explored by substitution of the aryl ring with different functional groups, and the impact on resulting ADC potency will be examined.

Successful arylboronic acid linkers should satisfy the following criteria:

- Linkers should be synthetically accessible
- Linkers should have fast kinetics of payload release in the presence of a pathologically relevant concentration of H_2O_2
- Linkers should have general stability in the absence of H_2O_2 (> 5 days) for example in circulation in plasma, at different pHs, and in the presence of biological nucleophiles
- The linker should enable conjugation to a relevant ADC payload, and the resulting linker-drug should be suitable for bioconjugation to an antibody: the linker should not cause significant antibody aggregation, and enable synthesis of ADCs with DARs close to 4
- Resulting arylboronic acid ADCs should possess comparable *in vitro* potency to ADCs comprising linker technology commonly used, such as cathepsin-cleavable dipeptides

1.2.2 Project Overview

The research described in Chapter 1 began with the exploration of a series of model arylboronic acid linkers comprising a fluorescent reporter molecule. Synthesis of three model linkers with different aryl substituents was achieved, as well as a non-cleavable control lacking the cleavable boronic acid moiety. HPLC analysis revealed the desired cleavage with H_2O_2 to release unmodified model payloads *via* 1,6-elimination. Further fluorometric analysis allowed a comparison of reaction rates of the panel of model linkers with different equivalents of H_2O_2, as well as their stability in the absence of H_2O_2, at different pH, in the presence of glutathione (GSH) and in unconditioned cell media. The superior stability of the arylboronic acid linkers in mouse plasma was exemplified by fluorometric and quantitative HPLC analysis, compared to a Val-Cit analogue which is commonly employed in FDA-approved ADCs.

The most promising arylboronic acid linkers were then elaborated by conjugation to potent cytotoxin MMAE and divinylpyrimidine (DVP) bioconjugation handles. This allowed bioconjugation to anti-HER2

antibody trastuzumab by re-bridging of the interchain disulfides, generating ADCs with average DARs close to 4 and minimal aggregation. The resulting ADCs were evaluated *in vitro* against a panel of HER2+ and HER2- breast cancer cell lines. Surprisingly, the peroxide-cleavable arylboronic acid ADCs were potent against all cell lines, regardless of HER2 antigen expression. Quantification of the extracellular H_2O_2 concentrations of these cell lines revealed that each HER2- cell line had significant levels of extracellular H_2O_2 compared to a negative control. Hence, it is proposed that the presence of extracellular H_2O_2 is responsible for the activity of the peroxide-cleavable ADCs in antigen-negative cell lines. This was further supported by treatment of cells with peroxide-scavenger catalase, which rendered the peroxide-cleavable ADCs non-toxic towards HER2- cell lines. Taken together, this suggested that extracellular peroxide was responsible for the ADC activity rather than instability or promiscuous reactivity.

Given the ability of the peroxide-cleavable linkers to cleave extracellularly without requiring internalisation of the ADC, the linkers were applied towards the generation of non-internalising anti-PD-L1 ADCs. As with trastuzumab, the interchain disulfide bonds of durvalumab were re-bridged with arylboronic acid-MMAE linkers to yield a peroxide-cleavable durvalumab ADC with minimal aggregation and average DAR close to 4. *In vitro* evaluation revealed potent dose-dependent cytotoxicity in PD-L1+ cell lines, which was significantly reduced upon catalase pre-treatment of the cells. This revealed the lack of internalisation of the PD-L1 ADC, and the successful design of the extracellularly-cleavable arylboronic acid linkers.

1.3 Results & Discussion

1.3.1 Synthesis of Model Linker-Payloads

1.3.1.1 Introduction

For initial investigation, it was envisioned that a series of model arylboronic acid linker-payloads could be constructed for evaluation of their ability to release a reporter molecule upon reaction with H_2O_2. The arylboronic acid motif displays extremely fast kinetics of oxidation with hydrogen peroxide, and the kinetics of the subsequent release can be influenced by aryl ring electronics.[114,118–120] Thus, capping of the widely used *para*-hydroxybenzyl spacer with a boronic acid was thought to enable extremely fast and selective antibody-payload cleavage upon exposure to high concentrations of ROS in the tumour microenvironment (Figure 27). An alkyne moiety included at the benzylic position could provide a functional handle for connection to the antibody using click chemistry. Additionally, alkyl-substitution at the benzylic position of such self-immolative spacers is known to enhance the rate of self-immolation.[118,121] 7-Amino-4-methyl coumarin (AMC) was chosen as the reporter molecule due to its tuneable fluorescence: when incorporated into a carbamate bond of the model linker its fluorescence is quenched.[98,122] However, when released from the linker following the desired H_2O_2-mediated oxidation and subsequent 1,6-elimination, the fluorescence is greatly increased, allowing facile monitoring of this process by fluorimetry (Figure 27).

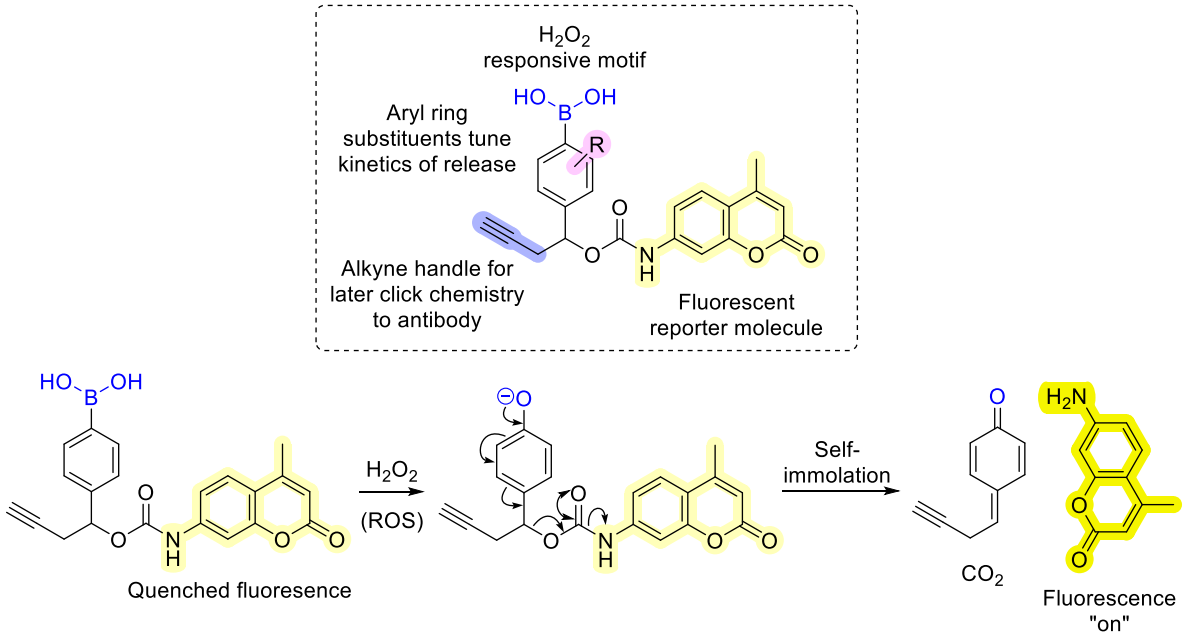

Figure 27: The structure of model linkers and their release of fluorescent reporter molecule by action of H_2O_2.

It was also envisioned that the rate of C-B oxidation and 1,6-immolation could be tuned by the incorporation of different functional groups on the aryl ring. Thus, a panel of model linkers with

different aryl ring substituents was designed for synthesis and investigation (Figure 28). In addition to an unsubstituted model linker (**1**), di-fluoro (**2**), mono-fluoro (**5**) and mono-nitro (**6**) linkers were chosen for investigation since C-B bond oxidation is facilitated by the presence of electron-withdrawing groups on the aromatic ring.[114,123] A Val-Cit model linker (**4**) would also be synthesised to allow comparison of kinetics to a cleavage motif commonly employed in ADCs. Finally, a non-cleavable linker (**3**) lacking the key boronic acid would also be synthesised, to confirm that the peroxide-responsive moiety is essential for payload release and that the carbamate bond is not inherently unstable.

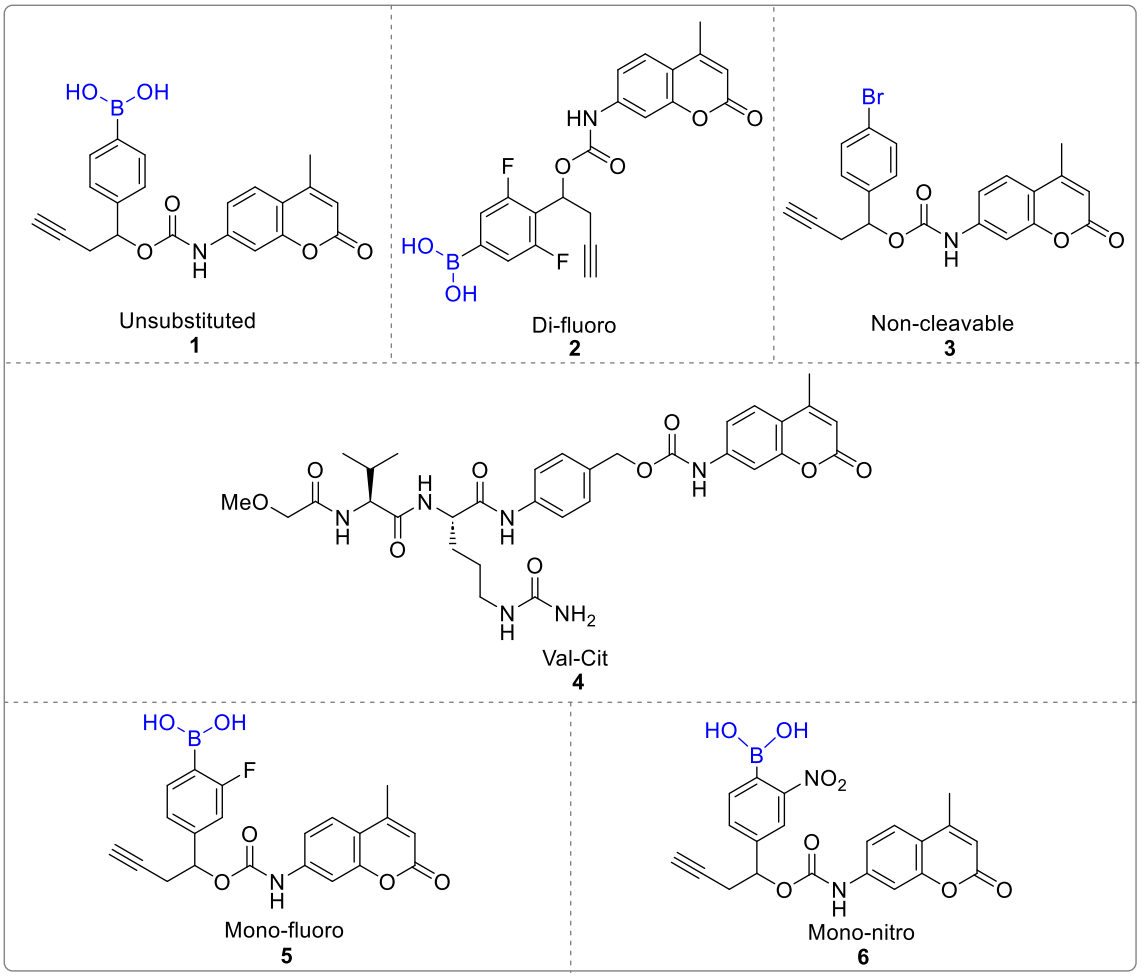

Figure 28: Panel of model linkers for synthesis and evaluation of the kinetics of payload release.

1.3.1.2 Synthesis

The first synthetic route towards model linkers employed a Miyaura borylation from an aryl halide as the last synthetic step to preclude any challenges with the handling and purification of boronic esters.[124] Commencing from commercially available 4-bromo benzaldehydes, a Barbier reaction with zinc and propargyl bromide could install the alkyne handle for later click chemistry to attach to the antibody (Scheme 1). This step also installs a benzylic alcohol for subsequent carbamate formation with AMC. Finally, Miyaura borylation could install a pinacol boronate from the aryl bromide, which

could be hydrolysed to the boronic acid if required. Since boronic esters rapidly hydrolyse to the boronic acids under physiological conditions,[114] whichever is more synthetically tractable will be pursued.

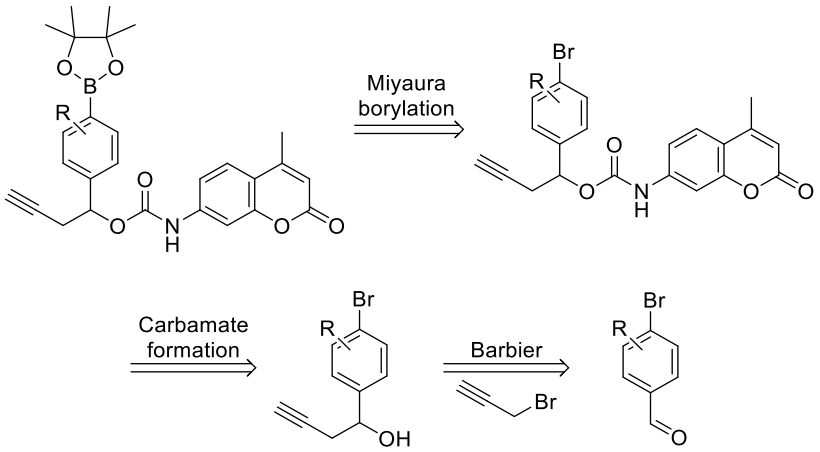

Scheme 1: Retrosynthetic route towards model linkers whereby the Miyaura borylation is performed as the last synthetic step.

For the unsubstituted analogue, Barbier reaction of 4-bromo benzaldehyde was successful in moderate yield to afford benzylic alcohol **7** (Scheme 2). Subsequent carbamate formation with AMC was successful in similar yields, affording carbamate **3** which corresponds to the non-cleavable control, since its only structural difference from the unsubstituted model linker **1** is the lack of the H_2O_2-responsive boronate.

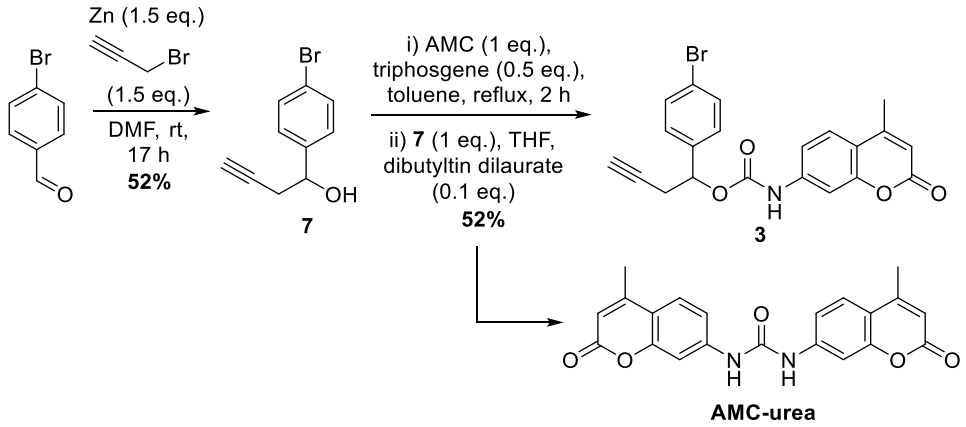

Scheme 2: Synthesis of non-cleavable linker **3** and undesired by-prodrug AMC-urea formation.

Formation of carbamate **3** involved generation of the AMC-isocyanate by triphosgene, catalysed by dibutyltin dilaurate.[125,126] The moderate yield of this reaction can be attributed to the formation of the AMC-urea (identified by the corresponding $[M+H]^+$ in LCMS) and challenging separation of this impurity from the desired product. However, yields were sufficient to access non-cleavable analogue **3** and attempt the Miyaura borylation to unsubstituted model linker **1**.

Unfortunately, Miyaura borylation of bromo-carbamate **3** was unsuccessful under two conditions, resulting only in starting material degradation (Table 1). In general, the carbamate bond appeared to be susceptible to hydrolysis upon heating in base, returning unmodified AMC as observed by the corresponding $[M+H]^+$ in LCMS.

Table 1: Attempted Miyaura borylation conditions to afford **1a**.

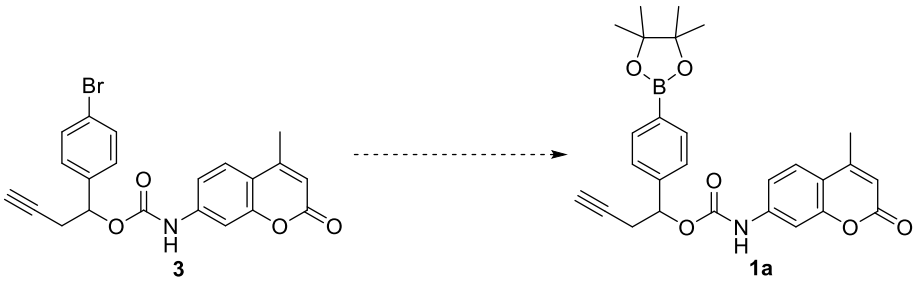

Entry	Conditions	Outcome
1	XPhos (0.025 eq.), XPhos-Pd-G2 (0.05 eq.), B_2Pin_2 (1.2 eq.), $K_3PO_4 \cdot 7H_2O$, EtOH	No reaction until heated to reflux, then degradation of starting material to free AMC.
2	$PdCl_2$(dppf) (0.03 eq.), B_2Pin_2 (1.1 eq.), KOAc (3 eq.), DMSO	No reaction until heated to 60 °C, then degradation of starting material to free AMC.

Given the inability to modify **3** in the basic conditions required for Miyaura borylation, a different synthetic route was considered whereby carbamate formation would be the final synthetic step (Scheme 3).

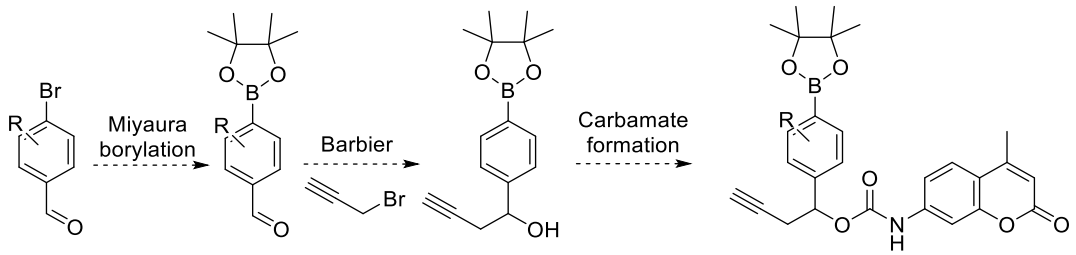

Scheme 3: Alternative synthetic route towards model linkers whereby carbamate formation is the final synthetic step.

For the unsubstituted linker, Miyaura borylation of 4-bromobenzaldehyde was successful in moderate yield, yielding pinacol boronate aldehyde **8** (Scheme 4). Barbier reaction of **8** with propargyl bromide was also initially successful in good yield, affording benzylic alcohol **9** without significant problems handling or purifying the boronic ester. However, the Barbier reaction was irreproducible for this

analogue and others, sometimes affording no desired reaction even with immediate pre-activation of zinc powder. Thus, more reliable conditions were required. Hence, reaction conditions which employed zinc pre-activation with diiodoethane and constant sonication were attempted.[127] The sonochemical reaction of aldehyde **8** was successful, albeit in lower yields than the original Barbier conditions. However, these conditions were significantly more reliable and gave consistent yields on repeat reactions.

Given previous carbamate formation attempts yielded significant AMC-urea by-product, alternative isocyanate formation conditions were employed. Pleasingly, the reaction of AMC and triphosgene with triethylamine at rt gave complete isocyanate formation within 15 minutes (confirmed by quenching an analytical sample with methanol and observing the isocyanate-methanol adduct mass by LCMS, Scheme 4). Without heating, formation of the undesired AMC-urea was greatly reduced. Subsequent reaction of AMC-isocyanate with benzylic alcohol **9** was successful, however, reverse-phase purification yielded mixtures of boronic ester (**1a**) and boronic acid (**1b**) product. Hence, upon repetition the reaction mixture was subjected to basic aqueous conditions after carbamate formation, which hydrolysed boronic pinacol ester **1a** to boronic acid **1b**. The new procedure afforded the final unsubstituted boronic acid linker **1b** in low yields, but in sufficient quantity and purity for further evaluation. Attention then turned to generate different analogues *via* the same synthetic route.

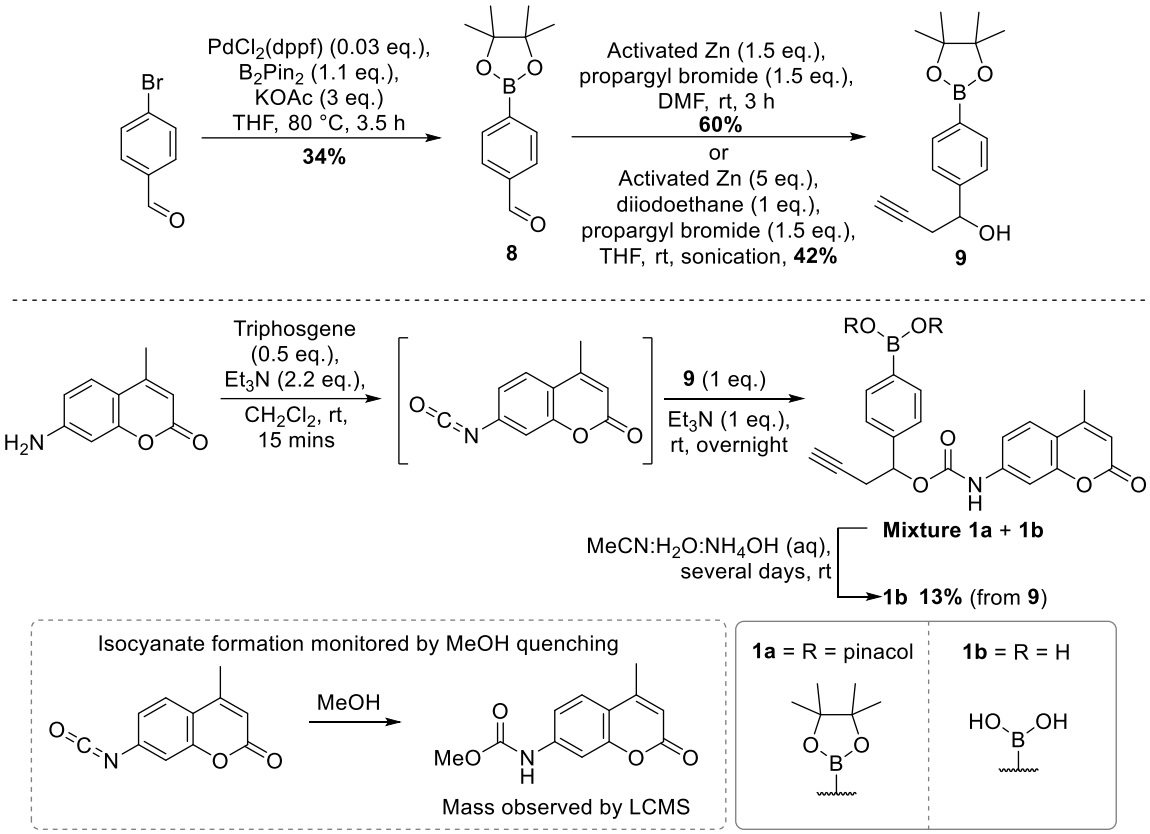

Scheme 4: Synthesis of unsubstituted model linker **1b**, including the quenching of isocyanate for observation by LCMS and hydrolysis of boronic ester and acid mixtures to obtain pure boronic acid **1b**.

Di-fluoro pinacol boronate **10** was obtained from the Miyaura borylation of 4-bromo-2,5-difluoro benzaldehyde, however, purification by flash column chromatography (FCC) only yielded impure product (Scheme 5). Upon repetition **10** was therefore carried forward crude without purification. The Barbier reaction of crude **10** was then successful, obtaining benzylic alcohol **11** in good yields over the two steps. Carbamate formation, followed by *in situ* hydrolysis of the boronic ester (**2a**) to the boronic acid (**2b**) yielded the final di-fluoro boronic acid linker **2b** in 29% yield.

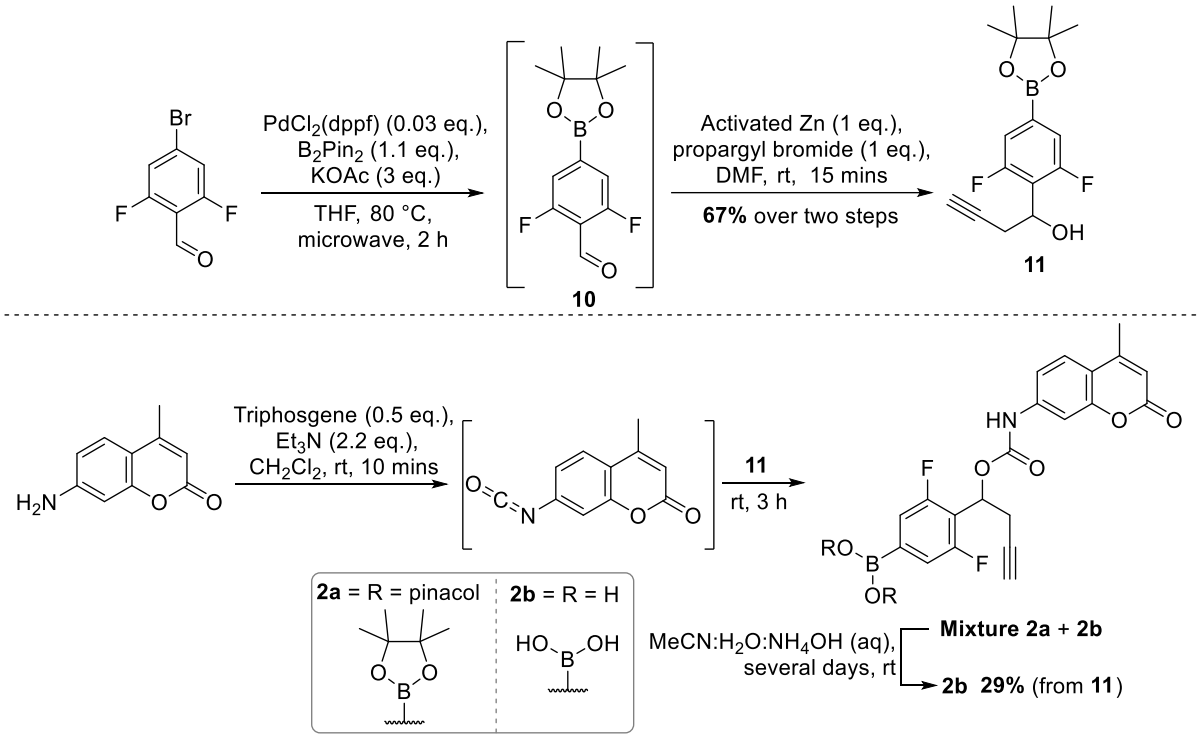

Scheme 5: Synthesis of the di-fluoro model linker **2b**.

Miyaura borylation of 3-fluoro-4-bromobenzaldehyde to afford **12** proceeded in moderate yield, and subsequent Barbier reaction also proceeded adequately, affording **13** with slightly improved yields when using the sonochemical method with diiodoethane (Scheme 6). Finally, carbamate formation with AMC was successful, yielding majority boronate ester **5a** in good yield, and a small amount of boronic acid **5b**. The boronate ester **5a** was then hydrolysed to boronic acid **5b**, overall affording **5b** in 13% yield from **13**.

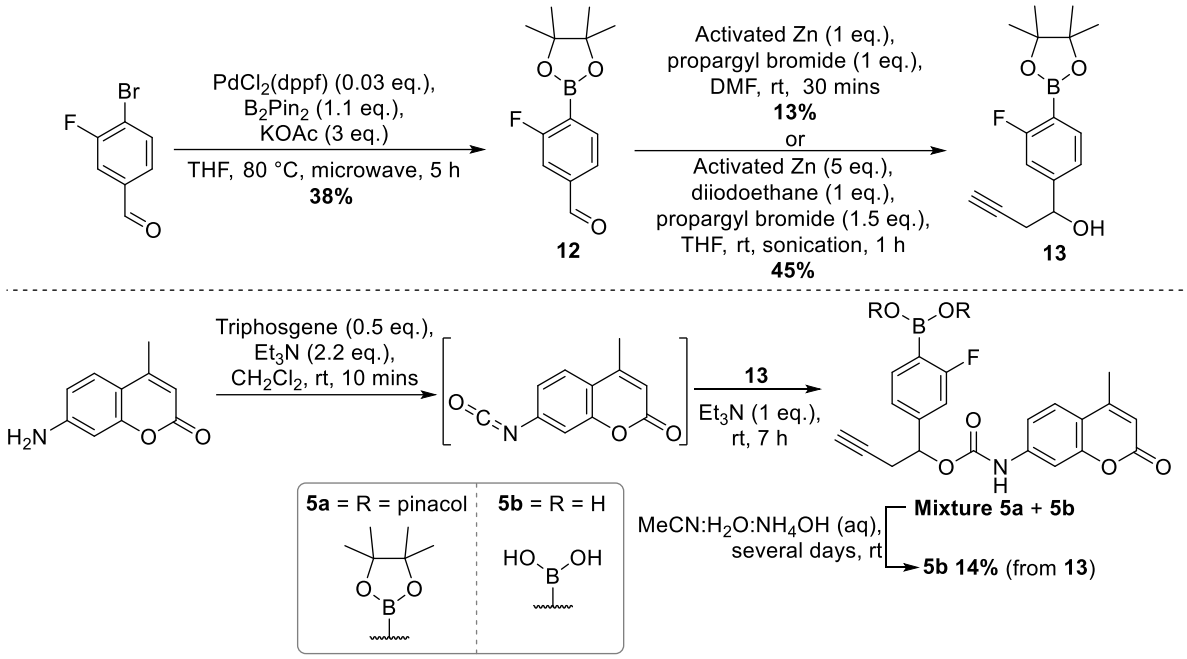

Scheme 6: Synthesis of mono-fluoro model linker **5b**.

Synthesis of mono-nitro analogue **6** commenced with Miyaura borylation of 3-nitro-4-bromobenzaldhehyde (Scheme 7). The reaction profile was complex when analysed by LCMS and formed a number of unidentified by-products, as well as the corresponding boronic acid. Hence only a moderate yield of **14** was achieved. Unfortunately, the subsequent Barbier reaction also gave a complex reaction mixture and proceeded with significant hydrolysis of the boronic ester to the boronic acid. As such, the boronic acid material **15** was isolated and carried forward impure. Although the desired product **6a** was observed to form in the subsequent carbamate formation step, multiple by-products also formed, and purification was challenging. Hence, final material **6a** was not obtained. In general, synthetic efforts towards the nitro analogue involved very complex reaction mixtures with difficult purification and thus no further attempts were made at synthesising **6a**. Moreover, it is known that drugs containing nitro groups can cause toxicity and consequently are often considered "structural alerts" to be avoided in drug design.[128,129]

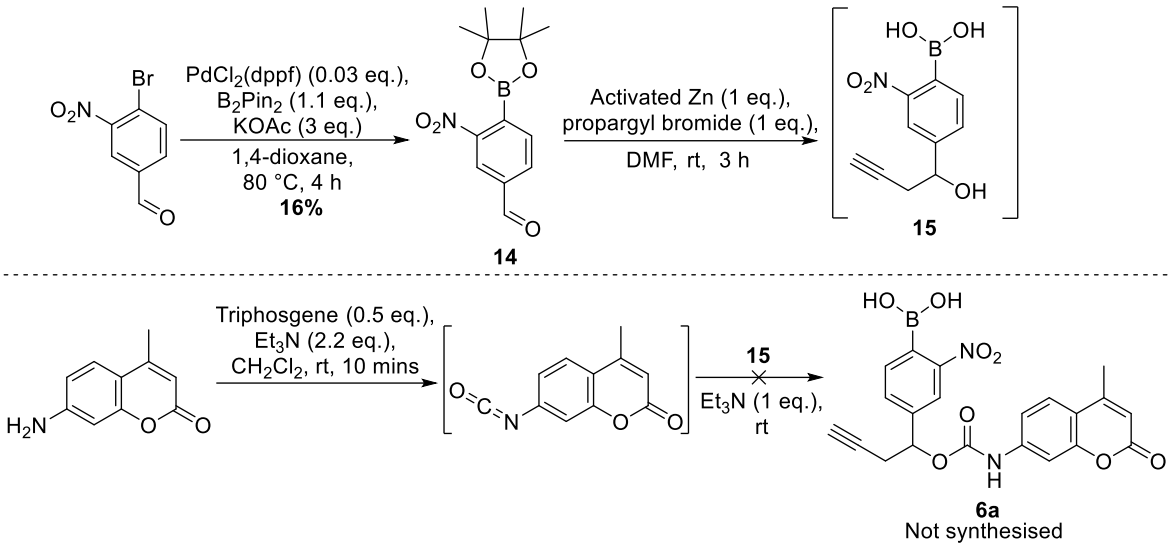

Scheme 7: Attempted synthesis of mono-nitro model linker **6a**.

Finally, Val-Cit model linker **4** was synthesised in moderate yields according to a previously published procedure (Scheme 8).[130]

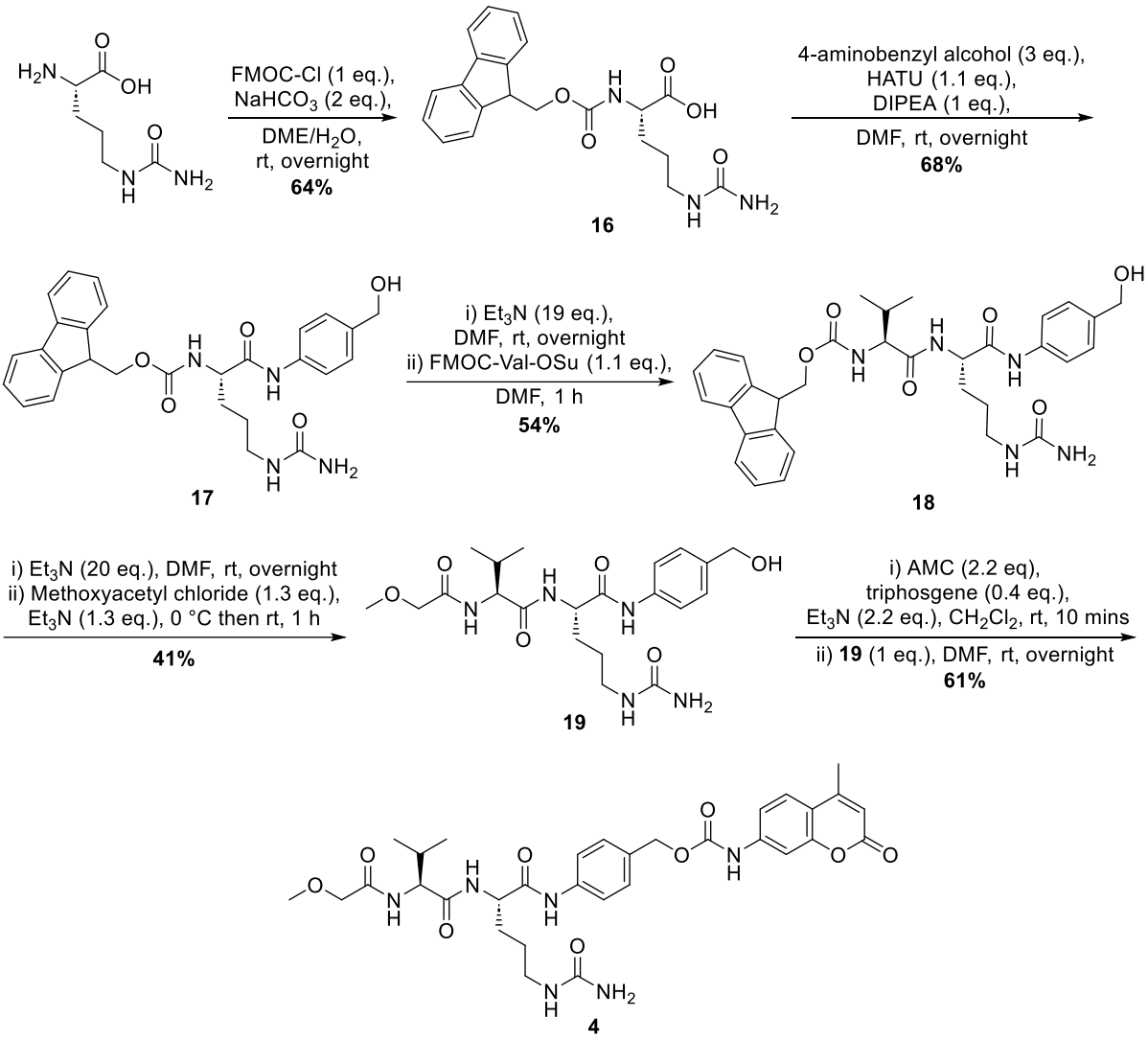

Scheme 8: Synthesis of Val-Cit AMC model linker **4**.

1.3.2 Evaluation of Payload Release from Model Linkers

1.3.2.1 HPLC kinetics

With model linkers **1b**, **2b**, **3**, **4** and **5b** in hand, HPLC analysis was performed to confirm the desired reactivity with H_2O_2. It was envisaged that this would give preliminary information regarding the extent and kinetics of AMC release. Arylboronic acid model linkers **1b, 2b** and **5b** were incubated with 10 equivalents (eq.) of H_2O_2 with caffeine as an internal standard. For the unsubstituted **1b** and di-fluoro linker **2b** (Figure 29A and Figure 29B respectively), boronic acid starting material was undetectable after 1 h incubation. For the mono-fluoro linker **5b**, cleavage was slower, with a trace of boronic acid starting material still remaining after 1 h incubation (Figure 29D). In each case, 1,6-elimination was sufficiently rapid such that the intermediate phenol was not observed. LCMS analysis allowed identification of the quinone methide (QM) formed from the 1,6-elimination (labelled **A** in Figure 29). Furthermore, another by-product was observed which corresponded to the mass of an AMC-quinone methide adduct (labelled **C** in Figure 29). Formation of similar by-products from addition to QMs has been observed in the literature, and is likely a result of the high concentrations used in the HPLC assay.[131,132] Other visible peaks could not be characterised by LCMS.

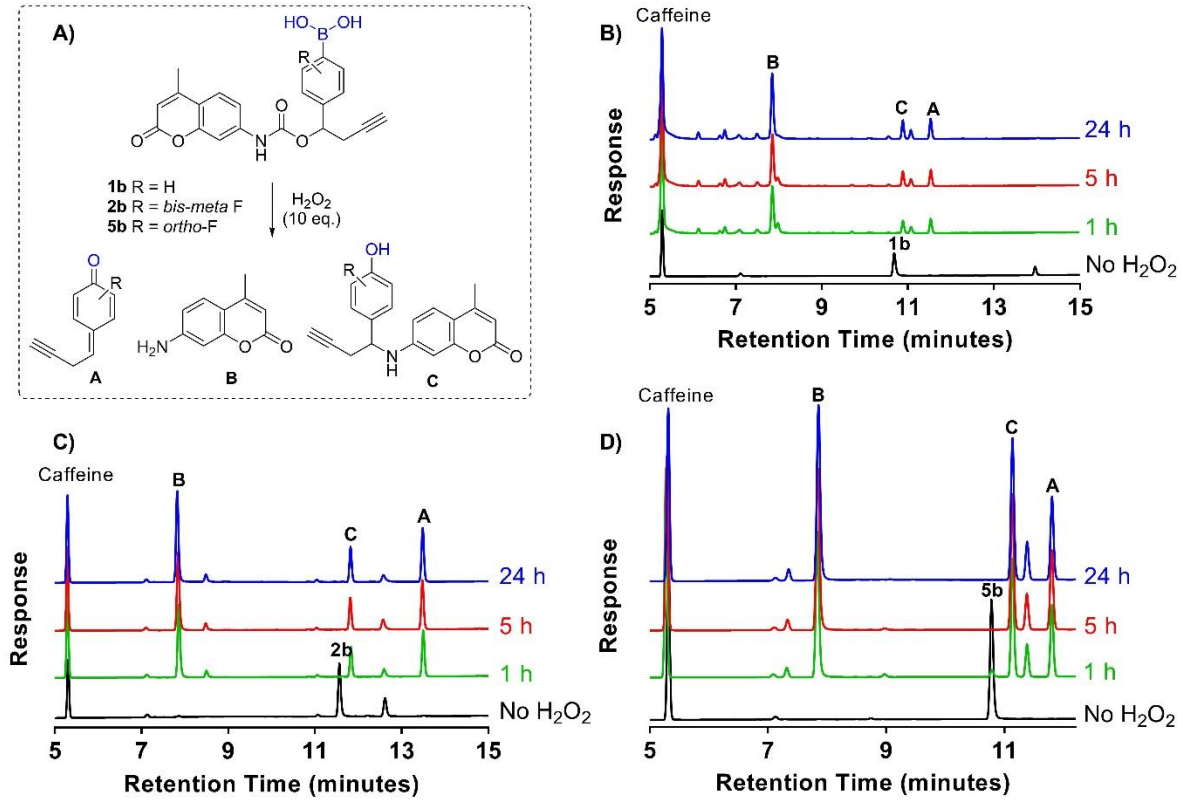

Figure 29: A) Linker cleavage with 10 equiv. H_2O_2 and the observed species formed by HPLC and LCMS, B) **1b** linker cleavage HPLC traces, C) **2b** linker cleavage HPLC traces, D) **5b** linker cleavage HPLC traces.

This preliminary HPLC assay demonstrated that arylboronate linkers **1b**, **2b** and **5b** displayed the desired reactivity and reporter molecule release with H_2O_2, warranting their further evaluation under more physiologically relevant conditions.

1.3.2.2 Fluorimetry kinetics

Release with different equivalents of H_2O_2

Fluorimetry offers a non-invasive, continuous analysis method to view the release of fluorescent AMC from the reaction of model linkers at low micromolar concentrations with H_2O_2. Hence, model linkers were incubated with various concentrations of H_2O_2 at 37 °C and fluorescence intensity was monitored over 24 h (5 µM linker, pH 7.4 PBS buffer).

In each case, AMC release was faster with increased equivalents of H_2O_2, and no fluorescence increase was observed in the absence of H_2O_2, suggesting stability of the model linkers (Figure 30A-C). Additionally, no fluorescence increase was observed with non-cleavable linker **3** (Figure 30D), highlighting that the boronic acid motif is key for the mechanism of AMC release. Comparison of each linker at 10 equiv. H_2O_2 (Figure 30E) shows that the di-fluoro linker **2b** cleaved the fastest ($t_{1/2}$ ~ 1h), followed by the unsubstituted **1b** ($t_{1/2}$ ~ 1.5 h) then the mono-fluoro linker **5b** ($t_{1/2}$ ~ 2 h).

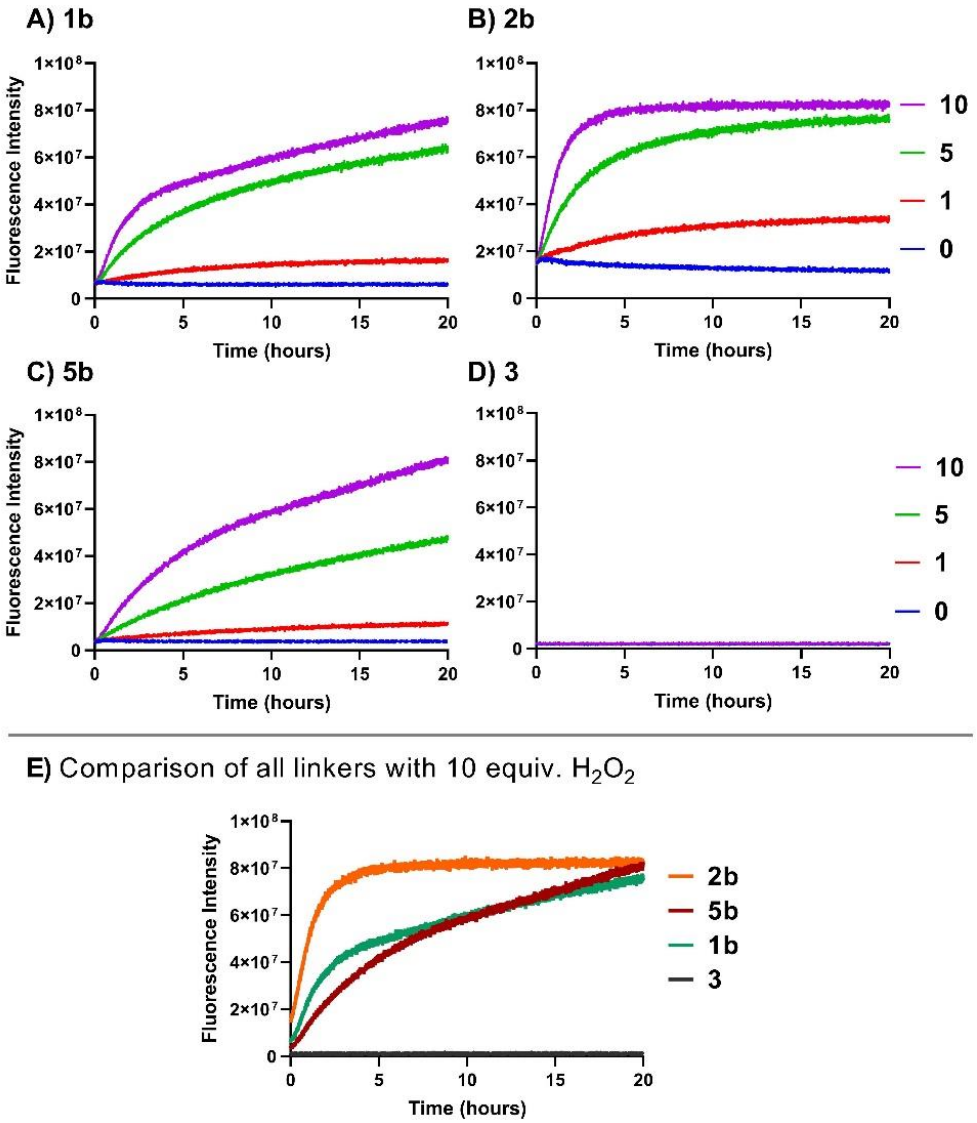

Figure 30: Kinetics of AMC release from H_2O_2-cleavable model linkers with different H_2O_2 equivalents. Legend 10, 5, 1, 0 refers to peroxide equivalents. A) Unsubstituted **1b**, B) Di-fluoro **2b**, C), Mono-fluoro **5b** and D) Non-cleavable **3**. E) Comparison of kinetics of AMC release from each linker with 10 equiv. H_2O_2.

Kinetics of release at different pH

Since linkers **1b** and **2b** seemed the most reactive in the initial kinetic studies, they were carried forward for further study. First, the kinetics of release was evaluated at different pH (Figure 31).

Release of AMC was accelerated at pH 9 compared to neutral pH 7.4. However, at acidic pH (4.5), which is more representative of lysosomes, release was significantly slower. Although most ADCs are designed to release their payload within lysosomes in the target cell, it is not essential for an efficacious ADC, and linker cleavage may also occur in the cytosol or extracellularly after diffusion from lysosomes.

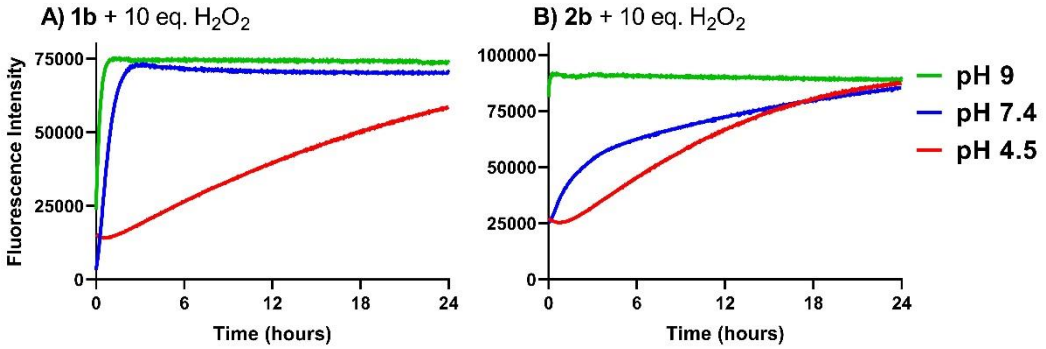

Figure 31: The release of fluorescent AMC from model linkers **1b** and **2b** with 10 equivalents (eq.) H_2O_2 at different pH.

Release in the presence of GSH

Next, release from the model linkers in the presence of glutathione (GSH) was evaluated to assess whether release would be hindered by the presence of other nucleophiles (Figure 32). Pleasingly, the rates of AMC release were similar with 10 eq. H_2O_2 with or without the presence of 10 eq. GSH, suggesting that linker cleavage and payload release would not largely be impeded by the presence of other nucleophiles.

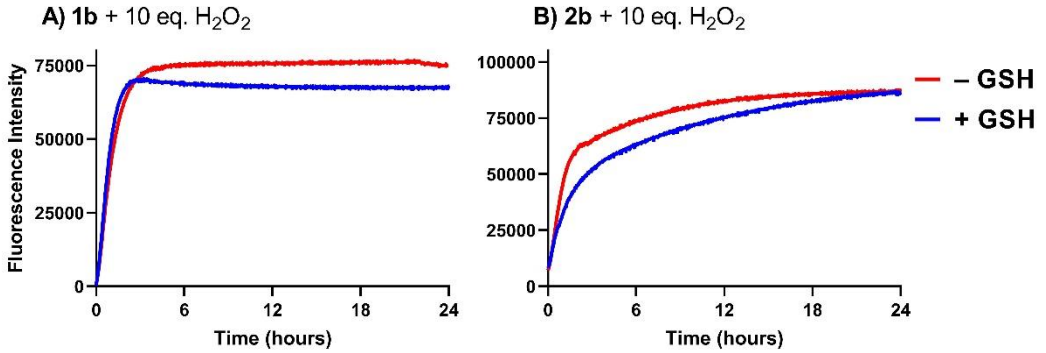

Figure 32: The release of fluorophore from model linkers A) **1b** and B) **2b** in the presence of 10 equiv. GSH and 10 equiv. H_2O_2. – GSH refers to no added GSH, + GSH refers to the addition of 10 equiv. GSH.

1.3.3 Stability Analysis

1.3.3.1 Stability at different pH

To further confirm the stability of model linkers, they were incubated in buffers with varying pHs (without H_2O_2). Both **1b** and **2b** were stable over 24 h with minimal fluorescence increase at pH 4.5, 7.4 and 9 (Figure 33).

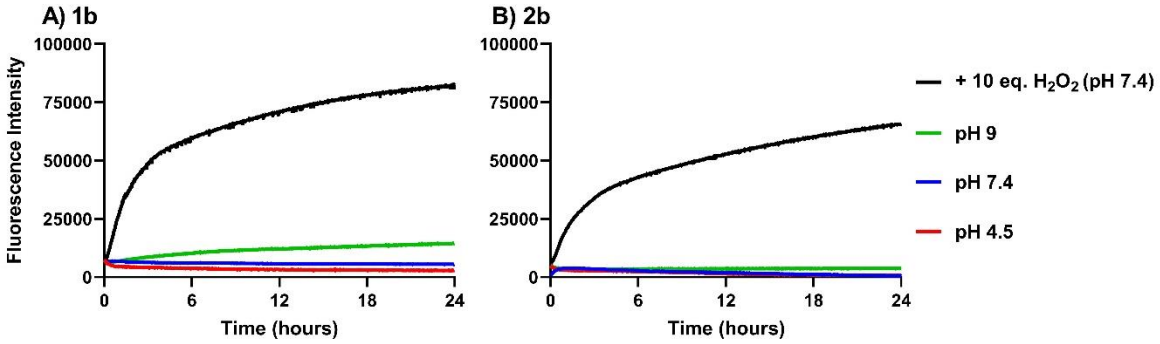

Figure 33: Stability of model linkers A) **1b** and B) **2b** at different pHs in the absence of H_2O_2 over 24 h. The fluorimetry when incubated with 10 equiv. H_2O_2 is include for comparison. pH 7.4 = PBS, pH 4.5 = ammonium acetate buffer, pH 9 = carbonate buffer.

Only when the unsubstituted linker **1b** was incubated for a further 10 days was significant fluorescence increase observed at pH 9, although it did not reach the same level as with 10 eq. H_2O_2 (Figure 34). Presumably, the carbamate bond is susceptible to hydrolysis in prolonged highly basic conditions (as was observed during the synthesis of **1** – see Table 1).

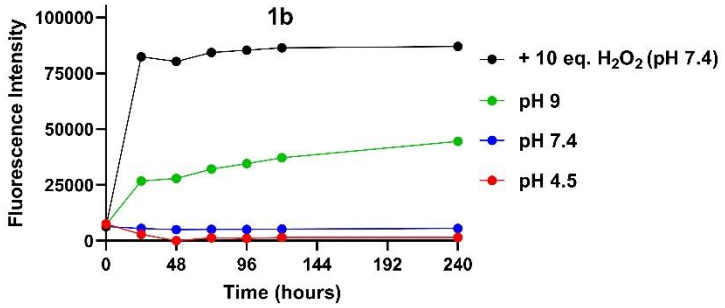

Figure 34: Stability of model linker **1b** at different pHs in the absence of H_2O_2 over 10 days. The fluorimetry when incubated with 10 equiv. H_2O_2 is include for comparison. pH 7.4 = PBS, pH 4.5 = ammonium acetate buffer, pH 9 = carbonate buffer.

1.3.3.2 Stability in the presence of GSH

When incubated for a prolonged period of time (10 days) in the presence of 10 eq. GSH at 37 °C, minimal fluorescence increase was observed from peroxide-cleavable linkers **1b** and **2b** (Figure 35). Di-fluoro linker **2b** displayed a small increase in fluorescence intensity over time, but it did not reach the high intensity that is obtained when the linker is incubated with 10 eq. H_2O_2, suggesting that only minimal levels of AMC are released with a large excess (10 eq.) of GSH.

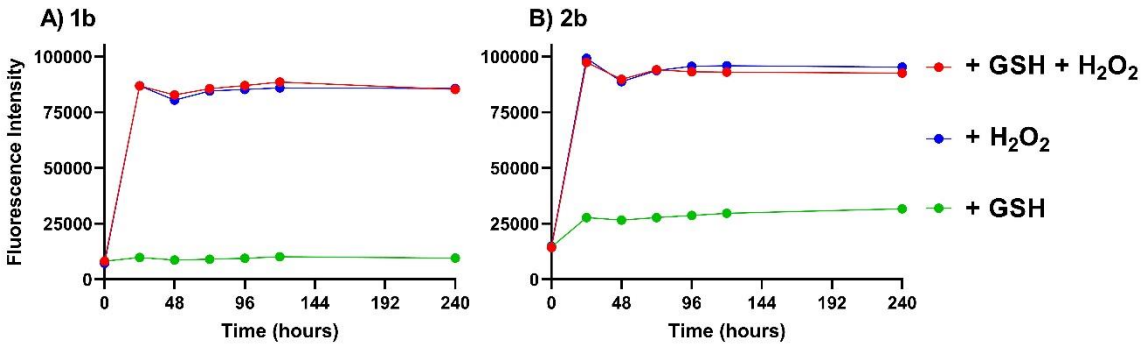

Figure 35: The release of AMC from model linkers A) **1b** and B) **2b** when incubated with GSH compared to when co-incubated with GSH and H_2O_2. + GSH refers to incubation with 10 eq. GSH, + H_2O_2 refers to incubation with 10 eq. H_2O_2.

1.3.3.3 Stability in cell media

To confirm that the linkers were not susceptible to degradation in the cell media used for *in vitro* studies, they were incubated with unconditioned cell media from each of the breast cancer cell lines examined (in the absence of cancer cells, the media does not contain any ROS). **1b** and **2b** were incubated with cell media at 37 °C, and fluorescence was monitored continuously for 24 h, then re-analysed every day for 4 days (the length of time of an *in vitro* assay) (Figure 36 and Figure 37).

For unsubstituted linker **1b**, there was a slight increase in fluorescence over time in RPMI and McCoy's media, but this did not reach the intensity of the linker when incubated with H_2O_2 (Figure 36). RMPI and McCoy's are the growth media for HER2-positive (HER2+) breast cancer cells (BT474 and SKBR3). **1b** was stable in DMEM, the media of HER2-negative (HER2-) breast cancer cells, hence no release of the payload in the non-target cell lines as a result of general instability in media was expected. However, the small amount of payload release from **1b** in the HER2+ media may contribute to the ADC activity in the target cells. Nevertheless, it should be considered that these small molecule linkers are only model compounds, and it is not entirely clear how applicable their stability is to the stability of the linker when incorporated into an ADC. Di-fluoro model linker **2b** was stable in all cell media, displaying no significant fluorescence increase during the 4-day incubation (Figure 37).

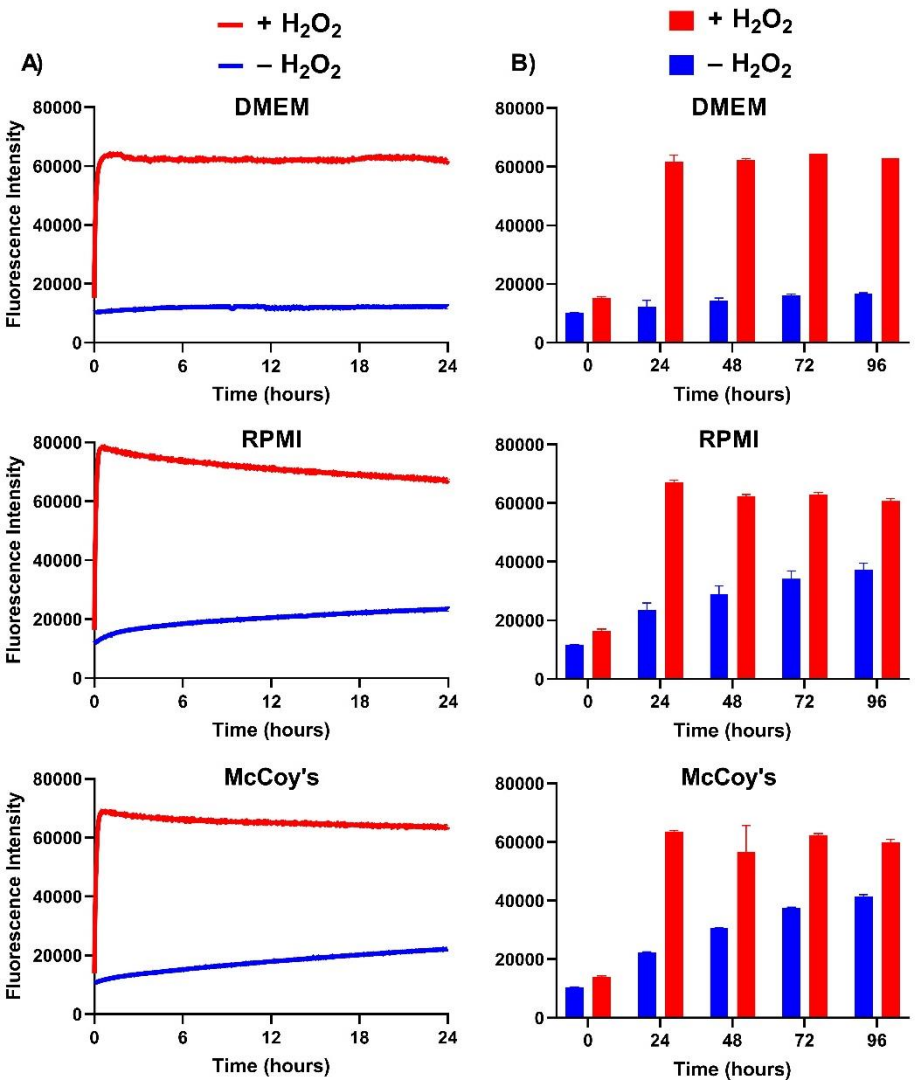

Figure 36: Stability of the unsubstituted model linker **1b** in cell media. (A) the fluorescence when incubated for 24 h at 37 °C, B) the fluorescence over 4 days at 37 °C, with (+) or without (-) co-incubation with 10 eq. H_2O_2. DMEM is the cell media for MCF7 and MDA-MB-468 cells, RPMI is the media for BT474 cells and McCoy's is the media for SKBR3 cells.

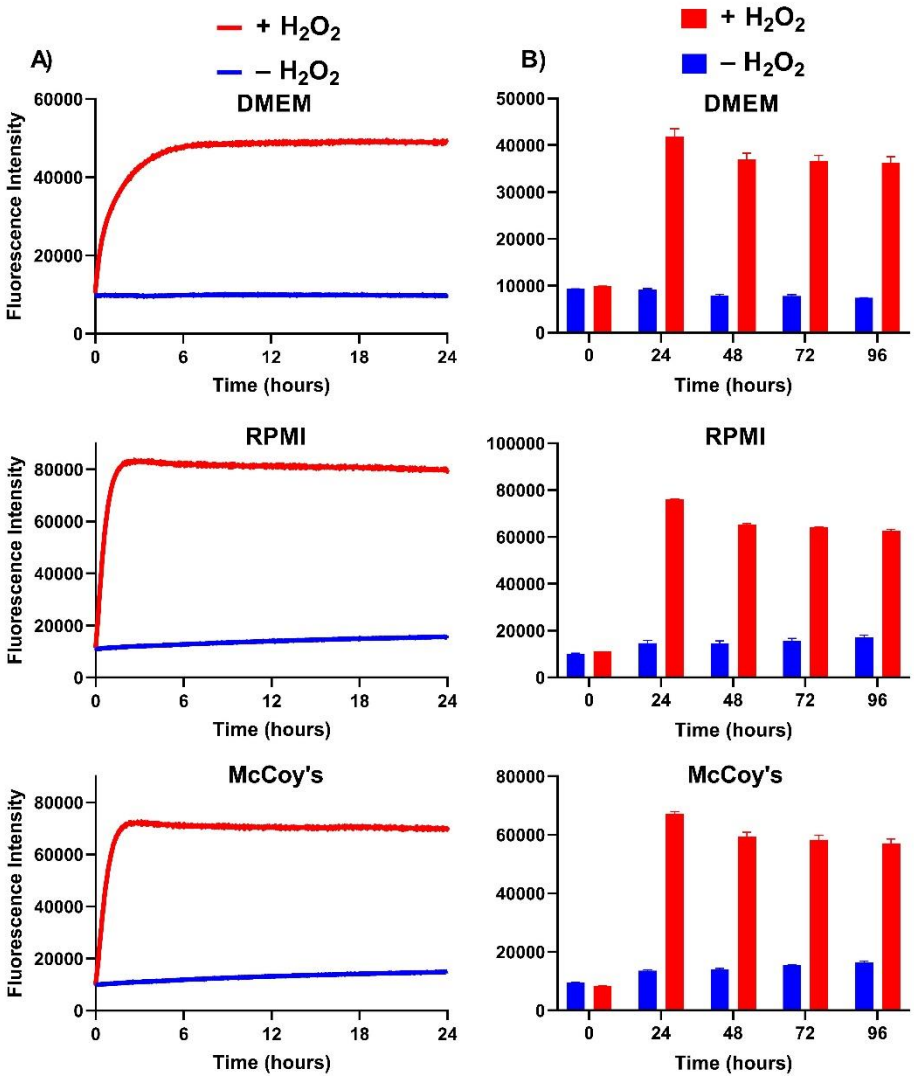

Figure 37: Stability of the unsubstituted model linker **2b** in cell media. (A) the fluorescence when incubated for 24 h at 37 °C, B) the fluorescence over 4 days at 37 °C, with (+) or without (-) co-incubation with 10 eq. H_2O_2. DMEM is the cell media for MCF7 and MDA-MB-468 cells, RPMI is the media for BT474 cells and McCoy's is the media for SKBR3 cells.

1.3.3.4 Stability in plasma

For initial assessment of model linker stability in human and mouse plasma, the di-fluoro linker **2b** was selected due to its apparent higher reactivity than the unsubstituted linker (Figure 30). Val-Cit model linker **4** was also evaluated in human and mouse plasma for comparison with linkers commonly used in ADCs. Comparing the stability of **2b** vs **4** in mouse plasma was of particular interest, since dipeptides have known instability to hydrolysis by the Ces1c hydrolase present in mouse plasma.[63–65] The assay was performed at 37 °C with caffeine as an internal standard, which allowed the quantitative analysis of linker degradation over time by HPLC analysis (Figure 38 and Figure 39).

In mouse plasma, Val-Cit model linker **4** was very unstable, with the starting material peak becoming completely undetectable within 10 days, and the appearance of a significant new peak (denoted with

an asterisk, Figure 38C). In contrast, di-fluoro linker **2b** was markedly more stable in the assay conditions (Figure 38B).

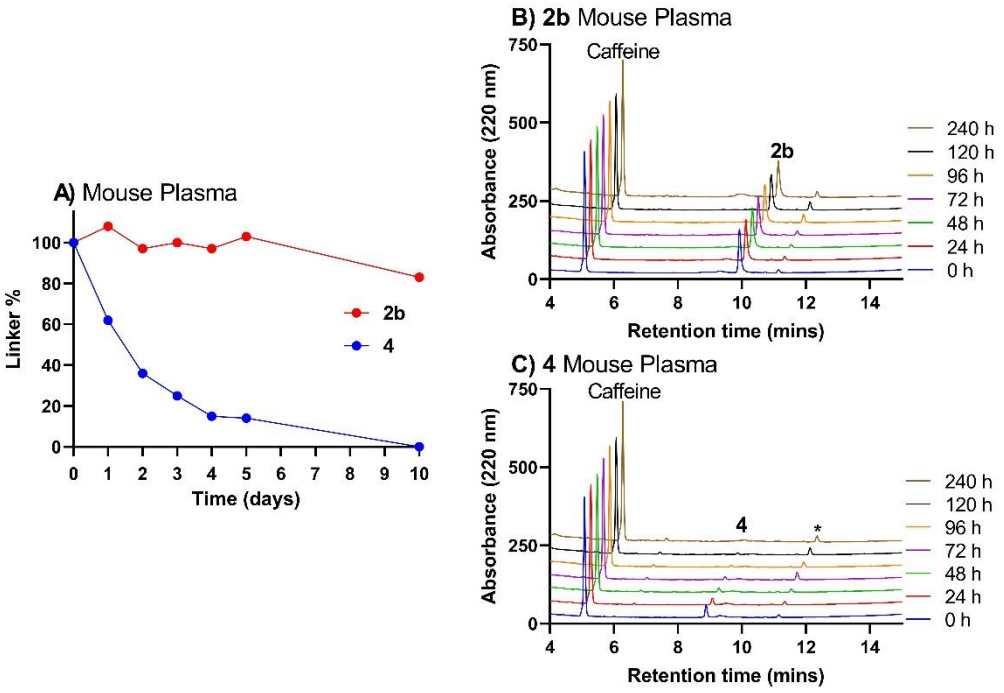

Figure 38: HPLC stability assay in mouse plasma. A) Quantitation of linker % over time calculated from the comparison of caffeine:linker peak area in the HPLC, B) HPLC traces of di-fluoro **2b** and C) Val-Cit **4** model linkers: the significant new peak from the degradation of linker **4** is denoted with an asterisk *. Raw HPLC data can be found in appendix 3.

In human plasma, the non-cleavable (**3**), di-fluoro (**2b**) and Val-Cit (**4**) linkers were comparably stable, with no significant degradation observed over 10 days.

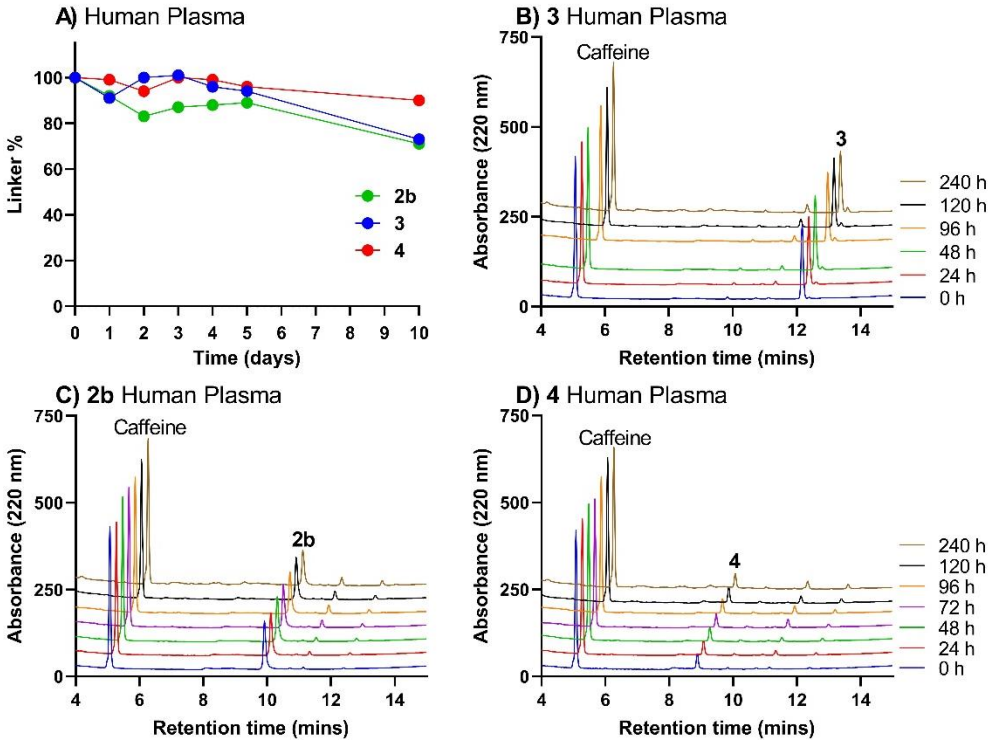

Figure 39: HPLC stability assay in human plasma. A) Quantitation of linker % over time calculated from the comparison of caffeine:linker peak area in the HPLC, B) HPLC traces of non-cleavable **3**, C) di-fluoro **2b**, and D) Val-Cit **4** model linkers. For the non-cleavable linker **3**, the HPLC trace at 72 h is not displayed due to inconsistencies in HPLC retention time, though the peak area could still be used for the quantitative analysis. Raw HPLC data can be found in appendix 3.

Although the HPLC assay gave good confidence that **2b** had improved stability over Val-Cit **4** in mouse plasma, the response from the linkers was at the lower limit of suitability for quantitation. It was envisioned that fluorimetry would also be a convenient way to confirm that the linkers do not degrade to release free "drug" (AMC) in the presence of plasma at more biologically relevant concentrations.

Thus, the unsubstituted **1b** and di-fluoro **2b** model linkers were incubated with human and mouse plasma and the fluorescence monitored over 20-24 h at 37°C (Figure 40). Pleasingly, no fluorescence increase was observed from incubation in either mouse or human plasma in comparison to the large fluorescence increase when incubated with 10 equiv. H_2O_2. Thus, the linkers do not degrade to release free "drug" in plasma.

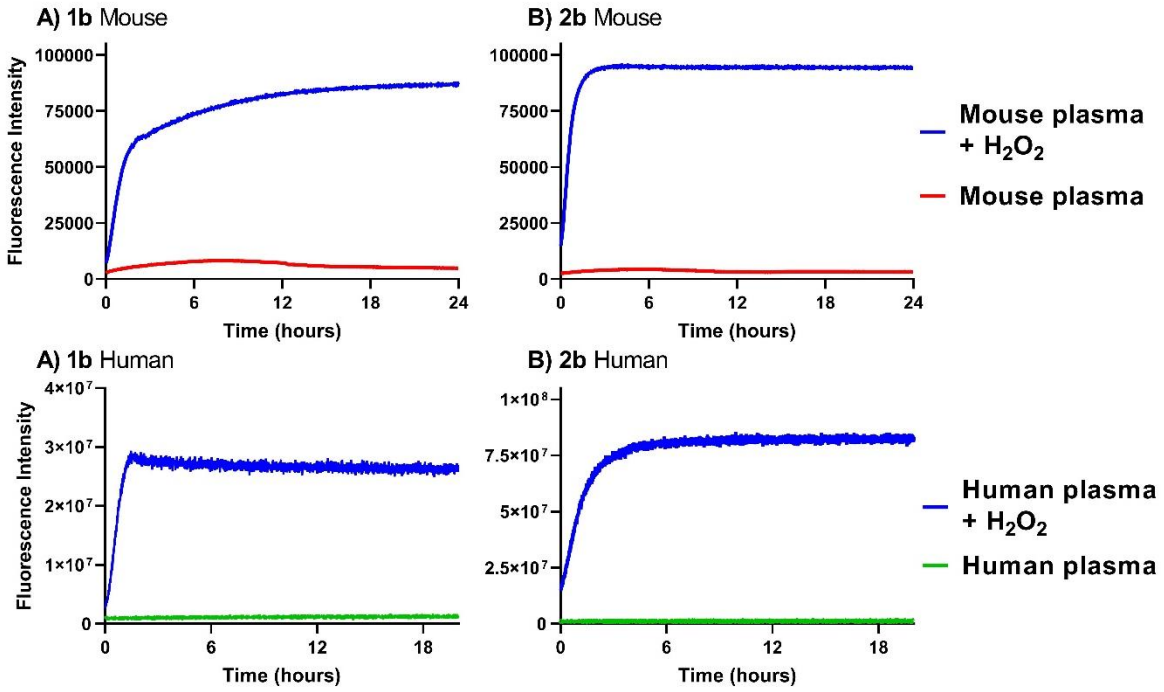

Figure 40: The fluorescence intensity of A) unsubstituted **1b** and B) di-fluoro linker **2b** when incubated with mouse plasma or C) **1b** and D) **2b** in human plasma over 20-24 h.

For further assurance, the linkers were evaluated over 10 days in human and mouse plasma. Similar to the results of the HPLC assay, the boronic acid linkers were stable in human and mouse plasma, with no significant increase in fluorescence over the 10 days, similar to the Val-Cit analogous linker **4** (Figure 41). However, in mouse plasma, **4** was highly unstable and displayed a significant increase in fluorescence intensity within 1 day. The fluorescence decrease observed for the remaining days is thought to be due to fluorescence quenching of the released fluorophore. The arylboronic acid linkers **1b** and **2b** do not display this major instability in mouse plasma, since a much lower fluorescence increase is observed.

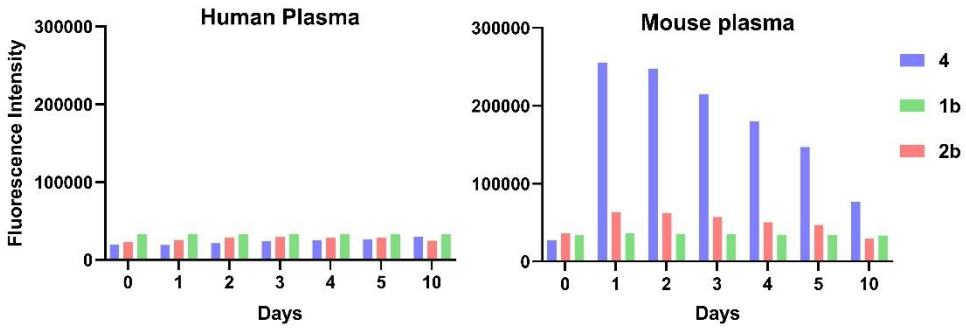

Figure 41: The long-term stability of unsubstituted **1b**, di-fluoro **2b** and Val-Cit **4** model linkers in human and mouse plasma. The decrease in fluorescence of **4** after initial increase is thought to be due to fluorescence quenching of the released fluorophore.

1.3.4 ADC Synthesis

Having confirmed the suitability of arylboronic acids for plasma stable and responsive peroxide-cleavable linkers, the unsubstituted and di-fluoro linkers were elaborated into ADCs which were expected to retain these favourable characteristics.

1.3.4.1 Linker synthesis

Synthetic intermediates from model linker synthesis (**9** and **11**) contain an alkyne for copper-catalysed azide–alkyne cycloaddition (CuAAC) to allow antibody attachment, and a benzylic alcohol for payload attachment. The Spring group have previously demonstrated the efficiency of DVP reagents for bioconjugation to trastuzumab, which generate re-bridged antibody species with an average drug-to-antibody ratio (DAR) of four.[36,37] Monomethyl auristatin E (MMAE) was chosen as the payload given its high cytotoxicity (sub-nanomolar IC_{50}) against a number of different cell lines and wide use in FDA-approved ADCs.

First, benzylic alcohols **9** and **11** were activated as *para*-nitro phenyl carbonates **20a** (unsubstituted) and **21b** (di-fluoro), for reaction with the amine residue of MMAE, affording linker-payloads **20b** and **21b** (Scheme 9). Then, CuAAC between alkynes **20b** and **21b** with DVP-azide **22** yielded the desired linker-payloads **20c** and **21c**.

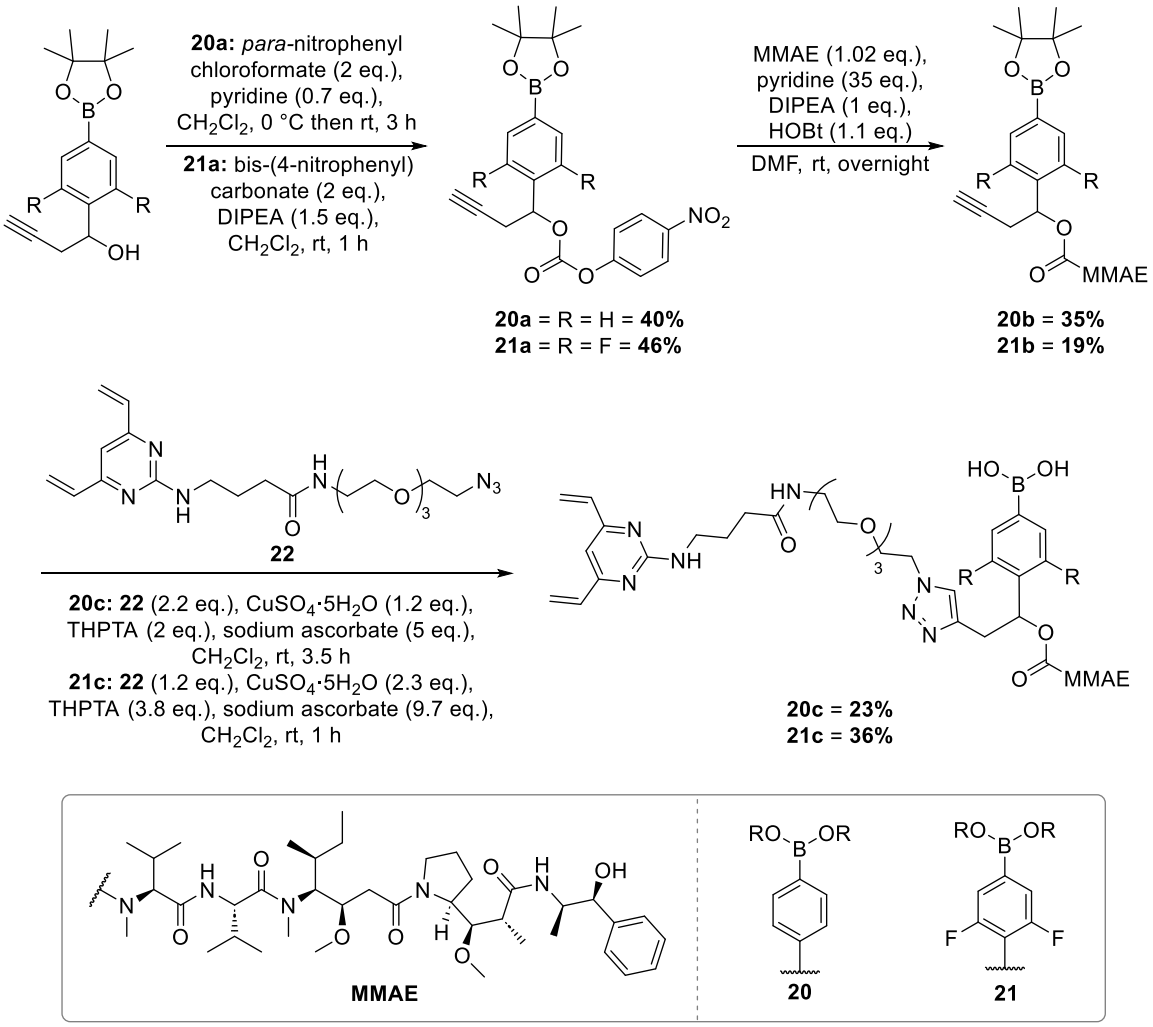

Scheme 9: Synthesis of arylboronic acid DVP-Linker-MMAE constructs **20c** (unsubstituted) and **21c** (di-fluoro). DVP-azide **22** was provided by Dr. Stephen Walsh.

Hence, the final DVP-linker-MMAE constructs **20c** and **21c** were obtained in moderate yield, primed for antibody bioconjugation. Non-cleavable DVP-linker **23** was provided by Dr Stephen Walsh for the synthesis of a control non-cleavable ADC, which has been utilised in previous work (Figure 42).[37,73] Additionally, Val-Cit-Linker-MMAE **24** was provided by Dr Stephen Walsh for use as a control (Figure 42).

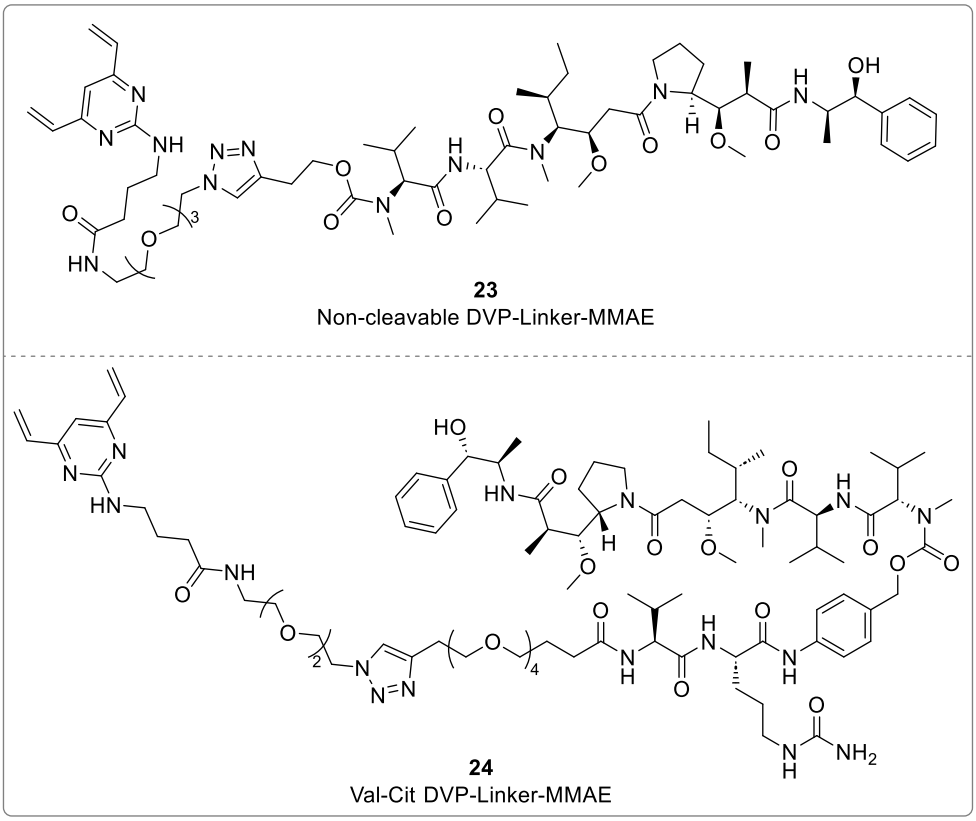

Figure 42: Structure of non-cleavable **23** and Val-Cit **24** DVP-Linker-MMAE constructs.

1.3.4.2 Bioconjugations

With the four DVP-linker-payloads **20c**, **21c**, **23** and **24** in hand, bioconjugation was required *via* antibody re-bridging to afford the final ADCs. Trastuzumab is an IgG antibody which targets human epidermal growth factor receptor (HER2), which is overexpressed in 20-30% of breast cancers.[133] Trastuzumab contains four interchain disulfide bonds which can be reduced to their free thiols by tris(2-carboxyethyl)phosphine (TCEP). Then, nucleophilic addition to the vinyl groups of a DVP-linker-MMAE can afford an antibody species whereby the native intrachain disulfide bonds are re-bridged, ideally attaching four drugs per antibody (DAR of 4).

Initial bioconjugation attempts employed standard conditions previously used in the Spring group,[37] with 10 eq. of TCEP·HCl at 37 °C in buffer (25 mM Tris HCl pH 8, 25 mM NaCl, 0.5 mM EDTA) with 2.5 mg/mL (16.7 µM) trastuzumab for 1 h, followed by incubation with 40 eq. of DVP-Linker-MMAE (10% DMSO co-solvent) for 2 h (Figure 43). Then, any remaining small-molecule contaminants were removed by a Zeba™ Spin Desalting Column (7K molecular weight cut-off) followed by successive diafiltration into PBS using an Amicon-Ultra centrifugal filter (10K molecular weight cut-off). The bioconjugation products were then analysed by SDS-Page and Hydrophobic Interaction Chromatography (HIC).

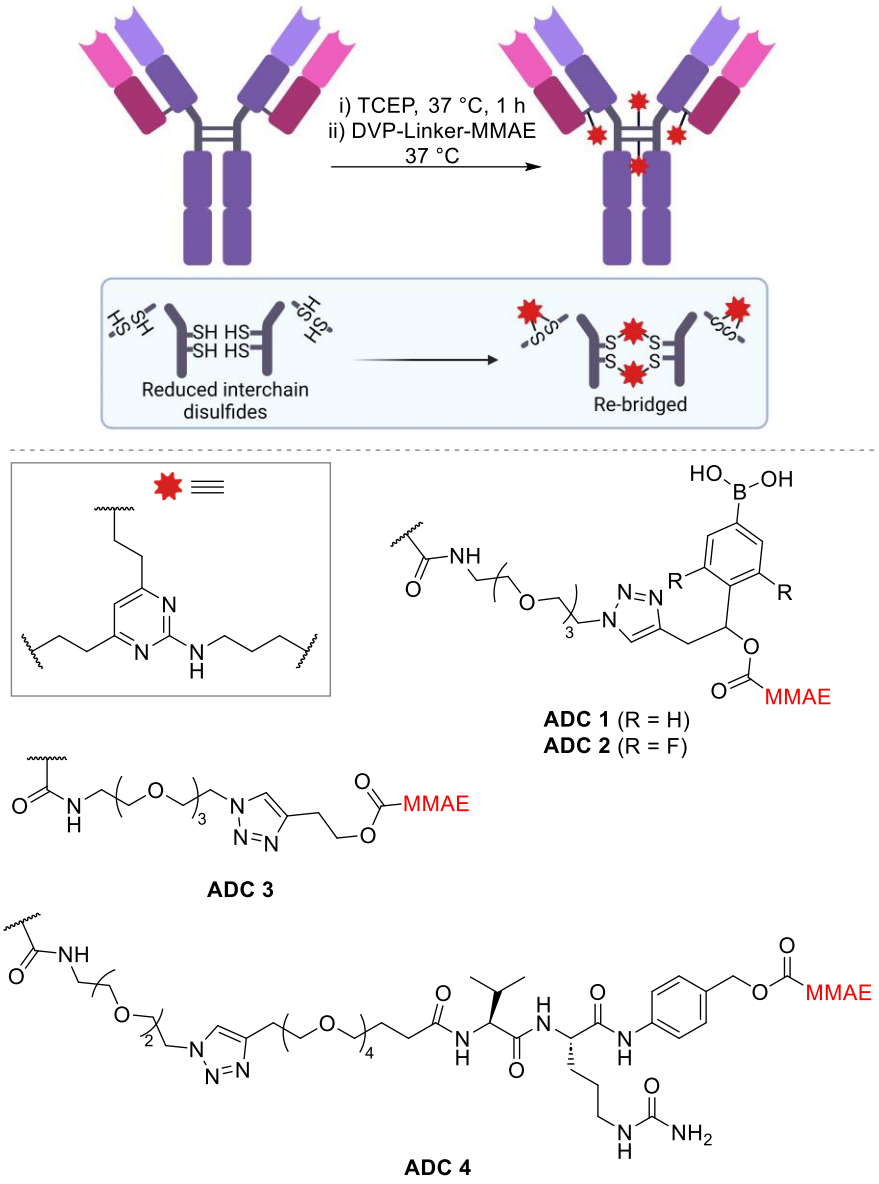

Figure 43: General schematic of the bioconjugation of trastuzumab to generate **ADCs 1-4**.

Bioconjugation yielded multiple species, as can be seen by SDS-page (Figure 44). When fully reduced, the IgG antibody can either be re-bridged by re-forming the covalent bond between two heavy chains, or it can undergo intra-chain re-bridging which forms a covalent bond within the same polypeptide chain, generating a "half-antibody" species. Despite no longer being covalently linked, the two heavy chains are held together by a number of non-covalent interactions, and thus the half-antibody is known to retain the antigen-binding and internalisation properties of the full antibody.[25,29,134] Hence, for this work, it was not considered problematic that bioconjugation yielded mainly the half-antibody. Pleasingly, reactions of all DVP-Linker-Payloads **20c**, **21c** and **24** yielded predominantly half-antibody **ADC 1**, **ADC 2** and **ADC 4**, with the arylboronate linkers giving similar distribution of product as the analogous Val-Cit linker.

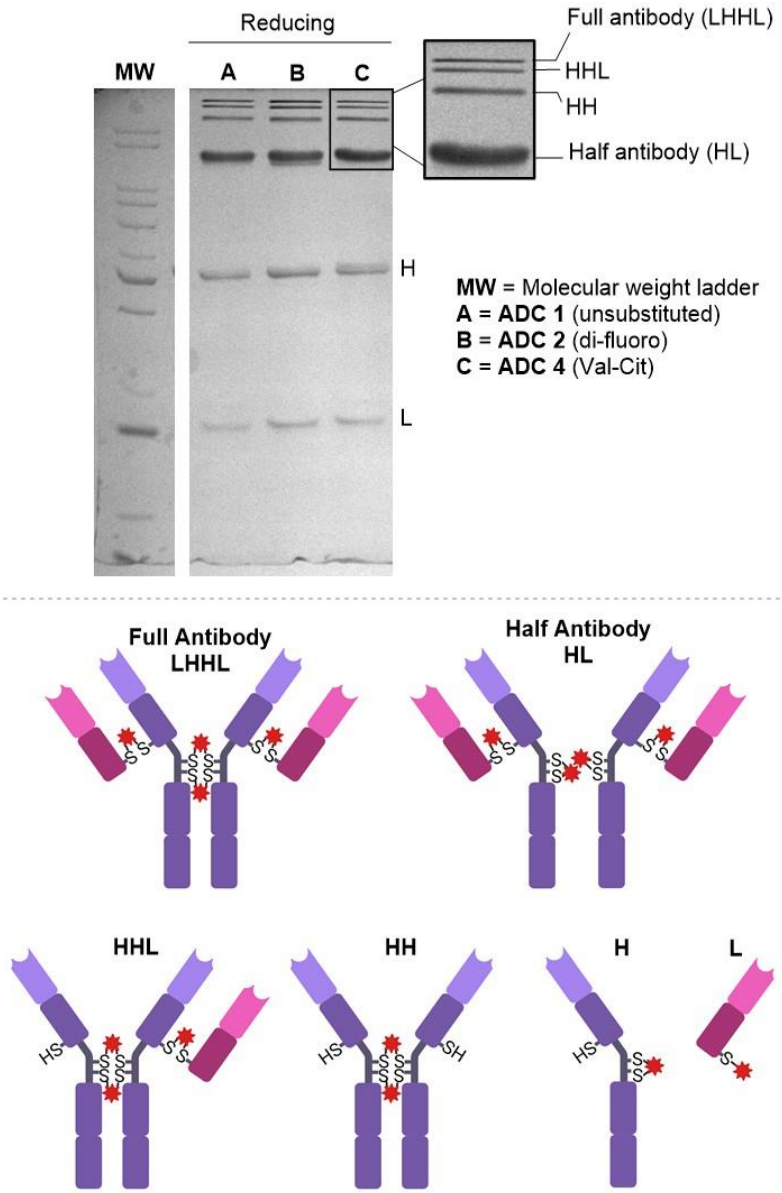

Figure 44: Initial bioconjugation conditions to afford **ADC 1** (lane A), **ADC 2** (lane B) and **ADC 4** (lane C). 12% acrylamide gel under reducing conditions with β-mercaptoethanol at 70 °C for 2 min prior to gel loading, stained with Coomassie blue. MW = molecular weight marker.

DARs were then analysed by Hydrophobic interaction chromatography (HIC). HIC separates ADC species based on their hydrophobicity, and since ADC species with increasing amounts of conjugated drug will be increasingly hydrophobic, the different ADC products can be separated according to the DAR. Average DAR is then calculated from equation (1), where DAR_x refers to the peak area corresponding to that DAR species. Pleasingly, HIC analysis revealed that all ADCs were generated with an average DAR close to 4 (Figure 45).

$$Average\ DAR = \frac{(DAR_1 + 2 \times DAR_2 + 3 \times DAR_3 + 4 \times DAR_4 + 5 \times DAR_5)}{(DAR_0 + DAR_1 + DAR_2 + DAR_3 + DAR_4 + DAR_5)} \quad (1)$$

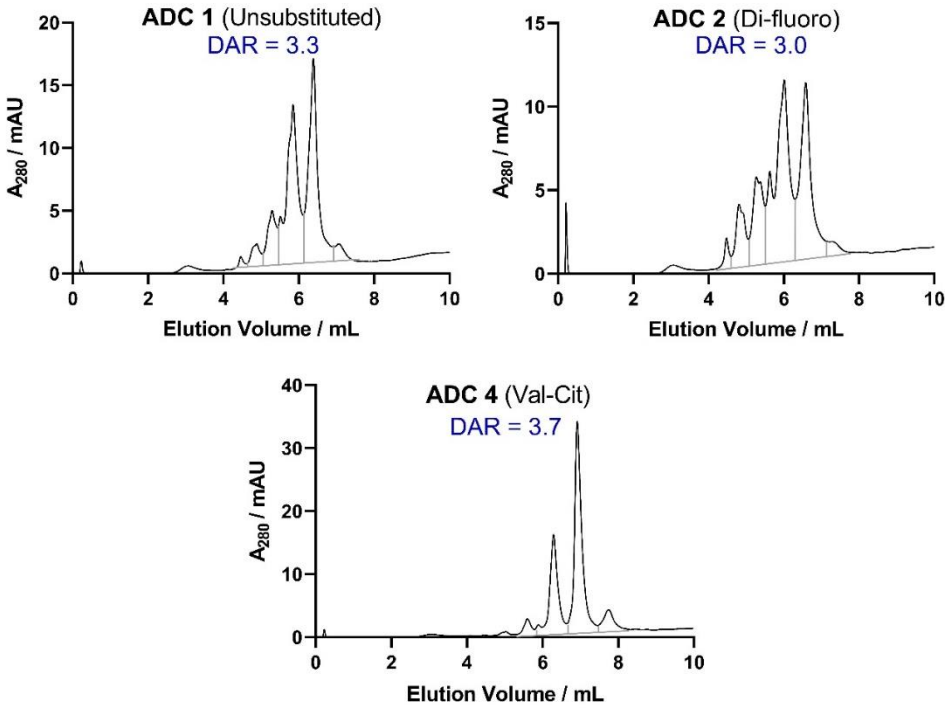

Figure 45: HIC traces for the initial bioconjugation to generate **ADC 1**, **ADC 2** and **ADC 4** including the calculated average DAR.

Having confirmed the successful bioconjugation by SDS-page gel and HIC, the conditions were optimised to try to improve conversion (Figure 46, Table 2). In most cases, increased linker equivalents and reaction times (80 equivalents, 4 h) resulted in greater conversion to high DAR species, giving improved average DAR. However, for unsubstituted **ADC 1**, the best DAR was achieved with lower equivalents (40 equivalents, 4 h).

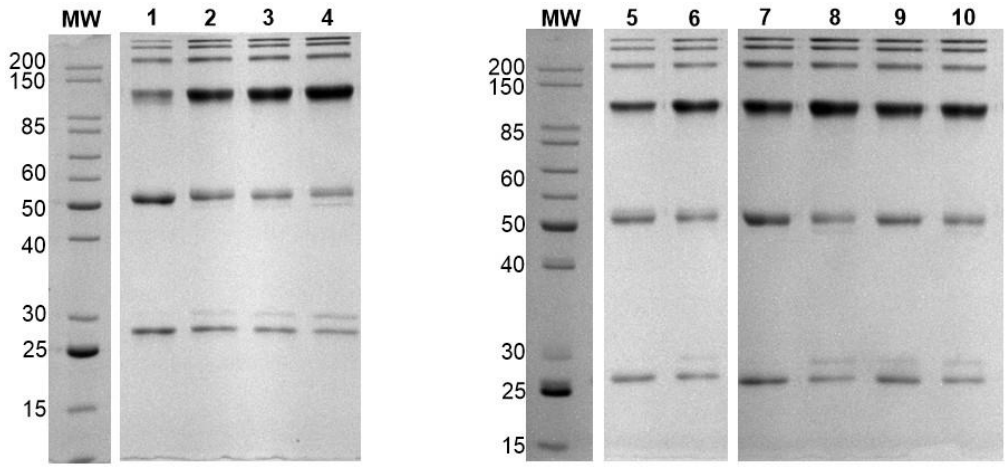

Figure 46: SDS-PAGE analysis of Table 2, 12% acrylamide gel under reducing conditions with β-mercaptoethanol at 70 °C for 2 min prior to gel loading, stained with Coomassie blue. MW = molecular weight marker. Lane numbering corresponds to entries in Table 2.

Table 2: Optimisation of the bioconjugation conditions to **ADC 1** (entries 7-10, linker **20c**), **ADC 2** (entries 1-4, linker **21c**), and **ADC 4** (entries 5-6, linker **24**). In each case the optimum condition is highlighted in bold.

Entry	ADC	DVP-Linker-MMAE	Linker equivalents	Time (h)	Average DAR
1	**ADC 2** (Di-fluoro)	Di-fluoro, **21c**	40	2	3.12
2		Di-fluoro, **21c**	40	4	3.41
3		Di-fluoro, **21c**	80	2	3.53
4		**Di-fluoro, 21c**	**80**	**4**	**3.74**
5	**ADC 4** (Val-Cit)	Val-Cit, **24**	40	2	3.50
6		**Val-Cit, 24**	**80**	**4**	**3.61**
7	**ADC 1** (Unsubstituted)	Unsubstituted, **20c**	40	2	2.86
8		**Unsubstituted, 20c**	**40**	**4**	**3.62**
9		Unsubstituted, **20c**	80	2	3.01
10		Unsubstituted, **20c**	80	4	3.08

With the optimised conditions in hand, the bioconjugations were scaled-up and the products fully characterised. Protein LCMS was initially performed at 150 cone voltage, whereby the mass of Val-Cit **ADC 4** was accurate within 2 Da and the non-cleavable **ADC 3** accurate within 1 Da of the expected half-antibody mass (Figure 47). However, larger mass inaccuracies were observed for the arylboronic acids **ADC 1** and **ADC 2**.

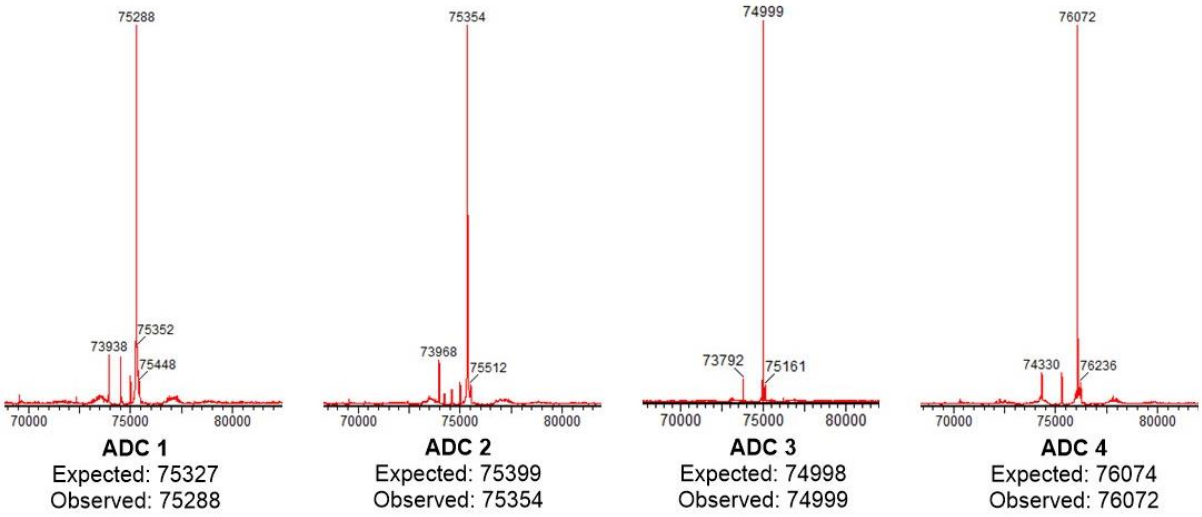

Figure 47: Deconvoluted protein mass spectra for **ADCs 1-4** at 150 cone voltage, including the expected mass (Da) vs. that observed. Mass spectra were reconstructed from the ion series using the MaxEnt 1 algorithm preinstalled on MassLynx 4.2 software according to the manufacturer's instructions. The raw ion series can be found in appendix 2.

The observed mass for unsubstituted **ADC 1** was 39 Da less than the expected value. Similarly, for the di-fluoro **ADC 2**, the observed mass was 46 Da less than the expected value. It was considered that this discrepancy might be a result of the high cone voltage used in the MS: perhaps some additional fragmentation related to the arylboronic acid linkers was occurring and resulting in the lower mass. Thus, **ADC 1** and **ADC 2** were re-evaluated at a lower cone voltage. In both cases (Table 3 and Table 4), decreasing the cone voltage from 150 to 40V increased the observed mass such that it was closer in accuracy to the expected mass. Changing from 40V to 20V had little impact on the observed mass. Since reducing the cone voltage resulted in an increase in the observed mass, it is reasonable to assume that the small discrepancy from the expected mass is a result of the accuracy of the analysis and is not reflective of incorrect characterisation of the ADC.

Table 3: Effect of changing cone voltage on the observed mass of **ADC 1** (unsubstituted) by protein LCMS.

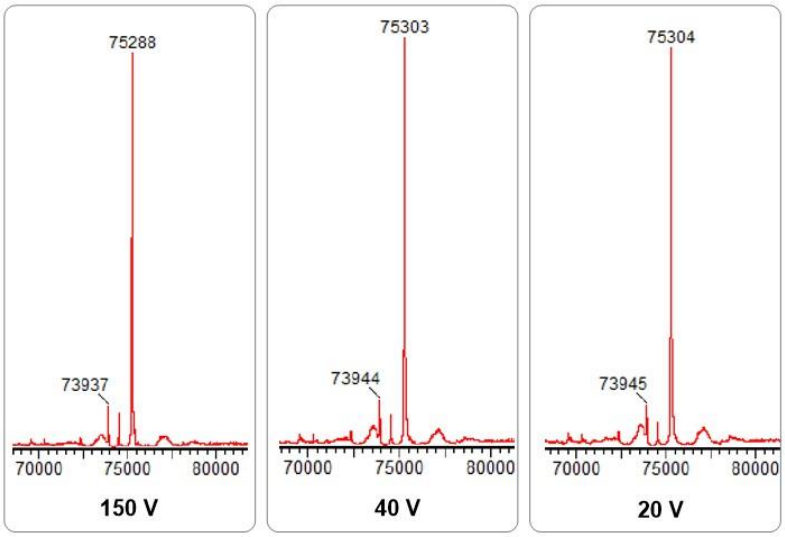

Entry	Cone Voltage	Expected Mass (Da)	Observed Mass (Da)	Difference in mass from expected (Da)
1	150	75,327	75,288	-39
2	40	75,327	75,303	-24
3	20	75,327	75,304	-23

Table 4: Effect of changing cone voltage on the observed mass of **ADC 2** (di-fluoro) by protein LCMS.

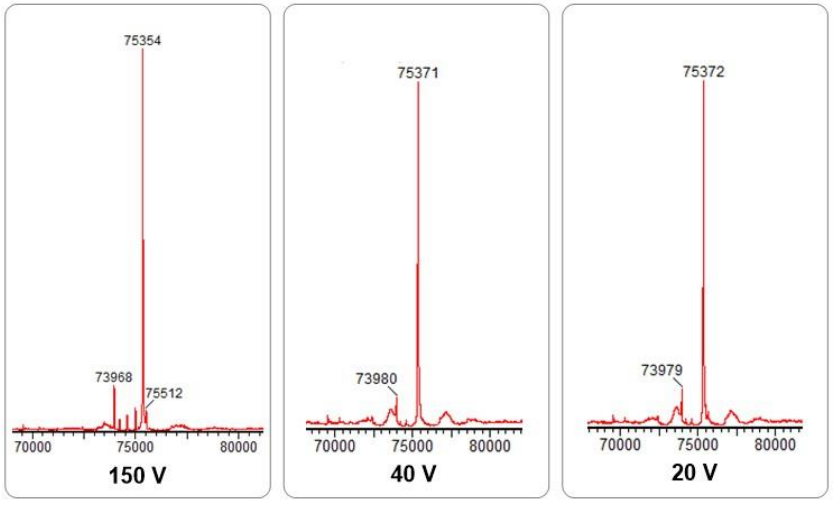

Entry	Cone Voltage	Expected Mass (Da)	Observed Mass (Da)	Difference in mass from expected (Da)
1	150	75,399	75,354	-45
2	40	75,399	75,371	-28
3	20	75,399	75,372	-27

For further assurance that the correct ADC had been synthesised, peroxide-cleavable **ADC 1** and **ADC 2** were incubated with H_2O_2 and the change in mass by protein MS monitored. Immolation of one drug followed by addition of water to the highly reactive quinone methide intermediate would result in an expected mass difference of -772 Da (Figure 48). Since the immolated species are identical, the expected mass change is the same for **ADC 1** and **ADC 2**.

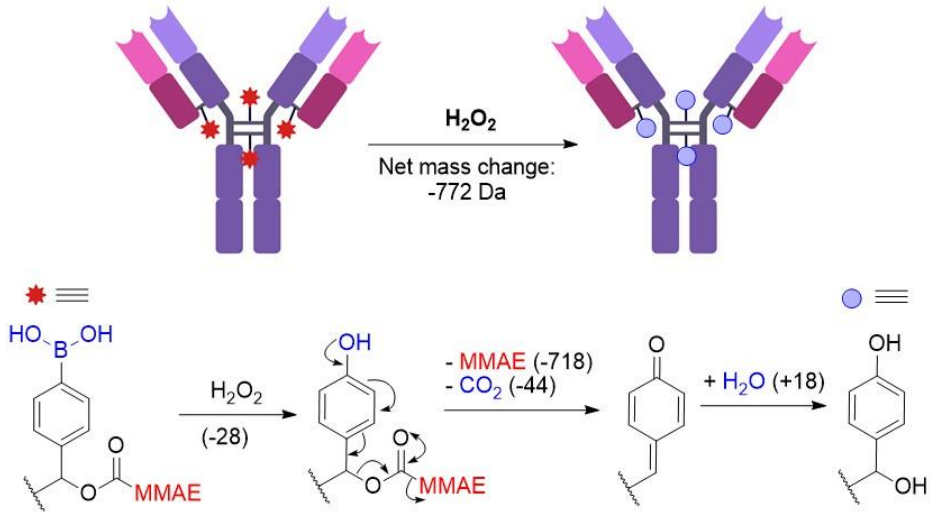

Figure 48: The expected mass loss from one drug immolation from a peroxide-cleavable ADC.

Hence, **ADC 1** and **ADC 2** were incubated with an excess of H_2O_2 and re-analysed by LCMS. Pleasingly, after 1 h incubation of **ADC 1** with H_2O_2, mass loss was observed from the half-antibody species corresponding to immolation of 2 drugs (Table 5). A minor peak in the MS corresponding to a singly re-bridged half-antibody species (possessing only one linker-drug), also showed the correct mass loss consistent with immolation of one drug (Table 5, Peaks 2 → 4).

Table 5: Protein LCMS changes upon addition of H_2O_2 to **ADC 1**.

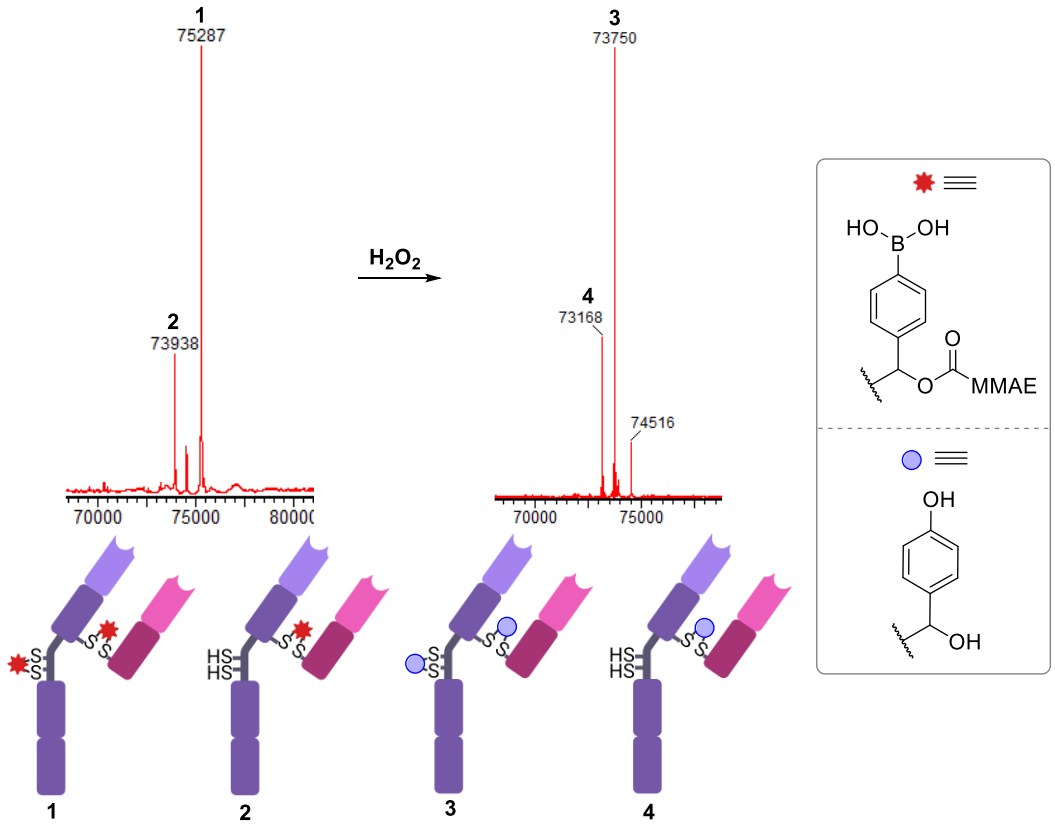

Peak Change	Start mass – H_2O_2 (Da)	End mass + H_2O_2 (Da)	Mass difference (Da)	Explanation
1 → 3	75287	73750	-1537	Immolation of 2 drugs
2 → 4	73938	73168	-770	Immolation of 1 drug

The di-fluoro **ADC 2** was incubated for 24 h, and similar mass losses were observed (Table 6).

Given that the ADCs undergo drug elimination in the presence of H_2O_2, and the protein mass spectrum accuracy could be improved at lower cone voltages, there can be a high confidence in the identity of the ADCs.

Table 6: Protein LCMS changes upon addition of H_2O_2 to **ADC 2**.

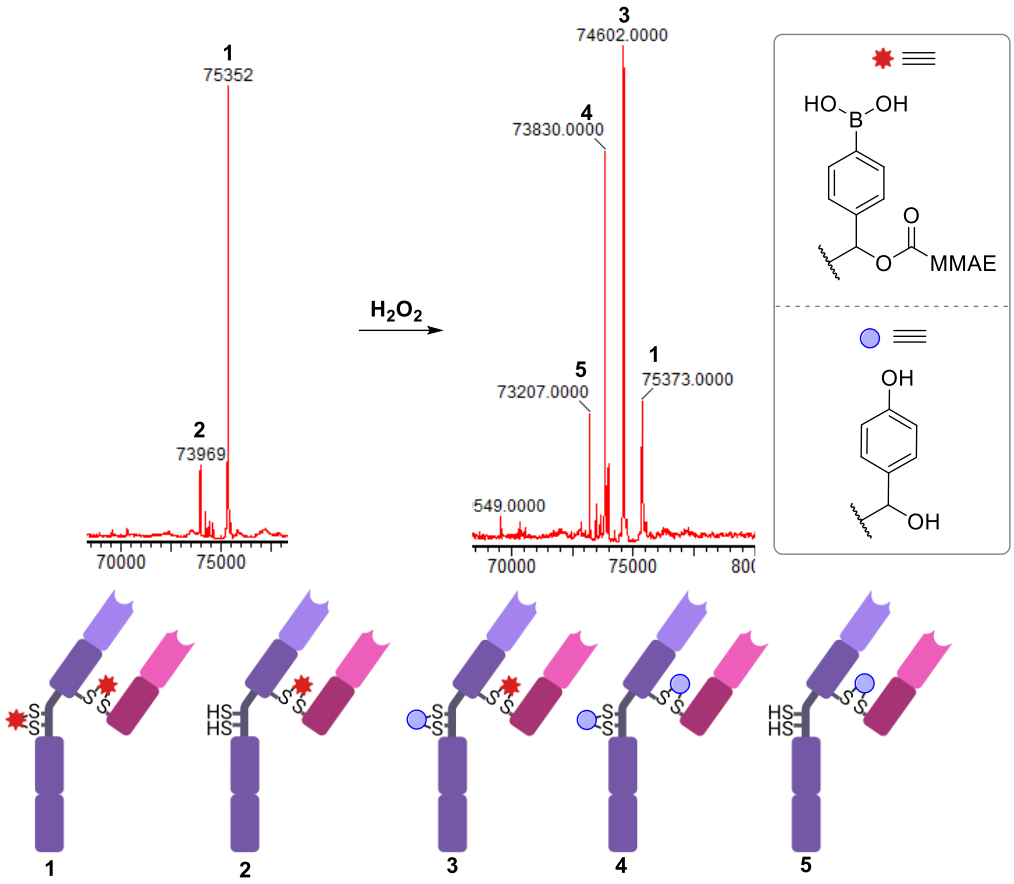

Peak Change	Start mass – H_2O_2 (Da)	End mass + H_2O_2 (Da)	Mass difference (Da)	Explanation
1 → 3	75352	74602	-750	Immolation of 1 drug
1 → 4	75352	73830	-1522	Immolation of 2 drugs
3 → 4	74602	73830	-772	Immolation of 1 drug
2 → 5	73969	73207	-762	Immolation of 1 drug

HIC chromatography then revealed in each case that the DAR 4 species was the major product, resulting in average DARs close to 4, comparable to the Val-Cit **ADC 4** (Figure 49).

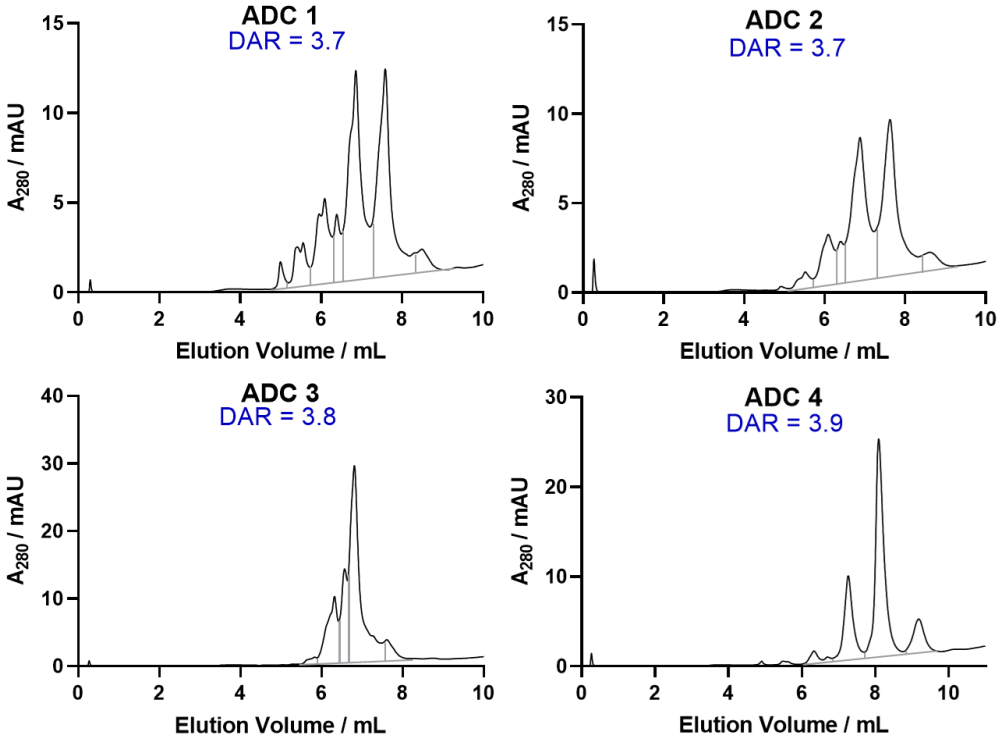

Figure 49: HIC traces of the optimised bioconjugations to generate **ADCs 1-4**. In each case DAR 4 is the major species, and the average DAR is close to 4.

Finally, the ADCs were analysed by size-exclusion chromatography (SEC). SEC separates species of different size as they pass through a resin-packed column, and thus enables the distinction of high molecular weight antibody aggregates from monomeric antibody species. For unsubstituted **ADC 1**, non-cleavable **ADC 3** and Val-Cit **ADC 4**, SEC analysis was facile, showing minimal aggregation <1% in all cases (Figure 50). However, for the di-fluoro **ADC 2**, no SEC analysis could be performed: upon injection, the resulting trace lacked any signal despite using similar concentrations to other ADCs, and the same analytical sample giving suitable HIC and MS spectra. It is proposed that for an unknown reason, **ADC 2** has higher affinity for the SEC column than other ADCs, and so is retained on the column. With other characterisation of **ADC 2** in hand (SDS-page gel, MS and HIC), the inability to acquire SEC data is considered acceptable, and does not reduce confidence in the identity of **ADC 2**. Additionally, the aggregation profile is predicted to be similar to the unsubstituted ADC since its only structural differences are substitution of the arylboronic acid ring and no protein precipitation was observed. If **ADC 2** does possess significant aggregation, then this should be reflected in the potency (or lack thereof) of the ADC during *in vitro* testing.

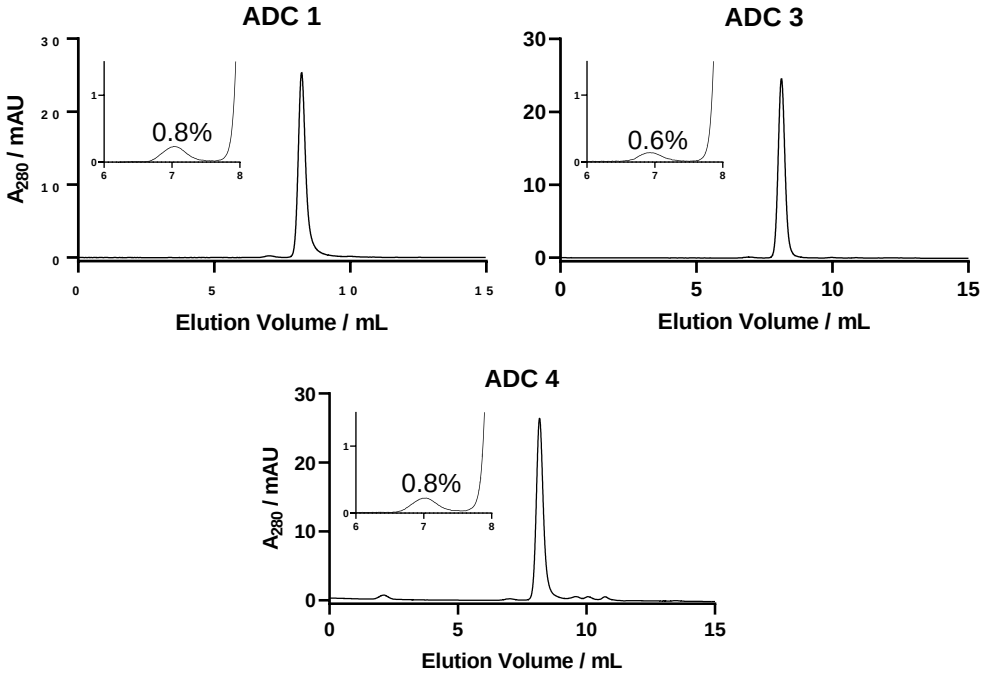

Figure 50: SEC traces for **ADC 1**, **ADC 3**, and **ADC 4**, indicating minimal (<1%) protein aggregation.

1.3.5 *In Vitro* Evaluation

With **ADCs 1-4** in hand, they were evaluated *in vitro*. A panel of four breast cancer cell lines were chosen, two of which overexpress the target receptor HER2 (SKBR3 and BT474 are HER2-positive, "HER2+") and two which do not overexpress HER2 (MCF7 and MDA-MB-468 are HER2-negative, "HER2-"). For a typical internalising ADC, it is expected that in HER2+ cell lines, the ADC should be able to bind HER2, internalise, then subsequently be degraded in lysosomes. The linker-payload metabolite is then expected to release the payload by H_2O_2-mediated linker cleavage (Figure 51A), most likely in the cytosol or extracellular space. The released payload can then exert its cytotoxic activity in the cell and cause cell death. In non-target HER2- cells, there should be little/no antibody-antigen binding, so there should be no intracellular breakdown of the ADC to release free drug and cause cell death (Figure 51B). Without internalisation, the ADC will remain in the extracellular medium for the duration of the *in vitro* assay.

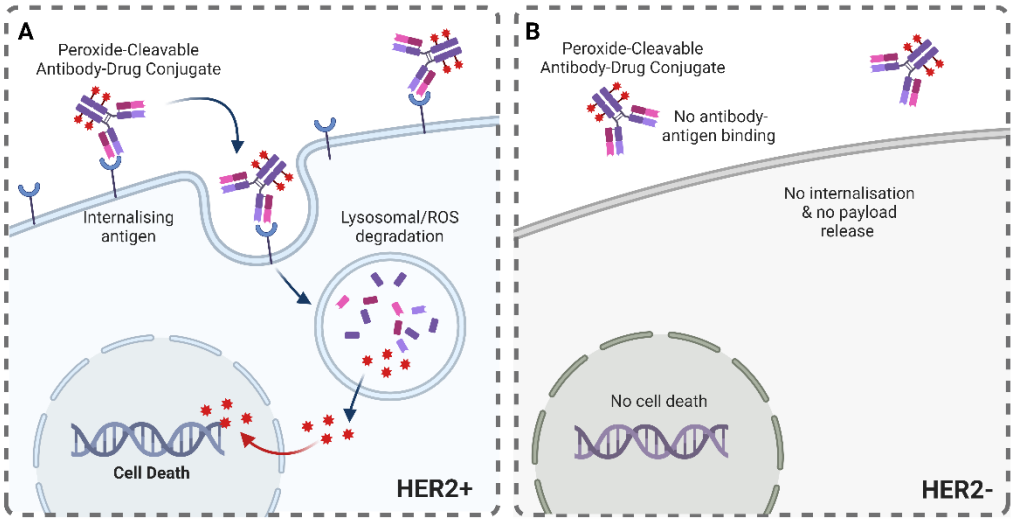

Figure 51: Expected mechanism of internalising peroxide-cleavable ADCs in A) target HER2+ cell lines, and B) non-target HER2- cells.

However, when incubated with HER2+ and HER2- cell lines, arylboronic acid **ADC 1** and **ADC 2** displayed potent dose-dependent cytotoxicity regardless of antigen expression (Figure 52, Table 7). In contrast, non-cleavable **ADC 3** and Val-Cit **ADC 4** were non-toxic in the HER2- cell lines. This suggests that the HER2- cell lines do not possess enough cell-surface HER2 for ADC internalisation (as expected), since these ADCs require internalisation for payload release. Therefore, the potency of **ADC 1** and **ADC 2** in HER2- cell lines is not presumed to result from receptor-mediated internalisation.

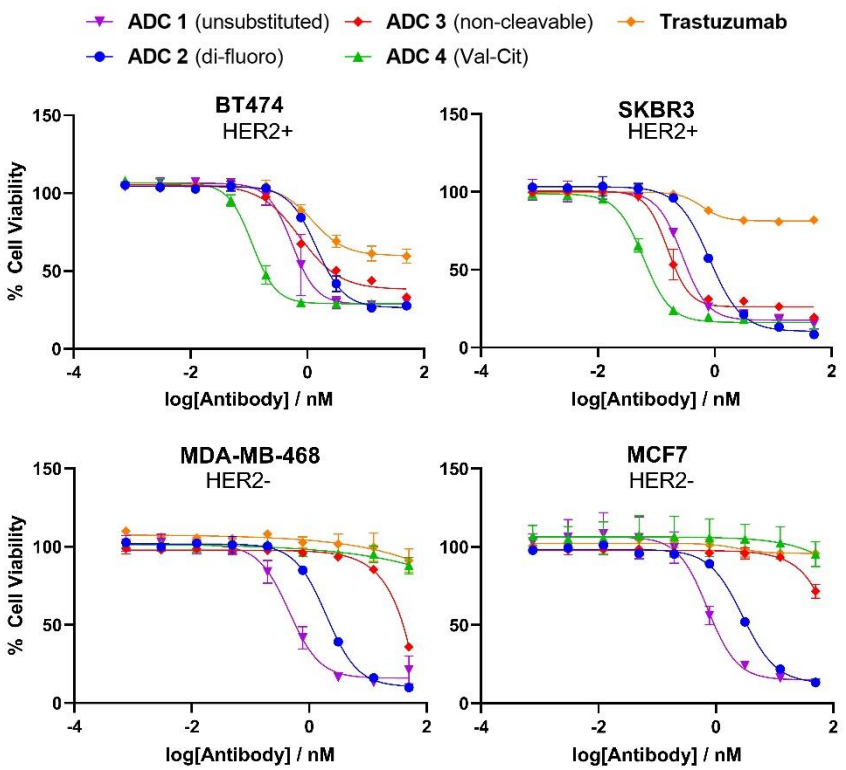

Figure 52: The *in vitro* cytotoxicity of **ADCs 1-4** and unconjugated trastuzumab in HER2-positive BT474 and SKBR3 cell lines and HER2-negative MDA-MB-468 and MCF7 cell lines. Viability data shown is the mean of three independent replicates and error bars represent standard error of the mean.

Table 7: Potency of **ADCs 1-4** against breast cancer cell lines. IC_{50} values (nM) were calculated using the log(inhibitor) vs. response curve fit with variable slope (four parameters) in GraphPad Prism.

	IC_{50} (nM)			
	BT474 (HER2+)	**SKBR3** (HER2+)	**MCF7** (HER2-)	**MDA-MB-468** (HER2-)
ADC 1	0.55	0.28	0.72	0.46
ADC 2	1.42	0.81	2.87	1.96
ADC 3	0.75	0.16	>50	>50
ADC 4	0.11	0.06	>50	>50

It is known that H_2O_2 is highly diffusible and membrane permeable, so is likely not restricted to the inside of cells.[106,107] Moreover, it has been reported that boron-containing prodrugs can be activated either intracellularly or extracellularly.[135] Therefore, the observed cytotoxicity of the peroxide-cleavable ADCs in non-target HER2- cell lines might result from extracellular linker cleavage. Despite not internalising, the ADCs remain in the presumably high ROS extracellular medium for the duration of the *in vitro* assay, during which the arylboronic acid linker could be cleaved to release MMAE. Since MMAE is membrane permeable, it can be envisioned that any extracellularly released payload could simply diffuse into the cell to cause cell death (Figure 53).

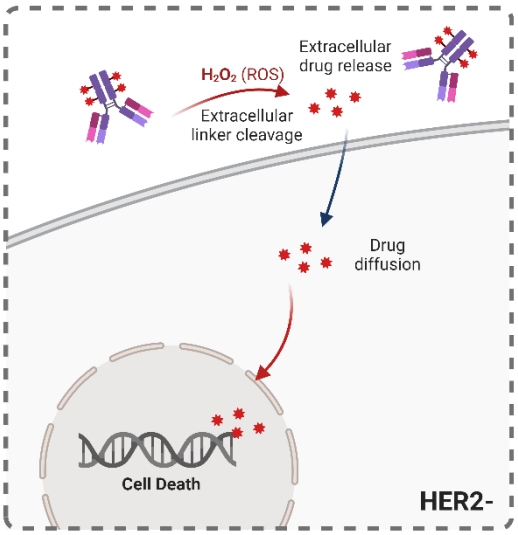

Figure 53: Hypothesis for the activity of peroxide-cleavable **ADC 1** and **ADC 2** in non-target HER2- cell lines.

To probe this hypothesis, a washout study was designed. It was envisioned that the ADCs could be incubated with the cancer cells for a sufficient time to allow antibody-antigen binding, then, media containing any unbound ADC could be removed and successively washed with fresh media. The cytotoxicity observed would therefore only result from ADC that was able to bind and internalise (Figure 54). In the case of HER2- cells, since very little binding is expected the ADCs should be non-toxic.

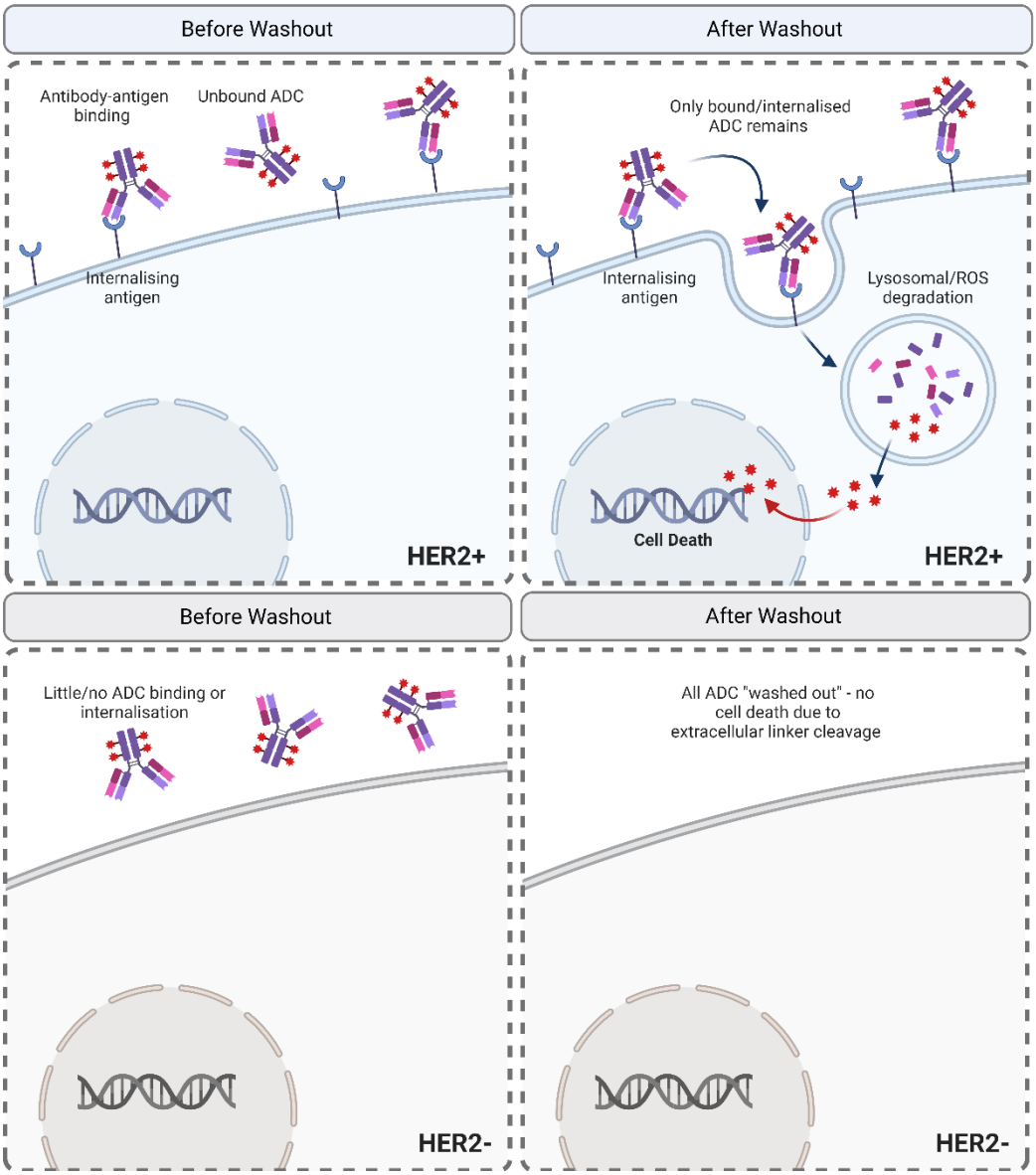

Figure 54: Diagram illustrating the principles of the washout study.

First, a 1 h washout was trialled: the peroxide-cleavable **ADC 1** and **ADC 2** were incubated with the cancer cells for 1 h before the media containing any unbound ADC was removed, and the cells washed with fresh media. Unfortunately, 1 h was not sufficient to allow binding and internalisation of the ADCs, as is demonstrated by the complete loss of activity in both HER2- and HER2+ cell lines (Figure 55).

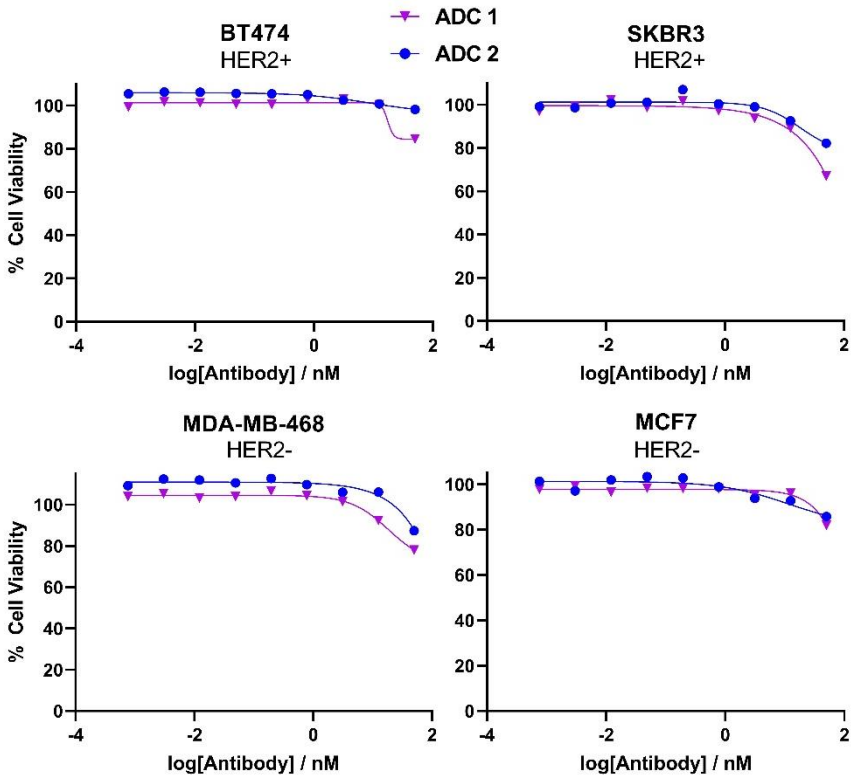

Figure 55: 1 h washout study of **ADC 1** and **ADC 2** in HER2+ and HER2- cell lines. Viability data shown is the mean of three technical replicates.

For the next attempt, ADCs were incubated for 24 h before the media was removed and replaced. Additionally, a reportedly non-toxic concentration of H_2O_2 (0.1 mM)[123,136,137] was added at the time of washout due to concerns that removing the cell media would also remove significant amounts of H_2O_2 which might impede the cleavage of the ADCs. With a 24 h washout, potent cytotoxicity was once again observed in each cell line regardless of HER2 expression (Figure 56). Hence, it was hypothesised that extracellular linker cleavage of the ADCs occurred within the longer 24 h incubation time.

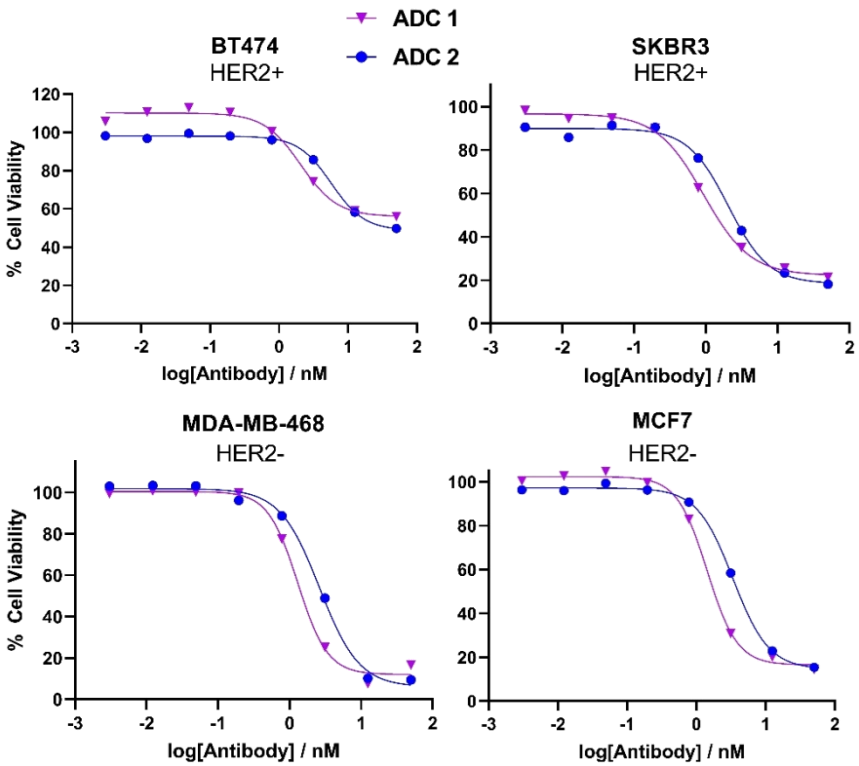

Figure 56: 24 h washout study of **ADC 1** and **ADC 2** in HER2+ and HER2- cell lines. Viability data shown is the mean of three technical replicates.

Repeating this experiment with incubations of **ADC 1** for 4 and 8 h before washout allowed some differentiation in cytotoxicity between HER2+ and HER2- cell lines (Figure 57). However, the impact of the addition of exogenous H_2O_2 was also more closely examined: MCF7 cells remained 99% viable with the addition 0.1 mM exogenous H_2O_2 (and no ADC). However, with the same concentration of H_2O_2, SKBR3 cells were reduced to 4.5% viability compared to completely untreated cells. Therefore, for the SKBR3 cell line, the number of viable cells had been significantly reduced irrespective of ADC treatment. Therefore, calculations of ADC potency in the SKBR3 cell line may not accurately reflect the cytotoxicity of ADC, since minor changes in cell numbers could account for large percent differences since the cell population was already greatly reduced by H_2O_2 treatment. Therefore, no conclusions could be drawn from this washout study.

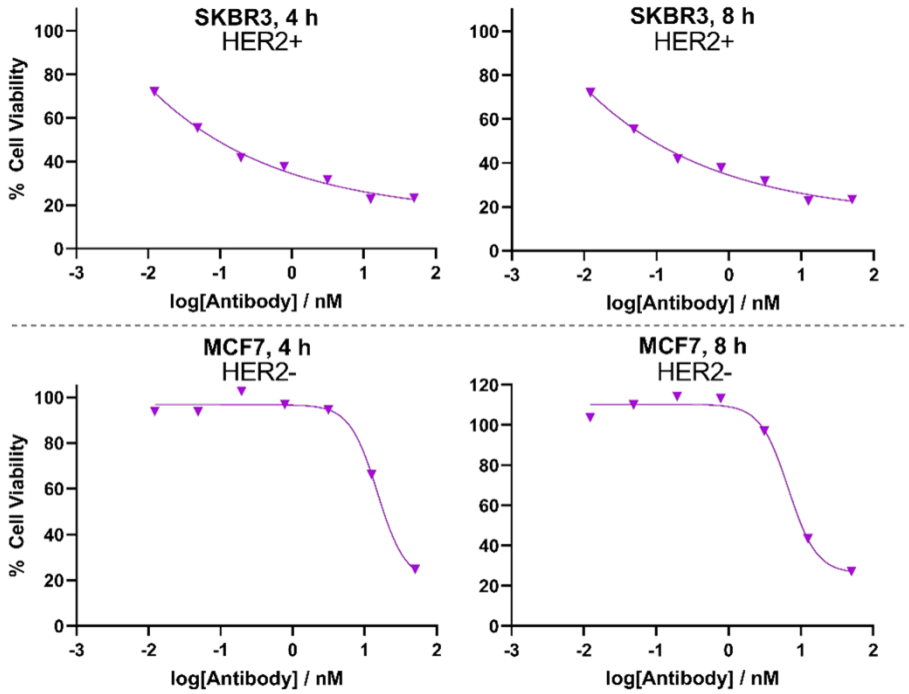

Washout Time	Cell Line	Average Luminescence		% Cell viability compared to untreated
		Untreated	+ 0.1 mM H_2O_2	
4h	SKBR3	1445000	64953	4.5%
	MCF7	1473000	1452667	99%
8h	SKBR3	1413667	226077	16%
	MCF7	1347333	1259333	93%

Figure 57: 4 and 8 h washout of **ADC 1** in HER2+ SKBR3 cells and HER2- MCF7 cells with addition of exogenous H_2O_2 (0.1 mM), and the impact of exogenous H_2O_2 on the cell viability. Viability data shown is the mean of three technical replicates.

To preclude complications with combined effects of H_2O_2 treatment and ADC treatment, the 4 h washout was repeated without the addition of exogenous H_2O_2 (Figure 58). Val-Cit **ADC 4** was potent against HER2+ SKBR3 cells, indicating that binding and internalisation of this ADC is sufficient in the 4 h incubation period prior to washout. In contrast, non-cleavable **ADC 3** displayed significantly lower potency against SKBR3 cells when compared to the previous experiment lacking the washout step (Figure 52). Potentially for **ADC 3**, an incubation time of 4 h before washout was insufficient to allow significant antigen binding and internalisation. Likewise, the ROS-cleavable **ADC 1** and **ADC 2** did not display high potency in either cell line, which may similarly suggest lack of significant internalisation in the 4 h incubation time before washout. Although the washout time could be increased, some cytotoxicity of **ADC 1** and **ADC 2** was already observed for both cell lines at the highest concentrations. Therefore, it is predicted that there is no suitable time whereby the ADC has sufficient time to bind/internalise, but the linker remains intact in the extracellular media. If ADC binding/internalisation

and extracellular linker cleavage occur on similar time-scales, it would be impossible to capture the effects of one without the other. Considering this, further attempts at designing a washout study to demonstrate the selectivity of **ADC 1** and **ADC 2** for antigen-positive cells were halted.

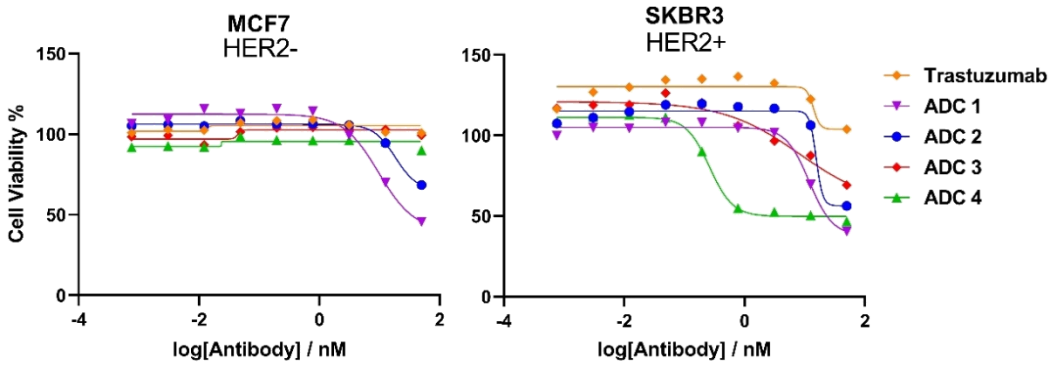

Figure 58: Potency of trastuzumab and **ADCs 1-4** against MCF7 and SKBR3 cell lines with a 4 h washout, without the addition of exogenous H_2O_2. Viability data shown is the mean of three technical replicates and error bars represent standard error of the mean.

A number of cell lines have been reported as "low ROS" in the literature, including the non-cancerous MCF10A cell line, which consists of non-cancerous mammalian breast tissue cells, and non-cancerous HEK-293T cells, which comprises human embryonic kidney cells. For example, a ROS-responsive small molecule prodrug of belinostat was potent against MCF7 breast cancer cells, but had low toxicity against MCF10A cells up to 10 µM, suggestive of insufficient activation to the active drug by H_2O_2.[138] Similarly, a ROS-activatable prodrug of vorinostat was inactive against HEK-293T with concentrations of 1000 nM, but displayed potent activity against breast cancer cell lines including MCF7 cells.[139] Hence, HEK-293T and MCF10A cells were next investigated as negative "low ROS" control cell lines to demonstrate the selectivity of the peroxide-cleavable ADCs.

Against HEK-293T cells, unsubstituted **ADC 1** achieved similar potency as treatment with MMAE, whereas the non-cleavable **ADC 3** was inactive, suggesting potency resulted from the cleavable linker rather than unspecific ADC internalisation (Figure 59). Hence, HEK-293T cells were discarded as a useful negative control. Similarly, against MCF10A cells, **ADC 1** and **ADC 2** displayed potent dose-dependent cytotoxicity, whereas Val-Cit **ADC 4** was inactive (Figure 59).

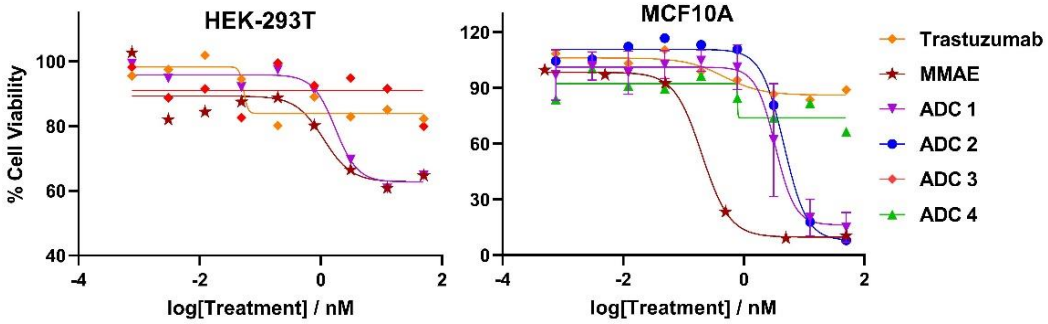

Figure 59: Potency of **ADCs 1-4** in non-cancerous HEK-293T and MCF10A cell lines. Viability data for HEK-293T cells were obtained after a 24 h treatment and are an average of three technical replicates. Viability data for the MCF10A cell line were obtained after a 4-day treatment with three technical replicates, and three independent replicates for **ADC 1**.

Whilst HEK-293T and MCF10A cell lines were reported as "low ROS" compared to breast cancer MCF7 cells (and thus did not result in the activation of belinostat and vorinostat prodrugs),[138,139] conflicting literature demonstrates that MCF10A and HEK-293T cells have similar H_2O_2 concentrations to breast cancer MCF7 cells. For example, Sarmiento-Salinas *et al.* demonstrated that MCF10A cells exhibited similar ROS levels to breast cancer MCF7 cells when stained with dihydroethidium and evaluated by fluorescence microscopy and flow cytometry.[140] This was supported by Hecht *et al.*, who demonstrated that MCF10A cells have similar intracellular ROS levels to breast cancer MCF7 cells.[141] Moreover, the extracellular concentrations of H_2O_2 were quantified, revealing that media from MCF10A cells had a greater extracellular concentration of H_2O_2 than breast cancer MCF7 and MDA-MB-231 cells.[141] Hence, the levels of extracellular H_2O_2 from MCF10A and HEK-293T cells may indeed be sufficient for extracellular linker cleavage from the peroxide-cleavable ADCs in the *in vitro* assay and thus are unsuitable negative controls.

To confirm the presence of extracellular H_2O_2 in the HER2- HEK-293T, MCF7, MDA-MB-468 and MDA-MB-231 cell lines, an Amplex™ Red detection assay was performed. The Amplex™ Red reagent is non-membrane permeable, and in the presence of horseradish peroxidase, is capable of oxidising by action of H_2O_2 to a highly fluorescent resorufin, thus allowing facile detection of extracellular H_2O_2 (Figure 60).[142,143]

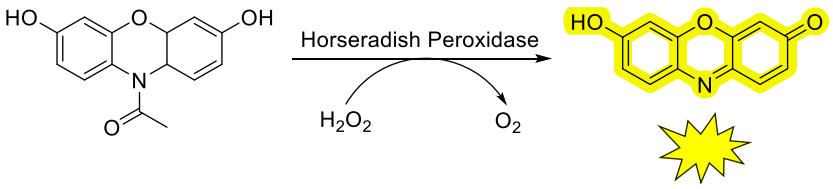

Figure 60: H_2O_2-mediated oxidation of Amplex™ Red to highly fluorescent resorufin in the presence of horseradish peroxidase.

All antigen negative cell lines displayed significantly enhanced fluorescence compared to a no cell negative control, with HEK-293T displaying the highest levels of fluorescence (Figure 61). Since each HER2- cell line possesses significant levels of extracellular ROS, it seems to support the hypothesis that the potency of **ADC 1** and **ADC 2** in these cell lines is a result of linker cleavage within the duration of the *in vitro* assays due to H_2O_2 in the extracellular media.

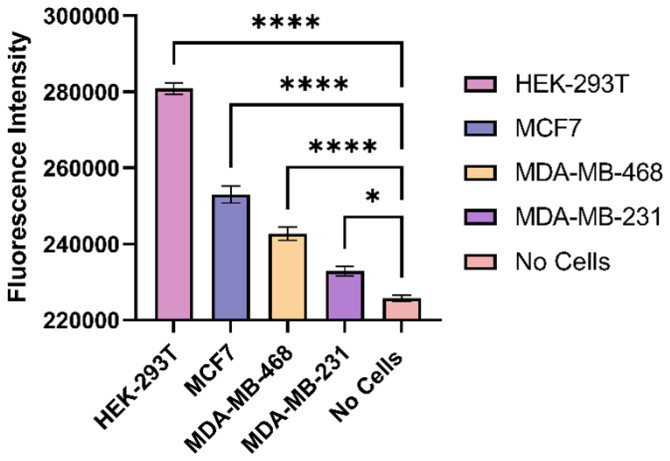

Figure 61: The fluorescence intensity from Amplex™ red reagent due to reaction with the extracellular hydrogen peroxide of different cell lines. The fluorescence of Amplex red™ was compared to the fluorescence in the absence of cancer cells. Data was analysed by an ordinary one-way ANOVA whereby * = $p < 0.05$, ** = $p < 0.01$, *** = $p < 0.001$, **** = $p < 0.001$. ns = non-significant, $p > 0.05$. Fluorescence data shown is the mean of 4-6 independent replicates and error bars represent standard error of the mean.

Given that a representative "low H_2O_2" cell line could not be found, a different approach was considered. Several species have been reported to "scavenge" H_2O_2 *in vitro*, such as catalase (CAT), which decomposes H_2O_2 to water and oxygen. It was hypothesised that removal of extracellular ROS with a suitable scavenger would preclude the extracellular linker cleavage of any non-internalised ADC, rendering the ADCs inactive against antigen-negative cell lines (Figure 62).

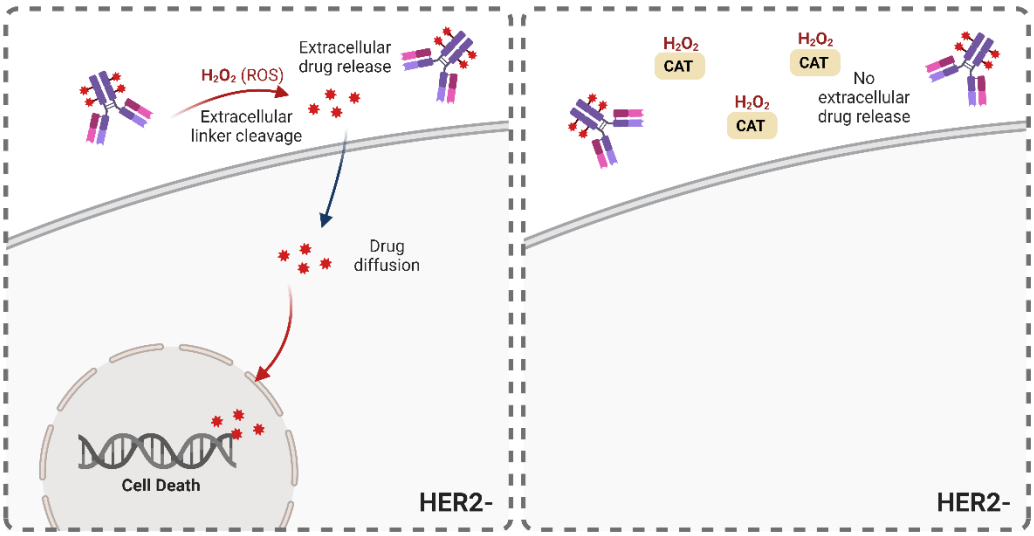

Figure 62: Illustration of the hypothesised activity of peroxide-cleavable ADCs in non-target cell lines, by extracellular linker cleavage (left) and the hypothesis that catalase (CAT) treatment of cells could remove extracellular H_2O_2, rendering peroxide-cleavable ADCs non-toxic towards HER2- cells (right).

For confirmation that CAT is indeed able to scavenge H_2O_2, model AMC linkers **1b** and **2b** were first incubated at 37 °C with H_2O_2 and catalase (CAT) and examined by fluorimetry (Figure 63). When co-incubated with H_2O_2 and CAT, no increase in fluorescence intensity was observed. Moreover, no fluorescence increase was observed with longer incubation times of 7-10 days, suggesting that CAT would be suitable for the long-term scavenging of H_2O_2 from cells during the course of an *in vitro* study.

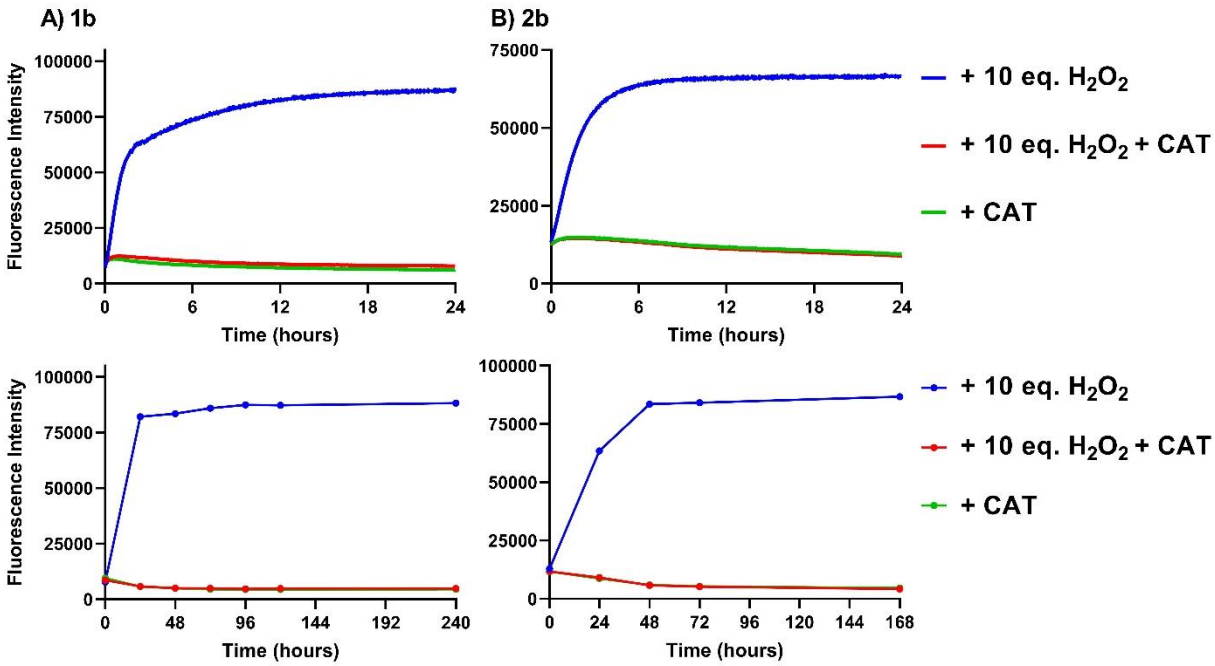

Figure 63: Fluorimetry of model linkers A) **1b** and B) **2b** in the presence of CAT: no fluorescence increase is observed when H_2O_2 is scavenged by CAT over 24 h (top), even with prolonged incubation times of 7-10 days (bottom). CAT = catalase.

For preliminary investigation *in vitro*, 80-200 units (U) CAT/well were incubated with HER2- MCF7 cells for 2 h, followed by addition of peroxide-cleavable **ADC 1**. However, no difference was observed in the cytotoxicity of **ADC 1** with or without the addition of CAT (Figure 64).

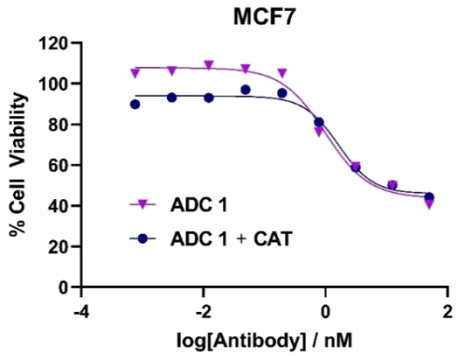

Figure 64: The cytotoxicity of **ADC 1** against MCF7 cells with or without CAT (80-200 U/well). Results shown are of three technical replicates.

To confirm the ability of CAT to scavenge H_2O_2 from cells *in vitro*, the Amplex™ Red detection assay was replicated with incubation of 400-1000 U CAT/well prior to measurement (5-fold higher concentrations of CAT compared to that used in Figure 64). In each cell line, the fluorescence produced by the Amplex™ red reagent was non-significant when compared to the fluorescence produced in the absence of cancer cells (Figure 65). Hence, it seemed that this concentration of CAT per well was sufficient at scavenging extracellular H_2O_2.

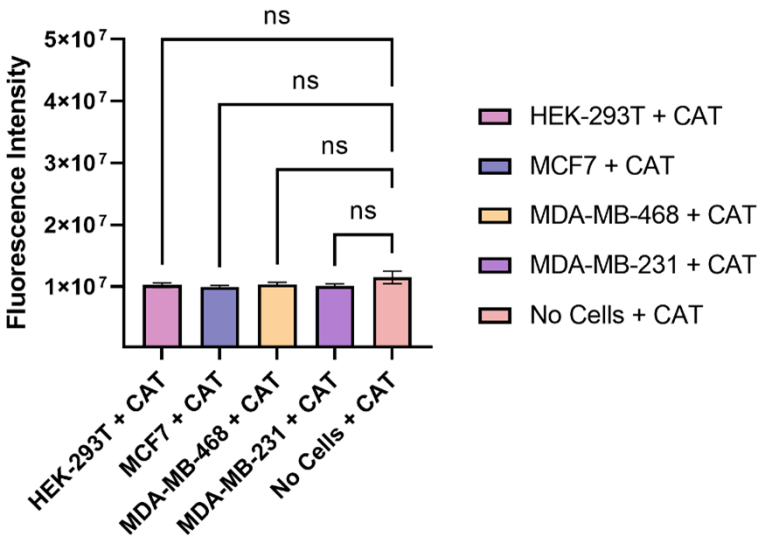

Figure 65: The fluorescence intensity from Amplex™ red reagent when cell lines were pre-treated with 400-1000 U/well CAT. Data was analysed by an ordinary one-way ANOVA whereby ns = non-significant, $p > 0.05$. Fluorescence data shown is the mean of two independent replicates and error bars represent standard error of the mean.

Hence, the cytotoxicity assay was repeated with this 5-fold higher concentration of CAT (400-1000 U/well). Pleasingly, CAT scavenging greatly reduced the potency of **ADC 1** compared to the potency without CAT (Figure 66A). Cell growth was also monitored continuously throughout the assay by live-cell imaging with an Incucyte® (Figure 66B). With CAT scavenging, the concentration of ADC treatment had non-significant effects on cell growth, in contrast to cell growth without CAT scavenging, where ADC treatment had significant dose-dependent effects (Figure 66B).

Since the presence of extracellular H_2O_2 is essential for the activity of **ADC 1** against antigen-negative MCF7 cells, support is provided for the proposed mechanism of action whereby potency of the peroxide-cleavable ADCs arises from extracellular H_2O_2-mediated linker cleavage and payload release.

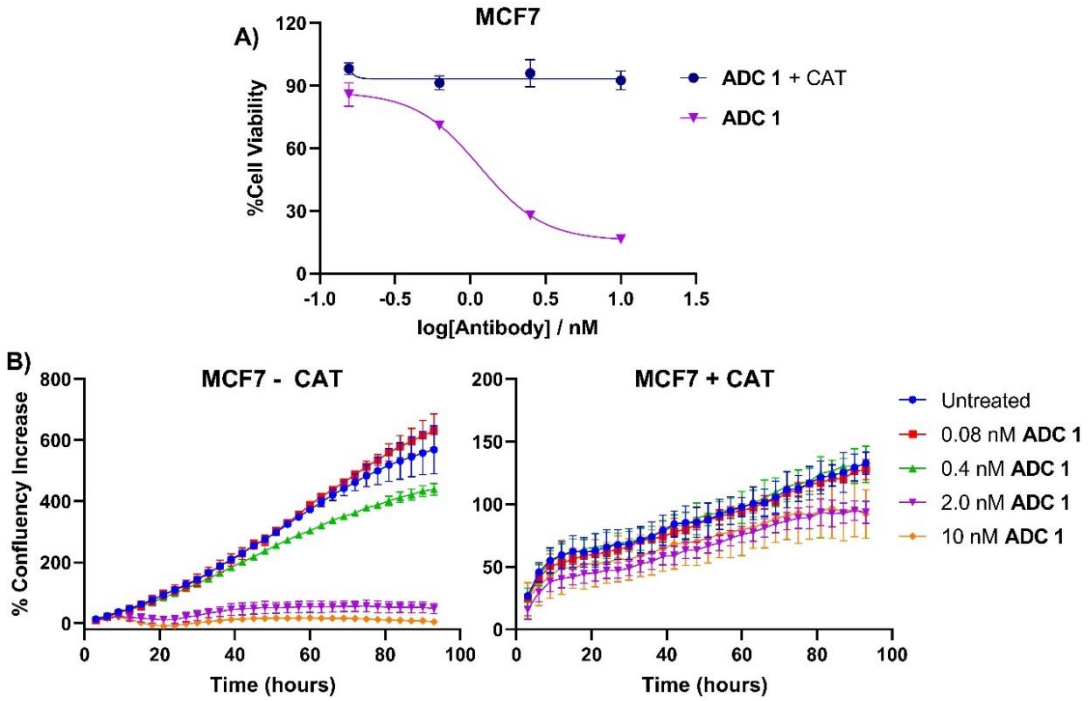

Figure 66: A) Cell viability endpoint reading for **ADC 1** against HER2- MCF7 cells with or without CAT treatment. Without CAT, **ADC 1** displays potent dose-dependent cell killing, but when the hydrogen peroxide is scavenged by CAT, no cell killing is observed. Viability data shown is the mean of two independent replicates and error bars represent standard error of the mean. B) Percent cell confluency increase of MCF7 cells when treated with varying concentrations of **ADC 1** in the absence and presence of CAT. Confluency data shown is one of two independent replicates and error bars represent standard error of the mean of the three technical replicates of one experiment.

1.3.6 Application Towards a Non-internalising ADC

1.3.6.1 Introduction

Although it was previously thought that internalisation of an ADC was essential for therapeutic activity, it is increasingly recognised that non-internalising ADCs may also be effective.[5] Indeed, non-internalising ADCs may offer several benefits over traditional internalising ADCs such as lower reliance on high expression of internalising antigens; ability to circumvent cancer resistance that results from disruptions to the internalisation process;[100,101] ability to treat a wider range of cancer targets and; potentially achieve improved tumour penetration and bystander effect.[102]

Efficacious non-internalising ADCs require linkers that can be cleaved extracellularly to release the payload. Given that peroxide-cleavable **ADC 1** and **ADC 2** were observed to kill cancer cells without requiring internalisation, it was envisaged that they could be utilised for the generation of efficacious non-internalising ADCs (Figure 67). For proof-of-concept investigation, programmed cell death-ligand 1 (PD-L1) was selected as a non-internalising antigen target.

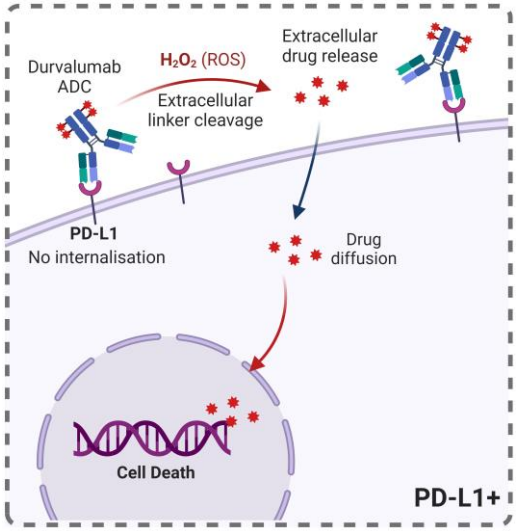

Figure 67: Proposed mechanism of action of a PD-L1 targeted non-internalising peroxide-cleavable ADC.

1.3.6.2 PD-L1 as a non-Internalising ADC target

PD-L1 is a transmembrane protein which inhibits the function of T cells by binding to programmed cell death protein-1 (PD-1). Hence, PD-L1 assists in cancer cell evasion of the immune system, and is upregulated in numerous solid cancers that are often associated with poor prognosis and reduced survival.[144] There are three anti-PD-L1 antibodies approved for use as immune checkpoint inhibitors which prevent the binding of PD-L1 to PD-1: avelumab (Bavencio®,[145] Merck), durvalumab (Imfinzi®,[146] AstraZeneca) and atezolizumab (Tecentriq®,[147] Roche).

There are few published studies on the internalisation of anti-PD-L1 antibodies. Some evidence has suggested that internalisation of PD-L1 is dependent on the specific recognition of certain antibody glycosylation sites.[148] However, internalisation of PD-L1 antibodies has been reported to be slow, for example Heskamp *et al.* observed that >75% of a radiolabelled anti-PD-L1 antibody remained membrane-bound after 24 h of incubation with PD-L1 overexpressing MDA-MB-231 cells.[149] Additionally, Xiao *et al*. observed that an avelumab-Val-Cit-MMAE ADC was <20% internalised after 2 h incubation and as a result, was ineffective as an internalising ADC *in vitro* against PD-L1 positive cell lines.[150]

Encouraged by these preliminary results of the slow internalisation of anti-PD-L1 antibodies, further work sought to investigate the application of arylboronic acid linkers towards non-internalising anti-PD-L1 ADCs. Durvalumab was chosen due to its availability from Cambridge University Hospital Addenbrookes, and similarity in structure to trastuzumab (IgG_1) which would allow bioconjugation in the same manner as trastuzumab modification.

1.3.6.3 ADC synthesis & bioconjugation

Since the unsubstituted trastuzumab **ADC 1** displayed slightly superior cytotoxicity *in vitro* than di-fluoro **ADC 2**, this linker was taken forward for generation of a durvalumab ADC. With unsubstituted DVP-linker-MMAE **20c** already in hand, durvalumab could be subjected to the same bioconjugation conditions as trastuzumab. Non-cleavable and Val-Cit durvalumab ADCs would also be synthesised (from DVP-linkers **23** and **24** respectively) to act as controls. Bioconjugation proceeded successfully to generate **ADC 5**, **ADC 6** and **ADC 7** (Figure 68), with the half antibody being the major component when viewed by SDS-page gel (Figure 69). HIC confirmed that the major species was DAR 4, and allowed calculations of average DAR which were close to 4 (Figure 70). SEC analysis revealed no observable aggregation (Figure 71). Finally, protein LCMS confirmed the correct identity of the ADCs, with the unsubstituted arylboronic **ADC 5** showing the same mass discrepancy (approx. - 40 Da) as observed with the trastuzumab ADCs (Figure 72).

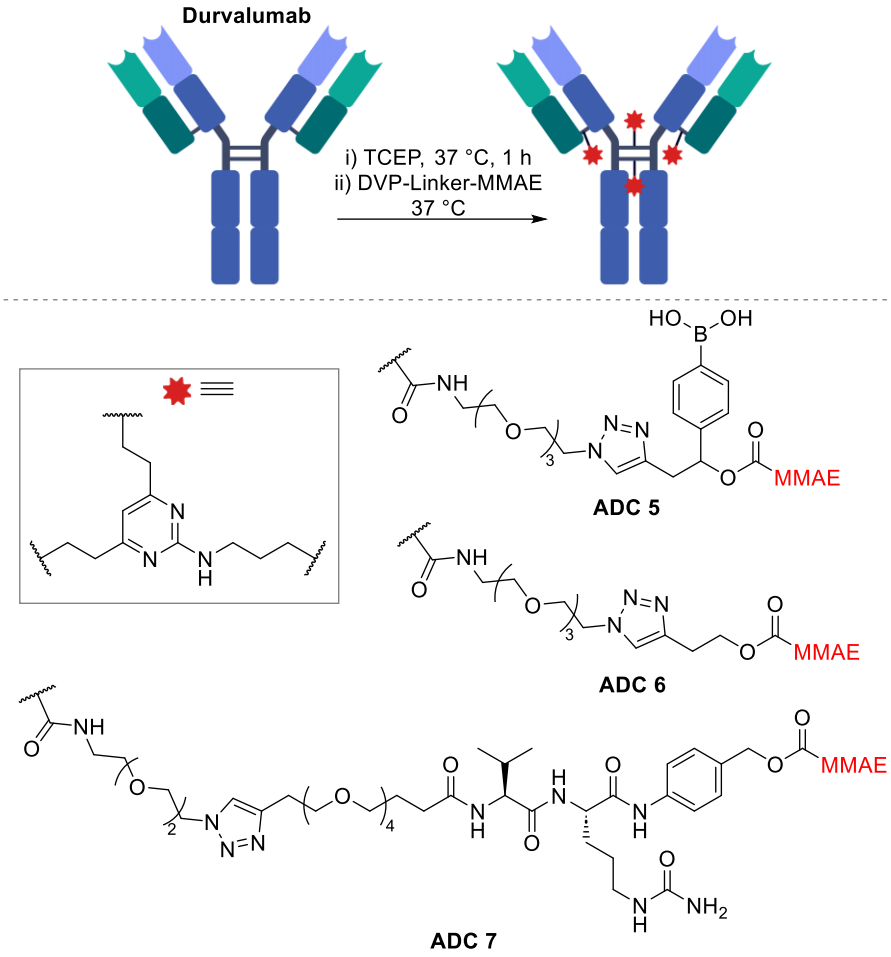

Figure 68: Bioconjugation reaction to Durvalumab **ADCs 5-7**.

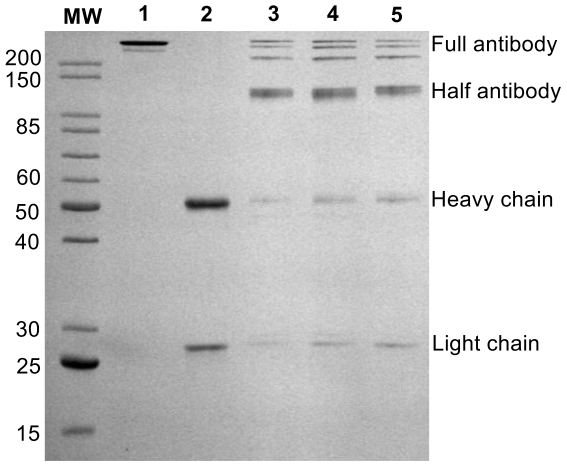

Figure 69: SDS-page gel for durvalumab bioconjugations. MW = molecular weight ladder Lane 1 = Durvalumab, 2 = Reduced durvalumab, 3 = **ADC 5** (unsubstituted), 4 = **ADC 6** (non-cleavable), 5 = **ADC 7** (Val-Cit). 12% acrylamide gel under reducing conditions with β-mercaptoethanol (lanes 2-5) at 70 °C for 2 min prior to gel loading, stained with Coomassie blue.

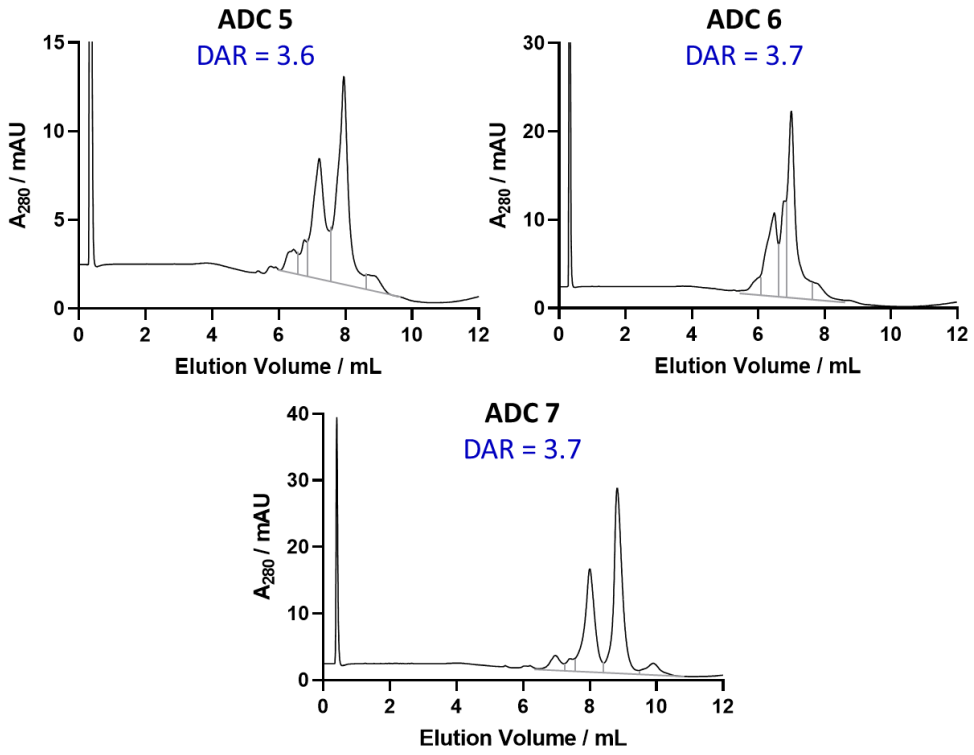

Figure 70: HIC traces for durvalumab **ADCs 5-7**. The major species corresponds to a DAR of 4 and the average DAR calculated from peak areas is shown.

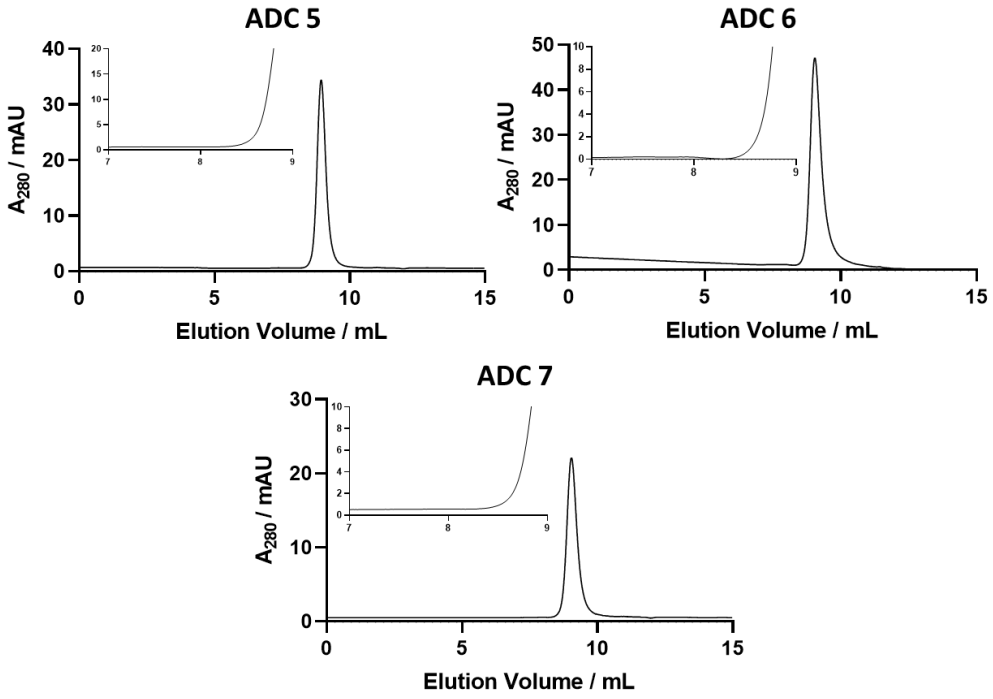

Figure 71: SEC traces for durvalumab **ADCs 5-7**. In each case, no aggregation was observed.

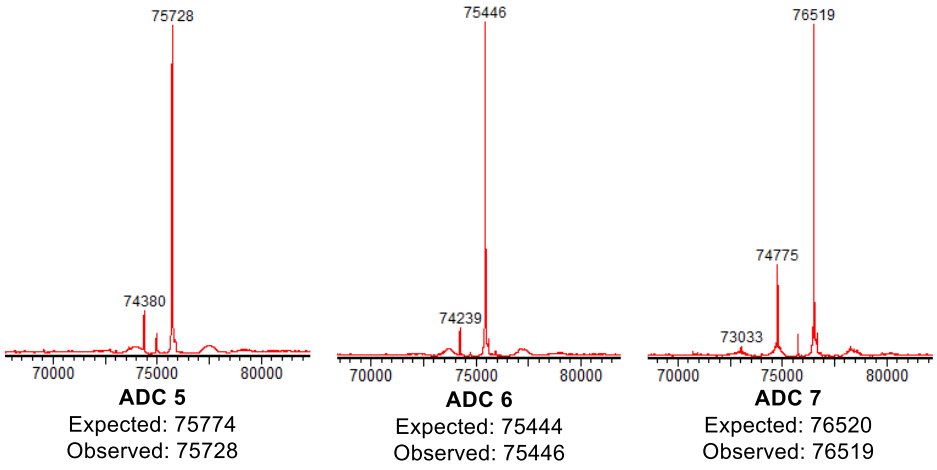

Figure 72: Protein LCMS of **ADCs 5-7**. Mass spectra were reconstructed from the ion series using the MaxEnt 1 algorithm preinstalled on MassLynx 4.2 software according to the manufacturer's instructions. The raw ion series can be found in appendix 2.

1.3.6.4 *In Vitro* evaluation

With durvalumab **ADCs 5-7** in hand, their cytotoxicity was evaluated *in vitro*. MCF7 cells have low levels of PD-L1 expression (PD-L1-) and MDA-MB-231 cells overexpress PD-L1 (PD-L1+).[151] Amplex™ Red quantitation previously demonstrated the presence of extracellular H_2O_2 in these cell lines (Figure 61). Hence, **ADCs 5-7** were incubated with MDA-MB-231 and MCF7 cells *in vitro* and their cytotoxicity examined (Figure 73, Table 8). Non-cleavable and Val-Cit durvalumab **ADC 6** and **ADC 7**, respectively, were non-toxic in both cell lines, suggestive of limited ADC internalisation. Conversely, peroxide-cleavable **ADC 5** possessed significant dose-dependent cytotoxicity in both cell lines, consistent with the ability of the linker to be cleaved in the extracellular media.

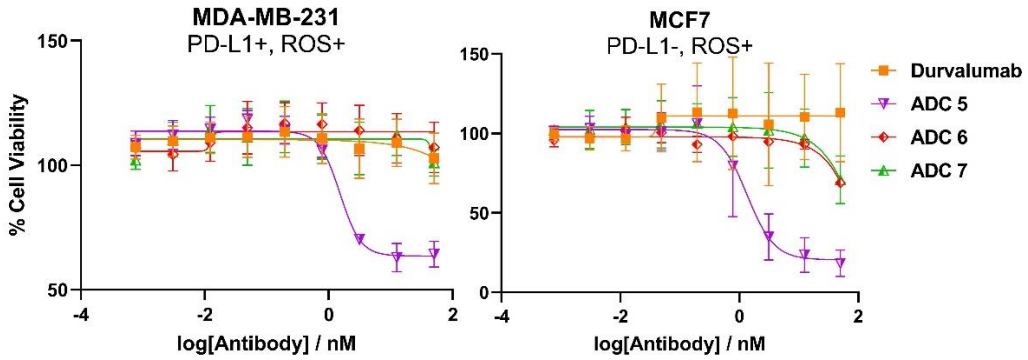

Figure 73: The *in vitro* cytotoxicity of **ADCs 5-7** and unconjugated durvalumab in PD-L1-positive MDA-MB-231 cells and PD-L1-negative MCF7 cells. Viability data shown is the mean of three independent replicates and error bars represent standard error of the mean.

Table 8: Potency of **ADCs 5-7** against breast cancer cell lines. IC_{50} values (nM) were calculated using the log(inhibitor) vs. response curve fit with variable slope (four parameters) in GraphPad Prism.

	IC_{50} (nM)	
	MDA-MB-231 (PD-L1+)	**MCF7** (PD-L1-)
ADC 5	1.52	1.35
ADC 6	>50	>50
ADC 7	>50	>50

To further confirm the cytotoxicity of **ADC 5** resulted from action of extracellular H_2O_2 (and not by intracellular ADC degradation following internalisation to release the payload), MCF7 and MDA-MB-231 cells were pre-treated with H_2O_2 scavenger CAT (Figure 74). Accordingly, the potency of **ADC 5** was greatly reduced in both PD-L1- and PD-L1+ cell lines when H_2O_2 was scavenged by CAT. Similar to trastuzumab **ADC 1** and **ADC 2**, with CAT scavenging, ADC concentration had no impact on cell growth, suggesting minimal payload release from the ADCs.

Taken together, these results support a non-internalising mechanism of action: if internalisation was sufficient, **ADC 6** and **ADC 7** would be cytotoxic as a result of intracellular processing of the antibody which releases payload or active payload metabolites. Moreover, if internalisation was sufficient, **ADC 5** would display cytotoxicity even with H_2O_2 scavenging, by similar intracellular processing to release active payload metabolites. However, it should be noted that these *in vitro* assays do not demonstrate binding to the target. As with the trastuzumab *in vitro* assays, the durvalumab **ADC 5** is potent even against PD-L1- MCF7 cells, presumably simply due to prolonged incubation in the extracellular high-H_2O_2 media. Hence, although a non-internalising mechanism of action is inferred, further biological evaluation is required to validate the ADCs as efficacious non-internalising ADCs which afford tissue-selectivity by binding only to overexpressing tumour cells.

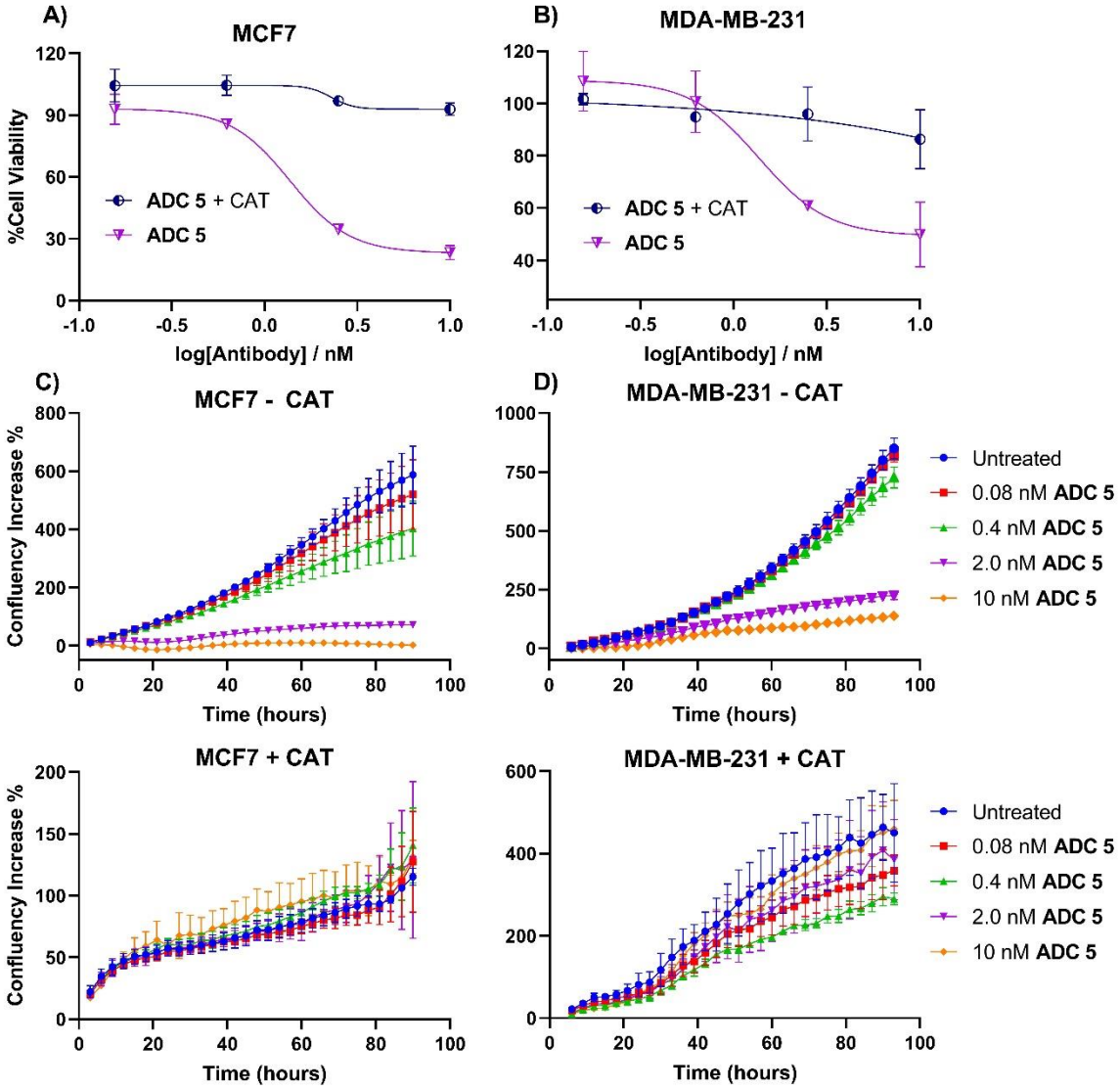

Figure 74: A) Cell titer glo endpoint reading for **ADC 5** in PD-L1-negative MCF7 and B) PD-L1 positive MDA-MB-231 cells. Without catalase, the ADC displays potent dose-dependent cell killing, but when the hydrogen peroxide is scavenged by CAT, no cell killing is observed. C) Confluency increase % of MCF7 and D) MDA-MB-231 cells when treated with varying concentrations of **ADC 5** in the absence and presence of scavenger CAT. Viability data shown is the mean of two independent replicates and error bars represent standard error of the mean. Confluency data shown is one of two independent replicates and error bars represent standard error of the mean of technical replicates of one experiment.

1.4 Conclusions

Peroxide-cleavable arylboronic acid linkers have been explored for their application towards ADCs with internalising or non-internalising mechanisms of action. Initial studies of model small molecule linkers with a fluorescent reporter payload revealed the desired reactivity of the arylboronic acids with H_2O_2 and relative stability in the absence of H_2O_2. Elaboration of the arylboronate linkers to anti-HER2 and anti-PD-L1 ADCs was then performed, and their properties evaluated *in vitro*.

Model linkers with fluorescent payload mimic AMC demonstrated that the aryl ring electronics impacted the kinetics of payload release. The fastest releasing model linker was the di-fluoro **2b** followed by the unsubstituted **1b**, and the slowest was the mono-fluoro **5**. Given the superior reactivity of the former two linkers, they were carried forward for evaluation of their stability. Both arylboronic acid linkers were stable at pH 4.5-9, in the presence of GSH, and in unconditioned cell media. Importantly, in mouse plasma, the di-fluoro arylboronic acid linker **2b** had superior stability (minimal degradation over 10 days) compared to analogous Val-Cit model linker **4**, which rapidly degraded. Although the stability of these small molecule model linkers are not complete representations of the stability of the resulting ADCs, they suggest that the general cleavable motif should be stable *in vivo*, with superior stability in mouse plasma compared with commonly utilised dipeptidic linkers.

With the promising reactivity and stability of the model linkers, the more reactive unsubstituted and di-fluoro linkers were elaborated into anti-HER2 ADCs successfully, obtaining **ADC 1** and **ADC 2** (respectively) with average DARs close to 4. *In vitro* evaluation revealed high potency towards HER2+ cell lines, but equal activity in HER2- cell lines. It was elucidated that the presence of extracellular H_2O_2 in non-target cell lines enabled extracellular linker cleavage and payload release. Scavenging of this extracellular H_2O_2 by catalase (CAT) rendered the peroxide-cleavable ADCs non-toxic in HER2- cell lines, demonstrating that H_2O_2 is essential for their activity, and that they are not otherwise unselective.

Given their ability to release payload extracellularly, the peroxide-cleavable linkers were used to generate a non-internalising ADC with anti-PD-L1 antibody durvalumab. When extracellular H_2O_2 was scavenged from PD-L1 positive cells, the peroxide-cleavable durvalumab ADC became non-toxic, demonstrating the importance of peroxide for the mechanism of action. Importantly, non-cleavable and Val-Cit durvalumab ADC analogues, which require internalisation and intracellular processing for payload release, were non-toxic against PD-L1+ cells. Taken together, this suggests that the durvalumab ADCs synthesised in this work were not significantly internalised, and peroxide-cleavable arylboronic acids are effective extracellularly-cleavable linkers.

In summary, this work presents arylboronic acids as suitable cleavable linkers for the generation of potent ADCs which may function most effectively by a non-internalising mechanism of action (Figure 75).

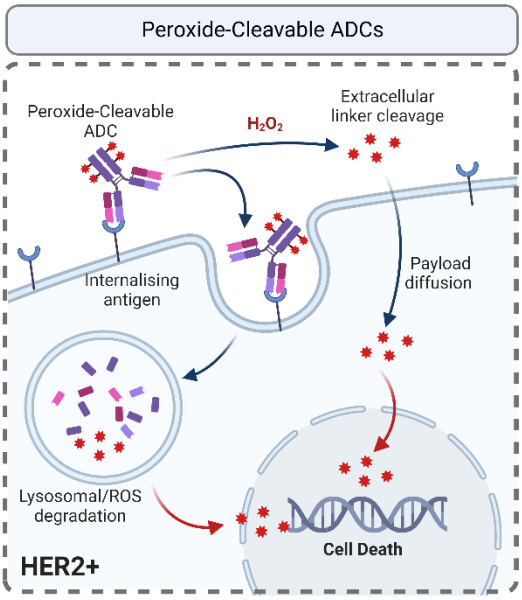

Figure 75: Schematic demonstrating the proposed mechanism of action of peroxide-cleavable ADCs, whereby internalising or non-internalising mechanism of action may occur.

1.5 Future Work

1.5.1 Kinetics of Release from ADCs

In this work, the kinetics of payload release were solely examined from the small molecule model linkers. This has drawbacks in that the payload mimic, AMC, does not entirely resemble the later payload incorporated in the ADCs, MMAE. Notably, AMC is appended from an aniline nitrogen, whereas MMAE is appended *via* an aliphatic nitrogen. Thus, the kinetics of payload release by immolation may be different for AMC vs MMAE, due to different leaving group abilities. For example, although the di-fluoro model linker **2b** displayed superior kinetics of release in the model linker studies, it displayed slightly inferior cytotoxicity *in vitro* compared to the unsubstituted ADC.

It would be useful therefore, to monitor the kinetics of release from the linkers when incorporated into ADCs. An experiment is envisioned whereby ADCs are incubated with a biologically relevant concentration of H_2O_2 at 37 °C, and aliquots taken at determined time intervals. The protein content could then be precipitated from the aliquot, and any cleaved drug should remain in the supernatant. Analysis of the supernatant by HPLC could then provide a quantitative readout of released MMAE when compared to a standard calibration curve of MMAE concentration vs HPLC response. Thus, this experiment would provide accurate kinetic data and allow comparison of the release performances of different ADCs.

Of course, factors other than release kinetics might influence the *in vitro* cytotoxicity of the ADCs. However, if the kinetics are well understood, this may allow greater interpretation of the *in vitro* results and aid future linker development.

1.5.2 Durvalumab Mechanism of Action

In this work the non-internalising nature of durvalumab ADCs was inferred from the inactivity of a non-cleavable and Val-Cit durvalumab **ADC 6** and **ADC 7** in PD-L1+ cells, and that the peroxide-cleavable **ADC 5** became less toxic when extracellular H_2O_2 was scavenged by CAT. However, further confirmation of the mechanism of action of durvalumab ADCs is required to confirm its non-internalising interaction with the PD-L1 antibody. It is envisioned that appendage of a fluorophore to the antibody of a durvalumab ADC would allow facile monitoring of ADC distribution by confocal microscopy. After different incubation times, the extent of internalisation of the durvalumab ADC could be monitored.

Furthermore, in this work, binding of the non-internalising ADCs to cell surface PD-L1 was only inferred. **ADC 5** would presumably display the same potency against PD-L1+ cell lines if it was not able to bind to the antigen, since it would be incubated with high-H_2O_2 extracellular cell media for the duration of the *in vitro* assay. For further verification therefore, binding assays of the ADCs to PD-L1

should be performed, to confirm they retain antigen binding affinity. Alternatively, the microscopy experiment previously described would probe the ability of ADC to bind to cells, since a washing step before microscopic analysis would remove any unbound ADC present in the extracellular media.

1.5.3 Further Validation *In Vivo*

Although the *in vitro* experiments described in this work are sufficient for a preliminary investigation of the suitability of arylboronic acids for incorporation as ADC linkers, *in vivo* experiments are essential to accurately evaluate their clinical potential. A major drawback of the plate-based *in vitro* assays is the inability to demonstrate cell targeting, since the ADCs are in close proximity to the cancer cells for the duration of the assay and can liberate the payload extracellularly regardless of internalisation. However, with *in vivo* administration, the ADC should circulate throughout the body and only be retained at the site where antibody-antigen binding can occur (in antigen-enriched tumours). An *in vivo* study could therefore reveal any true off-target toxicity of the ADCs. For example, healthy mice treated with ADC should remain healthy if the ADC does not lead to off-target MMAE release. In contrast, ADC treatment of mice with antigen-positive tumour xenografts should result in tumour reduction and improved survival.

1.5.4 Application Towards Other Antibodies and Cellular Targets

Given the promising non-internalising mechanism of action of the peroxide-cleavable linkers, further work could explore appendage to a number of different antibodies that do not appreciably internalise. In addition, numerous other extracellular targets are emerging which allow targeting of a wide range of cancers and require extracellular payload release. For example, non-internalising ADCs targeting CD20,[81,87] CD21,[50] CD72,[50] TAG72,[62,97] CEACAM5,[88] and NKA[152] have been described. Furthermore, peroxide-cleavable linkers could be explored for ADCs targeting components of the extracellular matrix, i.e. secreted proteins, or targeting the tumour stroma or vasculature.[5]

Section II: Peroxide-Activatable Prodrugs

II.1 Introduction

This section describes efforts towards the development of novel anti-cancer prodrugs activated by the hydrogen peroxide present in cancer. Here, the concept of small-molecule prodrugs is introduced, as well as the considerations needed for the design of self-immolative linking units, and an overview of peroxide-activatable prodrugs described in the literature.

II.1.1 Prodrug Approach

Chemotherapeutics are often unselective: upon administration to the body, the drugs circulate everywhere and exert their function on healthy cells as well as target cancer cells.[153] This leads to numerous problems, such as: undesired toxicity, harmful side effects, and the necessity for increased doses as only a portion of the administered drug acts on the desired target.[135,154] Hence, there has been increased interest in creating more selective therapies, where the drug only acts at the target site.[153]

Prodrugs are drug analogues with little to no biological activity. However, they comprise an intentional structural lability which allows selective "unmasking" of the active drug at the site of disease. The conversion of an inactive prodrug to the active drug is usually due to a chemical or enzymatic process, which occurs more frequently in diseased over healthy cells. This affords site-specific activation of the drug. The activity of a drug can be attenuated by protecting a functional group essential for the drugs activity with a "trigger".[155–158] This trigger can be cleaved by an effector (i.e. chemically or enzymatically) to reveal the parent, active drug directly (Figure 76A). Alternatively, a linker can be used to connect the trigger to the drug, which is designed to self-immolate after trigger activation to release an unmodified drug (Figure 76B). Such prodrug approaches have been widely investigated for small-molecule drugs,[139,153,157,159,160] fluorescent reporter systems,[161] and macromolecular systems.[113,162]

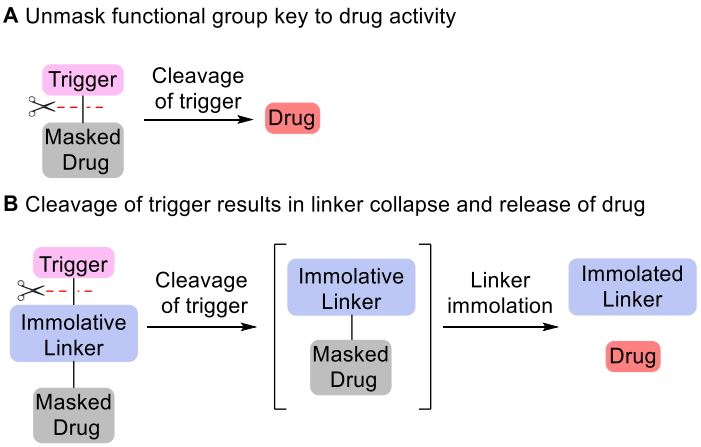

Figure 76: A) Simple functional group masking prodrug strategy, B) prodrug strategy involving immolation of a linker which connects the cleavage trigger to the drug.

For a simple functional group masking strategy, care must be taken that the structural alteration sufficiently attenuates the potency of the drug, since this can be difficult to achieve with only small functional-group protections.[135] Additionally, the presence of the protecting group/trigger in close proximity to the drug must not impede its capability to be cleaved or hinder drug release. Prodrugs with self-immolative linkers might offer an attractive alternative, whereby the trigger is spatially separated from the drug, ensuring pro-moiety cleavage is not hindered by steric clashes. In summary, for the development of a successful prodrug with a self-immolative linker, the pro-moiety must 1) sufficiently mask drug activity and 2) must site-selectively and effectively release the drug *via* linker immolation upon trigger activation.

There are many differences between healthy cells and diseased cells (e.g. in cancer), such as differences in pH and the elevated presence of different enzymes and other chemical species.[163] These differences can be exploited for the activation of a prodrug only at the site of disease. Commonly seen in both the ADC field and the prodrug field are the use of dipeptides, such as Val-Cit, which target the elevated levels of cathepsin enzymes in cancer compared to healthy cells.[164] Cleavage of these peptide linkers reveals an amine, either belonging to the native drug or to an immolative linker. Many other enzymes have also been used as effectors of linker cleavage, including: plasmin, β-glucuronidase, β-galactosidase, penicillin G amidase, azo/nitroreductases and many others (Figure 77).[165] Finally, boronic esters/acids have also been employed as prodrug triggers due to their favourable and selective reactivity with hydrogen peroxide.[135] Hydrogen peroxide and its high prevalence in cancer has been discussed previously in this report (Section I, Chapter 1).

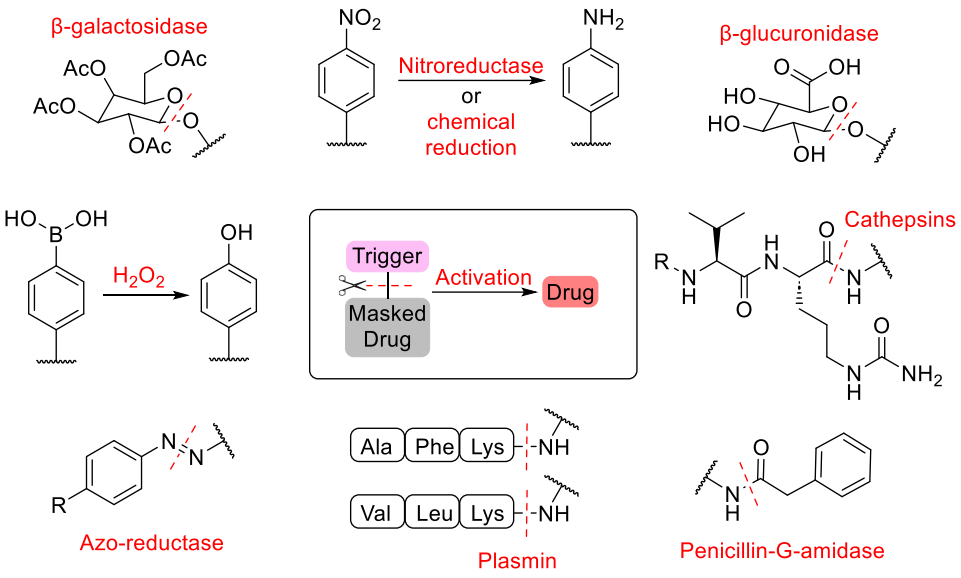

Figure 77: A non-exhaustive selection of various types of triggers that can be cleaved to release a drug (or linker-drug species primed for immolation) by an effector up-regulated at the site of disease.

II.1.2 Self-Immolative Linkers

Self-immolative linkers typically require an electron-rich aromatic ring containing an electron-donating substituent in conjugation with a suitable leaving group.[162] The electron-donating group lowers the energy barrier for dearomatisation and is only revealed after cleavage of the initial trigger unit.[162] One of the first and most common self-immolative linkers is the *para*-aminobenzyl moiety (PAB, Figure 78). Following trigger cleavage, an electron-rich aniline is revealed which can undergo a spontaneous 1,6-elimination electronic cascade to release a leaving group (LG) at the benzylic position. A *para*-hydroxybenzyl motif can also be utilised, whereby trigger cleavage reveals a phenol instead of an aniline. Both of these linkers release a highly electrophilic quinone methide intermediate, which is quickly hydrolysed in the presence of water to a benign alcohol.[111,112] However, these intermediates are also known to react with biological nucleophiles, such as glutathione (GSH) or DNA bases.[112] Although this may lead to undesirable toxicity, in the case of anti-cancer therapy the release of an additionally toxic quinone methide at the tumour site may contribute to the therapeutic effect.[113]

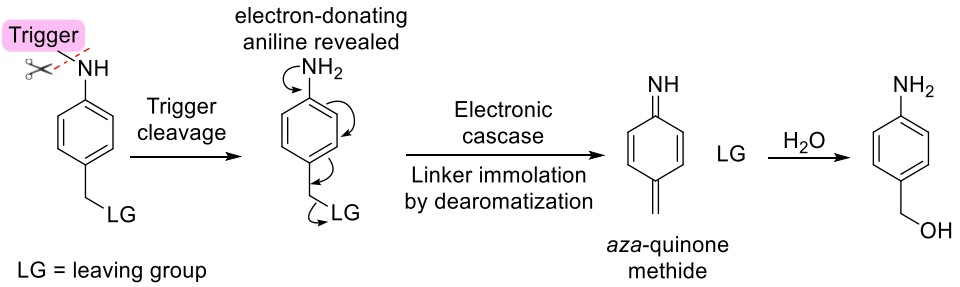

Figure 78: General *para*-aminobenzyl immolative spacer which undergoes immolation via 1,6-elimination following trigger cleavage.

The nature of the leaving group can vary depending on which drug functionality the self-immolative linker is connected to (Figure 79). For example, to release alcohol-containing drugs, a carbonate or ether linkage can be incorporated into the immolative linker design. For the release of amines, carbamate bonds are often employed.[166]

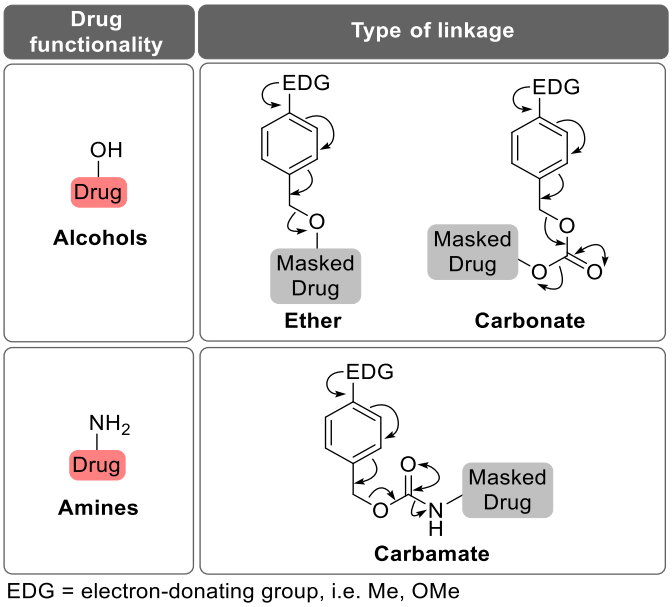

Figure 79: Common linkage moieties to release different drug functionalities. EDG = electron donating group, i.e. NH_2 or OH.

Numerous benzyl-based self-immolative linkers have been explored with different triggers and leaving groups, as well as linkers that disassemble by cyclisation-elimination or through extended conjugated systems beyond 1,6-eliminations.[113] For different types of linkers, the stability and kinetics of trigger-cleavage and subsequent immolation vary, and should be considered during the design of prodrugs.

II.1.2.1 Kinetics of Self-Immolation

Cleavage trigger

The type of motif that is revealed following trigger cleavage influences the ability of the linker to undergo immolation. For example, hydroxybenzyl groups have less favourable immolation kinetics than aminobenzyl groups due to the lower nucleophilicity of phenols compared to anilines.[162,167] Hence, only certain functional groups are sufficiently electron-donating to be able to undergo spontaneous 1,6-elimination after their unmasking, such as anilines, phenols and thiophenols.[162]

Substituents

The electronics of the ring have significant impact on the kinetics of self-immolation. For example, increasing electron-density with electron-donating substituents increases the energy of the aromatic ring HOMO. This strengthens the HOMO-LUMO interaction between the aromatic π molecular orbital

(MO) and the σ* MO of the C-LG (leaving group) bond. Hence, the $C_{benzene}$-$C_{benzylic}$ σ bond is strengthened, and the $C_{benzylic}$-LG σ bond weakened, which facilitates immolation and C-LG bond cleavage (Figure 80A). For this reason, the introduction of electron-donating groups (EDGs) such as methoxy (OMe) onto the self-immolative linker significantly enhances the rate of self-immolation.[115] In contrast, electron-withdrawing groups (EWGs) destabilise the partial positive charge which forms in the transition state at the benzylic position (Figure 80B). Hence, self-immolation is disfavoured and release from these linkers is much slower.[112,121,168] Aryl ring substituents have greater impact on self-immolation kinetics when they are conjugated to the benzylic leaving group (i.e. *ortho* or *para*). Finally, the incorporation of substituents at the benzylic position help to stabilise the developing positive charge on the benzylic carbon and hence enhance the rates of immolation (Figure 80A).[118,121]

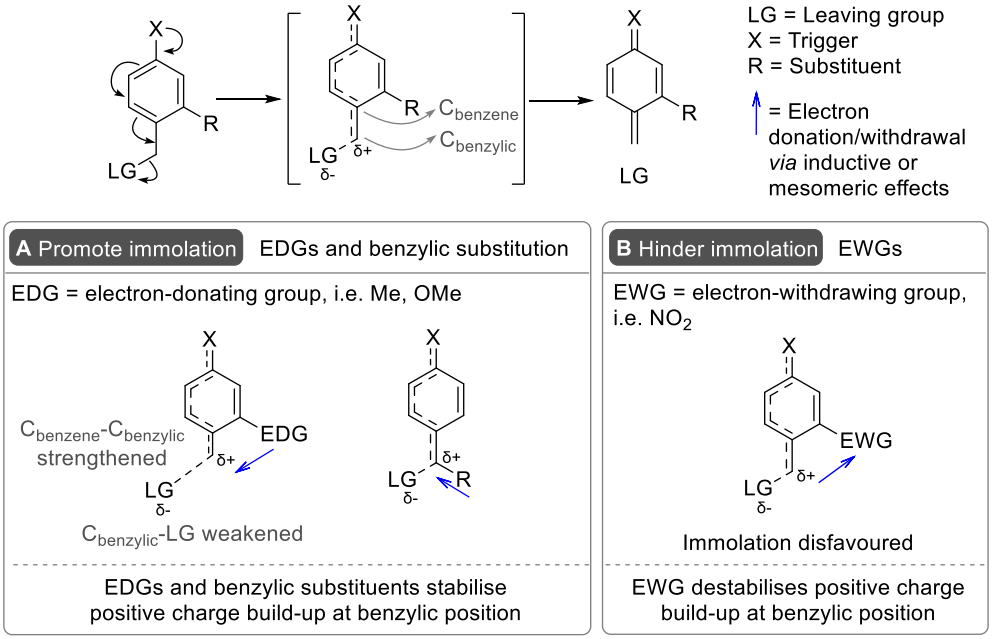

Figure 80: The effect of aryl ring substituents on immolation and leaving group release from benzylic spacers. A) Electron-donating groups (EDG) and benzylic substituents facilitate immolation, whereas B) electron-withdrawing groups (EWG) hinder immolation. Blue arrows represent the generic direction of electron donation/withdrawal by inductive or mesomeric effects.

Leaving group

Self-immolation is driven by the formation of thermodynamically stable products and the increase in entropy associated with generating multiple species from one linker-drug. In the case of carbamate or carbonate linkages (Figure 79), the release of CO_2 is a major entropic and thermodynamic driving force for immolation.[162] Hence, release through carbamates or carbonates tends to occur more quickly than release from ether bonds (which do not generate CO_2 upon immolation).

However, not all functional groups can be released by immolation under physiological conditions. For example, Toki *et al.* discovered that an aliphatic alcohol could not be liberated from a *para*-

aminobenzyl ether (PABE) linker, whereas a phenolic leaving group (1-naphthol) was successfully released from the same linkage (Figure 81).[169] This was attributed to the high pKa of the aliphatic alcohol leaving group.

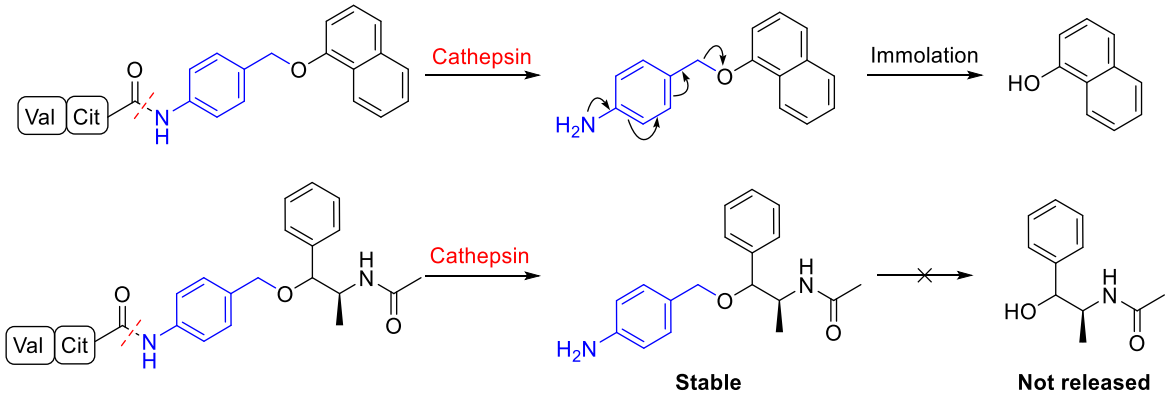

Figure 81: A cathepsin cleavable *para*-aminobenzyl ether linker (depicted in blue) was able to release a phenolic leaving group by cleavage of a benzylic ether bond, but was not able to release an aliphatic leaving group.[169]

The pKa of the released alcohol is important: even some phenols with higher pKa values are unable to be released by linker self-immolation.[119,170,171] For example, a phenolic pyrrolobenzodiazepine (PBD) dimer was not observed to be released from a *para*-aminobenzyl ether spacer following glutathione-mediated cleavage and cyclisation of the initial trigger (Figure 82).[170]

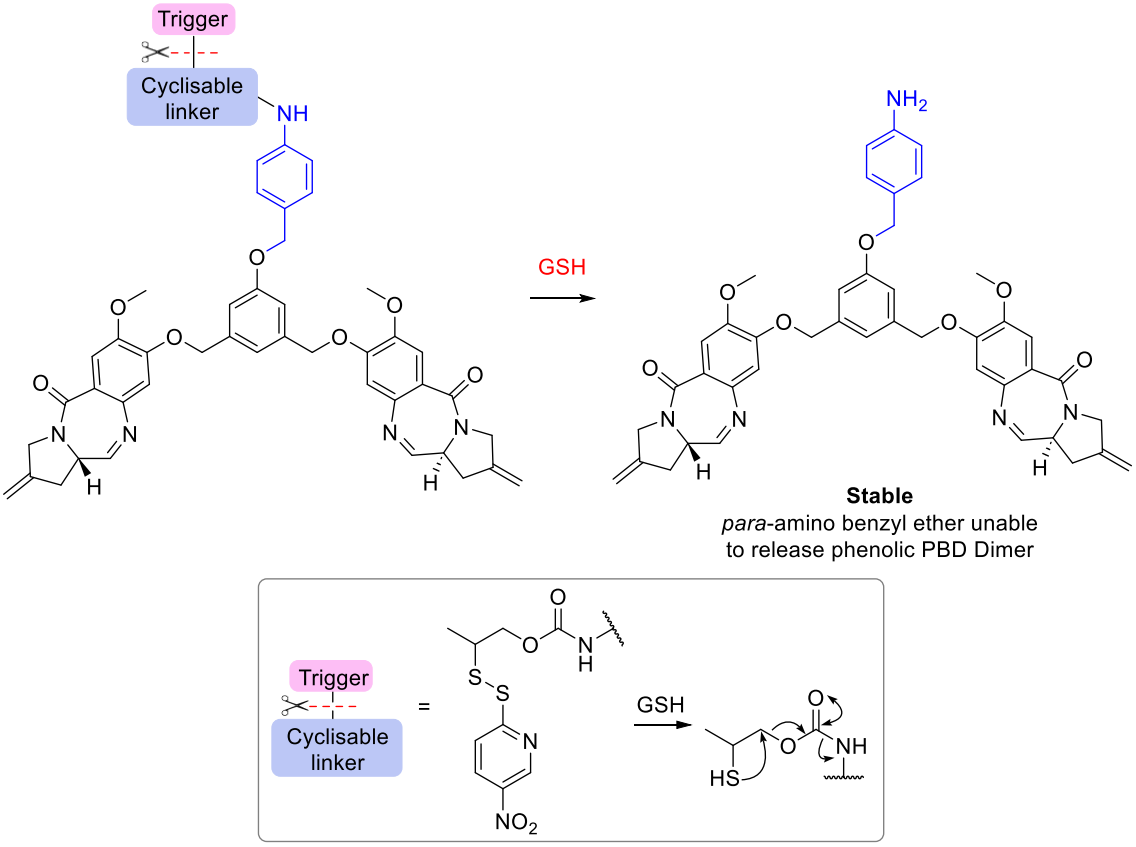

Figure 82: The pKa of the leaving group is important in determining whether self-immolation is possible. The high pKa of the phenolic PBD dimer prevents its release from a para-aminobenzyl ether spacer (depicted in blue).

Substituents on the leaving group can impact the pKa and thus influence their ability to be released by self-immolation. For example, in work described by Pillow *et al.,* effective immolation of a phenol from a *para*-aminobenzyl ether spacer was attributed to the presence of an electron-withdrawing carbonyl substituent able to stabilise the released phenolate (Figure 83).[170]

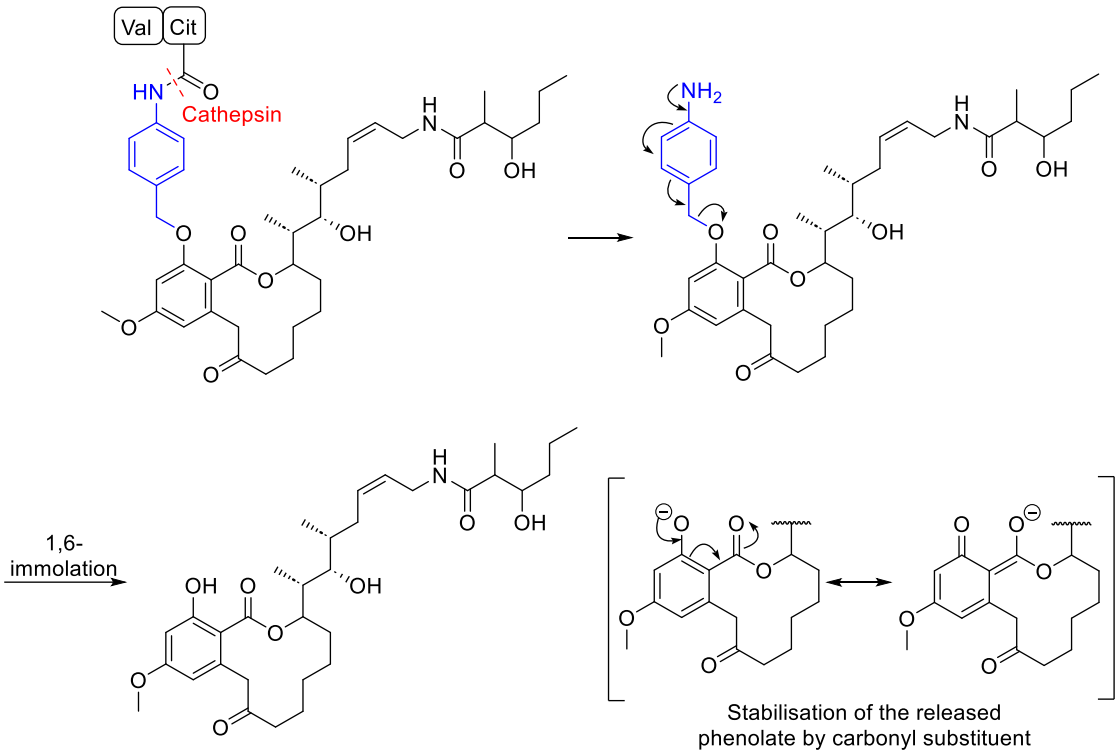

Figure 83: Release of a phenol from a para-aminobenzyl ether spacer was effective, attributed to the lowering of the phenolic pKa due to neighbouring electron-withdrawing carbonyl substituent.[170] The immolative linker is depicted in blue.

The direct release of amines through benzylamine linkers is necessary for amine leaving groups that are incapable of forming carbamate or amide bonds. However, the direct release of amines involves the cleavage of a benzyl C-N bond without the entropically favoured release of CO_2, and thus is often unfavourable. For example, Jourden *et al.* found that *para*-hydroxybenzyl linkers were unable to release aliphatic amines, anilines or sulfonamides (Figure 84).[172]

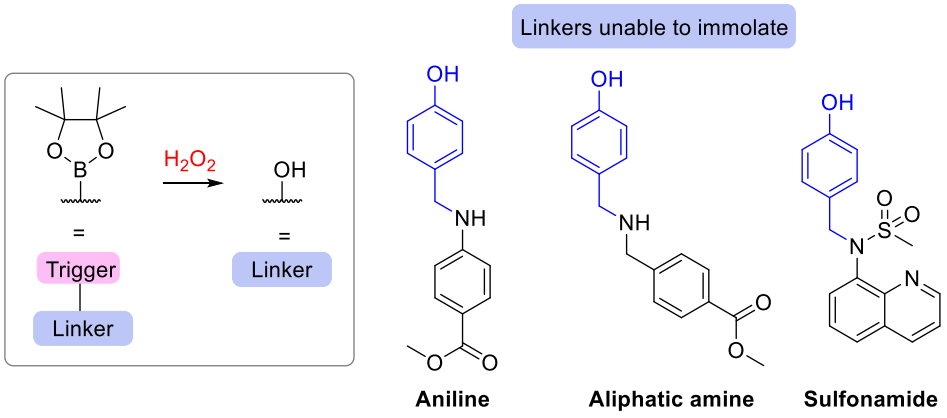

Figure 84: *Para*-hydroxybenzyl spacers connecting aniline, aliphatic amine and sulfonamide leaving groups were unable to self-immolate following trigger cleavage by H_2O_2. The linking unit is depicted in blue.

As an alternative for the direct release of amines, immolative linkers can incorporate quaternary ammonium ions. Primary amines can be incorporated as quaternary ammoniums by protonation

providing their pKa is sufficiently high at physiological pH: Rose *et al.* investigated a series of phenolic immolative linkers with primary aliphatic quaternary ammoniums as leaving groups (Figure 85A).[173] Release was possible at physiological pH 7.4, with electron-donating substituents on the immolative spacer enhancing the rate of release, as expected. More complex quaternary ammonium salts have also been explored, including aromatic heterocycles,[174] and cyclic tertiary amines[175] (Figure 85B).

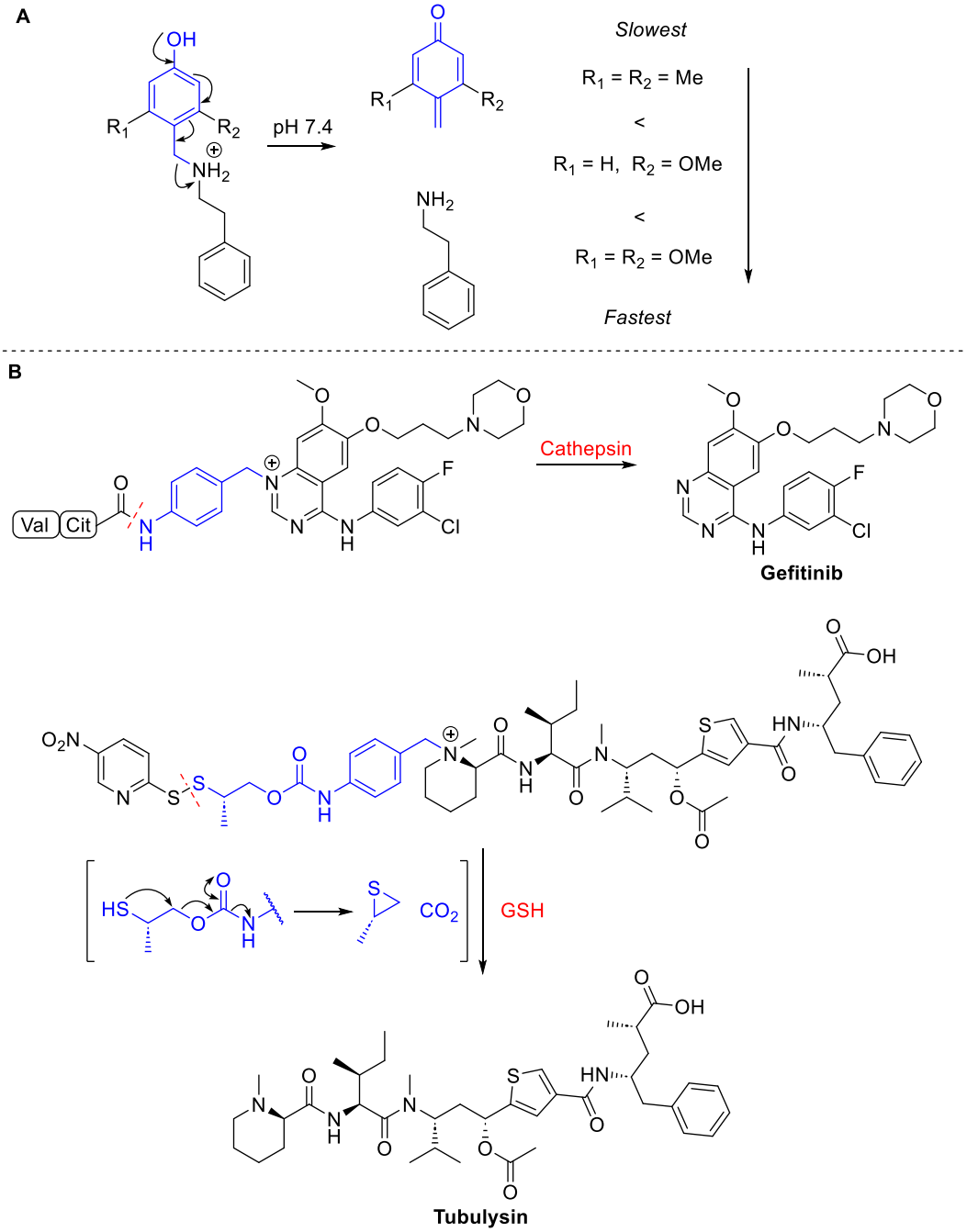

Figure 85: A) Release of a quaternary aliphatic amine from a para-hydroxybenzyl immolative spacer, whereby electron-donating substituents enhance the rate of leaving group release.[173] B) Additional examples of heteroaromatic,[174] and tertiary amines,[175] incorporated as quaternary ammoniums for release from self-immolative linkers. The immolative linker is depicted in blue.

Whilst most existing prodrug strategies release a leaving group *via* C-N or C-O bond cleavage, C-C bond cleavage is also possible. Both Dunsmore *et al.*[176] and Gong *et al*.[177] generated prodrugs of anti-cancer agent β-Lapachone by conjugation of an immolative spacer to the ketone, which is able to release the drug by benzyl C-C bond cleavage after trigger activation (Figure 86).

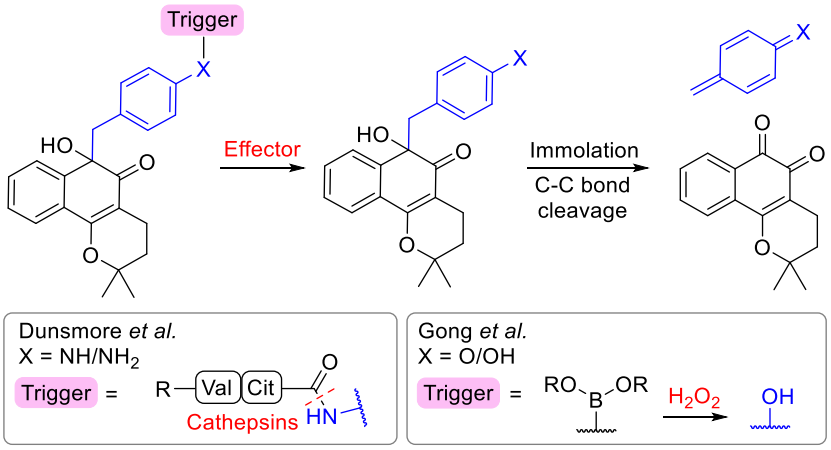

Figure 86: The release of β-Lapachone by benzylic C-C bond cleavage with different cleavage triggers described by Dunsmore *et al*.[176] and Gong *et al*.[177]. The self-immolative linker is depicted in blue.

In summary, although there are general trends which may help to predict whether self-immolation will occur (such as the combination of aryl ring electron-donating groups with good leaving groups), it remains difficult to predict whether immolation of different leaving groups will occur, and case-by-case evaluation is often required.[10,31–33]

II.1.3 ROS-Cleavable Prodrugs

As previously discussed in Section I, Chapter 1 of this report, reactive-oxygen-species (ROS) are essential for the maintenance of normal cell function, growth, migration, and apoptosis.[180] Whilst the endogenous levels of ROS are maintained at relatively low concentrations in healthy cells (approx. 20 nM),[154] in some pathological states, such as cancer, the concentrations of ROS can reach up to 100 µM.[181] This distinction between healthy and pathological cells makes ROS an attractive target for selective drug delivery.

H_2O_2 is the major target of ROS-cleavable self-immolative linkers since it has higher concentrations compared to the other ROS, and is more stable and long-lived.[108] The ability of H_2O_2 to oxidise arylboronates and arylboronic acids is well-established.[137] Boron possesses an empty p-orbital which is able to accept two electrons from H_2O_2. This leads to oxidation of the C-B bond, followed by hydrolysis, results in overall conversion of the arylboronate or boronic acid to a phenol. The phenol is then primed for immolation by 1,6-elimination of a suitable leaving group in the benzylic position (Figure 87).

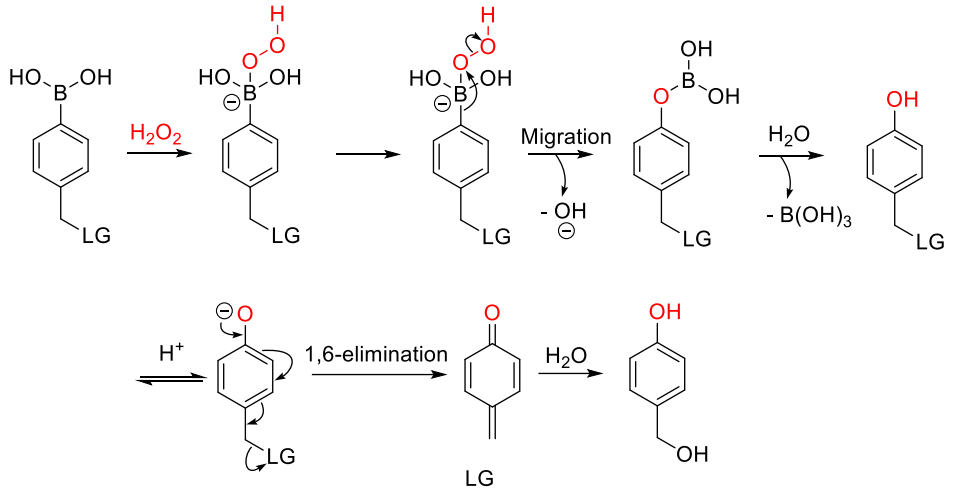

Figure 87: Mechanism for H_2O_2-mediated oxidation of an arylboronic acid, and the subsequent self-immolation that can occur if a suitable leaving group (LG) is present at the benzylic position.

Other moieties also undergo specific reactions with H_2O_2 such as thiazolidinones,[182,183] aryl oxalate esters,[184] thioketals,[185,186] and motifs containing sulfur,[187] selenium,[188,189] or tellurium[190,191] (Figure 88). However, the arylboronates/boronic acids are the most well-established H_2O_2-cleavable motif and will be the focus of this chapter.

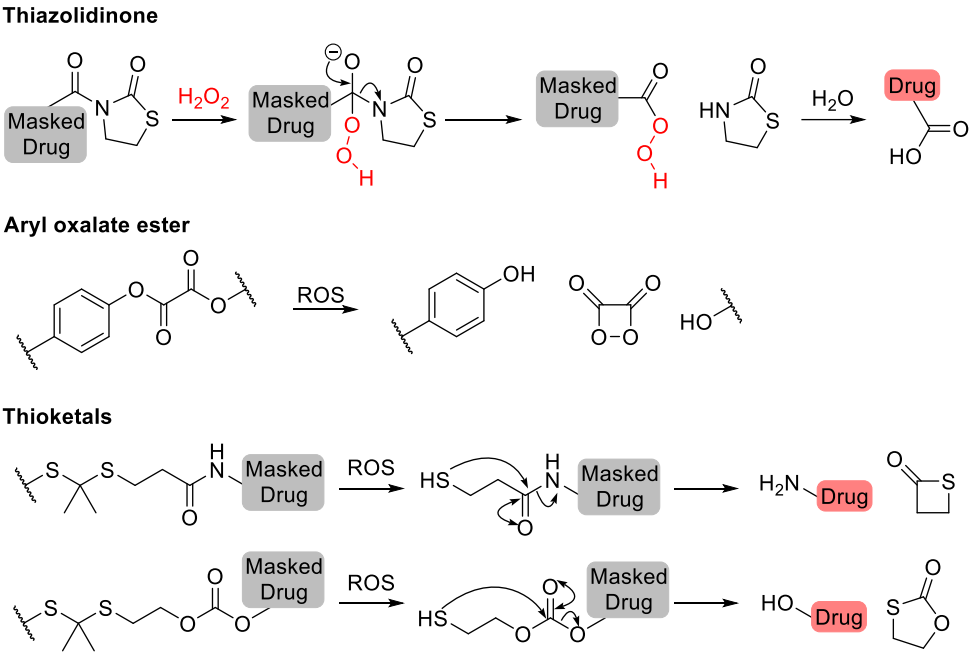

Figure 88: A variety of H_2O_2-responsive motifs utilised in ROS-responsive prodrugs and their mechanisms of cleavage.

Whilst arylboronates had been widely explored for H_2O_2-reporter systems, it wasn't until 2010 that they were first applied to peroxide-activatable prodrugs: Jourden *et al*. coupled benzyl arylboronate immolative linkers to matrix metalloproteinase inhibitors (MMPis) by carbonate or ether bonds (Figure 89).[110] These prodrugs gave responsive drug release in the presence of H_2O_2, with carbonate-

containing prodrug **C** cleaving the fastest (Figure 89). However, carbonate **C** suffered from low aqueous hydrolytic stability, with over 50% hydrolysis observed in 24 h. In general, the biological application of molecules containing carbonate linkages is limited due to their insufficient stability and tendency for non-specific hydrolysis.[171,192,193] Hence, the final prodrugs were synthesised with benzyl ether linkages which displayed >100-fold less activity compared to the parent drugs. Then, activity could be regained in the presence of H_2O_2 due to arylboronic acid oxidation, self-immolation and release of the parent inhibitors from the prodrugs.[110]

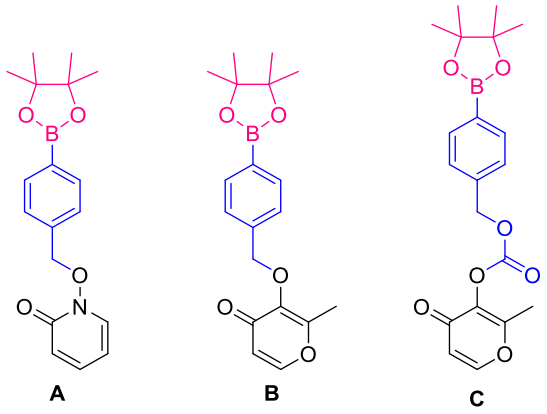

Figure 89: Model arylboronate prodrugs of MMP inhibitors studied by Jourden *et al*., possessing benzyl ether (A and B) or carbonate (C) linkages.[110] The ROS-responsive boronate is depicted in magenta, and the self-immolative linker is depicted in blue.

Having established that H_2O_2-activatable pro-moieties could generate efficacious prodrugs, many prodrugs of similar structure have since been explored.[111,120,154] A few examples have been described which directly mask a key hydroxyl group of a drug to render it inactive.[91,194–197] In this case, a self-immolative linker is not required, since H_2O_2 oxidation reveals the parent drug. Wang *et al.* showed that the key hydroxyl of SN-38 could be masked as a boronic acid and activated in the presence of cancer cells *in vitro*.[197] This resulted in a prodrug with comparable *in vivo* potency to the parent drug due to activation *in situ,* but with a potentially improved safety profile (Figure 90).[197]

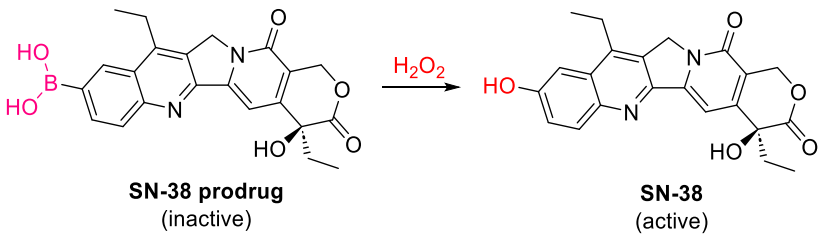

Figure 90: Direct functional group masking of SN-38 with a peroxide-responsive boronic acid.[197]

Kuang *et al.* utilised an arylboronic acid self-immolative unit to generate prodrugs of nitrogen mustards (Figure 91).[198] Nitrogen mustards are DNA cross-linking agents which suffer from severe side-effects due to their poor selectivity for cancer cells, hence, they are attractive candidates for a targeted

prodrug approach. First, the nitrogen mustards were modified as quaternary ammonium salts (Figure 91A). Whilst this was effective at generating prodrugs which only exhibited DNA cross-linking when activated by H_2O_2, the charged species were unable to cross cell-membranes. The authors later developed neutral nitrogen mustard prodrugs (Figure 91B), noting that direct masking of a phenol of a nitrogen mustard as a boronic acid sufficiently lowered its activity prior to activation by H_2O_2 *in vitro*.[199]

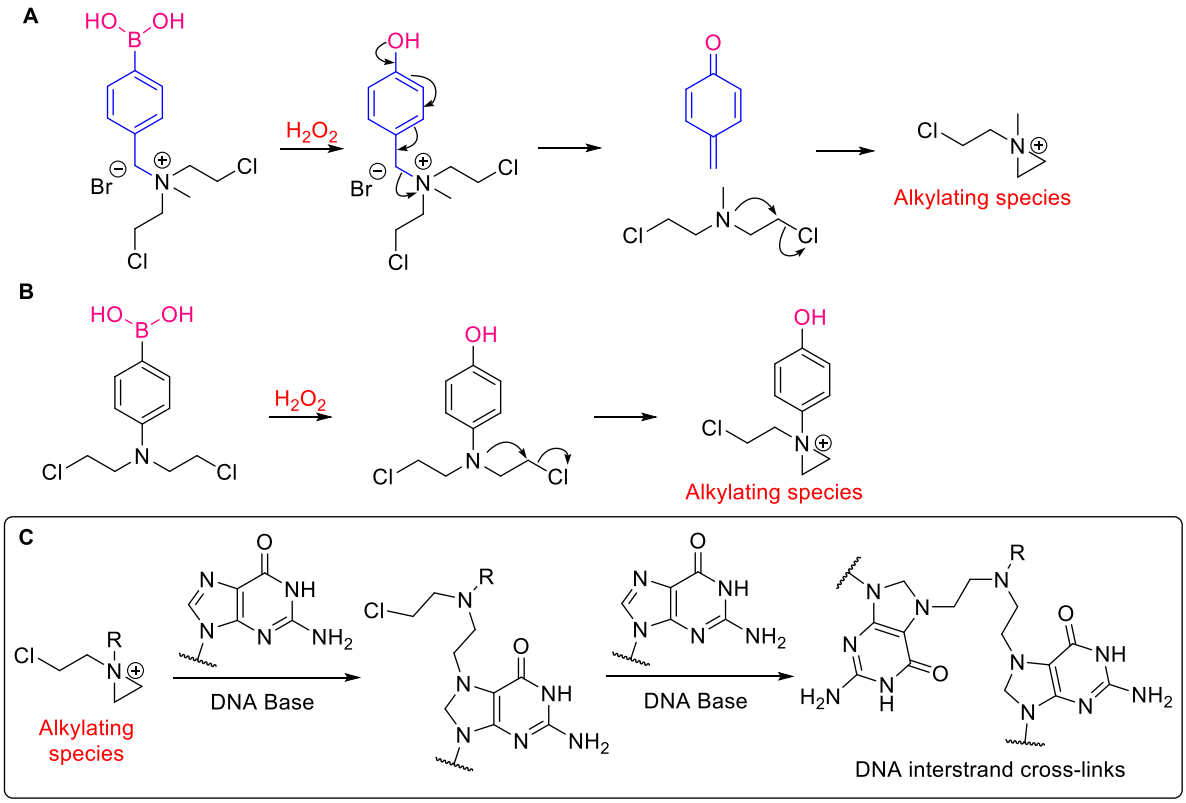

Figure 91: A) Quaternary ammonium nitrogen mustard prodrugs, B) neutral phenolic nitrogen mustard prodrugs, C) mechanism of action of DNA alkylation from the released nitrogen mustard. The H_2O_2 responsive unit is depicted in magenta and the self-immolative linker depicted in blue.

H_2O_2-activatable prodrugs of many other anti-cancer cytotoxic agents have also been described (Figure 92). The hydroxamic acid functional groups of histone deacetylase (HDAC) inhibitors vorinostat (SAHA) and belinostat have been used as an attachment point for a H_2O_2-responsive pro-moiety.[138,139,200] The carbonate containing SAHA-prodrug was stable in serum and had improved selectivity towards cancer cells with high levels of H_2O_2 compared to H_2O_2-deficient HEK-293T cells, and an ether linked analogue displayed comparable potency.[139] Similarly, an arylboronate belinostat prodrug was inactive against normal mammary epithelial MCF10A cells, but displayed potent cytotoxicity (IC_{50} = 1.46 µM) against breast cancer MCF7 cells.[138] An additional benefit of the prodrug approach was revealed in the superior potency of the belinostat prodrug over the parent drug *in vivo*, attributed to its improved bioavailability and therefore improved tumoral concentrations.[138] Additionally, an arylboronate

prodrug of a lysine-specific HDAC inhibitor, *trans*-2-phenylcyclopropylamine has been described.[201] The prodrug had selective activity against glioblastoma cell lines compared to healthy astrocytes. The anti-tumour agent evodiamine has also been modified with an arylboronate by a carbonate linkage and although the authors did not explore the hydrolytic stability of the carbonate, the evodiamine prodrug had good activity *in vitro* against multiple cancer cell lines.[202]

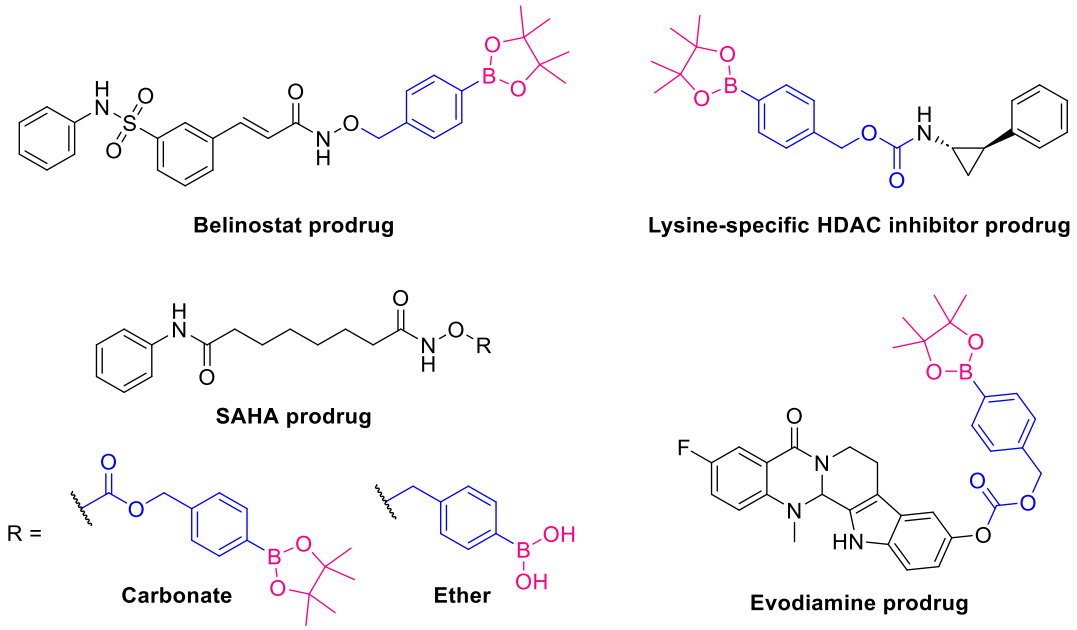

Figure 92: The structure of various arylboronate prodrugs of anti-cancer agents Belinostat, SAHA, evodiamine and a lysine-specific HDAC inhibitor. The H_2O_2 responsive unit is depicted in magenta, the self-immolative linker depicted in blue and the released drug depicted in black.

A variety of H_2O_2-responsive prodrugs of anti-metabolite agents have been described, which use carbamate bonds to release the native amine of the parent drugs: gemcitabine (GEM),[203] doxorubicin (DOX),[120] methotrexate (MTX),[123,182] and melatonin (MLT)[116] (Figure 93). All carbamate-containing prodrugs afforded selective drug release with H_2O_2, resulting in potent cancer cytotoxicity *in vitro* and *in vivo*.[116,120,123,182,203] The arylboronate GEM prodrug exhibited reduced myelosuppression *in vivo* compared to the parent drug, as a result of its selective activation in cancer cells.[203]

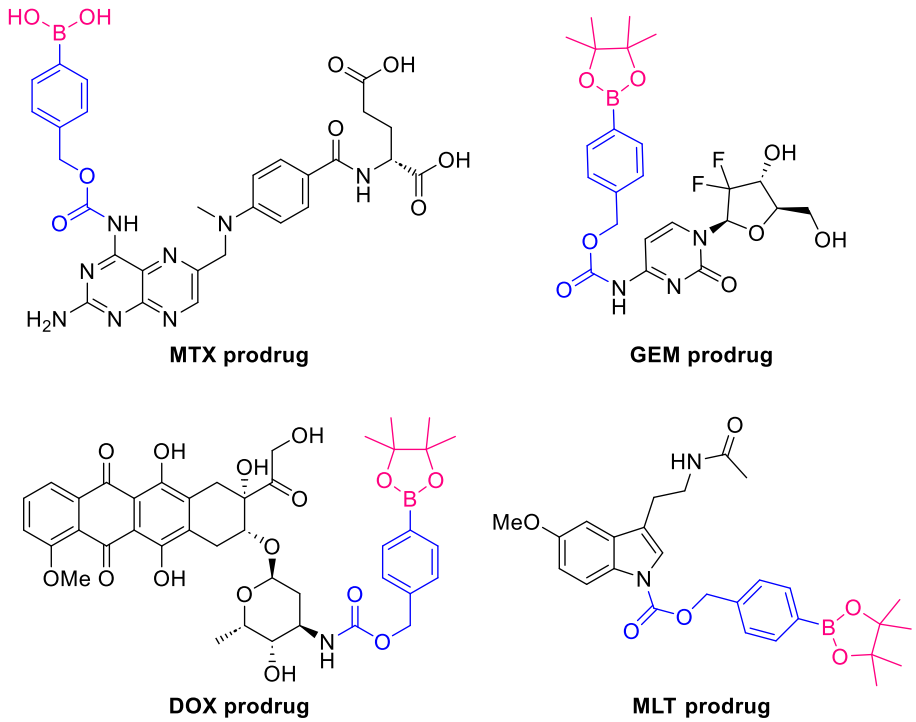

Figure 93: Structure of arylboronate anti-metabolite prodrugs of MTX,[123,182] GEM,[203] MLT,[116] and DOX.[120] The H_2O_2 responsive unit is depicted in magenta, the self-immolative linker depicted in blue and the released drug depicted in black.

Often, a carbamate bond is essential for facile release of amines by self-immolation. For example, a prodrug of aminotrexate (AMT) was examined with the pro-moiety directly attached to the aniline.[123] Whilst oxidation of the boronic acid to the phenol was complete within 2 h, immolation of the free drug by benzyl C-N cleavage was slow and remained incomplete after 48 h (Figure 94A).[123] Similarly, during the investigation of H_2O_2-responsive crizotinib prodrugs, a benzyl-linked aniline was unable to self-immolate, and remained as the stable phenolic intermediate (Figure 94B).[204] In contrast, an analogue bearing a carbamate linkage was able to self-immolate.[204]

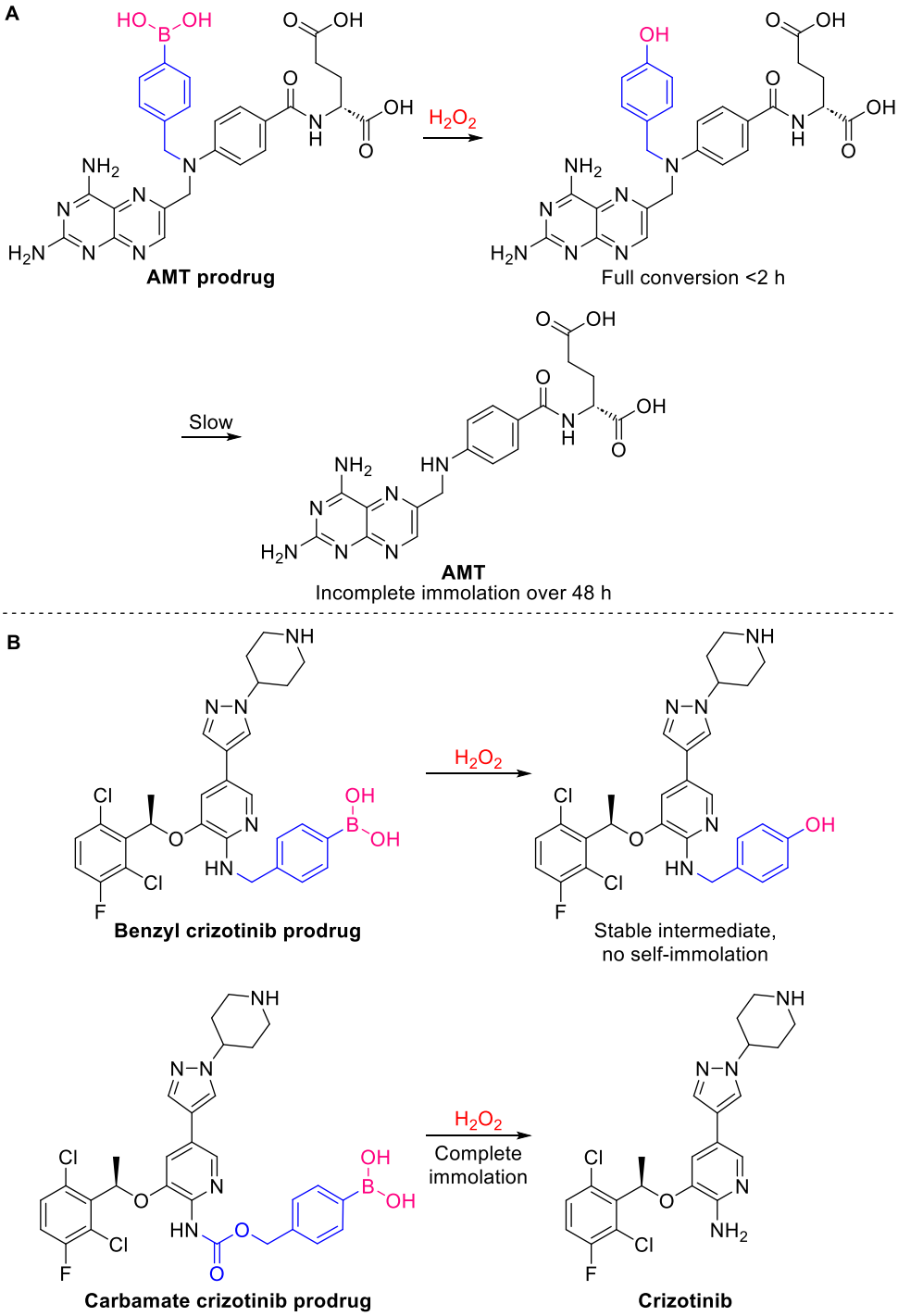

Figure 94: A) Unsuccessful self-immolation of an AMT prodrug where an aniline was attached to a para-hydroxybenzyl spacer directly,[123] B) unsuccessful self-immolation of a crizotinib prodrug where an aniline was attached to a para-hydroxybenzyl spacer directly, but successful self-immolative crizotinib prodrug when attached via a carbamate bond.[204] The H_2O_2 responsive unit is depicted in magenta, the self-immolative linker depicted in blue and the released drug depicted in black.

Arylboronate linkers have also been used to successfully liberate a heterocyclic amine, 5-fluorouracil (5-FU), to overcome serious side-effects of 5-FU treatment which include myelosuppression, central neurotoxicity and gastrointestinal toxicity (Figure 95).[205,206] The prodrug approach was also envisioned to minimise the metabolism of 5-FU, which limits its utility *in vivo*.[206] The 5-FU prodrug efficiently

reacted with H_2O_2 to liberate 5-FU, and gave potent growth inhibition against a panel of different cancer cell lines *in vitro*, but no toxicity against normal MEC1 cells up to 100 µM. Additionally the prodrug had improved safety and tolerability *in vivo*.

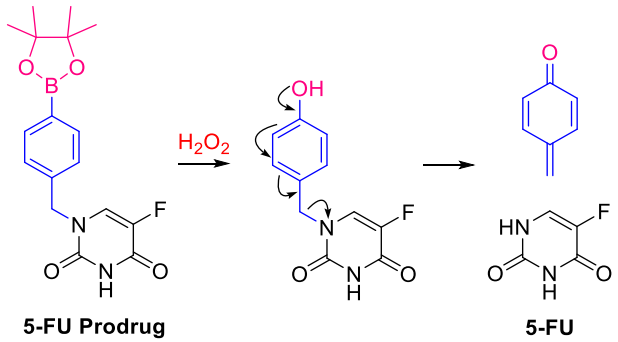

5-FU Prodrug 5-FU

Figure 95: Structure and activation of arylboronate 5-FU prodrug. The H_2O_2 responsive unit is depicted in magenta, the self-immolative linker depicted in blue and the released drug depicted in black.

H_2O_2-responsive prodrugs have also been generated of compounds which amplify the production of ROS for oxidation therapy: aminoferrocenes,[207–212] cinnamaldehyde,[213] and diethyldithiocarbamate.[214] Furthermore, the arylboronate/boronic acid prodrug approach has been applied to nanomaterials,[215–218] and theranostics,[137,212,219–221] whereby trigger activation releases the drug and a diagnostic agent simultaneously to allow concurrent treatment and imaging.

II.2 Aims & Outline

The utility of arylboronates as prodrug moieties has been exemplified by the large increase in interest in recent years. Several prodrugs have been explored and have demonstrated the ability of arylboronates and boronic acids to successfully modulate drug activity, whilst also allowing site-specific prodrug activation and thus improved tolerability and safety. Hence, there is continued interest in applying the H_2O_2-responsive prodrug strategy to other drugs with known off-target effects or safety shortcomings.

Section II of this thesis describes studies towards the development of H_2O_2-responsive prodrugs of small molecule anti-cancer agents: navitoclax, a drug that failed progression into the clinic due to activity against platelets which causes thrombocytopenia (Chapter 2),[222–224] and olaparib®, which suffers from off-target effects such as anaemia, thrombocytopenia, and neutropenia (Chapter 3).[225,226]

Chapter 2: Peroxide-Activatable Prodrug of Navitoclax

2.1 Introduction

2.1.1 BCL-2 Proteins as a Cancer Target

Apoptosis, or "programmed cell death" is highly regulated and involved in a number of biological processes such as normal cell turnover.[227] Apoptosis is controlled by members of the B-cell lymphoma (BCL-2) family of proteins which interact with each other by protein-protein interactions and are classified according to their role.[228–230] Anti-apoptotic or "pro-survival" proteins include Bcl-2, Bcl-x, Bcl-xL, Bcl-w and Mcl-1. Pro-apoptotic members include Bok, Bax and Bak, and also contain a sub-family of "BH3-only" proteins: Bid, Bad, Bim, Bik, Bmf, Puma, Noxa and Blk. The BH3-only proteins are antagonists of the anti-apoptotic proteins, inhibiting their activity upon binding. The balance of activity of the pro- or anti-apoptotic proteins is heavily regulated and ultimately determines whether a cell will live or die. However, this balance is often disrupted in pathological conditions. For example, upregulation of anti-apoptotic Bcl-2 protein expression allows increased binding of the pro-apoptotic BH3-only proteins, resulting in the protection of cancer cells from apoptosis. Bcl-xL and Bcl-2 are overexpressed in many cancers and are known to contribute to cell survival, tumour progression, and resistance to therapy.[230] Hence, the Bcl-2 family of proteins are an appealing druggable target for cancer therapy.

2.1.2 Small Molecule BCL-2 Inhibitors

There has been significant interest in the development of chemical inhibitors of the anti-apoptotic BCL-2 proteins, based on the premise that inhibitors occupying the hydrophobic BH3-binding groove would liberate pro-apoptotic BH3-proteins which can then fulfil their pro-apoptotic roles and cause cancer cell death.

Inhibitor development was largely pioneered by researchers at Abbott Laboratories (later Abbvie), who first performed high-throughput NMR-based structure-activity-relationship (SAR) experiments.[231] This resulted in the discovery of ABT-737 which was able to bind with sub nanomolar affinity to Bcl-xL, Bcl-2 and Bcl-w (Figure 96A). Crystallography of ABT-737 bound to human Bcl-xL revealed binding within two pockets: the chloro-biphenyl moiety binds in P2 and the thio-phenyl moiety engages P4.[232] However, despite achieving good binding affinity, ABT-737 suffered from poor oral bioavailability and aqueous solubility.[233] Efforts to improve the oral bioavailability then led to the development of ABT-263, later named navitoclax (Figure 96B-C).[233] Navitoclax retained high binding affinity, with a Ki of approx. 1 nM against Bcl-xL and Bcl-2, but impressively achieved 20-fold higher oral bioavailability than the original hit, ABT-737.[223,233]

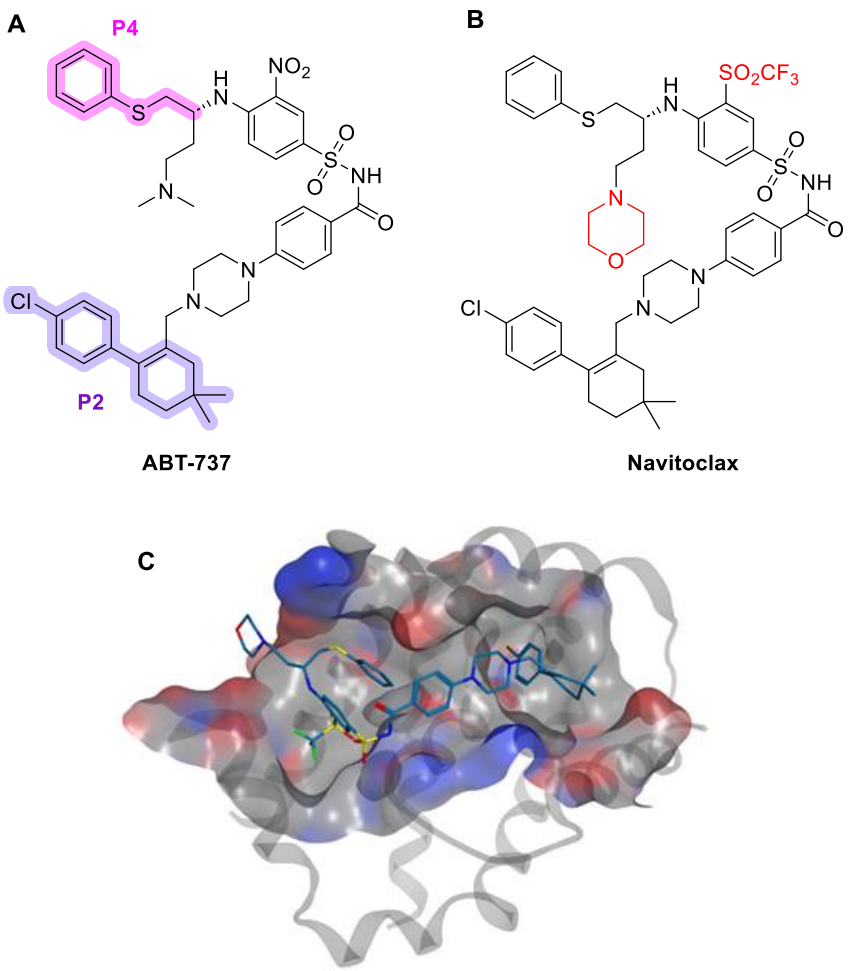

Figure 96: (A) The structure of ABT-737 with the moieties engaging P2 and P4 highlighted in purple and magenta respectively, (B) the structure of navitoclax, with the structural changes from ABT-737 highlighted in red, (C) the crystal structure of navitoclax (blue) bound to Bcl-xL (PDB: 4QNQ, visualised using MOE).

Although navitoclax progressed as a candidate to phase 2 clinical trials, its success was limited by a major dose-limiting toxicity, caused by "on-target" inhibition of Bcl-xL on circulating platelets. Since platelets rely on Bcl-xL for survival,[234,235] inhibition by navitoclax induces platelet apoptosis and thus causes dose-dependent thrombocytopenia.[222–224] Hence, the maximum efficacy that could be achieved by navitoclax whilst minimising platelet toxicity was inadequate for further clinical progression. Given that this side-effect only results from Bcl-xL inhibition, it was postulated that an inhibitor selective for Bcl-2 would prevent the toxicity against platelets. Although challenging, due to the high sequence homology between Bcl-2 and Bcl-xL, ABT-199 was developed (later named venetoclax, Venclexta®, Figure 97).[236] Venetoclax retained sub-nanomolar affinity for Bcl-2 (Ki <0.010 nM) but had 3-fold lower affinity than navitoclax for Bcl-xL (Ki = 48 nM) (Table 9).[236] Accordingly, the platelet activity was decreased >60-fold, and venetoclax had markedly reduced effects on platelets both *ex vivo* and *in vivo*.[236]

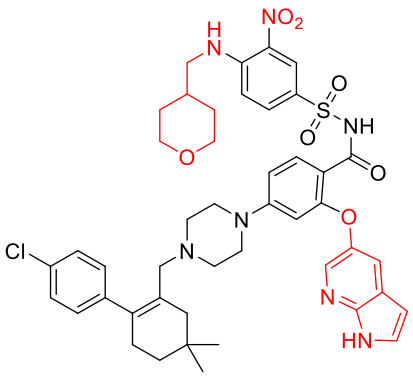

Venetoclax

Figure 97: The structure of Venetoclax (ABT-199) with structural differences from navitoclax highlighted in red.

Table 9: Comparison of the activities of navitoclax and venetoclax against Bcl-2 and Bcl-xL and their effect on platelets.

Drug	Binding affinity Bcl-2 (Ki)	Binding affinity Bcl-xL (Ki)	Platelet activity (EC_{50})	Comment
Navitoclax	~1 nM	~1 nM	0.08 µM	On-target platelet activity due to Bcl-xL inhibition causes dose-dependent thrombocytopenia
Venetoclax	<0.01 nM	48 nM	5.5 µM	Selective binding to Bcl-2 over Bcl-xL

Venetoclax has since been approved by the FDA for the treatment of chronic lymphocytic leukemia (CLL), small lymphocytic lymphoma (SLL), and in combination therapy for acute myeloid leukemia (AML).[237] However, for some solid tumours, treatment with venetoclax is ineffective because inhibition of Bcl-2 alone is inadequate.[228] Therefore, for the treatment of cancers which rely on both Bcl-2 and Bcl-xL for survival, dual inhibition of both proteins may be necessary. Furthermore, cancer cell resistance to venetoclax can be acquired by upregulation of Bcl-xL expression,[238] which decreases the reliance of the cancer on Bcl-2. Bcl-xL is also more commonly overexpressed in solid tumours and a subset of leukemia and lymphoma cells, therefore venetoclax has limited efficacy against these targets.[239–241] Taken together, there is still an unmet clinical need to develop a therapeutic which can target both Bcl-2 and Bcl-xL whilst avoiding on-target platelet toxicity, to enable application of Bcl-2 inhibitors to a wider range of cancers.

2.1.3 Bcl-2 PROTACs

PROTACs are proteolysis targeting chimeras, which are bifunctional molecules capable of binding a target protein and an E3 ligase simultaneously. The simultaneous binding and ternary complex formation initiates proteosome-mediated degradation of the target protein. Since E3 ligases are poorly

expressed in human platelets, but have high expression in various cancer cell lines, the PROTAC approach was considered for developing a cancer-selective targeted Bcl-xL/Bcl-2 therapeutic.[242–245]

Development of a PROTAC selective for Bcl-xL and Bcl-2 was explored by Zhou and Zheng *et al*.[238,244,245]: replacement of the solvent-exposed morpholine ring of navitoclax with a piperazine provided a linking amine for attachment of an E3 ligase binding unit (Figure 98). Although the resulting PROTAC DT2216 demonstrated rapid and long-lasting Bcl-xL protein degradation, moderate on-target platelet toxicity was still observed (but improved compared to navitoclax). In addition, the PROTAC was observed to only degrade Bcl-xL and not Bcl-2. This was a result of the lack of solvent-exposed lysine residues in Bcl-2 available for ubiquitination, meaning degradation of Bcl-2 could not be induced after Bcl-2 binding.[245] As a result, DT2216 had limited efficacy against cancers which rely on both Bcl-2 and Bcl-xL for survival.

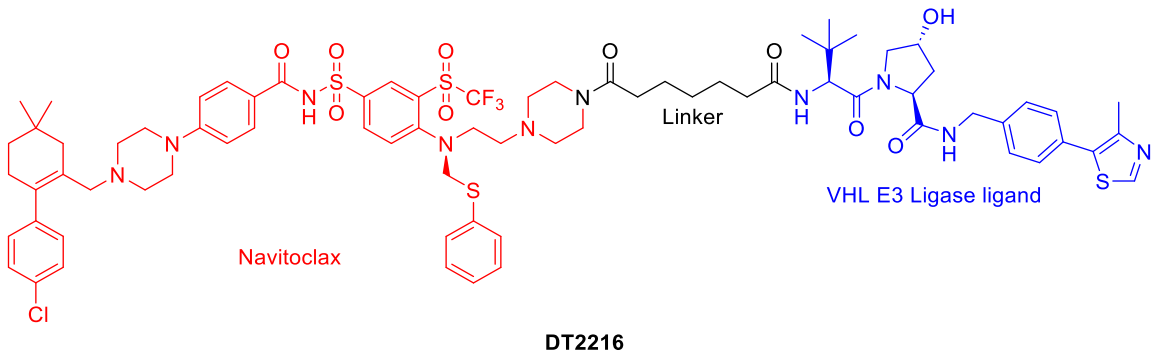

Figure 98: The structure of PROTAC DT2216, which acted as a Bcl-xL degrader, but was unable to cause Bcl-2 degradation.

It was envisioned that connecting a different position on navitoclax could encourage a different orientation of the Bcl-2 ternary complex formation, which could expose different lysines to enable ubiquitination of Bcl-2 as well as Bcl-xL. Thus, different PROTAC structures were investigated utilising an attachment point from the methyl group of the cyclohexene ring (Figure 99).[238] PROTAC 753b was 5-fold more potent at degrading Bcl-xL than DT2216 and importantly was also able to degrade Bcl-2.

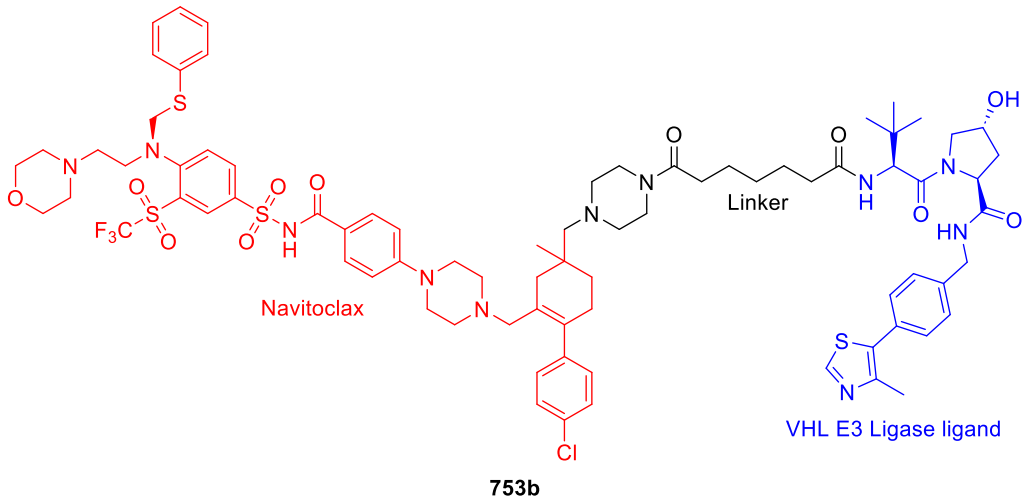

Figure 99: The structure of improved PROTAC 753b, which enabled degradation of both Bcl-2 and Bcl-xL.

A number of other dual Bcl-xL and Bcl-2 targeting PROTACs have been explored incorporating VHL or cereblon E3 ligase ligands and different Bcl-xL inhibitors, all of which displayed activity against cancer cells but not against platelets.[244,246]

2.1.4 BCL-2 Antibody-Drug Conjugate

Currently underway is a phase 1 clinical trial of ABBV-155 (mirzotamab clezutoclax),[247] an antibody-drug conjugate comprising a mirzotamab antibody targeting B7H3 (CD276) and Bcl-xL inhibitor clezutoclax. B7H3 is a transmembrane protein which is overexpressed in tumour tissues and has limited expression in normal tissues.[248] The proposed mechanism of action of the ADC involves binding to CD276 present on tumour cells followed by internalisation and linker cleavage to release Bcl-xL inhibitor clezutoclax, which then restores apoptotic processes in the cancer cell.[249] As a monotherapy or in combination therapy, mirzotamab clezutoclax has shown tolerable safety activity and anti-tumour activity in solid tumours.[250]

2.1.5 Navitoclax-Galactose Prodrug

Another method of achieving tumour-selective Bcl-2 inhibition is to develop site-activatable small molecule prodrugs. A navitoclax prodrug was explored by Muñoz-Espín *et al.* for specific targeting of senescent cells.[251]

The continued survival of senescent cells (cells which age, stop dividing but do not die) is commonly related to the overexpression of Bcl-xL.[251] The dysregulation of cellular senescence can cause accumulation of senescent cells, which can contribute to the development of multiple age-related disorders, cancers, and other diseases.[251–253] Hence, inhibition of Bcl-xL is an attractive approach to target senescent cells. To preclude the on-target platelet toxicity of navitoclax, it was modified by conjugation to an acetylated galactose, generating prodrug "Nav-gal" (Figure 100B). Since β-

galactosidases are often upregulated in senescent cells, the authors envisioned that Nav-gal could be site-selectively activated by β-galactosidase-cleavage of the pro-moiety (Figure 100A).

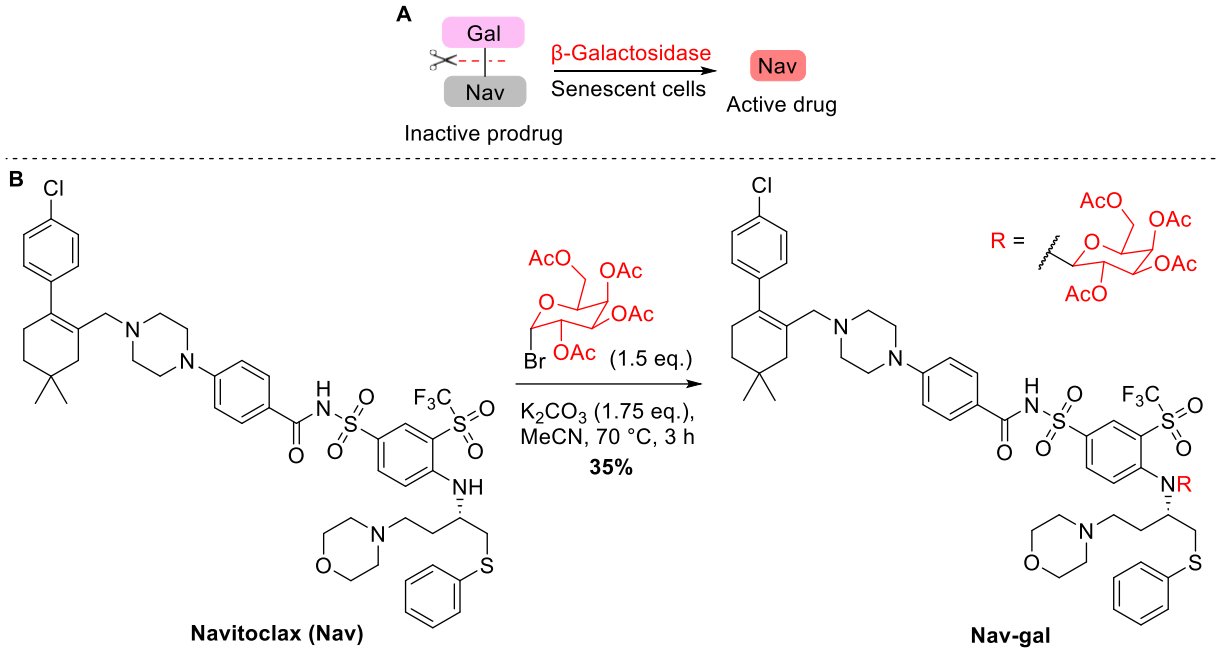

Figure 100: A) Activation of Nav-gal prodrug in senescent cells by β-galactosidase pro-moiety cleavage, B) the synthetic procedure for synthesis of Nav-gal prodrug. Red indicates the transformation.[251]

Like navitoclax, Nav-gal demonstrated greater activity against senescent cells compared to non-senescent cells (Table 10), presumably due to the increased importance of Bcl-xL in senescent cell survival. However, Nav-gal was able to achieve a greater "senolytic index", which indicates the difference in activity between senescent and non-senescent cells, due to its selective activation in cells with elevated β-galactosidases.

Table 10: Activity of navitoclax and Nav-Gal in various model senescent and non-senescent cell lines.

Cell Type	Navitoclax IC_{50} / μM	Nav-Gal IC_{50} / μM
Non-senescent A549	1.93	9.76
Senescent A549	0.12	0.28
"Selectivity" (senolytic index)	16-fold greater activity in senescent A549 cells	35-fold greater activity in senescent A549 cells
Non-senescent SK-Mel-103	0.028	0.125
Senescent SK-Mel-103	0.0011	0.0016
"Selectivity" (senolytic index)	25-fold greater activity in senescent SK-Mel-103 cells	78-fold greater activity in senescent SK-Mel-103 cells

When examined in cells with lowered β-galactosidase activity, navitoclax had similar potency, however, Nav-gal was significantly less potent, indicating that β-galactosidase was essential for the activity of the prodrug Nav-gal in senescent cells by activation *in situ*.

Finally, the platelet toxicity of Nav-gal was examined. *Ex vivo* experiments demonstrated that Nav-gal had significantly lower impact on platelet count compared to navitoclax in mice, and *in vivo,* Nav-gal did not cause thrombocytopenia in mice. In summary, the authors demonstrated that galacto-conjugation generated a prodrug with decreased activity in non-senescent cells, but potent activity in senescent cells due to activation by endogenous β-galactosidase.

2.2 Project Aims

Given the clinical significance of Bcl-2 and Bcl-xL for the treatment of cancer, new methods to target both proteins simultaneously whilst preventing the on-target toxicity on platelets experienced by navitoclax are desirable. Since success has been observed in generating a β-galactosidase-activatable prodrug, it was envisioned that a similar peroxide-activatable prodrug could be generated for broader targeting of cancer cells rather than senescent cells. To this end, navitoclax could be conjugated to an arylboronic acid prodrug handle, which would target the elevated levels of hydrogen peroxide in cancer.[103–105] Similar to Nav-gal, appendage of the arylboronic acid to the aniline of navitoclax is expected to modulate the activity of navitoclax in non-target cells, whilst enabling activation in the high-ROS environment of cancer (Figure 101). H_2O_2-mediated oxidation of the C-B bond to the resulting phenol could then undergo spontaneous 1,6-elimination to release the active drug at the site of action.

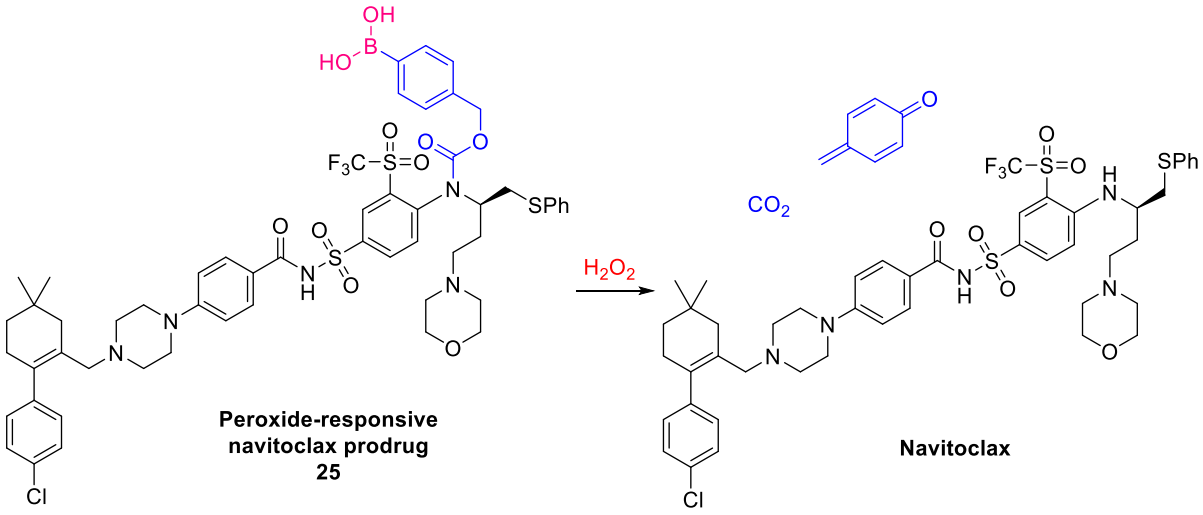

Figure 101: Proposed structure of a H_2O_2-activatable prodrug of navitoclax and its activation to release free navitoclax by boronic acid oxidation and linker self-immolation. The immolative linker is depicted in blue, and the ROS-responsive boronic acid in magenta.

Following synthesis of a peroxide-activatable navitoclax prodrug, its stability and kinetics of release with H_2O_2 will be investigated, and the activity examined compared to native drug. A successful prodrug should satisfy the following criteria:

1) Attachment of the H_2O_2-responsive aryl boronic acid moiety should significantly decrease the inhibitory activity of the prodrug against Bcl-xL compared to the native drug
2) The prodrug should be stable under physiological conditions, i.e., in plasma, to avoid off-target activity during circulation
3) The prodrug should be activated by pathologically relevant concentrations of H_2O_2, with favourable kinetics of immolation to release the active drug

4) The prodrug should achieve similar inhibitory potency *in vitro*/*in vivo* as the native drug and have an improved safety profile, including lower activity on platelets.

2.3 Results & Discussion

2.3.1 Aniline Analogue Synthesis

2.3.1.1 Late-stage functionalisation

PAB spacers are widely used as immolative linkers, and arylboronic acid linkers are able to release anilines through a carbamate bond by action of H_2O_2 (as demonstrated previously in this report: Section I, Chapter 1). Hence, initial prodrug design featured appendage of the arylboronic acid handle to the aniline of navitoclax via a carbamate bond (prodrug **25**, Scheme 10). Given the literature precedent for late-stage functionalisation of the aniline of navitoclax,[251] this was considered an attractive approach that could afford prodrug **25** in only one step from the commercial drug by reaction of the secondary aniline with an electrophile such as 4-BPin-benzyl chloroformate **26** (Scheme 10).

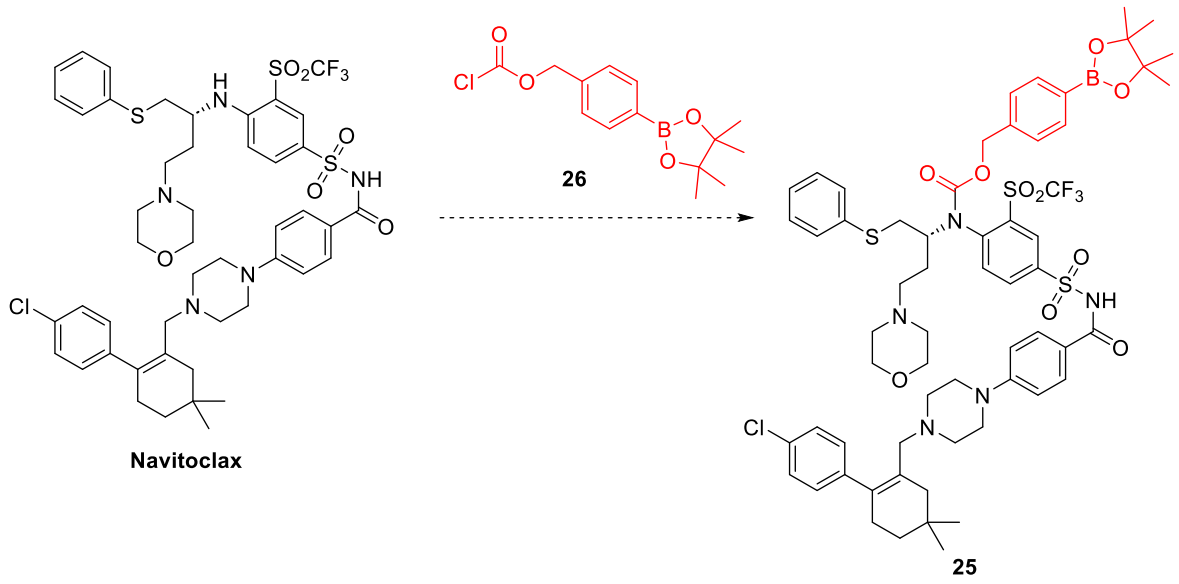

Scheme 10: Proposed reaction of 4-BPin-benzyl chloroformate **26** to afford H_2O_2-responsive carbamate prodrug **25**.

The synthesis and chromatographic isolation of BPin chloroformate **26** has previously been reported in the literature.[254] However, attempts to replicate reactions of 4-(Hydroxymethyl)phenylboronic acid pinacol ester **27** with triphosgene were unfruitful and it seemed in general that the product was too reactive to isolate (Table 11).

To preclude any complications associated with the handling and purification of boronic esters,[124] an alternative 4-Bromobenzyl chloroformate **28** was considered for synthesis, whereby a Miyaura borylation could install the boronic ester moiety after initial navitoclax modification (Scheme 11).

Table 11: Attempts to form chloroformate **26** by reaction of **27** with triphosgene.

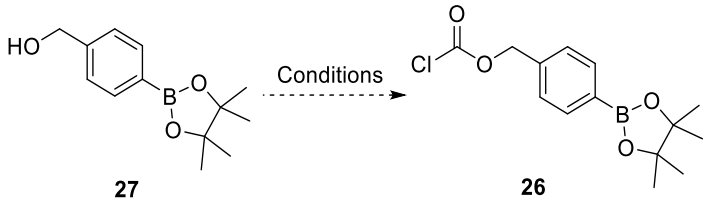

27 **26**

Entry	Conditions	Outcome
1	Triphosgene (0.7 eq.), NaOH (2 M, 1.7 eq.), CH_2Cl_2, rt	No desired reaction observed.
2	Triphosgene (0.5 eq.), pyridine (1.2 eq.), Et_3N (0.3 eq.), CH_2Cl_2, 0 °C then rt	Product degraded upon purification on silica.

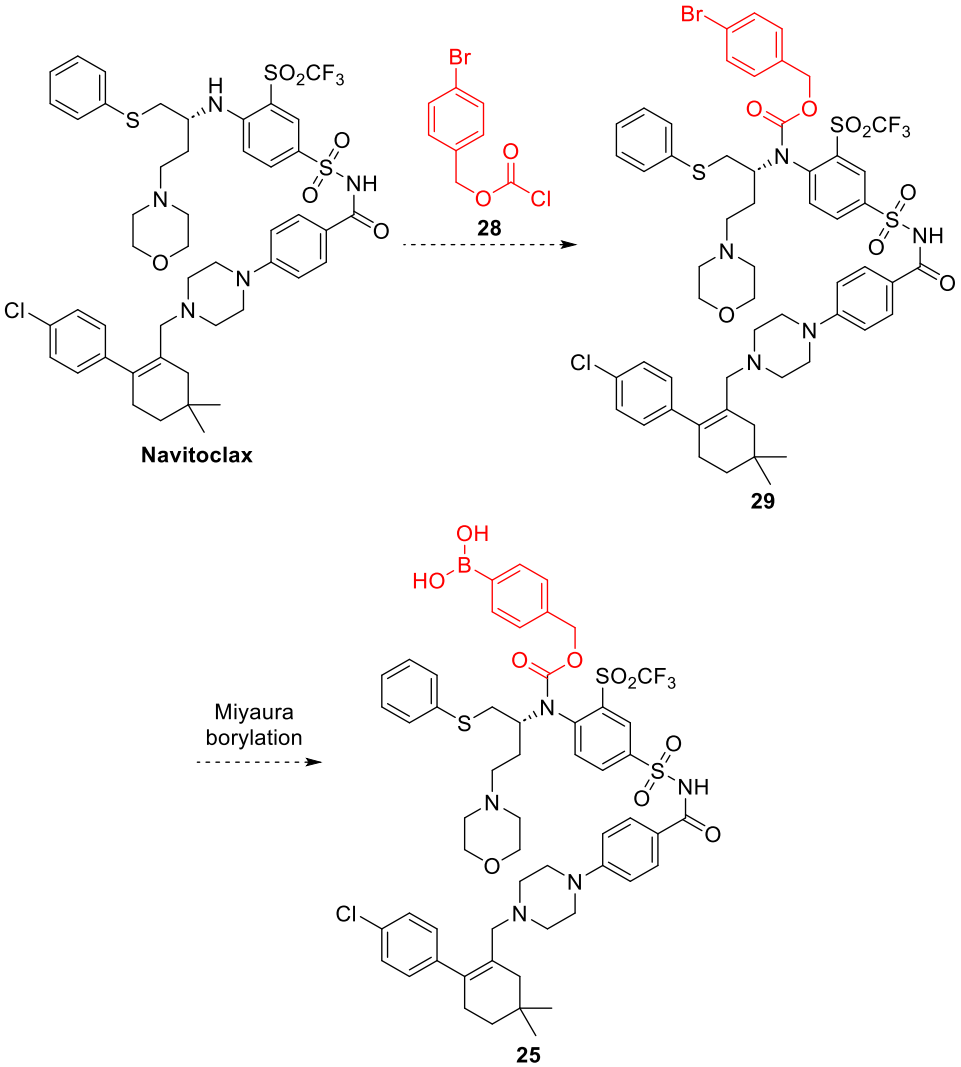

Scheme 11: Proposed alternative synthesis of navitoclax prodrug **25**, by reaction with 4-bromobenzyl chloroformate **28**, followed by Miyaura borylation.

However, synthesis of 4-bromobenzyl chloroformate **28** was also challenging due to the volatility of the product, which prevented its isolation after reverse-phase chromatography. The same problem was also encountered with the higher molecular weight iodo- analogue **30** (Scheme 12).

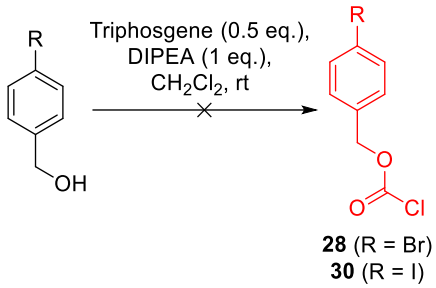

Scheme 12: Conditions for the attempted synthesis of 4-bromo- or iodo-benzyl chloroformates **28** and **30**.

Whilst attempts to isolate the product *via* distillation or by carrying forward crude into reaction with navitoclax were considered, success was achieved in the synthesis of alternative electrophiles **31** and **32**, activated as *para*-nitrophenyl carbonates (Table 12). Two different reaction conditions were employed, and electrophiles were generated with either the boronic ester group already installed (**32**), or a bromine (**31**) primed for later Miyaura borylation.

Table 12: Synthesis of activated para-nitrophenyl carbonates **31** and **32**.

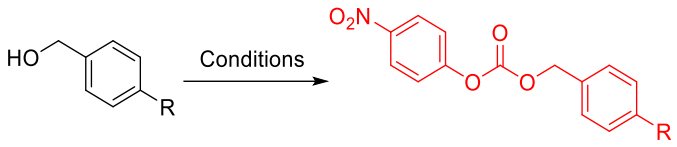

Entry	R =	Conditions	Yield
1	BPin (**32**)	Bis-4-nitrophenyl carbonate (2 eq.), DIPEA (1.5 eq.), CH_2Cl_2, rt, 1 h	63%
2	BPin (**32**)	4-nitrophenyl chloroformate (2 eq.), Et_3N (2.5 eq.), CH_2Cl_2, 0 °C then rt, 2 h	96%
3	Br (**31**)	4-nitrophenyl chloroformate (1.5 eq.), Et_3N (2.5 eq.), CH_2Cl_2, rt, 30 mins	96%

With activated BPin carbonate **32** in hand, the reaction with navitoclax was attempted using conditions previously used for the reaction of an amine (of MMAE) with an activated *para*-nitrophenyl carbonate (Table 13, Entry 1). However, in this case no desired reaction was observed, and the carbonate starting material **32** degraded. Alternative conditions sought to replicate the literature procedure for the

synthesis of the Gal-Nav prodrug,[251] which utilised K_2CO_3 in MeCN at elevated temperatures (Table 13, Entry 2). However again, no changes were observed other than carbonate degradation.

Table 13: Attempted reaction of activated carbonate **32** with navitoclax.

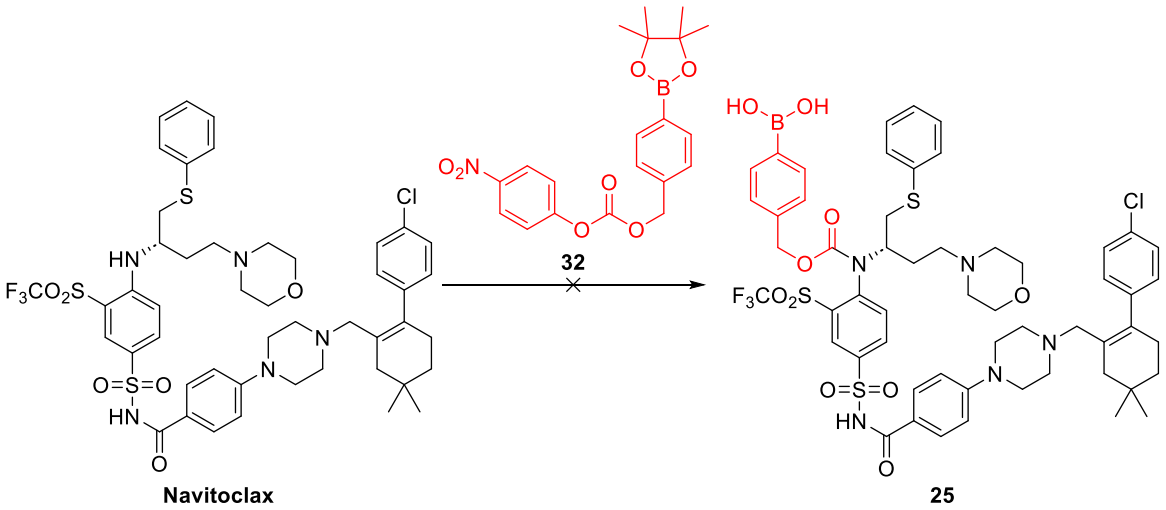

Entry	Conditions	Outcome
1	HOBt (1.5 eq.), DIPEA (1 eq.), pyridine (35 eq.), DMF, rt, 3 days	No reaction. Carbonate **32** degradation.
2	K_2CO_3 (1.75 eq.), MeCN, 70 °C, 3 days	No reaction. Carbonate **32** degradation.

It was discovered that the aniline of navitoclax is very unreactive: it is part of a very electron-poor ring bearing electron-withdrawing sulfonamide and triflate substituents. Thus, it is likely a very poor nucleophile, which might explain its inability to react with activated carbonate **32**. However, the aniline of navitoclax is reported to react in a substitution reaction with acetylated galactose-bromide (Figure 100).[251] Hence, it was envisioned that the reaction of navitoclax with a substituted aryl bromide might be similarly successful. This would generate benzyl analogue **33** which would require immolation *via* benzylamine C-N bond cleavage, which does not benefit from the entropic driving force of CO_2 release (Scheme 13). Although the release of anilines from such spacers is generally reported to be slow,[123,204] electron-withdrawing groups in conjugation with leaving groups are known to facilitate their release.[170] Since the aniline is part of an extremely electron-poor ring, it is hypothesised that self-immolation from **33** may be possible.

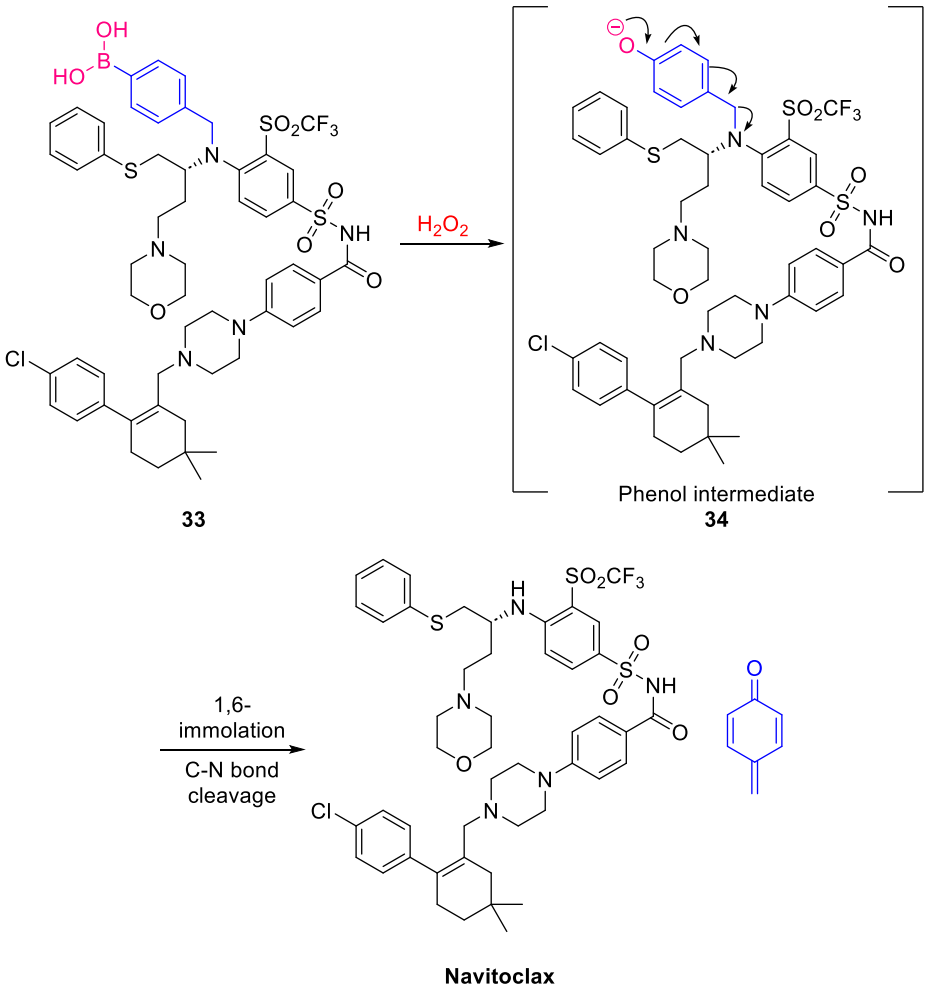

Scheme 13: Proposed mechanism of release from compound **33**, which involves cleavage of benzylamine C-N bond.

Using the conditions reported for the synthesis of Nav-gal,[251] reaction of navitoclax with 2-(4-(bromomethyl)phenyl)-4,4,5,5-tetramethyl-1,3,2-dioxaborolane **35** was attempted (Scheme 14). Reaction of navitoclax was observed by LCMS, however, multiple by-products formed, and conversion of starting material stalled at *ca*. 4 h.

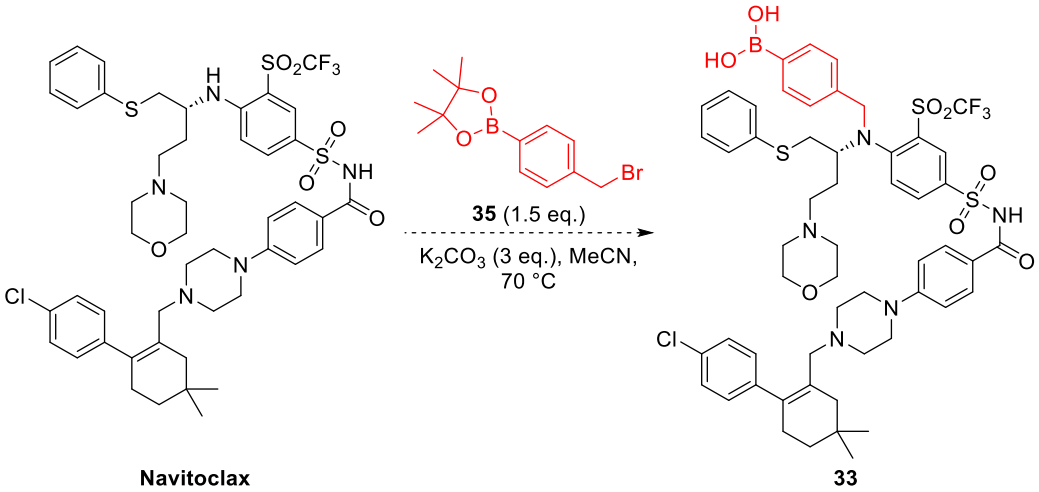

Scheme 14: Attempted synthesis of **33** *via* the substitution reaction of navitoclax with **35**.

Addition of potassium iodide accelerated the rate of conversion, during which an ion with mass corresponding to the boronic acid product **33** was observed by LCMS. Upon normal-phase purification, degradation of the reaction mixture was observed. The mixture was more stable to reverse-phase purification, however, the reaction profile contained multiple components which were poorly separated. With more careful inspection, it was clear that multiple structural isomers had formed, which are indistinguishable by mass spectrometry (Figure 102).

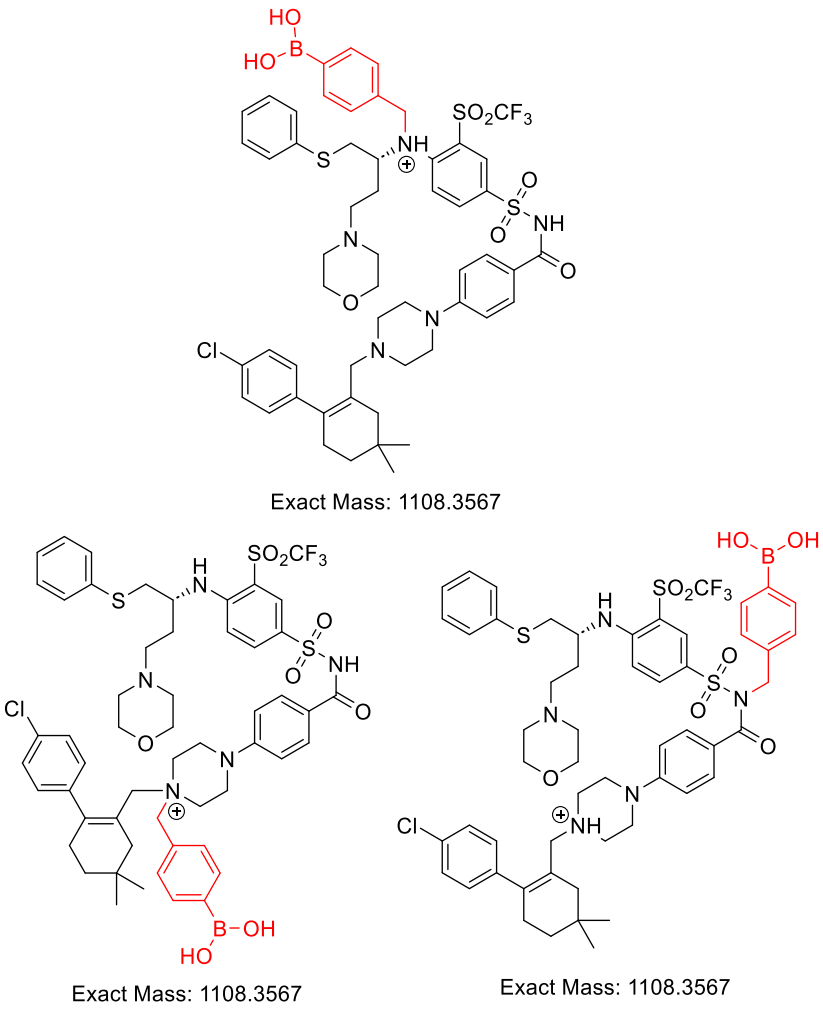

Figure 102: Proposed structural isomers formed during the substitution reaction of navitoclax with benzyl bromide **35**.

Given the difficultly in purifying the complex mixture that resulted from the reaction of navitoclax with pinacol boronate **35**, the reaction was repeated with the bromine analogue **36** instead (Scheme 15). This was envisioned to generate more easily separable products, by removing potential complications from the purification of mixtures of boronic acids and boronic esters.[124] Following successful synthesis of benzyl bromide **37**, a Miyaura borylation could then access **33**.

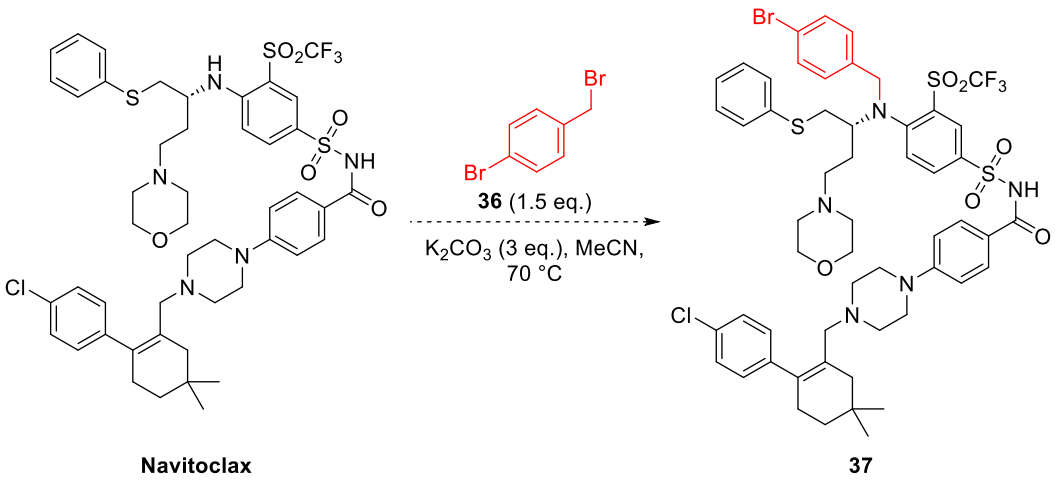

Scheme 15: Attempted synthesis of **37** *via* the substitution reaction of navitoclax with 4-bromobenzyl bromide **36**.

Unfortunately, the reaction profile for reaction of navitoclax with **36** was still extremely complex with the formation of multiple products, and purification was equally challenging as the boronic ester analogue. However, one pure chromatographic fraction was isolated, which was subjected to characterisation for regioisomeric identification. Each regioisomer should have distinct heteronuclear multiple bond correlations (HMBC) by NMR, which would allow reliable assignment (Figure 103). Additionally, if the isolated species was not modified at the desired aniline position, a HMBC coupling would be observed between the chiral carbon CH and the NH of the unfunctionalised aniline (magenta arrow, Figure 103). The aniline NH can be identified by its high chemical shift and lack of signal in ^{1}H-^{13}C HSQC spectra.

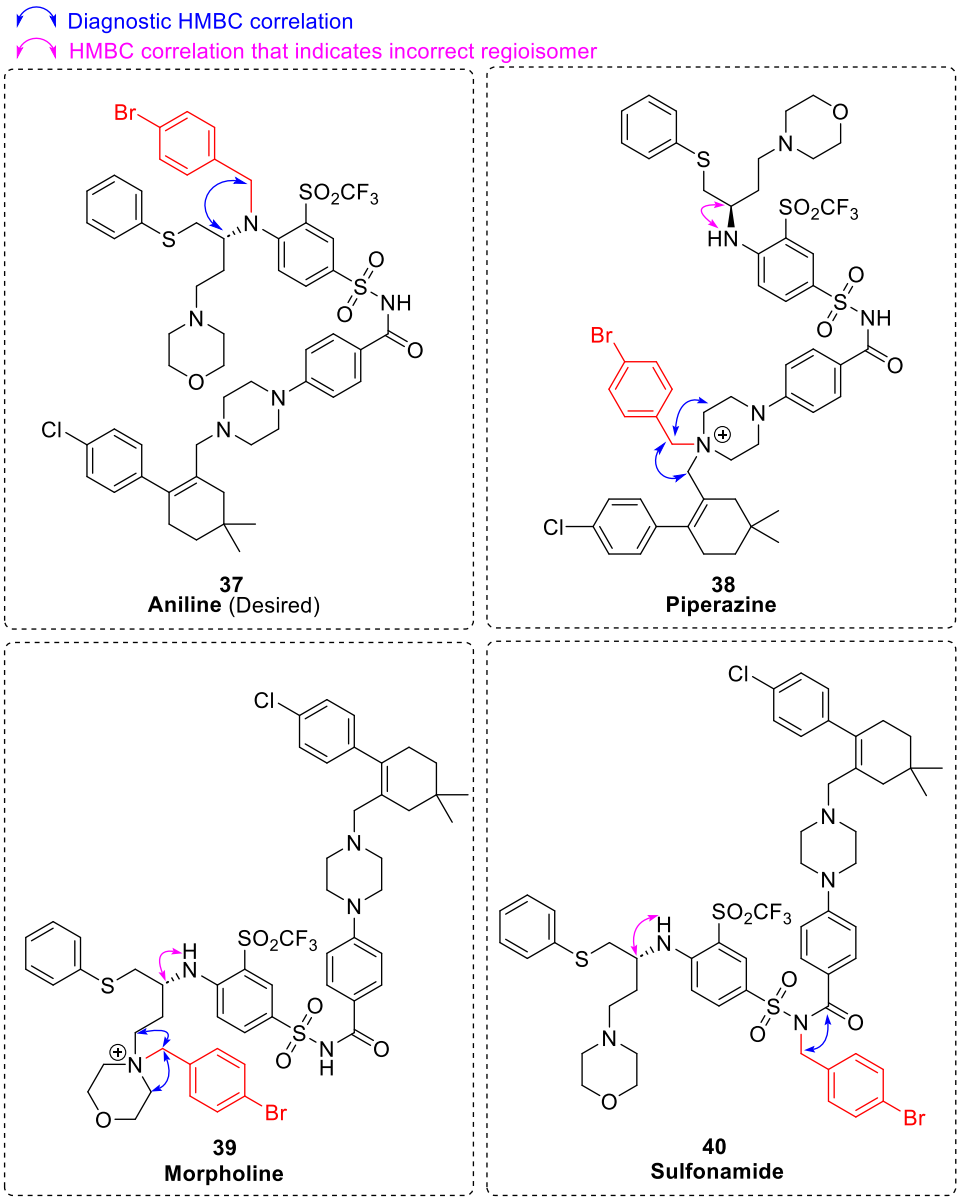

Figure 103: Proposed diagnostic HMBC correlations (blue arrows) for the various structural isomers produced by the reaction of navitoclax with 4-bromobenzyl bromide **36**. Magenta arrows indicate the diagnostic aniline ^{1}H-^{13}C HMBC correlation that would be observed for each regioisomer other than the desired.

Accordingly, 2D NMR analysis (HMBC and ROESY) confirmed that the isolated component was the morpholine isomer, **39** (Figure 104 and Figure 105). Although it may be interesting to investigate whether this regioisomer would act as an effective prodrug of navitoclax, insufficient material was isolated for further investigation. Given the poor reaction yields from the expensive drug starting material and challenging purification, re-synthesis of this isomer (or others) was not pursued further by late-stage functionalisation.

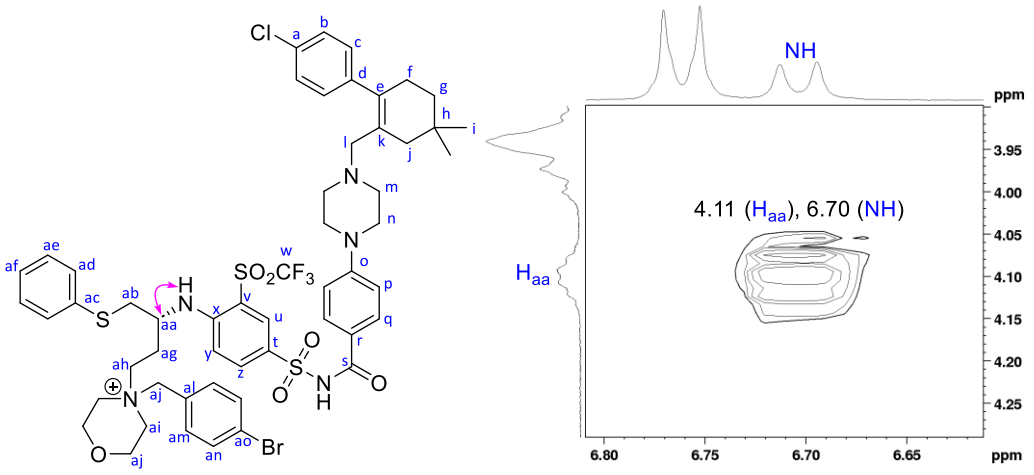

Figure 104: COSY correlation (magenta arrow) between aniline NH and H_{aa} indicates that the desired position has not been modified.

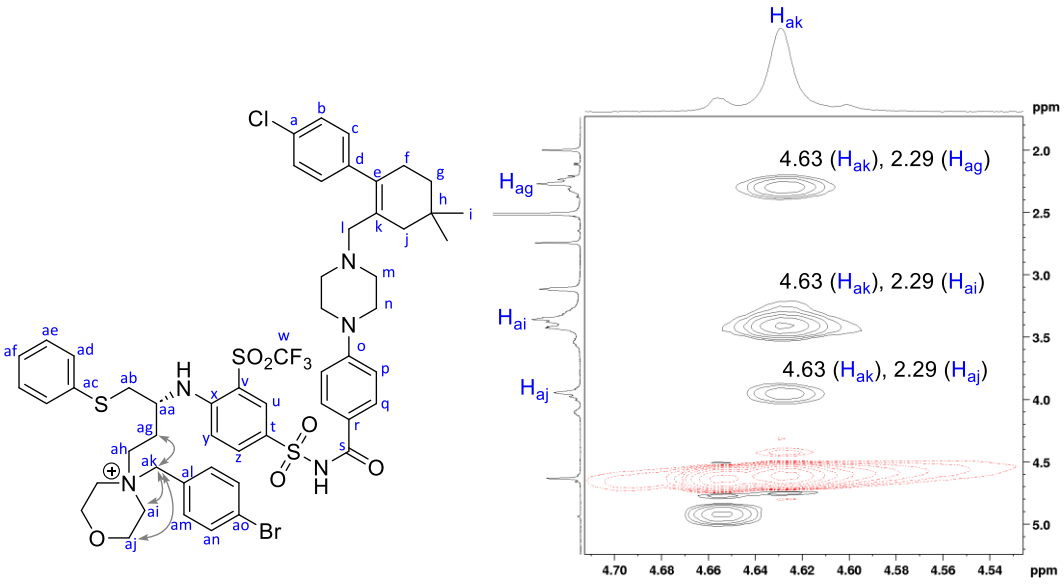

Figure 105: ROESY correlations confirm the morpholine substituted regioisomer structure 39. ROESY correlations are shown by grey arrows.

Other attempts for late-stage functionalisation of navitoclax included reductive amination with model benzaldehyde (Table 14, Entry 1) and amide formation using conditions reported to be successful for the reaction of unreactive, electron-deficient amines,[255] (Table 14, Entry 2). However, in all cases no reactivity was observed.

Table 14: Attempts at late-stage reductive amination or amide formation of the aniline of navitoclax.

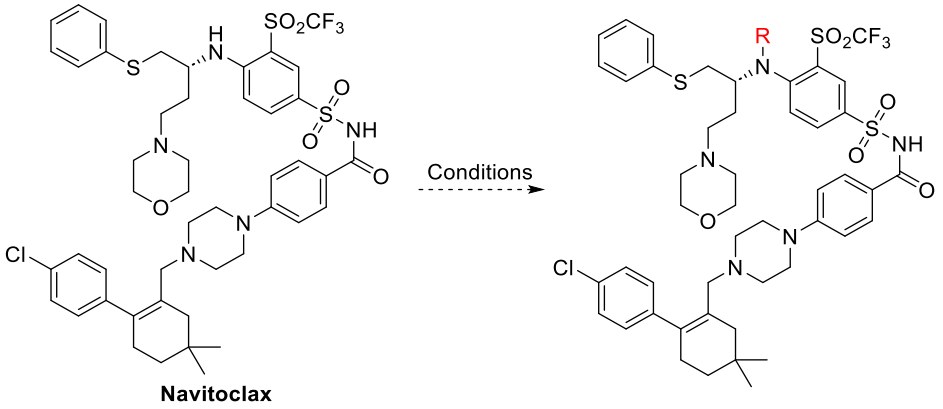

Entry	Reaction Type	R	Conditions	Outcome
1	Reductive amination	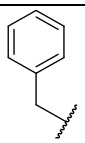	Benzaldehyde (1.1 eq.), $NaBH(OAc)_3$ (1.2 eq.), HOAc (0.5 eq.), DCE, rt.	No reaction
2	Amide formation	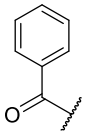	Benzoic acid (1.1 eq.), DIPEA (5 eq.), BTFFH[a] (1.1 eq.), CH_2Cl_2, 40 °C	No reaction
3	Amide formation	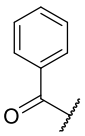	Benzoic acid (1.1 eq.), DIPEA (5 eq.), BTFFH[a] (1.1 eq.), CH_2Cl_2, microwave, 80 °C	No reaction

[a] BTFFH = Fluoro-N,N,N',N'-bis(tetramethylene)formamidinium hexafluorophosphate

Finally, to further investigate the reactivity and regioselectivity of the reactions of navitoclax, the reported literature reaction of navitoclax with 2,3,4,6-tetra-*O*-acetyl-α-D-galactopyranosyl bromide was attempted (Scheme 16).[251] ^{1}H NMR of the crude reaction mixture indicated complete consumption of navitoclax and new distinct signals, however, FCC purification of the mixture returned unfunctionalised navitoclax, suggesting degradation upon purification. Other components isolated by purification did not correspond to the desired product. Hence, no further information was gained on whether the reported literature reaction yields the correct regioisomer to aid further work towards the late-stage functionalisation of navitoclax.

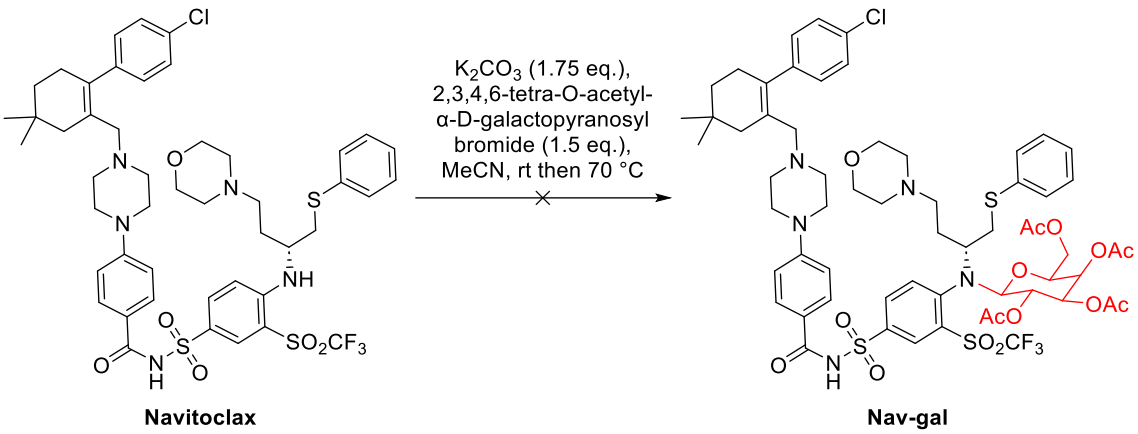

Scheme 16: Unsuccessful reaction towards Nav-gal following reported literature procedure.[251]

2.3.1.2 Fragment modification

Several challenges were discovered during attempts to modify navitoclax by late-stage functionalisation: (1) the aniline is unreactive and poorly nucleophilic due to the very electron-poor aryl ring, and (2) late-stage functionalisation yields complex mixtures due to the presence of multiple reactive amine sites, which were difficult to purify. Thus, an alternative fragment synthesis approach was considered whereby the reactive prodrug handle is introduced onto the aniline (1) prior to it becoming poorly reactive, and (2) before the introduction of competing basic amines in the molecule.

As such, retrosynthetic analyses of both "carbamate" (**25**) or "benzyl" (**33**) modified navitoclax prodrugs were performed (Scheme 17). First, it was considered that the boronic acid handle should be introduced in the last synthetic step to preclude challenges with handling and purification of boronic esters/acids.[124] This would be achieved by incorporating a Miyaura borylation from aryl bromide **29** or **37** as the final synthetic step. Aryl bromides **29** or **37** can be disconnected to reveal amide coupling partners, sulfonamides **41** and **42,** and carboxylic acid **43**, which can be synthesised in three synthetic steps reported in the literature.[256] Then, disconnection of the sulfonamide ring gives functionalised chiral amines **45** and **46** which could undergo S_NAr with commercially available sulfonamide **44**. Amines **45** and **46** could be synthesised from the reaction of commercially available chiral amine **49** with the electrophilic prodrug handles **36** or **48**.

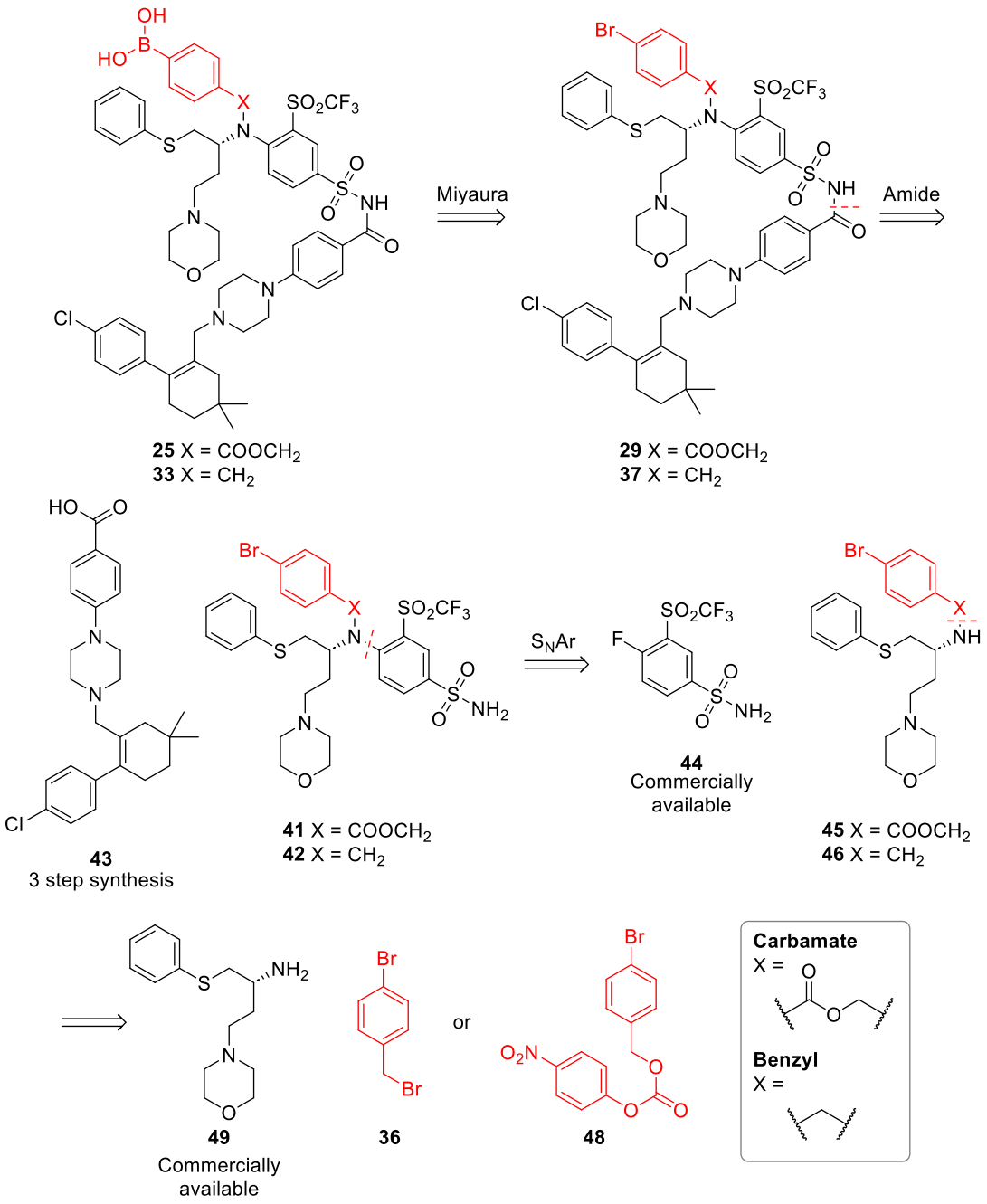

Scheme 17: Disconnection approach towards navitoclax prodrugs **33** and **25**, which installs the prodrug handle at the desired amine prior to its incorporation into an electron-poor aryl sulfonamide, and prior to the introduction of other competing basic amines.

In the forward synthesis, chiral amine **49** was reacted with 4-bromobenzyl bromide **36** to generate the benzyl amine **46**. Simple S_N2 reaction conditions were first employed, with slight excess of the amine starting material in an attempt to disfavour double alkylation (Table 15, Entry 1). This gave moderate yields, with minor product corresponding to double alkylation product **50**. Alternative conditions utilising reductive amination with 4-bromo benzaldehyde were also attempted (Table 15, Entry 2), however the double addition product **50** was still observed, and the overall yield was slightly lower owing to incomplete reduction of the imine, which was difficult to separate from the desired product.

Optimisation of this reaction could have included careful monitoring to ensure all starting amine was converted to the imine prior to the addition of reducing agent, as well as use of a stronger reducing agent such as $NaBH_4$ to ensure full imine reduction. However, enough material was obtained, so further reaction optimisation was not performed.

Table 15: Synthetic procedures to afford benzyl-modified chiral amine **46**.

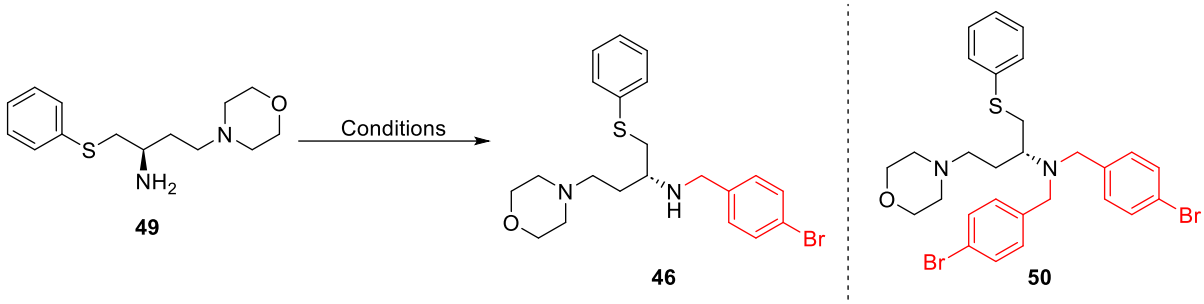

Entry	Reaction Type	Conditions	Outcome
1	Substitution	4-Bromobenzyl bromide (0.8 eq.), DIPEA (1 eq.), CH_2Cl_2, rt, 24 h	**46** (**55%**) Minor product = **50**
2	Reductive amination	4-Bromobenzaldehyde (1 eq.), $NaHB(OAc)_3$ (1.4 eq.), DCE, rt, 24 h	**46** (**36%**) Minor product = **50**

To generate the carbamate analogue **45**, two conditions were attempted. First, the isocyanate of chiral amine (**50**) was generated *in situ* with triphosgene for reaction with 4-bromobenzyl alcohol (Scheme 18). Although this was successful, the yield was poor, and a minor by-product was isolated corresponding to urea **51** from the self-reaction of the isocyanate with residual unfunctionalised **49**. Therefore, reaction with 4-bromobenzyl *para*-nitrophenyl carbonate **31** was investigated instead. First, **31** was synthesised in quantitative yields from the reaction of 4-bromobenzyl alcohol with *para*-nitrophenyl chloroformate. Then, reaction of **31** with amine **49** gave carbamate product **45** in moderate yield, with no major by-products.

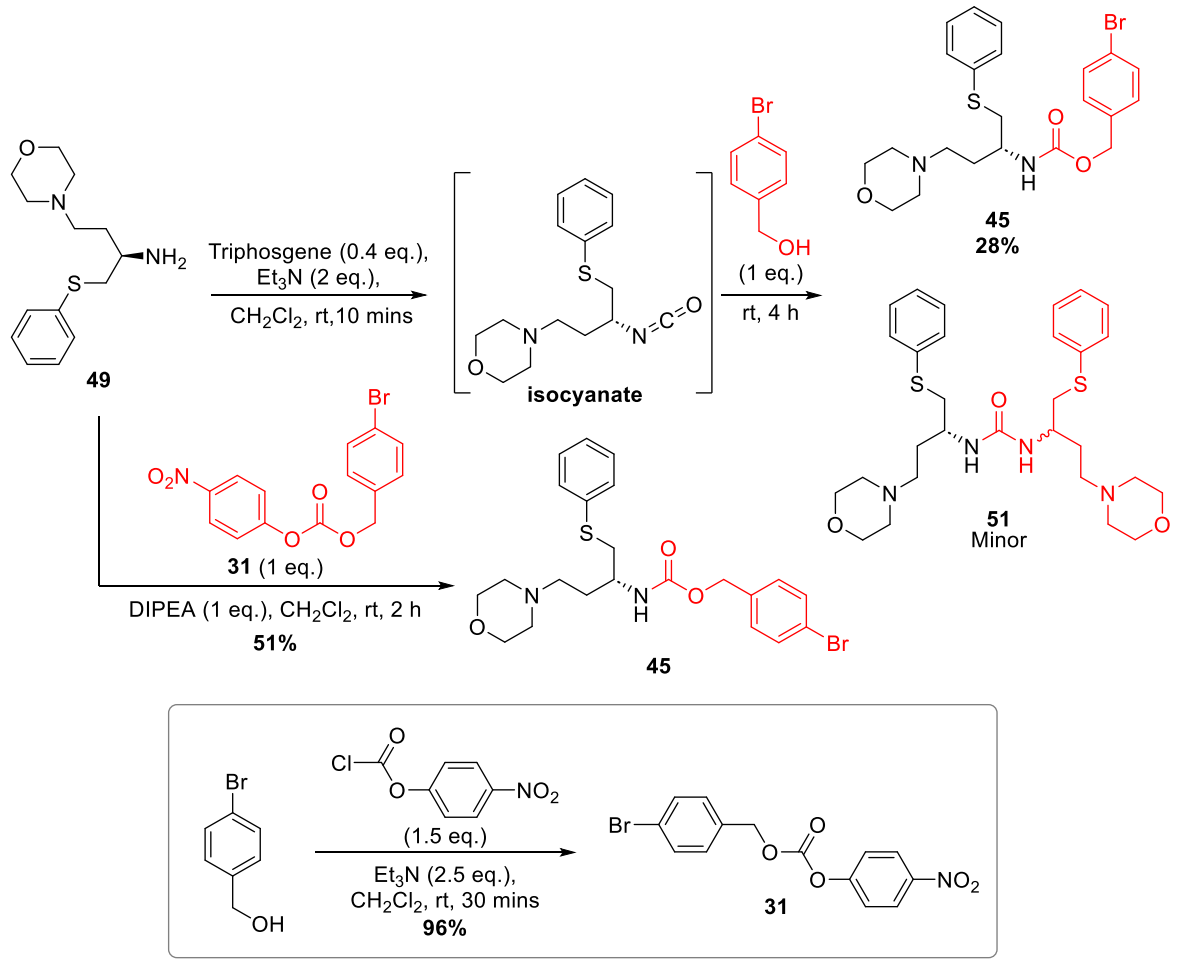

Scheme 18: Synthetic routes towards **45**.

With both prodrug-handle functionalised chiral amines **45** and **46** in hand, the ability of the amine to perform S_NAr reaction with sulfonamide **44** was investigated. Initially, both amines **45** and **46** were subjected to S_NAr conditions reported in the literature with DIPEA in DMSO (Scheme 19).[256] However, the desired product was not observed to form and instead, the reaction yielded unreacted starting material and by-product **52** formed by self-reaction of sulfonamide starting material **44**.

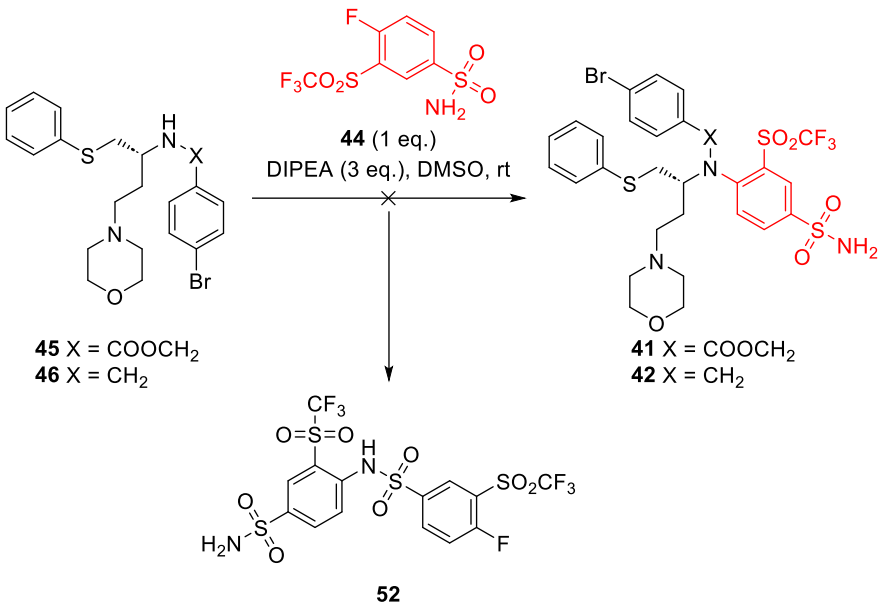

Scheme 19: The unsuccessful S_NAr reaction towards **41** and **42** which instead afforded bis-sulfonamide adduct **52**.

Attempts to change the order of addition, stirring amines **45**/**46** in base (DIPEA) and DMSO with slow addition of the sulfonamide **44** were also unsuccessful, returning a small amount of the bis-sulfonamide adduct **52** and unreacted starting material. There was little change in the reaction profile upon heating to 80 °C for a prolonged period of time (~20 h), except for an increase in bis-sulfonamide adduct **52**. Alternative conditions were attempted during which **45** and **46** were treated with LDA at -78 °C prior to the addition of the sulfonamide **44**. However, the reaction profiles for these reactions were extremely complex, with multiple by-products and no identification of the mass of the desired products by LCMS. Attempted reactions without any base present were also unsuccessful.

Given the inability to react amines **45** and **46** with the sulfonamide **44**, it was envisioned that protection of the sulfonamide nitrogen may prevent formation of the undesired bis-sulfonamide adduct **52** and allow the desired reaction to occur. Such protecting group would be removed following S_NAr reaction. *para*-Methoxy benzyl (PMB) and di-methoxy benzyl (DMB) groups are commonly used for sulfonamide protections and can be deprotected in mild acidic conditions.[257] Installation of PMB or DMB moieties usually commence from reaction of a sulfonyl chloride with protected PMB-amine (Scheme 20A). However, since the amine of the sulfonamide appears to be reactive, it was envisaged that an S_N2 reaction with PMB-Cl could install the desired protecting group (Scheme 20B). Unfortunately, in basic conditions (DIPEA), the only observed reaction was formation of the bis-sulfonamide adduct **52**. A second attempt without base saw no reaction when the sulfonamide **44** was added slowly to a solution of PMB-Cl, and even with heating to 80 °C overnight, no reaction was observed.

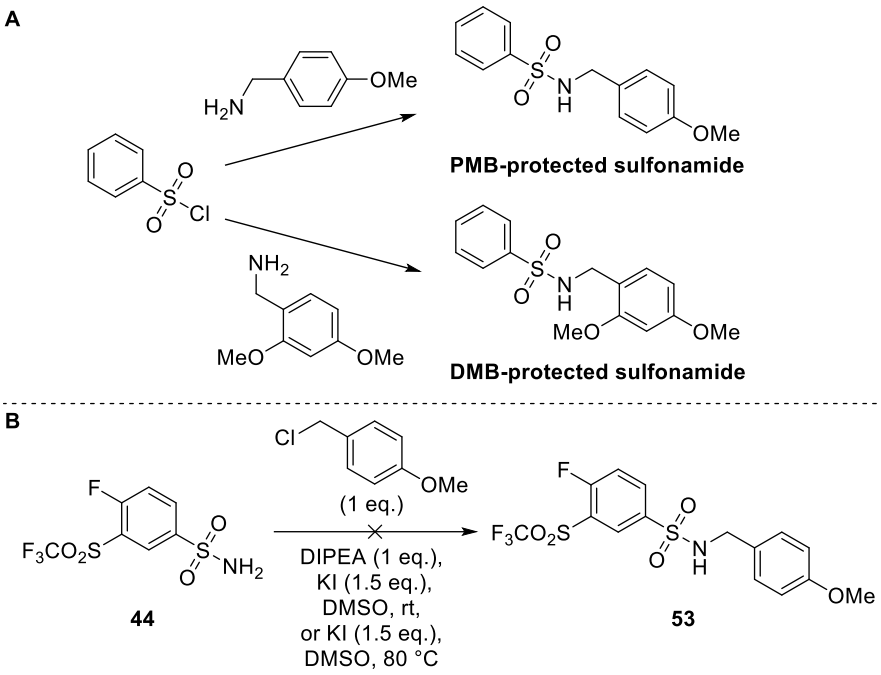

Scheme 20: A) Common methods for the generation of protected sulfonamides from sulfonyl chlorides, B) attempted PMB protection of sulfonamide **44** by S_N2 reaction.

tert-Butyloxycarbonyl (Boc) was then considered as an alternative protecting group. Pleasingly, reaction of sulfonamide **44** with Boc-anhydride yielded Boc-protected sulfonamide **54**, albeit in poor yield with long reaction times (Scheme 21).

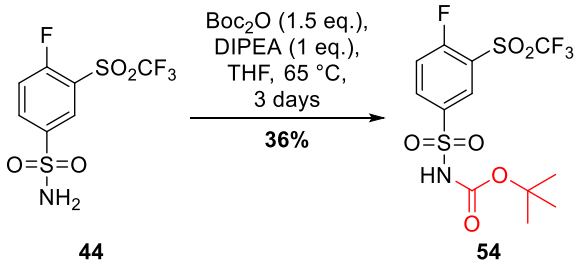

Scheme 21: Synthesis of Boc-protected sulfonamide **54**.

With protected sulfonamide **54** in hand, the S_NAr reaction with chiral amine **46** could be attempted (Table 16). After several days at rt, reaction of **46** was observed, and purification isolated a component with promising ^1H NMR spectra. On scale-up, however, no reaction was observed even with prolonged reaction times and heating to 80 °C (Table 16, Entry 1b). Alternative reaction conditions involving treatment of chiral amine with LDA at -78 °C prior to sulfonamide addition resulted in a complex mixture in which no desired product mass was observed by LCMS (Table 16, Entry 2).

Table 16: Attempted reaction of Boc-protected sulfonamide **54** with benzyl-modified amine **46**.

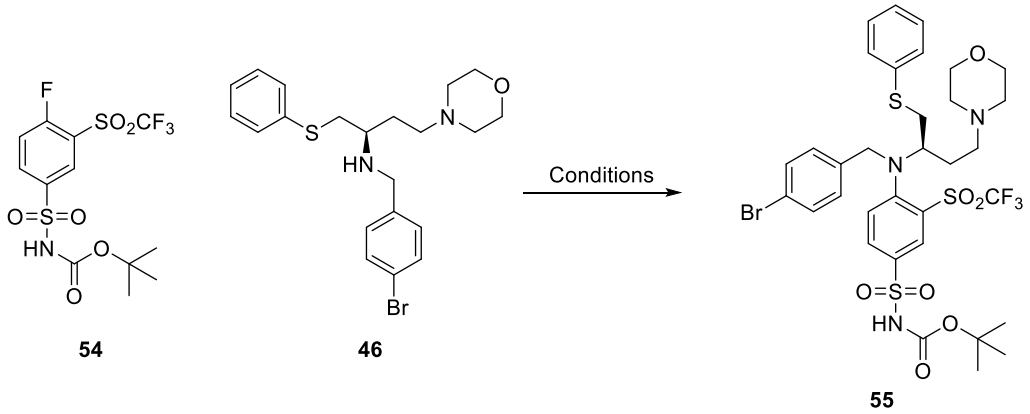

Entry		Conditions	Outcome
1	**a**	DIPEA (3 eq.), DMSO, rt, 3 weeks	Tentative isolation of product
	b	DIPEA (3 eq.), DMSO, rt, 3 weeks, then 80 °C	No reaction
2		**46** (1 eq.), LDA (1 eq.), -78 °C, then **54** -78 °C then rt	Complex mixture

Similarly, no reaction was observed between carbamate modified chiral amine **45** with Boc-protected sulfonamide **54** (Scheme 22). The LDA reaction was not attempted since it only returned a complex mixture with **46**.

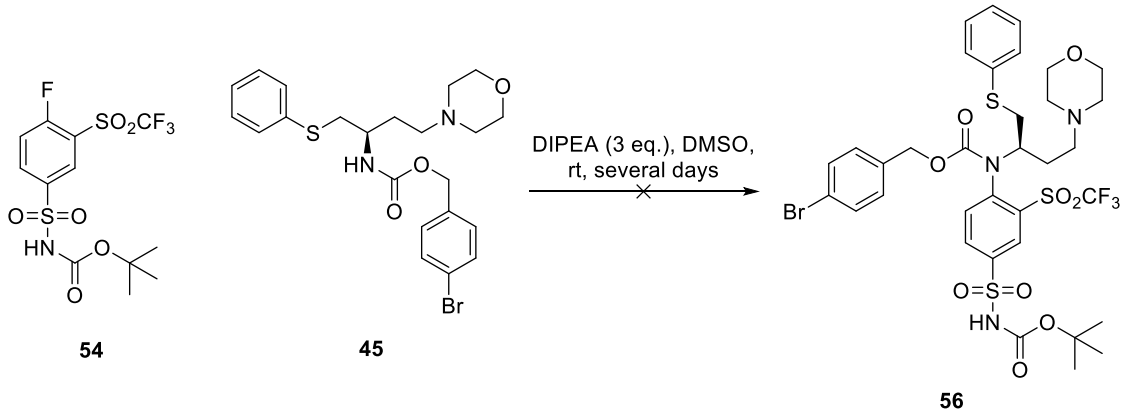

Scheme 22: Unsuccessful reaction of Boc-protected sulfonamide **54** with prodrug-modified amine **45**.

Failure to access tertiary amines **55** or **56** *via* S_NAr with Boc-protected sulfonamide **44**, combined with a lack of alternative synthetic routes which circumvent issues with the poor nucleophilicity of the amine once incorporated as an aniline, resulted in halting efforts to synthesise tertiary amine prodrugs **25** and **33**.

2.3.2 Alternative Analogues

Given that peroxide-cleavable navitoclax prodrugs modified at the aniline position were synthetically inaccessible, further work sought to investigate whether other positions of navitoclax could be modified to generate a prodrug. As was discovered during attempts to modify navitoclax at the aniline, there are many other reactive amines present in the structure of navitoclax. In fact, the only pure navitoclax analogue synthesised and isolated was substituted at the nitrogen of the morpholine ring (**39**, Figure 106).

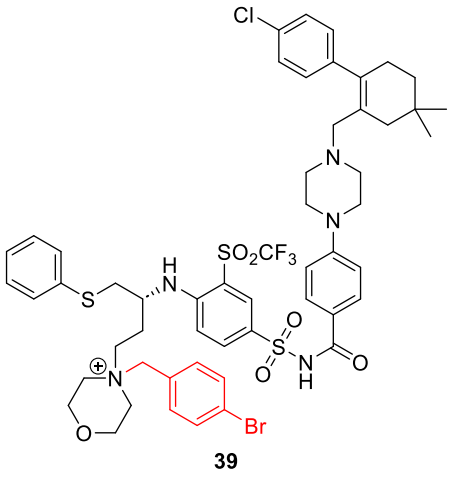

39

Figure 106: The only isolated analogue of navitoclax, substituted on the morpholine nitrogen, **39**.

To assess whether modification of the morpholine nitrogen may impact the binding ability of a navitoclax prodrug, the key ligand interactions in the crystal structure of navitoclax bound to Bcl-xL were examined (Figure 107, PDB: 4QNQ). The morpholine nitrogen has binding interactions with Glu96, therefore modification at this position might negatively impact the binding ability of navitoclax. Similarly, the piperazine motif seems to fit into a narrow binding pocket, therefore modification at this position also has the potential to disrupt binding to generate an inactive prodrug.

Prodrug handle installation at the morpholine or piperazine nitrogens would produce quaternary ammonium prodrugs, which are precedented as suitable self-immolative linker leaving groups (see Section II.1.2.1).[173–175,198] Release of such quaternary amines can occur through benzyl-amine linkages, without requiring carbamate bonds, hence these were considered for prodrug design.

The morpholine motif is quite solvent-accessible, whereas the piperazine motif fits more closely in the centre of the binding pocket. Additionally, a Bcl-xL PROTAC substituted the morpholine oxygen to allow linker attachment, and the resulting structure was still able to bind Bcl-xL.[238,244,245] Taken together, modification of the piperazine ring might have greater influence on Bcl-xL binding than modification of the morpholine ring, so a piperazine prodrug was considered first for synthesis (Figure 108).

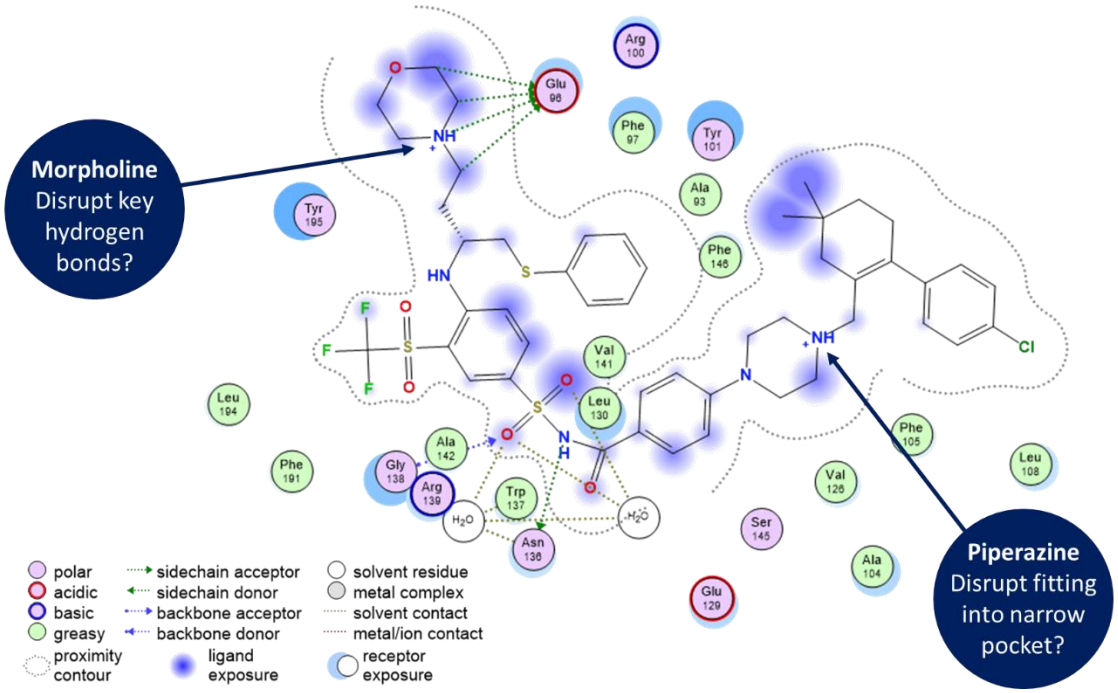

Figure 107: Ligand site interactions of navitoclax bound to Bcl-xL (PDB: 4QNQ).

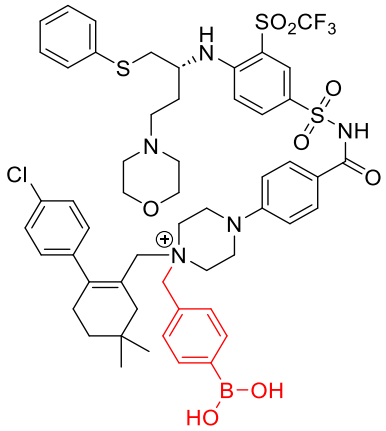

57
Piperazine-modified navitoclax prodrug

Figure 108: Structure of proposed piperazine-modified navitoclax prodrug, **57**.

2.3.2.1 Piperazine substituted analogue

A late-stage functionalisation approach for the synthesis of piperazine prodrug **57** was predicted to be problematic due to the presence of multiple basic amine sites, as previously experienced. Hence, a route was envisaged whereby the prodrug handle would be introduced early in the synthesis, possessing a bromo substituent for Miyaura borylation of **38** as the final synthetic step (Scheme 23). Care would need to be taken such that competitive Miyaura borylation at the aryl-chloride of **38** would not occur. Bromo benzyl piperazine analogue **38** can be disconnected to the commercially available chiral amine **49** and S_NAr electrophile **58**. An amide bond disconnection then gives **59** and commercially

available sulfonamide **44**. Attaching the sulfonamide nitrogen by the amide bond prior to S_NAr was envisioned to circumvent the known issues with self-S_NAr to form the bis-sulfonamide adduct **52** (*vide supra*). Then, the prodrug handle could be installed from piperazine **60**. The synthesis of **60** is reported in the literature, starting from the S_NAr of piperazine **65** with protected 4-fluorobenzoate **66**, followed by a Mannich reaction with 4,4-dimethyl cyclohexanone **63**, then Grignard addition of **61** and **62** followed by dehydration to give **60**.[256]

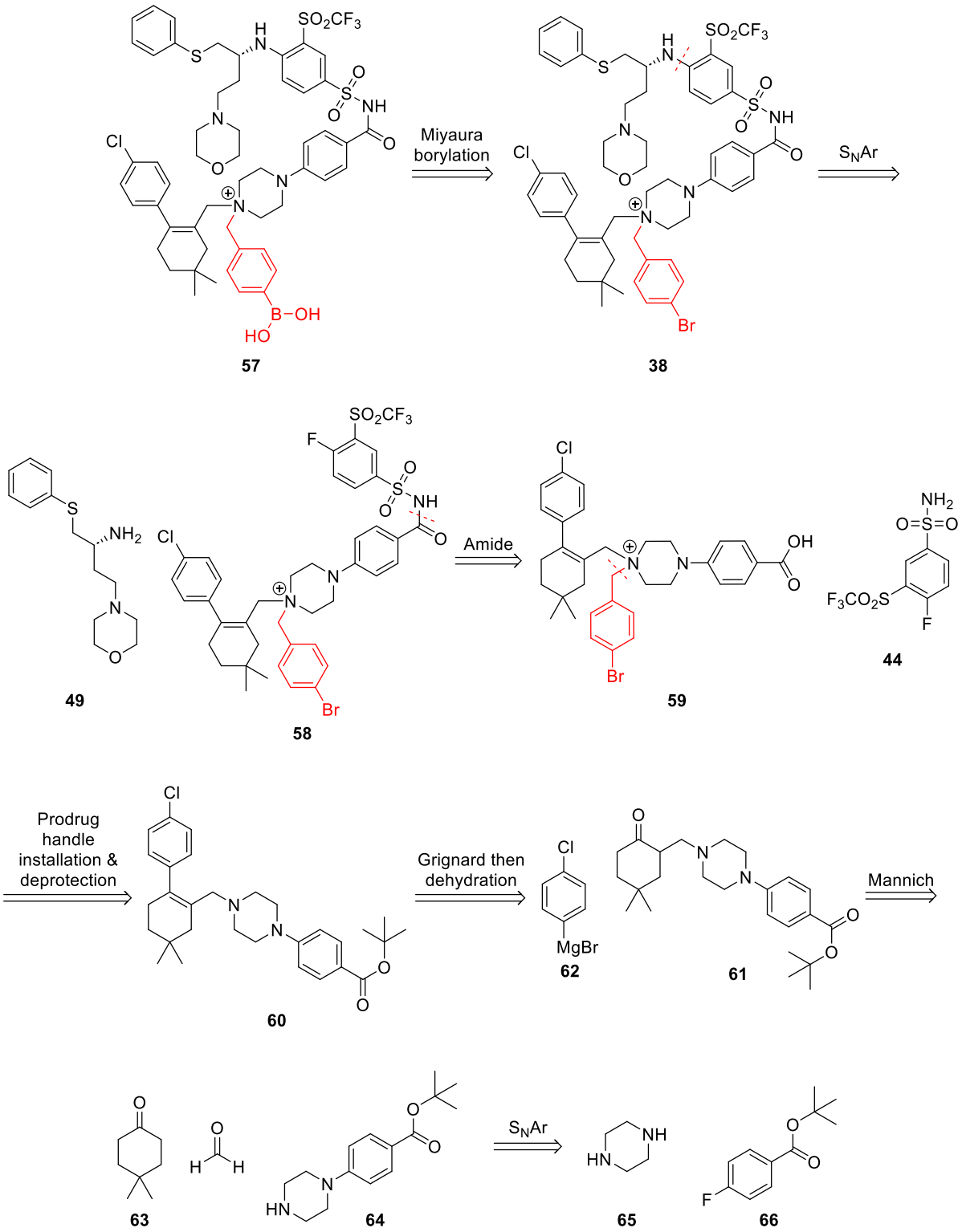

Scheme 23: Retrosynthetic analysis of piperazine prodrug **57**.

First, synthesis of tert-butyl 4-(piperazin-1-yl)benzoate **64** was successful *via* literature S_NAr reaction of *tert*-butyl 4-fluorobenzoate **66** in good yield (Scheme 24).

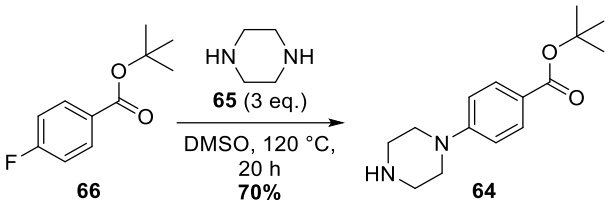

Scheme 24: Synthesis of **64** from the S_NAr reaction of tert-butyl 4-fluorobenzoate **66**.

However, the subsequent Mannich reaction with 4,4-dimethyl cyclohexanone **63** following literature conditions was unsuccessful (Table 17, Entry 1). Minimal conversion to a compound with the desired product mass was observed by LCMS and attempts to isolate this component by FCC as reported in the literature were unsuccessful. Alternative conditions were employed using DMSO instead of ^{t}BuOH for improved solubility, and with the addition of molecular sieves to remove water and encourage imine formation (Table 17, Entry 2). However, again, only minimal amounts of a compound with desired product mass were observed by LCMS, so purification and isolation were not pursued.

Table 17: Attempted Mannich reaction to form **61**.

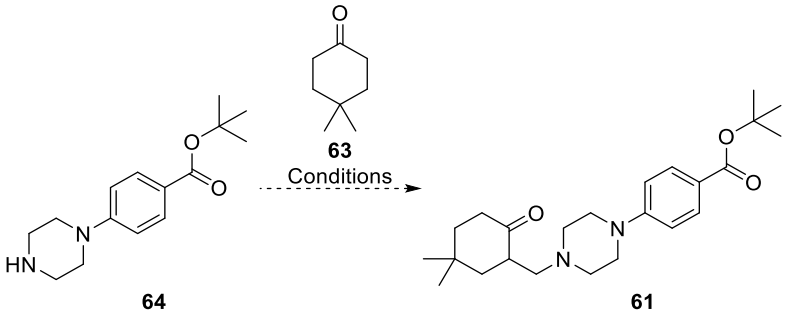

Entry	Conditions	Observations	Outcome
1	**63** (1.5 eq.), paraformaldehyde, conc. HCl, ^{t}BuOH, reflux >3 h	Suspension	Trace product mass observed by LCMS. Conversion stalled and could not be isolated by FCC.
2	**63** (1.5 eq.), paraformaldehyde, conc. HCl, DMSO, molecular sieves, 120 °C, 3 h	Full dissolution	Trace peak with product mass in LCMS. No conversion with further time. Isolation not pursued.

An alternative synthetic route reported in a patent employs a one-pot carbonylation/bromination of dimethylcyclohexanone **63** with DMF and PBr_3, followed by reductive amination with the piperazine analogue to afford the amino methylated compound **69** (Scheme 25)**.**[258] A Suzuki reaction between **69** and 4-chlorophenylboronic acid **70** followed by ester hydrolysis could then afford the final deprotected carboxylic acid **43**.

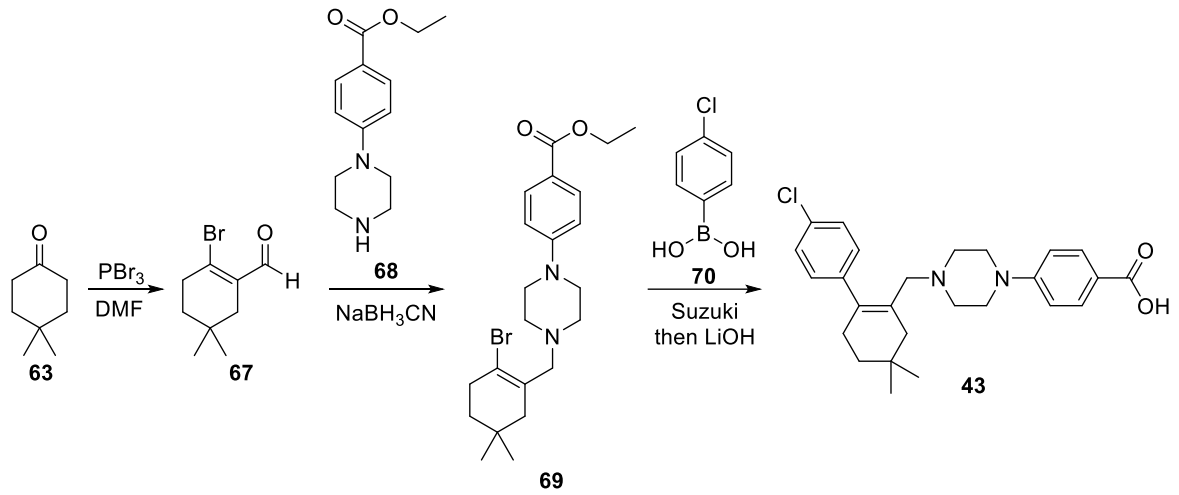

Scheme 25: Reported synthetic route towards fragment **43** utilising one-pot carbonylation/bromination followed by reductive amination then Suzuki reaction.[258]

Having already synthesised piperazine-*tert*-butyl benzoate **64**, the patent synthesis was attempted with this substrate, predicting that the small change in carboxylic acid protecting group would be equally tolerated (Scheme 26).

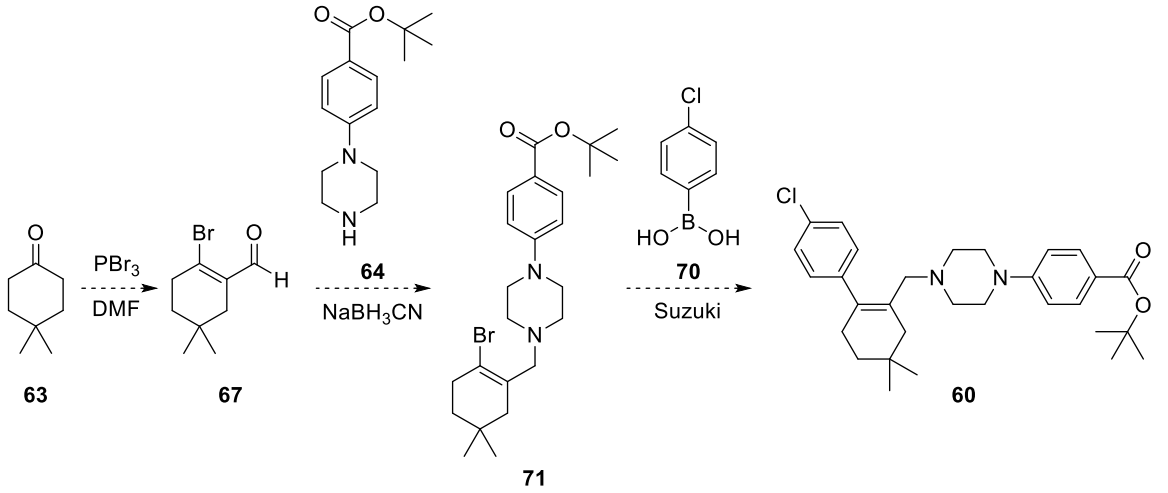

Scheme 26: Alternative synthetic route towards piperazine intermediate **60**.

Commencing from 4,4-dimethylcyclohexanone **63**, the literature reported one-pot bromination/carbonylation conditions were replicated in moderate yield to afford aldehyde **67** (Scheme 27).

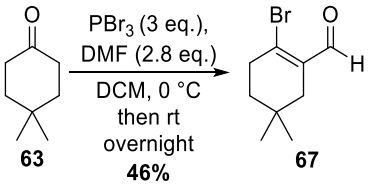

Scheme 27: Successful synthesis of aldehyde **67**.

Aldehyde **67** was then subjected to reductive amination with piperazine **64**. However, the one-pot reductive amination procedure reported in the patent yielded mainly reduced aldehyde (**72**, 28% yield), and only 6% desired product **71** (Table 18, Entry 1). A different approach sought to form the imine completely from **64** and **67** before addition of the reducing agent, to prevent unwanted aldehyde reduction (Table 18, Entry 2). However, a complex mixture was obtained, and normal-phase purification did not isolate any pure product. Subsequent reverse-phase purification also did not yield anything corresponding to the desired product. Using molecular sieves and alternative reducing agent $NaBH(OAc)_3$ was also unsuccessful (Table 18, Entry 3), as were attempts to change the solvent (Table 18, Entry 4).

Table 18: Attempted reductive amination to afford **71**.

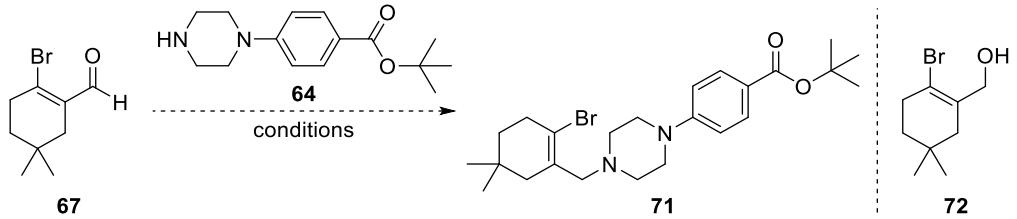

Entry	Solvent	Reducing Agent	Procedure	Outcome
1	EtOH	$NaBH_3CN$	Mix **64** and **67** in EtOH, add $NaBH_3CN$ then AcOH	**64** (65%), **72** (28%), **71** (6%)
2	EtOH	$NaBH_3CN$	Mix **64** and **67** overnight in EtOH, then add AcOH and $NaBH_3CN$	Messy normal-phase FCC, then subsequent reverse-phase FCC isolated unknown component not corresponding to product.
3	EtOH	$NaBH(OAc)_3$	Mix **64** and **67** in EtOH, molecular sieves, then add $NaBH(OAc)_3$	No reaction
4	THF and Toluene	$NaBH_3CN$	Mix **64** and $NaBH_3CN$ in THF, stir 15 mins, add **67** in toluene	No reaction

Given that the reductive amination towards **71** was unsuccessful, alkylation was considered as an alternative strategy. Since the product of single alkylation is a sterically hindered tertiary amine, it was predicted that double alkylation to generate **74** would be unfavourable and could be controlled by reaction conditions and the number of equivalents used. First, alkyl-bromide **73** required synthesis. It

was envisaged that it could be afforded easily from already synthesised aldehyde **67** *via* aldehyde reduction and PBr_3 substitution (Scheme 28).

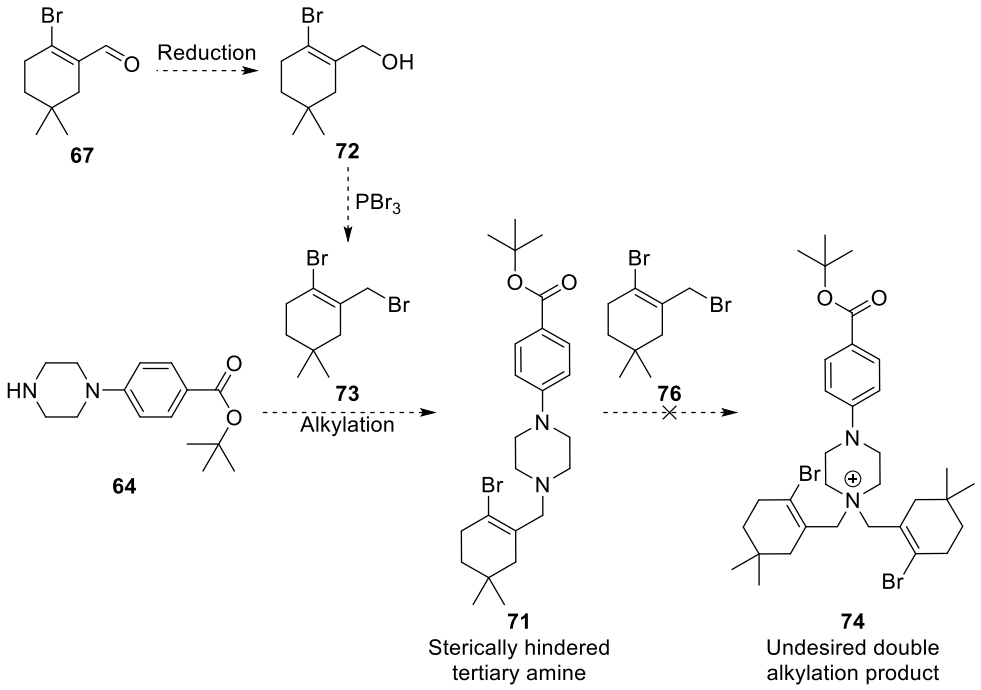

Scheme 28: Proposed alkylation strategy to **71**, whereby double alkylation to **74** could be controlled by reaction conditions. Synthesis of alkyl bromide **73** could be achieved from reduction and bromination of aldehyde **67**.

Reduction of **67** with $NaBH_4$ was successful, isolating **72** with small amounts of an unknown impurity, which was carried on crude. Subsequent bromination with PBr_3 was also successful, though the product **73** was also carried forward crude since its volatility hampered concentration from solvent. Then, during the alkylation of piperazine **64**, only singly alkylated product **71** was observed to form and was isolated in approx. 20% overall yield from **67** (Scheme 29).

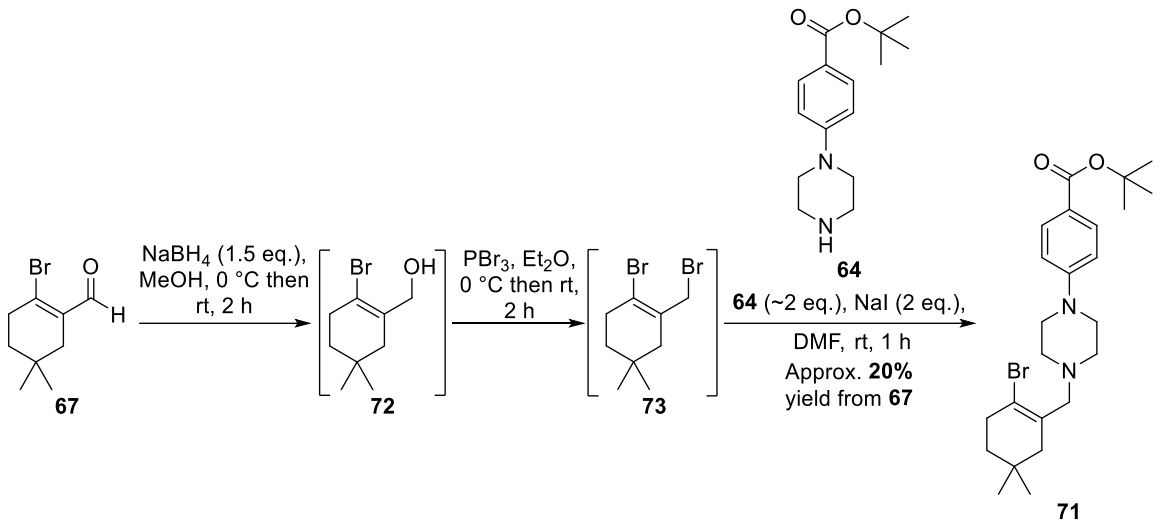

Scheme 29: Synthesis of **71** using the alkylation strategy.

2.4 Conclusions

This chapter described preliminary efforts towards synthesis of a peroxide-cleavable prodrug of Bcl-2 inhibitor navitoclax.

First, late-stage modification of the aniline of navitoclax was attempted, encouraged by the literature precedent for late-stage modification of this position (Figure 109). However, attempts to react navitoclax with activated *para*-nitrophenyl carbonates were unsuccessful, as were attempts to perform reductive aminations or amide formation reactions, presumably due to the poor nucleophilicity of the electron-poor aniline. However, modification of navitoclax was achieved by reaction with substituted benzyl bromides, although the reaction profile was extremely complex due to the formation of multiple regioisomers. In fact, the only pure isolated material corresponded to an analogue modified at the morpholine nitrogen, **39**, as identified by 2D NMR analysis. Hence, the desired aniline regioisomer, **37** was not isolated. Ultimately, the challenges associated with attempting late-stage functionalisation of a complex drug comprising multiple reactive amine sites and poorly nucleophilic desired aniline prompted us to consider an alternative fragment synthesis approach.

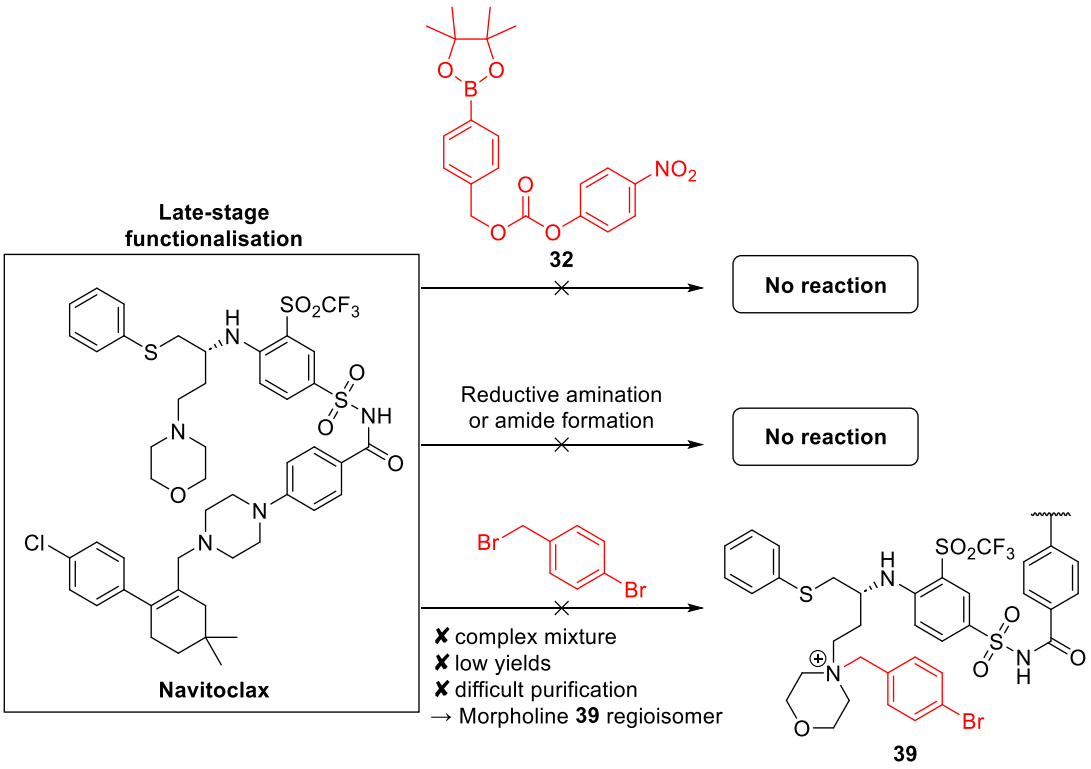

Figure 109: Summary of efforts towards late-stage functionalisation of navitoclax.

Fragment synthesis began from commercially available chiral amine **49**, whereby a benzylic and carbamate prodrug handle were installed to give **45** and **46** (Figure 110). However, the subsequent S_NAr reaction with sulfonamide **44** was unsuccessful due to unexpected formation of a bis-sulfonamide

adduct **52**. Reaction instead with Boc-protected sulfonamide **54** was still unfruitful, and the desired tertiary amines **41** and **42** could not be accessed.

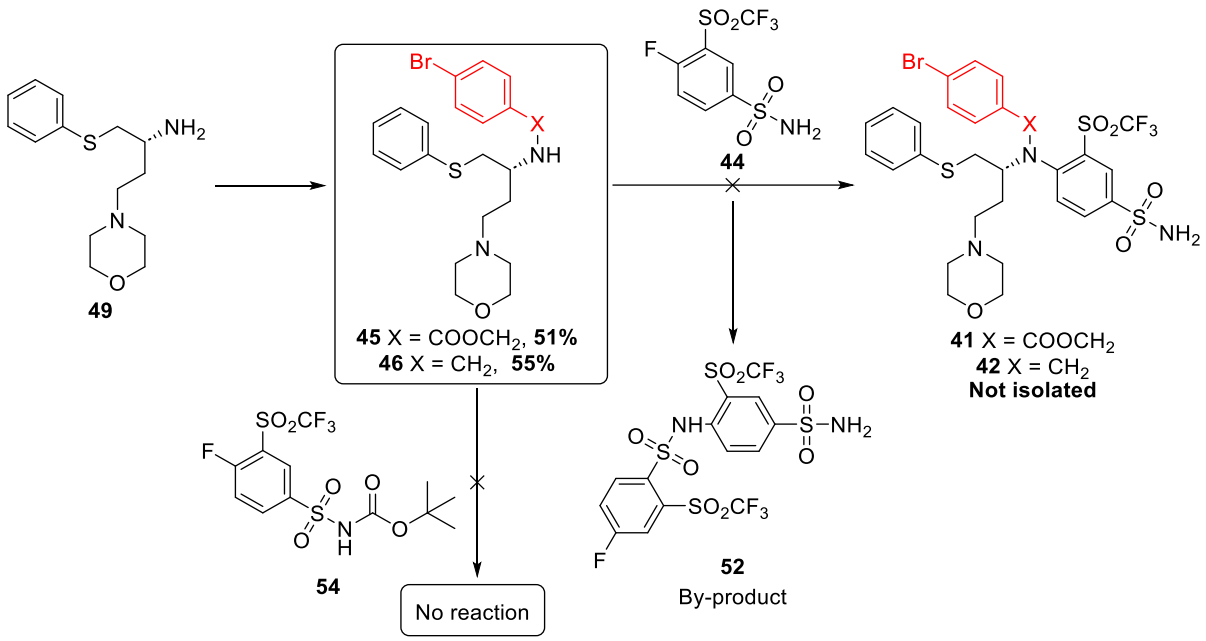

Figure 110: Summary of efforts towards fragment synthesis of a peroxide-responsive prodrug of navitoclax.

Since the aniline prodrug analogue was synthetically inaccessible, other modifiable positions were next investigated for prodrug synthesis. The piperazine was first selected for modification since unlike the morpholine ring, it is not solvent accessible, and it sits in a narrow pocket whereby introduction of a bulky benzyl substituent might hinder the ability of navitoclax to bind to Bcl-xL.

In the forward synthesis of the piperazine-substituted prodrug, the literature precedent for the Mannich reaction of piperazine **64** with 4,4-dimethylcyclohexanone **63** was attempted (Figure 111). However, the Mannich reaction was problematic and could not access sufficient product for continuation of the synthesis. Hence, an alternative synthetic precedent was pursued, which utilised a reductive amination for alternative reaction of **64**. However, once again, the reductive amination failed to provide sufficient material under various conditions. A final alternative synthetic route was considered, involving alkylation of **64** with alkyl bromide **73**, which was synthesised from aldehyde **67** in several telescoped steps. This reaction was successful, accessing piperazine intermediate **71** for further progression.

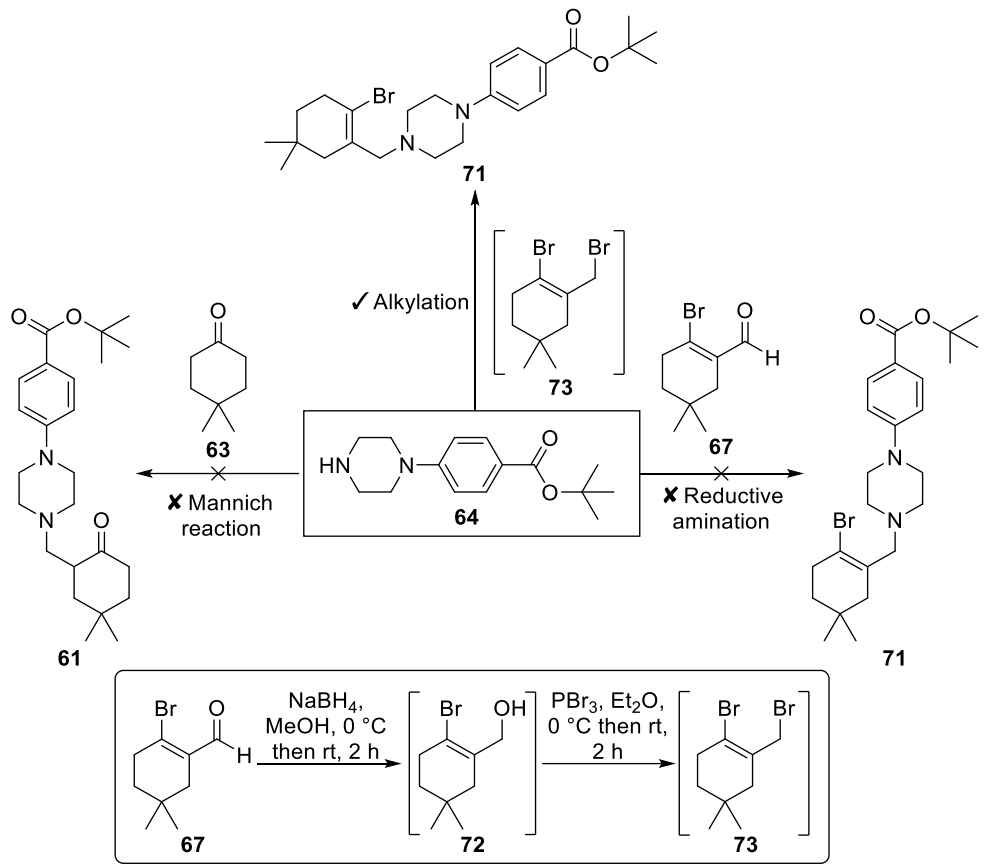

Figure 111: Summary of synthetic challenges towards piperazine intermediates for the synthesis of peroxide-cleavable prodrug of navitoclax.

2.5 Future Work

2.5.1 Synthesis

Having successfully developed an alternative synthetic route towards piperazine intermediate **71**, prior to attempting the synthesis of whole navitoclax prodrug **57**, the release of the quaternary ammonium from a model substrate should be investigated. With **71** in hand, the benzyl boronic acid handle should be introduced to generate model quaternary ammonium substrate **76** (Scheme 30A). Although double alkylation to the quaternary ammonium was not observed in the formation of intermediate **71**, harsher reaction conditions and elevated reaction temperatures may allow alkylation of intermediate with 4-bromobenzyl bromide to afford quaternary ammonium **75**. Subsequent Miyaura borylation could then afford prodrug handle modified intermediate **76**, but care should be taken to ensure the desired regioisomer is obtained rather than the isomer arising from borylation of the alkenyl bromide. It should then be confirmed that quaternary ammonium **76** is able to undergo self-immolation and C-N bond cleavage with H_2O_2 (Scheme 30B).

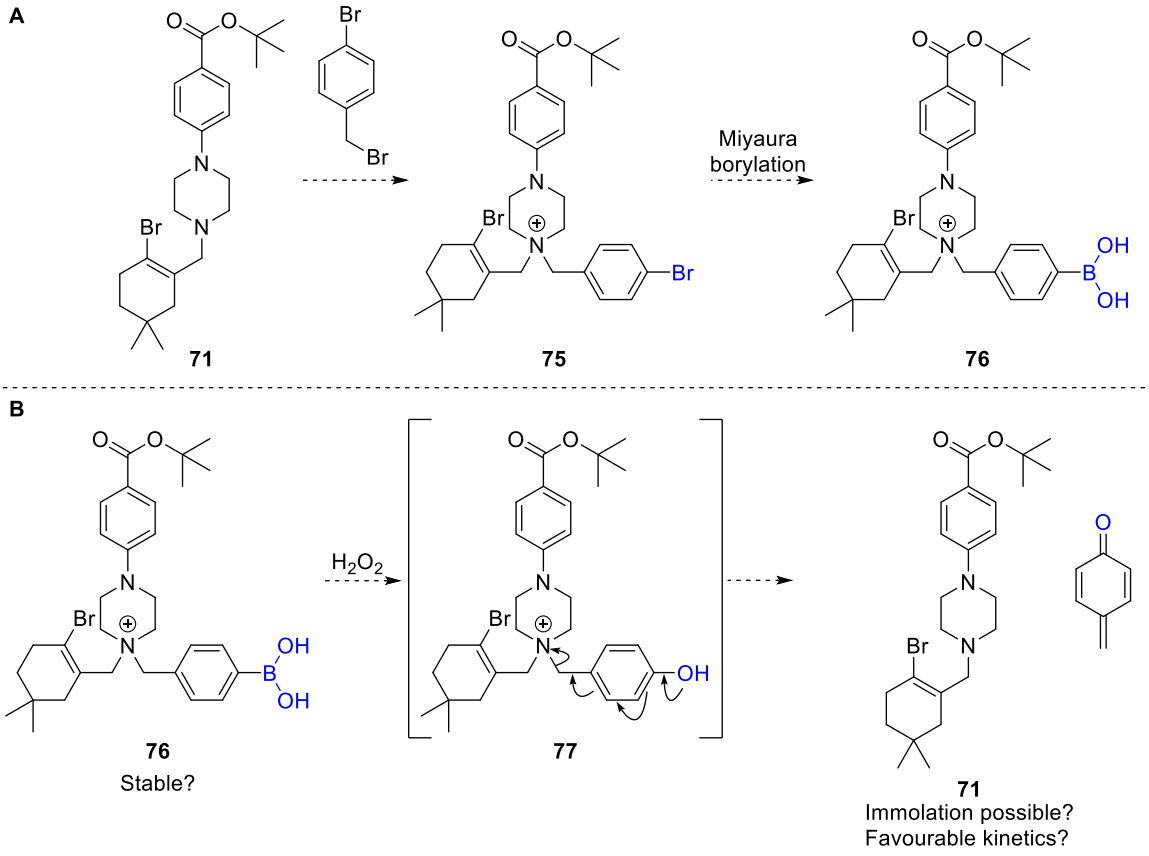

Scheme 30: A) Proposed generation of model quaternary ammonium prodrug mimic **76**, B) examination of the ability of **76** to release by immolation in the presence of peroxide.

Once the synthesis and release of intermediate **76** has been confirmed, full synthesis of a piperazine-modified navitoclax prodrug could be conducted. A Suzuki reaction of **71** should be performed prior

to prodrug handle installation to prevent regioselectivity issues during Miyaura borylation that may occur with the aryl bromide of the prodrug handle. Then, quaternary ammonium synthesis could be performed from chloro-intermediate **60**, prior to the introduction of any other reactive amines into the molecule. Subsequent amide bond formation with sulfonamide **44** could generate **58**, followed by S_NAr with chiral amine **49** to access **38**. Finally, a Miyaura borylation could afford the final prodrug **57** (Scheme 31).

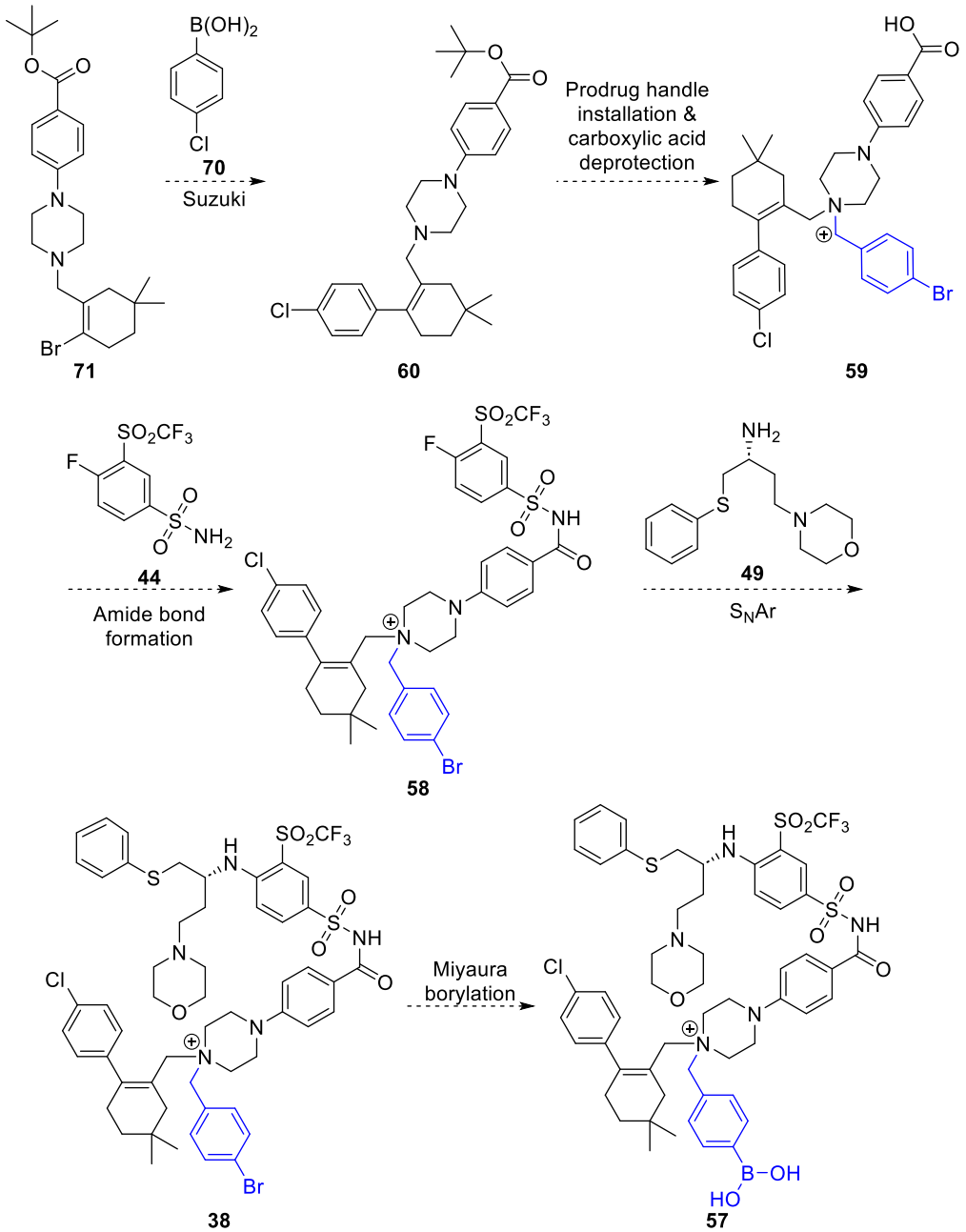

Scheme 31: Proposed synthesis of final piperazine modified prodrug of navitoclax **57**.

2.5.2 Kinetics of Release & Stability

Upon synthesis of final piperazine peroxide-cleavable prodrug **57**, its ability to release unmodified navitoclax in the presence of H_2O_2 should be examined. This could be achieved by an HPLC assay, which can track disappearance of the prodrug over time and appearance of free navitoclax when incubated at 37 °C with defined, biologically relevant concentrations of H_2O_2 in aqueous buffer. The stability of the prodrugs in the absence of peroxide should also be confirmed in the same conditions, as well as in plasma and at different pH.

2.5.3 Prodrug Validation

After confirming release and stability of the prodrug, it should be confirmed that modification at the piperazine position has sufficiently attenuated the ability of navitoclax to inhibit Bcl-xL. This could be investigated by an *in vitro* Bcl-xL activity assay which monitors the ability of Bcl-xL to bind a ligand (i.e. Bcl-xL Assay Kit #50223: BPS Bioscience). Incubation of the prodrug alone should have little to no impact on the ability of Bcl-xL to bind to the assay ligand, however, when activated by H_2O_2, the prodrug should inhibit the ability of Bcl-xL to bind the assay ligand to a similar extent as navitoclax.

2.5.4 Further Biological Evaluation

Finally, the prodrug should be examined for *in vitro* efficacy. The prodrug should display potent cytotoxicity in target cancer cells by activation *in situ* by the elevated levels of H_2O_2 and subsequent inhibition of Bcl-2/Bcl-xL. To confirm the activity of the prodrug is due to H_2O_2-mediated activation only, the cells could be pre-treated with peroxide-scavenger catalase to remove endogenous H_2O_2. Little/no potency should then be observed for the prodrug since it should be unable to bind to Bcl-2/Bcl-xL. *In vivo*, the effect of treatment with prodrug **57** on platelets should be carefully examined and compared to treatment with the parent drug. This would ultimately validate that a prodrug approach is effective at preventing the on-target platelet toxicity of navitoclax.

Chapter 3: Peroxide-Activatable Prodrug of Olaparib

3.1 Introduction

3.1.1 PARP & PARP Inhibitors

Poly(ADP-ribose)polymerases (PARP) are family of enzymes which synthesise poly(ADP-ribose) chains from nicotinamide adenine dinucleotide (NAD+).[259] PARP activity is essential for many processes such as the regulation of transcription, apoptosis, and the DNA damage response.[259] PARP1 is the most well understood PARP, and its role is to detect single-strand DNA damage and initiate DNA damage repair.[260] After binding to the damaged DNA in the binding domain, PARP1 synthesises poly(ADP-ribose) (PAR) and transfers it to acceptor proteins in a process known as PARylation. This in turn causes recruitment of other repair proteins to the damaged DNA site. PARP inhibitors (PARPi) are small molecule drugs designed to competitively bind to the PARP NAD+ active site, preventing the ability of PARPs to repair DNA damage. Hence, PARP inhibitors have been employed as anti-cancer agents in various contexts:

1) **Combination therapy of PARP inhibitors with other DNA-damaging chemotherapeutics.** Initial cancer cell DNA damage is caused by treatment with a traditional chemotherapeutic agent (or by radiotherapy). Repair of this DNA damage is prevented by cancer cell PARP inhibition. This is often described as PARP inhibitors "sensitizing" the cancer to the chemotherapeutic agent.[259]
2) **Treatment of cancer cells which already have limited ability to perform DNA-damage repair or have increased PARP dependence.** Some cancers have mutations in the homologous recombination (HR) genes Breast Cancer Associated 1 and 2 (BRCA1 and BRCA2): these cancer cells are unable to repair DNA-damage by homologous recombination and are more reliant on PARPs for DNA-damage repair. Thus, treatment with a PARP inhibitor further renders the cancer unable to repair DNA-damage, which can lead to cancer cell death.[261]

There are several other complex biological mechanisms by which PARP-inhibitors can encourage cancer cell death, however, they will not be discussed in detail in this report.[262–267]

Several PARP inhibitors have been granted FDA approval, namely olaparib (Lynparza®, 2014),[268] rucaparib (Rubraca®, 2016),[269] niraparib (Zejula®, 2017),[270] and talazoparib (Talzenna®, 2018),[271] for BRCA-deficient breast, ovarian, fallopian tube, and primary peritoneal cancers (Figure 112).[259,272] Additionally, over 200 clinical trials of PARP inhibitors are currently underway.[259]

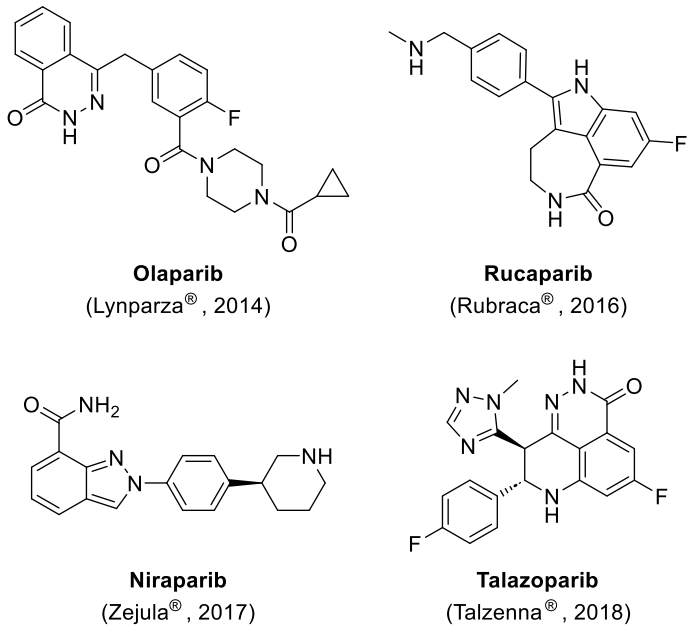

Figure 112: The structure of FDA-approved PARP inhibitors including their approval year.

Despite the successful FDA-approval of several PARP inhibitors, some studies have shown that the use of PARP inhibitors in combination therapies can result in normal tissue toxicity. Due to the similarity in their catalytic domain, PARP inhibitors designed to target PARP1 often inhibit the activity of other PARPs (i.e. PARP2 and PARP3).[265,273] PARP2 inhibition in particular has been discovered to impact the production of blood cells and platelets, which leads to severe hematologic toxicity, such as anaemia, thrombocytopenia and neutropenia.[226,274] Taken together, these off-target toxicities impose dose restrictions, and limit the clinical utility of PARP inhibitors as single agents, or in combination therapy.[275–282]

Hence, to preclude undesired off-target effects, there is a clinical interest in improving the tissue-selectivity of PARP inhibitors. A promising approach is the development of PARPi prodrugs, whereby an inactive form of the PARPi would be administered and only become activated at the site of cancer. There have been few investigations of PARPi prodrugs in the literature.[283–285]

3.1.1.1 Hypoxia-activated prodrug of olaparib

Hypoxia is a known feature of many solid tumours, which contributes to tumour progression.[286–289] In hypoxic environments, an aromatic nitro-moiety, such as 2-nitroimidazoles, can undergo a one-electron reduction. Fragmentation or further reduction of this pro-moiety can then lead to release of an active drug (Figure 113).[157,283,290]

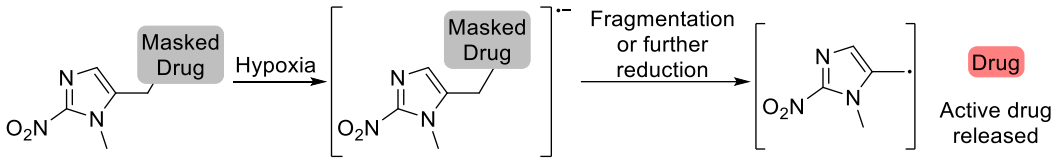

Figure 113: Ability of 2-nitroimidazoles to undergo a one-electron reduction in hypoxic environments which can lead to the release of an active drug.

Dickson *et al.* investigated conjugation of a similar 2-nitroimidazole trigger to the phthalazinone nitrogen of olaparib: this was envisioned to disrupt key hydrogen bonding interactions in the PARP2 binding site to render olaparib inactive.[283] A series of derivatives possessing the structural core of olaparib were generated with 2-nitroimidazole trigger groups attached to the phthalazinone nitrogen (Figure 114A). The prodrugs exhibited ~160-fold lower activity in a radiometric PARP1 inhibition assay, compared to the unfunctionalised core (Figure 114A). However, upon radiolytic reduction no released parent PARPi was detected. Instead, a hydroxylamine intermediate was formed that was proposed to be too stable to release the drug by fragmentation or reduction (Figure 114B).

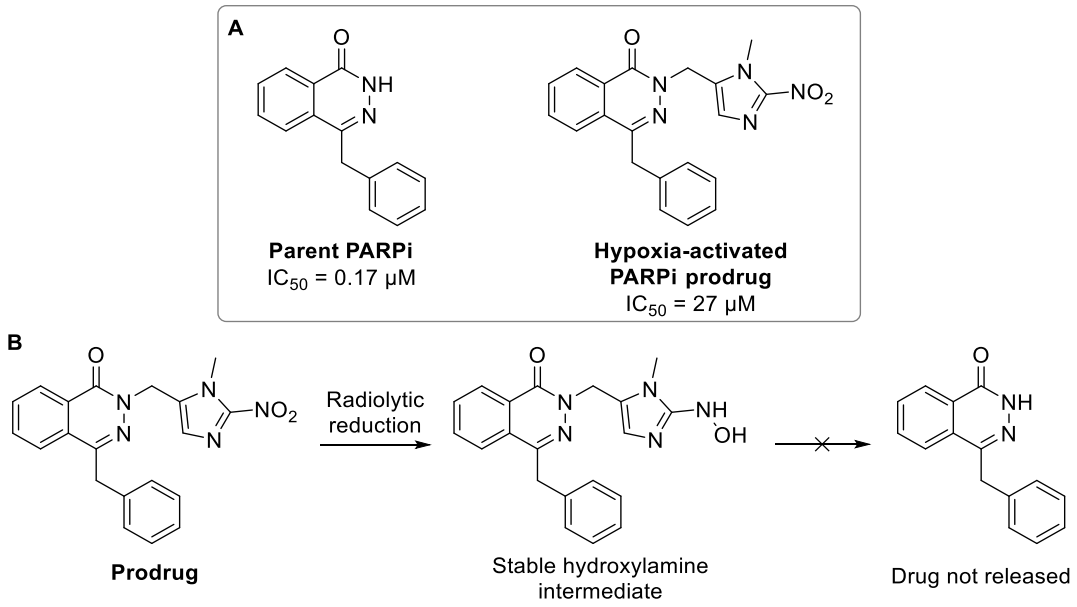

Figure 114: A) First attempt at generating a hypoxia-activated PARPi prodrug, including the reported IC_{50} values from a radiometric PARP1 inhibition assay. B) The prodrug was unable to release the drug upon radiolytic reduction due to formation of a stable hydroxylamine intermediate.[283]

Hence, an alternative linkage of the 2-nitroimidazole trigger was explored. A phenol was introduced to the phthalazinone core, which served as an attachment point for the 2-nitroimidazole trigger (Figure 115).[283] This prodrug was able to release the parent drug upon reduction, however the prodrug only exhibited approx. 9-fold lower activity than the parent drug. Further development is therefore required to identify a hypoxia-activatable prodrug which is able to effectively release the parent drug upon

reduction, but which also provides sufficient deactivation of PARPi activity for adequate site-selective activation.

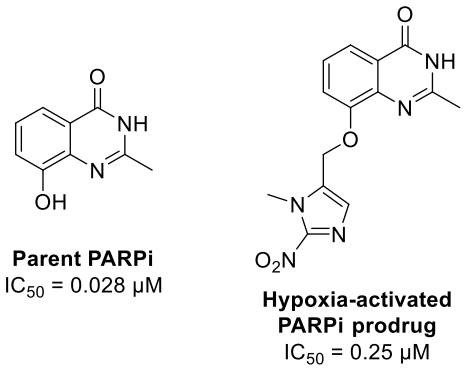

Figure 115: Alternative linking position of the hypoxia-activatable 2-nitroimidazolyl trigger to afford a prodrug which was able to release the parent drug upon reduction, but only provides *ca.* 9-fold deactivation of PARPi activity. (Reported IC_{50} values from a radiometric PARP1 inhibition assay).[283]

3.1.1.2 Photoactivatable prodrug of talazoparib

Talazoparib is one of the most potent FDA-approved PARP inhibitors, with an IC_{50} of 0.57 nM.[81] However, a serious risk of talazoparib treatment is myelodysplastic syndrome – a type of blood cancer where immature blood cells do not mature – and acute myeloid leukemia.[271] Hence, Li *et al.* sought to develop a talazoparib prodrug which could be activated by UV light.[284] By connecting an *ortho*-nitrobenzyl moiety to the phthalazinone nitrogen of talazoparib, an inactive prodrug was afforded which was no longer able to hydrogen bond to Gly863 and Ser904 of the PARP1 active site (Figure 116A). Accordingly, the prodrug showed 380-fold lower inhibitory activity (IC_{50} = 1.9 μM compared to parent drug IC_{50} = 0.005 μM) in an enzymatic assay. Moreover, *in vitro*, the prodrug was markedly less toxic than the parent drug (IC_{50} = 1.87 vs. 0.015 μM in BRCA1-defective MX-1 cells), but with UV irradiation for 1 minute, the IC_{50} was increased to 0.577 μM, demonstrating the successful release of talazoparib *in vitro* (Figure 116B). However, since UV light itself is damaging to cells, the irradiation time was limited by the tolerance of the cells to UV radiation in the absence of prodrug. Hence, the prodrug was unable to achieve the same potency as the parent drug, presumably due to incomplete release by UV-activation. Therefore, the utility of such UV-activatable prodrugs may be limited, since prolonged irradiation of the tumour site to afford full prodrug activation and talazoparib release would likely cause non-specific damage to surrounding healthy cells.

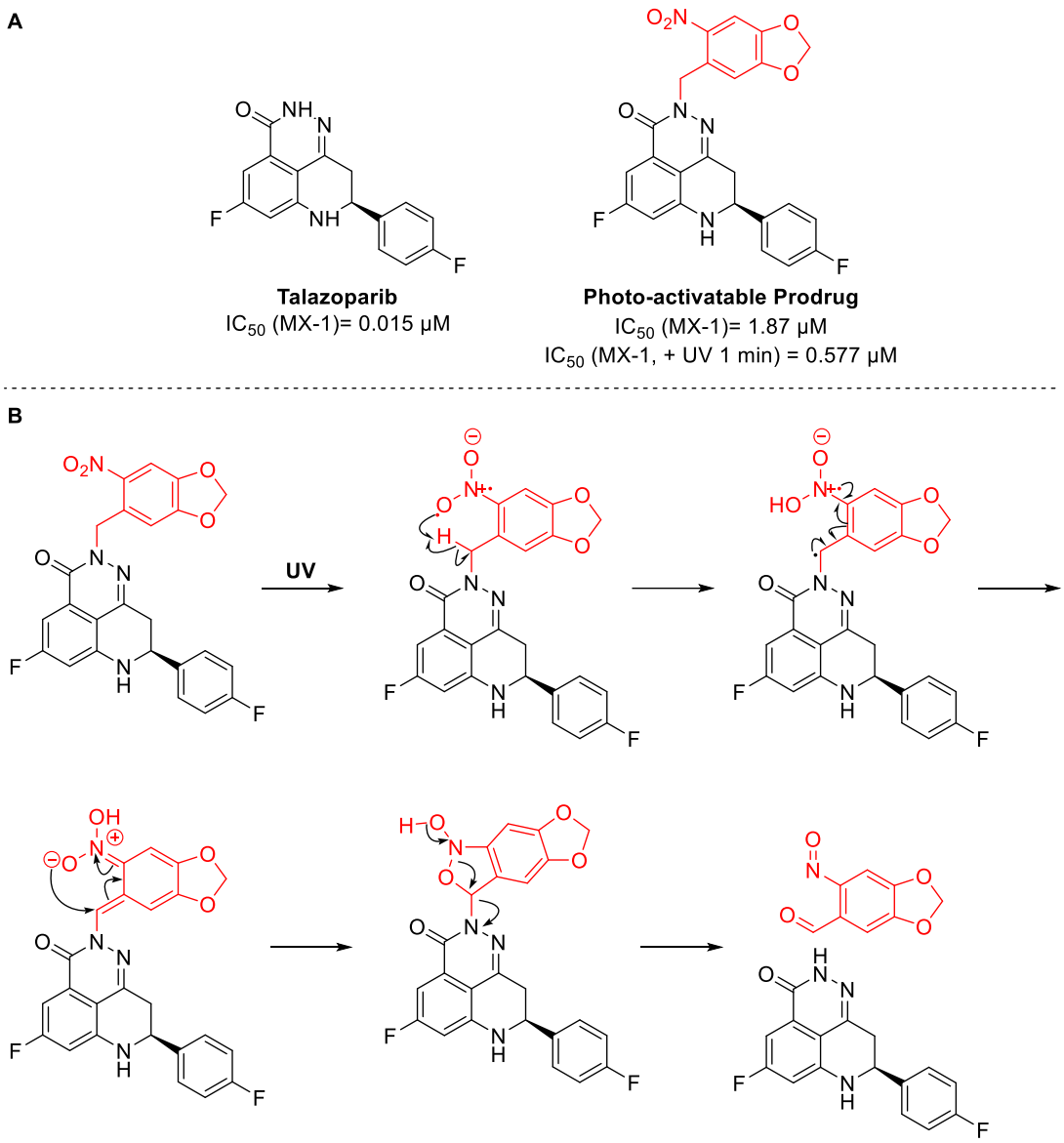

Figure 116: A) The structure of photoactivatable talazoparib prodrug, which has significantly lower activity than the parent drug unless irradiated with UV light, B) the mechanism of talazoparib release from the photoactivatable prodrug.[284]

3.1.1.3 Glucuronide prodrug of TSL-1502M

Recently, Wang *et al.* described the development of a PARPi prodrug which utilises the enhanced levels of β-glucuronidase in the tumour microenvironment.[285] By capping potent PARPi TSL-1502M with a glucuronide moiety, a prodrug TSL-1502 was generated, which exhibited significantly decreased inhibitory activity in a cell-free enzymatic assay (IC_{50} = >3000 nM compared to parent drug IC_{50} = 0.66 nM (PARP1), 0.87 nM (PARP2)) (Figure 117). Structural modelling revealed that the carbonyl moiety of TSL-1502M formed critical hydrogen bonding interactions in the PARP1 active site: glucuronide capping at this position introduced spatial conflict, and prevented formation of these hydrogen bonds, rendering the prodrug inactive.

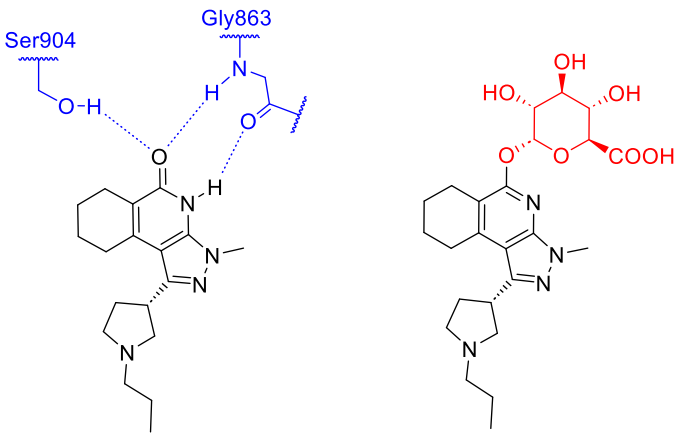

TSL-1502M
Parent Drug
IC_{50} = 0.66 - 0.87 nM

TSL-1502
Glucuronide Prodrug
IC_{50} >3000 nM

Figure 117: Structure of parent PARPi TSL-1502M and glucuronide prodrug TSL-1502.[285] The key hydrogen bond interactions to the PARP1 active site are shown in blue, and the glucuronide pro-moiety is highlighted in red. Capping of the drug at this position prevents the formation of key hydrogen bonds to the PARP active site.

When incubated with MDA-MB-436 cancer cells, TSL-1502 was observed to convert to the active drug TSL-1502M (determined by HPLC-MS analysis).[285] Additionally, *in vivo* pharmacokinetics detected high distributions of prodrug TSL-1502 in plasma, whereas active TSl-1502M was mainly distributed in the tumour, suggesting that prodrug TSL-1502 mainly liberates the active drug at the site of tumour.

However, *in vitro*, the prodrug was significantly less potent than the parent drug. For example, in MDA-MB-436 cells the parent drug TSL-1502M achieved an IC_{50} of 0.9 nM, whereas prodrug TSL-1502 displayed 87-fold lower potency, with an IC_{50} of 78.7 nM. It is suspected that this is due to incomplete conversion of the prodrug to the active form *in vitro*. Despite this, *in vivo*, prodrug TSL-1502 demonstrated dose-dependent tumour growth inhibition with no adverse effects and enhanced potency over FDA-approved PARPi olaparib.[285]

3.2 Project Aims

There are limited examples in the literature of PARPi prodrugs which fulfil the criteria of an efficacious prodrug: 1) ability to rapidly convert to the active form in the presence of a cancer-specific trigger, and 2) offer sufficient reduction of PARPi potency as a prodrug compared to the active form, for effective discrimination between healthy and target cells. Hence, it was envisioned that the arylboronic acid motif described in this report could be used to generate PARPi prodrugs which rapidly release the active drug in the presence of the high levels of H_2O_2 in cancer (Figure 118).

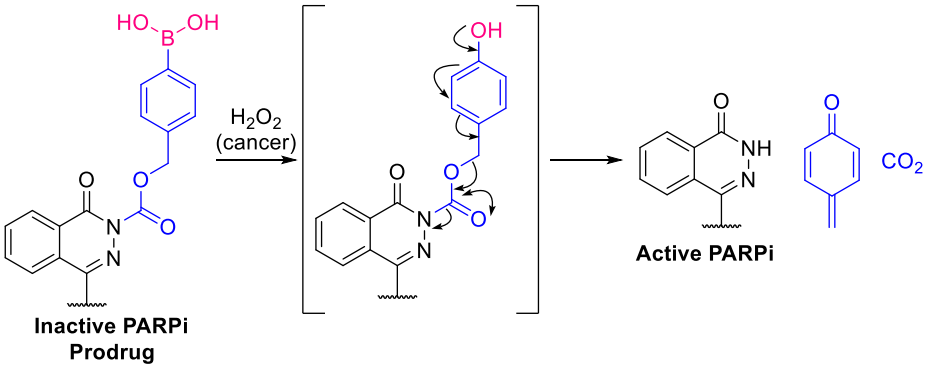

Figure 118: Generic representation of a ROS-sensitive PARPi prodrug utilising an arylboronic acid pro-moiety, which could release the drug by 1,6-elimination through a carbamate bond after H_2O_2-oxidation. The H_2O_2 responsive unit is depicted in magenta, the self-immolative linker depicted in blue and the released drug depicted in black.

For development of a successful peroxide-activatable PARPi prodrug, the prodrug must be inactive when modified with arylboronic acid responsive motif, stable under biological conditions in the absence of H_2O_2, and must rapidly convert to the active, unfunctionalised drug in the presence of H_2O_2.

3.3 Results & Discussion

Olaparib (Lynparza®) was selected for the generation of a ROS-cleavable prodrug due to its commercial availability and modifiable phthalazinone core. The binding mode of olaparib is known to involve a tridentate hydrogen bond network to Ser904 and Gly863.[267] For this reason, functionalisation of the phthalazinone nitrogen with the cleavage trigger was expected to disrupt these key binding interactions to render the inhibitor inactive (Figure 119), as has previously shown to be a successful approach in the literature.[283–285]

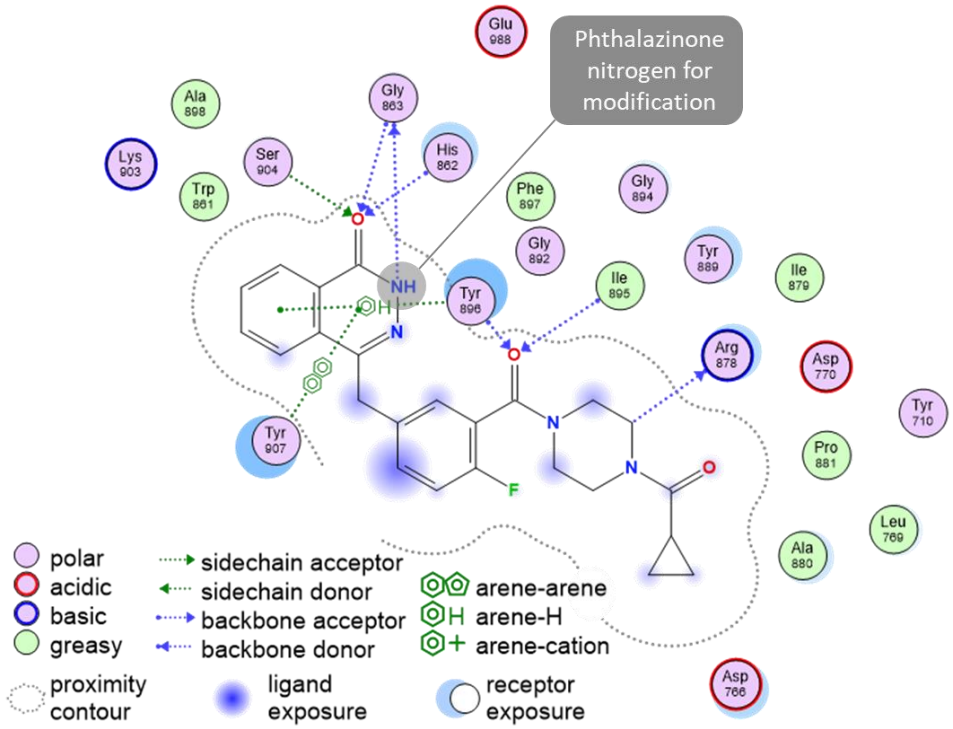

Figure 119: Olaparib bound to the catalytic active site of PARP1 (PDB: 7KK4, visualised using MOE), showing the tridentate hydrogen bond network to Ser904 and Gly863.

3.3.1 Benzyl Analogue Synthesis

It was envisioned that modification of the phthalazinone nitrogen of olaparib could be achieved *via* late-stage functionalisation of the final drug molecule. First, linkage of a benzyl-boronic acid to this position was investigated (Scheme 32). Although immolation of linkers *via* C-N bond cleavage is generally reported to be slow,[123,204] it is facilitated by the conjugation of electron-withdrawing groups.[170] Since the phthalazinone amine is conjugated to a carbonyl and adjacent aromatic ring, release *via* C-N bond cleavage may be possible.

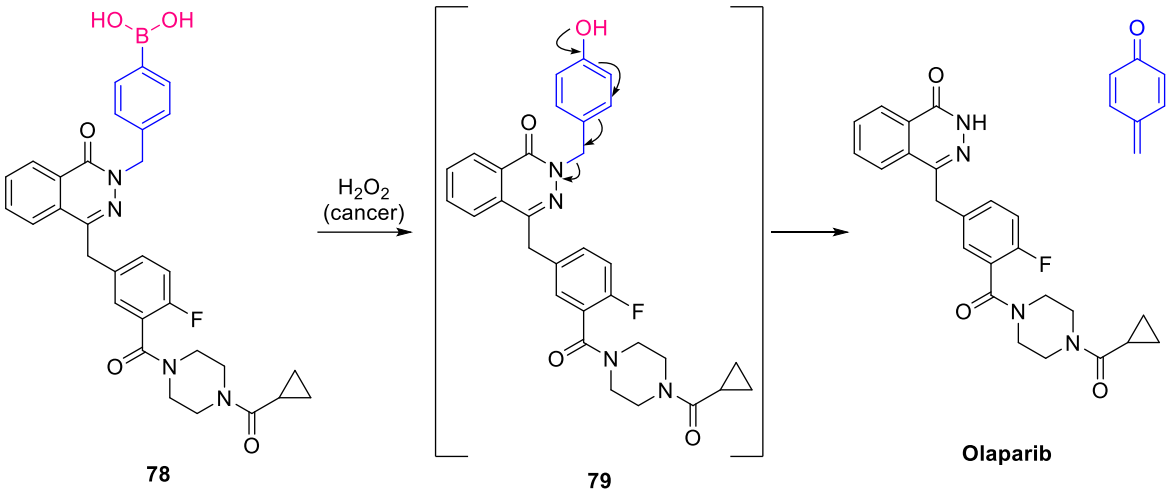

Scheme 32: Proposed benzyl-arylboronic acid olaparib prodrug **78** and its proposed conversion to free drug when exposed to H_2O_2. The H_2O_2 responsive unit is depicted in magenta, the self-immolative linker depicted in blue and the released drug depicted in black.

Reaction of olaparib with 4-bromobenzyl bromide was successful with short reaction times, affording **80** in good yields (Scheme 33). The disappearance of the phthalazinone NH signal at 10.3 ppm during the reaction suggested substitution on the desired phthalazinone nitrogen rather than on the piperazine ring (Figure 120). This was further confirmed by 2D NMR, whereby HMBC correlations could be observed from benzylic protons (Hw, Figure 121) to neighbouring carbonyl Cv, and quaternary carbon Co.

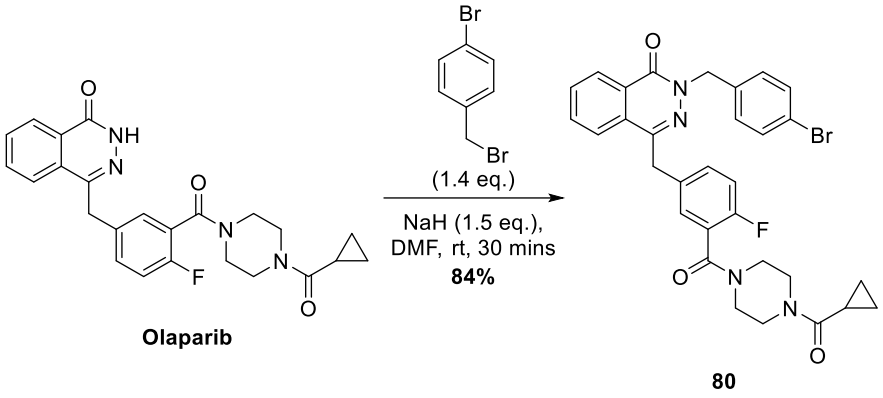

Scheme 33: Synthesis of benzyl-bromide modified olaparib **80**.

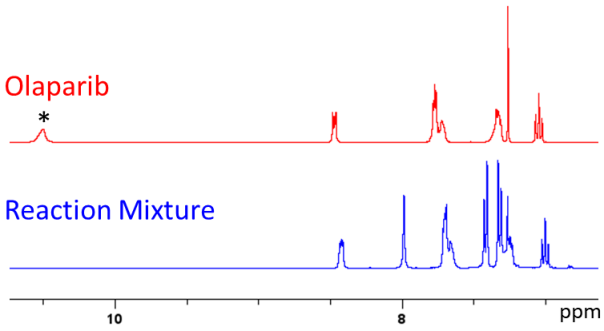

Figure 120: Disappearance of phthalazinone NH signal (*) in the ^{1}H proton NMR ($CDCl_3$) of the reaction mixture towards **80**.

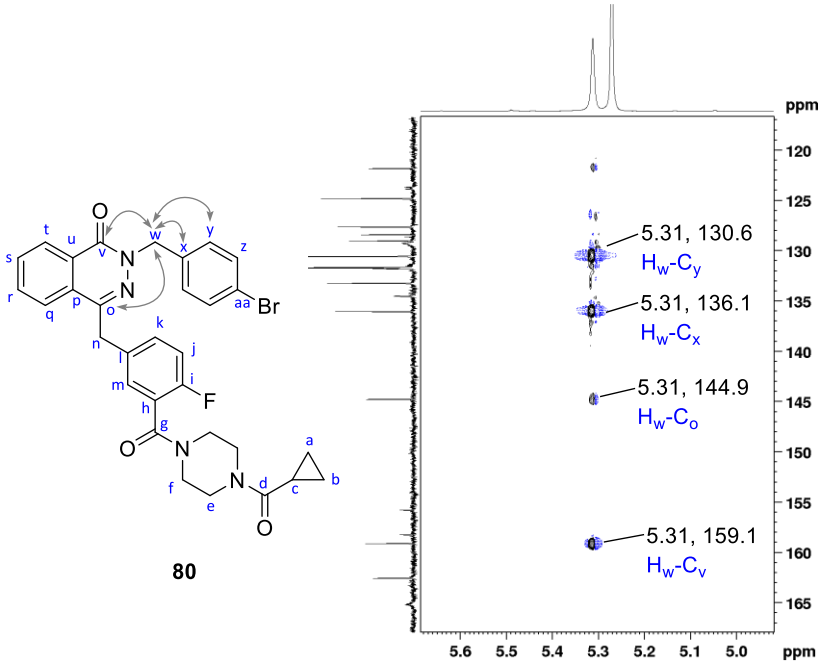

Figure 121: ^{1}H-^{13}C HMBC correlations between benzylic proton Hw to various carbons which support the formation of desired regioisomer **80**.

Having accessed benzyl bromide **80**, the final step involved Miyaura borylation to afford final benzyl boronic acid prodrug **78** (Scheme 34). This was successful in moderate yields using common Miyaura borylation conditions. Following work-up, partial hydrolysis of the boronic ester to the boronic acid was observed. However, these were successfully separated by reverse-phase FCC.

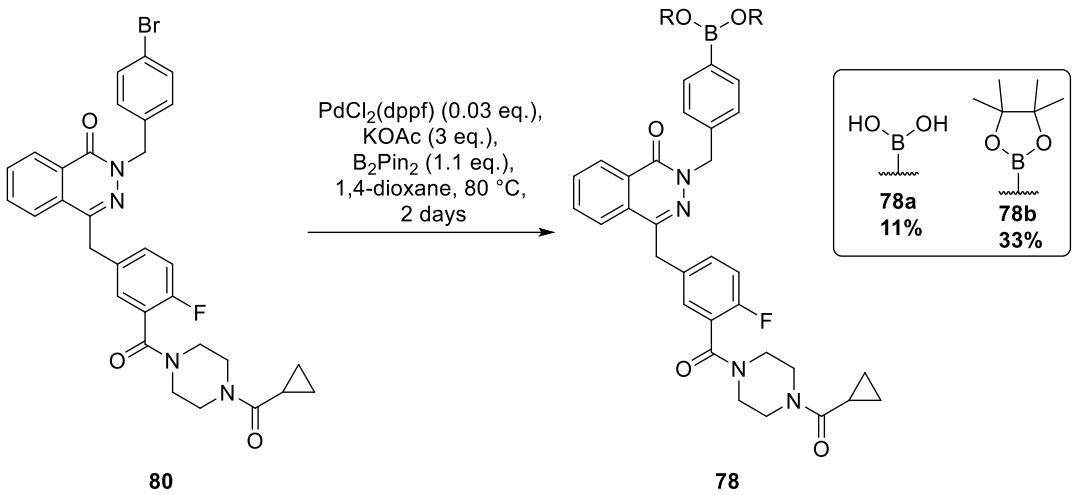

Scheme 34: Synthesis of benzyl boronic acid prodrug **78** by Miyaura borylation of **80**.

3.3.2 Benzyl Prodrug Release

Having successfully synthesised an olaparib analogue bearing a benzyl-arylboronic acid at the phthalazinone nitrogen, this analogue (**78a**) was then investigated for its ability to release olaparib in the presence of H_2O_2 by the expected 1,6-elimination. A small volume of 30 w/w% H_2O_2 was added to a crude sample of **78a** in 1:1 MeCN:H_2O at rt, and the mixture was monitored by HPLC and LCMS. Oxidation of the boronic acid to the phenol **79** was complete within 1 h (identified by complete conversion to the phenol $[M+H]^+$ by LCMS). However, even after 26 h incubation with H_2O_2, no elimination was observed to release the free drug (Figure 122). Presumably, the intermediate phenol **79** is stable under these conditions, and elimination involving cleavage of a C-N bond is unfavourable, despite the conjugation to electron-withdrawing carbonyl. Therefore, it was concluded that this benzyl-linked olaparib analogue **78** is an unsuitable peroxide-activatable prodrug.

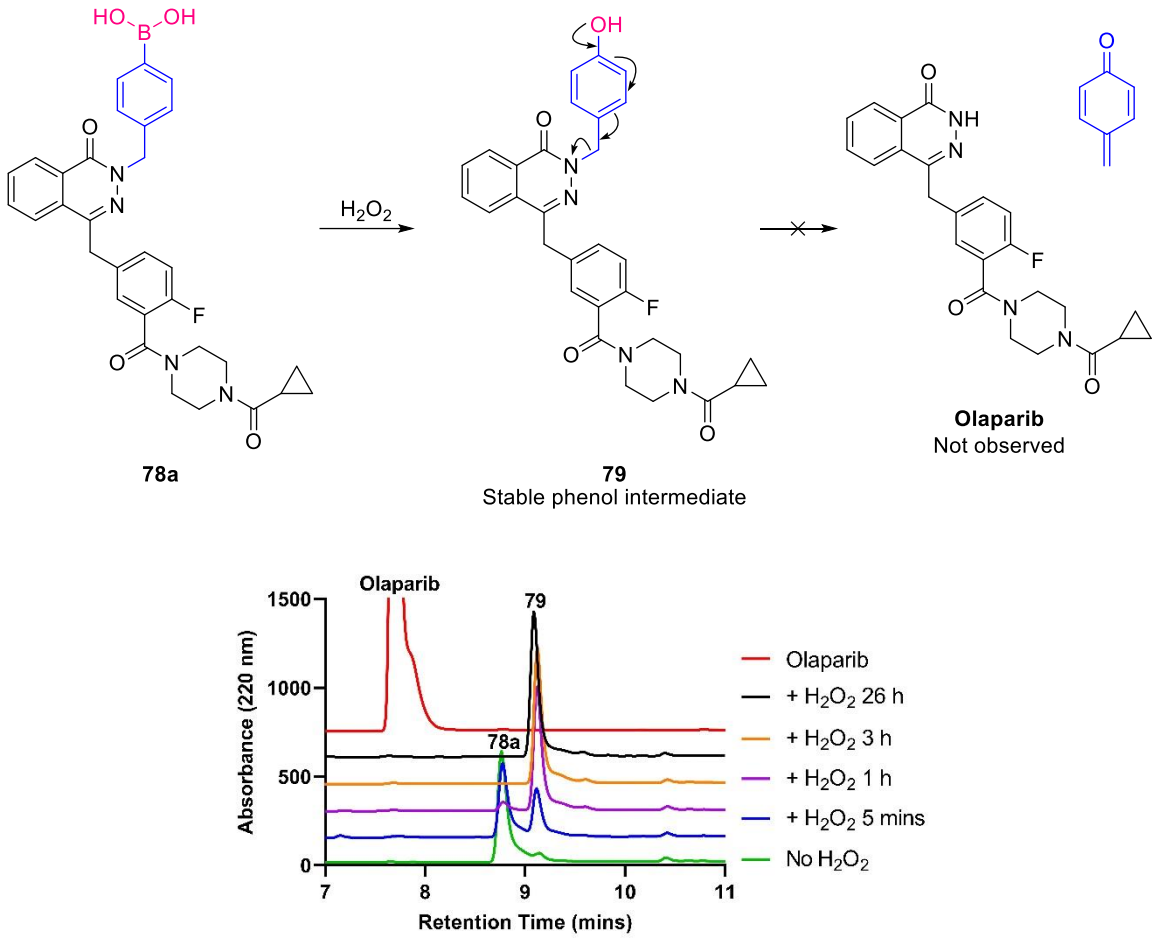

Figure 122: HPLC monitoring of **78a** incubated with H_2O_2: a stable phenol intermediate **79** formed within 1 h, which did not immolate to release free olaparib. The H_2O_2 responsive unit is depicted in magenta, the self-immolative linker depicted in blue and the released drug depicted in black.

3.3.3 Carbamate Analogue Synthesis

Release of drugs from self-immolative linkers is facilitated by the increase in entropy associated with the release of CO_2.[162] Hence, efforts now focussed on synthesising olaparib analogue **81**, which connects the ROS-responsive arylboronic acid *via* a carbamate bond.

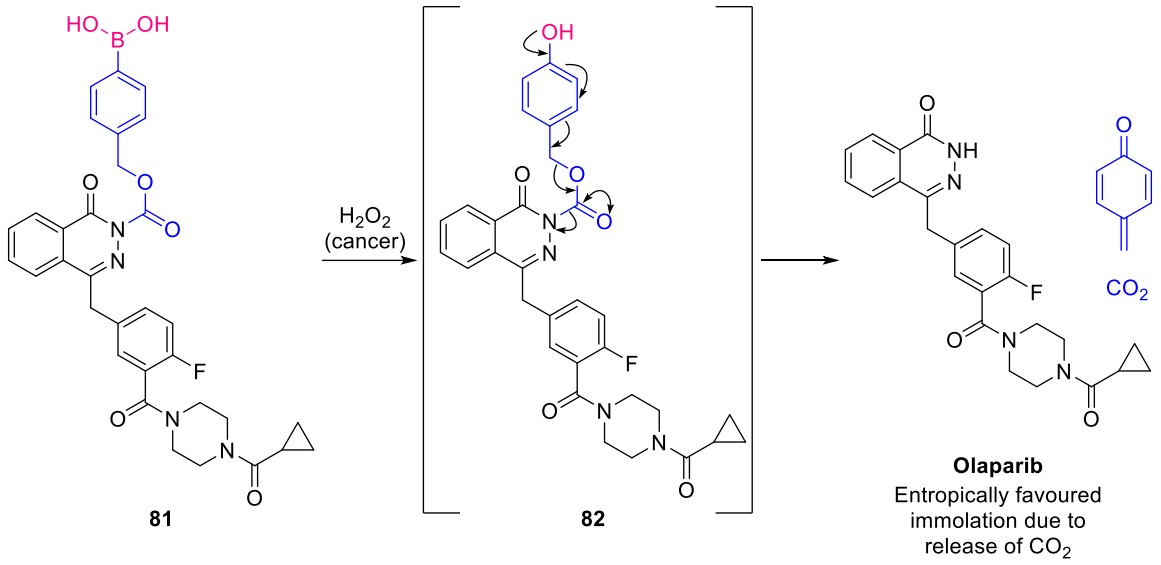

Scheme 35: Proposed release of olaparib from carbamate peroxide-cleavable prodrug **81**. The H_2O_2 responsive unit is depicted in magenta, the self-immolative linker depicted in blue and the released drug depicted in black.

With activated 4-bromobenzyl *para*-nitrophenyl carbonate **31** already in hand (Chapter 2), the reaction with olaparib was attempted under the same conditions that had previously allowed benzyl modification (Table 19). However, under these conditions, no desired reaction was observed, and the starting material carbonate degraded (Table 19, Entry 1). Hence, a selection of different bases, solvents and additives were screened for the synthesis of **83** from olaparib and carbonate **31**. Pleasingly, the addition of 18-crown-6 to the reaction of olaparib in DMF with NaH afforded complete reaction to **83** (Table 19, Entry 2). Despite classically being selective for the co-ordination of potassium ions, 18-crown-6 has been reported to also complex sodium ions.[291] Conducting the reaction using NaHMDS in THF with the addition of 18-crown-6 also afforded complete conversion to **83** (Table 19, Entry 9).

Table 19: Conditions screen for the reaction of olaparib with **31** to generate carbamate intermediate **83**. Optimal conditions are highlighted in bold. Observations are from *in situ* reaction monitoring only and product isolation was not performed.

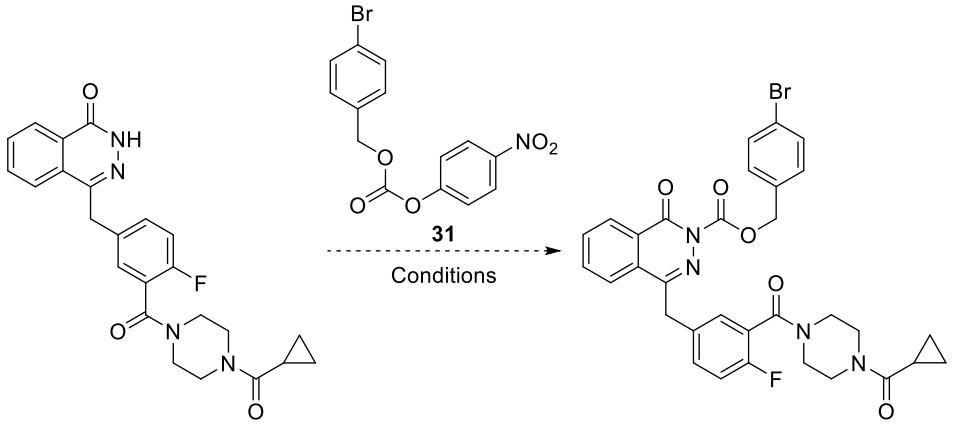

Entry	Base (1 eq.)	Solvent	Additive (1 eq.)	Temp	Observations[a]
1	NaH	DMF	-	rt	No reaction. Carbonate **31** degradation.
2	**NaH**	**DMF**	**18-crown-6**	**rt**	**Complete reaction to 83.**
3	NaH	THF	-	rt	Incomplete reaction. Minor **83** observed.
4	NaH	THF	18-crown-6	rt	Incomplete reaction. Minor **83** observed.
5	NaH	THF	18-crown-6	60 °C	No reaction.
6	DMAP	THF	-	rt	No reaction. Carbonate **31** degradation.
7	LiHMDS	THF	-	rt	Incomplete reaction. Minor **83** observed.
8	NaHMDS	THF	-	rt	Incomplete reaction. Minor **83** observed.
9	**NaHMDS**	**THF**	**18-crown-6**	**rt**	**Complete reaction to 83.**

[a]Observations from *in situ* reaction monitoring only. Product isolation was not performed.

Scale-up of Table 19, Entry 2 afforded 150 mg of **83** in moderate yield. Subsequent Miyaura borylation of **83** afforded final carbamate olaparib prodrug **81** in 82% overall conversion, obtained as a mixture

of boronic acid **81a** and ester **81b** product which was carried forward for testing without further purification (Scheme 36).

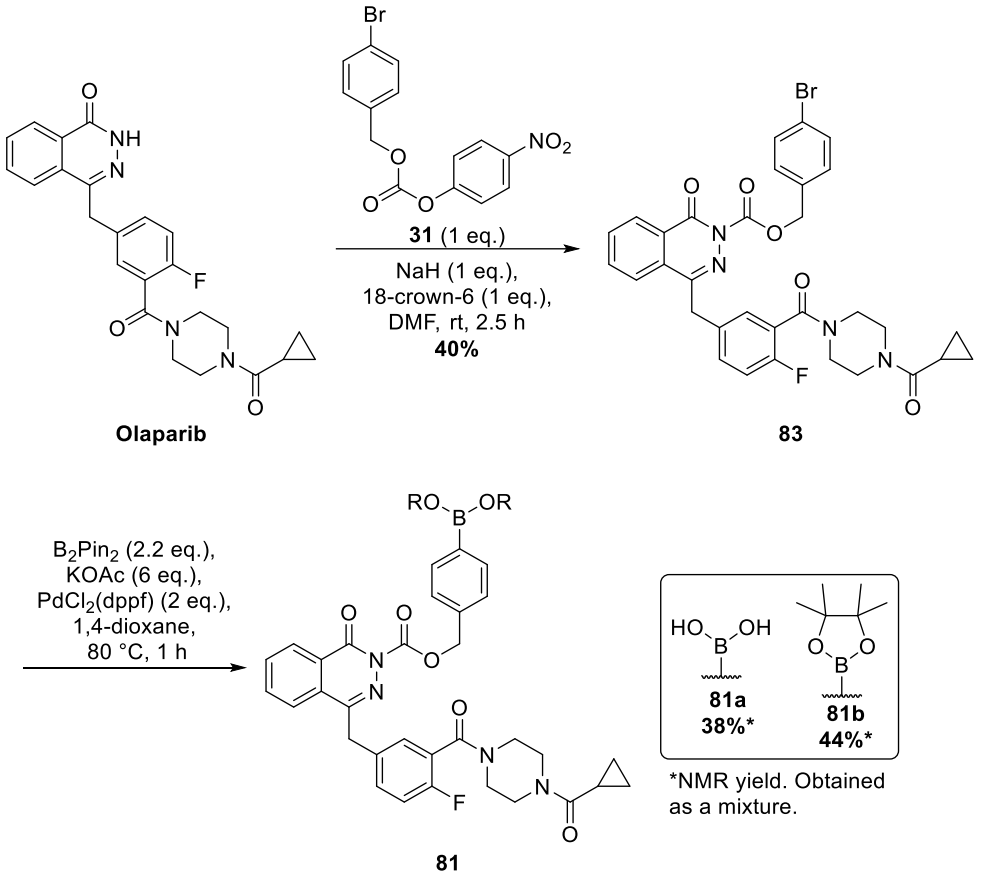

Scheme 36: Synthetic route towards carbamate olaparib prodrug **81**.

3.3.4 Carbamate Analogue Release

With the final carbamate prodrug mixture **81** in hand, a crude sample of the boronic ester/acid mixture was subjected to H_2O_2 at rt and monitored by HPLC (Figure 123). Pleasingly, after only 5 mins a signal appeared with the same HPLC retention time as olaparib, which was confirmed by observation of the correct $[M+H]^+$ in LCMS. The olaparib peak increased with 1.5 h incubation and after 24 h, no prodrug **81** remained, suggesting full release of olaparib from the prodrug. Phenol intermediate **82** was not observed, presumably because 1,6-elimination is too fast for detection.

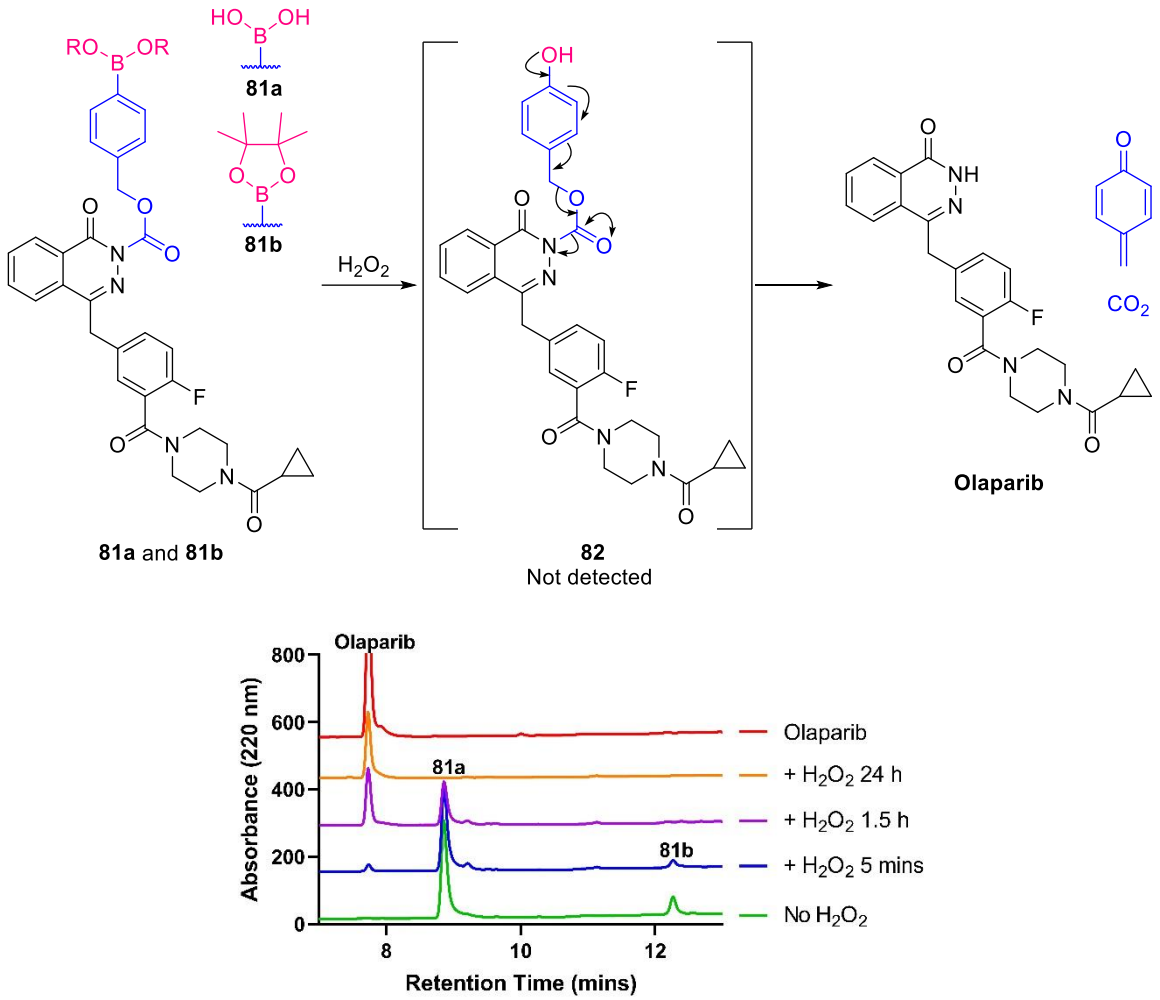

Figure 123: HPLC monitoring of **81a** and **81b** incubated with H_2O_2 at rt: no prodrug **81a** or **81b** remained after 24 h, suggestive of full release of olaparib. The H_2O_2 responsive unit is depicted in magenta, the self-immolative linker depicted in blue and the released drug depicted in black.

3.4 Conclusions & Future Work

Preliminary work has demonstrated the successful and facile two-step synthesis of carbamate-arylboronate/arylboronic acid modified olaparib **81**, which is able to release unfunctionalised olaparib in the presence of H_2O_2. An analogous benzyl linked arylboronic acid **78** was unable to release olaparib, likely due to the stability of the phenolic intermediate **79** formed after boronic acid oxidation. Further exploration of the properties of the carbamate prodrug **81** and biological investigation are required for completion of this work.

3.4.1 Kinetics & Stability Evaluation

Preliminary work has shown that carbamate prodrug **81** is able to release free olaparib in the presence of H_2O_2. However, more detailed evaluation of the kinetics of release under conditions representative of biological systems is required for validation of this approach. Briefly, the cleavage of prodrug **81** should be investigated in aqueous buffer at 37 °C, with pathologically relevant concentrations of H_2O_2. Cleavage should be monitored by HPLC over time, and the rate of release examined with different concentrations of H_2O_2 (similar to work described in Chapter 1.3). The prodrug should also be incubated in the same conditions in the absence of H_2O_2 to confirm that release is mediated solely by H_2O_2 and that the prodrug is not generically unstable under physiological conditions. Release from prodrug **81** and examination of stability could also be investigated at different pHs, to gauge how the prodrug would behave in different regions of the body. Finally, the plasma stability of prodrug **81** should be examined, to ensure off-target activation of the prodrug would not occur upon circulation in plasma in the body.

3.4.2 Examine Prodrug Activity

It should be confirmed that capping the phthalazinone nitrogen with the peroxide-responsive pro-moiety sufficiently reduces the inhibitory activity of olaparib. This could be investigated in a PARP activity assay kit, whereby the activity of PARP1 and PARP2 is monitored by their ability to generate poly(ADP-ribose), which generates a fluorescent read-out in the assay. Incubation of free olaparib should result in a reduction in PARP1 and PARP2 activity by PARP inhibition and thus a reduced fluorescence response. In contrast, incubation of prodrug **81** should have minimal effect on PARP activity compared to a negative control. However, activation of prodrug **81** with H_2O_2 should then result in similar reduced fluorescence as treatment with free olaparib, due to activation of the prodrug to the active PARPi. Taken together, these experiments would demonstrate that prodrug **81** effectively modulates the activity of olaparib until activated by H_2O_2.

3.4.3 *In Vitro* and *In Vivo* Evaluation

To finalise the evaluation of ROS-cleavable PARPi prodrug **81**, its potency should be evaluated *in vitro*. First, it should be confirmed that the prodrug **81** is active in cancer cell lines commonly treated with PARPi, such as those with BRCA-mutations. This would elucidate whether the endogenous H_2O_2 levels are sufficient for prodrug activation *in vitro*. Additionally, it could be demonstrated that with pre-treatment of cells with H_2O_2 scavenger catalase (see Chapter 1.3.5), the prodrug is no longer potent. This would demonstrate that the prodrug is stable *in vitro* and requires activation by H_2O_2 for inhibitory activity. *In vivo* evaluation, for example in mice xenograft models, could investigate the ability of prodrug **81** to achieve tumour reduction, without off-target toxicity. The tolerability and potency of the prodrug **81** could be compared to treatment with olaparib for validation of the prodrug approach to afford site-selectivity and reduced off-target effects.

3.4.4 Varying Aryl Ring Electronics

After validation of the peroxide-cleavable olaparib prodrug **81** *in vitro* and *in vivo*, attention could turn to optimizing the kinetics of drug release. As demonstrated in Chapter 1.3, tuning the electronics of the aryl ring can impact the rate of the oxidation/self-immolation process. Although the rates of release of small molecule model linkers did not correlate with the potency of the final ADCs in Chapter 1, in the case of small molecule prodrugs, the kinetics of drug release can be directly examined from the prodrug itself in biologically relevant conditions. Hence, a series of different prodrugs could be synthesised with various aryl ring and benzylic substituents, to explore which give fastest drug release (Figure 124).

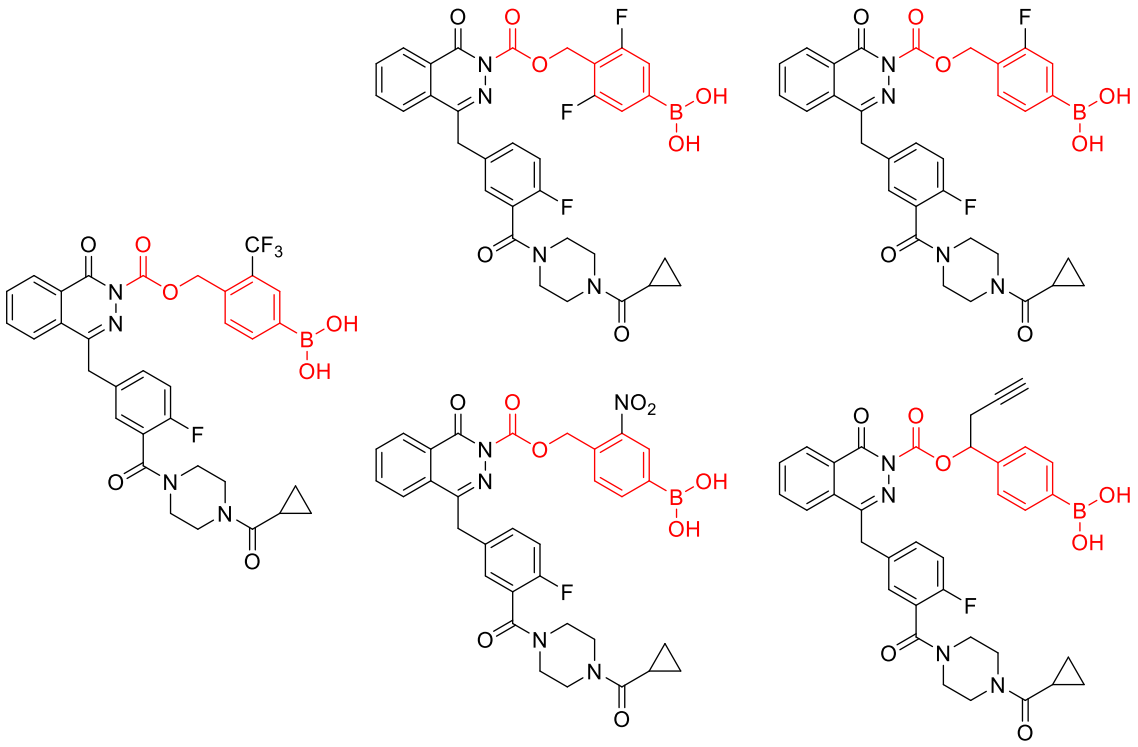

Figure 124: Non-exhaustive selection of alternative olaparib prodrugs with varying pro-moiety electronics and benzylic substitutions for evaluation of the impact on the kinetics of boronic acid oxidation and drug release.

3.4.5 Towards Other PARPi Prodrugs

Finally, if the previous experiments are promising, then the arylboronic acid pro-moiety could be utilised for the generation of prodrugs from a number of PARP inhibitors which suffer from off-target toxicities. Other FDA-approved PARP inhibitors possess a similar modifiable nitrogen involved in forming key binding interactions with the PARP active site. Thus, it is predicted that modification at these positions with an arylboronic acid prodrug handle could similarly yield inactive prodrugs (Figure 125). However, unlike olaparib, these PARPi also possess other amine positions where functionalisation might also occur. Therefore, a late-stage functionalisation approach might not be suitable for these prodrugs, and instead stepwise synthesis may be required.

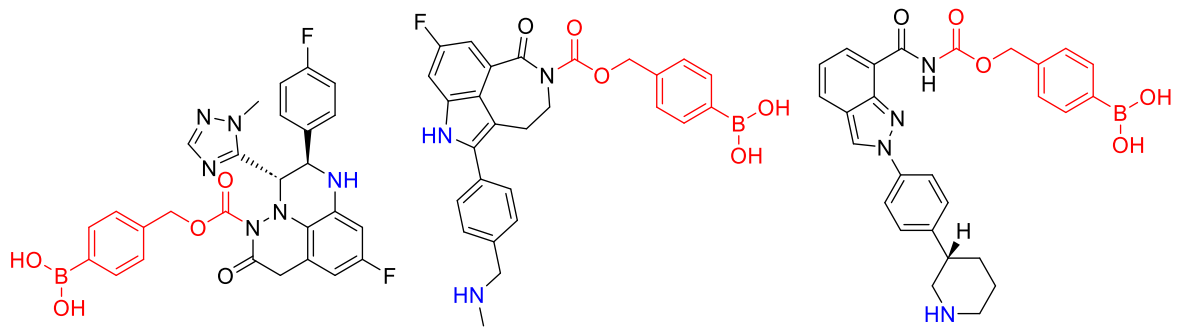

Figure 125: The structure of proposed ROS-cleavable prodrugs of other FDA-approved PARPi. The prodrug moiety is highlighted in red, and other potentially modifiable nitrogens which might hinder synthesis by late-stage functionalisation are highlighted in blue.

Chapter 4: Experimental

4.1 General Experimental

All non-aqueous reactions were conducted under a stream of dry nitrogen using oven-dried glassware. Temperatures of 0 °C were maintained using an ice-water bath. Room temperature (rt) refers to ambient temperature. Reactions performed under microwave irradiation were performed in sealed vials using a Biotage® Initiator+ microwave synthesizer.

Solvents: All solvents were used as received unless otherwise stated. Ethyl acetate (EtOAc), methanol (MeOH), dichloromethane (CH_2Cl_2), acetonitrile (MeCN) and toluene were distilled from calcium hydride. Petroleum ether (PE) refers to the fraction between 40–60 °C upon distillation. Tetrahydrofuran (THF) was dried using Na wire and distilled from a mixture of lithium aluminium hydride and calcium hydride with triphenylmethane as indicator. Anhydrous dimethylformamide (DMF), dimethyl sulfoxide (DMSO), 1,2-dimethoxyethane (DME), 1,2-dichloroethane (DCE) and 1,4-dioxane were purchased from commercial sources and used without further purification.

Reagents: Unless otherwise stated, all reagents were used as received from commercial sources and handled in accordance with COSHH regulations.

Yields: Yields refer to spectroscopically and chromatographically pure compounds unless otherwise stated. Any significant solvent peaks visible by NMR were factored into yield calculations.

Reaction monitoring: Reactions were monitored by thin layer chromatography (TLC) or liquid chromatography mass spectroscopy (LCMS). TLC was performed using glass plates pre-coated with Merck silica gel 60 F254 and visualised by UV fluorescence (λ_{max} = 254 nm) or by staining with potassium permanganate or vanillin. Retention factors (Rf) are quoted to 0.01. Where TLC Rfs were not obtained, the LCMS retention time is provided instead.

LCMS: LCMS analysis was performed using A) Waters ACQUITY H-Class UPLC with an ESCi Multi-Mode Ionisation Waters SQ Detector 2 spectrometer using MassLynx 4.1 software; LC system: solvent A: 2 mM NH_4OAc in H_2O/MeCN (95:5); solvent B: MeCN; solvent C: 2% HCO_2H; gradient: A/B/C, 90:5:5-0:95:5 over 1 min at a flow rate of 0.6 mL min^{-1} or B) CSH C18 reverse-phase silica, using a Waters Acquity UPLC CSH C18 column with dimensions 2.1 mm × 50 mm and particle size 1.7 µm with a gradient using decreasingly polar mixtures as eluent, for example, decreasingly polar mixtures of water (containing 0.1% formic acid or 0.1% ammonia) as solvent A and acetonitrile as solvent B. (A typical 2 min analytical UPLC method would employ a solvent gradient over 1.3 min, at approximately 1 mL/min, from a 97:3 mixture of solvents A and B respectively to a 3:97 mixture of solvents A and B.) Low resolution mass spectrometry (LRMS) data were obtained from these instruments.

Chromatography: Flash column chromatography (FCC) was carried out manually using Merck 9385 Kieselgel 60 SiO_2 (230-400 mesh) or using a Combiflash Rf200 automated chromatography system with Redisep® normal-phase silica flash columns (35−70 μm) or Redisep® reverse-phase C18-silica flash columns (20-40 μm).

HPLC: Analytical high performance liquid chromatography (HPLC) was performed on an Agilent 1260 Infinity machine, using a Supelcosil™ ABZ+PLUS column (150 mm × 4.6 4 mm, 3 μm) with a linear gradient system (solvent A: 0.05% (v/v) TFA in H_2O; solvent B: 0.05% (v/v) TFA in MeCN) over 20 min at a flow rate of 1 mL/min, and UV detection (λ_{max} = 220 – 254 nm).

IR: Infrared (IR) spectra were recorded neat on a Perkin-Elmer Spectrum One spectrometer with internal referencing. Selected absorption maxima (ν_{max}) are reported in wavenumbers (cm^{-1}) with peak intensity reported as w = weak, m = medium, s = strong, br = broad.

NMR: Proton and carbon nuclear magnetic resonance (NMR) were recorded using an internal deuterium lock on Bruker DPX-400 (400 MHz, 101 MHz), Bruker Avance 400 QNP (400 MHz, 101 MHz), Bruker Avance 500 Cryo Ultrashield (500 MHz, 126 MHz), Bruker Avance 600 BBI (600 MHz) and Bruker TXO Cryoprobe Avance II+ Ultrashield (700 MHz) spectrometers. For proton NMR, chemical shifts (δH) are reported in parts per million (ppm), to the nearest 0.01 ppm and are referenced to the residual non-deuterated solvent peak ($CDCl_3$: 7.26, DMSO-d_6: 2.50, CD_3OD (MeOD): 3.31, acetone-d_6: 2.05). Coupling constants (J) are reported in Hertz (Hz) to the nearest 0.1 Hz. Data are reported as follows: chemical shift, multiplicity (s = singlet; d = doublet; t = triplet; q = quartet; qn = quintet; sep = septet; m = multiplet; br = broad or a combination of these, e.g. dd, dt etc.), integration and coupling constant(s). For carbon NMR, chemical shifts (δC) are quoted in ppm, to the nearest 0.1 ppm, and are referenced to the residual non-deuterated solvent peak ($CDCl_3$: 77.16, DMSO-d_6: 39.52, MeOD: 49.00, acetone-d_6: 19.84, 206.26). Structural assignments are supported by DEPT-editing, ^{1}H-^{13}C HSQC, ^{1}H-^{13}C HMBC, ^{1}H-^{13}C ROESY or by analogy. Spectra were processed using TopSpin v. 4.1 (Bruker). Signals that could not be definitively assigned are described by their general characteristics, (i.e. aromatic, Ar) or as a selection of potential assignments (i.e. Ca/Cb). “Ha, Hb” refers to overlapping signals corresponding to Ha and Hb. Structural assignments are only provided for novel compounds and for known compounds a literature reference is provided which has agreeing spectral data.

HRMS: High resolution mass spectrometry (HRMS) measurements were recorded with a Micromass Q-TOF mass spectrometer or a Waters LCT Premier Time of Flight mass spectrometer. Mass values are reported within the error limits of ±5 ppm mass units. ESI refers to electrospray ionisation.

Protein LCMS: Protein LCMS was performed on a Xevo G2-S TOF mass spectrometer coupled to an Acquity UPLC system using an Acquity UPLC BEH300 C4 column (1.7 µm, 2.1 × 50 mm). H_2O with 0.1% formic acid (solvent A) and 95% MeCN and 5% water with 0.1% formic acid (solvent B), were used as the mobile phase at a flow rate of 0.2 mL/min. The gradient was programmed as follows: 95% A for 0.93 min, then a gradient to 100% B over 4.28 min, then 100% B for 1.04 minutes, then gradient to 95% A over 1.04 min. The electrospray source was operated with a capillary voltage of 2.0 kV and a cone voltage of 20 V, 40 V, 120 V or 150 V. Nitrogen was used as the desolvation gas at a total flow of 850 L/h. Total mass spectra were reconstructed from the ion series using the MaxEnt algorithm preinstalled on MassLynx software (v4.1 from Waters) according to the manufacturer's instructions. Only the region of the total ion chromatogram (TIC) between 3.25-3.75 min was analysed. Peaks outside of this range did not contain proteinogenic signals and were excluded. Trastuzumab and durvalumab samples were deglycosylated with PNGase F (New England Biolabs) prior to LCMS analysis.

Optical rotations ([α]D): Optical rotations were recorded on an Anton-Paar MCP polarimeter. The specific rotations are reported in deg dm^{-1} cm^3 g^{-1} at 589 nm, calculated from the optical rotation observed at a specific concentration and temperature. The temperature (°C) and solvent for the measurement are shown.

Fluorescence: Fluorescence was measured with a Pherastar FS plate reader using a 350/460 optic module or a CLARIOstar microplate reader.

Toxic reagent handling: Extreme care was taken when conducting reactions containing MMAE, olaparib and navitoclax. All handling was conducted in a fumehood while wearing full personal protective equipment (safety glasses, lab coat, nitrile gloves). Reactions were conducted on small scales, with local safety signage. All organic waste was disposed of immediately in appropriate waste containers.

4.2 Synthetic Procedures

Activation of Zn Powder

Zinc powder was activated by stirring with 1 M HCl (aq), followed by successive washing with H_2O, EtOH then Et_2O before rigorous drying under vacuum.

(4-(1-(((4-Methyl-2-oxo-*2H*-chromen-7-yl)carbamoyl)oxy)but-3-yn-1-yl)phenyl)boronic acid (1b)

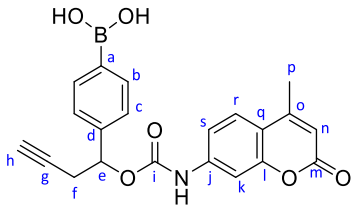

7-Amino-4-methylcoumarin (161 mg, 0.919 mmol) in CH_2Cl_2 (20 mL) was added triphosgene (114 mg, 0.383 mmol) then Et_3N (282 µL, 2.02 mmol). After 15 mins, 1-(4-(4,4,5,5-tetramethyl-1,3,2-dioxaborolan-2-yl)phenyl)but-3-yn-1-ol (**9**) (250 mg, 0.919 mmol) was added. After 1 h, additional Et_3N (128 µL, 0.918 mmol) was added and the mixture left to stir at rt overnight. H_2O (1 mL) was then added to the reaction mixture and then concentrated *in vacuo*. The residue was suspended in a mixture of MeCN:H_2O:NH_4OH (aq) until basic by pH paper. After stirring for several days, the mixture was concentrated *in vacuo* and purified by reverse-phase FCC (10-80% MeCN in H_2O), yielding 1-(4-(4,4,5,5-tetramethyl-1,3,2-dioxaborolan-2-yl)phenyl)but-3-yn-1-yl (4-methyl-2-oxo-2*H*-chromen-7-yl)carbamate (**1b**) (45.0 mg, 0.115 mmol, 13%) as an amorphous white solid.

LCMS (5-95% MeCN in H_2O, 2% formic acid) retention time 1.34 mins; **^{1}H NMR** (400 MHz, acetone-d_6): δ 8.02 (s, 1H, NH), 7.88 (d, 2H, *J* = 8.1 Hz, Hb), 7.69 (d, 1H, *J* = 8.7 Hz, Hr), 7.64 (d, 1H, *J* = 2.1 Hz, Hk), 7.52 (dd, 1H, *J* = 8.7, 2.1 Hz, Hs), 7.46 (d, 2H, *J* = 8.0 Hz, Hc), 6.17 (d, 1H, *J* = 1.1 Hz, Hn), 5.93 (t, 1H, *J* = 6.5 Hz, He), 2.82 (m, 2H, Hf), 2.44 (m, 4H, Hp, Hh); **^{13}C NMR*** (101 MHz, acetone-d_6): δ 160.6 (Cm), 155.1 (Cl), 153.3 (Co), 153.1 (Ci), 143.3 (Cd), 142.0 (Cj), 134.8 (Cb), 126.4 (Cc), 126.2 (Cr), 114.8 (Cs), 113.0 (Cn), 105.6 (Ck), 78.9 (Cg), 75.1 (Ce), 72.0 (Ch), 26.6 (Cf), 18.1 (Cp). **IR** ν_{max}/cm^{-1}: 3293 br (O-H), 1736 s (C=O), 1682 s (C=O), 1612 m (C=C); **HRMS (ESI)**: m/z calcd for $[M+H]^+$: 392.1305; found: 392.1312.

*Cq and Ca could not be identified due to low intensity.

(3,5-Difluoro-4-(1-(((4-methyl-2-oxo-2*H*-chromen-7-yl)carbamoyl)oxy)but-3-yn-1-yl)phenyl)boronic acid (2b)

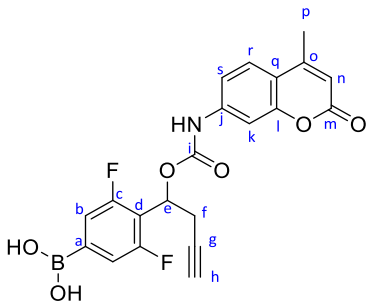

7-Amino-4-methylcoumarin (171 mg, 0.976 mmol) in CH_2Cl_2 (22 mL) was added triphosgene (115 mg, 0.388 mmol) then Et_3N (300 µL, 2.15 mmol). After 10 mins, 1-(2,6-difluoro-4-(4,4,5,5-tetramethyl-1,3,2-dioxaborolan-2-yl)phenyl)but-3-yn-1-ol (**11**) (300 mg, 0.974 mmol) was added. After 3 h, the reaction mixture was concentrated *in vacuo* then suspended in a mixture of MeCN:H_2O:NH_4OH (aq) until basic by pH paper. After stirring overnight, the mixture was concentrated *in vacuo* and purified by reverse-phase FCC (10-80% MeCN in H_2O), yielding (3,5-difluoro-4-(1-(((4-methyl-2-oxo-2*H*-chromen-7-yl)carbamoyl)oxy)but-3-yn-1-yl)phenyl)boronic acid (**2b**) (120 mg, 0.280 mmol, 29%) as an amorphous white solid.

LCMS (5-95% MeCN in H_2O, 2% formic acid) retention time 1.34 mins; **^{1}H NMR** (400 MHz, Acetone-d_6): δ 7.68 (d, 1H, *J* = 8.7 Hz, Hr), 7.60 (d, 1H, *J* = 2.0 Hz, Hk), 7.51 (dd, 1H, *J* = 8.7, 2.1 Hz, Hs), 7.42 (m, 2H, Hb), 6.26 (t, 1H, *J* = 7.7 Hz, He), 6.16 (br s, 1H, Hn), 3.00 (m, 2H, Hf), 2.46 (t, 1H, *J* = 2.6 Hz, Hh), 2.43 (br s, 3H, Hp); **^{13}C NMR** (101 MHz, Acetone-d_6): δ 163.3-160.8 (dd, *J* = 250.5, 6.7 Hz, Cc), 161.3 (Cm), 155.7 (Cl), 154.0 (Co), 153.5 (Ci), 143.6 (Cj), 127.0 (Cr), 117.8-117.3 (Cb, Cd, Ca), 116.3 (Cq), 115.5 (Cs), 113.6 (Cn), 106.2 (Ck), 79.8 (Cg), 72.8 (Ch), 67.5 (Ce), 24.5 (Cf), 18.7 (Cp); **IR** ν_{max} /cm^{-1}: 3300 br (O-H), 2924 s (C-H alkyne), 1687 s (C=O), 1615 m (C=O); **HRMS (ESI)**: m/z calcd for $[M+H]^+$: 428.1117; found: 428.1110.

1-(4-Bromophenyl)but-3-yn-1-yl (4-methyl-2-oxo-2*H*-chromen-7-yl)carbamate (3)

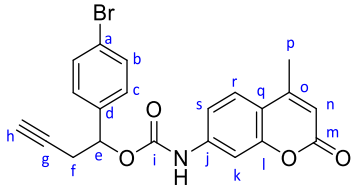

7-Amino-4-methylcoumarin (156 mg, 0.890 mmol) and triphosgene (131 mg, 0.441 mmol) were suspended in toluene (32 mL) and heated to reflux. After 2 h, the reaction mixture was cooled to rt and evaporated under a stream of nitrogen before a solution of 1-(4-bromophenyl)but-3-yn-1-ol (**7**)

(200 mg, 0.889 mmol) in THF (32 mL) was added. Dibutyltin dilaurate (53.0 µL, 0.0895 mmol) was added to the resulting suspension and stirred at rt for approx. 18 h before being quenched with H_2O (3 mL) and concentrated *in vacuo*. The crude residue was then purified by reverse-phase FCC (10-80% MeCN in 0.5% formic acid (aq)), yielding 1-(4-bromophenyl)but-3-yn-1-yl (4-methyl-2-oxo-2*H*-chromen-7-yl)carbamate (**3**) (196 mg, 0.460 mmol, 52%) as an amorphous white solid.

LCMS (5-95% MeCN in H_2O, 2% formic acid) retention time 1.51 mins; **^{1}H NMR** (400 MHz, $CDCl_3$): δ 7.52 (m, 3H, Hb/Hc and Hs/Hr/Hk), 7.38 (m, 2H, Hs/Hr/Hk), 7.31 (m, 2H, Hb/Hc), 6.19 (br s, 1H, Hn), 5.87 (t, 1H, *J* = 6.5 Hz, He), 2.78 (m, 2H, Hf), 2.40 (br s, 3H, Hp), 2.03 (t, 1H, *J* = 2.7 Hz, Hh); **^{13}C NMR** (101 MHz, $CDCl_3$): δ 161.1 (Cm), 154.5 (Cl), 152.3 (Co), 151.8 (Ci), 141.1 (Cd), 137.7 (Cj), 131.9 (Ar), 128.3 (Cb/Cc), 125.5 (Ar), 123.0 (Ca), 115.9 (Cq), 114.5 (Cs/Cr/Ck), 113.5 (Cn), 106.2 (Ar), 79.0 (Cg), 74.4 (Ce), 71.7 (Ch), 26.5 (Cf), 18.9 (Cp); **IR** ν_{max} /cm^{-1}: 3274 s (C-H alkyne), 1682 s (C=O), 1584 m (C=O); **HRMS (ESI)**: m/z calcd for $[M+H]^+$: 426.0342; found: 426.0343.

4-((*S*)-2-((*S*)-2-(2-Methoxyacetamido)-3-methylbutanamido)-5-ureidopentanamido)benzyl (4-methyl-2-oxo-2*H*-chromen-7-yl)carbamate (4)

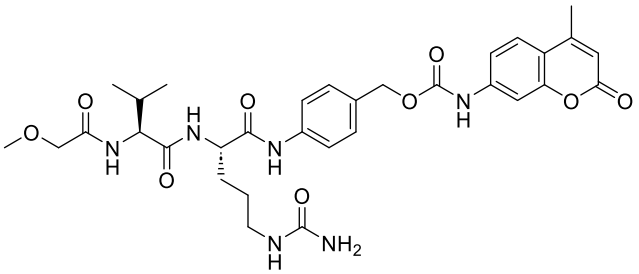

7-Amino-4-methylcoumarin (52.0 mg, 0.297 mmol) in CH_2Cl_2 (5 mL) was added triphosgene (15.0 mg, 50.5 µmol) then Et_3N (35.0 µL, 0.251 mmol). After 10 mins, (*S*)-*N*-(4-(hydroxymethyl)phenyl)-2-((*S*)-2-(2-methoxyacetamido)-3-methylbutanamido)-5-ureidopentanamide (**19**) (52.0 mg, 0.115 mmol) in DMF (1 mL) was added. After stirring overnight, the reaction mixture was quenched with H_2O (0.5 mL), concentrated under a stream of N_2 and then purified by FCC (10-15% MeOH in CH_2Cl_2) yielding 4-((*S*)-2-((*S*)-2-(2-methoxyacetamido)-3-methylbutanamido)-5-ureidopentanamido)benzyl (4-methyl-2-oxo-2*H*-chromen-7-yl)carbamate (**4**) (46.0 mg, 70.5 µmol, 61%) as an amorphous white solid.

LCMS (5-95% MeCN in H_2O, 2% formic acid) retention time 1.56 mins; **^{1}H NMR** (500 MHz, DMSO-d_6): δ 10.27 (br s, 1H), 10.16 (br s, 1H), 8.36 (d, 1H, *J* = 7.5 Hz), 7.69 (d, 1H, *J* = 9.0 Hz), 7.61 (d, 2H, *J* = 8.4 Hz), 7.56 (d, 1H, *J* = 1.9 Hz), 7.47 (d, 1H, *J* = 8.8 Hz), 7.41 (dd, 1H, *J* = 8.9, 2.0 Hz), 7.38 (d, 2H, *J* = 8.6 Hz), 6.23 (d, 1H, *J* = 1.6 Hz), 6.08 (t, 1H, *J* = 5.9 Hz), 5.41 (br s, 2H), 5.13 (s, 2H), 4.40 (m, 1H), 4.30 (m, 1H), 3.86 (d, 2H, *J* = 1.2 Hz), 3.32 (s, 3H) 2.97 (m, 2H), 2.38 (d, 3H, *J* = 1.2 Hz), 2.00 (m, 1H), 1.70 (m, 1H), 1.59 (m, 1H), 1.44 (m, 1H), 1.36 (m, 1H), 0.86 (d, 3H, *J* = 6.9 Hz), 0.81 (d, 3H, *J* = 6.8 Hz); **^{13}C NMR**

(101 MHz, DMSO-d_6): δ 170.8, 170.6, 168.7, 160.1, 158.9, 153.8, 153.2, 142.8, 139.0, 130.8, 129.1, 126.1, 119.0, 114.4, 114.3, 111.9, 104.4, 71.2, 66.0, 58.6, 56.7, 53.2, 38.4, 31.0, 29.2, 22.1, 19.2, 18.01, 18.00.

Spectroscopic data are in accordance with the literature.[73]

(2-Fluoro-4-(1-(((4-methyl-2-oxo-2*H*-chromen-7-yl)carbamoyl)oxy)but-3-yn-1-yl)phenyl)boronic acid (5b)

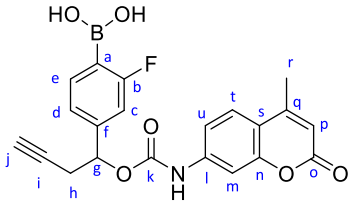

7-Amino-4-methyl-2*H*-chromen-2-one (123 mg, 0.700 mmol) in CH_2Cl_2 (20 mL) was added triphosgene (82.9 mg, 0.279 mmol) followed by Et_3N (216 µL, 1.55 mmol). After 10 mins, 1-(3-fluoro-4-(4,4,5,5-tetramethyl-1,3,2-dioxaborolan-2-yl)phenyl)but-3-yn-1-ol (**13**) (203 mg, 0.698 mmol) in CH_2Cl_2 (1.5 mL) was added at rt. After 1 h, additional Et_3N (97.0 µL, 0.695 mmol) was added and stirred for an additional 6 h. Then, the reaction was quenched with H_2O (3 mL), concentrated *in vacuo* then purified by reverse-phase FCC (10-100% MeCN in H_2O) and lyophilised to yield a mixture of boronic ester and acid product. The boronic ester 1-(3-fluoro-4-(4,4,5,5-tetramethyl-1,3,2-dioxaborolan-2-yl)phenyl)but-3-yn-1-yl (4-methyl-2-oxo-2*H*-chromen-7-yl)carbamate (**5a**) (91.3 mg, 0.186 mmol) was subjected to hydrolysis by stirring in 1:1 H_2O:MeCN with addition of NH_4OH (aq) until basic by pH paper. After stirring overnight at rt and combined with the boronic acid material isolated originally, (2-fluoro-4-(1-(((4-methyl-2-oxo-2*H*-chromen-7-yl)carbamoyl)oxy)but-3-yn-1-yl)phenyl)boronic acid (**5b**) (53.5 mg, 0.100 mmol, 14%) was afforded as an amorphous white powder.

LCMS (5-95% MeCN in H_2O, 2% formic acid) retention time 1.33 mins; **^{1}H NMR** (400 MHz, Acetone-d_6): δ 7.76 (app t, 1H, *J* = 7.1 Hz, Ht), 7.70 (d, 1H, *J* = 8.7 Hz, He), 7.66 (d, 1H, *J* = 2.0 Hz, Hc), 7.53 (dd, 1H, *J* = 8.7, 2.1 Hz, Hd), 7.32 (dd, 1H, *J* = 7.7, 1.0 Hz, Hu), 7.21 (d, 1H, *J* = 10.6 Hz, Hm), 6.18 (d, 1H, *J* = 1.2 Hz, Hp), 5.95 (t, 1H, *J* = 6.2 Hz, Hg), 2.90 (m, 2H, Hh), 2.48 (t, 1H, *J* = 2.6 Hz, Hj), 2.45 (d, 3H, *J* = 1.2 Hz, Hr); **^{13}C NMR** (101 MHz, Acetone-d_6): δ 168.0-165.6 (d, *J* = 244.9 Hz, Cb), 159.8 (Co), 154.5 (Ck), 152.6 (Cn/Cq), 152.3 (Cn/Cq), 144.4-144.3 (d, *J* = 8.4 Hz, Cf), 136.2 (Ct), 136.1 (Cl), 125.8 (Ce), 121.8 (Ca), 115.1 (Cs), 114.2 (Cd), 113.0 (Cu), 112.7 (Cm), 112.5 (Cp), 105.1 (Cc), 79.2 (Ci), 73.5 (Cg), 71.7 (Cj), 25.8 (Ch), 17.5 (Cr); **IR** ν_{max} /cm^{-1}: 3292 br (O-H), 2986 m (C-H alkyne), 1685 m (C=O), 1620 m (C=C); **HRMS (ESI)**: m/z calcd for $[M+H]^+$: 410.1211; found: 410.1209.

1-(4-Bromophenyl)but-3-yn-1-ol (7)

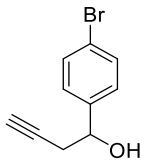

Method 1: Activated Zn powder (264 mg, 4.05 mmol) and propargyl bromide (80 wt% in toluene) (720 µL, 6.46 mmol) were stirred in DMF (15 mL) until the solution turned deep black. 4-bromobenzaldehyde (501 mg, 2.71 mmol) was then added at rt. After approx. 16 h, 1 N HCl (40 mL) was added to the reaction mixture and extracted with EtOAc (3 x 40 mL). The combined organic phases were then washed with 3 M LiCl (aq) (4 x 50 mL), dried over Na_2SO_4 then purified by FCC (20% EtOAc in PE) yielding 1-(4-bromophenyl)but-3-yn-1-ol (**7**) (318 mg, 1.41 mmol, 52%) as an orange oil.

Method 2 (Sonochemical Barbier): 4-Bromobenzaldehyde (500 mg, 2.70 mmol), activated Zn powder (882 mg, 13.5 mmol), diiodoethane (765 mg, 2.71 mmol) and propargyl bromide (80 wt% in toluene) (450 µL, 4.04 mmol) were suspended in THF (10 mL) and sonicated at rt for 2 h. 1 N HCl (40 mL) was then added to the reaction mixture and was extracted with EtOAc (4 x 40 mL). The combined organic phases were washed with brine (40 mL), dried over Na_2SO_4 and concentrated *in vacuo*. The crude residue was purified by FCC (20% EtOAc in PE) yielding 1-(4-bromophenyl)but-3-yn-1-ol (**7**) (325 mg, 1.28 mmol, 68%) as a pale-yellow oil.

R_f = 0.16 (20% EtOAc in PE); **^{1}H NMR** (400 MHz, $CDCl_3$): δ 7.51 (d, 2H, *J* = 7.9 Hz), 7.29 (d, 2H, *J* = 7.6 Hz), 4.86 (t, 1H, *J* = 6.3 Hz), 2.63 (m, 2H), 2.10 (m, 1H); **^{13}C NMR** (101 MHz, $CDCl_3$): δ 141.4, 131.6, 127.5, 121.8, 80.2, 71.7, 71.4, 29.4.

Spectroscopic data are in accordance with the literature.[292]

4-(4,4,5,5-Tetramethyl-1,3,2-dioxaborolan-2-yl)benzaldehyde (8)

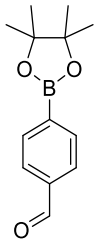

$PdCl_2(dppf)\cdot CH_2Cl_2$ (134 mg, 0.164 mmol), B_2Pin_2 (1.51 g, 5.95 mmol) and KOAc (1.59 g, 16.2 mmol) were suspended in DMSO (20 mL), and 4-bromobenzaldehyde (994 mg, 5.37 mmol) was added. The mixture was heated at 80 °C for 3.5 h, cooled to rt, then filtered through a pad of celite. The filtrate

was concentrated *in vacuo* then purified by FCC (5% EtOAc in PE) yielding 4-(4,4,5,5-tetramethyl-1,3,2-dioxaborolan-2-yl)benzaldehyde (**8**) (427 mg, 1.84 mmol, 34%) as a yellow oil.

R_f = 0.36 (2:1 EtOAc:PE); **^{1}H NMR** (400 MHz, $CDCl_3$): δ 9.95 (s, 1H), 7.88 (d, 2H, *J* = 7.7 Hz), 7.77 (d, 2H, *J* = 7.7 Hz), 1.28 (s, 12H); **^{13}C NMR*** (101 MHz, $CDCl_3$): δ 192.4, 138.1, 135.2, 128.6, 84.2, 24.8.

Spectroscopic data are in accordance with the literature.[293] *The carbon connected to boron could not be identified due to low intensity.

1-(4-(4,4,5,5-Tetramethyl-1,3,2-dioxaborolan-2-yl)phenyl)but-3-yn-1-ol (9)

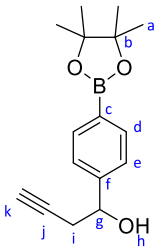

Method 1: Activated Zn powder (22.0 mg, 0.336 mmol) and propargyl bromide (80 wt% in toluene) (36.0 µL, 0.380 mmol) were stirred in DMF (750 µL) until the solution turned deep black. 4-(4,4,5,5-Tetramethyl-1,3,2-dioxaborolan-2-yl)benzaldehyde (**8**) (50.0 mg, 0.215 mmol) was then added at rt. After 3 h, 1 N HCl (5 mL) was added to the reaction mixture and extracted with EtOAc (3 x 10 mL). The combined organic phases were then washed with 3 M LiCl (3 x 20 mL), dried over Na_2SO_4, concentrated *in vacuo*, then purified by FCC (50% EtOAc in PE) yielding 1-(4-(4,4,5,5-tetramethyl-1,3,2-dioxaborolan-2-yl)phenyl)but-3-yn-1-ol (**9**) (34.9 mg, 0.128 mmol, 60%) as a yellow oil.

Method 2 (Sonochemical Barbier): 4-(4,4,5,5-Tetramethyl-1,3,2-dioxaborolan-2-yl)benzaldehyde (**8**) (199 mg, 0.857 mmol), activated Zn powder (282 mg, 4.31 mmol), diiodoethane (278 mg, 0.879 mmol) and propargyl bromide (80 wt% in toluene) (140 µL, 1.26 mmol) were suspended in THF (5 mL) and sonicated at rt overnight. 1 N HCl (30 mL) was then added to the reaction mixture and was extracted with EtOAc (4 x 30 mL). The combined organic phases were washed with brine (30 mL), dried over Na_2SO_4 and concentrated *in vacuo*. The crude residue was purified by FCC (40% EtOAc in PE) yielding 1-(4-(4,4,5,5-tetramethyl-1,3,2-dioxaborolan-2-yl)phenyl)but-3-yn-1-ol (**9**) (98.1 mg, 0.360 mmol, 42%) as a yellow oil.

R_f = 0.64 (50% EtOAc in PE); **^{1}H NMR** (400 MHz, $CDCl_3$): δ 7.80 (d, 2H, *J* = 7.9 Hz, Hd/He), 7.39 (d, 2H, *J* = 8.0 Hz, Hd/He), 4.89 (t, 1H, *J* = 5.8 Hz, Hg), 2.64 (m, 2H, Hi), 2.06 (t, 1H, *J* = 2.6 Hz, Hk) 1.34 (s, 12H, Ha); **^{13}C NMR*** (101 MHz, $CDCl_3$): δ 145.5 (Cf), 135.0 (Cd/Ce), 125.0 (Cd/Ce), 83.8 (Cb), 80.5 (Cj), 72.3 (Cg), 71.1 (Ck), 29.4 (Ci), 24.9 (Ca); **IR ν_{max}** /cm^{-1}: 3430 br (O-H), 3288 s (C-H alkyne); **HRMS (ESI)**: m/z calcd for $[M+H]^+$: 273.1657; found: 273.1661.

*Cc could not be identified due to low intensity.

2,6-Difluoro-4-(4,4,5,5-tetramethyl-1,3,2-dioxaborolan-2-yl)benzaldehyde (10)

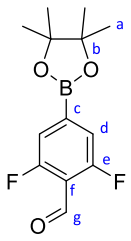

4-Bromo-2,6-difluorobenzaldehyde (50.0 mg, 226 µmol), $PdCl_2(dppf)\cdot CH_2Cl_2$ (18.5 mg, 22.7 µmol), KOAc (66.5 mg, 678 µmol) and B_2Pin_2 (63.0 mg, 248 µmol) were suspended in THF (23 mL) and irradiated in a microwave at 80 °C for 2 h. After cooling to rt, the reaction mixture was filtered through a pad of celite and the filtrate concentrated *in vacuo* and purified by FCC (5-100% EtOAc in PE) yielding 2,6-difluoro-4-(4,4,5,5-tetramethyl-1,3,2-dioxaborolan-2-yl)benzaldehyde (**10**) (103 mg) as a colourless oil with an impurity related to B_2Pin_2.

R_f = 0.25 (10% EtOAc in PE); **^{1}H NMR** (500 MHz, $CDCl_3$): δ 10.38 (s, 1H, Hg), 7.38 (m, 2H, Hd), 1.35 (s, 12H, Ha); **^{13}C NMR** (126 MHz, $CDCl_3$): δ 185.0 (Cg), 163.5-161.4 (dd, *J* = 263.9, 4.7 Hz, Ce), 117.9-117.8 (dd, *J* = 19.6, 4.5 Hz, Cd), 115.6 (app t, *J* = 11.1 Hz, Cf), 85.0 (Cb), 25.0 (Ca); **IR** ν_{max} /cm^{-1}: 2980 s (C-H), 1705 s (C=O), 1367 m (C-H aldehyde); **HRMS (ESI)**: m/z calcd for $[M+H]^+$: 269.1155; found: 269.1152.

*Cc could not be identified due to low intensity.

1-(2,6-Difluoro-4-(4,4,5,5-tetramethyl-1,3,2-dioxaborolan-2-yl)phenyl)but-3-yn-1-ol (11)

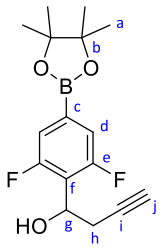

Activated Zn powder (26.4 mg, 404 µmol) and propargyl bromide (80 wt% in toluene) (45.0 µL, 475 µmol) were stirred in DMF (1 mL) until the solution turned deep black. 2,6-Difluoro-4-(4,4,5,5-tetramethyl-1,3,2-dioxaborolan-2-yl)benzaldehyde (**10**) (103 mg, impure) was then added and the mixture cooled to 0 °C. After 30 mins, additional Zn powder (26.4 mg, 404 µmol) was added. After 15 mins, the reaction mixture was diluted with EtOAc (10 mL), then 1 N HCl (10 mL) was added and extracted. The organic phase was then washed with 5% LiCl (20 mL), dried over Na_2SO_4, concentrated *in vacuo*, then purified by FCC (10% EtOAc in PE) yielding 1-(2,6-difluoro-4-(4,4,5,5-tetramethyl-1,3,2-

dioxaborolan-2-yl)phenyl)but-3-yn-1-ol (**11**) (38.5 mg, 125 µmol, 67% from 4-bromo-2,6-difluorobenzaldehyde) as an amorphous white solid.

R_f = 0.25 (66% EtOAc in PE); **^{1}H NMR** (500 MHz, $CDCl_3$): δ 7.31 (m, 2H, Hd), 5.27 (t, 1H, *J* = 6.9 Hz, Hg) 2.83 (m, 2H, Hh), 2.01 (t, 1H, *J* = 2.6 Hz, Hj), 1.34 (s, 12H, Ha); **^{13}C NMR*** (126 MHz, $CDCl_3$): δ 161.6-159.5 (dd, *J* = 249.8, 7.0 Hz, Ce), 120.2 (t, *J* = 16.5 Hz, Cf), 117.5-117.3 (dd, *J* = 20.0, 5.0 Hz, Cd), 84.6 (Cb), 79.5 (Ci), 70.8 (Cj), 65.2 (Cg), 27.2 (Ch), 24.8 (Ca); **IR** ν_{max} /cm^{-1}: 3429 br (O-H), 3420 s (C-H alkyne); **HRMS (ESI)**: m/z calcd for $[M+H]^+$: 309.1468; found: 309.1482.

*Cc could not be identified due to low intensity.

3-Fluoro-4-(4,4,5,5-tetramethyl-1,3,2-dioxaborolan-2-yl)benzaldehyde (12)

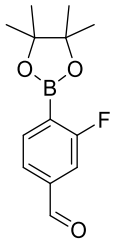

4-Bromo-3-fluorobenzaldehyde (99.0 mg, 0.488 mmol), $PdCl_2(dppf)\cdot CH_2Cl_2$ (12.1 mg, 14.8 µmol), B_2Pin_2 (138 mg, 0.543 mmol) and KOAc (145 mg, 1.48 mmol) were suspended in THF (5 mL) and then irradiated in a microwave at 80 °C for 5 h. After cooling to rt, the reaction mixture was filtered through a pad of celite and the filtrate concentrated *in vacuo* and purified by FCC (10% EtOAc in PE) yielding 3-fluoro-4-(4,4,5,5-tetramethyl-1,3,2-dioxaborolan-2-yl)benzaldehyde (**12**) (49.6 mg, 0.198 mmol, 38%) as a colourless oil.

R_f = 0.63 (2:1 EtOAc:PE); **^{1}H NMR** (400 MHz, $CDCl_3$): δ 9.99 (s, 1H), 7.89 (m, 1H), 7.62 (d, 1H, *J* = 7.6 Hz), 7.49 (d, 1H, *J* = 8.2 Hz), 1.36 (s, 12H); **^{13}C NMR*** (101 MHz, $CDCl_3$): δ 191.09-191.07 (d, *J* = 2.1 Hz), 168.5-166.0 (d, *J* = 253.7 Hz), 140.5-140.4 (d, *J* = 6.9 Hz), 137.7-137.6 (d, *J* = 8.0 Hz), 124.84-124.81 (d, *J* = 3.2 Hz), 115.4-115.1 (d, *J* = 24.8 Hz), 84.4, 24.8.

Spectroscopic data are in accordance with the literature.[294] *Cc could not be identified due to low intensity.

1-(3-Fluoro-4-(4,4,5,5-tetramethyl-1,3,2-dioxaborolan-2-yl)phenyl)but-3-yn-1-ol (13)

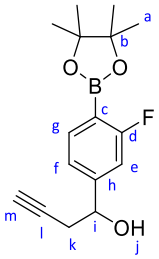

Method 1: Activated Zn powder (19.5 mg, 0.298 mmol) and propargyl bromide (80 wt% in toluene) (32.7 µL, 0.345 mmol) were stirred in DMF (400 µL) until the solution turned deep black. 3-Fluoro-4-(4,4,5,5-tetramethyl-1,3,2-dioxaborolan-2-yl)benzaldehyde (**12**) (49.0 mg, 0.196 mmol) was then added at rt. After 30 mins, 1 N HCl (5 mL) was added to the reaction mixture and extracted with EtOAc (3 x 10 mL). The combined organic phases were then washed with 3 M LiCl (3 x 20 mL), dried over Na_2SO_4, concentrated *in vacuo*, then purified by FCC (40% EtOAc in PE) yielding 1-(3-fluoro-4-(4,4,5,5-tetramethyl-1,3,2-dioxaborolan-2-yl)phenyl)but-3-yn-1-ol (**13**) (7.20 mg, 24.8 µmol, 13%) as a colourless oil.

Method 2 (Sonochemical Barbier): 3-Fluoro-4-(4,4,5,5-tetramethyl-1,3,2-dioxaborolan-2-yl)benzaldehyde (**12**) (167 mg, 0.668 mmol), activated Zn powder (216 mg, 3.30 mmol), diiodoethane (187 mg, 0.665 mmol) and propargyl bromide (80 wt% in toluene) (110 µL, 0.988 mmol) were suspended in THF (3.5 mL) and sonicated at rt for 1 h. 1 N HCl (15 mL) was then added to the reaction mixture and was extracted with EtOAc (4 x 20 mL). The combined organic phases were washed with brine (20 mL), dried over Na_2SO_4 and concentrated *in vacuo*. The crude residue was purified by FCC (30% EtOAc in PE) yielding 1-(3-fluoro-4-(4,4,5,5-tetramethyl-1,3,2-dioxaborolan-2-yl)phenyl)but-3-yn-1-ol (**13**) (87.9 mg, 0.303 mmol, 45%) as a colourless oil.

R_f = 0.50 (40% EtOAc in PE); **^{1}H NMR** (400 MHz, $CDCl_3$): δ 7.73 (m, 1H, Hg), 7.12 (m, 2H, He, Hf), 4.88 (m, 1H, Hi), 2.63 (m, 2H, Hk), 2.07 (t, 1H, *J* = 2.7 Hz, Hm), 1.36 (s, 12H, Ha); **^{13}C NMR*** (101 MHz, $CDCl_3$): δ 168.5-166.0 (d, *J* = 251.3 Hz, Cd), 148.5-148.4 (d, *J* = 7.9 Hz, Ch), 137.0-136.9 (d, *J* = 8.4 Hz, Cg), 120.9-120.8 (d, *J* = 3.0 Hz, Cf), 112.7-112.5 (d, *J* = 25.2 Hz, Ce), 83.9 (Cb), 71.54 (Cl), 71.52 (Ci), 71.4 (Cm), 29.4 (Ck), 24.8 (Ca); **IR** ν_{max} /cm^{-1}: 3518 br (O-H), 3300 s (C-H alkyne), 1703 s (C=O), 1624 s (C=O); **HRMS (ESI)**: m/z calcd for $[M+H]^+$: 291.1562; found: 291.1573.

*Cc could not be identified due to low intensity.

3-Nitro-4-(4,4,5,5-tetramethyl-1,3,2-dioxaborolan-2-yl)benzaldehyde (14)

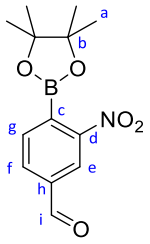

$PdCl_2(dppf)\cdot CH_2Cl_2$ (53.7 mg, 65.8 μmol), B_2Pin_2 (607 mg, 2.39 mmol) and KOAc (640 mg, 6.52 mmol) were suspended in 1,4-dioxane (10 mL), and 4-bromo-3-nitrobenzaldehyde (501 mg, 2.18 mmol) was added. The mixture was shielded from light and heated at 80 °C for 4 h, cooled to rt, then filtered through a pad of celite. The filtrate was concentrated *in vacuo* then purified by reverse-phase FCC (10-100% MeCN in 0.5% formic acid (aq)), yielding 3-nitro-4-(4,4,5,5-tetramethyl-1,3,2-dioxaborolan-2-yl)benzaldehyde (**14**) (97.0 mg) as an impure yellow solid.

R_f = 0.49 (66% EtOAc in PE); **^{1}H NMR** (700 MHz, $CDCl_3$): δ 10.10 (s, 1H, Hi), 8.62 (s, 1H, He), 8.16 (d, 1H, *J* = 7.1 Hz, Hf), 7.73 (d, 1H, *J* = 7.0 Hz, Hg), 1.43 (s, 12H, Ha); **^{13}C NMR*** (176 MHz, $CDCl_3$): δ 189.8 (Ci), 137.8 (Cd), 134.0 (Cg), 133.4 (Cf), 123.9 (Ce), 85.2 (Cb), 24.7 (Ca).

Spectroscopic data are in accordance with the literature.[295] *Cc was not identified due to low intensity.

(4-(1-Hydroxybut-3-yn-1-yl)-2-nitrophenyl)boronic acid (15)

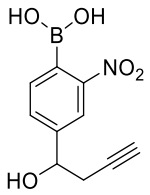

Activated Zn powder (21.8 mg, 0.333 mmol) and propargyl bromide (80 wt% in toluene) (36.2 μL, 0.382 mmol) were stirred in DMF (1 mL) until the solution turned deep black. Impure 3-nitro-4-(4,4,5,5-tetramethyl-1,3,2-dioxaborolan-2-yl)benzaldehyde (**14**) (60.0 mg) in DMF (200 μL) was then added at rt. After 3 h, 1 N HCl (5 mL) was added to the reaction mixture and extracted with EtOAc (3 x 10 mL). The combined organic phases were then washed with 3 M LiCl (3 x 20 mL), dried over Na_2SO_4, concentrated *in vacuo*, then purified by FCC (2:1 EtOAc:PE) yielding impure (4-(1-hydroxybut-3-yn-1-yl)-2-nitrophenyl)boronic acid (**15**) (10.0 mg) as an impure orange oil. The material was carried forward without further purification or characterisation.

(*S*)-2-((((9*H*-Fluoren-9-yl)methoxy)carbonyl)amino)-5-ureidopentanoic acid (16)

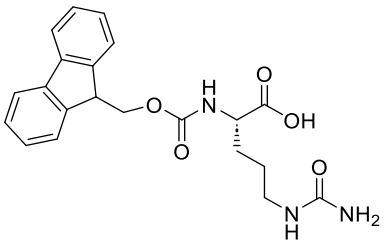

To a suspension of citrulline (499 mg, 2.85 mmol) in H_2O (24 mL) was added $NaHCO_3$ (479 mg, 5.71 mmol). After 1 h at rt, FMOC-Cl (670 mg, 2.59 mmol) in DME (12 mL) was added. After stirring at rt overnight, DME was removed under vacuum and the mixture was extracted with EtOAc (3 x 30 mL). The aqueous layer was then acidified with 1 N HCl (15 mL). The aqueous phase was extracted with 10% iPrOH:EtOAc (3 x 50 mL) and then the combined organic phases dried over Na_2SO_4 then concentrated *in vacuo*. Et_2O (20 mL) was added to the clear viscous liquid, and the resulting white precipitate was collected by vacuum filtration, with successive washings with Et_2O yielding (*S*)-2-((((9*H*-fluoren-9-yl)methoxy)carbonyl)amino)-5-ureidopentanoic acid (**16**) (724 mg, 1.82 mmol, 64%) as an amorphous white solid.

LCMS (5-95% MeCN in H_2O, 2% formic acid) retention time 1.27 mins; **^{1}H NMR** (400 MHz, DMSO-d_6): δ 12.58 (br s, 1H), 7.90 (d, 2H, *J* = 7.5 Hz), 7.73 (d, 2H, *J* = 7.4 Hz), 7.67 (d, 1H, *J* = 8.0 Hz), 7.43 (app t, 2H, *J* = 7.4 Hz), 7.34 (app t, 2H, *J* = 7.3 Hz), 5.94 (br t, 1H), 5.38 (br s, 2H), 4.25 (m, 3H), 3.93 (m, 1H), 2.96 (m, 2H), 1.70 (m, 1H), 1.57 (m, 1H), 1.43 (m, 2H); **^{13}C NMR** (101 MHz, DMSO-d_6): δ 173.9, 158.7, 156.1, 143.9, 143.8, 140.7, 127.6, 127.1, 125.3, 120.1, 65.6, 53.7, 46.6, 28.2, 26.8.

Spectroscopic data are in accordance with the literature.[130]

(9*H*-Fluoren-9-yl)methyl(*S*)-(1-((4-(hydroxymethyl)phenyl)amino)-1-oxo-5-ureidopentan-2-yl)carbamate (17)

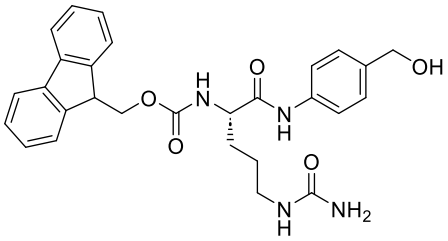

(*S*)-2-((((9*H*-fluoren-9-yl)methoxy)carbonyl)amino)-5-ureidopentanoic acid (**16**) (720 mg, 1.81 mmol) and 4-aminobenzyl alcohol (672 mg, 5.45 mmol) in DMF (18 mL) was added DIPEA (317 µL, 1.82 mmol) and stirred at rt for 15 mins. Then, HATU (760 mg, 2.00 mmol) was added and the reaction mixture was stirred in the dark overnight. The reaction mixture was then concentrated *in vacuo* and purified

by FCC (2-10% MeOH in CH_2Cl_2), yielding (9*H*-fluoren-9-yl)methyl (*S*)-(1-((4-(hydroxymethyl)phenyl)amino)-1-oxo-5-ureidopentan-2-yl)carbamate (**17**) (623 mg, 1.24 mmol, 68%) as a pale-orange amorphous solid.

LCMS (5-95% MeCN in H_2O, 2% formic acid) retention time 1.64 mins; **^{1}H NMR** (400 MHz, DMSO-d_6): δ 9.98 (s, 1H), 7.89 (d, 2H, *J* = 7.5 Hz), 7.75 (m, 2H), 7.67 (d, 1H, *J* = 7.9 Hz), 7.56 (d, 2H, *J* = 8.1 Hz), 7.42 (app t, 2H, *J* = 7.3 Hz), 7.34 (m, 2H), 7.24 (d, 2H, *J* = 8.1 Hz), 6.00 (br t, 1H), 5.43 (br s, 2H), 4.43 (s, 2H), 4.21 (m, 4H), 3.00 (m, 2H), 1.64 (m, 2H), 1.44 (m, 2H); **^{13}C NMR** (101 MHz, DMSO-d_6): δ 171.0, 158.9, 156.1, 143.9, 140.7, 137.6, 137.4, 127.7, 127.1, 126.9, 125.4, 120.1, 118.9, 65.7, 62.6, 55.0, 46.7, 38.6, 29.3, 26.9.

Spectroscopic data are in accordance with the literature.[130]

(9*H*-Fluoren-9-yl)methyl ((*S*)-1-(((*S*)-1-((4-(hydroxymethyl)phenyl)amino)-1-oxo-5-ureidopentan-2-yl)amino)-3-methyl-1-oxobutan-2-yl)carbamate (18)

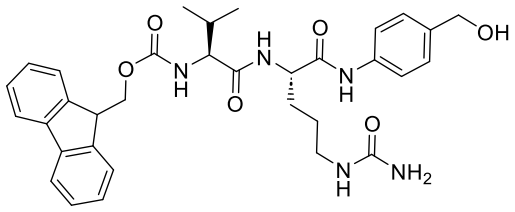

(9*H*-Fluoren-9-yl)methyl (*S*)-(1-((4-(hydroxymethyl)phenyl)amino)-1-oxo-5-ureidopentan-2-yl)carbamate (**17**) (376 mg, 0.748 mmol) in DMF (4 mL) was added Et_3N (2.00 mL, 14.3 mmol) and stirred at rt overnight. DMF and Et_3N were removed under a stream of N_2, then DMF (6 mL) was added followed by fmoc-L-valine *N*-hydroxysuccinimide ester (FMOC-Val-OSu) (359 mg, 0.822 mmol) and the mixture stirred at rt for 1 h. The reaction mixture was concentrated by a stream of N_2 then purified by FCC (2-10% MeOH in CH_2Cl_2) to yield (9*H*-fluoren-9-yl)methyl ((*S*)-1-(((*S*)-1-((4-(hydroxymethyl)phenyl)amino)-1-oxo-5-ureidopentan-2-yl)amino)-3-methyl-1-oxobutan-2-yl)carbamate (**18**) (244 mg, 0.406 mmol, 54%) as an amorphous pale-pink solid.

LCMS (5-95% MeCN in H_2O, 2% formic acid) retention time 1.66 mins; **^{1}H NMR** (400 MHz, DMSO-d_6): δ 10.00 (s, 1H), 8.11 (d, 1H, *J* = 7.5 Hz), 7.88 (d, 2H, *J* = 7.5 Hz), 7.74 (m, 2H), 7.55 (d, 2H, *J* = 8.1 Hz), 7.42 (m, 3H), 7.32 (m, 2H), 7.23 (d, 2H, *J* = 8.1 Hz), 6.05 (t, 1H, *J* = 5.2 Hz), 5.43 (s, 2H), 5.12 (br t, 1H), 4.42 (m, 3H), 4.26 (m, 3H), 3.92 (m, 1H), 3.11 (m, 2H), 2.10 (m, 1H), 1.71 (m, 1H), 1.60 (m, 1H), 1.41 (m, 2H), 0.87 (m, 6H); **^{13}C NMR** (101 MHz, DMSO-d_6): δ 171.3, 170.5, 159.0, 156.2, 144.0, 143.8, 140.8, 137.6, 127.7, 127.1, 127.0, 125.4, 120.1, 118.9, 65.8, 62.7, 60.2, 54.9, 53.1, 46.8, 30.7, 29.6, 26.8, 19.3, 18.3.

Spectroscopic data are in accordance with the literature.[73]

(*S*)-*N*-(4-(Hydroxymethyl)phenyl)-2-((*S*)-2-(2-methoxyacetamido)-3-methylbutanamido)-5-ureidopentanamide (19)

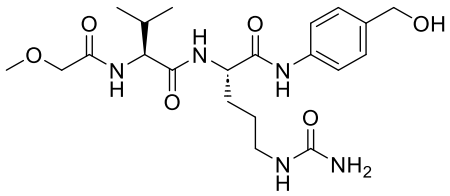

(9*H*-fluoren-9-yl)methyl ((*S*)-1-(((*S*)-1-((4-(hydroxymethyl)phenyl)amino)-1-oxo-5-ureidopentan-2-yl)amino)-3-methyl-1-oxobutan-2-yl)carbamate (**18**) (275 mg, 0.458 mmol) in DMF (2 mL) was added Et_3N (1.30 mL, 9.32 mmol) and stirred at rt overnight. The reaction mixture was concentrated by a stream of N_2, then DMF (1 mL) was added and the solution cooled to 0 °C. Methoxyacetyl chloride (54.0 µL, 0.591 mmol) was then added, followed by Et_3N (83.0 µL, 0.595 mmol). After 30 mins, the reaction was warmed to rt, then stirred for 1 h. The reaction mixture was then quenched with H_2O (1 mL) and concentrated under a stream of N_2, then purified by FCC (10-15% MeOH CH_2Cl_2) yielding (*S*)-*N*-(4-(hydroxymethyl)phenyl)-2-((*S*)-2-(2-methoxyacetamido)-3-methylbutanamido)-5-ureidopentanamide (**19**) (80.0 mg, 0.177 mmol, 41%) as an amorphous pale-pink solid.

LCMS (5-95% MeCN in H_2O, 2% formic acid) retention time 1.20 mins; **^{1}H NMR** (400 MHz, DMSO-d_6) δ 9.98 (s, 1H), 8.31 (d, 1H, *J* = 7.3 Hz), 7.51 (m, 2H), 7.22 (d, 2H, *J* = 8.2 Hz), 6.05 (t, 1H, *J* = 5.6 Hz), 5.43 (br s, 2H), 5.18 (t, 1H, *J* = 5.5 Hz), 4.38 (m, 3H), 4.28 (m, 1H), 3.86 (s, 2H), 3.32 (s, 3H), 2.98 (m, 2H), 1.99 (m, 1H), 1.64 (m, 2H), 1.40 (m, 2H), 0.85 (d, 3H, *J* = 6.7 Hz), 0.81 (d, 3H, *J* = 6.7 Hz); **^{13}C NMR** (101 MHz, DMSO-d_6) δ 171.0, 170.5, 169.1, 159.2, 137.7, 137.6, 127.1, 119.1, 71.3, 62.8, 58.8, 57.0, 53.4, 38.6, 31.1, 29.4, 26.9, 19.3, 18.2.

Spectroscopic data are in accordance with the literature.[73]

4-Nitrophenyl (1-(4-(4,4,5,5-tetramethyl-1,3,2-dioxaborolan-2-yl)phenyl)but-3-yn-1-yl) carbonate (20a)

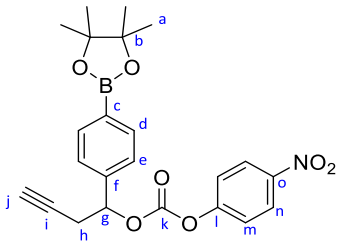

para-Nitrophenyl chloroformate (59.7 mg, 0.296 mmol), 1-(4-(4,4,5,5-tetramethyl-1,3,2-dioxaborolan-2-yl)phenyl)but-3-yn-1-ol (**9**) (40.0 mg, 0.147 mmol), in CH_2Cl_2 (1 mL) were cooled to 0 °C before the addition of pyridine (17.0 µL, 0.211 mmol). The solution was then allowed to warm to rt over 3 h. The

reaction mixture was then diluted with CH_2Cl_2 (10 mL) and extracted with sat. aq. $NaHCO_3$ (10 mL). The aqueous phase was then re-extracted with CH_2Cl_2 (2 x 10 mL). The combined organic phases were then dried over Na_2SO_4 then concentrated *in vacuo* before purifying by FCC (20-50% EtOAc in PE), then a second FCC (20% EtOAc in PE), yielding 4-nitrophenyl (1-(4-(4,4,5,5-tetramethyl-1,3,2-dioxaborolan-2-yl)phenyl)but-3-yn-1-yl) carbonate (**20a**) (26.0 mg, 59.5 µmol, 40%) as a colourless oil.

R_f = 0.21 (20% EtOAc in PE); **^{1}H NMR** (400 MHz, $CDCl_3$): δ 8.27 (d, 2H, *J* = 9.3 Hz, Hn), 7.89 (d, 2H, *J* = 8.2 Hz, Hd), 7.47 (d, 2H, *J* = 7.6 Hz, He), 7.38 (d, 2H, *J* = 9.3 Hz, Hm), 5.87 (t, 1H, *J* = 6.6 Hz, Hg), 2.90 (m, 2H, Hh), 1.37 (s, 12H, Ha); **^{13}C NMR** (101 MHz, $CDCl_3$): δ 155.6 (Cl), 151.6 (Ck), 145.5 (Co), 140.3 (Cf), 135.2 (Cd/Ce), 130.1 (Cc), 125.8 (Cd/Ce), 125.3 (Cm), 121.8 (Cn), 84.1 (Cb), 79.0 (Cg), 78.4 (Ci), 71.4 (Cj), 26.5 (Ch), 24.9 (Ca); **IR** ν_{max} /cm^{-1}: 3295 s (C-H alkyne), 2978 m (C-H alkyne), 1765 m (C=O), 1524 m (N-O); **HRMS (ESI)**: m/z calcd for $[M+H]^+$: 438.1719; found 438.1715.

Unsubstituted-alkyne-MMAE (20b)

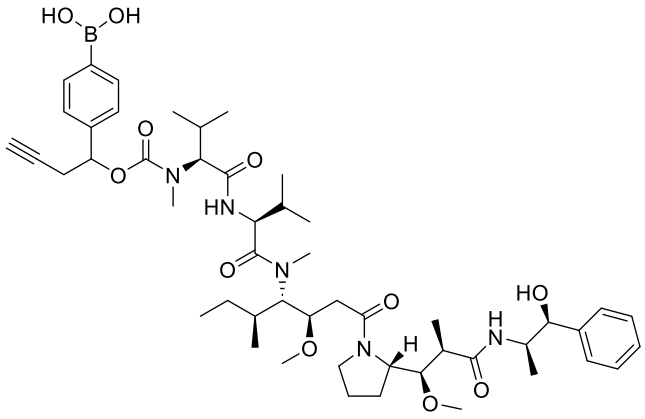

4-Nitrophenyl (1-(4-(4,4,5,5-tetramethyl-1,3,2-dioxaborolan-2-yl)phenyl)but-3-yn-1-yl) carbonate (**20a**) (16.6 mg, 38.0 µmol) and MMAE (27.0 mg, 37.6 µmol) in DMF (1 mL) were added pyridine (82.5 µL, 1.33 mmol), DIPEA (6.60 µL, 37.9 µmol) and HOBt (80 wt%) (7.00 mg, 41.5 µmol). After stirring overnight at rt, the reaction mixture was concentrated *in vacuo* then purified by reverse-phase FCC (10-80% MeCN in H_2O). Any boronic ester product was subjected to hydrolysis in H_2O:NH_4OH (aq), stirred at rt overnight, then lyophilised yielding unsubstituted-alkyne-MMAE (**20b**) (12.5 mg, 13.4 µmol, 35%) as an amorphous white powder.

HPLC (5-95% MeCN/H_2O over 20 min) retention time 11.847 min; **HPLC** (20-80% MeCN/H_2O over 20 min) retention time 11.325 min; **LRMS** (ESI) m/z calcd for $[M+H]^+$: 934.9; found: 934.7.

Unsubstituted-DVP-MMAE (20c)

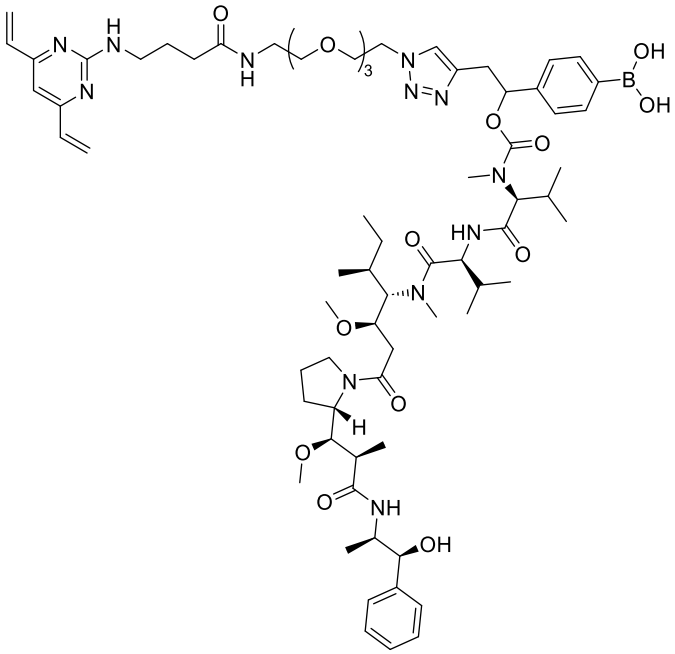

To a solution of unsubstituted-alkyne-MMAE (**20b**) (12.5 mg, 13.4 µmol) and DVP-azide (**22**) (12.9 mg, 29.8 µmol) in CH_2Cl_2 (1.8 mL), was added a solution of $CuSO_4 \cdot 5H_2O$ (4.00 mg, 16.0 µmol), THPTA (11.5 mg, 26.5 µmol) and sodium ascorbate (13.3 mg, 67.1 µmol) in $H_2O/^tBuOH$ (3.6 mL, 1:1) and the reaction mixture was stirred at rt for 3.5 h. The reaction mixture was then concentrated *in vacuo* and purified by reverse-phase FCC (10-80% MeCN in 0.1 M NH_4OH (aq)). Lyophilisation yielded unsubstituted-DVP-MMAE (**20c**) (4.20 mg, 3.07 µmol, 23%) as an amorphous white powder.

HPLC (5-95% MeCN/H_2O over 20 min) retention time 9.831 min; **HPLC** (20-80% MeCN/H_2O over 20 min) retention time 9.158 min; **HRMS (ESI)**: m/z calcd for $[M+H]^+$: 1366.8162; found 1366.8156.

1-(2,6-Difluoro-4-(4,4,5,5-tetramethyl-1,3,2-dioxaborolan-2-yl)phenyl)but-3-yn-1-yl (4-nitrophenyl) carbonate (21a)

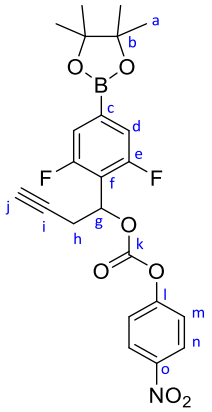

1-(2,6-Difluoro-4-(4,4,5,5-tetramethyl-1,3,2-dioxaborolan-2-yl)phenyl)but-3-yn-1-ol (**11**) (92.8 mg, 301 µmol) in DMF (1 mL) was added bis(4-nitrophenyl) carbonate (182 mg, 600 µmol), followed by DIPEA (78.7 µL, 451 µmol) and the mixture stirred at rt for 1 h. The reaction mixture was then diluted with CH_2Cl_2 (10 mL) and washed with sat. Na_2CO_3 (10 mL). The aqueous phase was then extracted with CH_2Cl_2 (2 x 10 mL) and the combined organic phases dried over Na_2SO_4, concentrated *in vacuo* then purified by reverse-phase FCC (10-100% MeCN in H_2O), yielding 1-(2,6-difluoro-4-(4,4,5,5-tetramethyl-1,3,2-dioxaborolan-2-yl)phenyl)but-3-yn-1-yl (4-nitrophenyl) carbonate (**21a**) (65.7 mg, 139 µmol, 46%) as an amorphous white solid.

LCMS (5-95% MeCN in H_2O, 2% formic acid) retention time 1.81 mins; **^{1}H NMR*** (400 MHz, $CDCl_3$): δ 8.28 (d, 2H, *J* = 8.5 Hz, Hn), 7.35 (m, 4H, Hm, Hd), 6.24 (t, 1H, *J* = 7.0 Hz, Hg), 3.10 (m, 2H, Hh), 2.00 (s, 1H, Hj), 1.36 (s, 9H, Ha); **^{13}C NMR†** (101 MHz, $CDCl_3$): δ 161.98-159.4 (dd, *J* = 253.3, 0.1 Hz, Ce), 155.4 (Cl/Co), 151.6 (Ck), 145.4 (Cl/Co), 125.3 (Cn), 121.7 (Cm), 117.6-117.4 (d, *J* = 23.6 Hz, Cd), 115.5-115.4 (d, *J* = 16.1 Hz, Cf), 84.7 (Cb), 77.8 (Ci), 71.3 (Cj), 70.6 (Cg), 24.8 (Ca), 23.7 (Ch); **IR** ν_{max} /cm^{-1}: 3305 s (C-H alkyne), 1777 m (C=O), 1530 m (N-O). Due to poor ionisation, no MS data could be obtained for this compound.

*Ha does not integrate to 12H presumably due to partial hydrolysis to boronic acid material. †Cc could not be identified due to low intensity.

Di-fluoro-alkyne-MMAE (21b)

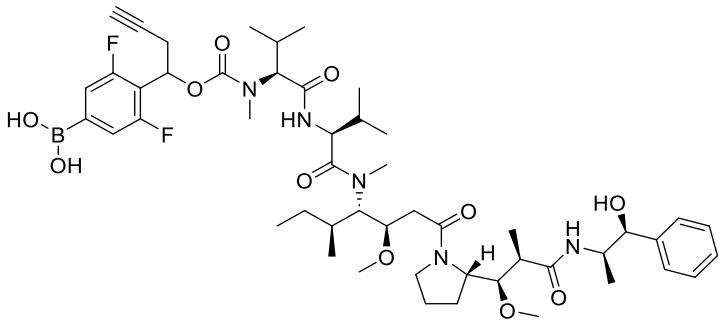

1-(2,6-Difluoro-4-(4,4,5,5-tetramethyl-1,3,2-dioxaborolan-2-yl)phenyl)but-3-yn-1-yl (4-nitrophenyl) carbonate (**21a**) (17.0 mg, 35.9 µmol) and MMAE (26.3 mg, 36.6 µmol) in DMF (1 mL) was added pyridine (100 µL, 1.24 mmol), DIPEA (6.30 µL, 36.2 µmol) and HOBt (80 wt%) (6.10 mg, 56.4 µmol). After stirring overnight at rt, the reaction mixture was concentrated *in vacuo* then purified by reverse-phase FCC (10-80% MeCN in H_2O) and lyophilised yielding di-fluoro-alkyne-MMAE (**21b**) (6.70 mg, 6.91 µmol, 19%) as an amorphous white powder.

HPLC (5-95% MeCN/H_2O over 20 min) retention time 12.590 min; **HPLC** (20-80% MeCN/H_2O over 20 min) retention time 12.978 min; **HRMS (ESI)**: m/z calcd for $[M+H]^+$: 969.5555; found 969.5554.

Difluoro-MMAE-DVP (21c)

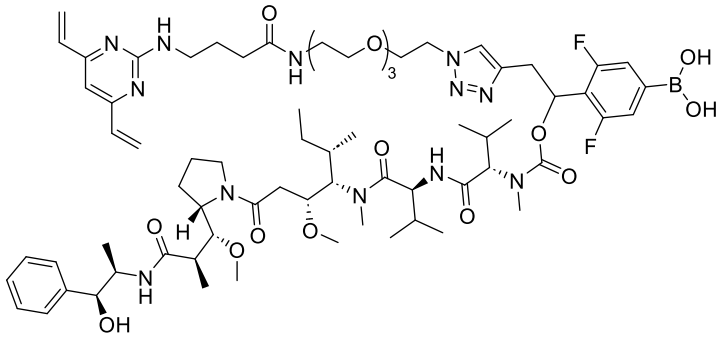

To a solution of difluoro-alkyne-MMAE (**21b**) (6.70 mg, 6.91 µmol) and DVP-azide (**22**) (3.50 mg, 8.07 µmol) in CH_2Cl_2 (1 mL), was added a solution of $CuSO_4 \cdot 5H_2O$ (4.00 mg, 16.0 µmol), THPTA (11.5 mg, 26.5 µmol) and sodium ascorbate (13.3 mg, 67.1 µmol) in $H_2O/^tBuOH$ (3.6 mL, 1:1) and the reaction mixture was stirred at rt for 1 h. The reaction mixture was then concentrated *in vacuo* and purified by reverse-phase FCC (10-80% MeCN in 0.1 M NH_4OH (aq)). Lyophilisation yielded unsubstituted-DVP-MMAE (**21c**) (3.50 mg, 2.49 µmol, 36%) as an amorphous white powder.

HPLC (5-95% MeCN/H_2O over 20 min) retention time 10.187 min; **HPLC** (20-80% MeCN/H_2O over 20 min) retention time 9.709 min; **HRMS (ESI)**: m/z calcd for $[M+H]^+$: 1402.8000; found 1402.7993.

DVP-Azide (22) - provided by Stephen Walsh.

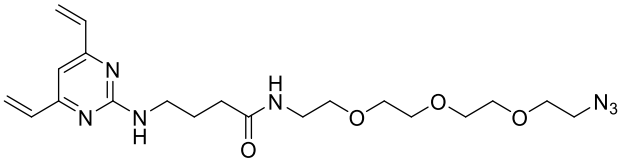

Non-cleavable DVP-Linker-MMAE (23) - provided by Stephen Walsh.

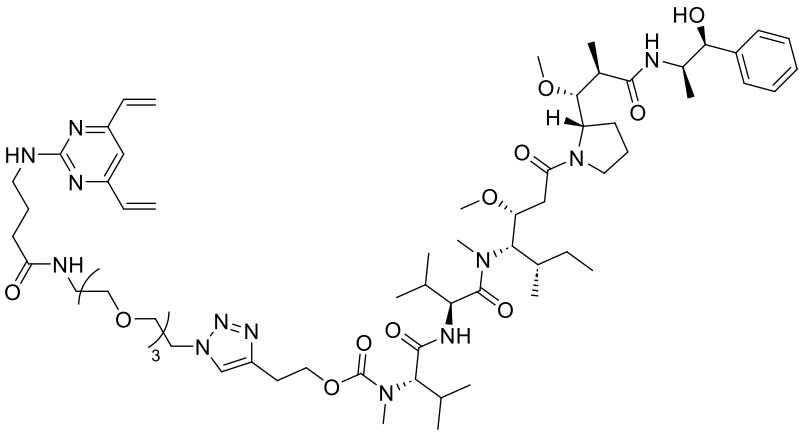

Val-Cit DVP-Linker-MMAE (24) - provided by Stephen Walsh.

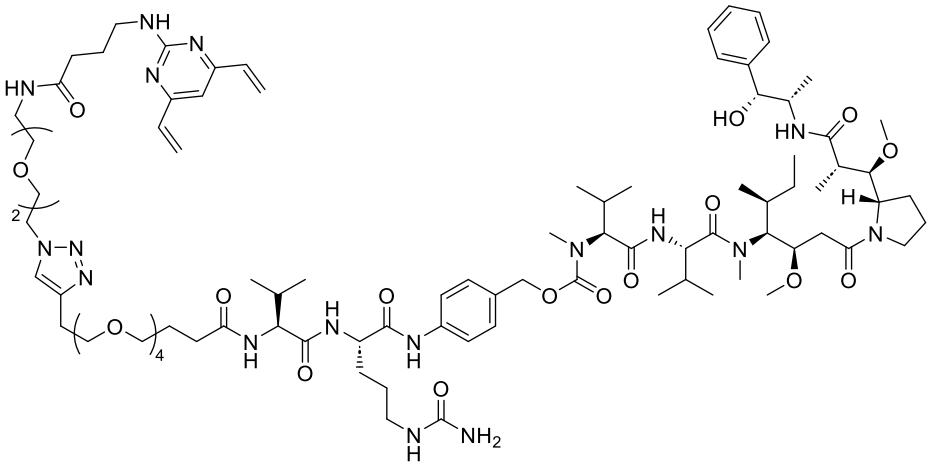

4-Bromobenzyl (4-nitrophenyl) carbonate (31)

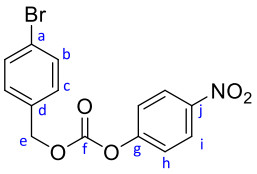

(4-Bromophenyl)methanol (150 mg, 0.802 mmol) in CH_2Cl_2 (4 mL) was added 4-nitrophenyl carbonochloridate (242 mg, 1.20 mmol) followed by Et_3N (0.279 mL, 2.00 mmol) at rt. After 30 mins, the reaction was diluted with CH_2Cl_2 (20 mL), washed with 1 N HCl (30 mL) and the aqueous washed

with CH_2Cl_2 (20 mL). The combined organic phases were dried over Mg_2SO_4 and concentrated in vacuo before purification by FCC (0-20% EtOAc in *n*-heptane) to afford 4-bromobenzyl (4-nitrophenyl) carbonate (**31**) (270 mg, 0.767 mmol, 96%) as an amorphous white solid.

R_f = 0.82 (1:1 EtOAc:*n*-heptane); **^{1}H NMR** (500 MHz, $CDCl_3$): δ 8.20 (d, 2H, *J* = 8.2 Hz, Hi), 7.48 (d, 2H, *J* = 8.5 Hz, Hb), 7.30 (d, 2H, *J* = 9.2 Hz, Hh), 7.25 (d, 2H, *J* = 7.7 Hz, Hc), 5.17 (s, 2H, Ce); **^{13}C NMR** (126 MHz, $CDCl_3$): δ 154.4 (Cg), 151.4 (Cf), 144.5 (Cj), 132.2 (Cd), 131.0 (Cb), 129.3 (Cc), 124.3 (Ci), 122.3 (Ca), 120.7 (Ch), 69.1 (Ce); **IR** ν_{max} /cm^{-1}: 1754 s (C=O), 1513 s (N-O), 1219 br (C-O); **HRMS (ESI)**: m/z calcd for $[M+H]^+$: 351.9821; found: 351.9823.

4-Nitrophenyl (4-(4,4,5,5-tetramethyl-1,3,2-dioxaborolan-2-yl)benzyl) carbonate (32)

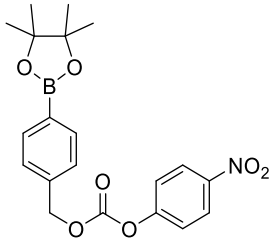

Method 1: A slurry of bis(4-nitrophenyl) carbonate (318 mg, 1.05 mmol) in CH_2Cl_2 (2 mL) was added to a stirred solution of (4-(4,4,5,5-tetramethyl-1,3,2-dioxaborolan-2-yl)phenyl)methanol (123 mg, 0.525 mmol) and DIPEA (0.112 mL, 0.643 mmol) in CH_2Cl_2 (4 mL) at rt. After 1 h, the reaction mixture was diluted with CH_2Cl_2 (15 mL), then extracted with sat. Na_2CO_3 (20 mL). The aqueous phase was then extracted with CH_2Cl_2 (3 x 20 mL) and the combined organic phases dried over Na_2SO_4 and concentrated *in vacuo*. The crude was purified by FCC (10-30% EtOAc in *n*-heptane), affording 4-nitrophenyl (4-(4,4,5,5-tetramethyl-1,3,2-dioxaborolan-2-yl)benzyl) carbonate (**32**) (131 mg, 0.328 mmol, 63%) as an amorphous white solid.

Method 2: Et_3N (177 µL, 1.27 mmol) was slowly added to a solution of (4-(4,4,5,5-tetramethyl-1,3,2-dioxaborolan-2-yl)phenyl)methanol (119 mg, 0.508 mmol) and 4-nitrophenyl carbonochloridate (207 mg, 1.03 mmol) in CH_2Cl_2 (4 mL) at 0 °C. The reaction was allowed to warm to rt and stirred for 1 h. The reaction mixture was then diluted with EtOAc, then extracted with sat. $NaHCO_3$ (20 mL). The aqueous phase was then extracted with CH_2Cl_2 (3 x 20 mL) and the organic phases combined and dried over Na_2SO_4 then concentrated *in vacuo.* The crude was then purified by reverse-phase preparative

LCMS (50-95% MeCN in 0.1% formic acid (aq)) to yield 4-nitrophenyl (4-(4,4,5,5-tetramethyl-1,3,2-dioxaborolan-2-yl)benzyl) carbonate (**32**) (195 mg, 0.488 mmol, 96%) as an amorphous white solid.

R_f = 0.57 (30% EtOAc in *n*-heptane); **^{1}H NMR** (500 MHz, $CDCl_3$): δ 8.19 (d, 2H, *J* = 8.3 Hz), 7.77 (d, 2H, *J* = 8.0 Hz), 7.36 (d, 2H, *J* = 8.0 Hz), 7.31 (d, 2H, *J* = 8.4 Hz), 5.24 (s, 2H), 1.28 (s, 12H); **^{13}C NMR** (126 MHz, $CDCl_3$): δ 154.5, 151.4, 144.4, 136.0, 134.2, 133.0, 126.6, 124.3, 120.8, 83.0, 69.8, 23.9.

Spectroscopic data are in accordance with the literature.[120]

(*R*)-4-(4-Bromobenzyl)-4-(3-((4-(N-(4-(4-((4'-chloro-4,4-dimethyl-3,4,5,6-tetrahydro-[1,1'-biphenyl]-2-yl)methyl)piperazin-1-yl)benzoyl)sulfamoyl)-2-((trifluoromethyl)sulfonyl)phenyl)amino)-4-(phenylthio)butyl)morpholin-4-ium (39)

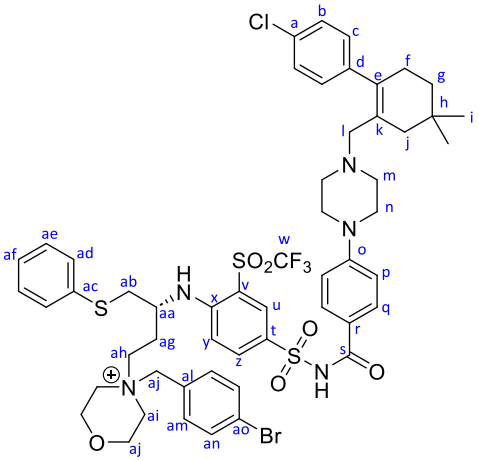

(*R*)-4-(4-((4'-chloro-4,4-dimethyl-3,4,5,6-tetrahydro-[1,1'-biphenyl]-2-yl)methyl)piperazin-1-yl)-*N*-((4-((4-morpholino-1-(phenylthio)butan-2-yl)amino)-3-((trifluoromethyl)sulfonyl)phenyl)sulfonyl)benzamide (**Navitoclax**) (50.3 mg, 51.6 µmol), K_2CO_3 (24.8 mg, 179 µmol), potassium iodide (15.0 mg, 90.4 µmol) and 1-bromo-4-(bromomethyl)benzene (20.2 mg, 80.8 µmol) were suspended in MeCN (1 mL) and heated to 70 °C. After 4 h, the reaction was cooled to rt and concentrated under a stream of compressed air. The crude solid was dissolved in EtOAc (10 mL), then washed with brine (10 mL) and the aqueous washed with EtOAc (10 mL). The combined organic phases were dried over Mg_2SO_4 and concentrated *in vacuo* before purification by reverse-phase FCC (0-100% MeCN in 0.1% formic acid (aq)) to yield the morpholine analogue product, (*R*)-4-(4-bromobenzyl)-4-(3-((4-(N-(4-(4-((4'-chloro-4,4-dimethyl-3,4,5,6-tetrahydro-[1,1'-biphenyl]-2-yl)methyl)piperazin-1-yl)benzoyl)sulfamoyl)-2-((trifluoromethyl)sulfonyl)phenyl)amino)-4-(phenylthio)butyl)morpholin-4-ium (**39**) (6.00 mg, 5.24 µmol, 10%) as an orange residue.

^{1}H NMR (500 MHz, DMSO-d_6): δ 8.10 (d, 1H, *J* = 2.1 Hz, Hu), 7.97 (dd, 1H, *J* = 9.1, 1.9 Hz, Hz), 7.71 (d, 2H, *J* = 8.9 Hz, Hq), 7.66 (d, 2H, *J* = 8.5 Hz, Han), 7.50 (d, 2H, *J* = 8.4 Hz, Ham), 7.35 (m, 6H, Hb, Had,

Hae), 7.22 (m, 1H, Haf), 7.12 (d, 2H, *J* = 8.5 Hz, Hc), 6.91 (d, 1H, *J* = 9.4 Hz, Hy), 6.76 (d, 2H, *J* = 9.0 Hz, Hp), 6.70 (d, 1H, *J* = 9.2 Hz, aniline NH), 4.63 (s, 2H, Hak), 4.11 (m, 1H, Haa), 3.94 (m, 4H, Haj), 3.54 (m, 1H, Hah'), 3.36 (m, 7H, Hai, Hab, Hah''), 3.11 (m, 4H, Hn), 2.74 (s, 2H, Hl), 2.28 (m, 8H, Hag, Hm, Hf), 2.00 (br s, 2H, Hj), 1.43 (app t, 2H, *J* = 6.4 Hz, Hg), 0.97 (s, 6H, Hi); **^{13}C NMR*** (126 MHz, DMSO-d_6): δ 169.8 (Cs), 152.0 (Co), 137.6 (Cz), 134.8 (Cam), 133.3 (Ce), 132.0 (Cu), 131.6 (Can), 129.9 (Cc), 129.3 (Ck), 129.2 (Cq), 128.8 (Cad and Cae), 127.7 (Cb), 126.0 (Cal), 124.4 (Cao), 113.0 (Cp), 112.5 (Cy), 62.4 (Cak), 59.5 (Cl), 59.2 (Caj), 56.4 (Cai), 52.2 (Cah, Cm), 49.7 (Caa), 47.2 (Cn), 40.9 (Cj), 34.9 (Cg), 30.0 (Cf), 28.5 (Ch), 27.5 (Ci), 25.1 (Cag); **IR** ν_{max} /cm^{-1}: 1599 m (N-H), 1462 m (C-H), 1326 s (S=O); **HRMS (ESI)**: m/z calcd for $[M+H]^+$: 1142.2608; found: 1142.2607.

NMR characterisation was performed by David Longmire. *Carbon signals were identified by 2D NMR correlations (HSQC, HMBC, ROESY). However, the carbon spectrum was not suitable intensity for all signals to be visible above the noise. Hence, some quaternary carbon signals could not be identified by 2D NMR alone on this minimal amount of material, and the carbon spectrum is not included in this thesis. Due to the small amount of material obtained, an α_D could not be obtained.

4-Bromobenzyl (*R*)-(4-morpholino-1-(phenylthio)butan-2-yl)carbamate (45)

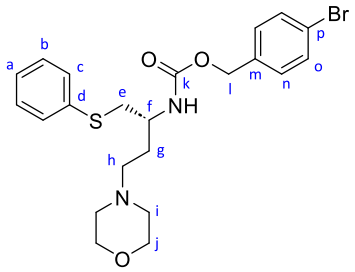

Method 1: To a solution of (*R*)-4-morpholino-1-(phenylthio)butan-2-amine (0.121 mL, 0.636 mmol) in CH_2Cl_2 (3 mL) was added bis(trichloromethyl) carbonate (95.0 mg, 0.320 mmol) followed by Et_3N (0.178 mL, 1.28 mmol). After 10 mins, (4-bromophenyl)methanol (119 mg, 0.636 mmol) was added and the reaction stirred at rt. After 4 h, the reaction was quenched with H_2O (500 µL) and then diluted with CH_2Cl_2 (15 mL) and extracted with H_2O. The organic phase was dried over Mg_2SO_4 and concentrated *in vacuo*. The crude was then purified by reverse-phase FCC (10-100% MeCN in 1% NH_4OH (aq)) and lyophilized to afford 4-bromobenzyl (*R*)-(4-morpholino-1-(phenylthio)butan-2-yl)carbamate (**45**) (87.0 mg, 0.181 mmol, 28%) as a colourless oil.

Method 2: 4-Bromobenzyl (4-nitrophenyl) carbonate (66.1 mg, 0.190 mmol) was added to a solution of (*R*)-4-morpholino-1-(phenylthio)butan-2-amine (50.0 mg, 0.190 mmol) in CH_2Cl_2 (500 µL), followed by DIPEA (33.0 µL, 0.190 mmol). After 2 h, the reaction was concentrated under a steam of compressed air and purified by reverse-phase FCC (10-100% MeCN in 1% NH_4OH (aq)), to afford 4-bromobenzyl

(*R*)-(4-morpholino-1-(phenylthio)butan-2-yl)carbamate (**45**) (46.1 mg, 96.2 µmol, 51%) as a white residue.

R_f = 0.15 (50% EtOAc in *n*-heptane), 0.42 (10% MeOH in CH_2Cl_2); **^{1}H NMR** (500 MHz, MeOD): δ 7.47 (d, 2H, *J* = 8.3 Hz, Ho), 7.38 (d, 2H, *J* = 7.63 Hz, Hc), 7.26 (m, 4H, Hn, Hb), 7.15 (m, 1H, Ha), 5.00 (m, 2H, Hl), 3.77 (m, 1H, Hf), 3.61 (m, 4H, Hj), 3.06 (m, 2H, He), 2.35 (m, 6H, Hh, Hi), 1.90 (m, 1H, Hg), 1.64 (m, 1H, Hg′); **^{13}C NMR** (126 MHz, MeOD): δ 158.7 (Ck), 138.2 (Cm), 138.0 (Cd), 133.1 (Co), 131.2 (Cc), 131.1 (Cb/Cn), 130.6 (Cb/Cn), 127.8 (Ca), 123.3 (Cp), 68.2 (Cj), 67.1 (Cl), 57.1 (Ch/Ci), 55.1 (Ch/Ci), 51.5 (Cf), 40.1 (Ce), 31.6 (Cg); **IR** ν_{max} /cm^{-1}: 1684 s (C=O), 1541 m (C-H); **HRMS (ESI)**: m/z calcd for $[M+H]^+$: 479.0999; found: 479.0997; $[\alpha]_D^{20.6}$**:** -10.0 ($CHCl_3$).

(*R*)-*N*-(4-bromobenzyl)-4-morpholino-1-(phenylthio)butan-2-amine (46)

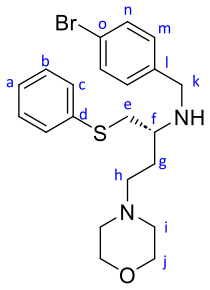

Method 1: 1-Bromo-4-(bromomethyl)benzene (230 mg, 0.920 mmol) was added (*R*)-4-morpholino-1-(phenylthio)butan-2-amine (294 mg, 1.10 mmol) in CH_2Cl_2 (4 mL). DIPEA (0.161 mL, 0.924 mmol) was then added at rt and stirred for 24 h. The reaction was then concentrated under a stream of compressed air, then purified by reverse-phase FCC (0-100% MeCN in 1% NH_4OH (aq)) and lyophilized to afford (*R*)-*N*-(4-bromobenzyl)-4-morpholino-1-(phenylthio)butan-2-amine (**46**) (220 mg, 0.505 mmol, 55%) as a colourless oil.

Method 2: (*R*)-4-Morpholino-1-(phenylthio)butan-2-amine (173 mg, 0.650 mmol) and 4-bromobenzaldehyde (120 mg, 0.650 mmol) in 1,2-dichloroethane (3 mL) was stirred for 15 mins. Then, sodium triacetoxyborohydride (193 mg, 0.91 mmol) was added at rt. The resulting slurry was stirred for 24 h, then diluted with EtOAc (20 mL), quenched with $NaHCO_3$ (20 mL) and the aqueous extracted with EtOAc (3 x 5 mL). The combined organic phases were dried over Mg_2SO_4 then concentrated *in vacuo*. The crude was purified by reverse-phase FCC (0-100% MeCN in 1% NH_4OH (aq)) then lyophilized to afford (*R*)-*N*-(4-bromobenzyl)-4-morpholino-1-(phenylthio)butan-2-amine (**46**) (103 mg, 0.237 mmol, 36%) as a yellow oil.

R_f = 0.43 (10% MeOH in CH_2Cl_2); **^{1}H NMR** (500 MHz, MeOD): δ 7.39 (m, 2H, Hn), 7.29 (m, 4H, Hb, Hc), 7.20 (m, 1H, Ha), 7.14 (m, 2H, Hm), 3.69 (m, 2H, Hk), 3.61 (m, 4H, Hj), 3.03 (d, 2H, *J* = 6.2 Hz, He), 2.69

(m, 1H, Hf) 2.35 (m, 6H, Hi, Hh) 1.72 (m, 2H, Hg); **^{13}C NMR** (126 MHz, MeOD): δ 140.1 (Cl), 137.0 (Cd), 132.5 (Cn), 131.5 (Cm), 131.0 (Cc), 130.1 (Cb), 127.5 (Ca), 121.8 (Co), 67.7 (Cj), 56.7(Ch/Ci), 55.1 (Cf), 54.6 (Ch/Ci), 50.7 (Ck), 49.4 (Ck), 38.9 (Ce), 30.2 (Cg); **IR** ν_{max} /cm^{-1}: 2945 s (N-H), 1483 m (C-H); **HRMS (ESI)**: m/z calcd for [M+H]$^+$: 435.1110; found: 435.1106; $[\alpha]_D^{20.3}$**:** -1.86 (EtOH).

(*R*)-*N*,*N*-Bis(4-bromobenzyl)-4-morpholino-1-(phenylthio)butan-2-amine (50)

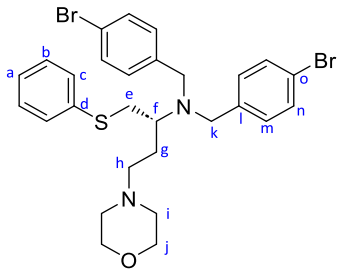

Method: By-product from the synthesis of **46**.

LCMS (5-95% MeCN in H_2O, 2% formic acid) retention time 0.99 mins; **^{1}H NMR** (500 MHz, MeOD): δ 7.40 (m, 6H, Hc, Hn), 7.29 (m, 2H, Hb), 7.24 (m, 1H, Ha), 7.04 (m, 4H, Hm), 3.49 (m, 8H, Hj, Hk), 3.36 (m, 1H, He'), 2.79 (m, 2H, Hf, He''), 2.25 (m, 6H, Hh', Hh'', Hi), 1.81 (m, 2H, Hg', Hg''); **^{13}C NMR** (126 MHz, MeOD): δ 140.6 (Cl), 137.6 (Cd), 132.3 (Cn), 132.1 (Cm), 131.6 (Cc), 130.1 (Cb), 127.5 (Ca), 121.6 (Co), 67.7 (Cj), 57.3 (Ch/Ci), 56.4 (Cf), 54.6 (Ch/Ci), 53.7 (Ck), 35.4 (Ce), 27.4 (Cg); **IR** ν_{max} /cm^{-1}: 1484 s (C-H); **HRMS (ESI)**: m/z calcd for [M+H]$^+$: 603.0684; found: 603.0680; $[\alpha]_D^{20.7}$**:** 19.5 ($CHCl_3$).

1,3-Bis((*R*)-4-morpholino-1-(phenylthio)butan-2-yl)urea (51)

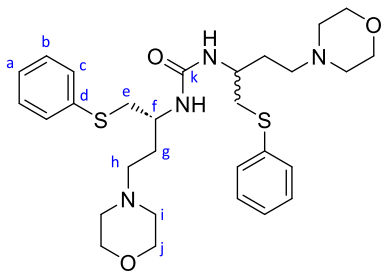

Method: By-product from the synthesis of **45** (Method 1): yielded (**51**) (18.9 mg 33.8 µmol, 5%).

LCMS (5-95% MeCN in H_2O, 2% formic acid) retention time 0.62 mins; **^{1}H NMR** (500 MHz, MeOD): δ 7.38 (d, 4H, *J* = 8.3 Hz, Hc), 7.27 (app t, 4H, *J* = 7.6 Hz, Hb), 7.16 (app tt, 2H, *J* = 7.4, 1.2 Hz, Ha), 3.91 (m, 2H, Hf), 3.64 (m, 8H, Hj), 3.09 (m, 4H, He' and He''), 2.40 (m, 12H, Hh' and Hh'' and Hi' and Hi''), 1.89 (m, 2H, Hg'), 1.61 (m, 2H, Hg''); **^{13}C NMR** (126 MHz, MeOD) δ: 160.1 (Ck) 138.0 (Cd) 130.3 (Cc) 130.1 (Cb) 127.1 (Ca) 67.6 (Cj) 56.7 (Ch/Ci) 54.8 (Ch/Ci) 49.5 (Cf) 40.2 (Ce) 31.7 (Cg); **IR** ν_{max} /cm^{-1}: 1609

s (C=O), 1458 m (C-H), 1458 m (C-H); **HRMS (ESI)**: m/z calcd for $[M+H]^+$: 559.2776; found: 559.2777; $[\alpha]_D^{20.7}$**:** -29.7 (EtOH).

4-Fluoro-*N*-(4-sulfamoyl-2-((trifluoromethyl)sulfonyl)phenyl)-3 ((trifluoromethyl)sulfonyl)-benzenesulfonamide (52)

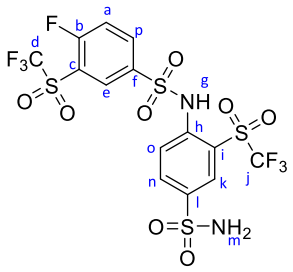

4-Bromobenzyl (*R*)-(4-morpholino-1-(phenylthio)butan-2-yl)carbamate (**45**) (58.1 mg, 0.121 mmol) was dissolved in DMSO (600 µL) and 4-fluoro-3-((trifluoromethyl)sulfonyl)benzenesulfonamide (37.2 mg, 0.121 mmol) was added, followed by DIPEA (63.0 µL, 0.362 mmol) at rt. After 24 h, additional DIPEA (25.0 µL, 0.144 mmol) was added. After 3 h, the reaction was diluted with EtOAc (10 mL), washed with 1 N HCl (10 mL), then H_2O (10 mL), then brine (10 mL). The organic phase was washed again with 3 N HCl (20 mL), then the organic dried over Na_2SO_4 and concentrated *in vacuo*. Reverse-phase FCC (10-100% MeCN in 0.1 M NH_4OH (aq)) yielded impure 4-fluoro-*N*-(4-sulfamoyl-2-((trifluoromethyl)sulfonyl)phenyl)-3-((trifluoromethyl)sulfonyl)benzenesulfonamide (**52**) by-product.

LCMS (5-95% MeCN in H_2O, 2% formic acid) retention time 1.30 mins; **^{1}H NMR** (700 MHz, MeOD): δ 8.58 (dd, 1H, $^4J_{HF}$ = 6.3 Hz, $^4J_{HH}$ = 2.2 Hz, He), 8.52 (m, 1H, Hp), 8.31 (d, 1H, $^5J_{HF}$ = 2.4Hz, Hk), 7.86 (dd, 1H, $^3J_{HH}$ = 9.0 Hz, $^4J_{HH}$ = 2.2 Hz, Hn), 7.63 (d, 1H, $^3J_{HH}$ = 8.8 Hz, Ho), 7.62 (d, 1H, $^3J_{HH}$ = 9.1 Hz, Ha); **^{13}C NMR** (176 MHz, MeOD): δ 162.7-161.2 (d, $^1J_{CF}$ = 267 Hz, Hb), 154.4 (Cl), 143.12-143.11 (d, $^4J_{CF}$ = 3 Hz, Hf), 137.9-137.8 (d, $^3J_{CF}$ = 10 Hz, He), 133.3 (Cn), 131.5 (Cp), 131.2 (Ch), 130.9 (Ck), 121.0 (Co), 120.43-120.39 (q, $^3J_{CF}$ = 2 Hz, Hi), 123.1-117.5 (q, $^1J_{CF}$ = 326 Hz, Hj), 122.4-116.9 (q, $^1J_{CF}$ = 325 Hz), 119.2-119.1 (dq, $^2J_{CF}$ = 14 Hz, $^3J_{CF}$ = 1.5 Hz), 118.5-118.4 (d, $^2J_{CF}$ = 22 Hz); **IR** ν_{max} /cm^{-1}: 1344 m (S=O); **HRMS (ESI)**: m/z calcd for $[M+H]^+$: 594.9203; found: 594.9187.

***tert*-Butyl ((4-fluoro-3-((trifluoromethyl)sulfonyl)phenyl)sulfonyl)carbamate (54)**

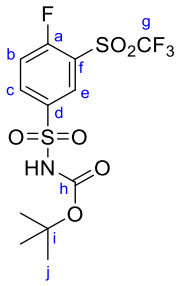

Boc anhydride (180.0 mg, 0.825 mmol) in THF (1.5 mL) was added DIPEA (95.0 µL, 0.545 mmol). Then, 4-fluoro-3-((trifluoromethyl)sulfonyl)benzenesulfonamide (**44**) (167.0 mg, 0.544 mmol) in THF (1.5 mL) was added slowly and the resulting solution heated to 65 °C for 3 days. The reaction mixture was concentrated under a stream of nitrogen, then purified by reverse-phase FCC (10-100% MeCN in 0.5% formic acid (aq)) to yield *tert*-butyl ((4-fluoro-3 ((trifluoromethyl)sulfonyl)phenyl)sulfonyl)carbamate (**54**) (79.4 mg, 0.195 mmol, 36%) as a pale-yellow amorphous solid.

LCMS (5-95% MeCN in H_2O, 2% formic acid) retention time 1.50 mins; **^{1}H NMR** (500 MHz, MeOD): δ 8.59 (m, 1H, He), 8.55 (m, 1H, Hc), 7.80 (app t, 1H, *J* = 9.2 Hz, Hb), 1.39 (s, 9H, Hj); **^{13}C NMR*** (126 MHz, MeOD): δ 164.5-162.3 (d, $^1J_{CF}$ = 270.6 Hz, Ca), 150.2 (Ch), 139.5-139.4 (d, $^3J_{CF}$ = 11.1 Hz, Cc), 137.93 – 137.90 (d, $^4J_{CF}$ = 3.8 Hz, Cd), 133.5 (br s, Ce), 120.1-119.9 (dd, $^2J_{CF}$ = 15.0 Hz, $^3J_{CF}$ = 1.5 Hz, Cf), 119.6-119.5 (d, $^2J_{CF}$ = 22.9 Hz, Cb), 83.3 (Ci), 26.7 (Cj); **IR** ν_{max} /cm^{-1}: 1640 s (C=O), 1370 s (S=O); **HRMS (ESI)**: m/z calcd for $[M+H]^+$: 408.0193; found: 408.0176.

*Cg could not be identified in the ^{13}C NMR spectra, presumably due to large $^1J_{CF}$ coupling of a quaternary carbon peak which renders the peak intensity too low to distinguish from the noise.

***tert*-Butyl 4-(piperazin-1-yl)benzoate (64)**

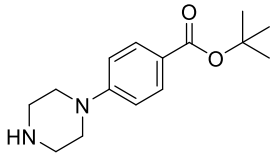

tert-Butyl 4-fluorobenzoate (900 µL, 5.10 mmol) and piperazine (1.30 g, 15.1 mmol) were suspended in DMSO (4 mL) and heated to 120 °C for 20 h. The reaction was cooled to rt, then diluted with EtOAc (40 mL) and extracted with brine (40 mL), then H_2O (40 mL). The combined organic phases were dried over Na_2SO_4 and concentrated *in vacuo.* The crude was then purified by normal-phase FCC (0-10% MeOH in CH_2Cl_2) to yield *tert*-butyl 4-(piperazin-1-yl)benzoate (**64**) (935 mg, 3.56 mmol, 70%) as an amorphous white solid.

R_f = 0.10 (5% MeOH in CH_2Cl_2); **^{1}H NMR** (400 MHz, $CDCl_3$): δ 7.88 (d, 2H, *J* = 8.9 Hz), 6.86 (d, 2H, *J* = 8.9 Hz), 3.30 (m, 4H), 3.06 (m, 4H), 1.59 (s, 9H); **^{13}C NMR** (101 MHz, $CDCl_3$): δ = 165.9, 154.2, 131.0, 122.0, 113.8, 80.1, 48.7, 45.7, 28.3.

Spectroscopic data are in accordance with the literature.[296]

2-Bromo-5,5-dimethylcyclohex-1-ene-1-carbaldehyde (67)

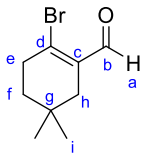

DMF (170 µL, 2.20 mmol) in CH_2Cl_2 (1 mL) was cooled to 0 °C. Then, PBr_3 (230 µL, 2.42 mmol) was added dropwise and stirred for 40 mins. Then, 4,4-dimethyl cyclohexanone (**63**) (101 mg, 0.800 mmol) was added and the solution left to warm to rt overnight. The reaction was then cooled to 0 °C and quenched by the slow addition of ice-cold H_2O (10 mL). The phases were separated and solid $NaHCO_3$ was added to the aqueous phase until pH paper indicated pH 6-7. The phases were re-mixed and extracted, then the aqueous further extracted with CH_2Cl_2 (2 x 10 mL). The combined organic phases were dried over Na_2SO_4, then concentrated *in vacuo* and purified by FCC (0-10% EtOAc in PE), yielding 2-bromo-5,5-dimethylcyclohex-1-ene-1-carbaldehyde (**67**) (79.3 mg, 0.365 mmol, 46%) as a colourless oil.

R_f = 0.60 (10% EtOAc in PE); **^{1}H NMR** (400 MHz, $CDCl_3$): δ 10.02 (s, 1H), 2.73 (tt, 2H, *J* = 6.5, 2.2 Hz), 2.07 (t, 2H, *J* = 2.3 Hz), 1.51 (t, 2H, *J* = 6.5 Hz), 0.94 (s, 9H); **^{13}C NMR** (101 MHz, $CDCl_3$): 194.0, 142.7, 134.2, 38.4, 36.90, 36.87, 28.6, 27.7.

Spectroscopic data are in accordance with the literature.[297,298]

***tert*-Butyl 4-(4-((2-bromo-5,5-dimethylcyclohex-1-en-1-yl)methyl)piperazin-1-yl)benzoate (71)**

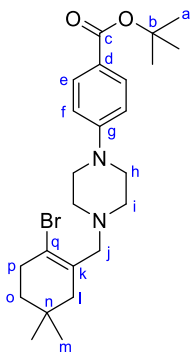

Method 1: 2-Bromo-5,5-dimethylcyclohex-1-ene-1-carbaldehyde (**67**) (20.0 mg, 92.1 µmol) and *tert*-butyl 4-(piperazin-1-yl)benzoate (**64**) (25.6 mg, 97.6 µmol) were dissolved in EtOH (200 µL) and

$NaBH_3CN$ (9.00 mg, 143 µmol) was added. Concentrated acetic acid was added until indicator paper showed pH = 5. After overnight stirring, the reaction mixture was concentrated *in vacuo* and purified by FCC (10-20% EtOAc in PE) yielding *tert*-butyl 4-(4-((2-bromo-5,5-dimethylcyclohex-1-en-1-yl)methyl)piperazin-1-yl)benzoate (**71**) (2.60 mg, 5.61 µmol, 6%) as a colourless oil.

Method 2: *tert*-Butyl 4-(piperazin-1-yl)benzoate (**64**) (372 mg, 1.42 mmol) in DMF (10 mL) was added Et_3N (198 µL, 1.42 mmol), NaI (213 mg, 1.42 mmol) and 1-bromo-2-(bromomethyl)-4,4-dimethylcyclohex-1-ene (**73**) (*ca*. 400 mg of crude material), and the mixture stirred at rt for 1 h. The reaction mixture was concentrated under a stream of N_2 then purified by reverse-phase chromatography (10-100% MeCN in 0.5% formic (aq)) to afford *tert*-Butyl 4-(4-((2-bromo-5,5-dimethylcyclohex-1-en-1-yl)methyl)piperazin-1-yl)benzoate (**71**) as a red oil (280.4 mg, 0.606 mmol, approx. 20% overall from **67**).

R_f = 0.45 (30% EtOAc in PE); **^{1}H NMR** (400 MHz, $CDCl_3$): δ 7.86 (d, 2H, *J* = 9.0 Hz, He), 6.84 (d, 2H, *J* = 9.0 Hz, Hf), 3.29 (m, 4H, Hh), 3.15 (s, 2H, Hj), 2.56 (m, 6H, Hi, Hp), 2.04 (m, 2H, Hl), 1.57 (s, 9H, Ha), 1.47 (t, 2H, *J* = 6.5 Hz, Ho), 0.94 (s, 6H, Hm); **^{13}C NMR** (176 MHz, $CDCl_3$): δ 166.0 (Cc), 154.0 (Cg), 131.9 (Ck), 131.0 (Ce), 121.7 (Cd), 121.4 (Cq), 113.7 (Cf), 80.1 (Cb), 63.0 (Cj), 52.5 (Ci), 47.6 (Ch), 43.7 (Cl), 37.3 (Co), 35.0 (Cp), 29.3 (Cn), 28.3 (Ca), 27.8 (Cm); **IR** ν_{max} /cm^{-1}: 1701 s (C=O), 1162 s (C-O), 797 w (C=C); **HRMS (ESI)**: m/z calcd for $[M+H]^+$: 463.1955; found: 463.1942.

(2-Bromo-5,5-dimethylcyclohex-1-en-1-yl)methanol (72)

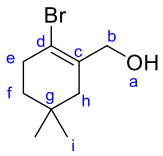

Method 1: By-product of reaction to make **71**: yielded (2-bromo-5,5-dimethylcyclohex-1-en-1-yl)methanol (**72**) (5.70 mg, 26.0 µmol, 28%) as a colourless oil.

Method 2: 2-Bromo-5,5-dimethylcyclohex-1-ene-1-carbaldehyde (**67**) (100 mg, 0.461 mmol), in MeOH (1 mL) was cooled to 0 °C, then $NaBH_4$ (26.0 mg, 0.687 mmol) was added slowly and left to warm to rt overnight. TLC indicated residual aldehyde starting material, so the mixture was cooled to 0 °C again, and additional $NaBH_4$ (9.00 mg, 0.238 mmol) was added and the mixture left to warm to rt overnight. The reaction mixture was then cooled to 0 °C and cold H_2O (10 mL) was added. The mixture was then extracted with CH_2Cl_2 (10 mL) and the organic phase washed with sat. NaCl (10 mL), dried over Na_2SO_4 and concentrated *in vacuo*. FCC (10% EtOAc in PE) yielded (2-bromo-5,5-dimethylcyclohex-1-en-1-yl)methanol (**72**) as an impure colourless oil which was carried forward to the next step without further purification.

R_f = 0.32 (30% EtOAc in PE); **^{1}H NMR** (400 MHz, $CDCl_3$): δ 4.23 (s, 2H, Hb), 2.54 (m, 2H, He), 2.08 (m, 2H, Hh), 1.48 (app t, 2H, *J* = 6.5 Hz, Hf), 0.97 (s, 6H, Hi); **^{13}C NMR** (101 MHz, $CDCl_3$): 134.1 (Cc), 120.2 (Cd), 66.4 (Cb), 42.9 (Ch), 37.2 (Cf), 34.5 (Ce), 29.2 (Cg), 27.8 (Ci); **IR** ν_{max} /cm^{-1}: 3298 br (O-H), 664 s (C=C); **HRMS (ESI)**: m/z calcd for $[M+H]^+$: 219.0379; found: 219.0374.

1-Bromo-2-(bromomethyl)-4,4-dimethylcyclohex-1-ene (73)

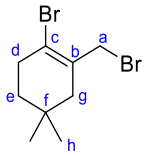

An estimated amount of impure (2-bromo-5,5-dimethylcyclohex-1-en-1-yl)methanol (**72**) (approx. 500 mg), was dissolved in Et_2O (10 mL) and cooled to 0 °C. PBr_3 (214 µL, 0.610 mmol) was added slowly and the reaction stirred overnight, allowing warming to rt. The reaction was cooled to 0 °C, then quenched with the slow addition of ice-cold H_2O (20 mL). The phases were separated, the aqueous cooled to 0 °C and added solid $NaHCO_3$ portion-wise until neutral pH was observed by pH indicator paper. The aqueous and organic phases were re-combined, extracted then the aqueous washed with CH_2Cl_2 (2 x 50 mL). The organic phases were combined, dried over Na_2SO_4, concentrated *in vacuo* followed by FCC (0-10% EtOAc in PE) to yield 1-bromo-2-(bromomethyl)-4,4-dimethylcyclohex-1-ene (**73**) as an impure, volatile colourless oil (1.07 g).

R_f = 0.74 (10% EtOAc in PE); **^{1}H NMR** (400 MHz, $CDCl_3$): δ 4.11 (s, 2H, Ha), 2.57 (2H, m, He), 2.11 (2H, t, *J* = 2.2 Hz, Hg), 1.50 (2H, t, *J* = 6.5 Hz, Hd), 0.99 (s, 6H, Hh); **^{13}C NMR** (176 MHz, $CDCl_3$): δ 131.4 (Cb), 123.6 (Cc), 43.1 (Cg), 37.1 (Cd), 36.9 (Ca), 34.8 (Ce), 29.4 (Cf), 27.6 (Ch).

Due to limited amount of sample and impurity, no further characterisation was performed, and the material was carried on crude.

(4-((4-(3-(4-(Cyclopropanecarbonyl)piperazine-1-carbonyl)-4-fluorobenzyl)-1-oxophthalazin-2(*1H*)-yl)methyl)phenyl)boronic acid (78a) and 4-(3-(4-(cyclopropanecarbonyl)piperazine-1-carbonyl)-4-fluorobenzyl)-2-(4-(4,4,5,5-tetramethyl-1,3,2-dioxaborolan-2-yl)benzyl)phthalazin-1(*2H*)-one (78b)

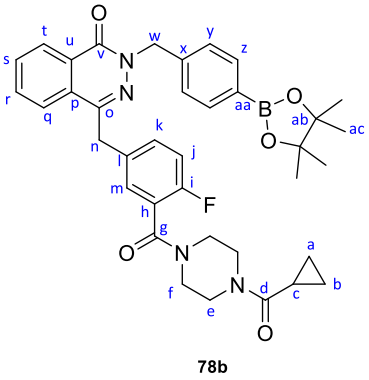

78b

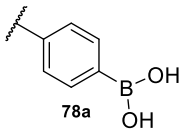

78a

2-(4-Bromobenzyl)-4-(3-(4-(cyclopropanecarbonyl)piperazine-1-carbonyl)-4-fluorobenzyl)phthalazin-1(2*H*)-one (**80**) (21.8 mg, 36.1 µmol), $PdCl_2(dppf)\cdot CH_2Cl_2$ (1.00 mg, 1.22 µmol), KOAc (10.1 mg, 103 µmol) and B_2Pin_2 (10.1 mg, 39.8 µmol) were suspended in degassed 1,4-dioxane (800 µL) and heated to 80 °C for 2 days. During this time, additional $PdCl_2(dppf)\cdot CH_2Cl_2$ (1.00 mg, 1.22 µmol), KOAc (10.1 mg, 103 µmol) and B_2Pin_2 (4.60 mg, 18.8 µmol) were added to aid conversion. Then, the reaction mixture was diluted with EtOAc (10 mL), filtered through a pad of celite, washed with EtOAc and concentrated *in vacuo*. The crude was then purified by reverse-phase FCC (10-100% MeCN in 0.5% formic acid (aq)) to yield 4-(3-(4-(cyclopropanecarbonyl)piperazine-1-carbonyl)-4-fluorobenzyl)-2-(4-(4,4,5,5-tetramethyl-1,3,2-dioxaborolan-2-yl)benzyl)phthalazin-1(2*H*)-one (**78b**) (7.67 mg†, 11.8 µmol, 33%) and (4-((4-(3-(4-(cyclopropanecarbonyl)piperazine-1-carbonyl)-4-fluorobenzyl)-1-oxophthalazin-2(1*H*)-yl)methyl)phenyl)boronic acid (**78a**) (2.23 mg†, 3.93 µmol, 11%) as an amorphous white solid mixture.

†Calculated NMR yield of the mixture of boronic ester and acid products.

LCMS (5-95% MeCN in H_2O, 2% formic acid) retention time ester **78b**: 1.49 mins; acid **78a**: 1.22 mins; **^{1}H NMR** (400 MHz, $CDCl_3$): δ 8.46 (m, 1H, Ht), 7.76 (d, 2H, *J* = 8.1 Hz, Hz), 7.71 (m, 3H, Hs, Hr, Hq), 7.44 (d, 2H, *J* = 7.9 Hz, Hy), 7.34 (m, 1H, Hm), 7.23 (m, 1H, Hk), 7.00 (app t, 1H, *J* = 8.7 Hz, Hj), 5.41 (s, 2H, Hw), 4.25 (s, 2H, Hn), 3.81 (br, 4H, He/Hf), 3.56-3.24 (br, 4H, He/Hf), 1.69 (br, 1H, Hc), 1.32 (s, 9H*, Hac), 1.00 (m, 2H, Ha/Hb), 0.81 (br, 2H, Ha/Hb); **^{13}C NMR** (176 MHz, $CDCl_3$): δ 172.4 (Cd), 165.4 (Cg), 159.2 (Cv), 157.7-156.3 (d, $^1J_{CF}$ = 247.0 Hz, Ci), 144.5 (Co), 140.1 (Cx), 135.0 (Cz), 135.6-134.6 (d, $^4J_{CF}$ = 3.1 Hz, Cl), 134.1 (Cp), 133.1 (Cs/Cr/Cq), 131.75-131.70 (d, $^3J_{CF}$ = 8.2 Hz, Ck), 131.5 (Cs/Cr/Cq), 129.2 (Cm), 129.0 (Cu), 128.8 (Ch), 128.4 (Caa), 127.9 (Cy), 127.7 (Ct), 124.7 (Cs/Cr/Cq), 116.2 (br m, Cj), 83.8 (Cab), 54.6 (Cw), 47.0-45.4 (br, Ce/Cf), 42.2 (br, Ce/Cf), 37.8 (Cn), 24.9 (Cac), 11.1 (Cc), 7.8 (br, Ca, Cb);

IR ν_{max} /cm^{-1}: 3053 w (O-H), 1638 s (C=O), 1264 m (B-O); **HRMS (ESI)**: m/z calcd for $[M+H]^+$ (**78a**): 569.2366; found: 569.2388.

*This material is a mixture of the boronic ester and acid, whereby proton signals between the two species are indistinguishable. Therefore, the pinacol protons Hac do not integrate to 12H as expected for pure boronic ester material.

2-(4-Bromobenzyl)-4-(3-(4-(cyclopropanecarbonyl)piperazine-1-carbonyl)-4-fluorobenzyl)-phthalazin-1(*2H*)-one (80)

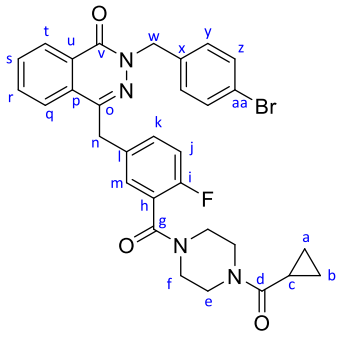

Olaparib (50.5 mg, 0.116 mmol) and NaH (60% dispersion in mineral oil) (7.00 mg, 0.175 mmol), were dissolved in DMF (300 µL) and stirred at rt for 25 mins. Then, 1-bromo-4-(bromomethyl)benzene (40.2 mg, 0.161 mmol) was added at rt and stirred for 30 mins. Then, the reaction was cooled to 0 °C and diluted with EtOAc (10 mL) then quenched with sat. NH_4Cl (aq) (10 mL). The aqueous phase was extracted with EtOAc (3 x 10 mL) and the combined organic phases washed with H_2O (2 x 10 mL). The aqueous phase still contained product by TLC, so was made more basic (~pH 8) with the addition of solid $NaHCO_3$, then extracted with EtOAc (10 mL). The combined organic phases were dried over Na_2SO_4 then concentrated *in vacuo* before FCC (0-5% MeOH in CH_2Cl_2) to yield 2-(4-bromobenzyl)-4-(3-(4-(cyclopropanecarbonyl)piperazine-1-carbonyl)-4-fluorobenzyl)phthalazin-1(2H)-one (**80**) (59.0 mg, 0.0977 mmol, 84%) as an amorphous white solid.

$\mathbf{R_f}$ = 0.27 (5% MeOH in CH_2Cl_2); **^{1}H NMR** (400 MHz, $CDCl_3$): δ 8.42 (m, 1H, Ht), 7.70 (m, 3H, Hs, Hr, Hq), 7.41 (d, 2H, *J* = 8.2 Hz, Hz), 7.32 (d, 2H, *J* = 8.3 Hz, Hy), 7.24 (m, 2H, Hm, Hk), 7.00 (app t, 1H, *J* = 8.8 Hz, Hj), 5.31 (s, 2H, Hw), 4.24 (s, 2H, Hn), 3.77 (br, 4H, He/Hf), 3.54 (br, 2H, He/Hf), 3.23 (br, 2H, He/Hf), 1.70 (br, 1H, Hc), 0.97 (br m, 2H, Ha/Hb), 0.78 (br m, 2H, Ha/Hb); **^{13}C NMR** (101 MHz, $CDCl_3$): 172.3 (Cd), 165.2 (Cg), 159.0 (Cv), 157.9-155.9 (d, $^1J_{CF}$ = 247.9 Hz, Ci), 144.6 (Co), 135.9 (Cx), 134.4 (Cl), 133.1 (Cs/Cr/Cq), 131.63 (Cs/Cr/Cq/Cz/Ck), 131.56 (Cs/Cr/Cq/Cz/Ck), 131.5 (Cs/Cr/Cq/Cz/Ck), 130.4 (Cy), 129.1 (m, Cm), 128.9 (Cu), 128.3 (Cp), 127.5 (Ct), 124.7 (Cs/Cr/Cq), 123.7-123.6 (d, $^2J_{CF}$ = 18.6 Hz, Hh), 121.7 (Caa), 116.1-116.0 (d, $^2J_{CF}$ = 24.5 Hz, Hj), 53.9 (Cw), 46.7-45.1 (br, Ce/Cf), 42.2 (Ce/Cf), 37.6 (Cn),

11.0 (Cc), 7.7 (br, Ca, Cb). **IR** ν_{max} /cm^{-1}: 1631 s (C=O), 1584 s (C=O); **HRMS (ESI)**: m/z calcd for [M+H]$^+$: 603.1402; found: 603.1402.

(4-(((4-(3-(4-(Cyclopropanecarbonyl)piperazine-1-carbonyl)-4-fluorobenzyl)-1-oxo-1,2-dihydrophthalazine-2-carbonyl)oxy)methyl)phenyl)boronic acid (81a) and 4-(4,4,5,5-tetramethyl-1,3,2-dioxaborolan-2-yl)benzyl 4-(3-(4-(cyclopropanecarbonyl)piperazine-1-carbonyl)-4-fluorobenzyl)-1-oxophthalazine-2(1*H*)-carboxylate (81b)

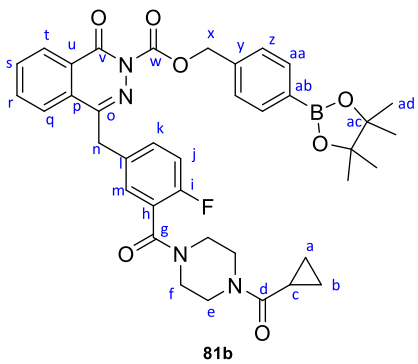

81b

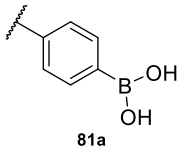

81a

4-Bromobenzyl 4-(3-(4-(cyclopropanecarbonyl)piperazine-1-carbonyl)-4-fluorobenzyl)-1-oxophthalazine-2(1H)-carboxylate (**83**) (25.0 mg, 38.6 µmol), $PdCl_2(dppf)\cdot CH_2Cl_2$ (63.0 mg, 77.1 µmol), B_2Pin_2 (21.6 mg, 85.1 µmol) and KOAc (22.8 mg, 232 µmol) were suspended in degassed 1,4-dioxane (1 mL) and heated to 80 °C for 1 h. The cooled mixture was filtered through a celite pad, then concentrated *in vacuo* followed by reverse-phase FCC (10-100% MeCN in 0.5% formic acid (aq)) then lyophilised to yield a mixture of boronic ester product, 4-(4,4,5,5-tetramethyl-1,3,2-dioxaborolan-2-yl)benzyl 4-(3-(4-(cyclopropanecarbonyl)piperazine-1-carbonyl)-4-fluorobenzyl)-1-oxophthalazine-2(1H)-carboxylate (**81b**) (11.7 mg†, 16.8 µmol, 44%) and boronic acid product (4-(((4-(3-(4-(cyclopropanecarbonyl)piperazine-1-carbonyl)-4-fluorobenzyl)-1-oxo-1,2-dihydrophthalazine-2-carbonyl)oxy)methyl)phenyl)boronic acid (**81a**) (8.97 mg†, 14.6 µmol, 38%).

†Calculated NMR yield of the mixture of boronic ester and acid products.

LCMS (5-95% MeCN in H_2O, 2% formic acid) retention time 1.42 mins; **^{1}H NMR*** (700 MHz, $CDCl_3$): δ 8.51 (br, 1H, Ht), 7.86 (m, 2H, Haa), 7.75 (m, 3H, Hs/Hr/Hq), 7.51 (m, 2H, Hz), 7.37 (m, 2H, Hm, Hk), 7.07 (br, 1H, Hj), 5.55 (s, 2H, Hx), 4.33 (s, 2H, Hn), 3.79 (br, 4H, He/Hf), 3.62 (br, 2H, He/Hf), 3.29 (2H, br, He/Hf), 1.78 (br, 1H, Hc), 1.36 (m, 6H, Had†), 1.03 (s, 2H, Ha/Hb), 0.84 (br, 2H, Ha/Hb); **^{13}C NMR**‡ (700 MHz, $CDCl_3$): δ 172.3 (Cd), 165.2 (Cg), 158.4 (Cv), 158.4-157.8 (d, $^1J_{CF}$ = 247.8 Hz, Ci), 152.4 (Cw), 146.1 (Co), 135.1 (Caa), 134.4 (Cs/Cr/Cq), 133.7 (Cl), 133.5 (Cy), 132.3 (Cs/Cr/Cq), 131.7 (Cm/Ck), 129.3 (Cm/Ck), 128.9 (Cp/Cu/Cab), 128.8 (Cp/Cu/Cab), 128.6 (Cp/Cu/Cab), 128.4 (Ct), 127.5 (Cz), 125.3 (Cs/Cr/Cq), 116.3 (Cj), 83.9 (Cac), 70.1 (Cx), 46.8-45.2 (Ce/Cf), 42.3 (br, Ce/Cf), 38.1 (Cn), 24.9 (Cad),

11.1 (Cc), 7.8 (Ca, Cb); **IR** ν_{max} /cm^{-1}: 3490 br (O-H), 1654 s (C=O), 1621 s (C=O); **HRMS (ESI)**: m/z calcd for [M+H]$^+$ (**81b**): 695.3047; found: 695.3038, [M+H]$^+$ (**81a**): 613.2264; found: 613.2276.

*The proton NMR of this compound has broad signals, presumably due to the presence of boronic acid. †The pinacol protons do not integrate to 12H because the sample contains a mixture of the boronic ester and acid form. ‡Ch could not be identified. Because it is a quaternary carbon and has $^2J_{CF}$ coupling, it is presumed splitting renders it too low intensity to observe within the noise.

4-Bromobenzyl 4-(3-(4-(cyclopropanecarbonyl)piperazine-1-carbonyl)-4-fluorobenzyl)-1-oxophthalazine-2(1*H*)-carboxylate (83)

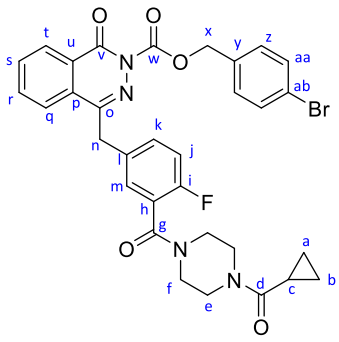

Olaparib (250 mg, 0.575 mmol) was suspended in DMF (2.5 mL) and NaH (60% dispersion in mineral oil) (23.0 mg, 0.575 mmol) and 18-crown-6 (152 mg, 0.575 mmol) were added and stirred at rt for 10 mins until the cloudy solution became clear. Then, 4-bromobenzyl (4-nitrophenyl) carbonate (**31**) (203 mg, 0.577 mmol) was added and stirred at rt for 2.5 h. The reaction was concentrated under a stream of N_2 and then purified by reverse-phase FCC (10-100% MeCN in 0.5% formic acid (aq)) then lyophilised to yield 4-bromobenzyl 4-(3-(4-(cyclopropanecarbonyl)piperazine-1-carbonyl)-4-fluorobenzyl)-1-oxophthalazine-2(1*H*)-carboxylate (**83**) (149 mg, 0.231 mmol, 40%) as an amorphous white powder.

LCMS (5-95% MeCN in H_2O, 2% formic acid) retention time 1.42 mins; **^{1}H NMR** (400 MHz, $CDCl_3$): δ 8.47 (m, 1H, Ht), 7.76 (m, 2H, Hs/Hr/Hq), 7.66 (m, 1H, Hs/Hr/Hq), 7.52 (d, 2H, *J* = 8.5 Hz, Haa), 7.39 (d, 2H, *J* = 8.5 Hz, Hz), 7.34 (m, 2H, Hm, Hk), 7.03 (app t, 1H, *J* = 8.9 Hz, Hj), 5.45 (s, 2H, Hx), 4.31 (s, 2H, Hn), 3.83-3.26 (br, 8H, He, Hf), 1.75-1.65 (br, 1H, Hc), 1.01 (m, 2H, Ha/Hb), 0.81 (br, 2H, Ha/Hb); **^{13}C NMR** (176 MHz, $CDCl_3$): δ 172.5 (Cd), 165.2 (Cg), 158.4 (Cv), 158.1-156.1 (d, $^1J_{CF}$ = 249.4 Hz, Ci), 152.4 (Cw), 146.3 (Co), 134.5 (Cs/Cr/Cq), 133.7 (d, $^4J_{CF}$ = 3.1 Hz, Cl), 133.6 (Cy), 132.4 (Cs/Cr/Cq), 131.9 (Caa), 131.7 (d, $^3J_{CF}$ = 7.7 Hz, Cm/Ck), 130.1 (Cz), 129.3 (m, Cm/Ck), 128.8 (Cp), 128.5 (Cu), 128.4 (Ct), 125.4 (Cs/Cr/Cq), 122.8 (Cab), 116.4 (d, $^2J_{CF}$ = 20.7 Hz, Cj), 69.4 (Cx), 47.0- 45.2 (br, Ce/Cf), 42.3 (br, Ce/Cf), 38.1 (Cn), 11.1 (Cc), 7.8 (Ca, Cb); **IR** ν_{max} /cm^{-1}: 1773 s (C=O), 1636 s (C=O); **HRMS (ESI)**: m/z calcd for [M+H]$^+$: 647.1300; found: 647.1268.

*Ch could not be identified. Because it is a quaternary carbon and has $^{2}J_{CF}$ coupling, it is presumed splitting renders it too low intensity to observe within the noise.

4.3 Bioconjugations

To a solution of trastuzumab or durvalumab (40 µL, 16.9 µM, 2.5 mg/mL) in tris-buffered saline (TBS) (25 mM Tris HCl pH 8, 25 mM NaCl, 0.5 mM EDTA) was added TCEP (10 eq.). The mixture was vortexed and incubated at 37 °C for 1 h with shaking at 400 rpm. A solution of DVP-linker-payload (20 mM in DMSO) was added with additional DMSO (final concentration of 0.61 mM, for 40 eq. of linker or 1.22 mM for 80 eq of linker, 10% DMSO (v/v)) and the reaction mixture incubated at 37 °C for 4 h with shaking at 400 rpm. The excess reagents were removed by size-exclusion chromatography with a Zeba Spin desalting column (40K MWCO, 0.5 mL) and exchanged into PBS with an Amicon-Ultra centrifugal filter (10K MWCO, Merck Millipore).

Table 20: Summary of final bioconjugation reaction conditions of trastuzumab and durvalumab to generate **ADCs 1-4** and **ADCs 5-7** respectively.

ADC	Antibody	Linker	Linker eq.	Reaction time	Average DAR
1	Trastuzumab	DVP-unsubstituted-MMAE (**20c**)	40	4 h	3.7
2	Trastuzumab	DVP-difluoro-MMAE (**21c**)	80	4 h	3.7
3	Trastuzumab	DVP-non-cleavable-MMAE (**23**)	80	4 h	3.8
4	Trastuzumab	DVP-Val-Cit-MMAE (**24**)	80	4 h	3.9
5	Durvalumab	DVP-unsubstituted-MMAE (**20c**)	40	4 h	3.6
6	Durvalumab	DVP-non-cleavable-MMAE (**23**)	40	4 h	3.7
7	Durvalumab	DVP-Val-Cit-MMAE (**24**)	40	4 h	3.7

4.4 SDS-PAGE

Non-reducing Tris-Glycine SDS-PAGE with 12% acrylamide with 4% stacking gel was performed as standard. Broad range molecular weight marker (10-200 kDa, New England BioLabs) was run in all gels. Samples (5 µL, 2.5 µg unless stated otherwise) were prepared with reducing loading dye (5 µL, containing β-mercaptoethanol) and heated to 90 °C for 5 min before loading. Gels were run at constant voltage (200 V) for 45-60 min in 1 x Laemmli running buffer (LRB). All gels were stained with Coomassie blue dye and imaged on a Syngene gel imaging system.

4.5 Size-Exclusion Chromatography (SEC)

Analytical size-exclusion chromatography (SEC) was carried out on an AKTA pure chromatography system using a Superdex™ 200 Increase 10/300 GL column. Samples were injected at a concentration of 1 mg/mL and eluted with TBS pH 8 (25 mM Tris HCl, 200 mM NaCl, 0.5 mM EDTA) at a flow rate of 0.5 mL/min.

4.6 Hydrophobic Interaction Chromatography (HIC)

Analytical hydrophobic interaction chromatography (HIC) was carried out on a Tosoh Bioscience TSKgel Butyl-NPR column (3.5 cm × 4.6 mm, 2.5 μm). Samples were injected at a concentration of 1 mg/mL and eluted with a linear gradient of solvent A in solvent B (solvent A: 1.5 M ammonium sulfate, 25 mM NaPi, pH 7 and solvent B: 25% isopropyl alcohol in 25 mM NaPi, pH 7 at a flow rate of 0.6 mL/min. The drug-to-antibody ratio was calculated by the integration of the signals at 280 nm:

$$Average\ DAR = \frac{(DAR_1 + 2 \times DAR_2 + 3 \times DAR_3 + 4 \times DAR_4 + 5 \times DAR_5)}{(DAR_0 + DAR_1 + DAR_2 + DAR_3 + DAR_4 + DAR_5)}$$

4.7 Chapter 1: Model linker peroxide-cleavage studies

Data from all cleavage studies were processed using GraphPad Prism Version 9.3.0.

Human and mouse plasma were obtained from Sigma Aldrich.

4.7.1 Release from model linkers 1b, 2b, 5b and 3 with 0, 1, 5, 10 equivalents of hydrogen peroxide

Model linkers **1b**, **2b**, **5b** and **3** (7.2 μL, 2.5 mM DMSO) were vortexed with PBS (280.8 μL) before adding hydrogen peroxide solution (72.0 μL at 1, 5 or 10 equivalents – final concentration of 50 μM, 250 μM and 500 μM respectively). 340 μL of the resulting solution was added to a 96-well plate (Greiner, black, clear flat bottomed). Fluorescence intensity was monitored at λ_{em} = 441 nm over 20 h at 37 °C. An adhesive film (BioRad) was used to prevent solvent evaporation. Readings were taken at 30-35 second intervals. The reactions were performed in triplicate, with three technical replicates for each set of conditions. Control wells contained water (72.0 μL) instead of hydrogen peroxide.

4.7.2 Release from 1b and 2b at different pH

Model linkers **1b** and **2b**, (7.2 μL, 2.5 mM DMSO) were vortexed with either PBS (pH 7.4), sodium acetate buffer (pH 4.5) or carbonate buffer (pH 9) (280.8 μL). Hydrogen peroxide solution (72.0 μL, 10 equivalents, 500 μM final concentration) was then added to the solutions and 340 μL of the resulting solution was added to a 96-well plate (Greiner, black, clear flat bottomed). Fluorescence intensity was monitored at λ_{em} = 441 nm over 25 h at 37 °C. An adhesive film (BioRad) was used to prevent solvent

evaporation. Readings were taken at 1.5-minute intervals. The reactions were performed in duplicate, with three technical replicates for each set of conditions.

4.7.3 Release in the presence of GSH, and hydrogen peroxide scavenger CAT

Model linkers **1b** and **2b**, (7.2 µL, 2.5 mM DMSO) were vortexed with either PBS (280.8 µL) containing 10 equivalents of reduced glutathione (GSH), or PBS containing ~2000 U/mL catalase (CAT) from bovine liver. Hydrogen peroxide solution (72.0 µL, 10 equivalents) or water (72.0 µL) for control wells, was then added to the solutions and 340 µL of the resulting solution was added to a 96-well plate (Greiner, black, clear flat bottomed). Fluorescence intensity was monitored at λ_{em} = 441 nm over 25 h at 37 °C. An adhesive film (BioRad) was used to prevent solvent evaporation. Readings were taken at 1.5-minute intervals. The reactions were performed in triplicate with three technical replicates for each set of conditions. Catalase was obtained from MERCK LIFE SCIENCE UK LTD.

4.7.3.1 Long term release in the presence of scavenger CAT

Once complete, the plate was covered in foil and placed in an incubator at 37 °C for 7 days. Additional fluorimetry measurements were taken at t = 24, 48, 72 and 168 h. This was performed in duplicate, with three technical replicates of each condition.

4.8 Chapter 1: Model linker stability studies

4.8.1 Stability of 1b and 2b by fluorimetry in the presence of different pH and GSH

Model linkers **1b** and **2b**, (7.2 µL, 2.5 mM DMSO) were vortexed with either PBS (pH 7.4), sodium acetate buffer (pH 4.5), carbonate buffer (pH 9) or PBS containing 10 equivalents of reduced glutathione (GSH) (all 280.8 µL). Water (72.0 µL) was then added to the solutions and 340 µL of the resulting solution was added to a 96-well plate (Greiner, black, clear flat bottomed). An adhesive film (BioRad) was used to prevent solvent evaporation. Fluorescence was monitored at λ_{em} = 441 nm. The reactions were performed in duplicate, with three technical replicates for each set of conditions.

4.8.2 Stability of 1b and 2b in unconditioned cell media

Unconditioned cell media used had not been in contact with cancer cells. McCoy's = High glucose McCoy's 5A medium, supplemented with GlutaMAX™. RPMI = RPMI1640 medium supplemented with 2 mM L-glutamine. DMEM = Dulbecco's Modified Eagle Medium (DMEM) supplemented with 2 mM L-glutamine. All cell media were supplemented with 10% heat-inactivated foetal-bovine serum FBS (HI-FBS), 50 U/mL penicillin and 50 µg/mL streptomycin.

Model linkers **1b** and **2b**, (7.2 µL, 2.5 mM DMSO) were vortexed with unconditioned cell media (280.8 µL) and then 272 µL of the resulting solution was added to a 96-well plate (Greiner, black, clear flat bottomed). Water (68 µL) or hydrogen peroxide solution (68 µL, 10 eq.), was then added to the

appropriate wells and fluorescence was monitored at λ_{em} = 441 nm over 24 h at 37 °C. An adhesive film (BioRad) was used to prevent solvent evaporation. The reactions were performed in triplicate, with three technical replicates for each set of conditions.

4.8.2.1 Long term release in the presence of unconditioned cell media

Once complete, the plate containing linkers in unconditioned cell media were covered in foil and placed in an incubator at 37 °C for the remaining 3 days. Additional fluorimetry measurements were taken at t = 48, 72 and 96 h. This was performed in triplicate, with three technical replicates of each condition.

4.8.3 Stability of **2b**, **3** and **4** in human and mouse plasma – HPLC study

2c, **3** and **4** (10 mM) were incubated with PBS (149 µL), human/mouse plasma (265 µL), DMSO (86 µL) and caffeine (10 µL, 15 mg/mL, internal standard) at 37 °C for 10 days. 50 µL aliquots of the mixture were taken at t = 1, 2, 3, 4, 5, 10 days and flash frozen in liquid nitrogen and stored at -20 °C before HPLC analysis of all samples on the same day. After thawing, the samples were precipitated with 1:1 EtOH:DMSO (100 µL), centrifuged (17,000G, 3 mins) and 50 µL of the supernatant analysed by HPLC. The linker peak area was calibrated to the caffeine internal standard for quantification of degradation over time.

For raw HPLC data, please see appendix 3, Table 21-Table 25.

4.8.4 Stability of **1b** and **2b** in human and mouse plasma – Fluorimetry, 20 h

Model linkers **1b** and **2b** (36.0 µL, 2.5 mM DMSO) were vortexed with PBS (774 µL) and 153 µL of the resulting solution was added to a 96-well plate (Greiner, black, clear flat bottomed). Then, human plasma (187 µL) was added to each well. Fluorescence intensity was monitored at λ_{em} = 441 nm over 20 h at 37 °C. An adhesive film (BioRad) was used to prevent solvent evaporation. Readings were taken at 30-35 second intervals. The reactions were performed in triplicate, with three technical replicates for each set of conditions.

4.8.5 Stability of **1b**, **2b** and **4** in human and mouse plasma – Fluorimetry, 10 days

Linkers **1b**, **2b** and **4** (28 µL, 2.5 mM in DMSO) were vortexed with PBS (602 µL) and 90 µL of this solution was added to the wells of a 96-well plate (Greiner, black, clear flat bottomed). To this, plasma (from human or mouse, 110 µL) was added. An adhesive film (BioRad) was used to prevent solvent evaporation. Control wells replaced plasma with PBS. Each condition had three technical replicates. The plate was incubated at 37 °C for 10 days, with readings at λ_{em} = 441 nm at t = 1, 2, 3, 4, 5, 7, 10 days.

4.9 Cell Lines

SKBR3, MDA-MB-231 and BT474 cells were obtained from the American Type Culture Collection (ATCC) and HER2-negative MCF7 and MDA-MB-468 cells were obtained from the European Collection of Authenticated Cell Cultures (ECACC).

SKBR3 cells were maintained in high glucose McCoy's 5A medium, supplemented with GlutaMAX™. MCF7, MDA-MB-468, MDA-MB-231 and HEK-293T cells were maintained in Dulbecco's Modified Eagle Medium (DMEM) supplemented with 2 mM L-glutamine. BT474 and MDA-MB-231 cells were maintained in RPMI1640 medium supplemented with 2 mM L-glutamine. SKBR3, MCF7, HEK-293T, BT474, MDA-MB-468 and MDA-MB-231 cells were maintained in media supplemented with 10% HI-FBS and 50 U/mL penicillin and 50 µg/mL streptomycin. MCF10A cells were maintained in Mammary Epithelial Cell Growth Basal Medium (MEBM) with mammary epithelial cell growth medium additive (MEGM, Lonza). All cell lines were incubated at 37 °C with 5% CO_2.

4.10 General Cell Viability Protocol

Cells were seeded in 96-well plates for 24 h at 37 °C with 5% CO_2. SKBR3 cells were seeded at 15,000 cells/well, BT474 cells were seeded at 20,000 cells/well, MCF7 cells were seeded at 7,500 cells/well, MDA-MB-468 cells were seeded at 10,000 cells/well, MCF10A cells were seeded at 5,000 cells/well, HEK-293T cells were seeded at 1,000 cells/well and MDA-MB-231 cells were seeded at 5,000 cells/well. Serial dilutions of ADCs or trastuzumab/durvalumab were added to the cells in complete growth medium and incubated at 37 °C with 5% CO_2 for 96 h. Cell viability was determined using a CellTiter-Glo viability assay (Promega) according to the manufacturer's instructions. Cell viability was plotted as a percentage of that of untreated cells. Each measurement was taken in triplicate unless stated otherwise. Three independent replicates were performed. Data was processed using GraphPad Prism Version 9.3.0 and best-fit IC_{50} values of each compound were calculated using the log (inhibitor) vs response (variable slope) function.

4.11 *In Vitro* Cytotoxicity with Washout

Cells were seeded in 96-well plates for 24 h at 37 °C with 5% CO_2. Serial dilutions of ADCs or trastuzumab were added to the cells in complete growth medium and incubated at 37 °C with 5% CO_2 for 1 h, 4 h, 8 h or 24 h. After the selected washout time, the cell media was removed and replaced with complete growth medium. The medium was removed once again and replaced with complete growth medium. For experiments where exogenous H_2O_2 was introduced, the media replacement contained 0.1 mM H_2O_2. After washout, the cells were incubated for the remaining time to allow a 4 day-treatment.

4.12 *In Vitro* Cytotoxicity with Catalase Scavenger

Cells were seeded in 96-well plates for 24 h at 37 °C with 5% CO_2. Cell media was then removed and replaced with 100 µL complete growth media containing catalase (400-1000 U/well) and incubated at 37 °C for 2 h. Then serial dilutions of ADCs in 100 µL complete growth media were added and cell growth was monitored on an IncuCyte® S3 Live-Cell Analysis System for 96 h with incubation at 37 °C and 5% CO_2. Cell viability was determined using a CellTiter-Glo viability assay (Promega) according to the manufacturer's instructions. Cell viability was plotted as a percentage of that of untreated cells. Each measurement was taken in triplicate. Two independent replicates were performed. Data was processed using GraphPad Prism Version 9.3.0 and best-fit IC_{50} values of each compound were calculated using the log (inhibitor) vs response (variable slope) function. Confluency increase was calculated using the equation: $[\frac{confluency_{final} - confluency_{initial}}{confluency_{initial}}] * 100$ whereby $confluency_{initial}$ is the % cell confluency at t = 3h after ADC treatment, and $confluency_{final}$ is the % cell confluency at approx. t = 96 h.

4.13 Quantification of Extracellular Hydrogen Peroxide with Amplex™ Red

Amplex™ Red Hydrogen Peroxide/Peroxidase Assay Kit (Invitrogen) was used following the manufacturer's instructions. Briefly, 20,000 cells/well were seeded in 100 µL F-12 Ham's nutrient mixture (for the no cell control, wells contained only F-12 Ham's nutrient mixture). After seeding for 24 h at 37 °C with 5% CO_2, 100 µL of the Amplex™ Red reaction mixture was added to each well and the fluorescence intensity monitored on a CLARIOstar plate reader over 30 minutes. Data shown is the reading at t = 30 minutes.

For catalase scavenging, after seeding, the media was removed and replaced with Ham's nutrient mixture containing catalase (approx. 400-1000 U/well) (100 µL) and incubated at 37 °C, 5% CO_2 for 2 h. Then, 100 µL of the Amplex™ Red reaction mixture was added to each well and the fluorescence intensity monitored on a CLARIOstar plate reader over 30 minutes. Data shown is the reading at t = 30 minutes.

4.14 Chapter 3: Crude Olaparib Prodrug Cleavage Study

A solution of **78a/78b** or **81a/81b** in MeCN:H_2O was added 30 w/w% H_2O_2 (10 µL) at rt and analysed by HPLC at various time intervals with UV detection (λ_{max} = 220 nm). In-between HPLC analysis, the same sample was analysed by LCMS for identification of masses corresponding to the observed HPLC peaks.

References

1 American Cancer Society Journal, Cancer Facts & Figures 2023, https://www.cancer.org/research/cancer-facts-statistics/all-cancer-facts-figures/2023-cancer-facts-figures.html.

2 World Health Organization, Cancer, https://www.who.int/news-room/fact-sheets/detail/cancer.

3 V. V. Padma, *Biomed.*, 2015, **5**, 1–6.

4 S. D. Barnscher, The Clinical Landscape Of ADCs In 2023: Diverse Technologies, Narrow Target, https://www.clinicalleader.com/doc/the-clinical-landscape-of-adcs-in-diverse-technologies-narrow-target-0001.

5 N. Ashman, J. D. Bargh and D. R. Spring, *Chem. Soc. Rev*, 2022, **51**, 9182–9202.

6 E. Wagner-Rousset, M. C. Janin-Bussat, O. Colas, M. Excoffier, D. Ayoub, J. F. Haeuw, I. Rilatt, M. Perez, N. Corvaïa and A. Beck, *MAbs*, 2014, **6**, 173–184.

7 R. V. J. Chari, M. L. Miller and W. C. Widdison, *Angew. Chemie - Int. Ed.*, 2014, **53**, 3796–3827.

8 R. P. Lyon, T. D. Bovee, S. O. Doronina, P. J. Burke, J. H. Hunter, H. D. Neff-Laford, M. Jonas, M. E. Anderson, J. R. Setter and P. D. Senter, *Nat. Biotechnol.*, 2015, **33**, 733–735.

9 J. Mantaj, P. J. M. Jackson, K. M. Rahman and D. E. Thurston, *Angew. Chemie - Int. Ed.*, 2017, **56**, 462–488.

10 N. Jain, S. W. Smith, S. Ghone and B. Tomczuk, *Pharm. Res.*, 2015, **32**, 3526–3540.

11 R. P. Lyon, J. R. Setter, T. D. Bovee, S. O. Doronina, J. H. Hunter, M. E. Anderson, C. L. Balasubramanian, S. M. Duniho, C. I. Leiske, F. Li and P. D. Senter, *Nat. Biotechnol.*, 2014, **32**, 1059–1062.

12 M. E. B. Smith, F. F. Schumacher, C. P. Ryan, L. M. Tedaldi, D. Papaioannou, G. Waksman, S. Caddick and J. R. Baker, *J. Am. Chem. Soc.*, 2010, **132**, 1960–1965.

13 J. D. Sadowsky, T. H. Pillow, J. Chen, F. Fan, C. He, Y. Wang, G. Yan, H. Yao, Z. Xu, S. Martin, D. Zhang, P. Chu, J. Dela Cruz-Chuh, A. O'Donohue, G. Li, G. Del Rosario, J. He, L. Liu, C. Ng, D. Su, G. D. Lewis Phillips, K. R. Kozak, S. F. Yu, K. Xu, D. Leipold and J. Wai, *Bioconjug. Chem.*, 2017, **28**, 2086–2098.

14 D. N. Toda, D. S. Asano and P. D. C. F. Barbas III, *Angew Chem Int Ed*, 2013, **52**, 12592–12596.

15 O. Koniev, G. Leriche, M. Nothisen, J. S. Remy, J. M. Strub, C. Schaeffer-Reiss, A. Van Dorsselaer,

R. Baati and A. Wagner, *Bioconjug. Chem.*, 2014, **25**, 202–206.

16 M. J. Matos, C. D. Navo, T. Hakala, X. Ferhati, A. Guerreiro, D. Hartmann, B. Bernardim, K. L. Saar, I. Compañón, F. Corzana, T. P. J. Knowles, G. Jiménez-Osés and G. J. L. Bernardes, *Angew. Chemie - Int. Ed.*, 2019, **58**, 6640–6644.

17 B. Bernardim, P. M. S. D. Cal, M. J. Matos, B. L. Oliveira, N. Martínez-Saéz, I. S. Albuquerque, E. Perkins, F. Corzana, A. C. B. Burtoloso, G. Jiménez-Osés and G. J. L. Bernardes, *Nat. Commun.*, 2016, **7**, 1–9.

18 S. C. Alley, D. R. Benjamin, S. C. Jeffrey, N. M. Okeley, D. L. Meyer, R. J. Sanderson and P. D. Senter, *Bioconjug. Chem.*, 2008, **19**, 759–765.

19 S. L. Vinogradova, Ekaterina V; Zhang, Chi; Spokoyny, Alexander M; Pentelute, Bradley L; Buchwald, *Nature*, 2015, **526**, 687–691.

20 S. J. Walsh, J. D. Bargh, F. M. Dannheim, A. R. Hanby, H. Seki, A. J. Counsell, X. Ou, E. Fowler, N. Ashman, Y. Takada, A. Isidro-Llobet, J. S. Parker, J. S. Carroll and D. R. Spring, *Chem. Soc. Rev.*, 2021, **50**, 1305–1353.

21 G. Badescu, P. Bryant, M. Bird, K. Henseleit, J. Swierkosz, V. Parekh, R. Tommasi, E. Pawlisz, K. Jurlewicz, M. Farys, N. Camper, X. Sheng, M. Fisher, R. Grygorash, A. Kyle, A. Abhilash, M. Frigerio, J. Edwards and A. Godwin, *Bioconjug. Chem.*, 2014, **25**, 1124–1136.

22 P. Bryant, M. Pabst, G. Badescu, M. Bird, W. McDowell, E. Jamieson, J. Swierkosz, K. Jurlewicz, R. Tommasi, K. Henseleit, X. Sheng, N. Camper, A. Manin, K. Kozakowska, K. Peciak, E. Laurine, R. Grygorash, A. Kyle, D. Morris, V. Parekh, A. Abhilash, J. W. Choi, J. Edwards, M. Frigerio, M. P. Baker and A. Godwin, *Mol. Pharm.*, 2015, **12**, 1872–1879.

23 M. Pabst, W. McDowell, A. Manin, A. Kyle, N. Camper, E. De Juan, V. Parekh, F. Rudge, H. Makwana, T. Kantner, H. Parekh, A. Michelet, X. B. Sheng, G. Popa, C. Tucker, F. Khayrzad, D. Pollard, K. Kozakowska, R. Resende, A. Jenkins, F. Simoes, D. Morris, P. Williams, G. Badescu, M. P. Baker, M. Bird, M. Frigerio and A. Godwin, *J. Control. Release*, 2017, **253**, 160–164.

24 C. R. Behrens, E. H. Ha, L. L. Chinn, S. Bowers, G. Probst, M. Fitch-Bruhns, J. Monteon, A. Valdiosera, A. Bermudez, S. Liao-Chan, T. Wong, J. Melnick, J. W. Theunissen, M. R. Flory, D. Houser, K. Venstrom, Z. Levashova, P. Sauer, T. S. Migone, E. H. Van Der Horst, R. L. Halcomb and D. Y. Jackson, *Mol. Pharm.*, 2015, **12**, 3986–3998.

25 F. F. Schumacher, J. P. M. M. Nunes, A. Maruani, V. Chudasama, M. E. B. B. Smith, K. A. Chester, J. R. Baker and S. Caddick, *Org. Biomol. Chem.*, 2014, **12**, 7261–7269.

26 M. Morais, J. P. M. Nunes, K. Karu, N. Forte, I. Benni, M. E. B. Smith, S. Caddick, V. Chudasama and J. R. Baker, *Org. Biomol. Chem.*, 2017, **15**, 2947–2952.

27 J. P. M. Nunes, M. Morais, V. Vassileva, E. Robinson, V. S. Rajkumar, M. E. B. Smith, R. B. Pedley, S. Caddick, J. R. Baker and V. Chudasama, *Chem. Commun.*, 2015, **51**, 10624–10627.

28 E. Robinson, J. P. M. Nunes, V. Vassileva, A. Maruani, J. C. F. Nogueira, M. E. B. Smith, R. B. Pedley, S. Caddick, J. R. Baker and V. Chudasama, *RSC Adv.*, 2017, **7**, 9073–9077.

29 S. Shao, M. H. Tsai, J. Lu, T. Yu, J. Jin, D. Xiao, H. Jiang, M. Han, M. Wang and J. Wang, *Bioorganic Med. Chem. Lett.*, 2018, **28**, 1363–1370.

30 A. Maruani, M. E. B. Smith, E. Miranda, K. A. Chester, V. Chudasama and S. Caddick, *Nat. Commun.*, 2015, **6**, 2–10.

31 F. Bryden, A. Maruani, J. M. M. Rodrigues, M. H. Y. Cheng, H. Savoie, A. Beeby, V. Chudasama and R. W. Boyle, *Bioconjug. Chem.*, 2018, **29**, 176–181.

32 A. N. Marquard, J. C. T. Carlson and R. Weissleder, *Bioconjug. Chem.*, 2020, **31**, 1616–1623.

33 B. Shi, M. Wu, Z. Li, Z. Xie, X. Wei, J. Fan, Y. Xu, D. Ding, S. H. Akash, S. Chen and S. Cao, *Cancer Med.*, 2019, **8**, 1793–1805.

34 O. Koniev, I. Dovgan, B. Renoux, A. Ehkirch, J. Eberova, S. Cianférani, S. Kolodych, S. Papot and A. Wagner, *Medchemcomm*, 2018, **9**, 827–830.

35 WO/2014/083505, 2014.

36 S. J. Walsh, S. Omarjee, F. M. Dannheim, D.-L. Couturier, D. Bexheti, L. Mendil, G. Cronshaw, T. Fewster, C. Gregg, C. Brodie, J. L. Miller, R. Houghton, J. S. Carroll and D. R. Spring, *Chem. Commun.*, 2022, **58**, 1962–1965.

37 S. J. Walsh, S. Omarjee, W. R. J. D. Galloway, T. T. L. Kwan, H. F. Sore, J. S. Parker, M. Hyvönen, J. S. Carroll and D. R. Spring, *Chem. Sci.*, 2019, **10**, 694–700.

38 J. R. Junutula, K. M. Flagella, R. A. Graham, K. L. Parsons, E. Ha, H. Raab, S. Bhakta, T. Nguyen, D. L. Dugger, G. Li, E. Mai, G. D. L. Phillips, H. Hiraragi, R. N. Fuji, J. Tibbitts, R. Vandlen, S. D. Spencer, R. H. Scheller, P. Polakis and M. X. Sliwkowski, *Clin. Cancer Res.*, 2010, **16**, 4769–4778.

39 J. R. Junutula, H. Raab, S. Clark, S. Bhakta, D. D. Leipold, S. Weir, Y. Chen, M. Simpson, S. P. Tsai, M. S. Dennis, Y. Lu, Y. G. Meng, C. Ng, J. Yang, C. C. Lee, E. Duenas, J. Gorrell, V. Katta, A. Kim, K. McDorman, K. Flagella, R. Venook, S. Ross, S. D. Spencer, W. Lee Wong, H. B. Lowman, R.

Vandlen, M. X. Sliwkowski, R. H. Scheller, P. Polakis and W. Mallet, *Nat. Biotechnol.*, 2008, **26**, 925–932.

40 C. J. Noren, S. J. Anthony-cahill, M. C. Griffith and P. G. Schultz, *Science (80-.).*, 1989, **244**, 182–188.

41 S. Jeger, K. Zimmermann, A. Blanc, J. Grünberg, M. Honer, P. Hunziker, H. Struthers and R. Schibli, *Angew. Chemie*, 2010, **49**, 9995–9997.

42 C. Belmant, L. Gauthier, F. Lhospice and R. Schibli, *Bioconjug. Chem.*, 2014, **25**, 569–578.

43 S. Dickgiesser, M. Rieker, D. Mueller-Pompalla, C. Schröter, J. Tonillo, S. Warszawski, S. Raab-Westphal, S. Kühn, T. Knehans, D. Könning, J. Dotterweich, U. A. K. Betz, J. Anderl, S. Hecht and N. Rasche, *Bioconjug. Chem.*, 2020, **31**, 1070–1076.

44 P. Agarwal, R. Kudirka, A. E. Albers, R. M. Bar, G. W. De Hart, P. M. Drake, L. C. Jones and D. Rabuka, *Bioconjug. Chem.*, 2013, **24**, 846–851.

45 P. M. Drake, A. E. Albers, J. Baker, S. Banas, R. M. Bar, A. S. Bhat, G. W. De Hart, A. W. Garofalo, P. Holder, L. C. Jones, R. Kudirka, J. Mcfarland, W. Zmolek and D. Rabuka, *Bioconjug. Chem.*, 2014, **25**, 1331–1341.

46 R. R. Beerli, T. Hell, A. S. Merkel and U. Grawunder, *PLoS*, 2015, **10**, 1–17.

47 L. Waldmeier, T. Hell, M. Escher, N. Stefan, F. I. Wolter, U. Grawunder and R. R. Beerli, *Mol. Cancer Ther.*, 2017, **11**, 879–893.

48 L. Ducry and B. Stump, *Bioconjug. Chem.*, 2010, **21**, 5–13.

49 P. D. Senter, *Curr. Opin. Chem. Biol.*, 2009, **13**, 235–244.

50 R. Gebleux, M. Stringhini, R. Casanova, A. Soltermann and D. Neri, *Int. J. Cancer*, 2017, **140**, 1670–1679.

51 F. Giansanti, E. Capone, S. Ponziani, E. Piccolo, R. Gentile, A. Lamolinara, A. Di Campli, M. Sallese, V. Iacobelli, A. Cimini, V. De Laurenzi, R. Lattanzio, M. Piantelli, R. Ippoliti, G. Sala and S. Iacobelli, *J. Control. Release*, 2019, **294**, 176–184.

52 M. N. Saleh, S. Sugarman, J. Murray, J. B. Ostroff, D. Healey, D. Jones, C. R. Daniel, D. LeBherz, H. Brewer, N. Onetto and A. F. LoBuglio, *J. Clin. Oncol.*, 2000, **18**, 2282–2292.

53 H. Xie, C. Audette, M. Hoffee, J. M. Lambert and W. Blättler, *J. Pharmacol. Exp. Ther.*, 2004, **310**, 844.

54 S. V. Govindan, T. M. Cardillo, R. M. Sharkey, F. Tat, D. V. Gold and D. M. Goldenberg, *Mol. Cancer Ther.*, 2013, **12**, 968–978.

55 V. H. J. Van Der Velden, J. G. Te Marvelde, P. G. Hoogeveen, I. D. Bernstein, A. B. Houtsmuller, M. S. Berger and J. J. M. Van Dongen, *Blood*, 2001, **97**, 3197–3204.

56 S. O. Doronina, B. E. Toki, M. Y. Torgov, B. A. Mendelsohn, C. G. Cerveny, D. F. Chace, R. L. DeBlanc, R. P. Gearing, T. D. Bovee, C. B. Siegall, J. A. Francisco, A. F. Wahl, D. L. Meyer and P. D. Senter, *Nat. Biotechnol.*, 2003, **21**, 778–784.

57 G. J. L. Bernardes, G. Casi, S. Trüssel, I. Hartmann, K. Schwager, J. Scheuermann and D. Neri, *Angew. Chemie - Int. Ed.*, 2012, **51**, 941–944.

58 F. Javaid, C. Pilotti, C. Camilli, D. Kallenberg, C. Bahou, J. Blackburn, J. R. Baker, J. Greenwood, S. E. Moss and V. Chudasama, *RSC Chem. Biol.*, 2021, **2**, 1206–1220.

59 A. G. Polson, J. Calemine-Fenaux, P. Chan, W. Chang, E. Christensen, S. Clark, F. J. De Sauvage, D. Eaton, K. Elkins, J. Michael Elliott, G. Frantz, R. N. Fuji, A. Gray, K. Harden, G. S. Ingle, N. M. Kljavin, H. Koeppen, C. Nelson, S. Prabhu, H. Raab, S. Ross, J. P. Stephan, S. J. Scales, S. D. Spencer, R. Vandlen, B. Wranik, S. F. Yu, B. Zheng and A. Ebens, *Cancer Res.*, 2009, **69**, 2358–2364.

60 R. Gébleux, M. Stringhini, R. Casanova, A. Soltermann, D. Neri, R. Gebleux, M. Stringhini, R. Casanova, A. Soltermann, D. Neri, R. Gébleux, M. Stringhini, R. Casanova, A. Soltermann and D. Neri, *Int. J. Cancer*, 2017, **140**, 1670–1679.

61 A. Dal Corso, R. Gébleux, P. Murer, A. Soltermann and D. Neri, *J. Control. Release*, 2017, **264**, 211–218.

62 R. Rossin, R. M. Versteegen, J. Wu, A. Khasanov, H. J. Wessels, E. J. Steenbergen, W. Ten Hoeve, H. M. Janssen, A. H. A. M. Van Onzen, P. J. Hudson and M. S. Robillard, *Nat. Commun.*, 2018, **9**, 1–11.

63 P. Strop, S. Liu, M. Dorywalska, K. Delaria, R. G. Dushin, T. Tran, W. Ho, S. Farias, M. G. Casas, Y. Abdiche, D. Zhou, R. Chandrasekaran, C. Samain, C. Loo, A. Rossi, M. Rickert, S. Krimm, T. Wong, S. M. Chin, J. Yu, J. Dilley, J. Chaparro-riggers, G. F. Filzen, C. J. O. Donnell, F. Wang, J. S. Myers, J. Pons, D. L. Shelton and A. Rajpal, *Chem. Biol.*, 2013, **20**, 161–167.

64 M. Dorywalska, P. Strop, J. A. Melton-Witt, A. Hasa-Moreno, S. E. Farias, M. Galindo Casas, K. Delaria, V. Lui, K. Poulsen, C. Loo, S. Krimm, G. Bolton, L. Moine, R. Dushin, T.-T. Tran, S.-H. Liu, M. Rickert, D. Foletti, D. L. Shelton, J. Pons and A. Rajpal, *Bioconjug. Chem.*, 2015, **26**, 650–659.

65 M. Dorywalska, R. Dushin, L. Moine, S. E. Farias, D. Zhou, T. Navaratnam, V. Lui, A. Hasa-Moreno, M. G. Casas, T. T. Tran, K. Delaria, S. H. Liu, D. Foletti, C. J. O'Donnell, J. Pons, D. L. Shelton, A. Rajpal and P. Strop, *Mol. Cancer Ther.*, 2016, **15**, 958–970.

66 W. Dokter, R. Ubink, M. Van Der Lee, M. Van Der Vleuten, T. Van Achterberg, D. Jacobs, E. Loosveld, D. Van Den Dobbelsteen, D. Egging, E. Mattaar, P. Groothuis, P. Beusker, R. Coumans, R. Elgersma, W. Menge, J. Joosten, H. Spijker, T. Huijbregts, V. De Groot, M. Eppink, G. De Roo, G. Verheijden and M. Timmers, *Mol. Cancer Ther.*, 2014, **13**, 2618–2629.

67 Y. Wang, S. Fan, W. Zhong, X. Zhou and S. Li, *Int. J. Mol. Sci.*, 2017, **18**, 1860.

68 P. J. Burke, P. D. Senter, D. W. Meyer, J. B. Miyamoto, M. Anderson, B. E. Toki, G. Manikumar, M. C. Wani, D. J. Kroll and S. C. Jeffrey, *Bioconjug. Chem.*, 2009, **20**, 1242–1250.

69 M. C. Mathieu, L. Massaad, C. Toussaint, J. Morizet, O. Parise, A. Gouyette and G. G. Chabot, *Cancer Res.*, 1993, **53**, 3541–3546.

70 S. Ahmed, C. Owen, K. James, L. Sampson and C. Patel, *Curr. Med. Chem.*, 2012, **9**, 263–273.

71 Y. Miyoshi, A. Ando, S. Hasegawa, M. Ishitobi, T. Taguchi, Y. Tamaki and S. Noguchi, *Clin. Cancer Res.*, 2003, **9**, 2288–2293.

72 T. Suzuki, Y. Miki, Y. Nakamura, K. Ito and H. Sasano, *Cancer Res.*, 2003, **63**, 2762–2770.

73 J. D. Bargh, S. J. Walsh, A. Isidro-Llobet, S. Omarjee, J. S. Carroll and D. R. Spring, *Chem. Sci.*, 2020, **11**, 2375–2380.

74 F. Li, K. K. Emmerton, M. Jonas, X. Zhang, J. B. Miyamoto, J. R. Setter, N. D. Nicholas, N. M. Okeley, R. P. Lyon, D. R. Benjamin and C. L. Law, *Cancer Res.*, 2016, **76**, 2710–2719.

75 S. C. Jeffrey, J. B. Andreyka, S. X. Bernhardt, K. M. Kissler, T. Kline, J. S. Lenox, R. F. Moser, M. T. Nguyen, N. M. Okeley, I. J. Stone, X. Zhang and P. D. Senter, *Bioconjug. Chem.*, 2006, **17**, 831–840.

76 S. Kolodych, C. Michel, S. Delacroix, O. Koniev, A. Ehkirch, J. Eberova, S. Cianférani, B. Renoux, W. Krezel, P. Poinot, C. D. Muller, S. Papot and A. Wagner, *Eur. J. Med. Chem.*, 2017, **142**, 376–382.

77 J. C. Kern, D. Dooney, R. Zhang, L. Liang, P. E. Brandish, M. Cheng, G. Feng, A. Beck, D. Bresson, J. Firdos, D. Gately, N. Knudsen, A. Manibusan, Y. Sun and R. M. Garbaccio, *Bioconjug. Chem.*, 2016, **27**, 2081–2088.

78 J. C. Kern, M. Cancilla, D. Dooney, K. Kwasnjuk, R. Zhang, M. Beaumont, I. Figueroa, S. C. Hsieh, L. Liang, D. Tomazela, J. Zhang, P. E. Brandish, A. Palmieri, P. Stivers, M. Cheng, G. Feng, P. Geda, S. Shah, A. Beck, D. Bresson, J. Firdos, D. Gately, N. Knudsen, A. Manibusan, P. G. Schultz, Y. Sun and R. M. Garbaccio, *J. Am. Chem. Soc.*, 2016, **138**, 1430–1445.

79 P. E. Brandish, A. Palmieri, S. Antonenko, M. Beaumont, L. Benso, M. Cancilla, M. Cheng, L. Fayadat-Dilman, G. Feng, I. Figueroa, J. Firdos, R. Garbaccio, L. Garvin-Queen, D. Gately, P. Geda, C. Haines, S. Hseih, D. Hodges, J. Kern, N. Knudsen, K. Kwasnjuk, L. Liang, H. Ma, A. Manibusan, P. L. Miller, L. Y. Moy, Y. Qu, S. Shah, J. S. Shin, P. Stivers, Y. Sun, D. Tomazela, H. C. Woo, D. Zaller, S. Zhang, Y. Zhang and M. Zielstorff, *Bioconjug. Chem.*, 2018, **29**, 2357–2369.

80 J. D. Bargh, S. J. Walsh, N. Ashman, A. Isidro-Llobet, J. S. Carroll and D. R. Spring, *Chem. Commun.*, 2021, **57**, 3457–3460.

81 A. G. Polson, J. Calemine-Fenaux, P. Chan, W. Chang, E. Christensen, S. Clark, F. J. De Sauvage, D. Eaton, K. Elkins, J. Michael Elliott, G. Frantz, R. N. Fuji, A. Gray, K. Harden, G. S. Ingle, N. M. Kljavin, H. Koeppen, C. Nelson, S. Prabhu, H. Raab, S. Ross, J. P. Stephan, S. J. Scales, S. D. Spencer, R. Vandlen, B. Wranik, S. F. Yu, B. Zheng, A. Ebens, A. G. Polson, J. Calemine-Fenaux, P. Chan, W. Chang, E. Christensen, S. Clark, F. J. De Sauvage, D. Eaton, K. Elkins, J. Michael Elliott, G. Frantz, R. N. Fuji, A. Gray, K. Harden, G. S. Ingle, N. M. Kljavin, H. Koeppen, C. Nelson, S. Prabhu, H. Raab, S. Ross, J. P. Stephan, S. J. Scales, S. D. Spencer, R. Vandlen, B. Wranik, S. F. Yu, B. Zheng and A. Ebens, *Cancer Res.*, 2009, **69**, 2358–2364.

82 Y. Wang, L. Liu, S. Fan, D. Xiao, F. Xie, W. Li, W. Zhong and X. Zhou, *Cancers (Basel).*, 2020, **12**, 744.

83 L. Borsi, B. Carnemolla, G. Nicolò, B. Spina, G. Tanara and L. Zardi, *Int. J. Cancer*, 1992, **52**, 688–692.

84 M. Dueck, S. Riedl, U. Hinz, A. Tandara, P. Möller, C. Herfarth and A. Faissner, *Int. J. Cancer*, 1999, **82**, 477–483.

85 M. Adams, J. L. Jones, R. A. Walker, J. H. Pringle and S. C. Bell, *Cancer Res.*, 2002, **62**, 3289–3297.

86 C. R. Justus, L. Dong and L. V. Yang, *Front. Physiol.*, 2013, **4**, 1–9.

87 J. F. DiJoseph, M. M. Dougher, D. C. Armellino, L. Kalyandrug, A. Kunz, E. R. Boghaert, P. R. Hamann and N. K. Damle, *Cancer Immunol. Immunother.*, 2007, **56**, 1107–1117.

88 S. V Govindan, T. M. Cardillo, S. Moon, H. J. Hansen and D. M. Goldenberg, *Clin. Cancer Res.*,

2009, **15**, 6052–6061.

89 S. J. Moon, S. V. Govindan, T. M. Cardillo, A. Christopher, D. Souza, H. J. Hansen, D. M. Goldenberg, C. A. D'Souza, H. J. Hansen and D. M. Goldenberg, *J. Med. Chem.*, 2008, **51**, 6916–6926.

90 R. M. Sharkey, H. Karacay, S. V. Govindan and D. M. Goldenberg, *Mol. Cancer Ther.*, 2011, **10**, 1072–1081.

91 D. M. Goldenberg, T. M. Cardillo, S. V. Govindan, E. A. Rossi and R. M. Sharkey, *Oncotarget*, 2020, **11**, 942.

92 M. Yasunaga, S. Manabe, D. Tarin and Y. Matsumura, *Bioconjug. Chem.*, 2011, **22**, 1776–1783.

93 M. Yasunaga, S. Manabe and Y. Matsumura, *Cancer Sci.*, 2011, **102**, 1396–1402.

94 H. Fuchigami, S. Manabe, M. Yasunaga and Y. Matsumura, *Sci. Rep.*, 2018, **8**, 1–9.

95 E. A. Love, A. Sattikar, H. Cook, K. Gillen, J. M. Large, S. Patel, D. Matthews and A. Merritt, *ChemBioChem*, 2019, **20**, 754–758.

96 Y. Ino, M. Gotoh, M. Sakamoto, K. Tsukagoshi and S. Hirohashi, *Proc. Natl. Acad. Sci. U. S. A.*, 2002, **99**, 365–370.

97 R. Rossin, P. R. Verkerk, S. M. Van Den Bosch, R. C. M. Vulders, I. Verel, J. Lub and M. S. Robillard, *Angew. Chemie - Int. Ed.*, 2010, **49**, 3375–3378.

98 B. J. Stenton, B. L. Oliveira, M. J. Matos, L. Sinatra and G. J. L. Bernardes, *Chem. Sci.*, 2018, **9**, 4185–4189.

99 B. L. Oliveira, B. J. Stenton, V. B. Unnikrishnan, C. R. De Almeida, J. Conde, M. Negrão, F. S. S. Schneider, C. Cordeiro, M. G. Ferreira, G. F. Caramori, J. B. Domingos, R. Fior and G. J. L. Bernardes, *J. Am. Chem. Soc.*, 2020, **142**, 10869–10880.

100 M. Barok, H. Joensuu and J. Isola, *Breast Cancer Res.*, 2014, **6**, 130–146.

101 F. Loganzo, X. Tan, M. Sung, G. Jin, J. S. Myers, E. Melamud, F. Wang, V. Diesl, M. T. Follettie, S. Musto, M. H. Lam, W. Hu, M. B. Charati, K. Khandke, K. S. K. Kim, M. Cinque, J. Lucas, E. Graziani, A. Maderna, C. J. O'Donnell, K. T. Arndt and H. P. Gerber, *Mol. Cancer Ther.*, 2015, **14**, 952–963.

102 N. Joubert, C. Denevault-Sabourin, F. Bryden and M. C. Viaud-Massuard, *Eur. J. Med. Chem.*, 2017, **142**, 393–415.

103 S. Toyokuni, K. Okamoto, J. Yodoi and H. Hiai, *FEBS Lett.*, 1995, **358**, 1–3.

104 P. Hileman, Elizabeth A; Achanta, Geetha; Huang, *Expert Opin. Ther. Targets*, 2001, **5**, 697–710.

105 L. Behrend, G. Henderson and R. Zwacka, *Biochem. Soc. Transcations*, 2003, **31**, 1441–1444.

106 G. Y. Liou and P. Storz, *Free Radic. Res.*, 2010, **44**, 479–496.

107 W. K. Lee and F. Thévenod, *Am. J. Physiol. - Cell Physiol.*, 2006, **291**, 195–202.

108 M. Giorgio, M. Trinei, E. Migliaccio and P. G. Pelicci, *Nat. Rev. Mol. Cell Biol.*, 2007, **8**, 722–728.

109 H. Pelicano, D. Carney and P. Huang, *Drug Resist. Updat.*, 2004, **7**, 97–110.

110 J. L. M. Jourden and S. Choen, *Angew Chem Int Ed*, 2010, **49**, 6795–6797.

111 J. Peiró Cadahiá, V. Previtali, N. S. Troelsen and M. H. Clausen, *Medchemcomm*, 2019, **10**, 1531–1549.

112 E. E. Weinert, R. Dondi, S. Colloredo-Melz, K. N. Frankenfield, C. H. Mitchell, M. Freccero and S. E. Rokita, *J. Am. Chem. Soc.*, 2006, **128**, 11940–11947.

113 A. G. Gavriel, M. R. Sambrook, A. T. Russell and W. Hayes, *Polym. Chem.*, 2022, **13**, 3188–3269.

114 S. Cao, R. Christiansen and X. Peng, *Chem. - A Eur. J.*, 2013, **19**, 9050–9058.

115 A. Alouane, R. Labruère, T. Le Saux, F. Schmidt and L. Jullien, *Angew. Chemie - Int. Ed.*, 2015, **54**, 7492–7509.

116 A. Bedini, A. Fraternale, R. Crinelli, M. Mari, S. Bartolucci, L. Chiarantini and G. Spadoni, *Chem. Res. Toxicol.*, 2019, **32**, 100–112.

117 J. P. M. António, A. S. Inês Carvalho, Joana André, J. N. R. Dias, H. Aguiar, Sandra I. Faustino, L. F. Lopes, Ricardo M. R. M. Veiros and G. J. L. Bernardes, *Angew Chem Int Ed*, 2021, **60**, 25914–25921.

118 R. A. Mosey and P. E. Floreancig, *Org. Biomol. Chem.*, 2012, **10**, 7980–7985.

119 K. M. Schmid, L. Jensen and S. T. Phillips, *J. Org. Chem.*, 2012, **77**, 4363–4374.

120 C. Skarbek, S. Serra, H. Maslah, E. Rascol and R. Labruère, *Bioorg. Chem.*, 2019, **91**, 103158.

121 M. P. Hay, *J. Chem. Soc. perkin Trans. 1*, 1999, **19**, 2759–2770.

122 A. Barrett, *Biochem. J.*, 1980, **187**, 909–912.

123 J. Peiró Cadahía, J. Bondebjerg, C. A. Hansen, V. Previtali, A. E. Hansen, T. L. Andresen and M. H. Clausen, *J. Med. Chem.*, 2018, **61**, 3503–3515.

124 N. Oka, T. Yamada, H. Sajiki, S. Akai and T. Ikawa, *Org. Lett.*, 2022, **24**, 3510–3514.

125 P. Franco, M. Lämmerhofer, P. M. Klaus and W. Lindner, *Chromatographia*, 2000, **51**, 139–146.

126 P. J. Boratyński, M. Zielińska-Błajet and J. Skarżewski, *Alkaloids Chem. Biol.*, 2019, **82**, 29–145.

127 A. S. Y. Lee, S. F. Chu, Y. T. Chang and S. H. Wang, *Tetrahedron Lett.*, 2004, **45**, 1551–1553.

128 K. Nepali, H. Y. Lee and J. P. Liou, *J. Med. Chem.*, 2019, **62**, 2851–2893.

129 S. Patterson and S. Wyllie, *Trends Parasitol.*, 2014, **30**, 289–298.

130 D. Mondal, J. Ford and K. G. Pinney, *Tetrahedron Lett.*, 2018, **59**, 3594–3599.

131 B. M. Sykes, M. P. Hay, D. Bohinc-Herceg, N. A. Helsby, C. J. O'Connor and W. A. Denny, *J. Chem. Soc. Perkin Trans. 1*, 2000, 1601–1608.

132 S. Daum, M. S. V. Reshetnikov, M. Sisa, T. Dumych, M. D. Lootsik, R. Bilyy, E. Bila, C. Janko, C. Alexiou, M. Herrmann, L. Sellner and A. Mokhir, *Angew. Chemie - Int. Ed.*, 2017, **56**, 15545–15549.

133 I. L. Andrulis, S. B. Bull, M. E. Blackstein, D. Sutherland, C. Mak, S. Sidlofsky, K. P. H. Pritzker, R. W. Hartwick, W. Hanna, L. Lickley, R. Wilkinson, A. Qizilbash, U. Ambus, M. Lipa, H. Weizel, A. Katz, M. Baida, S. Mariz, G. Stoik, P. Dacamara, D. Strongitharm, W. Geddie and D. McCready, *J. Clin. Oncol.*, 1998, **16**, 1340–1349.

134 S. Sun, P. Akkapeddi, M. C. Marques, N. Martínez-Sáez, V. M. Torres, C. Cordeiro, O. Boutureira and G. J. L. Bernardes, *Org. Biomol. Chem.*, 2019, **17**, 2005–2012.

135 H. Maslah, C. Skarbek, S. Pethe and R. Labruère, *Eur. J. Med. Chem.*, 2020, **207**, 112670.

136 Q. Bao, L. Zhang, N. Wang, B. Gabet, W. Yang, X. Gao, Q. You and Z. Jiang, *ACS Med. Chem. Lett.*, 2020, **11**, 2182–2189.

137 E. J. Kim, S. Bhuniya, H. Lee, H. M. Kim, C. Cheong, S. Maiti, K. S. Hong and J. S. Kim, *J. Am. Chem. Soc.*, 2014, **136**, 13888–13894.

138 S. Zheng, S. Guo, Q. Zhong, C. Zhang, J. Liu, L. Yang, Q. Zhang and G. Wang, *ACS Med. Chem. Lett.*, 2018, **9**, 149–154.

139 S. D. Bhagat, U. Singh, R. K. Mishra and A. Srivastava, *ChemMedChem*, 2018, **13**, 2073–2079.

140 F. L. Sarmiento-Salinas, A. Delgado-Magallón, J. B. Montes-Alvarado, D. Ramírez-Ramírez, J. C. Flores-Alonso, P. Cortés-Hernández, J. Reyes-Leyva, I. Herrera-Camacho, M. Anaya-Ruiz, R.

Pelayo, L. Millán-Pérez-Peña and P. Maycotte, *Front. Oncol.*, 2019, **9**, 1–13.

141 F. Hecht, J. M. Cazarin, C. E. Lima, C. C. Faria, A. A. da C. Leitão, A. C. F. Ferreira, D. P. Carvalho and R. S. Fortunato, *Life Sci.*, 2016, **158**, 7–13.

142 F. A. Summers, B. Zhao and R. P. Mason, in *Free Radical Biology and Medicine*, 2012, vol. 53, pp. 1–17.

143 G. J. DeYulia, J. M. Cárcamo, O. Bórquez-Ojeda, C. C. Shelton and D. W. Golde, *Proc. Natl. Acad. Sci. U. S. A.*, 2005, **102**, 5044–5049.

144 T. Okazaki and T. Honjo, *Int. Immunol.*, 2007, **19**, 813–824.

145 E. S. Kim, *Drugs*, 2017, **77**, 929–937.

146 Y. Y. Syed, *Drugs*, 2017, **77**, 1369–1376.

147 A. Markham, *Drugs*, 2016, **76**, 1227–1232.

148 C. W. Li, S. O. Lim, E. M. Chung, Y. S. Kim, A. H. Park, J. Yao, J. H. Cha, W. Xia, L. C. Chan, T. Kim, S. S. Chang, H. H. Lee, C. K. Chou, Y. L. Liu, H. C. Yeh, E. P. Perillo, A. K. Dunn, C. W. Kuo, K. H. Khoo, J. L. Hsu, Y. Wu, J. M. Hsu, H. Yamaguchi, T. H. Huang, A. A. Sahin, G. N. Hortobagyi, S. S. Yoo and M. C. Hung, *Cancer Cell*, 2018, **33**, 187-201.e10.

149 S. Heskamp, W. Hobo, J. D. M. Molkenboer-Kuenen, D. Olive, W. J. G. Oyen, H. Dolstra and O. C. Boerman, *Cancer Res.*, 2015, **75**, 2928–2936.

150 D. Xiao, L. Luo, J. Li, Z. Wang, L. Liu, F. Xie, J. Feng and X. Zhou, *Bioorg. Chem.*, 2021, **116**, 105366.

151 S. Azadi, H. Aboulkheyr Es, S. Razavi Bazaz, J. P. Thiery, M. Asadnia and M. Ebrahimi Warkiani, *Biochim. Biophys. Acta - Mol. Cell Res.*, 2019, **1866**, 118526.

152 D. J. Marshall, S. S. Harried, J. L. Murphy, C. A. Hall, M. S. Shekhani, C. Pain, C. A. Lyons, A. Chillemi, F. Malavasi, H. L. Pearce, J. S. Thorson and J. R. Prudent, *Mol. Ther.*, 2016, **24**, 1760–1770.

153 H. H. Han, H. M. Wang, P. Jangili, M. Li, L. Wu, Y. Zang, A. C. Sedgwick, J. Li, X. P. He, T. D. James and J. S. Kim, *Chem. Soc. Rev.*, 2023, **52**, 879–920.

154 P. Wang, Q. Gong, J. Hu, X. Li and X. Zhang, *J. Med. Chem.*, 2020, **64**, 298–325.

155 A. Albert, *Nature*, 1958, **182**, 421–423.

156 N. J. Harper, *J. Med. Chem.*, 1959, **1**, 467–500.

157 A. K. Sinhababu and D. R. Thakker, *Adv. Drug Deliv. Rev.*, 1996, **19**, 241–273.

158 V. J. Stella, *J. Med. Chem.*, 1980, **23**, 1275–1282.

159 J. Rautio, H. Kumpulainen, T. Heimbach, R. Oliyai, D. Oh, T. Järvinen and J. Savolainen, *Nat. Rev. Drug Discov.*, 2008, **7**, 255–270.

160 P. Wang, X. Jin, J. Cai, J. Chen and M. Ji, *Anticancer agents Med. Chem.*, 2014, **14**, 418–439.

161 M. Eun Jun, B. Roy and K. Han Ahn, *Chem. Commun.*, 2011, **47**, 7583–7601.

162 C. A. Blencowe, A. T. Russell, F. Greco, W. Hayes and D. W. Thornthwaite, *Polym. Chem.*, 2011, **2**, 773–790.

163 I. Giang, E. L. Boland and G. M. K. Poon, *AAPS J.*, 2014, **16**, 899–913.

164 G.-J. Tan, Z.-K. Peng, J.-P. Lu and F.-Q. Tang, *World J. Biol. Chem.*, 2013, **4**, 91.

165 X. Li, F. Huo, Y. Zhang, F. Cheng and C. Yin, *J. Mater. Chem. B*, 2022, **10**, 5504–5519.

166 A. K. Ghosh and M. Brindisi, *J. Med. Chem.*, 2015, **58**, 2895–2940.

167 I. Tranoy-Opalinski, A. Fernandes, M. Thomas, J. P. Gesson and S. Papot, *Anticancer. Agents Med. Chem.*, 2008, **8**, 617–637.

168 A. Alouane, R. Labruère, T. Le Saux, I. Aujard, S. Dubruille, F. Schmidt and L. Jullien, *Chem. - A Eur. J.*, 2013, **19**, 11717–11724.

169 B. E. Toki, C. G. Cerveny, A. F. Wahl and P. D. Senter, *J. Org. Chem.*, 2002, **67**, 1866–1872.

170 D. Zhang, H. Le, J. Dela Cruz-Chuh, S. Bobba, J. Guo, L. Staben, C. Zhang, Y. Ma, K. R. Kozak, G. D. Lewis Phillips, B. S. Vollmar, J. D. Sadowsky, R. Vandlen, B. Wei, D. Su, P. Fan, P. S. Dragovich, S. C. Khojasteh, C. E. C. A. Hop and T. H. Pillow, *Bioconjug. Chem.*, 2018, **29**, 267–274.

171 S. S. Matikonda, J. M. Fairhall, J. D. A. Tyndall, S. Hook and A. B. Gamble, *Org. Lett.*, 2017, **19**, 528–531.

172 J. L. M. Jourden, K. B. Daniel and S. M. Cohen, *Chem. Commun.*, 2011, **47**, 7968–7970.

173 D. A. Rose, J. W. Treacy, Z. J. Yang, J. H. Ko, K. N. Houk and H. D. Maynard, *J. Am. Chem. Soc.*, 2022, **144**, 6050–6058.

174 L. R. Staben, S. G. Koenig, S. M. Lehar, R. Vandlen, D. Zhang, J. Chuh, S. F. Yu, C. Ng, J. Guo, Y. Liu, A. Fourie-O'Donohue, M. Go, X. Linghu, N. L. Segraves, T. Wang, J. Chen, B. Wei, G. D. L. Phillips, K. Xu, K. R. Kozak, S. Mariathasan, J. A. Flygare and T. H. Pillow, *Nat. Chem.*, 2016, **8**,

1112–1119.

175 L. R. Staben, S. F. Yu, J. Chen, G. Yan, Z. Xu, G. Del Rosario, J. T. Lau, L. Liu, J. Guo, B. Zheng, J. Dela Cruz-Chuh, B. C. Lee, R. Ohri, W. Cai, H. Zhou, K. R. Kozak, K. Xu, G. D. Lewis Phillips, J. Lu, J. Wai, A. G. Polson and T. H. Pillow, *ACS Med. Chem. Lett.*, 2017, **8**, 1037–1041.

176 L. Dunsmore, C. D. Navo, J. Becher, E. G. de Montes, A. Guerreiro, E. Hoyt, L. Brown, V. Zelenay, S. Mikutis, J. Cooper, I. Barbieri, S. Lawrinowitz, E. Siouve, E. Martin, P. R. Ruivo, T. Rodrigues, F. P. da Cruz, O. Werz, G. Vassiliou, P. Ravn, G. Jiménez-Osés and G. J. L. Bernardes, *Nat. Chem.*, 2022, **14**, 754–765.

177 Q. Gong, X. Li, T. Li, X. Wu, J. Hu, F. Yang and X. Zhang, *Angew. Chemie - Int. Ed.*, 2022, **61**, 1–9.

178 K. Matsuo, R. Kamada, K. Mizusawa, H. Imai, Y. Takayama, M. Narazaki, T. Matsuda, Y. Takaoka and I. Hamachi, *Chem. - A Eur. J.*, 2013, **19**, 12875–12883.

179 C. J. M. Stirling, *Acc. Chem. Res.*, 1979, **12**, 198–203.

180 K. H. Krause, *Exp. Gerontol.*, 2007, **42**, 256–262.

181 C. F. Szatrowski, T P; Nathan, *Cancer Res.*, 1991, **51**, 794–798.

182 N. S. Andersen, J. Peiró Cadahía, V. Previtali, J. Bondebjerg, C. A. Hansen, A. E. Hansen, T. L. Andresen and M. H. Clausen, *Eur. J. Med. Chem.*, 2018, **156**, 738–746.

183 C. Perez, J. P. Monserrat, Y. Chen and S. M. Cohen, *Chem. Commun.*, 2015, **51**, 7116–7119.

184 M. Wu, L. Wu, J. Li, D. Zhang, S. Lan, X. Zhang, X. Lin, G. Liu, X. Liu and J. Liu, *Theranostics*, 2019, **9**, 20–33.

185 N. Oddone, F. Pederzoli, J. T. Duskey, C. A. De Benedictis, A. M. Grabrucker, F. Forni, M. Angela Vandelli, B. Ruozi and G. Tosi, *Int. J. Pharm.*, 2019, **570**, 1–11.

186 N. Oddone, F. Boury, E. Garcion, A. M. Grabrucker, M. C. Martinez, F. Da Ros, A. Janaszewska, F. Forni, M. A. Vandelli, G. Tosi, B. Ruozi and J. T. Duskey, *Front. Pharmacol.*, 2020, **11**, 1–15.

187 K. Wang, B. Yang, H. Ye, X. Zhang, H. Song, X. Wang, N. Li, L. Wei, Y. Wang, H. Zhang, Q. Kan, Z. He, D. Wang and J. Sun, *ACS Appl. Mater. Interfaces*, 2019, **11**, 18914–18922.

188 Z. Pan, J. Zhang, K. Ji, V. Chittavong, X. Ji and B. Wang, *Org. Lett.*, 2018, **20**, 8–11.

189 N. Ma, Y. Li, H. Xu, Z. Wang and X. Zhang, *J. Am. Chem. Soc.*, 2010, **132**, 442–443.

190 W. Cao, Y. Gu, T. Li and H. Xu, *Chem. Commun.*, 2015, **51**, 7069–7071.

191 R. Fang, H. Xu, W. Cao, L. Yang and X. Zhang, *Polym. Chem.*, 2015, **6**, 2817–2821.

192 J. Ferriz, J M; Vinsova, *Curr. Pharm. Des.*, 2010, **16**, 2033–2052.

193 S. J. Hecker and M. D. Erion, *J. Med. Chem.*, 2008, **51**, 2328–2345.

194 C. Zhang, Q. Zhong, Q. Zhang, S. Zheng, L. Miele and G. Wang, *Breast Cancer Res. Treat.*, 2015, **152**, 283–291.

195 J. Liu, S. Zheng, V. L. Akerstrom, C. Yuan, Y. Ma, Q. Zhong, C. Zhang, Q. Zhang, S. Guo, P. Ma, E. V. Skripnikova, M. R. Bratton, A. Pannuti, L. Miele, T. E. Wiese and G. Wang, *J Med Chem*, 2016, **59**, 8134–8140.

196 J. Liu, S. Zheng, S. Guo, C. Zhang, Q. Zhong, Q. Zhang, P. Ma, E. V Skripnikova, M. R. Bratton, T. E. Wiese and G. Wang, *ACS Med. Chem. Lett.*, 2017, **8**, 102–106.

197 L. Wang, S. Xie, L. Ma, Y. Chen and W. Lu, *Eur. J. Med. Chem.*, 2016, **116**, 84–89.

198 Y. Kuang, K. Balakrishnan, V. Gandhi and X. Peng, *J. Am. Chem. Soc.*, 2011, **133**, 19278–19281.

199 W. Chen, K. Balakrishnan, Y. Kuang, Y. Han, M. Fu, V. Gandhi and X. Peng, *J. Med. Chem.*, 2014, **57**, 4498–4510.

200 Y. Liao, L. Xu, S. Ou, H. Edwards, D. Luedtke, Y. Ge and Z. Qin, *ACS Med. Chem. Lett.*, 2018, **9**, 635–640.

201 M. Engel, Y. S. Gee, D. Cross, A. Maccarone, B. Heng, A. Hulme, G. Smith, G. J. Guillemin, B. W. Stringer, C. J. T. Hyland and L. Ooi, *J. Neurochem.*, 2019, **149**, 535–550.

202 X. Li, S. Wu, G. Dong, S. Chen, Z. Ma, D. Liu and C. Sheng, *ACS Med. Chem. Lett.*, 2020, **11**, 439–444.

203 K. Matsushita, T. Okuda, S. Mori, M. Konno, H. Eguchi, A. Asai, J. Koseki, Y. Iwagami, D. Yamada, H. Akita, T. Asaoka, T. Noda, K. Kawamoto, K. Gotoh, S. Kobayashi, Y. Kasahara, K. Morihiro, T. Satoh, Y. Doki, M. Mori, H. Ishii and S. Obika, *ChemMedChem*, 2019, **14**, 1384–1391.

204 B. Bielec, I. Poetsch, E. Ahmed, P. Heffeter, B. K. Keppler and C. R. Kowol, *Molecules*, 2020, **25**, 1–18.

205 Y. Ai, O. N. Obianom, M. Kuser, Y. Li, Y. Shu and F. Xue, *ACS Med. Chem. Lett.*, 2019, **10**, 127–131.

206 J. S. Macdonald, *Oncology (Williston Park).*, 1999, **13**, 33–34.

207 H. Hagen, P. Marzenell, E. Jentzsch, F. Wenz, M. R. Veldwijk and A. Mokhir, *J. Med. Chem.*, 2012, **55**, 924–934.

208 P. Marzenell, H. Hagen, L. Sellner, T. Zenz, R. Grinyte, V. Pavlov, S. Daum and A. Mokhir, *J. Med. Chem.*, 2013, **56**, 6935–6944.

209 S. Daum, V. F. Chekhun, I. N. Todor, N. Y. Lukianova, Y. V. Shvets, L. Sellner, K. Putzker, J. Lewis, T. Zenz, I. A. M. De Graaf, G. M. M. Groothuis, A. Casini, O. Zozulia, F. Hampel and A. Mokhir, *J. Med. Chem.*, 2015, **58**, 2015–2024.

210 M. Schikora, A. Reznikov, L. Chaykovskaya, O. Sachinska, L. Polyakova and A. Mokhir, *Bioorganic Med. Chem. Lett.*, 2015, **25**, 3447–3450.

211 S. Daum, S. Babiy, H. Konovalova, W. Hofer, A. Shtemenko, N. Shtemenko, C. Janko, C. Alexiou and A. Mokhir, *J. Inorg. Biochem.*, 2018, **178**, 9–17.

212 S. Daum, J. Toms, V. Reshetnikov, H. G. Özkan, F. Hampel, S. Maschauer, A. Hakimioun, F. Beierlein, L. Sellner, M. Schmitt, O. Prante and A. Mokhir, *Bioconjug. Chem.*, 2019, **30**, 1077–1086.

213 J. Noh, B. Kwon, E. Han, M. Park, W. Yang, W. Cho, W. Yoo, G. Khang and D. Lee, *Nat. Commun.*, 2015, **6**, 1–9.

214 Q. Pan, B. Zhang, X. Peng, S. Wan, K. Luo, W. Gao, Y. Pu and B. He, *Chem. Commun.*, 2019, **55**, 13896–13899.

215 M. Ye, Y. Han, J. Tang, Y. Piao, X. Liu, Z. Zhou, J. Gao, J. Rao and Y. Shen, *Adv. Mater.*, 2017, **29**, 1–10.

216 Y. Xu, W. Shi, H. Li, X. Li and H. Ma, *ChemMedChem*, 2019, **14**, 1079–1085.

217 J. Li, A. Dirisala, Z. Ge, Y. Wang, W. Yin, W. Ke, K. Toh, J. Xie, Y. Matsumoto, Y. Anraku, K. Osada and K. Kataoka, *Angew. Chemie - Int. Ed.*, 2017, **56**, 14025–14030.

218 C. Dong, Q. Zhou, J. Xiang, F. Liu, Z. Zhou and Y. Shen, *J. Control. Release*, 2020, **321**, 529–539.

219 O. Redy-Keisar, S. Ferber, R. Satchi-Fainaro and D. Shabat, *ChemMedChem*, 2015, **10**, 999–1007.

220 X. Gao, J. Cao, Y. Song, X. Shu, J. Liu, J. Z. Sun, B. Liu and B. Z. Tang, *RSC Adv.*, 2018, **8**, 10975–10979.

221 G. Ravikumar, M. Bagheri, D. K. Saini and H. Chakrapani, *Chem. Commun.*, 2017, **53**, 13352–

13355.

222 W. H. Wilson, O. A. O. Connor, M. S. Czuczman, A. S. Lacasce, J. F. Gerecitano, J. P. Leonard, A. Tulpule, K. Dunleavy, H. Xiong, Y. Chiu, Y. Cui, T. Busman, S. W. Elmore, S. H. Rosenberg, A. P. Krivoshik, S. H. Enschede and R. A. Humerickhouse, *Lancet Oncol.*, 2010, **11**, 1149–1159.

223 C. Tse, A. R. Shoemaker, J. Adickes, M. G. Anderson, J. Chen, S. Jin, E. F. Johnson, K. C. Marsh, M. J. Mitten, P. Nimmer, L. Roberts, S. K. Tahir, Y. Xiao, X. Yang, H. Zhang, S. Fesik and S. W. Ros, *Cancer Res.*, 2008, **68**, 3421–3428.

224 A. W. Roberts, J. F. Seymour, J. R. Brown, W. G. Wierda, T. J. Kipps, S. L. Khaw, D. A. Carney, S. Z. He, D. C. S. Huang, H. Xiong, Y. Cui, T. A. Busman, E. M. Mckeegan, A. P. Krivoshik, S. H. Enschede and R. Humerickhouse, *J. Clin. Oncol.*, 2023, **30**, 488–496.

225 C. J. LaFargue, G. Z. Dal Molin, A. K. Sood and R. L. Coleman, *Lancet Oncol.*, 2019, **20**, e15–e28.

226 J. Farreś, J. Martín-Caballero, C. Martínez, J. J. Lozano, L. Llacuna, C. Ampurdanés, C. Ruiz-Herguido, F. Dantzer, V. Schreiber, A. Villunger, A. Bigas and J. Yélamos, *Blood*, 2013, **122**, 44–54.

227 S. Elmore, *Toxicol. Pathol.*, 2007, **35**, 495–516.

228 A. Negi and A. S. Voisin-Chiret, *ChemBioChem*, 2022, **23**, e202100689.

229 M. Giam, D. C. S. Huang and P. Bouillet, *Oncogene*, 2008, **27**, S128–S136.

230 V. Kirkin, S. Joos and M. Zörnig, *Biochim. Biophys. Acta - Mol. Cell Res.*, 2004, **1644**, 229–249.

231 T. Oltersdorf, S. W. Elmore, A. R. Shoemaker, R. C. Armstrong, D. J. Augeri, B. A. Belli, M. Bruncko, T. L. Deckwerth, J. Dinges, P. J. Hajduk, M. K. Joseph, S. Kitada, S. J. Korsmeyer, A. R. Kunzer, A. Letai, C. Li, M. J. Mitten, D. G. Nettesheim, S. C. Ng, P. M. Nimmer, J. M. O'Connor, A. Oleksijew, A. M. Petros, J. C. Reed, W. Shen, S. K. Tahir, C. B. Thompson, K. J. Tomaselli, B. Wang, M. D. Wendt, H. Zhang, S. W. Fesik and S. H. Rosenberg, *Nature*, 2005, **435**, 677–681.

232 E. F. Lee, P. E. Czabotar, B. J. Smith, K. Deshayes, K. Zobel, P. M. Colman and W. D. Fairlie, *Cell Death Differ.*, 2007, **14**, 1711–1713.

233 C. Park, M. Bruncko, J. Adickes, J. Bauch, H. Ding, A. Kunzer, K. C. Marsh, P. Nimmer, A. R. Shoemaker, X. Song, S. K. Tahir, C. Tse, X. Wang, M. D. Wendt, X. Yang, H. Zhang, S. W. Fesik, S. H. Rosenberg and S. W. Elmore, *J. Med. Chem.*, 2008, **51**, 6902–6915.

234 K. D. Mason, M. R. Carpinelli, J. I. Fletcher, J. E. Collinge, A. A. Hilton, S. Ellis, P. N. Kelly, P. G.

Ekert, D. Metcalf, A. W. Roberts, D. C. S. Huang and B. T. Kile, *Cell*, 2007, **128**, 1173–1186.

235 H. Zhang, P. M. Nimmer, S. K. Tahir, J. Chen, R. M. Fryer, K. R. Hahn, L. A. Iciek, S. J. Morgan, M. C. Nasarre, R. Nelson, L. C. Preusser, G. A. Reinhart, M. L. Smith, S. H. Rosenberg, S. W. Elmore and C. Tse, *Cell Death Differ.*, 2007, **14**, 943–951.

236 A. J. Souers, J. D. Leverson, E. R. Boghaert, S. L. Ackler, N. D. Catron, J. Chen, B. D. Dayton, H. Ding, S. H. Enschede, W. J. Fairbrother, D. C. S. Huang, S. G. Hymowitz, S. Jin, S. L. Khaw, P. J. Kovar, L. T. Lam, J. Lee, H. L. Maecker, K. C. Marsh, K. D. Mason, M. J. Mitten, P. M. Nimmer, A. Oleksijew, C. H. Park, C. Park, D. C. Phillips, A. W. Roberts, D. Sampath, J. F. Seymour, M. L. Smith, G. M. Sullivan, S. K. Tahir, C. Tse, M. D. Wendt, Y. Xiao, J. C. Xue, H. Zhang, R. A. Humerickhouse, S. H. Rosenberg and S. W. Elmore, *Nat. Med.*, 2013, **19**, 202–208.

237 L. M. Juárez-salcedo, V. D. Ba and S. Dalia, *Drugs Context*, 2019, **8**, 212574.

238 D. Lv, P. Pal, X. Liu, Y. Jia, D. Thummuri, P. Zhang, W. Hu, J. Pei, Q. Zhang, S. Zhou, S. Khan, X. Zhang, N. Hua, Q. Yang, S. Arango, W. Zhang, D. Nayak, S. K. Olsen, S. T. Weintraub, R. Hromas, M. Konopleva, Y. Yuan, G. Zheng and D. Zhou, *Nat. Commun.*, 2021, **12**, 1–14.

239 J. Mihalyova, T. Jelinek, K. Growkova, M. Hrdinka and M. Simicek, *Exp. Hematol.*, 2018, **61**, 10–25.

240 G. F. Perini, G. N. Ribeiro, J. Vaz, P. Neto, L. T. Campos and N. Hamerschlak, *J. Hematol. Oncol.*, 2018, **11**, 1–15.

241 M. Vogler, *Adv. Med.*, 2014, **2014**, 943648.

242 A. Kissopoulou, J. Jonasson, T. L. Lindahl and A. Osman, *PLoS One*, 2013, **8**, 1–16.

243 P. F. Bray, S. E. Mckenzie, L. C. Edelstein, S. Nagalla, K. Delgrosso, A. Ertel, J. Kupper, Y. Jing, E. Londin, P. Loher, H. Chen, P. Fortina and I. Rigoutsos, *BMC Genomics*, 2013, **14**, 1–15.

244 X. Zhang, D. Thummuri, X. Liu, W. Hu, P. Zhang, S. Khan, Y. Yuan, D. Zhou and G. Zheng, *Eur. J. Med. Chem.*, 2020, **192**, 112186.

245 S. Khan, X. Zhang, D. Lv, Q. Zhang, Y. He, P. Zhang, X. Liu, D. Thummuri, Y. Yuan, J. S. Wiegand, J. Pei, A. Sharma, C. R. Mccurdy, V. M. Kuruvilla, A. A. Ferrando, Y. Kim, A. Rogojina, P. J. Houghton, G. Huang, R. Hromas, M. Konopleva and G. Zheng, *Nat. Med.*, 2020, **25**, 1938–1947.

246 X. Zhang, D. Thummuri, Y. He, X. Liu, P. Zhang and G. Zheng, *Chem. Commun.*, 2020, **55**, 14765–14768.

247 U.S National Library of Medicine, A Study With ABBV-155 Alone and in Combination With Taxane Therapy in Adults With Relapsed and/or Refractory Solid Tumors, https://www.clinicaltrials.gov/ct2/show/NCT03595059.

248 W. Zhou and W. Jin, *Front. Immunol.*, 2021, **12**, 1–13.

249 National Cancer Institute, Mirzotamab Clezutoclax (Code C158279), https://ncit.nci.nih.gov/ncitbrowser/pages/concept_details.jsf?dictionary=NCI_Thesaurus&version=23.03d&code=C157279&ns=ncit&type=all&key=null&b=1&n=0&vse=null.

250 A. W. Tolcher, B. A. Carneiro, A. Dowlati, A. R. A. Razak, Y. K. Chae, J. A. Villella, S. Coppola, S. Englert, A. C. Phillips, A. J. Souers, Z. Salman, S. Penugonda, J. D. Powderly and P. LoRusso, *J. Clin. Oncol.*, 2021, **39**, 3015.

251 E. G. M. P. B. Lozano-torres, D. Macias, J. R. Wilson, I. I. I. Cristina, S. M. Zhenguang, Z. Araceli, L. J. F. Blandez, A. Bernardos, F. Sancenón, M. Rovira, L. Fruk, C. P. Martins, M. Serrano, G. J. Doherty and D. Muñoz-espín, *Aging Cell*, 2020, **19**, 1–19.

252 D. Mchugh and J. Gil, *J. Cell Biol.*, 2018, **217**, 65–77.

253 B. G. Childs, M. Gluscevic, D. J. Baker, R. Laberge, J. Dananberg, J. M. Van Deursen, M. Clinic and M. Clinic, *Nat. Rev. Drug Discov.*, 2018, **16**, 718–735.

254 X. Liu, M. Yan, Z. Chen, B. Zhang, N. Yao, S. Zhao, X. Zhao, T. Zhang and G. Hai, *Spectrochim. Acta Part A Mol. Biomol. Spectrosc.*, 2022, **286**, 1–9.

255 M. E. Due-Hansen, S. K. Pandey, E. Christiansen, R. Andersen, S. V. F. Hansen and T. Ulven, *Org. Biomol. Chem.*, 2016, **14**, 430–433.

256 G. Wang, H. Zhang, J. Zhou, C. Ha, D. Pei and K. Ding, *Synthesis (Stuttg).*, 2008, **15**, 2398–2404.

257 P. G. M. Wuts and T. W. Greene, *Greene's Protective Groups in Organic Synthesis*, John Wiley and Sons Inc., Hoboken, New Jersey, 5th edn., 2006.

258 WO2017123616A1, 2017, 66–68.

259 M. Rose, J. T. Burgess, K. O'Byrne, D. J. Richard and E. Bolderson, *Front. Cell Dev. Biol.*, 2020, **8**, 1–22.

260 A. Chen, *Chin. J. Cancer*, 2011, **30**, 463–471.

261 H. E. Bryant, N. Schultz, H. D. Thomas, K. M. Parker, D. Flower, E. Lopez, S. Kyle, M. Meuth, N. J. Curtin and T. Helleday, *Nature*, 2005, **434**, 913–917.

262 T. Helleday, *Mol. Oncol.*, 2011, **5**, 387–393.

263 F. Dantzer, V. Schreiber, C. Niedergang, C. Trucco, E. Flatter, G. D. La Rubia, J. Oliver, V. Rolli, J. Ménissier-de Murcia and G. De Murcia, *Biochimie*, 1999, **81**, 69–75.

264 C. E. Ström, F. Johansson, M. Uhlén, C. A. K. Szigyarto, K. Erixon and T. Helleday, *Nucleic Acids Res.*, 2011, **39**, 3166–3175.

265 J. Murai, S. N. Huang, B. B. Das, A. Renaud, Y. Zhang, J. H. Doroshow, J. Ji, S. Takeda and Y. Pommier, *Cancer Res.*, 2013, **72**, 5588–5599.

266 J. Y. Murai, S. N. Huang, A. Renaud, Y. Zhang, J. Ji, S. Takeda, J. Morris, B. Teicher, J. H. Doroshow and Y. Pommier, *Mol. Cancer Ther.*, 2014, **13**, 433–443.

267 Y. Shen, M. Aoyagi-scharber and B. Wang, *J. Pharmacol. Exp. Ther.*, 2015, 446–457.

268 S. Arora, S. Balasubramaniam, H. Zhang, T. Berman, P. Narayan, D. Suzman, E. Bloomquist, S. Tang, Y. Gong, R. Sridhara, F. R. Turcu, D. Chatterjee, B. Saritas-Yildirim, S. Ghosh, R. Philip, A. Pathak, J. J. Gao, L. Amiri-Kordestani, R. Pazdur and J. A. Beaver, *Oncologist*, 2021, **26**, e164–e172.

269 Y. Y. Syed, *Drugs*, 2017, **77**, 585–592.

270 L. J. Scott, *Drugs*, 2017, **77**, 1029–1034.

271 S. M. Hoy, *Drugs*, 2018, **78**, 1939–1946.

272 R. Pal, PARP Inhibitors: Where Are We in 2020 and What's Coming Next?, https://blog.crownbio.com/parp-inhibitors-2020#:~:text=PARP inhibitors are approved as,resistance to these targeted agents.

273 A. A. Antolin, M. Ameratunga, U. Banerji, P. A. Clarke, P. Workman and B. Al-Lazikani, *Sci. Rep.*, 2020, **10**, 1–14.

274 S. A. Hurvitz, A. Gonçalves, H. S. Rugo, K.-H. Lee, L. Fehrenbacher, L. A. Mina, S. Diab, J. L. Blum, J. Chakrabarti, M. Elmeliegy, L. DeAnnuntis, E. Gauthier, A. Czibere, I. C. Tudor, R. G. W. Quek, J. K. Litton and J. Ettl, *Oncologist*, 2020, **25**, e439–e450.

275 A. Dréan, C. J. Lord and A. Ashworth, *Crit. Rev. Oncol. Hematol.*, 2016, **108**, 73–85.

276 A. M. Oza, D. Cibula, A. O. Benzaquen, C. Poole, R. H. J. Mathijssen, G. S. Sonke, N. Colombo, J. Špaček, P. Vuylsteke, H. Hirte, S. Mahner, M. Plante, B. Schmalfeldt, H. Mackay, J. Rowbottom, E. S. Lowe, B. Dougherty, J. C. Barrett and M. Friedlander, *Lancet Oncol.*, 2015, **16**, 87–97.

277 A. Rajan, C. A. Carter, R. J. Kelly, M. Gutierrez, S. Kummar, M. A. Yancey, J. Ji, B. Mannargudi, S. Woo, W. D. Figg and G. Giaccone, *Clin Cancer Res*, 2019, **18**, 2344–2351.

278 J. H. Kummar, Shivaani; Chen, Alice; Ji, Jiuping; Zhang, Yiping; Ried, Joel M; Ames, Matthew; Jia, Lee; Weil, Marcie; Speranza, Giovanna; Murgo, Anthony J; Kinders, Robert; Wang, Lihua; Parchment, Ralph E; Carter, John; Stotler, Howard; Rubinstein, Larry; Holli, *Cancer Res.*, 2011, **71**, 5626–5637.

279 R. Plummer, C. Jones, M. Middleton, R. Wilson, J. Evans, A. Olsen, N. Curtin, A. Boddy, P. McHugh, D. Newell, A. Harris, P. Johnson, H. Steinfeldt, R. Dewji, D. Wang, L. Robson and H. Calvert, *Clin. Cancer Res.*, 2008, **14**, 7917–7923.

280 R. Plummer, P. Stephens, L. Aissat-Daudigny, A. Cambois, G. Moachon, P. D. Brown and M. Campone, *Cancer Chemother. Pharmacol.*, 2014, **74**, 257–265.

281 J. Samol, M. Ranson, E. Scott, E. MacPherson, J. Carmichael, A. Thomas and J. Cassidy, *Invest. New Drugs*, 2012, **30**, 1493–1500.

282 J. F. Liu, W. T. Barry, M. Birrer, J.-M. Lee, R. J. Buckanovich, B. J. Fleming, Gini F; Rimel, M. K. Buss, S. Nattam, J. Hurteau, W. Luo, P. Quy, C. Whalen, L. Obermayer, H. Lee, E. P. Winer, E. C. Kohn, P. S. Ivy and U. A. Matulonis, *Lancet Oncol.*, 2014, **15**, 1207–1214.

283 B. D. Dickson, W. W. Wong, W. R. Wilson and M. P. Hay, *Molecules*, 2019, **24**, 1–20.

284 J. Li, D. Xiao, L. Liu, F. Xie, W. Li, W. Sun, X. Yang and X. Zhou, *Molecules*, 2020, **25**, 1–14.

285 L. Wang, X. Zhu, L. Li, L. Li, L. Fu, Y. Li, H. Fu, X. Chen and L. Lou, *Am. J. Cancer Res.*, 2021, **11**, 1632–1645.

286 W. R. Wilson and M. P. Hay, *Nat. Rev. Cancer*, 2011, **11**, 393–410.

287 P. Vaupel and A. Mayer, *Cancer Metastasis Rev.*, 2007, **26**, 225–239.

288 R. M. Phillips, *Cancer Chemother. Pharmacol.*, 2016, **77**, 441–457.

289 A. L. Harris, *Nat. Rev. Cancer*, 2002, **2**, 38–47.

290 G. J. Weiss, J. R. Infante, E. G. Chiorean, M. J. Borad, J. C. Bendell, J. R. Molina, R. Tibes, R. K. Ramanathan, K. Lewandowski, S. F. Jones, M. E. Lacouture, V. K. Langmuir, H. Lee, S. Kroll and H. A. Burris, *Clin. Cancer Res.*, 2011, **17**, 2997–3004.

291 S. N. Igumnov, M. N. Mamontov and I. A. Uspenskaya, *J. Chem. Eng. Data*, 2012, **57**, 456–461.

292 B. Mondal, U. Adhikari, P. P. Hajra and U. K. Roy, *New J Chem*, 2021, **45**, 7163–7173.

293 R. Bisht and B. Chattopadhyay, *J. Am. Chem. Soc.*, 2016, **138**, 84–87.

294 E. E. Stache, A. B. Ertel, T. Rovis and A. G. Doyle, *ACS Catal.*, 2018, **8**, 11134–11139.

295 WO2020057592 (A1), 2018, 102.

296 T. Scattolin, T. Gharbaoui and C. Y. Chen, *Org. Lett.*, 2022, **24**, 3736–3740.

297 WO2022026717 (A1), 2021, 57.

298 R. J. Binder, M. J. Hatfield, L. Chi and P. M. Potter, *Eur. J. Med. Chem.*, 2018, **149**, 79–89.

Appendix 1: NMR Spectra

(4-(1-(((4-Methyl-2-oxo-2*H*-chromen-7-yl)carbamoyl)oxy)but-3-yn-1-yl)phenyl)boronic acid (1b)

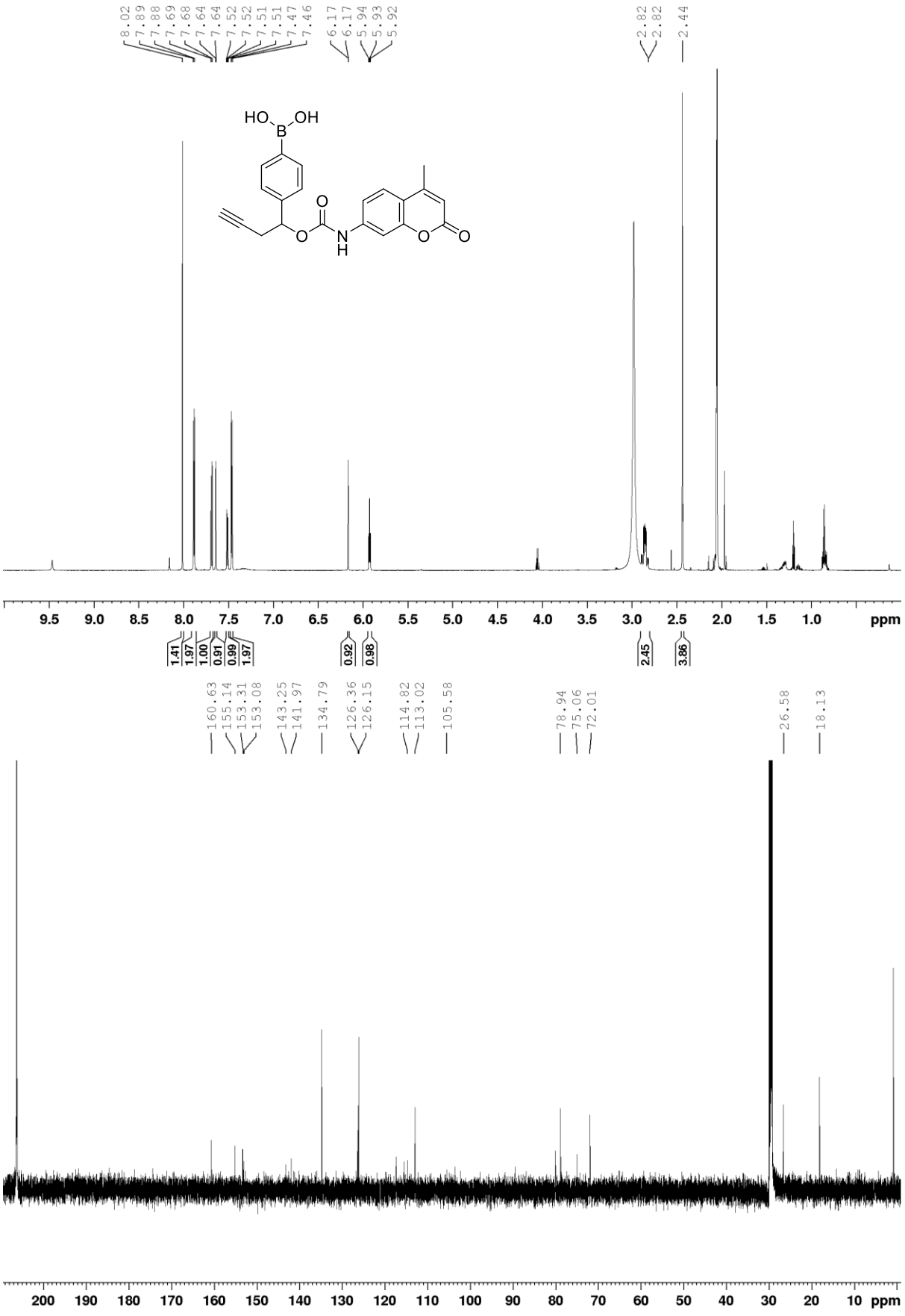

(3,5-Difluoro-4-(1-(((4-methyl-2-oxo-2*H*-chromen-7-yl)carbamoyl)oxy)but-3-yn-1-yl)phenyl)boronic acid (2b)

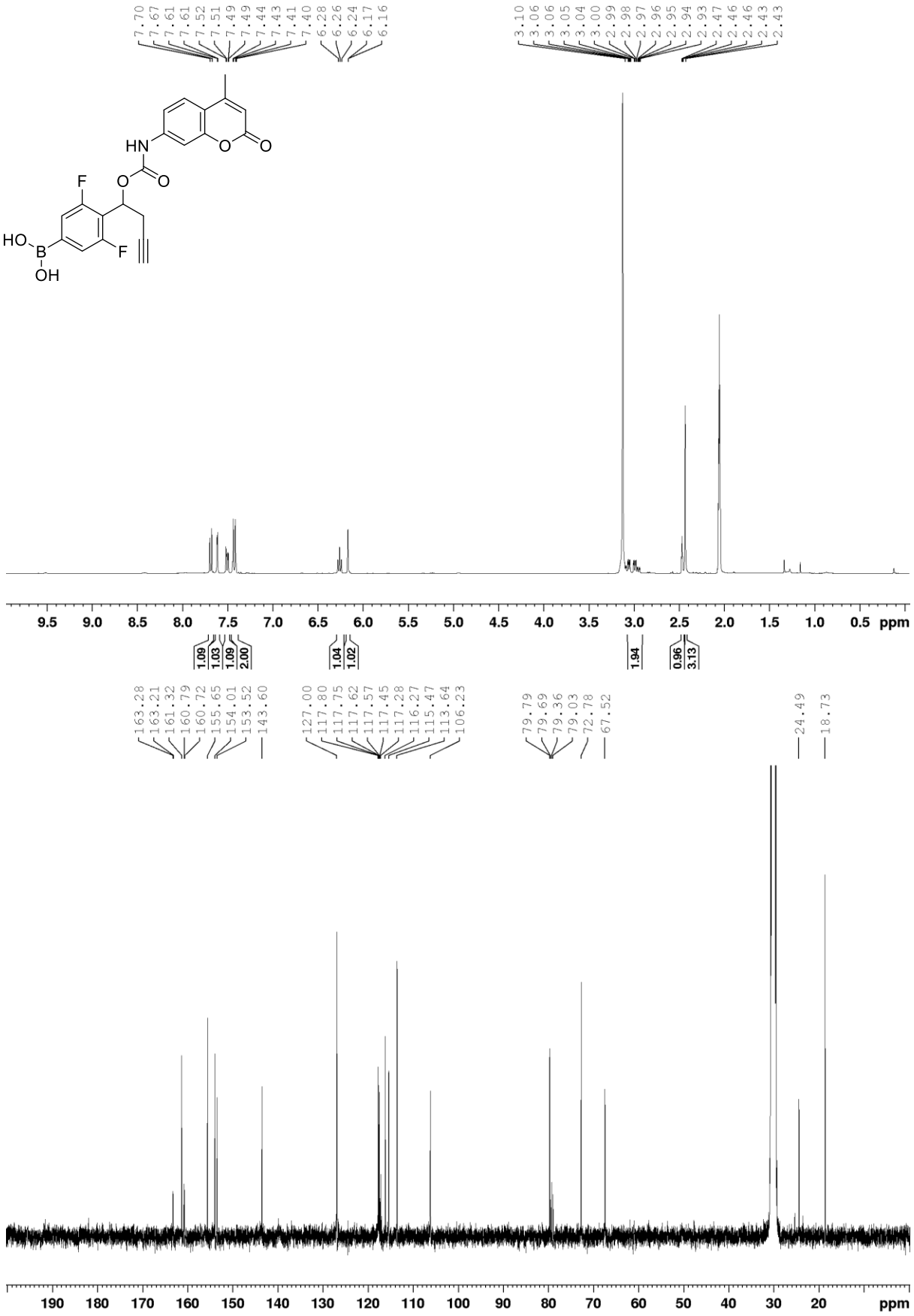

1-(4-Bromophenyl)but-3-yn-1-yl (4-methyl-2-oxo-2*H*-chromen-7-yl)carbamate (3)

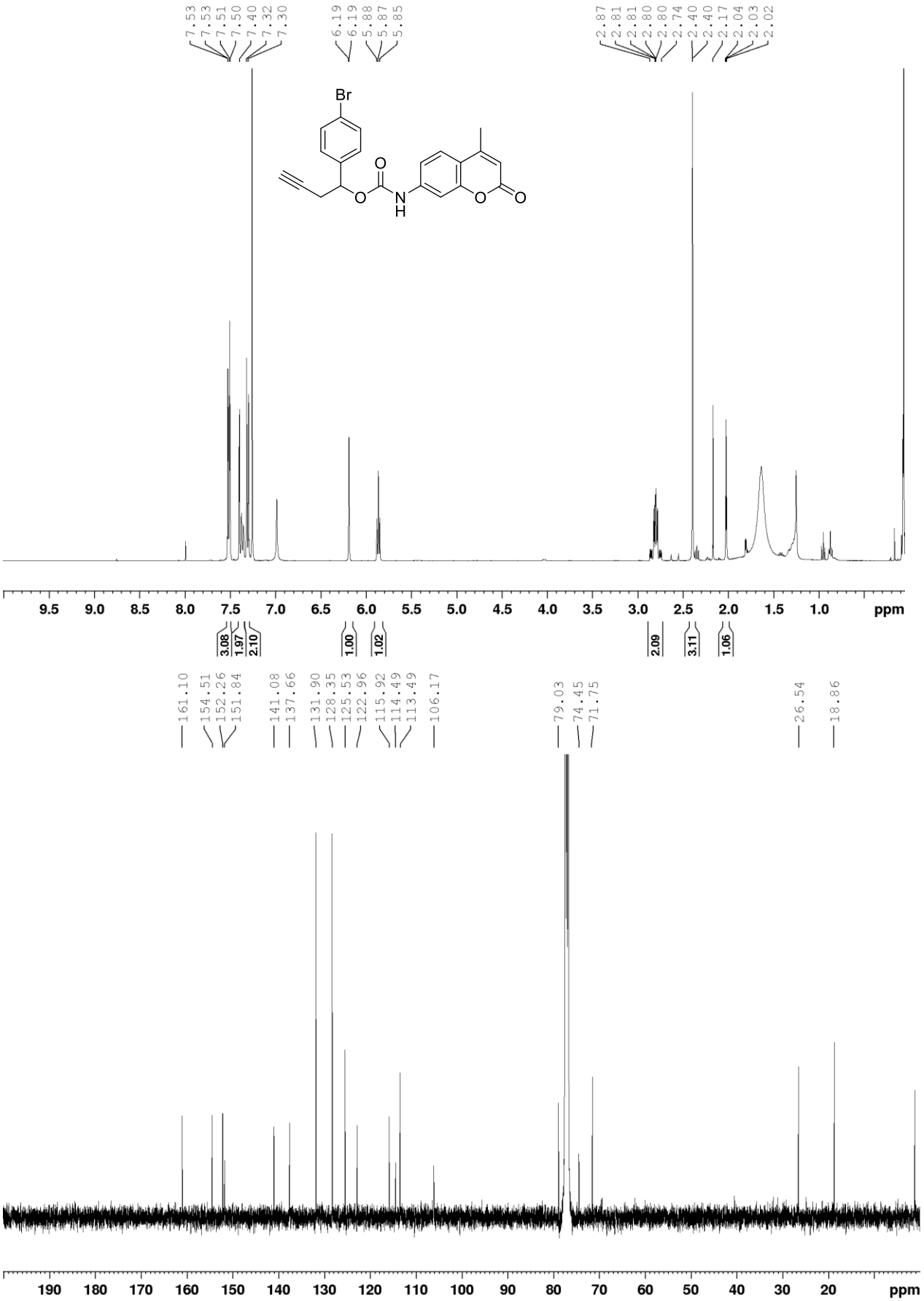

4-((*S*)-2-((*S*)-2-(2-Methoxyacetamido)-3-methylbutanamido)-5-ureidopentanamido)benzyl (4-methyl-2-oxo-2*H*-chromen-7-yl)carbamate (4)

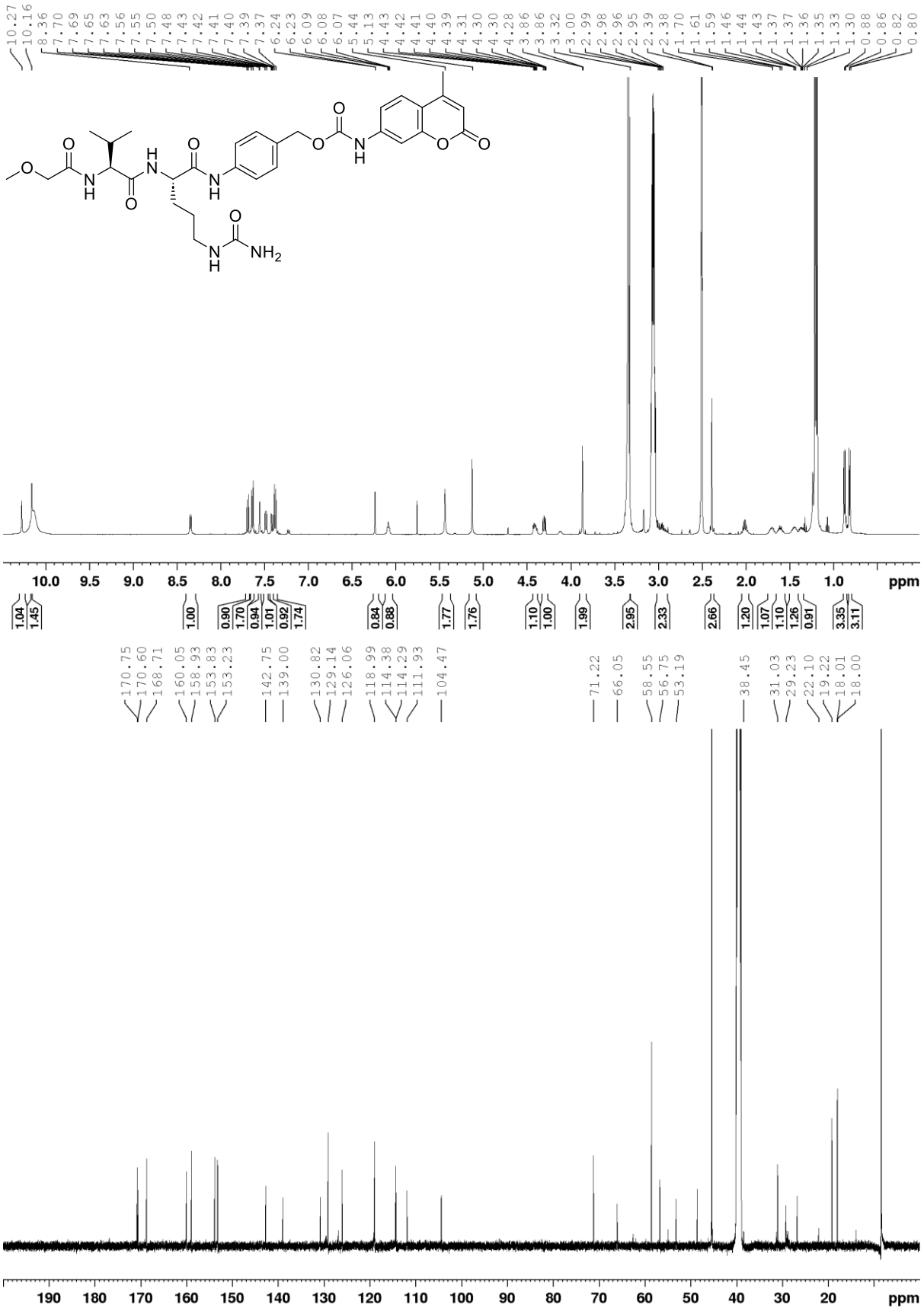

(2-Fluoro-4-(1-(((4-methyl-2-oxo-2*H*-chromen-7-yl)carbamoyl)oxy)but-3-yn-1-yl)phenyl)boronic acid (5b)

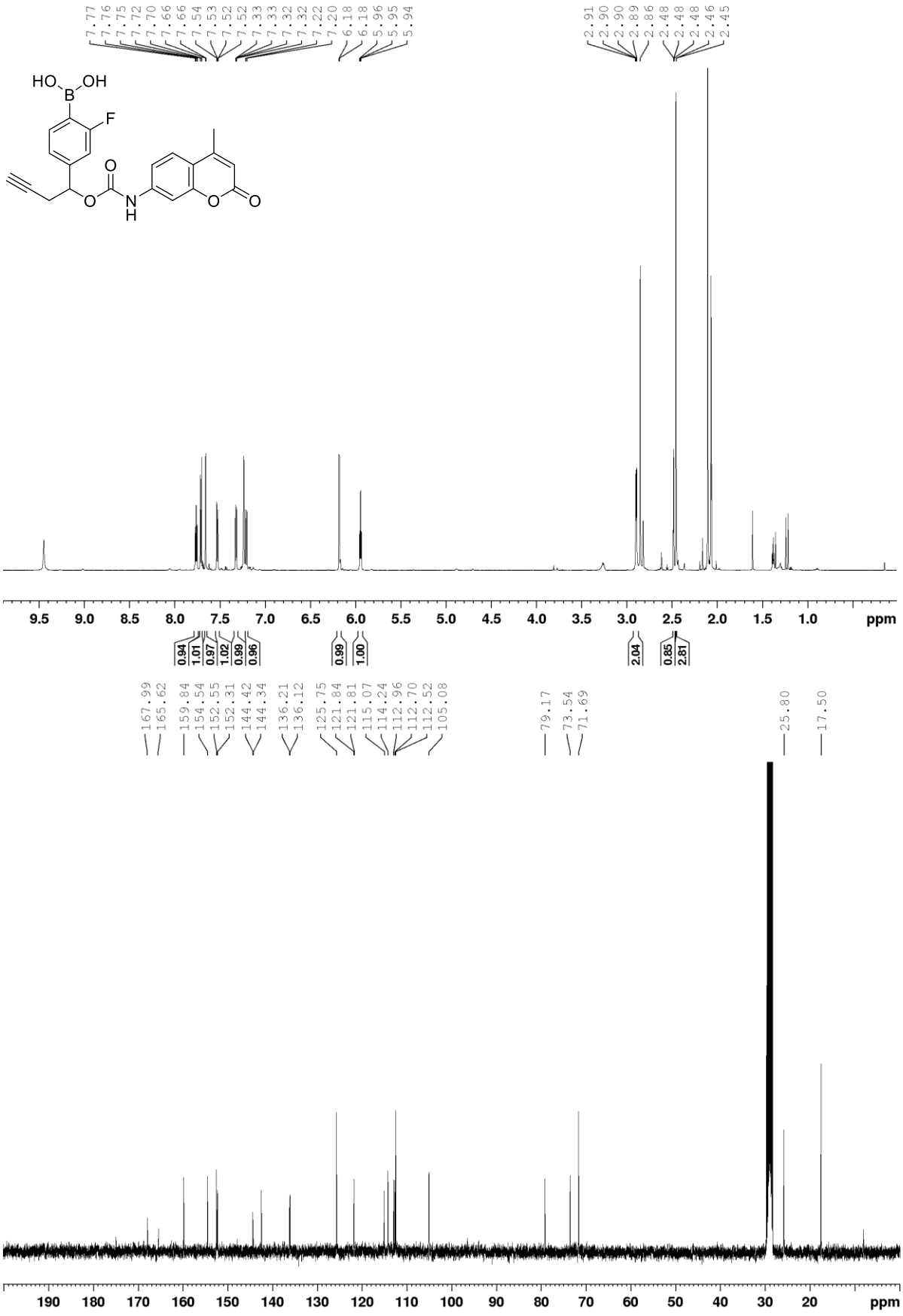

1-(4-Bromophenyl)but-3-yn-1-ol (7)

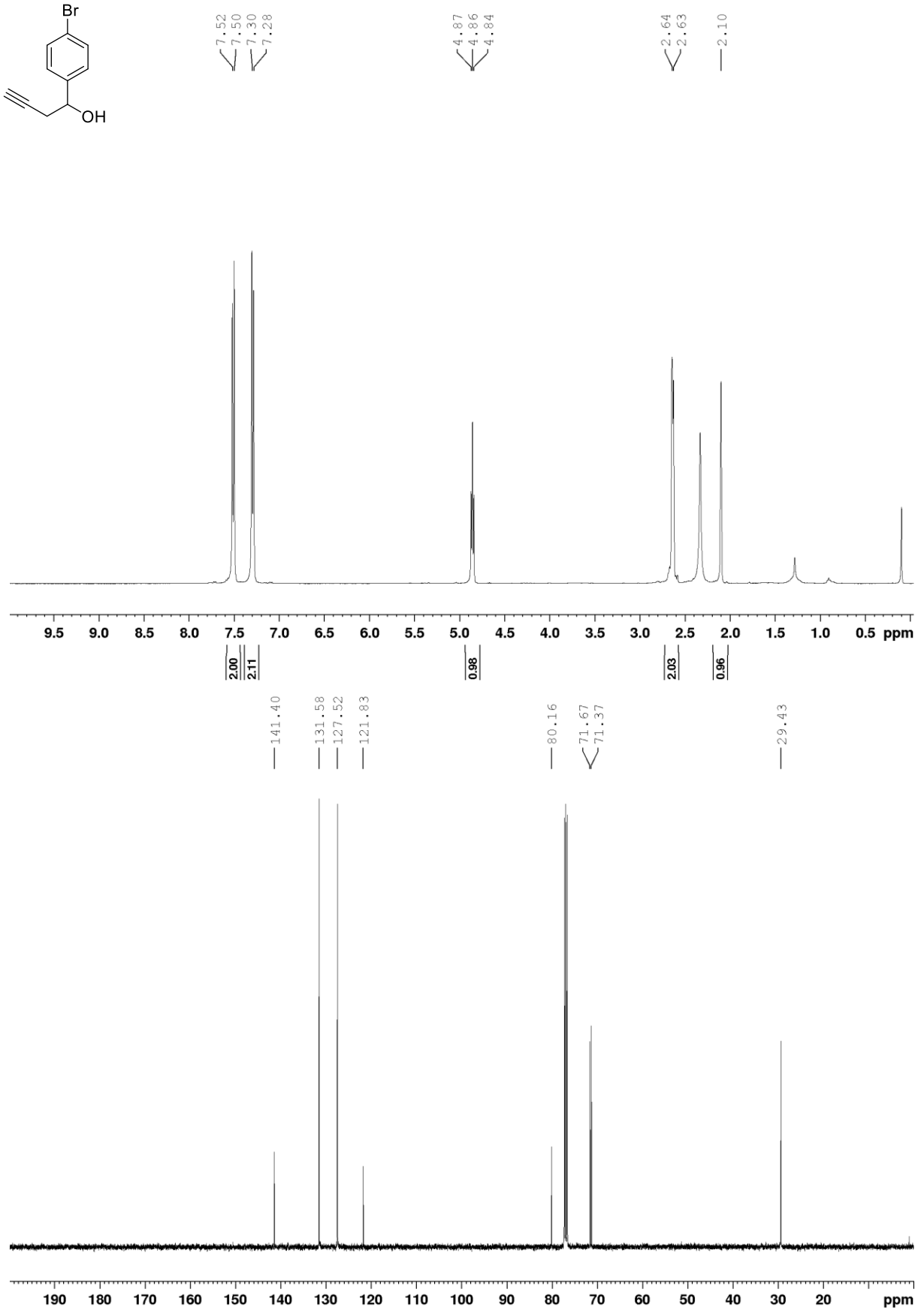

4-(4,4,5,5-Tetramethyl-1,3,2-dioxaborolan-2-yl)benzaldehyde (8)

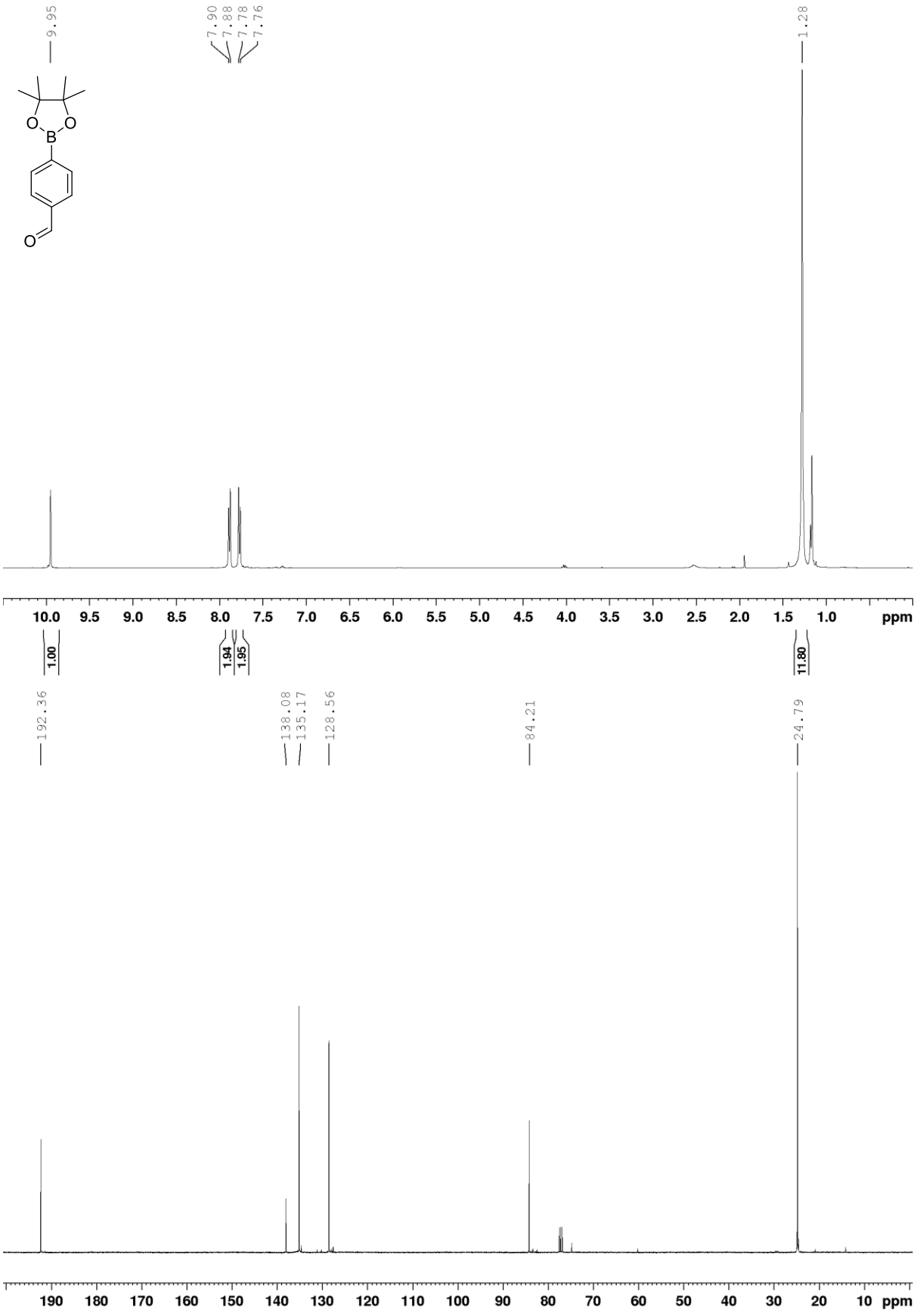

1-(4-(4,4,5,5-Tetramethyl-1,3,2-dioxaborolan-2-yl)phenyl)but-3-yn-1-ol (9)

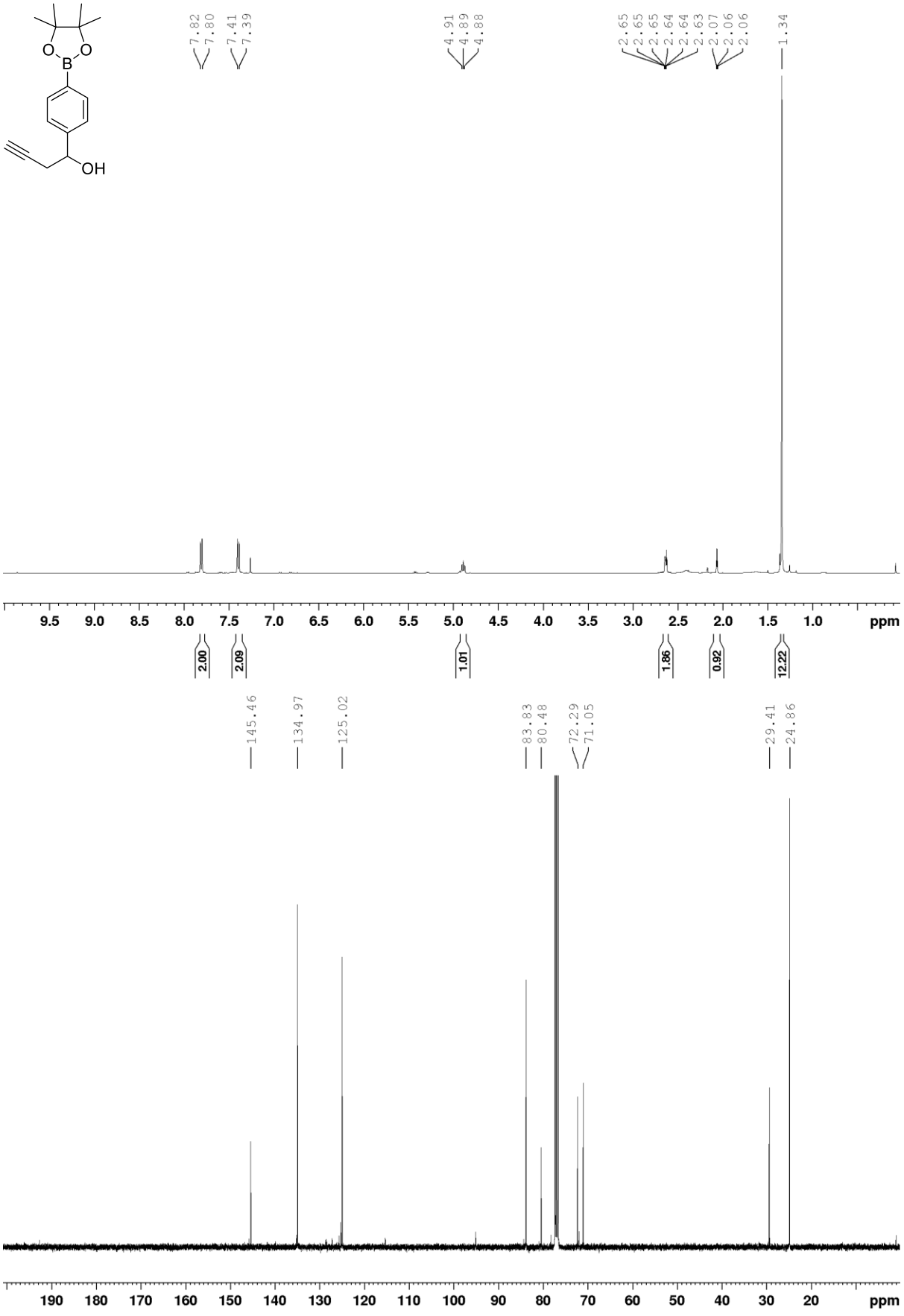

2,6-Difluoro-4-(4,4,5,5-tetramethyl-1,3,2-dioxaborolan-2-yl)benzaldehyde (10)

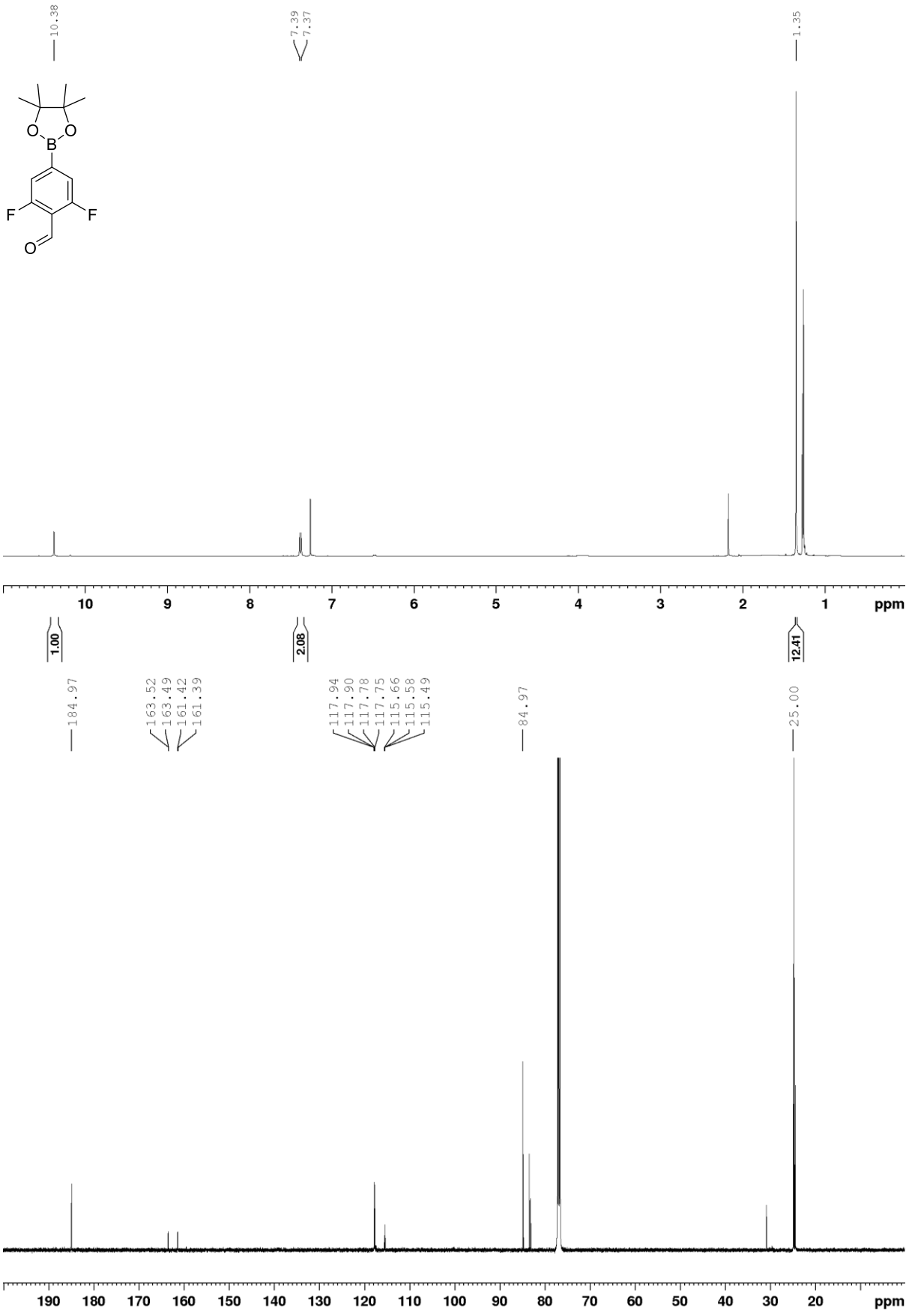

1-(2,6-Difluoro-4-(4,4,5,5-tetramethyl-1,3,2-dioxaborolan-2-yl)phenyl)but-3-yn-1-ol (11)

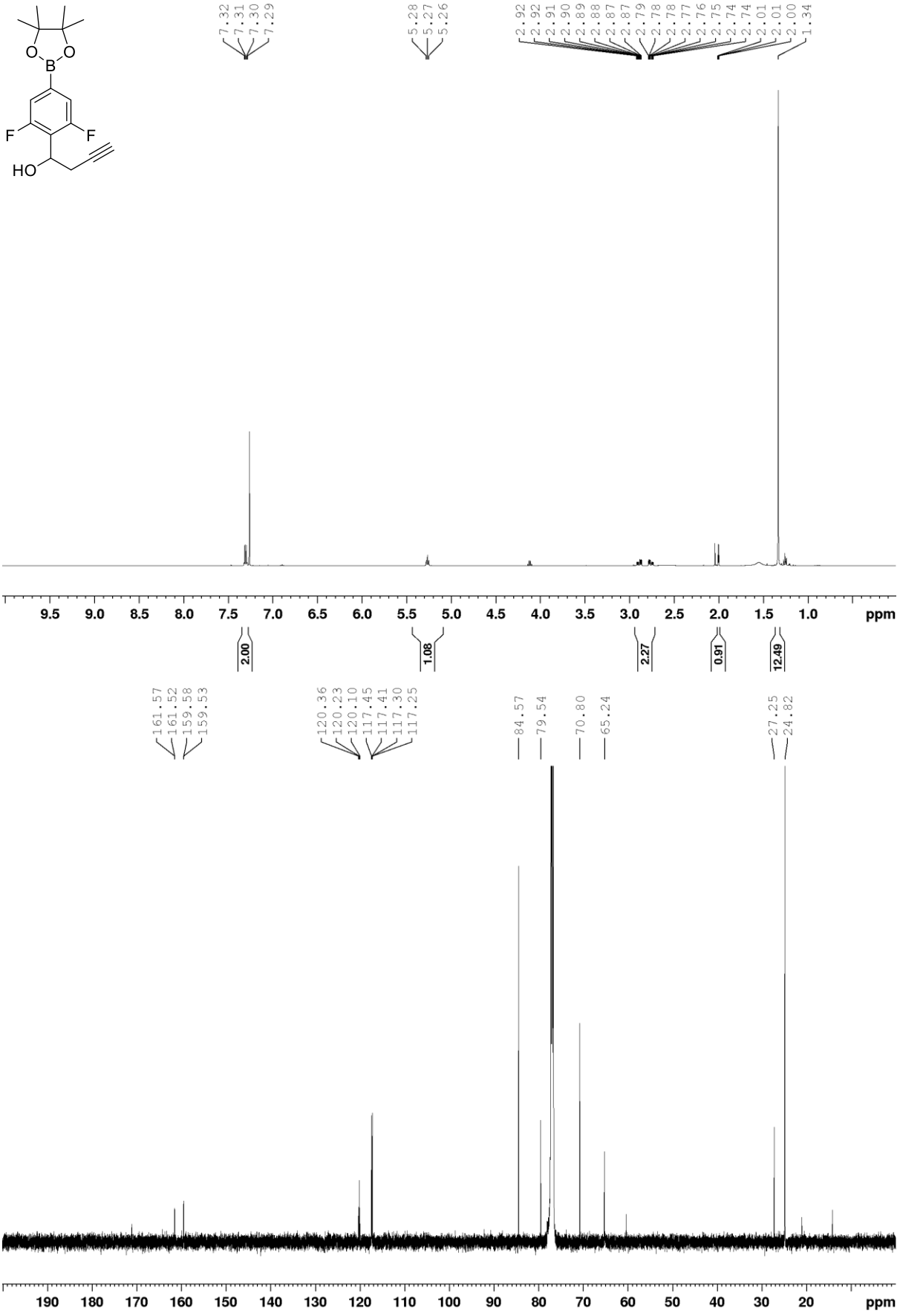

3-Fluoro-4-(4,4,5,5-tetramethyl-1,3,2-dioxaborolan-2-yl)benzaldehyde (12)

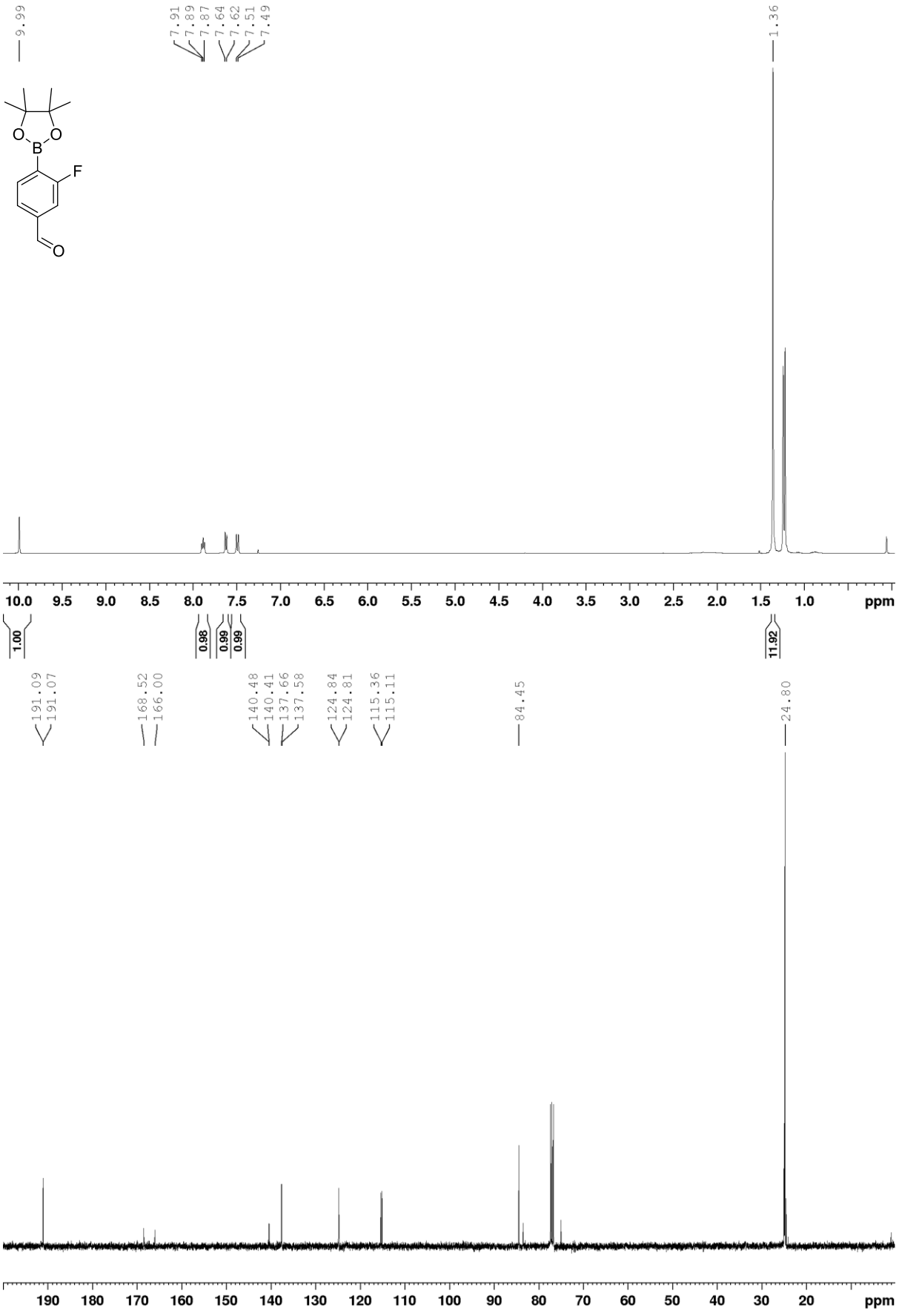

1-(3-Fluoro-4-(4,4,5,5-tetramethyl-1,3,2-dioxaborolan-2-yl)phenyl)but-3-yn-1-ol (13)

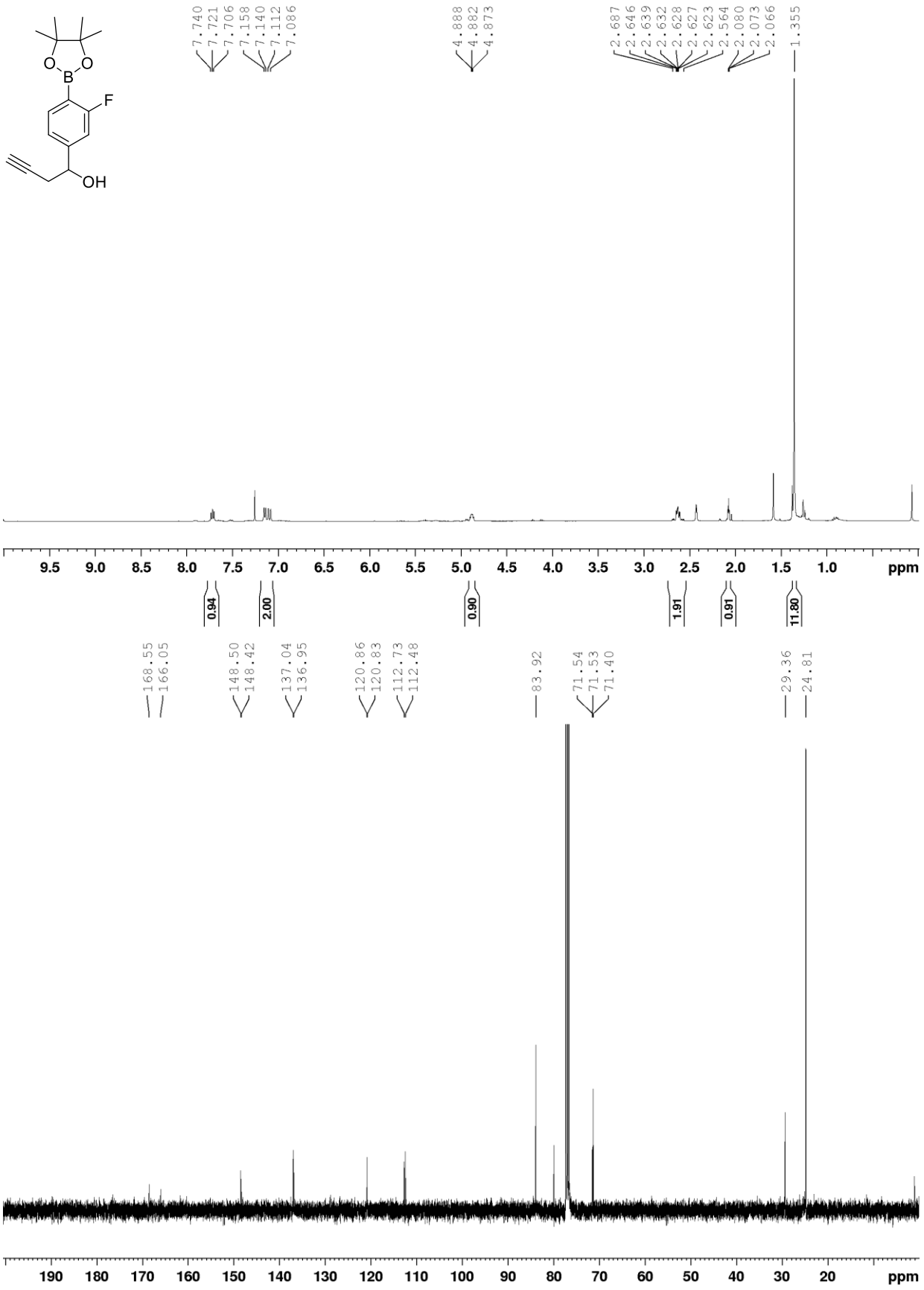

3-Nitro-4-(4,4,5,5-tetramethyl-1,3,2-dioxaborolan-2-yl)benzaldehyde (14)

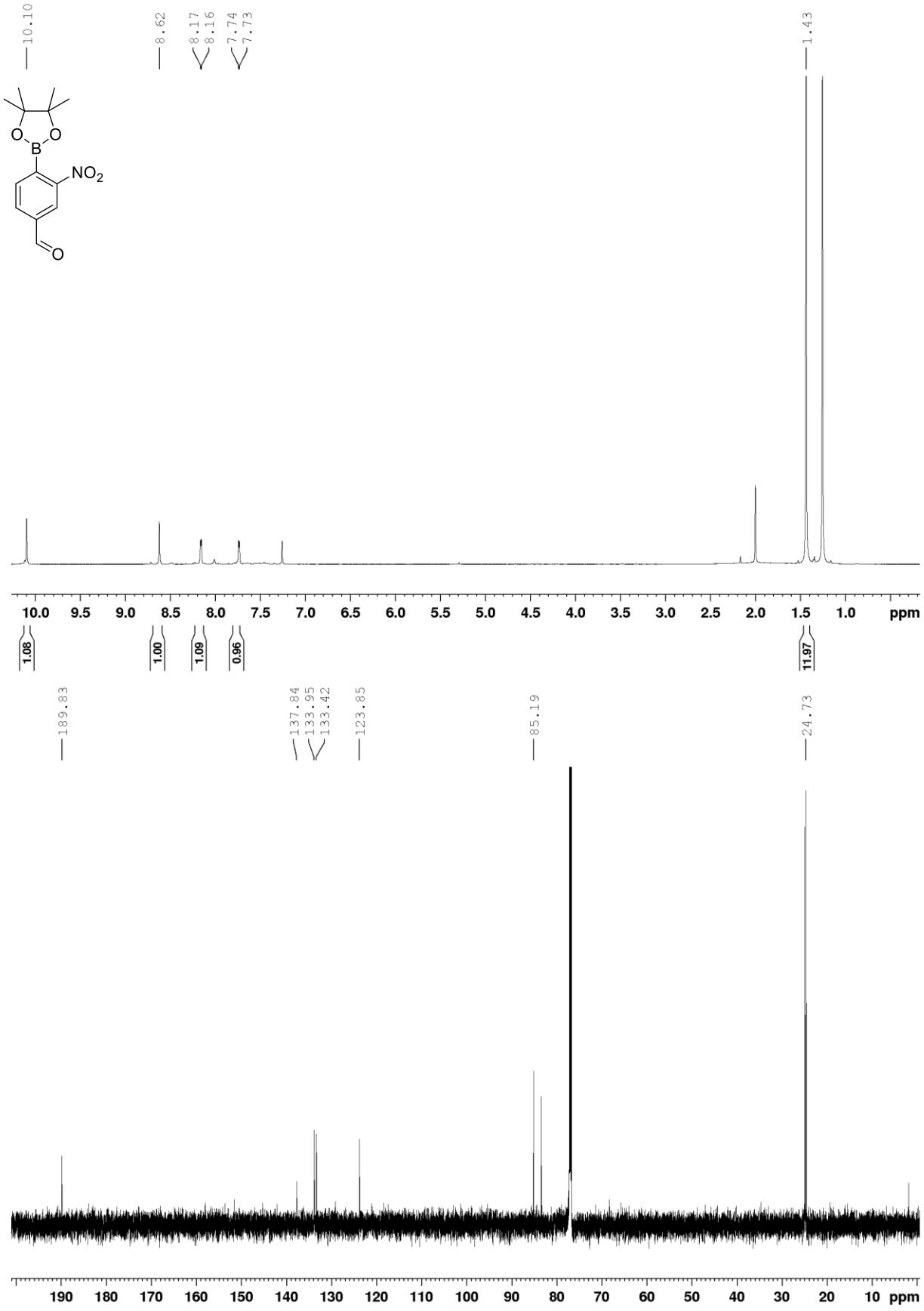

(*S*)-2-((((9*H*-Fluoren-9-yl)methoxy)carbonyl)amino)-5-ureidopentanoic acid (16)

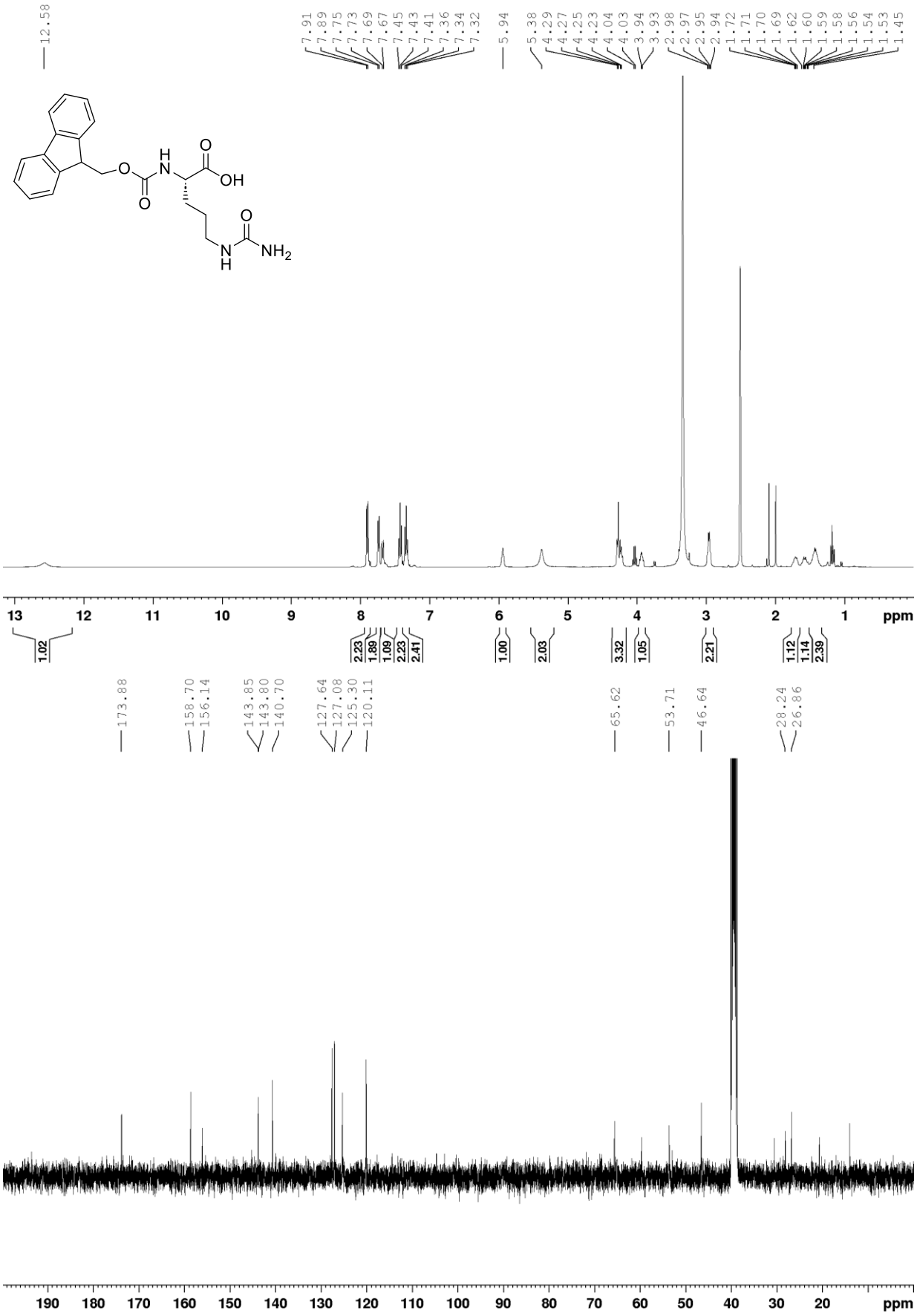

(9*H*-Fluoren-9-yl)methyl(*S*)-(1-((4-(hydroxymethyl)phenyl)amino)-1-oxo-5-ureidopentan-2-yl)carbamate (17)

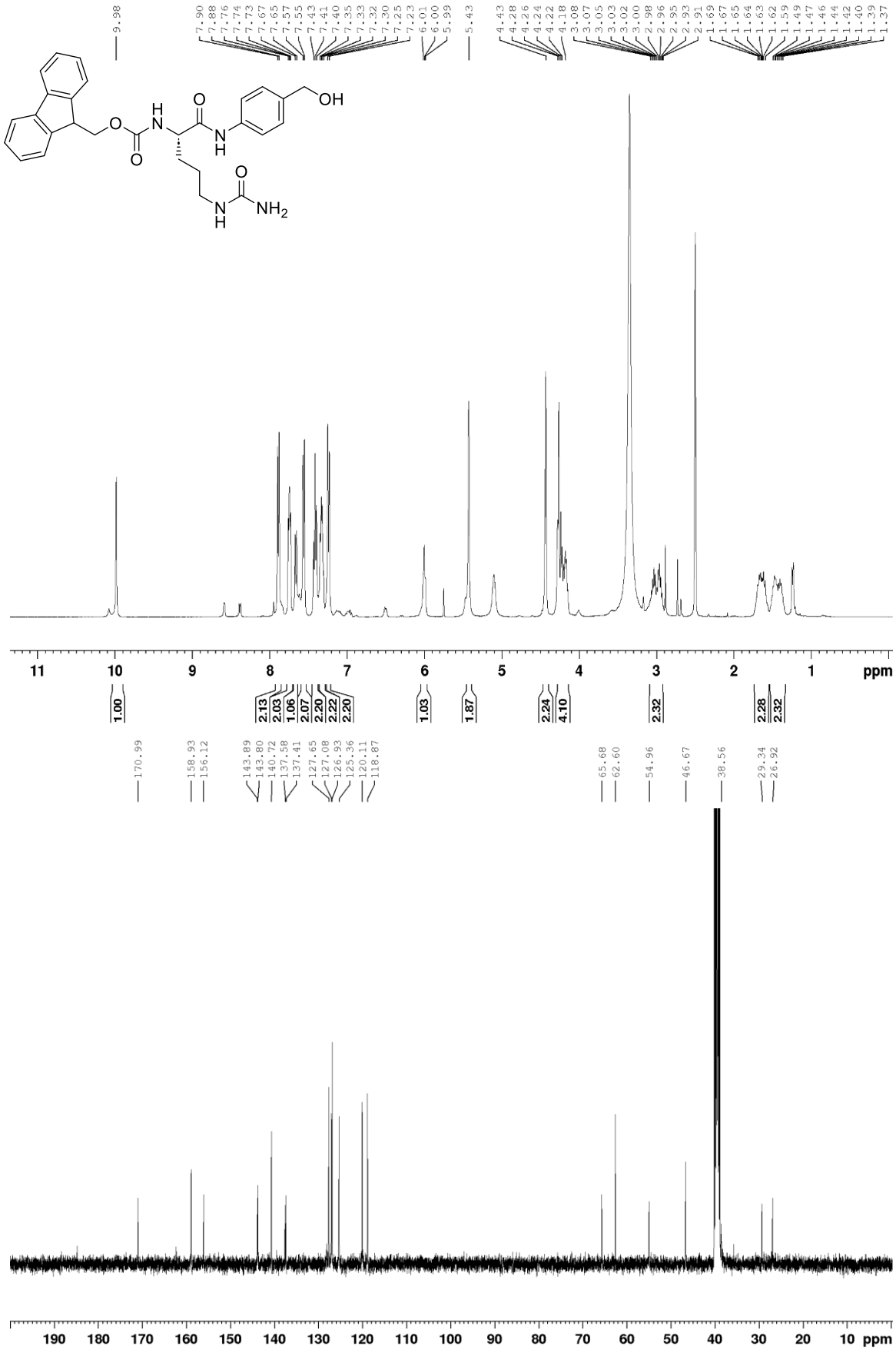

(9*H*-Fluoren-9-yl)methyl ((*S*)-1-(((*S*)-1-((4-(hydroxymethyl)phenyl)amino)-1-oxo-5-ureidopentan-2-yl)amino)-3-methyl-1-oxobutan-2-yl)carbamate (18)

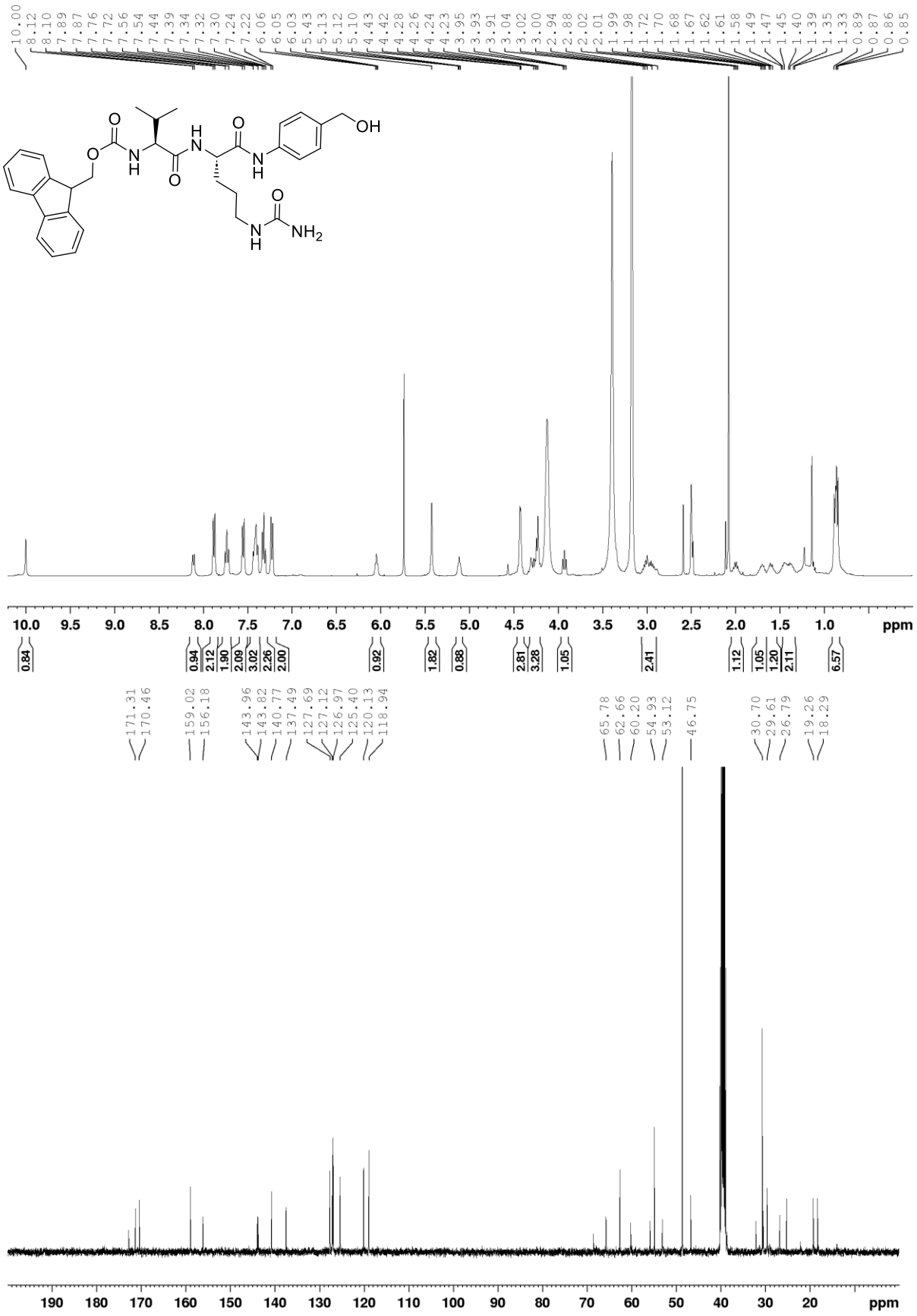

(*S*)-*N*-(4-(hydroxymethyl)phenyl)-2-((*S*)-2-(2-methoxyacetamido)-3-methylbutanamido)-5-ureidopentanamide (19)

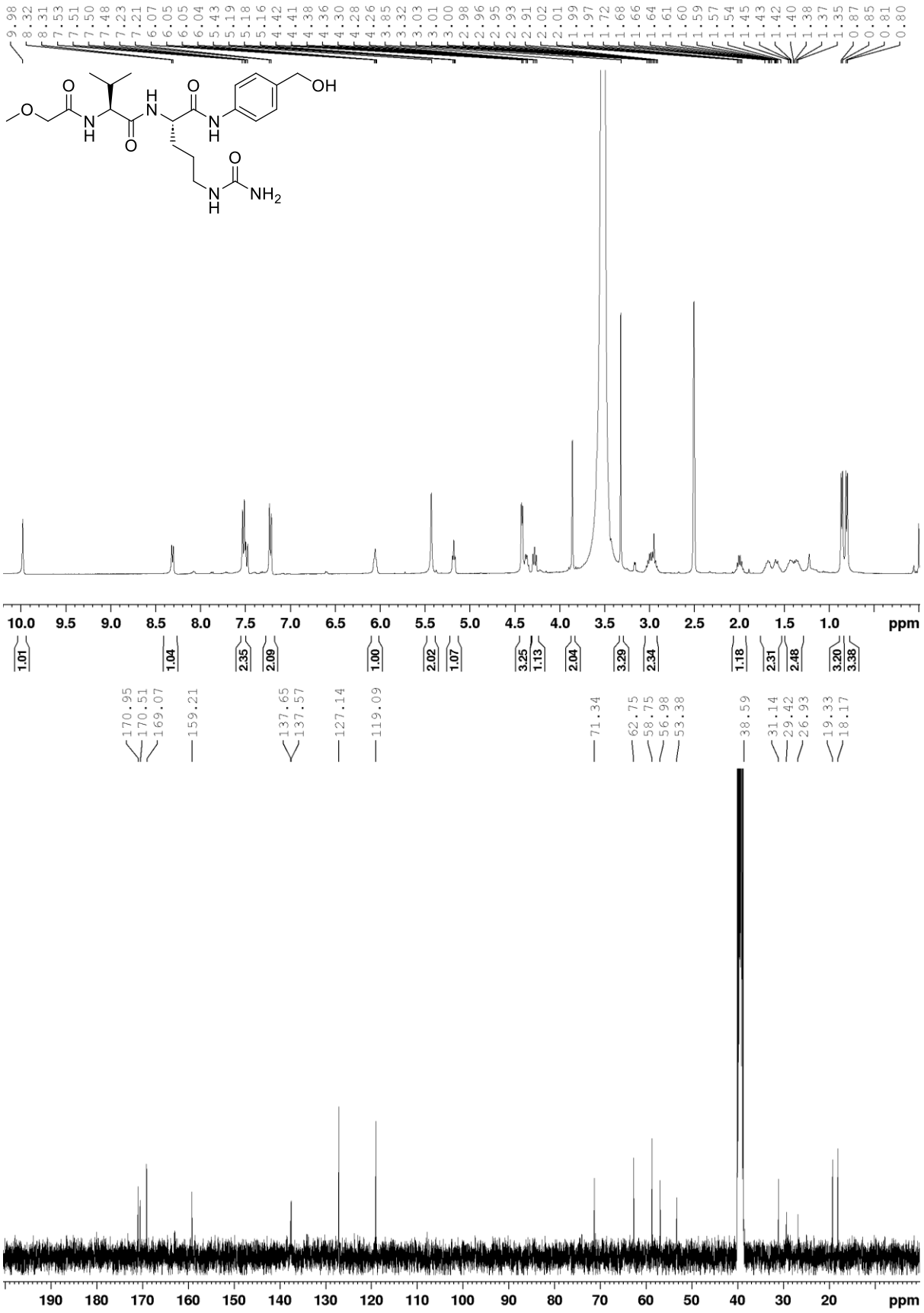

4-Nitrophenyl (1-(4-(4,4,5,5-tetramethyl-1,3,2-dioxaborolan-2-yl)phenyl)but-3-yn-1-yl) carbonate (20a)

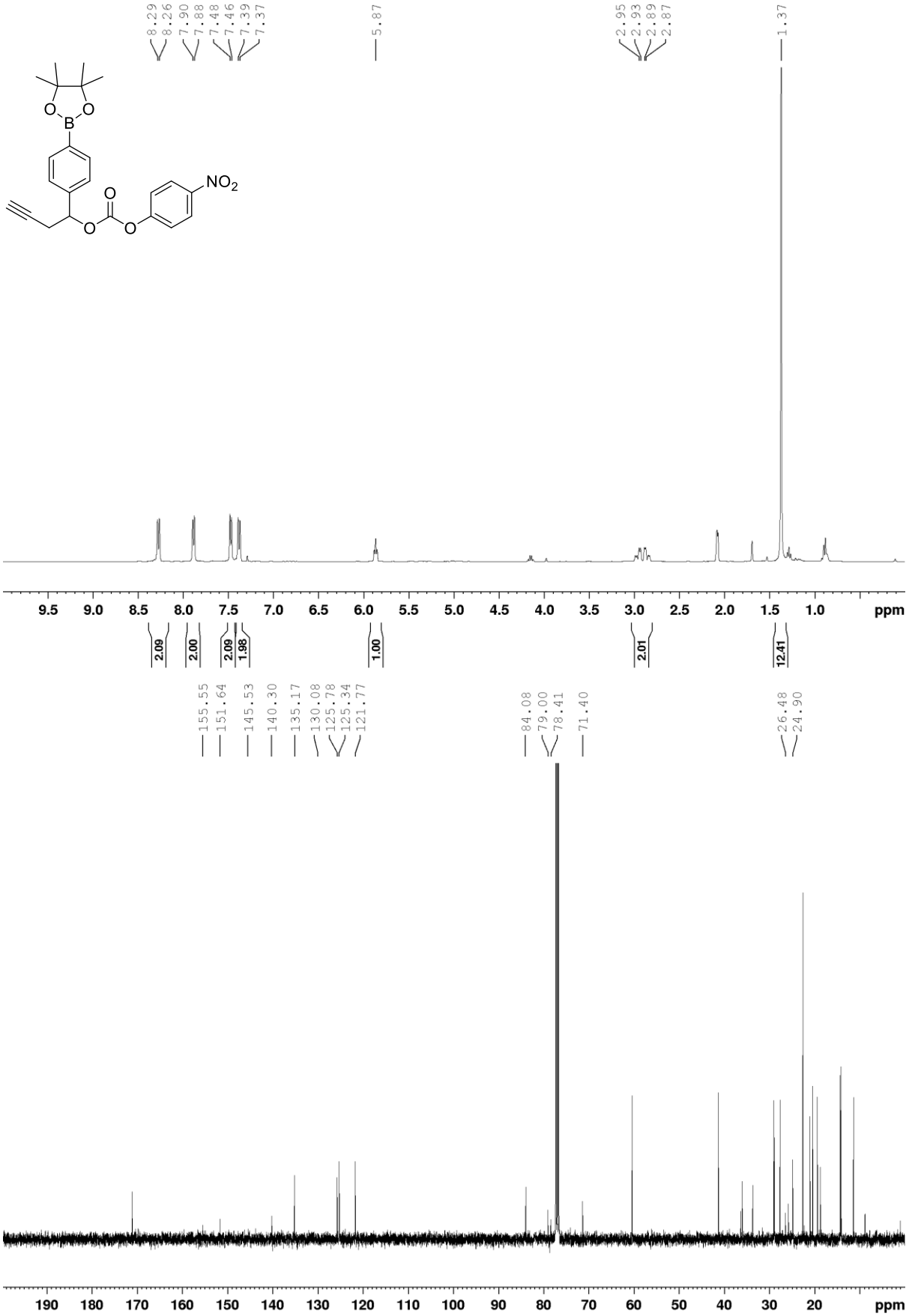

1-(2,6-Difluoro-4-(4,4,5,5-tetramethyl-1,3,2-dioxaborolan-2-yl)phenyl)but-3-yn-1-yl (4-nitrophenyl) carbonate (21a)

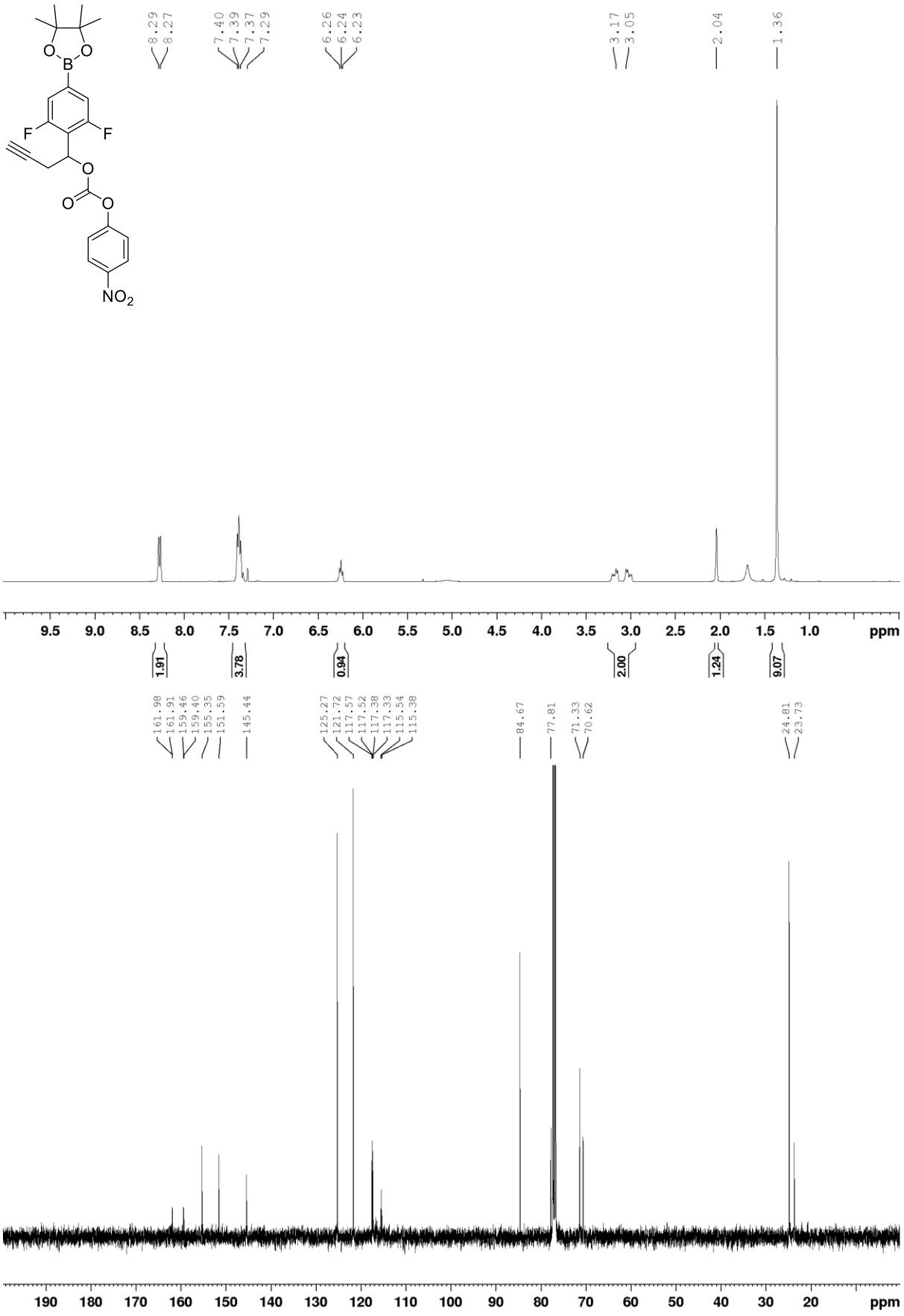

4-Bromobenzyl (4-nitrophenyl) carbonate (31)

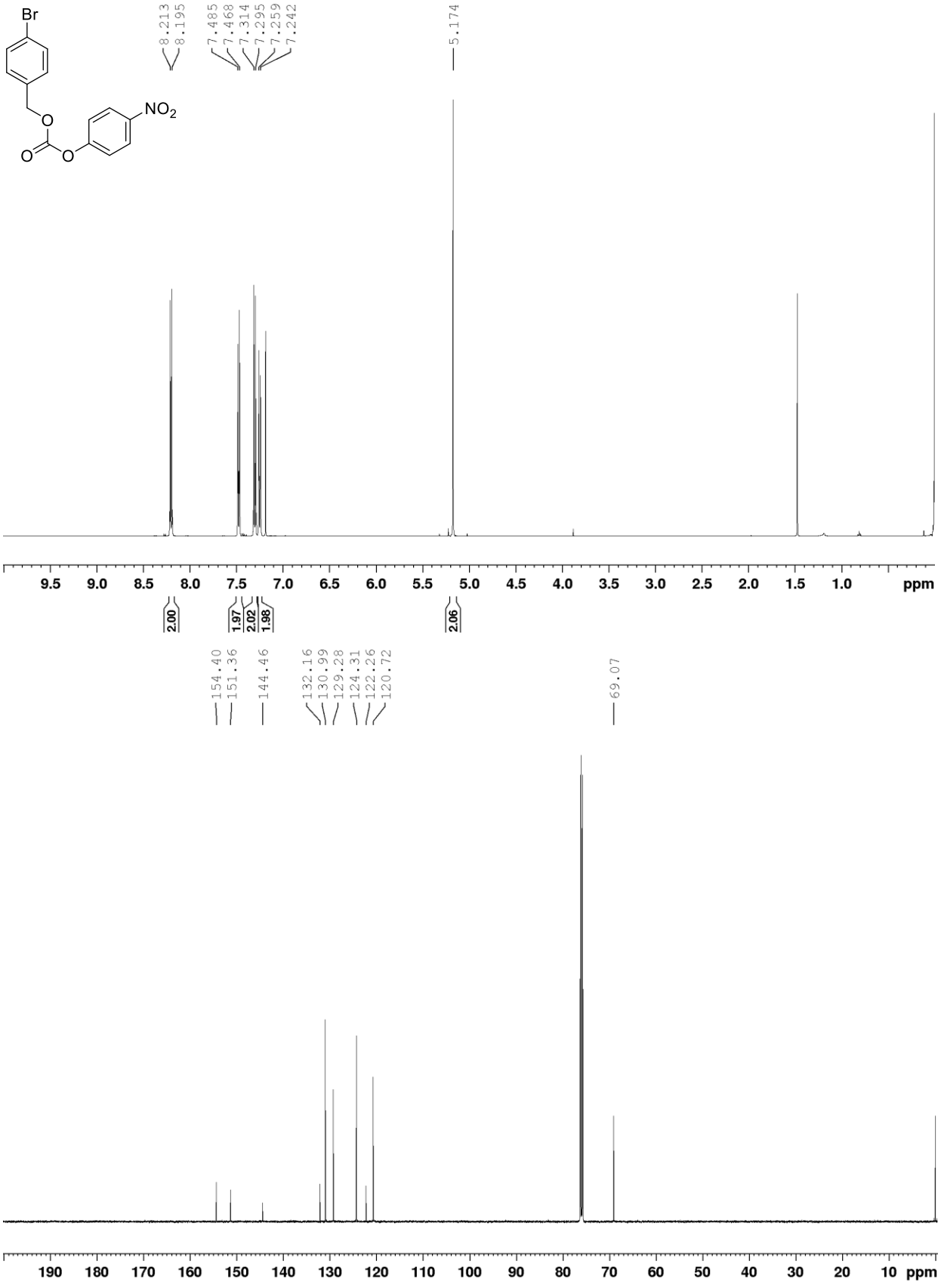

4-Nitrophenyl (4-(4,4,5,5-tetramethyl-1,3,2-dioxaborolan-2-yl)benzyl) carbonate (32)

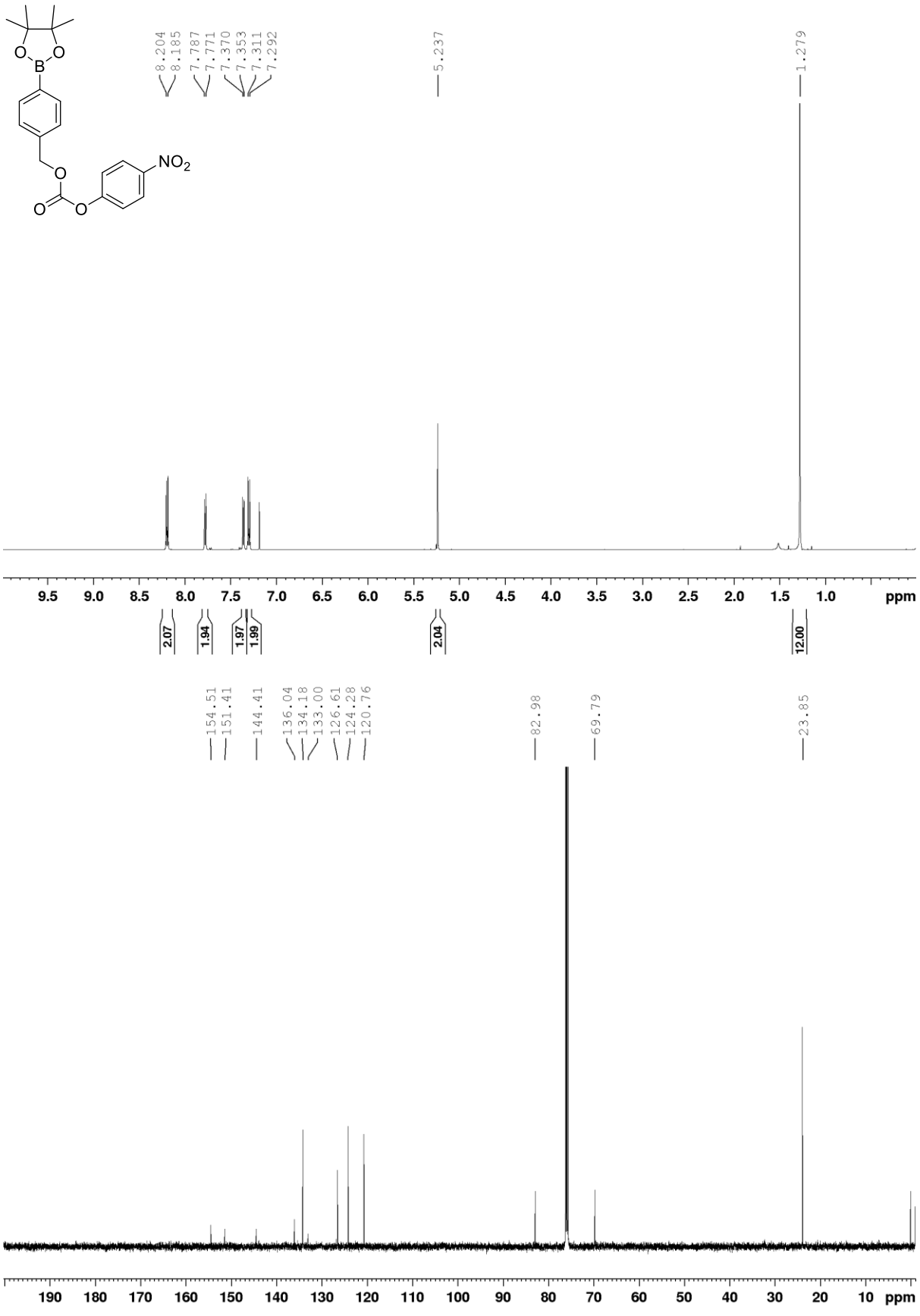

(*R*)-4-(4-Bromobenzyl)-4-(3-((4-(*N*-(4-(4-((4'-chloro-4,4-dimethyl-3,4,5,6-tetrahydro-[1,1'-biphenyl]-2-yl)methyl)piperazin-1-yl)benzoyl)sulfamoyl)-2-((trifluoromethyl)sulfonyl)phenyl)amino)-4-(phenylthio)butyl)morpholin-4-ium (39)

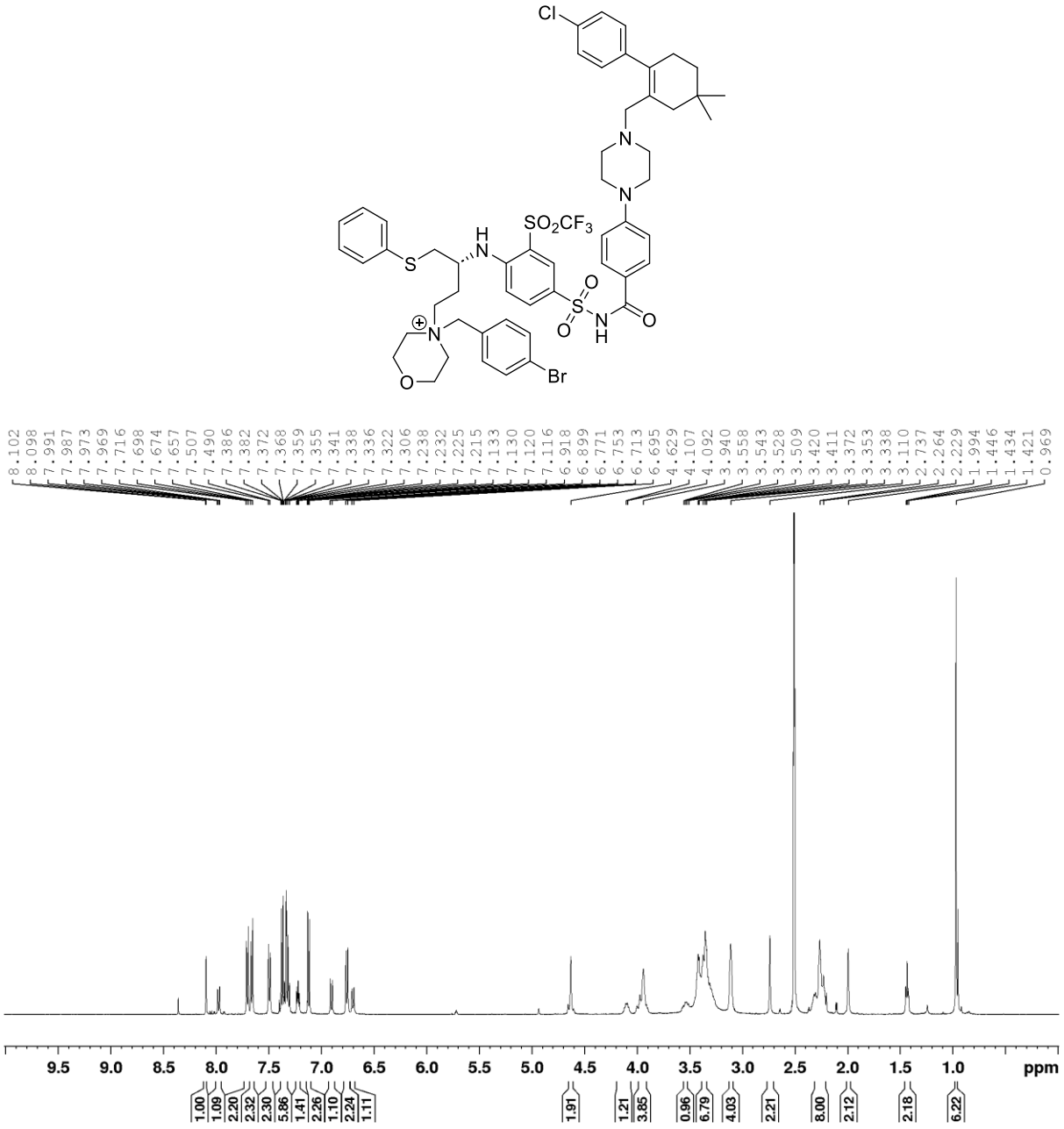

4-Bromobenzyl (*R*)-(4-morpholino-1-(phenylthio)butan-2-yl)carbamate (45)

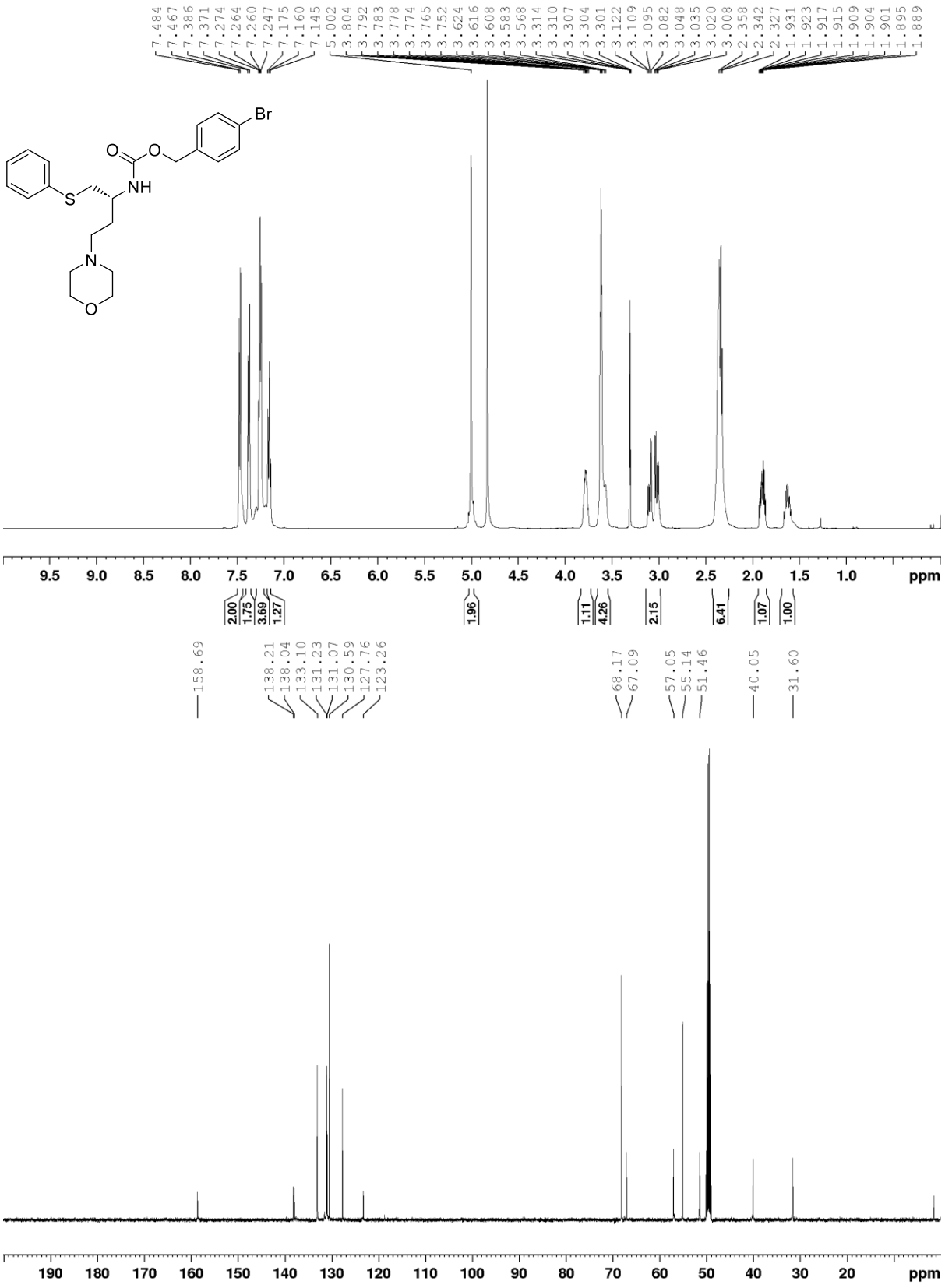

(*R*)-*N*-(4-Bromobenzyl)-4-morpholino-1-(phenylthio)butan-2-amine (46)

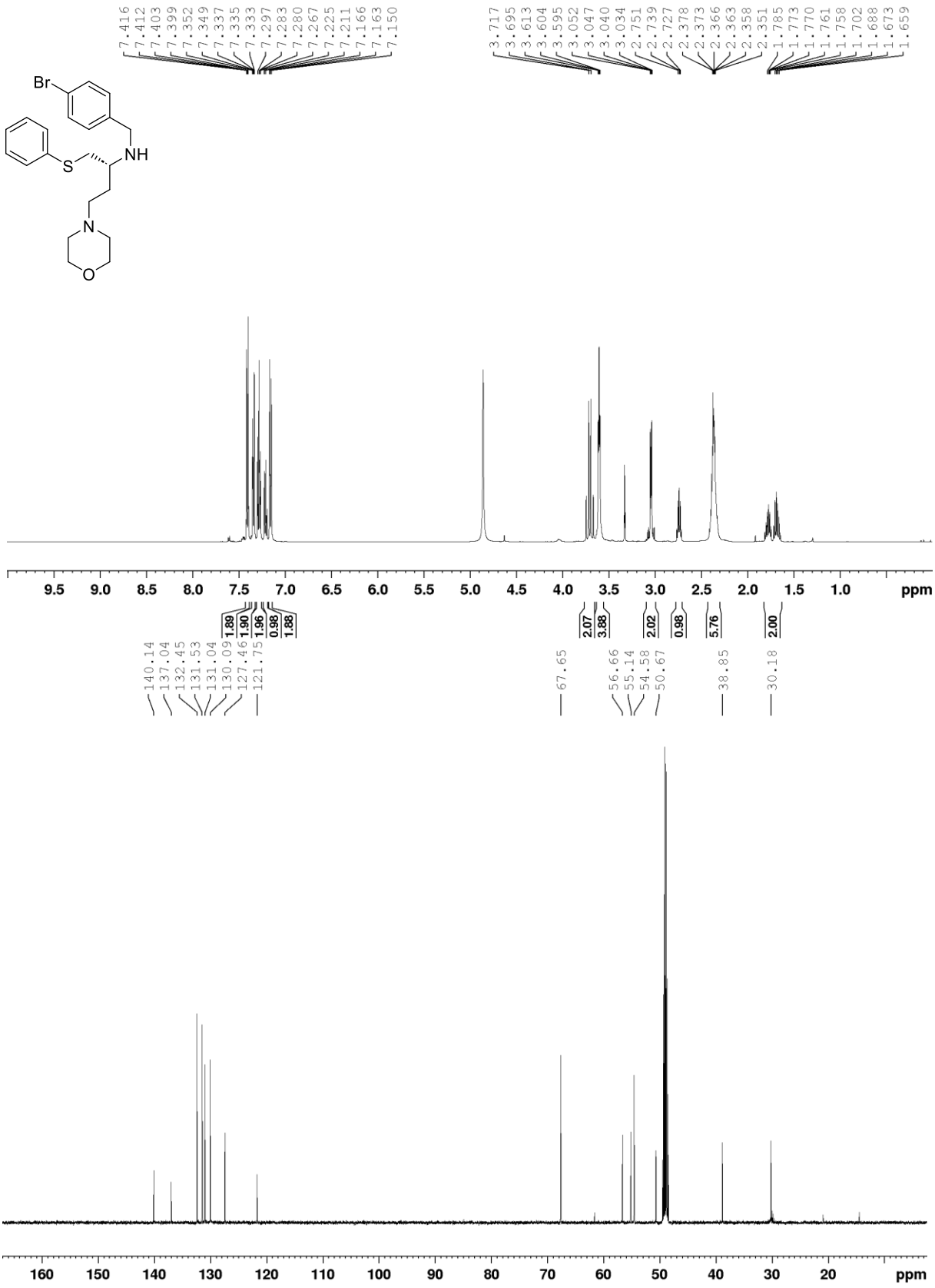

(*R*)-*N,N*-bis(4-bromobenzyl)-4-morpholino-1-(phenylthio)butan-2-amine (50)

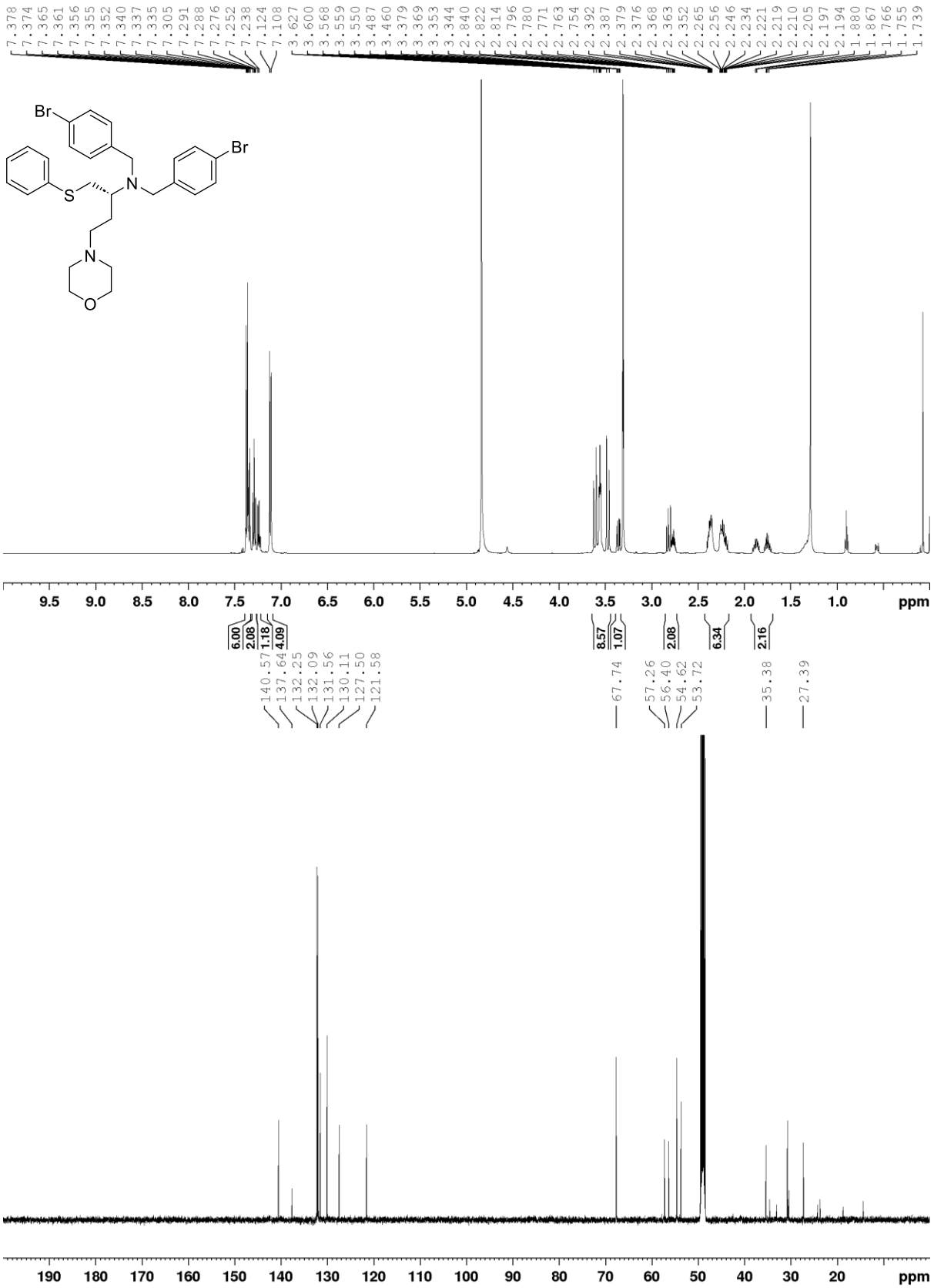

1,3-Bis((*R*)-4-morpholino-1-(phenylthio)butan-2-yl)urea (51)

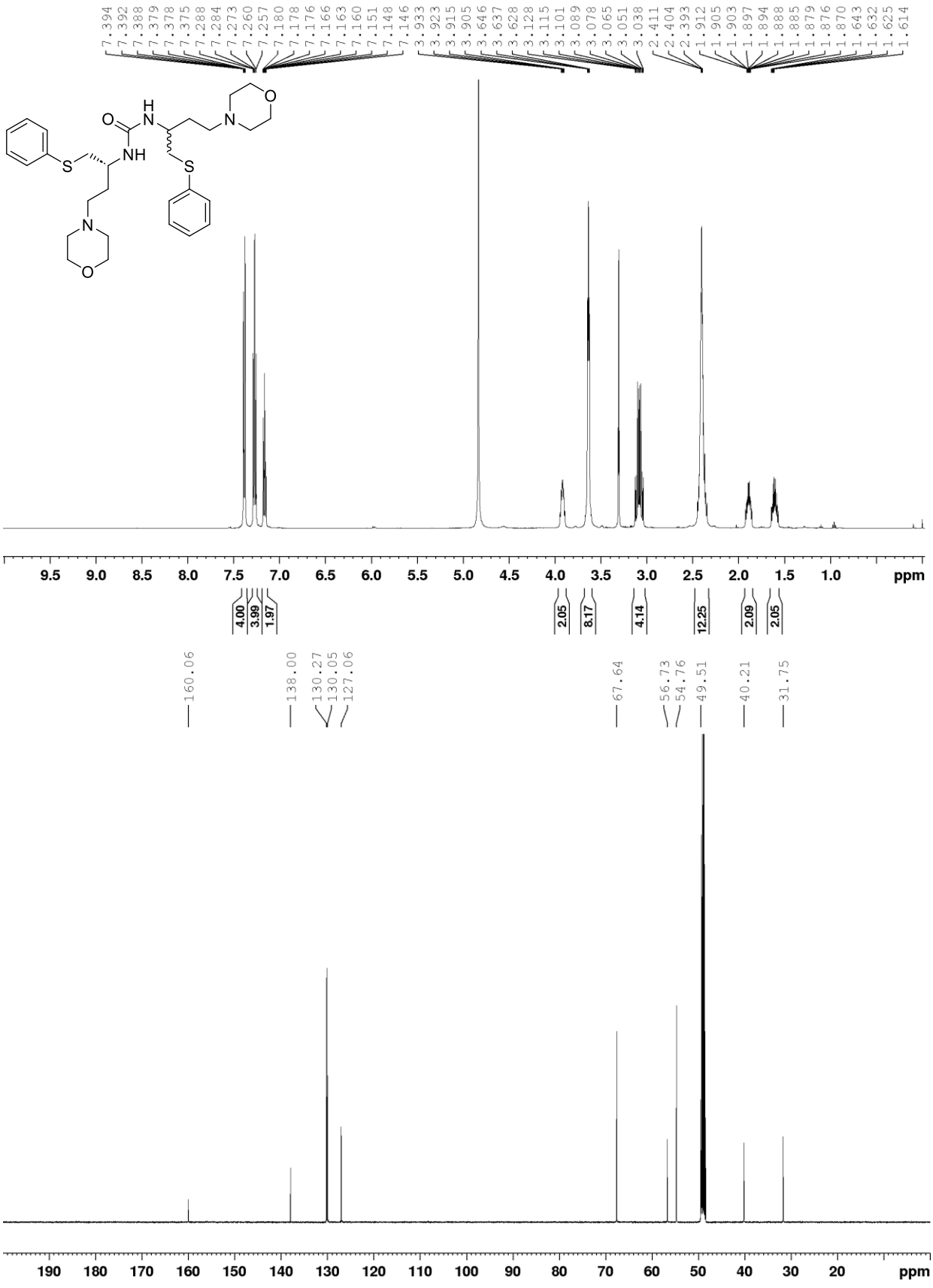

4-Fluoro-*N*-(4-sulfamoyl-2-((trifluoromethyl)sulfonyl)phenyl)-3 ((trifluoromethyl)sulfonyl)-benzenesulfonamide (52)

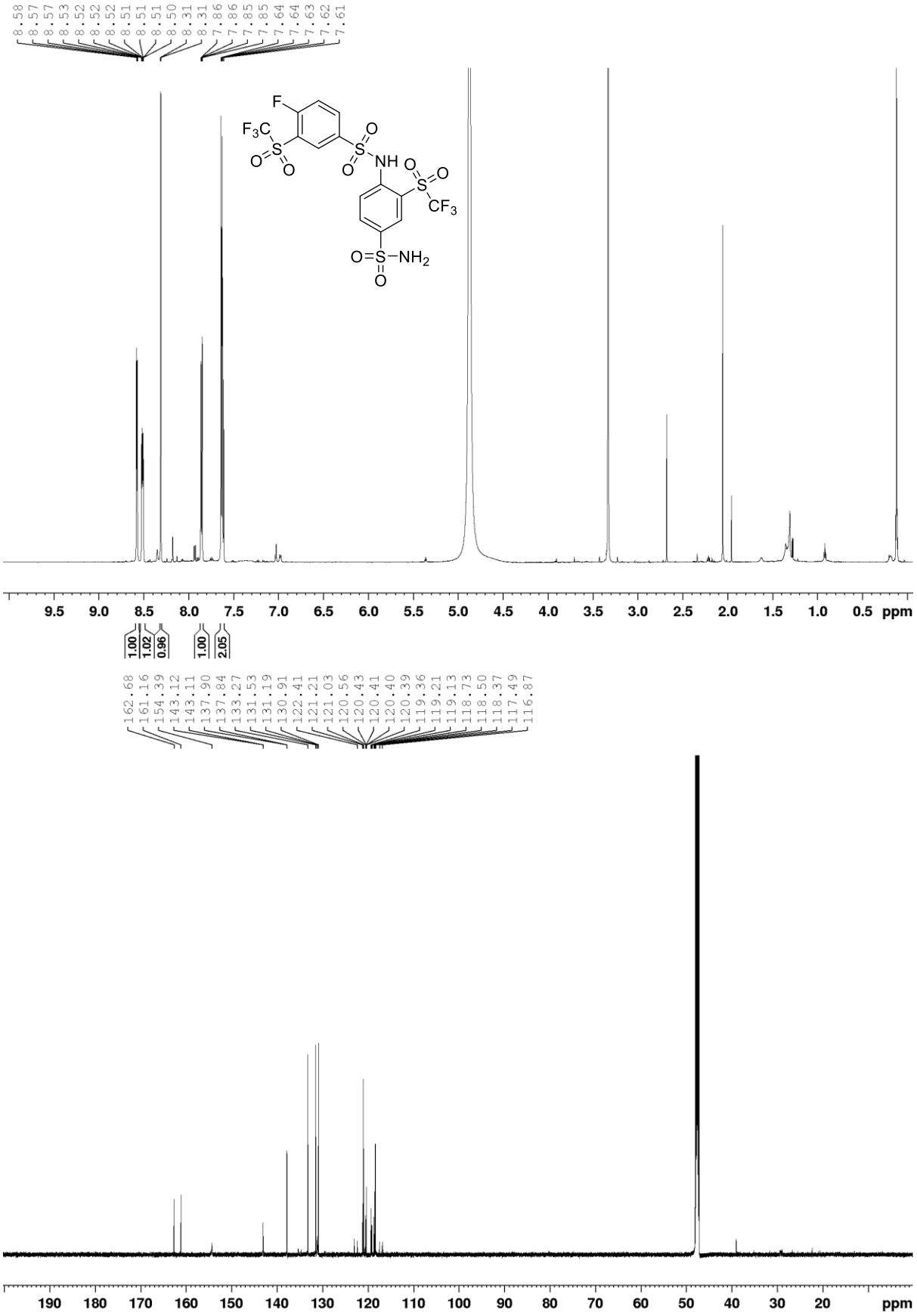

***tert*-Butyl ((4-fluoro-3-((trifluoromethyl)sulfonyl)phenyl)sulfonyl)carbamate (54)**

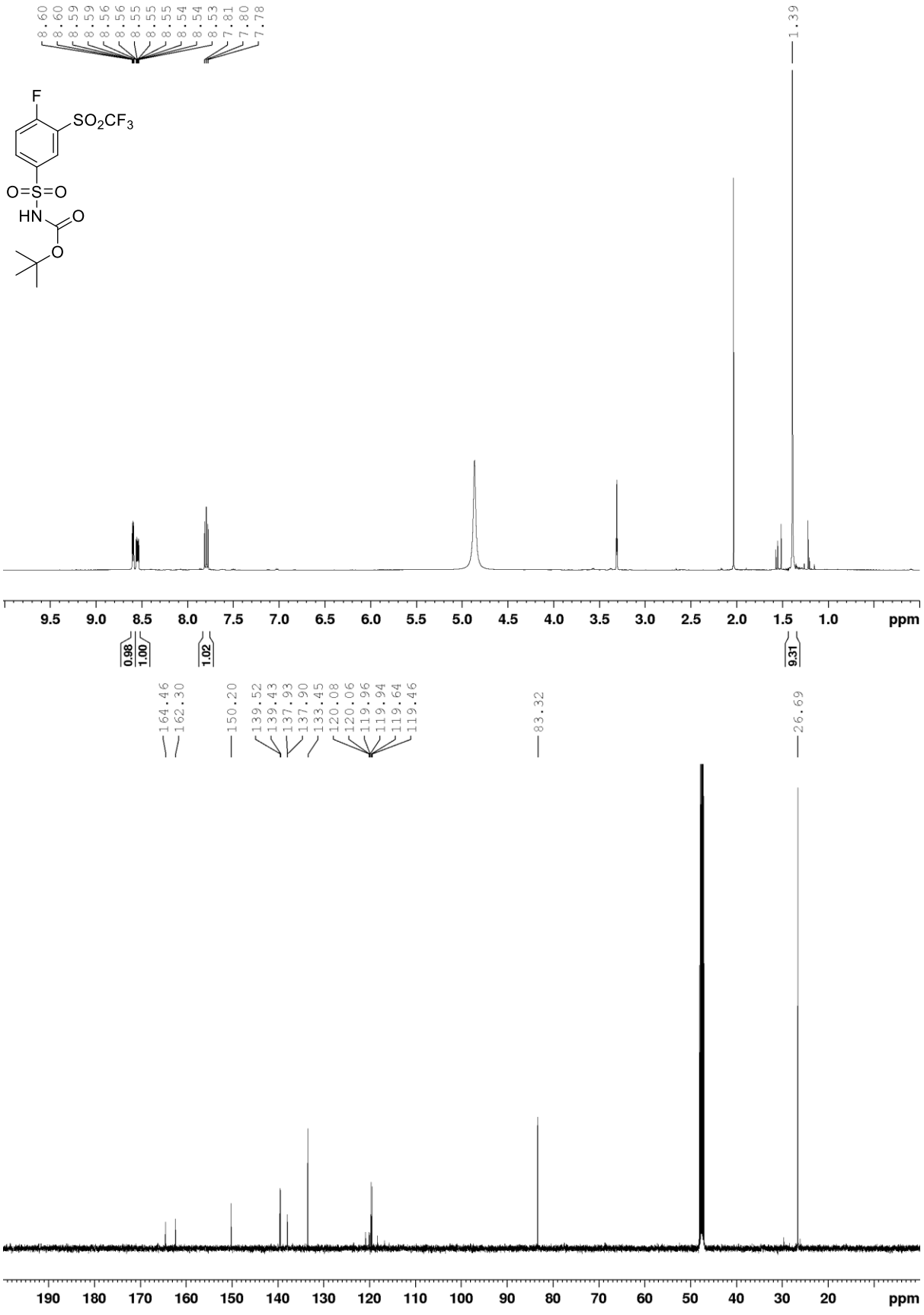

***tert*-Butyl 4-(piperazin-1-yl)benzoate (64)**

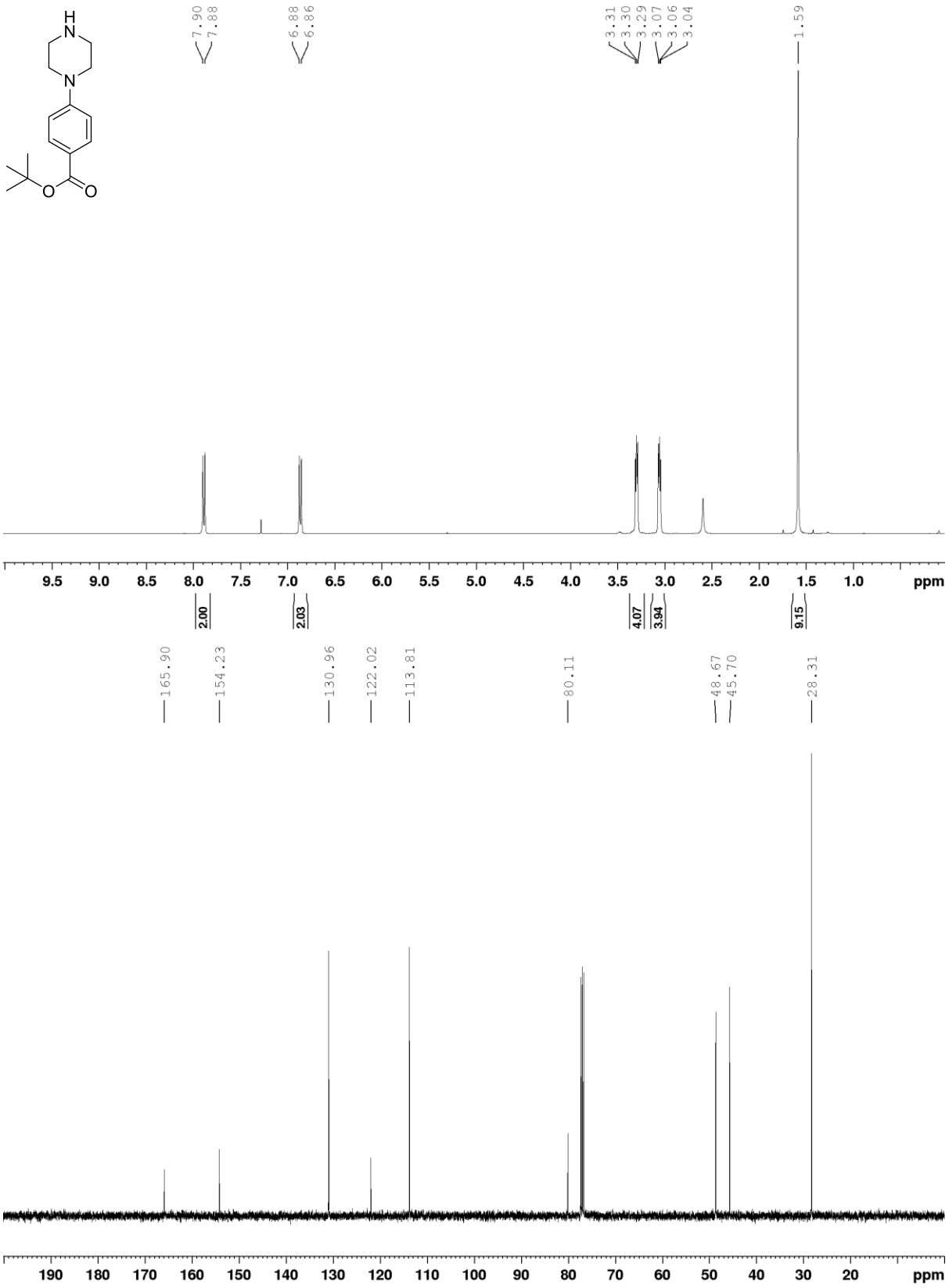

2-Bromo-5,5-dimethylcyclohex-1-ene-1-carbaldehyde (67)

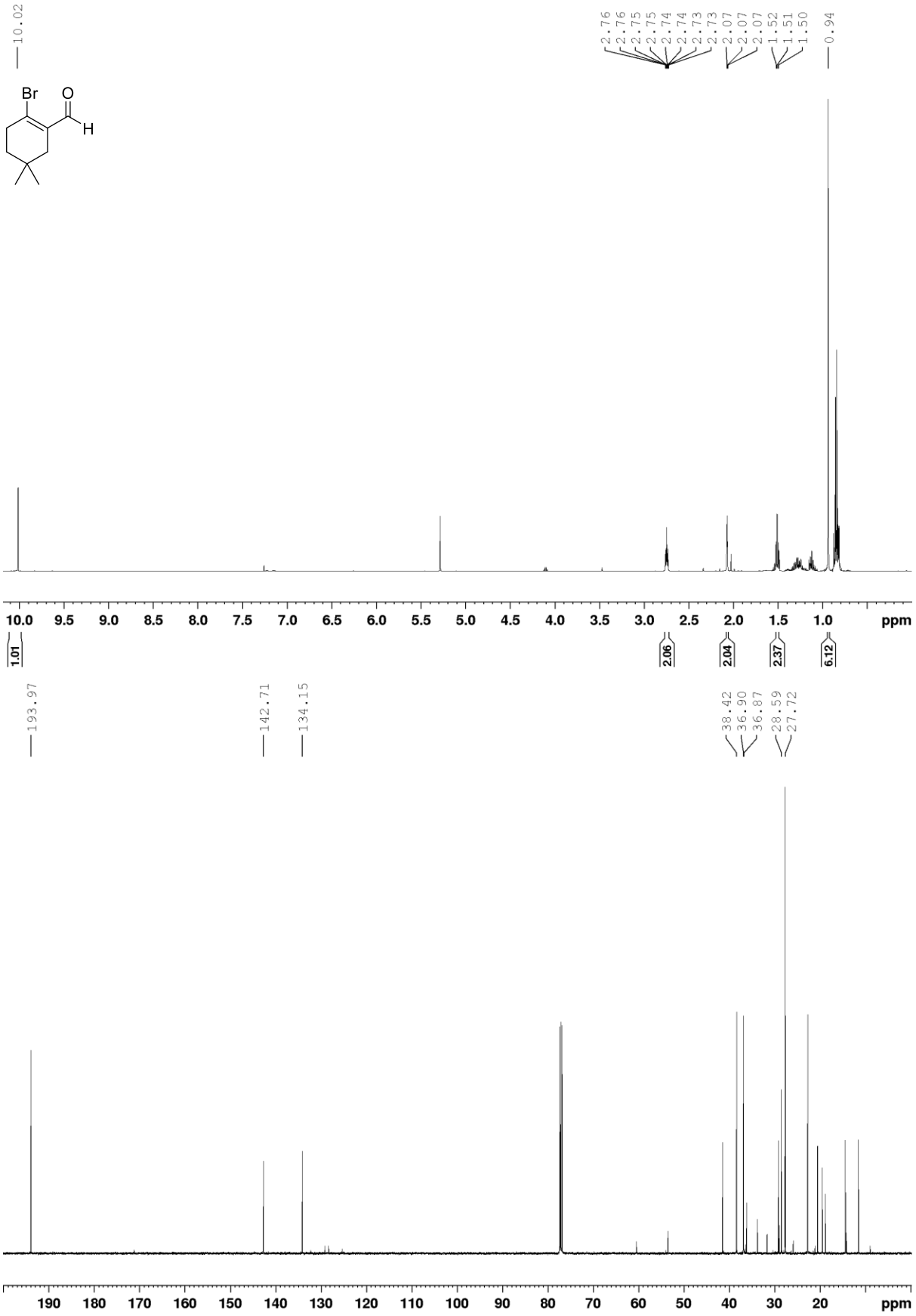

tert-Butyl 4-(4-((2-bromo-5,5-dimethylcyclohex-1-en-1-yl)methyl)piperazin-1-yl)benzoate (71)

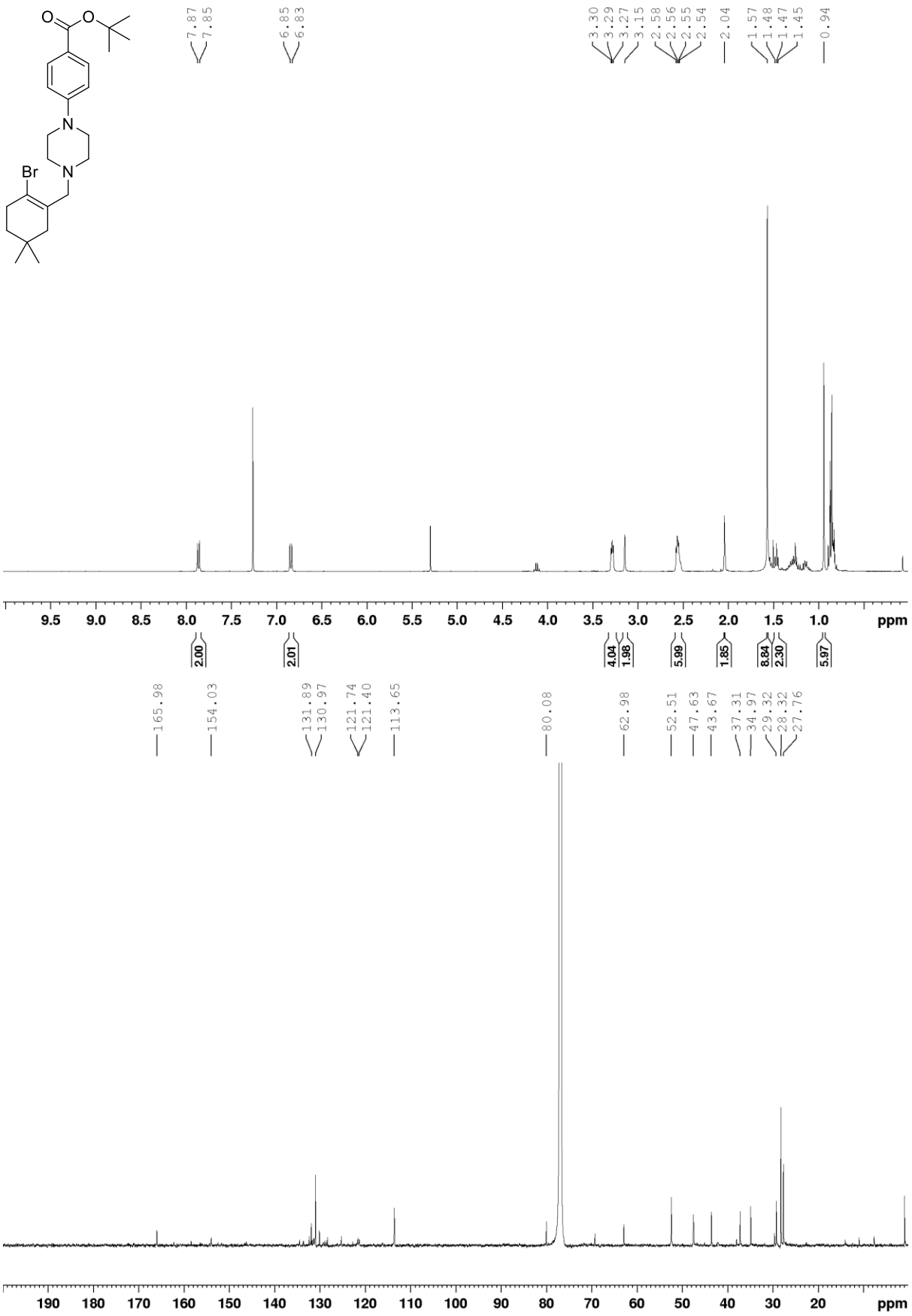

(2-Bromo-5,5-dimethylcyclohex-1-en-1-yl)methanol (72)

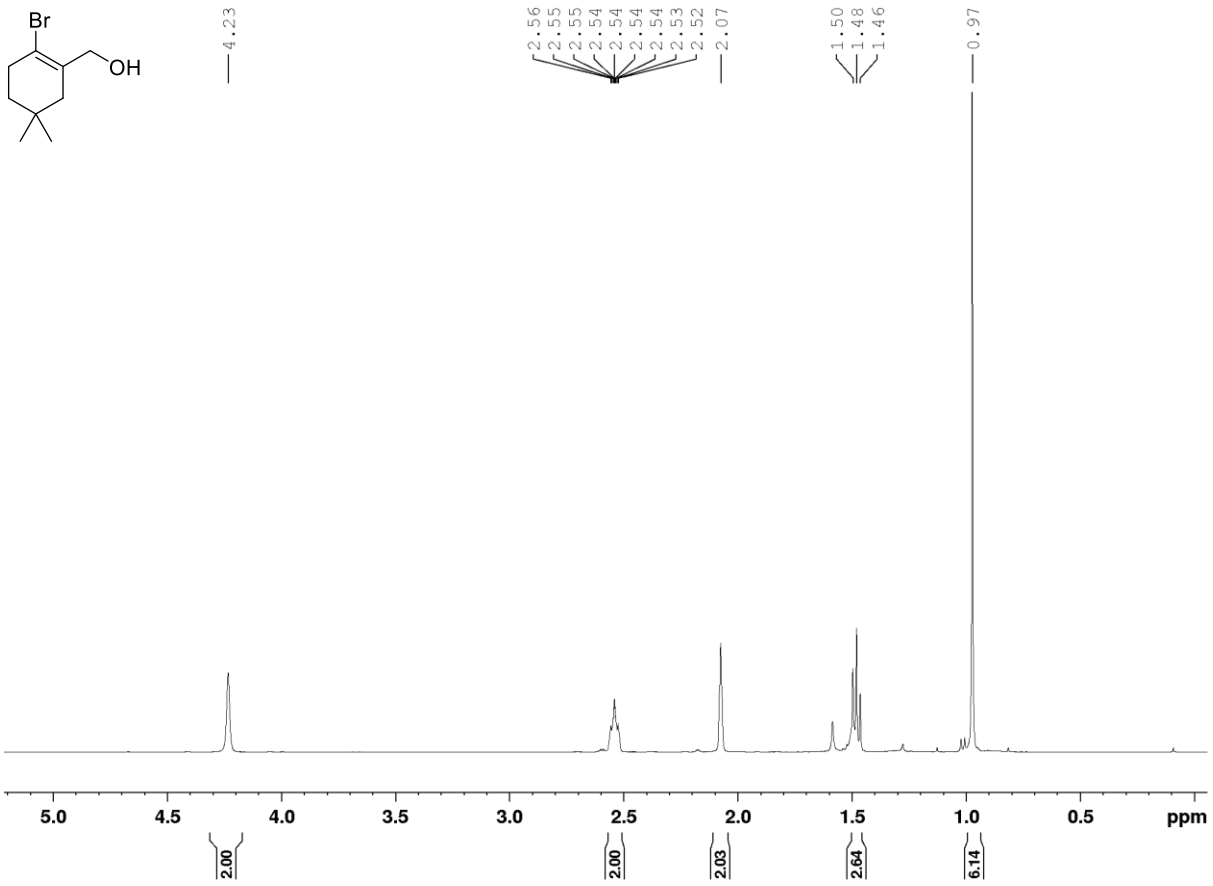

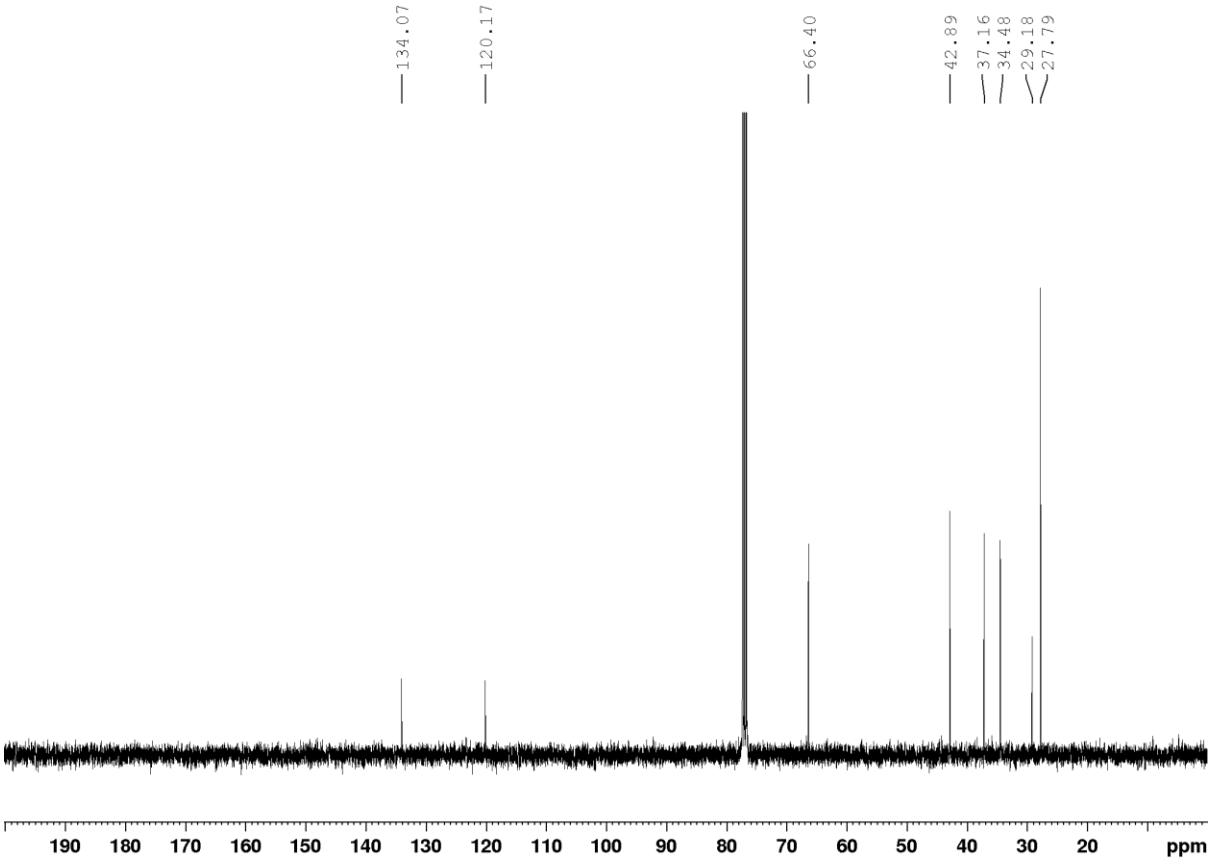

1-Bromo-2-(bromomethyl)-4,4-dimethylcyclohex-1-ene (73)

Impure

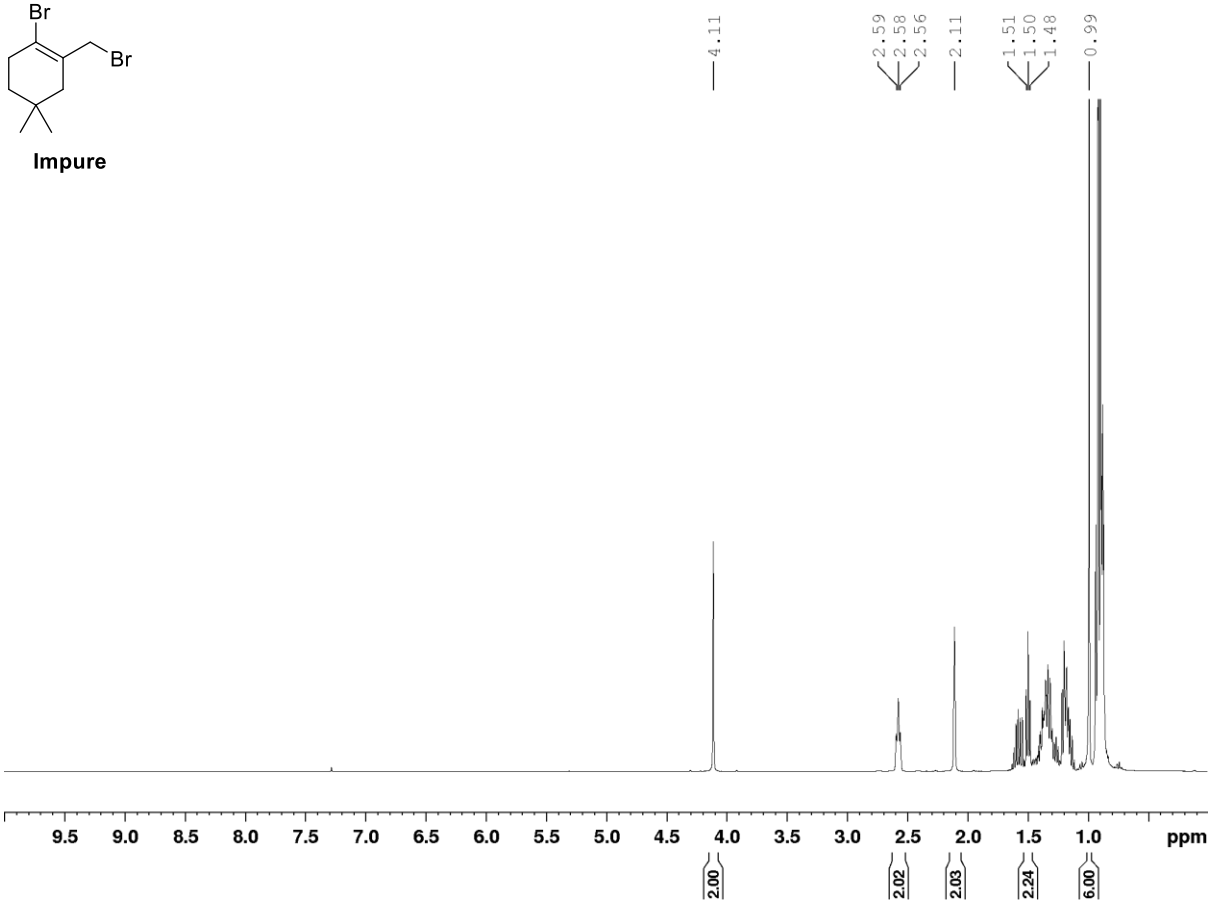

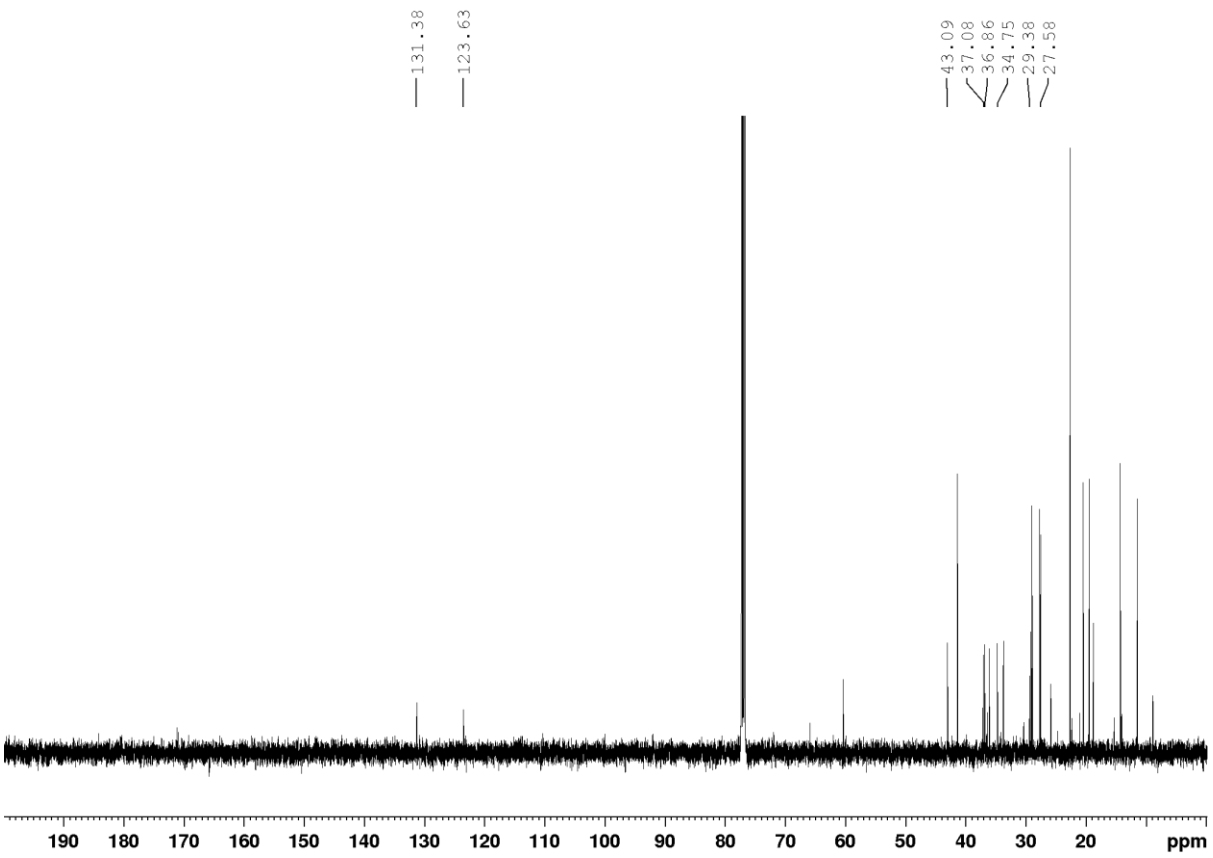

(4-((4-(3-(4-(Cyclopropanecarbonyl)piperazine-1-carbonyl)-4-fluorobenzyl)-1-oxophthalazin-2(*1H*)-yl)methyl)phenyl)boronic acid (78a) and 4-(3-(4-(cyclopropanecarbonyl)piperazine-1-carbonyl)-4-fluorobenzyl)-2-(4-(4,4,5,5-tetramethyl-1,3,2-dioxaborolan-2-yl)benzyl)phthalazin-1(*2H*)-one (78b)

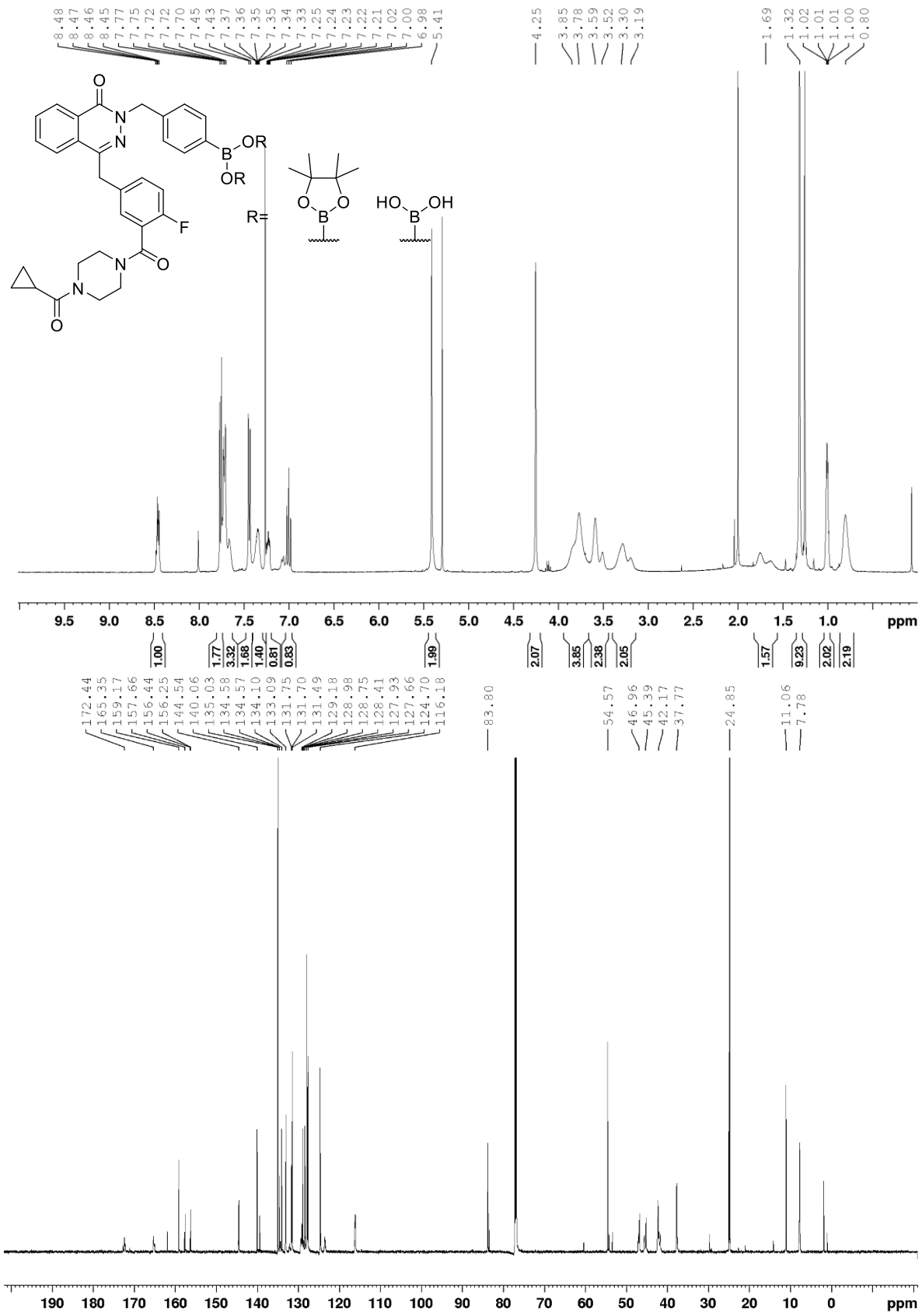

2-(4-Bromobenzyl)-4-(3-(4-(cyclopropanecarbonyl)piperazine-1-carbonyl)-4-fluorobenzyl)-phthalazin-1(*2H*)-one (80)

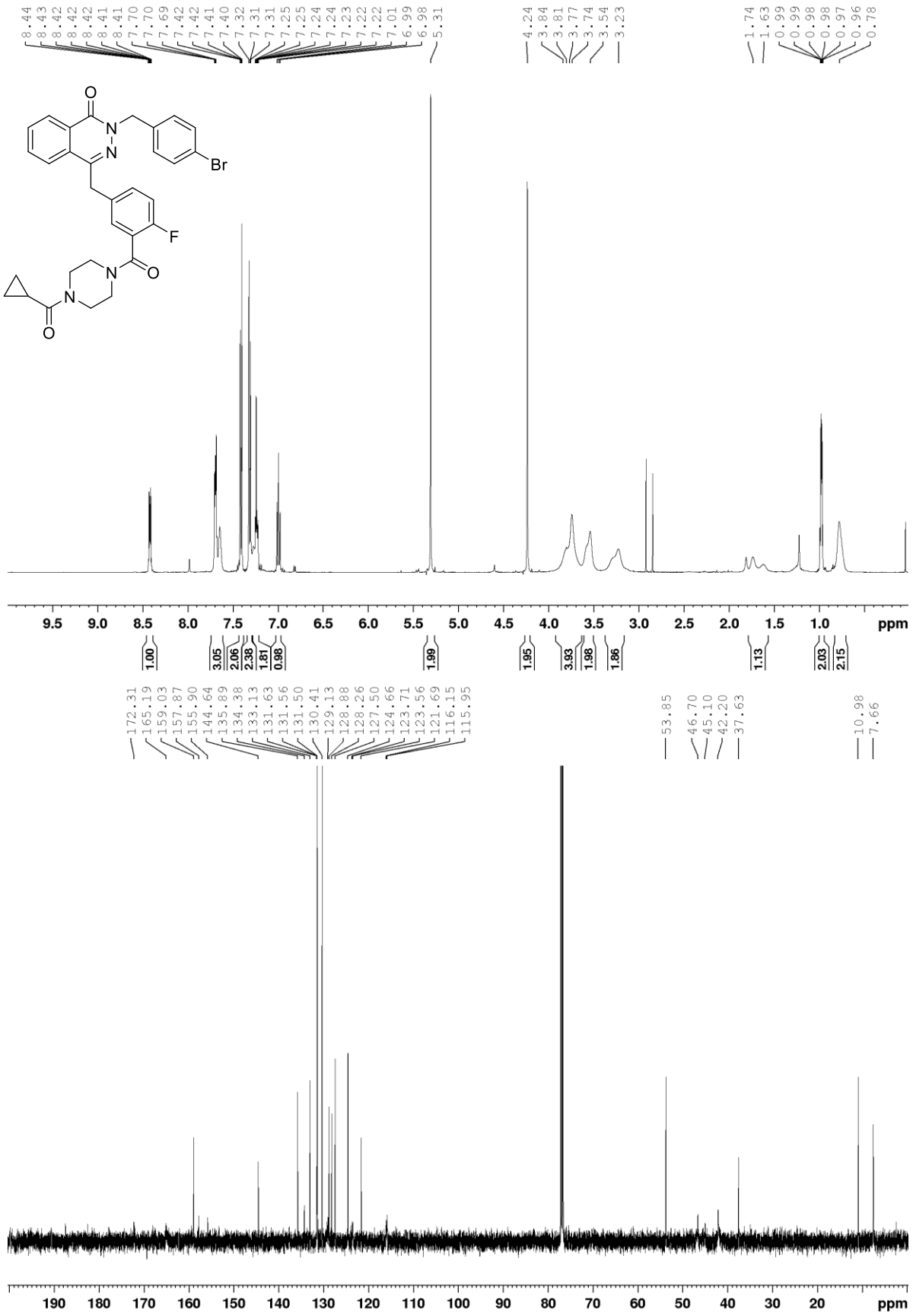

(4-(((4-(3-(4-(Cyclopropanecarbonyl)piperazine-1-carbonyl)-4-fluorobenzyl)-1-oxo-1,2-dihydrophthalazine-2-carbonyl)oxy)methyl)phenyl)boronic acid (81a) and 4-(4,4,5,5-tetramethyl-1,3,2-dioxaborolan-2-yl)benzyl 4-(3-(4-(cyclopropanecarbonyl)piperazine-1-carbonyl)-4-fluorobenzyl)-1-oxophthalazine-2(1*H*)-carboxylate (81b)

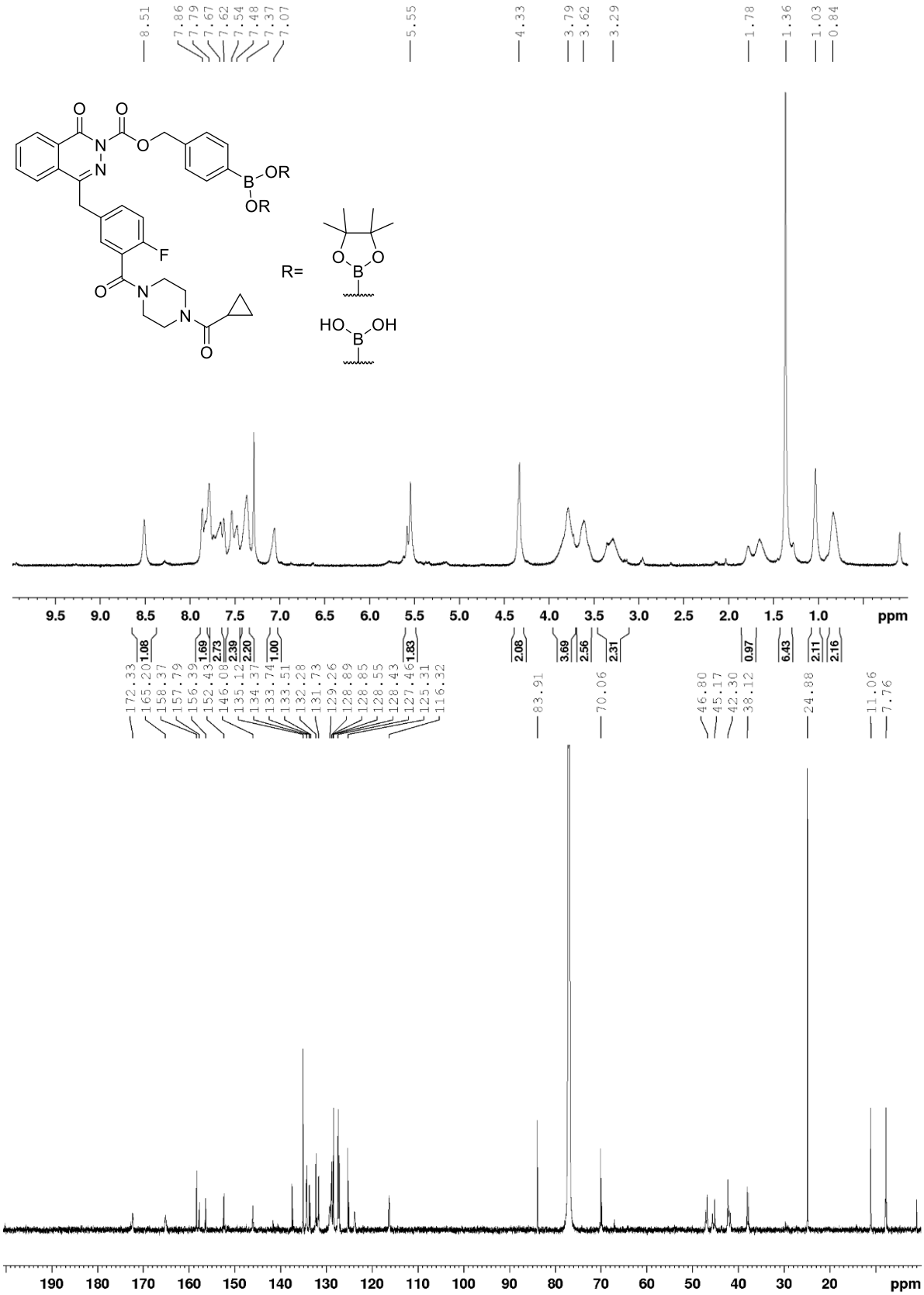

4-Bromobenzyl 4-(3-(4-(cyclopropanecarbonyl)piperazine-1-carbonyl)-4-fluorobenzyl)-1-oxophthalazine-2(1*H*)-carboxylate (83)

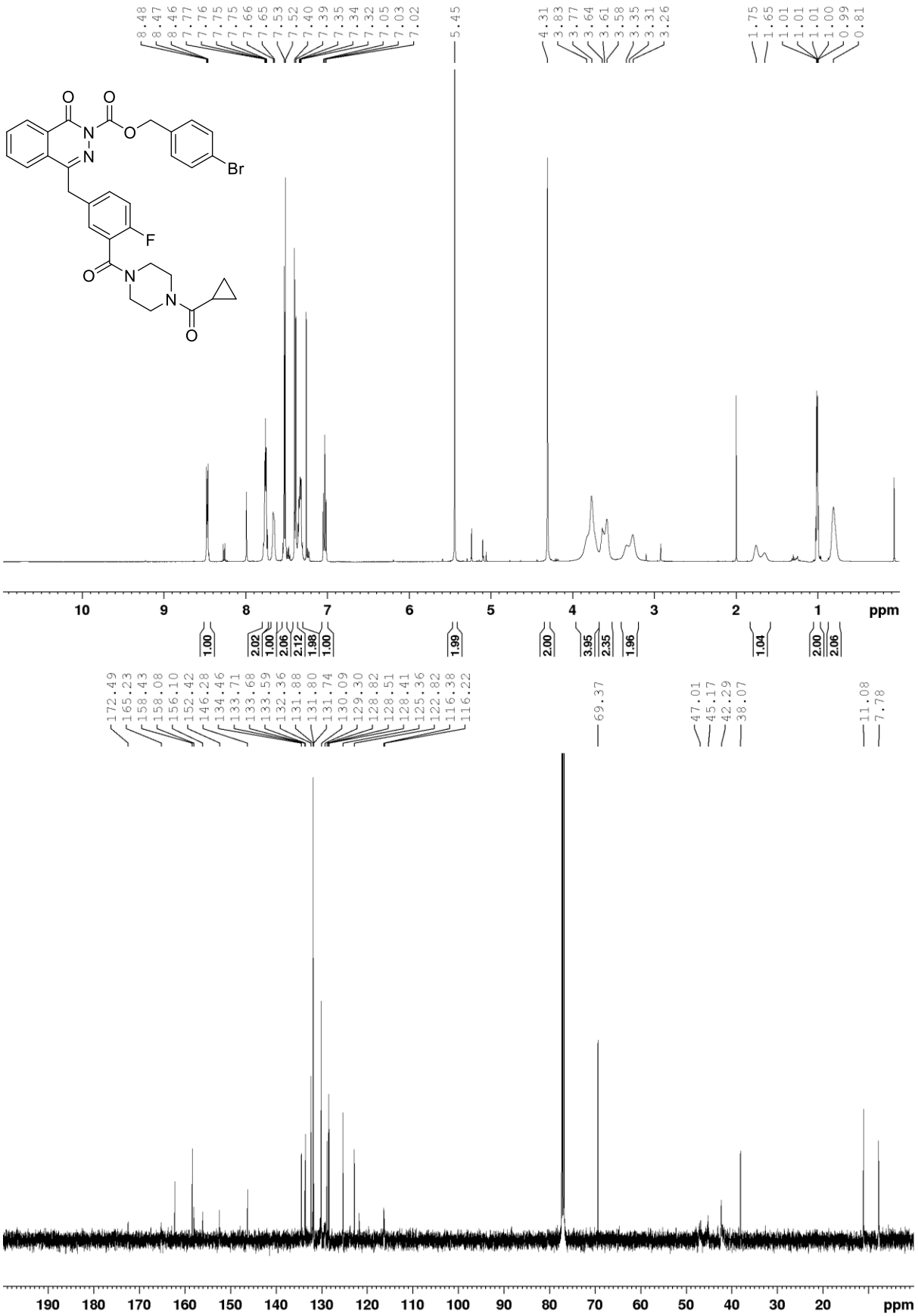

Appendix 2: Protein LCMS

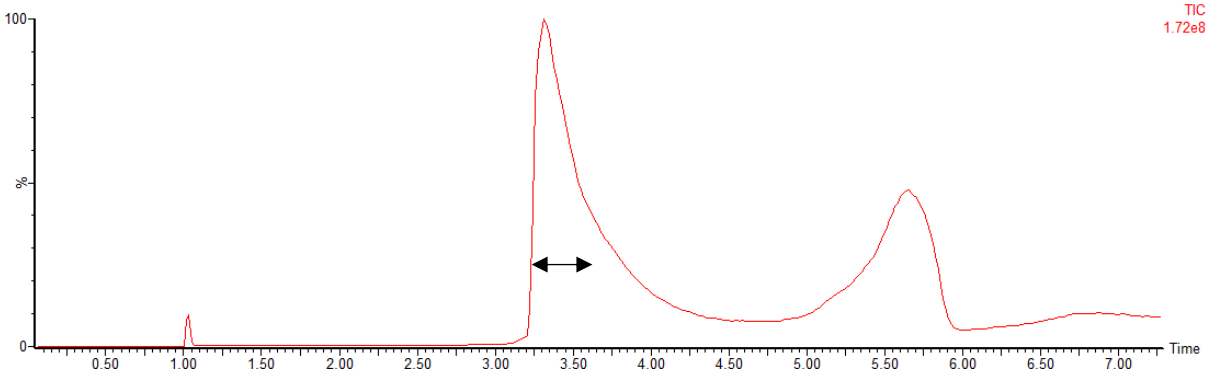

Figure 126: Typical TIC trace of trastuzumab sample with arrow indicating region of analysis.

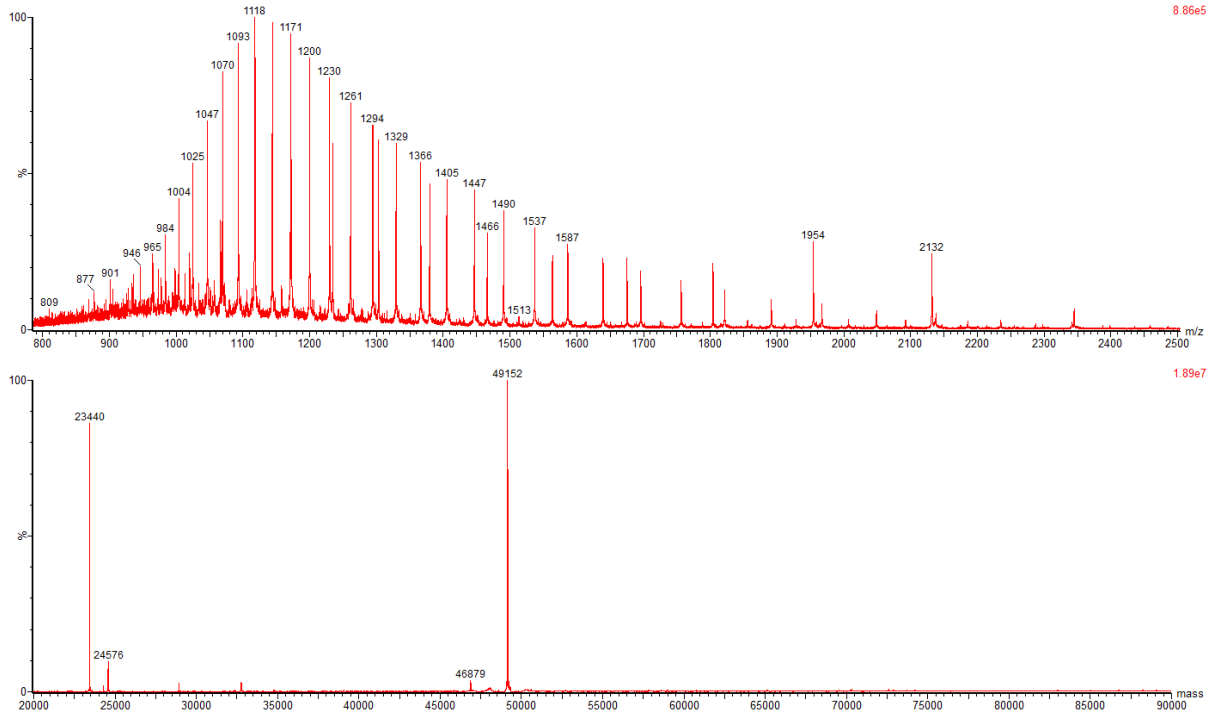

Figure 127: LCMS of unmodified, deglycosylated, reduced trastuzumab. Top = non-deconvoluted MS. Bottom = deconvoluted MS; heavy chain expected 49,153 Da, observed 49,152 Da; light chain expected 23,439 Da, observed 23,440 Da.

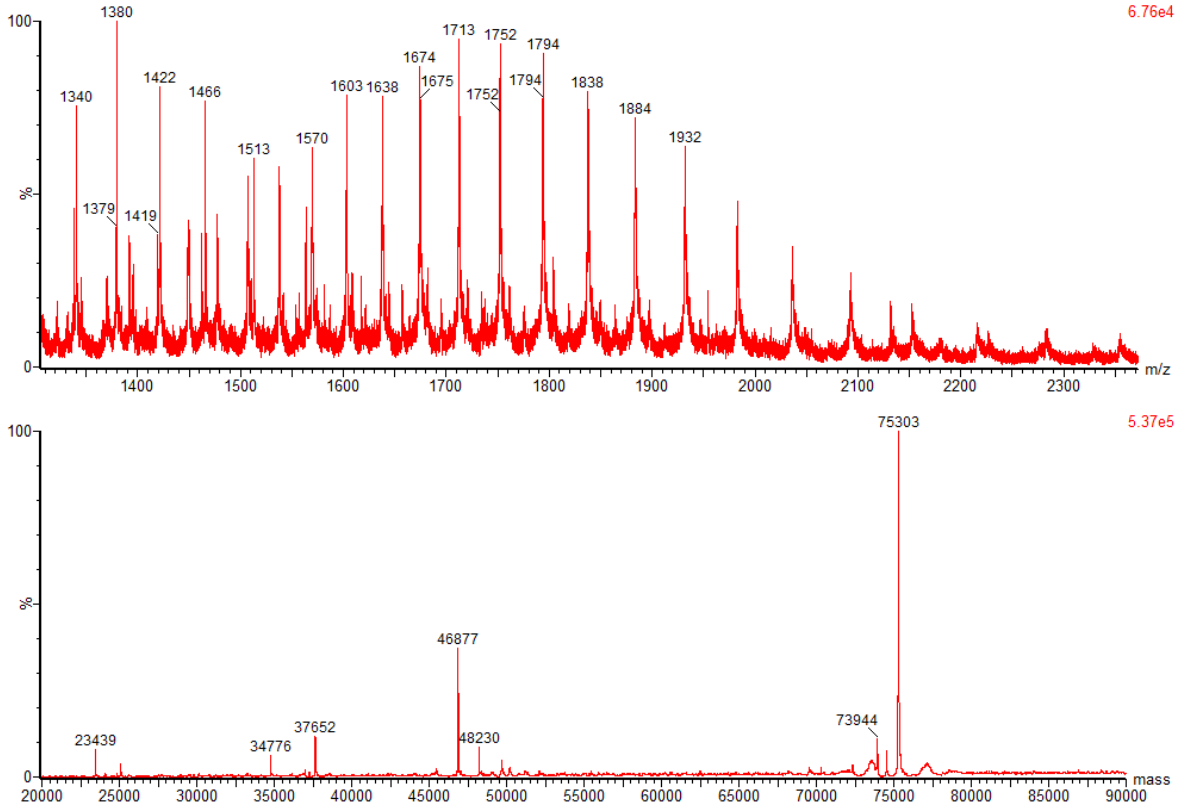

Figure 128: LCMS of **ADC 1**. Top = non-deconvoluted MS. Bottom = deconvoluted MS; expected 75,327 Da, observed 75,303 Da. (40 V cone voltage).

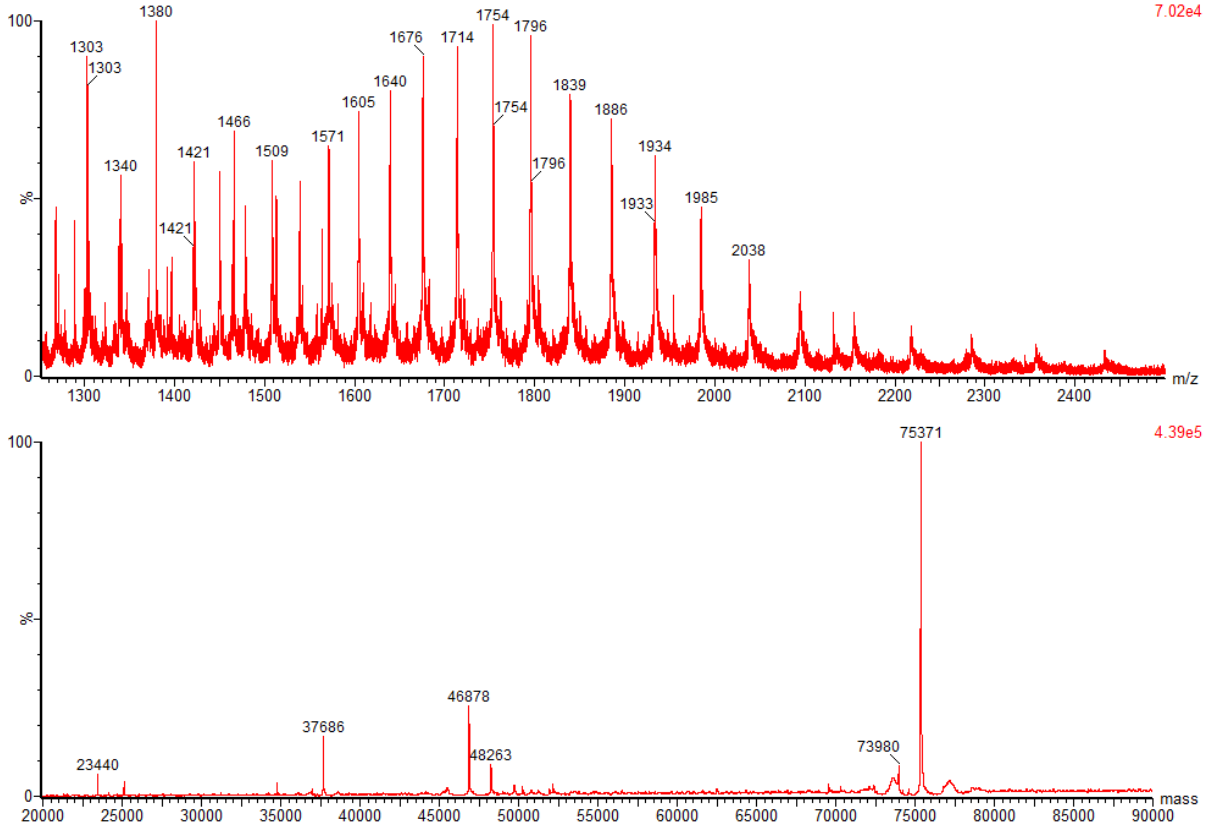

Figure 129: LCMS of **ADC 2**. Top = non-deconvoluted MS. Bottom = deconvoluted MS; expected 75,399 Da, observed 75,371 Da. (40 V cone voltage).

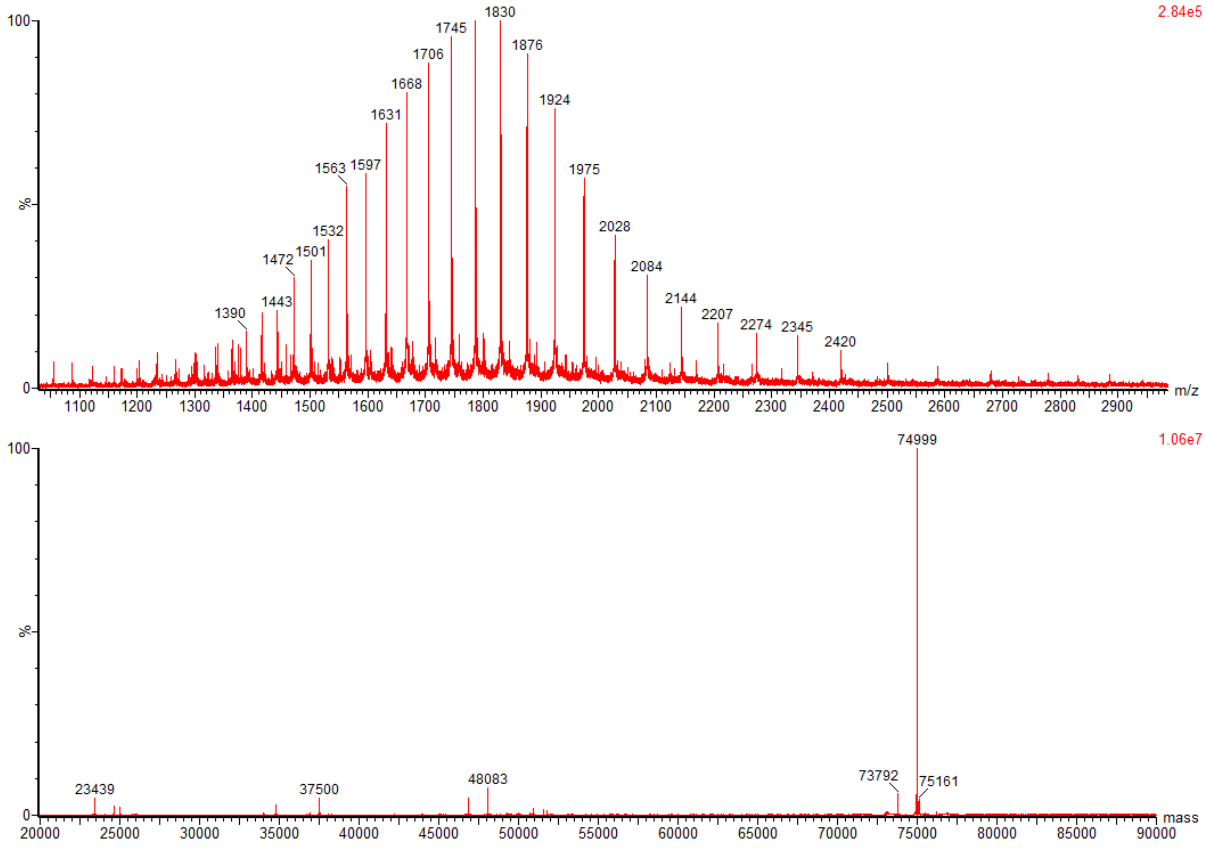

Figure 130: LCMS of **ADC 3**. Top = non-deconvoluted MS. Bottom = deconvoluted MS; expected 74,998 Da, observed 74,999 Da.

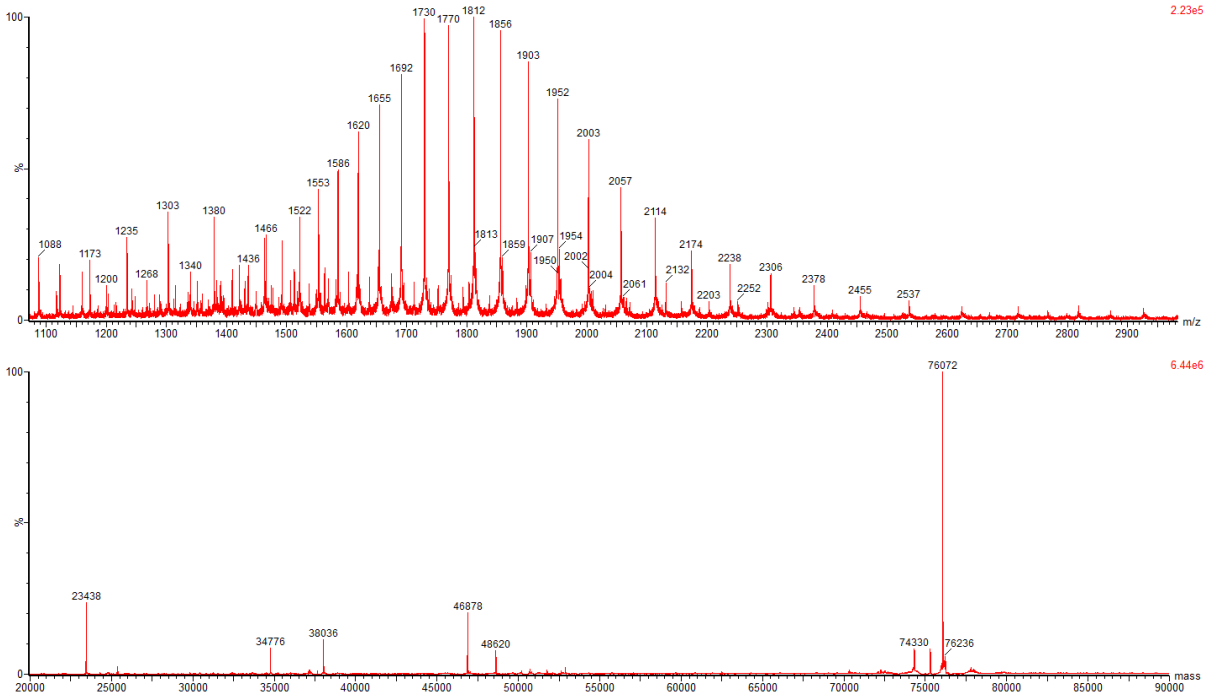

Figure 131: LCMS of **ADC 4**. Top = non-deconvoluted MS. Bottom = deconvoluted MS; expected 76,074 Da, observed 76,072 Da.

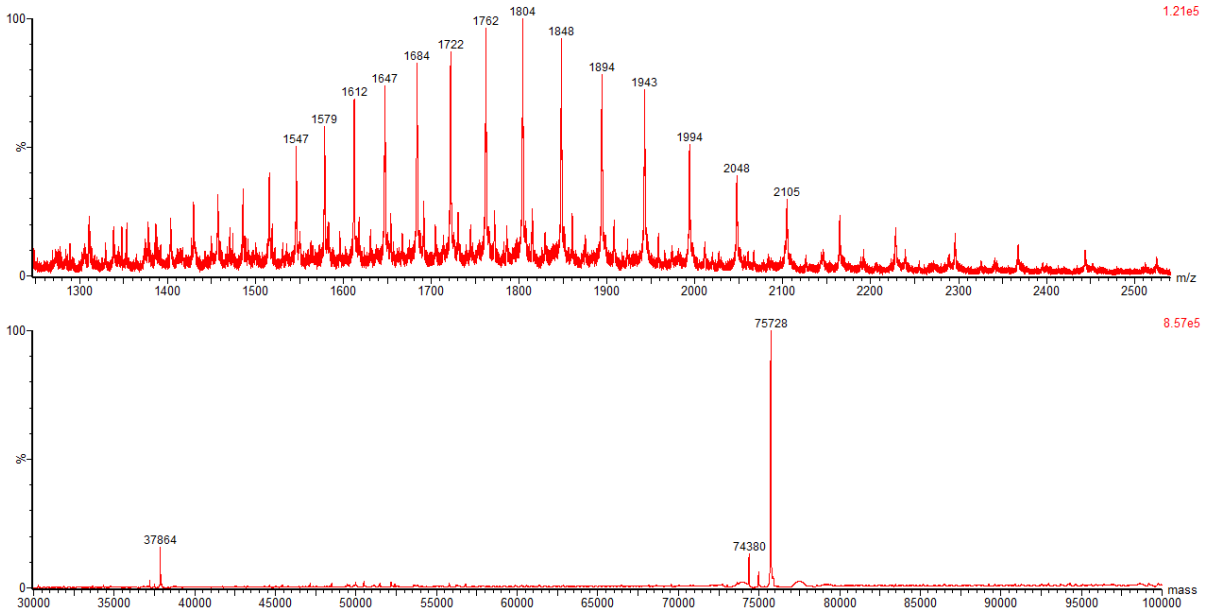

Figure 132: LCMS of **ADC 5**. Top = non-deconvoluted MS. Bottom = deconvoluted MS; expected 75,774 Da, observed 75,728 Da.

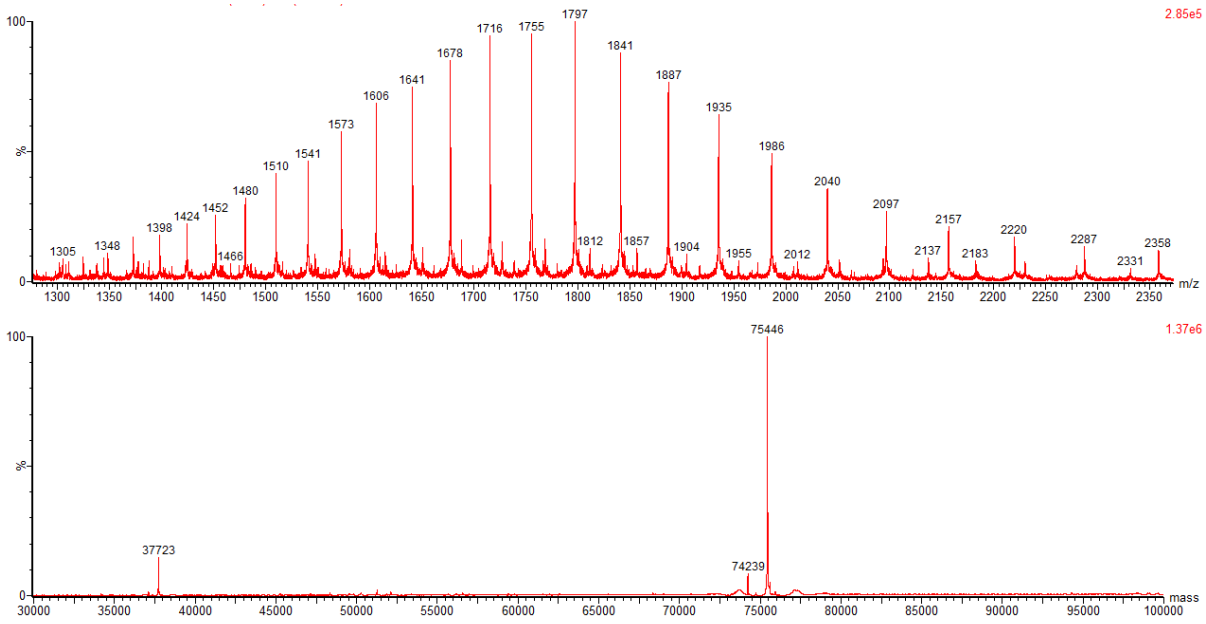

Figure 133: LCMS of **ADC 6**. Top = non-deconvoluted MS. Bottom = deconvoluted MS; expected 75,444 Da, observed 75,446 Da.

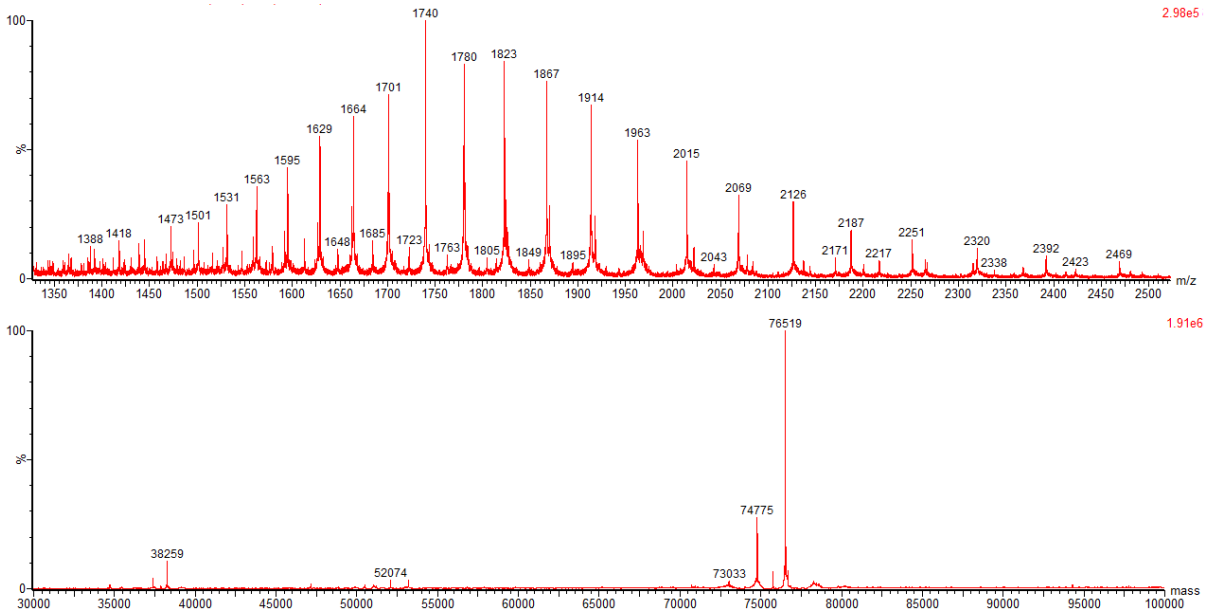

Figure 134: LCMS of **ADC 7**. Top = non-deconvoluted MS. Bottom = deconvoluted MS; expected 76,520 Da, observed 76,519 Da.

Appendix 3: Small-molecule HPLC

Table 21: Val-Cit model linker **4** HPLC assay stability in human plasma.

Time (days)	Linker Peak Area	Caffeine Peak Area	Linker/ Caffeine	Normalised Linker %
0	193.9	1605.6	0.121	100
1	189.6	1581.1	0.120	99
2	184.3	1628.6	0.113	94
3	181.2	1493.4	0.121	100
4	195.2	1625.4	0.120	99
5	200.6	1729.7	0.116	96
10	180.6	1661.7	0.109	90

Table 22: Val-Cit model linker **4** HPLC assay stability in mouse plasma

Time (days)	Linker Peak Area	Caffeine Peak Area	Linker/ Caffeine	Normalised Linker %
0	185.1	1548.1	0.120	100
1	115.9	1564.4	0.074	62
2	65.9	1547.8	0.043	36
3	48.7	1658.5	0.029	25
4	29.0	1578.0	0.018	15
5	25.1	1547.3	0.016	14
10	0.0	1873.3	0.000	0

Table 23: Di-fluoro model linker **2b** HPLC assay stability in human plasma

Time (days)	Linker Peak Area	Caffeine Peak Area	Linker/ Caffeine	Normalised Linker %
0	421.2	1075.9	0.391	100
1	783.4	2299.7	0.341	87
2	662.2	2205.9	0.300	77
3	1009.5	3215.4	0.314	80
4	672.4	2111.7	0.318	81
5	608.3	2022.6	0.301	77
10	517.7	1989.2	0.260	66

Table 24: Di-fluoro model linker **2b** HPLC assay stability in mouse plasma

Time (days)	Linker Peak Area	Caffeine Peak Area	Linker/ Caffeine	Normalised Linker %
0	1317.7	1743.6	0.756	100
1	1330.4	1607.6	0.828	110
2	1486.9	1712.3	0.868	115
3	1321.4	1634.9	0.808	107
4	1394.4	1649.7	0.845	112
5	1193.8	1537.1	0.777	103
10	1335.6	1646.1	0.811	107

Table 25: Non-cleavable model linker **3** HPLC assay stability in human plasma

Time (hours)	Linker Peak Area	Caffeine Peak Area	Linker/ Caffeine	Normalised Linker %
0	1597.7	1028.2	0.644	100
24	1596.5	934.6	0.585	91
48	1629.4	1046.3	0.642	100
72	1496.4	970.3	0.648	101
96	1547.6	959.5	0.620	96
120	1599.8	963.5	0.602	94
240	1811.0	852.9	0.471	73

Appendix 4: Protein HPLC

Hydrophobic Interaction Chromatography

Average DAR values were calculated using the following equation, where DAR_x refers to the peak area corresponding to that DAR species.

$$Average\ DAR = \frac{(DAR_1 + 2 \times DAR_2 + 3 \times DAR_3 + 4 \times DAR_4 + 5 \times DAR_5)}{(DAR_0 + DAR_1 + DAR_2 + DAR_3 + DAR_4 + DAR_5)}$$

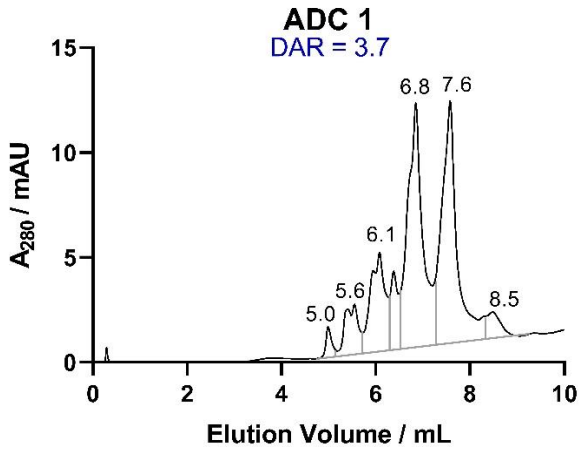

DAR Species	Elution Volume / mL	Peak Area
0	5.0	1.8
1	5.6	6.4
2	6.1	13.1
3	6.8	33.4
4	7.6	34.5
5	8.5	5.3

Figure 135: HIC trace for **ADC 1** including the peak areas used for calculation of average DAR.

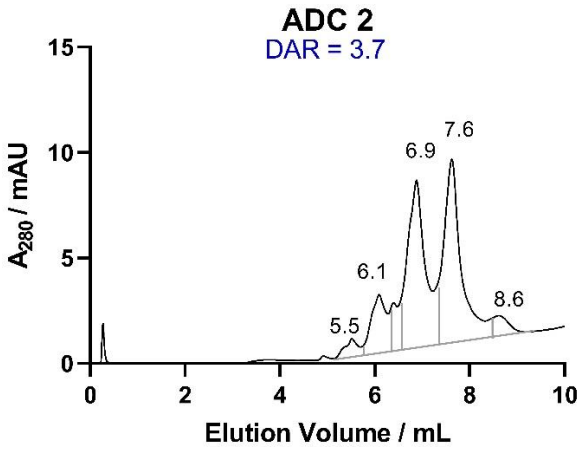

DAR Species	Elution Volume / mL	Peak Area
1	5.5	2.7
2	6.1	10.7
3	6.9	35.4
4	7.6	40.1
5	8.6	5.5

Figure 136: HIC trace for **ADC 2** including the peak areas used for calculation of average DAR.

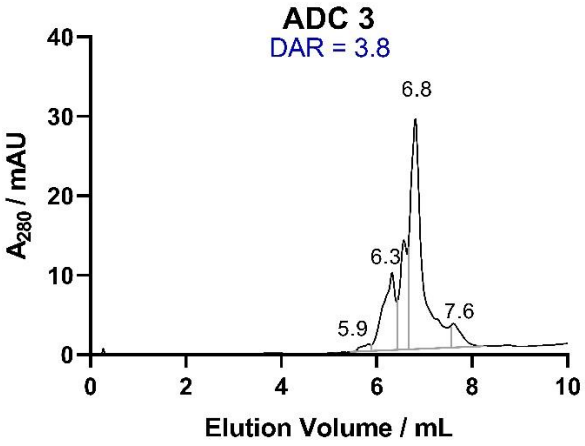

DAR Species	Elution Volume / mL	Peak Area
2	5.9	1.7
3	6.3	20.7
4	6.8	53.5
5	7.6	6.0

Figure 137: HIC trace for **ADC 3** including the peak areas used for calculation of average DAR.

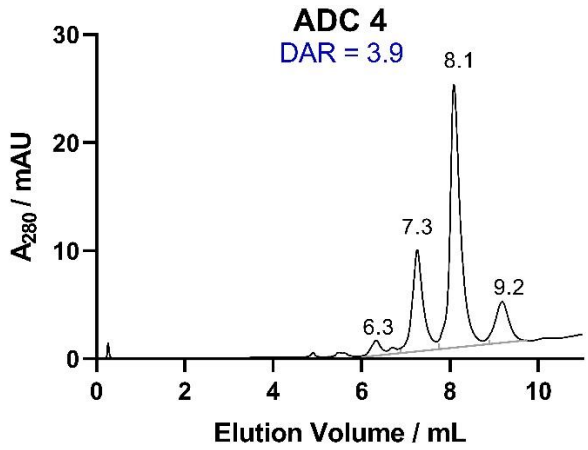

DAR Species	Elution Volume / mL	Peak Area
2	6.3	3.9
3	7.3	24.4
4	8.1	57.3
5	9.2	12.7

Figure 138: HIC trace for **ADC 4** including the peak areas used for calculation of average DAR.

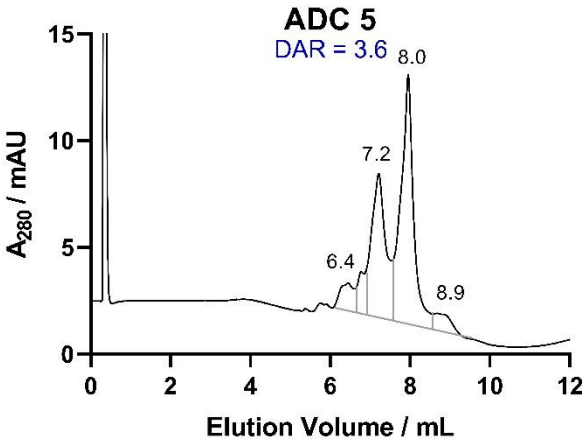

DAR Species	Elution Volume / mL	Peak Area
2	6.4	7.2
3	7.2	31.9
4	8.0	50.2
5	8.9	5.6

Figure 139: HIC trace for **ADC 5** including the peak areas used for calculation of average DAR.

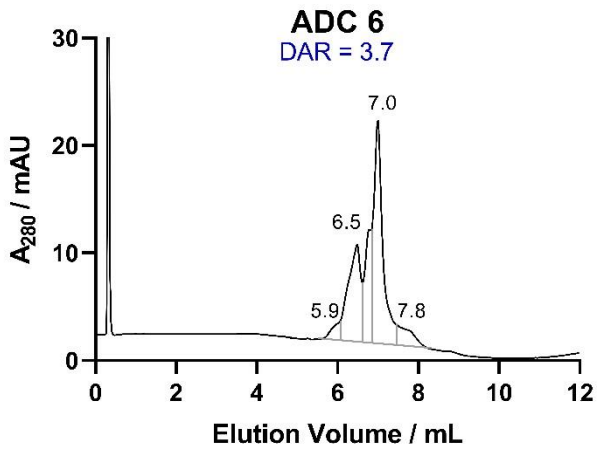

DAR Species	Elution Volume / mL	Peak Area
2	5.9	4.2
3	6.5	26.2
4	7.0	43.7
5	7.8	7.7

Figure 140: HIC trace for **ADC 6** including the peak areas used for calculation of average DAR.

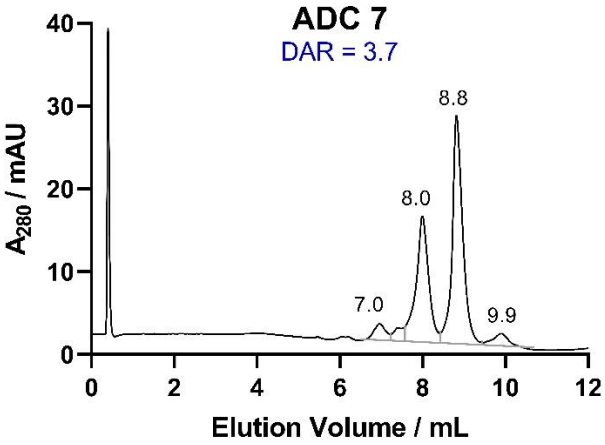

DAR Species	Elution Volume / mL	Peak Area
2	7.0	5.5
3	8.0	34.4
4	8.8	50.9
5	9.9	6.0

Figure 141: HIC trace for **ADC 7** including the peak areas used for calculation of average DAR.

Size-Exclusion Chromatography

Size-exclusion chromatography could not be obtained for **ADC 2**. **ADCs 5-7** are not included here since no aggregated species were observed.

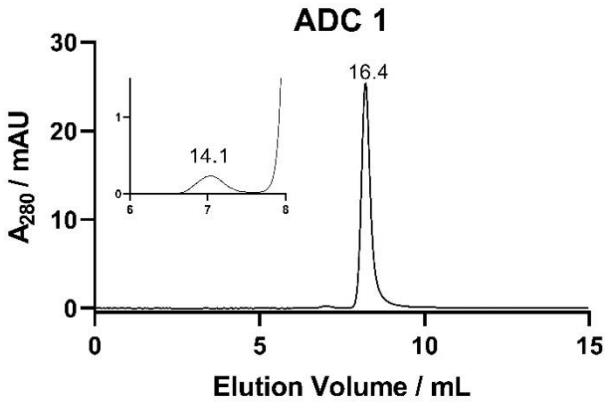

Species	Elution Volume / mL	Peak Area
Aggregate	14.1	0.8
ADC	16.4	99.2

Figure 142: SEC trace for **ADC 1** including a zoom of the peak corresponding to aggregated antibody species.

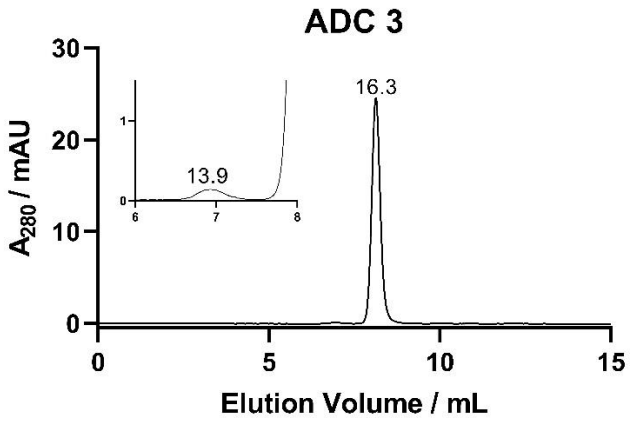

Species	Elution Volume / mL	Peak Area
Aggregate	13.9	0.6
ADC	16.3	99.4

Figure 143: SEC trace for **ADC 3** including a zoom of the peak corresponding to aggregated antibody species.

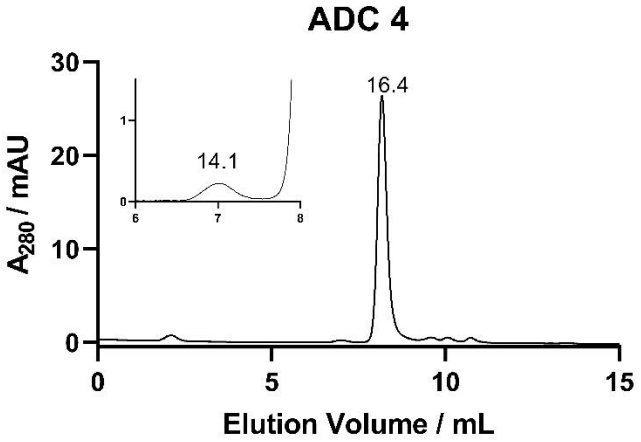

Species	Elution Volume / mL	Peak Area
Aggregate	14.1	0.8
ADC	16.4	99.2

Figure 144: SEC trace for **ADC 4** including a zoom of the peak corresponding to aggregated antibody species.

Appendix 5: Publications List

Peroxide-Cleavable Linkers for Antibody-Drug Conjugates, N. Ashman, J. D. Bargh, S. J. Walsh, R. D. Greenwood, A. Tiberghien, J. S. Carroll, D. R. Spring, *Chem. Commun*. **2023**, 59, 1841-1844.

Non-internalising antibody-drug conjugates, N. Ashman, J. D. Bargh, D. R. Spring, *Chem. Soc. Rev*. **2022**, 51, 9182-9202.

Antibody dual-functionalisation enabled through a modular divinylpyrimidine disulfide rebridging strategy, A. R. Hanby, S. J. Walsh, A. J. Counsell, N. Ashman, K. T. Mortensen, J. S. Carroll, D. R. Spring, *Chem. Commun.* **2022**, *58*, 9401-9404.

A dual-enzyme cleavable linker for antibody-drug conjugates, J. D. Bargh, S. J. Walsh, N. Ashman, A. Isidro-Llobet, J. S. Carroll, D. R. Spring, *Chem. Commun.* **2021**, *57*, 3457-3460.

Site-selective modification strategies in antibody-drug conjugates, S. J. Walsh, J. D. Bargh, F. M. Dannheim, A. R. Hanby, H. Seki, A. J. Counsell, X. Ou, E. Fowler, N. Ashman, Y. Takada, A. Isidro-Llobet, J. S. Parker, J. S. Carroll, D. R. Spring, *Chem. Soc. Rev.* **2021**, *50*, 1305-1353.